WETLAND ECOLOGY AND BIOGEOCHEMISTRY UNDER NATURAL AND HUMAN DISTURBANCE

EDITED BY: Jianghua Wu, Matthias Peichl, Ligang Xu, Junwei Luan and John Connolly

PUBLISHED IN: Frontiers in Earth Science, Frontiers in Environmental Science and Frontiers in Ecology and Evolution

frontiers Research Topics

ISSN 1664-8714
ISBN 978-2-88971-822-1
DOI 10.3389/978-2-88971-822-1

About Frontiers

Frontiers is more than just an open-access publisher of scholarly articles: it is a pioneering approach to the world of academia, radically improving the way scholarly research is managed. The grand vision of Frontiers is a world where all people have an equal opportunity to seek, share and generate knowledge. Frontiers provides immediate and permanent online open access to all its publications, but this alone is not enough to realize our grand goals.

Frontiers Journal Series

The Frontiers Journal Series is a multi-tier and interdisciplinary set of open-access, online journals, promising a paradigm shift from the current review, selection and dissemination processes in academic publishing. All Frontiers journals are driven by researchers for researchers; therefore, they constitute a service to the scholarly community. At the same time, the Frontiers Journal Series operates on a revolutionary invention, the tiered publishing system, initially addressing specific communities of scholars, and gradually climbing up to broader public understanding, thus serving the interests of the lay society, too.

Dedication to Quality

Each Frontiers article is a landmark of the highest quality, thanks to genuinely collaborative interactions between authors and review editors, who include some of the world's best academicians. Research must be certified by peers before entering a stream of knowledge that may eventually reach the public - and shape society; therefore, Frontiers only applies the most rigorous and unbiased reviews.
Frontiers revolutionizes research publishing by freely delivering the most outstanding research, evaluated with no bias from both the academic and social point of view. By applying the most advanced information technologies, Frontiers is catapulting scholarly publishing into a new generation.

What are Frontiers Research Topics?

Frontiers Research Topics are very popular trademarks of the Frontiers Journals Series: they are collections of at least ten articles, all centered on a particular subject. With their unique mix of varied contributions from Original Research to Review Articles, Frontiers Research Topics unify the most influential researchers, the latest key findings and historical advances in a hot research area! Find out more on how to host your own Frontiers Research Topic or contribute to one as an author by contacting the Frontiers Editorial Office: frontiersin.org/about/contact

WETLAND ECOLOGY AND BIOGEOCHEMISTRY UNDER NATURAL AND HUMAN DISTURBANCE

Topic Editors:
Jianghua Wu, Memorial University of Newfoundland, Canada
Matthias Peichl, Swedish University of Agricultural Sciences, Sweden
Ligang Xu, Nanjing Institute of Geography and Limnology (CAS), China
Junwei Luan, International Center for Bamboo and Rattan, China
John Connolly, Trinity College Dublin, Ireland

Cover Image taken by Topic Editor Jianghua Wu

Citation: Wu, J., Peichl, M., Xu, L., Luan, J., Connolly, J., eds. (2021). Wetland Ecology and Biogeochemistry Under Natural and Human Disturbance. Lausanne: Frontiers Media SA. doi: 10.3389/978-2-88971-822-1

Table of Contents

frontiers in Earth Science

EDITORIAL
published: 15 October 2021
doi: 10.3389/feart.2021.752101

Editorial: Wetland Ecology and Biogeochemistry Under Natural and Human Disturbance

Jianghua Wu[1]*, *Matthias Peichl*[2], *Junwei Luan*[3], *John Connolly*[4] and *Ligang Xu*[5]

[1]Environment and Sustainability, School of Science and the Environment, Memorial University of Newfoundland, Corner Brook, NL, Canada, [2]Department of Forest Ecology and Management, Swedish University of Agricultural Sciences, Umea, Sweden, [3]Institute of Resources and Environment, International Centre for Bamboo and Rattan, Beijing, China, [4]Department of Geography, Trinity College Dublin, The University of Dublin, Dublin, Ireland, [5]Nanjing Institute of Geography and Limnology, Chinese Academy of Sciences, Nanjing, China

Keywords: wetlands, climate change, human disturbance, biogeochemistry, ecosystem function, greenhouse gas emissions

Editorial on the Research Topic

Wetland Ecology and Biogeochemistry Under Natural and Human Disturbance

INTRODUCTION

Wetlands are areas where the water level is present either at or near the surface of the soil all year or for varying periods of time during the year (Zedler and Kercher, 2005). They provide essential ecosystem services such as water purification, flood control, biodiversity conservation, carbon sequestration, and greenhouse gas (GHG) regulation (Paar et al.; Zhang et al.). These wetland functions are vulnerable to climate change and human disturbances, however, the extent and direction of their future changes are highly uncertain at present. This has caused a significant uncertainty over how climate change and human disturbances would have affected the ecosystem function of wetlands.

This special issue attempted to help address this knowledge gap with a compilation of 12 original papers and one corrigendum which reported recent findings on the effects of climate change and human disturbances on wetland ecosystem functions. Moreover, various restoration methods proposed by several articles in this special issue have been put forward to evaluate the opportunities and limitations in returning biogeochemical functions in disturbed wetlands towards their natural state.

THE IMPACTS OF CLIMATE CHANGE AND HUMAN DISTURBANCES ON THE WETLAND C BALANCE

Temperature and precipitation regime alterations are two essential climatic changes predicted for the future. On the one hand, global warming, which is likely coinciding with lower water table levels, may increase organic matter lability and accelerate decomposition in wetlands, thus emitting more greenhouse gases and aggravating global warming (AminiTabrizi et al.). On the other hand, warming may increase vegetation productivity and photosynthetic carbon dioxide (CO_2) uptake in wetlands (Li et al., 2021). Increased substrate supply due to greater vegetation might, however, also enhance CH_4 production (Li et al., 2021). Meanwhile, warmer conditions might coincide with lowered WTL which may enhance CH_4 oxidation and thus decrease net CH_4 emissions. The net effect of warming on the carbon sink function and GHG balance of wetlands depends on these two contrasting effects. Drought spells could lead to an increase in carbon emissions from wetlands (Keane et al.), while

OPEN ACCESS

Edited and reviewed by:
Edward A. Johnson,
University of Calgary, Canada

***Correspondence:**
Jianghua Wu
jwu@grenfell.mun.ca

Received: *02 August 2021*
Accepted: *06 October 2021*
Published: *15 October 2021*

Citation:
Wu J, Peichl M, Luan J, Connolly J and Xu L (2021) Editorial: Wetland Ecology and Biogeochemistry Under Natural and Human Disturbance. Front. Earth Sci. 9:752101. doi: 10.3389/feart.2021.752101

flooding could increase algal production, while it would also decrease decomposition and enhance methane emissions, which benefits carbon uptake and could become important to estimate carbon balance in wetlands (Kane et al.).

Besides climate change, wetlands are vulnerable to human disturbances, resulting in the loss of more than half of the world's inland wetlands (Zedler and Kercher, 2005). Many wetlands have been drained with the purpose to gain land for agricultural, forestry and industrial use. The lowered water table level (WTL) following drainage alters the microbial communities and their activity which can lead to increased carbon emissions (Kitson and Bell, 2020). Transforming a wetland to rice paddy can increase nutrient concentration, which impacts bryophyte distribution (Ma et al.). Moreover, a network of seismic lines due to industrial activities for resource extraction can increase mineralization rates and carbon loss from wetlands (Davidson et al.). Road and dam construction significantly altered the hydrological regime and also influenced nutrients and metals retention, as well as wetland types (Rideout et al.; Sun et al.). Thus, altogether, these special issue contributions highlight that human disturbances considerably impact wetland functions.

RESTORATION METHODS FOR DISTURBED WETLANDS

In order to re-establish key wetland functions, various restoration methods have been put forward and evaluated in the literature (e.g., Taft et al., 2018; Wen et al., 2018; Liu et al., 2020; Evans et al., 2021), and several special methods have been proposed and studied by several contributed papers in this special issue. One common restoration method is rewetting (i.e. raising the WTL by ditch blocking) which can result in reduced CO_2 and N_2O emissions and thus mitigate the climate impact (Taft et al., 2018; Liu et al., 2020). However, rewetting drained wetlands can increase methane (CH_4) emissions (Wen et al., 2018), which may weaken their potential to mitigate global warming. Consequently, the critical point of raising water level has been investigated (Evans et al., 2021). In addition, Lemmer et al. introduced one alternate restoration method which is based on partial removal of the well pad's construction materials to near the water table level and the surface elevation of the surrounding ecosystem. They find that this approach is the most effective restoration method to sequester carbon, compared to the method where the foreign clay was partially removed and typical fen plant species were introduced (Lemmer et al.). Furthermore, Leppä et al. demonstrated that selection cutting is an effective tool to control water table level, which plays an essential role in the biogeochemical function of wetland ecosystems. However, Yavitt et al. demonstrate that it is challenging to restore key soil properties and functioning in highly degraded wetlands. Altogether, these contributions highlight the need for improved understanding of various restoration techniques and their effectiveness in restoring the biogeochemical functions of degraded peatlands.

Overall, these 12 Special Issue papers brought together a wide range of aspects related to the impacts of climate change and human disturbances on wetland ecosystems and thereby contribute significantly to an improved understanding of carbon cycling and greenhouse gas emissions from wetlands, wetland hydrology, ecosystem ecology and biogeochemical dynamics of wetlands. In addition, different special restoration methods for disturbed wetlands were tested with the goal to develop management strategies that restore and maintain the natural ecosystem functions of global wetlands.

AUTHOR CONTRIBUTIONS

JW, as the leading guest editor, wrote the first draft of this editorial, and MP and JL helped edit, revise and improve this editorial. All authors contributed to manuscript revision, read, and approved the submitted version.

REFERENCES

Evans, C. D., Peacock, M., Baird, A. J., Artz, R. R. E., Burden, A., Callaghan, N., et al. (2021). Overriding Water Table Control on Managed Peatland Greenhouse Gas Emissions. *Nature* 593, 548–552. doi:10.1038/s41586-021-03523-1

Kitson, E., and Bell, N. G. A. (2020). The Response of Microbial Communities to Peatland Drainage and Rewetting. A Review. *Front. Microbiol.* 11, 582812. doi:10.3389/fmicb.2020.582812

Li, Q., Gogo, S., Leroy, F., Guimbaud, C., and Laggoun-Défarge, F. (2021). Response of Peatland CO_2 and CH_4 Fluxes to Experimental Warming and the Carbon Balance. *Front. Earth Sci.* 9, 631368. doi:10.3389/feart.2021.631368

Liu, H., Wrage-Mönnig, N., and Lennartz, B. (2020). Rewetting Strategies to Reduce Nitrous Oxide Emissions from European Peatlands. *Commun. Earth Environ.* 1, 17. doi:10.1038/s43247-020-00017-2

Taft, H. E., Cross, P. A., and Jones, D. L. (2018). Efficacy of Mitigation Measures for Reducing Greenhouse Gas Emissions from Intensively Cultivated Peatlands. *Soil Biol. Biochem.* 127, 10–21. doi:10.1016/j.soilbio.2018.08.020

Wen, X., Unger, V., Jurasinski, G., Koebsch, F., Horn, F., Rehder, G., et al. (2018). Predominance of Methanogens over Methanotrophs in Rewetted Fens Characterized by High Methane Emissions. *Biogeosciences* 15, 6519–6536. doi:10.5194/bg-15-6519-2018

Zedler, J. B., and Kercher, S. (2005). WETLAND RESOURCES: Status, Trends, Ecosystem Services, and Restorability. *Annu. Rev. Environ. Resour.* 30, 39–74. doi:10.1146/annurev.energy.30.050504.144248

Conflict of Interest: The authors declare that the research was conducted in the absence of any commercial or financial relationships that could be construed as a potential conflict of interest.

frontiers in Earth Science

ORIGINAL RESEARCH
published: 24 February 2020
doi: 10.3389/feart.2020.00032

Environmental Together With Interspecific Interactions Determine Bryophyte Distribution in a Protected Mire of Northeast China

Jin-Ze Ma[1,2,3,4], Xu Chen[5], Azim Mallik[1,6], Zhao-Jun Bu[1,3,4], Ming-Ming Zhang[1,3,4], Sheng-Zhong Wang[1,3,4]* and Sebastian Sundberg[7,8]*

[1] Key Laboratory of Geographical Processes and Ecological Security in Changbai Mountains, Ministry of Education, School of Geographical Sciences, Northeast Normal University, Changchun, China, [2] Research Center for Environmental Engineering and Technology, School of Geography and Environmental Engineering, Gannan Normal University, Ganzhou, China, [3] State Environmental Protection Key Laboratory of Wetland Ecology and Vegetation Restoration, Institute for Peat and Mire Research, Northeast Normal University, Changchun, China, [4] Jilin Provincial Key Laboratory for Wetland Ecological Processes and Environmental Change in the Changbai Mountains, Changchun, China, [5] State Key Laboratory of Biogeology and Environmental Geology, School of Earth Sciences, China University of Geosciences, Wuhan, China, [6] Department of Biology, Lakehead University, Thunder Bay, ON, Canada, [7] Evolutionary Biology Centre, Department of Plant Ecology and Evolution, Uppsala University, Uppsala, Sweden, [8] Swedish Species Information Centre, Swedish University of Agricultural Sciences, Uppsala, Sweden

OPEN ACCESS

Edited by:
Matthias Peichl, Department of Forest Ecology & Management, Swedish University of Agricultural Sciences, Sweden

Reviewed by:
Heinjo During, Utrecht University, Netherlands
Michal Hájek, Masaryk University, Czechia
Nele Ingerpuu, University of Tartu, Estonia

***Correspondence:**
Zhao-Jun Bu
buzhaojun@nenu.edu.cn
Sheng-Zhong Wang
szwang@nenu.edu.cn

Specialty section:
This article was submitted to Biogeoscience, a section of the journal Frontiers in Earth Science

Received: *19 November 2019*
Accepted: *29 January 2020*
Published: *24 February 2020*

Citation:
Ma J-Z, Chen X, Mallik A, Bu Z-J, Zhang M-M, Wang S-Z and Sundberg S (2020) Environmental Together With Interspecific Interactions Determine Bryophyte Distribution in a Protected Mire of Northeast China. Front. Earth Sci. 8:32. doi: 10.3389/feart.2020.00032

Question: What environmental variables and plant–plant interactions affect mire bryophyte distribution and does the surrounding landscape with human disturbance play a role in the mire bryophyte distribution?

Location: Jinchuan mire, Northeast China.

Methods: We studied the spatial distribution of bryophytes in 100 1 × 1 m quadrats in the mire. Spatial variables were simulated by analysis of the distance-based Moran's eigenvector maps (dbMEM). Variation partitioning analysis was used to reveal the relative contribution of spatial and environmental variables to bryophytes. The relationship between environmental variables and bryophytes was tested by redundancy analysis (RDA). We used co-occurrence and niche overlap models to detect interactions among bryophytes. We also studied the influence of the surrounding landscape on the distribution of bryophytes in relation to water chemistry.

Results: The eight bryophytes occupying part of the mire had both a general distribution trend and a local spatial structure. Over 40% of the total variation in cover among bryophytes could be explained by spatial and environmental variables. In this fraction, the environmental variables explained 29.7% of the variation, of which only 4.5% was not spatially structured. RDA showed the contribution of dwarf shrub cover (SC), Na, and P to the bryophyte distribution was relatively large. Concentration of Na and SC decreased gradually from north to south, and contributed most to the variation in species composition along the first axis. The concentrations of P decreased from east to west, and contributed along the second axis. All the bryophyte species were spatially isolated but with large niche overlaps, indicating that the bryophyte community was structured by interspecific competition.

Conclusion: Sodium mainly originating from the volcanic hill and P from the paddy fields were the main environmental factors affecting the bryophyte distribution. Concentrations of Na and P showed spatial structure, and resulted in induced spatial dependence (ISD) playing a major role in the spatial structure of the bryophyte community. Dwarf shrubs affected by nutrient distribution in the mire significantly influenced the bryophyte distribution in the mire. We conclude that the surrounding ecosystems had important influence on bryophyte distribution via nutrient influx. Furthermore, competitive interactions exacerbated the spatial separation of bryophytes.

Keywords: dbMEM, induced spatial dependence, tephra, human activity, interspecific competition, niche overlap

INTRODUCTION

Mires, as peat accumulating ecosystems, play a critical role in the global carbon cycle by virtue of their enormous carbon storage (Potvin et al., 2015), which is attributed to slow decomposition in waterlogged and anoxic conditions (van Breemen, 1995). During the past century, mires have become severely degraded globally due to human impact, which has negatively influenced their species composition and carbon storage functioning (Chambers et al., 2007; Klimkowska et al., 2010). For mire ecologists and conservationists, it is pivotal to understand which factors are important for the distribution of mire plants. Mires are usually dominated by bryophytes (mainly *Sphagnum*), and associated wetland vascular plants. Here, plant distribution is strongly affected by environmental variables such as WTD (Andrus, 1986; Breeuwer et al., 2008; Bu et al., 2013), shade (Gignac and Vitt, 1990), pH (Benavides and Vitt, 2014; Plesková et al., 2016), and cation concentrations (Kooijman, 1993).

Mire water chemistry shows a strong relationship with pH and the availability of cations, usually Ca and/or Mg, which makes up the poor-rich vegetation gradient (Tahvanainen, 2004; Johnson et al., 2015). For instance, with increasing K availability, the survival of calcifugous sphagna (Vicherová et al., 2015) and of more nutrient-demanding species increases (Hájek et al., 2015). Minerotrophic mires receive water supply mainly from groundwater or surrounding ecosystems (Rydin and Jeglum, 2013). The surrounding landscape can supply macro-nutrients, mainly N and P, and thus create gradients of nutrients in minerotrophic mires (Bragazza and Gerdol, 2002; Tahvanainen et al., 2002). Surrounding landscapes can also influence mire plant distribution and biodiversity by affecting the quantity and quality of water input (Moore and Wilmott, 1976), rainfall (Sjögren and Lamentowicz, 2008), humidity, and wind (Mitchell et al., 2001).

In ecosystems, most environmental variables are spatially patterned, which in turn produce spatial structures in plant distribution. This is referred to as ISD (Borcard et al., 2011; Mikulyuk et al., 2011). The influence of ISD on community structure can be assessed by partitioning of environmental and spatial variables (Dray et al., 2006; Verleyen et al., 2009). ISD of plant distribution is widespread in various ecosystems (Hájek et al., 2011; Mikulyuk et al., 2011; Grimaldo et al., 2016). It can also result from spatially structured historical processes that influence both environmental and biotic variables (Borcard et al., 2011) and could occur at multiple spatial scales, which are generally broad. Therefore, the plant distribution data are not completely independent, but have some spatial connection and correlation.

Interspecific interaction is a key process in shaping plant communities. In bryophyte dominated ecosystems, niche overlaps among bryophytes are often high (Goffinet and Shaw, 2009) and competitive exclusion appears to be rare (Rydin, 1993; Mälson and Rydin, 2009). However, besides stress tolerance, interspecific interaction still is an important factor affecting *Sphagnum* distribution (Rydin, 1993; Bragazza, 1997; Goffinet and Shaw, 2009; Bu et al., 2013). Hollow species usually dominate in the more nutrient-rich hollows by virtue of their strong competitive ability while hummock species are mainly distributed in nutrient-poor hummocks due to their superior water transport and storage capacity. Interspecific relations interact with other environmental variables, such as nitrogen or phosphorus, leading to the patterning of bryophyte distributions and mire vegetation (Bu et al., 2011).

Addition experiments (Rydin, 1993; Breeuwer et al., 2008; Bu et al., 2011) or removal experiments (Bates, 1988) are commonly used in studies on interspecific interaction among bryophytes but they have the drawback that they may cause disturbance and changes in bryophyte growth. Alternatively, null model and niche overlap studies in natural bryophyte communities can be utilized. Null model is generally used to evaluate the effect of biotic interactions on community composition (Peres-Neto, 2004). If a plant community is structured by competition, the checkerboard score and the number of checkerboard species pairs are usually larger, and the observed number of species combinations and variance ratio are smaller in null model analysis of co-occurrence patterns (Gotelli, 2000). However, differences in species dispersal abilities, environmental requirements, or phylogenetic processes may produce plant communities similar to the competitively structured community (Gotelli and Entsminger, 2004; Peres-Neto, 2004). Niche overlap reflects the degree of mutual resource utilization by two species (Bragazza, 1997). In a microhabitat, a greater niche overlap implies a greater tendency to compete, while the opposite is true for macrohabitat (Schoener, 1983; Decaëns, 2010). These types

Abbreviations: dbMEM, distance-based Moran's eigenvector maps; EC, electrical conductivity; HC, herb cover; ISD, induced spatial dependence; ORP, oxidation–reduction potential; RDA, redundancy analysis; SC, dwarf shrub cover; SES, standardized effect size; VPC, vascular plant cover; WTD, water table depth.

of interactions may be revealed by a combination of null model and niche overlap.

We conducted a study in a bryophyte-dominated mire (Jinchuan) of northeastern China. This mire is at the base of a volcanic landform, in north neighbored by a volcanic hill (**Figure 1**). One side of this 100 ha mire has been protected from human disturbances by an upland forest acting as a natural barrier but the opposite side is heavily influenced by agricultural activities from a rice paddy. Our objective was to reveal the relative contributions of environmental variables, biotic interactions, and spatial variables on the bryophyte community. In particular, we tested the hypotheses: (1) environmental variables are spatial structured, and ISD plays a major role in bryophyte community structuring; (2) the surrounding landscape has important influence on mire plant distribution by affecting spatial structure of environmental variables in the mire; and (3) competitive interactions are the most important reason for local spatial structuring of bryophytes in the mire.

STUDY SITES AND METHODS

Study Site

We conducted this study in Jinchuan mire (42°20′N, 126°22′E; 618 m a.s.l.), located near the Changbai Mountains, Northeast China (**Figure 1A**). As a part of the National Nature Reserves of Longwan, the mire has been protected with a fence since 2004. The mire was initiated during the middle Holocene, about 6800 years ago (Zhang et al., 2019). The peat thickness of the mire is generally 4–6 m, with a maximum of 9 m, and peat storage is estimated up to 10 billion kg (Zhao, 1999). The mire is situated at the base of a volcanic landform, in north neighbored by a volcanic hill (about 40 m high above the mire surface level) with forest cover and cornfields (Wang et al., 2017), and has a 0.6° north to south slope. The surface tephra of the volcanic hill was formed from the latest eruption about 2000 B.P. and is rich in K and Na (Mao et al., 2009). The area to the east was originally covered by forest and swamp but was transformed into a rice paddy in the 1950s (Wang et al., 2017). A river to the south separates the mire hydrologically from other cultivated lands (**Figure 1B**). Water pH in the mire ranges from 5.5 to 6.5 and calcium concentrations vary from 0.4 to 11.6. Although Ca concentrations in this mire is rather low, its pH is higher than that of bogs and poor fens (Sjörs and Gunnarsson, 2002; Vitt et al., 2009; Rydin and Jeglum, 2013). Hence, Jinchuan mire should be classified as an intermediate fen. There are at least 82 vascular plants in the mire, and average coverage of which is about 40%. The dominant vascular plants are *Carex limosa* L., *Carex lasiocarpa* Ehrh., *Carex schmidtii* Meinsh, *Thelypteris palustris* Schott, and *Phragmites australis* (Cav.) Trin. The dominant bryophytes are *Sphagnum flexuosum* Dozy and Molk, *Sphagnum imbricatum* Hornsch. Ex Russ., and *Sphagnum subsecundum* Nees. The region is characterized by a temperate monsoon climate, with a mean annual temperature of 5.8°, relative humidity of 68%, and precipitation of 780 mm, mainly falling as rain during July and August. A warming trend was observed from 1955 to 2010 (Meteorological data were obtained from the China meteorological data service center[1]).

Sampling Surveys

In September 2010, we set up six transects, in which three transects roughly oriented along a north–south axis and three along east–west axis crisscrossing Jinchuan mire and surveyed

[1]http://data.cma.cn/

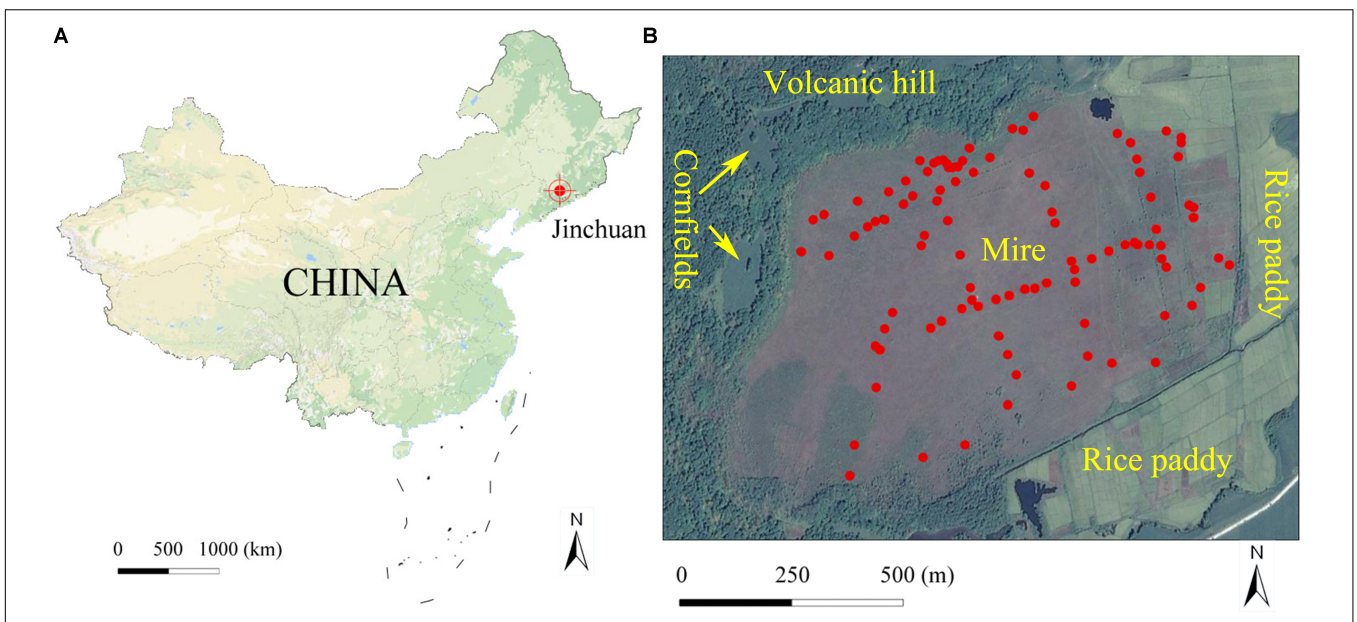

FIGURE 1 | Location of Jinchuan mire in China **(A)** and quadrat location in the mire **(B)**. The quadrats were marked with red points. The map image data comes from Google map.

100 1 × 1 m random quadrats along these transects by sample throwing method. We adjusted the position slightly to avoid surveying quadrats lacking bryophytes (**Figure 1B**). In each quadrat, we recorded the presence and cover of each bryophyte species, VPC, SC, HC, geographical coordinates (Garmin etrex VENTURE), and altitude (Alt). The bryophytes *Atrichum undulatum* (Hedw.) p. Beauv, *Aulacomnium palustre* (Hedw.) Schwägr., *Calliergonella cuspidata* (Hedw.) Loesk., and *Campylium stellatum* (Hedw.) C.E.O. Jensen, *S. flexuosum*, *S. imbricatum*, *S. subsecundum*, and *Sphagnum warnstorfii* Russow were chosen as the main study species since they were common species in the mire. *S. imbricatum* and *S. warnstorfii* formed low hummocks, and *A. palustre* occasionally grew in these hummocks. *S. flexuosum*, *S. subsecundum*, *A. undulatum*, and *C. cuspidata* generally grew in hollows.

Water Sampling and Chemical Analyses

At the same time as the sampling surveys, the vertical distance between the average position of bryophyte surface and the free water surface was measured by a steel measuring tape and recorded as WTD. At 5 cm under the water table of the edge of each quadrat, EC and pH of mire water were determined using a portable multifunction instrument (model: Sanxin PD-501), and adjusted ORP of water was measured by a portable pH meter (model: thermo scientific orion 3 star). Two 100 mL water samples were collected with polythene bottles at the same position (Gignac and Vitt, 1990). Two drops of concentrated sulfuric acid or nitric acid were added to the bottles, respectively, to prevent microbial growth and precipitation from affecting element concentrations. All the water samples were deep-frozen stored in the laboratory until analysis. Elemental K, Ca, Mg, and Na in the water samples with concentrated nitric acid were analyzed by flame atomic absorption spectrometry (model: Spectr AA220FS). Total N and P in the water samples with concentrated sulfuric acid were determined by the alkaline potassium persulfate digestion UV spectrophotometric method (MEPC, 2012) and the ammonium molybdate spectrophotometric method (MEPC, 1989), respectively.

Statistical Analysis

The dbMEM analysis (Dray et al., 2006; Gao et al., 2014; Legendre and Gauthier, 2014) was used to reveal the influence of spatial variables on the community structure. According to the geographical coordinates of each quadrat, a matrix of Euclidean distances among quadrats was constructed (Dray et al., 2006). Truncated this matrix to retain only the distances among close neighbors, and computed a principal coordinate analysis (PCoA) of the truncated distance matrix. The eigenvectors (dbMEMs) with positive spatial correlation were used as spatial variables of community variation in analyses (Borcard et al., 2011). According to the sizes of the eigenvectors, dbMEMs can be divided into two scales: broad and fine scale, which represent global and local spatial structure, respectively (Borcard et al., 2011).

Environmental variables included altitude (Alt), WTD, EC, ORP, pH, calcium (Ca), magnesium (Mg), potassium (K), sodium (Na), nitrogen (N), phosphorus (P), VPC, SC, and HC. Spatial variables included 31 dbMEMs. To reduce the explanatory variables and prevent the inflation of the overall type I error, the analysis of forward selection with Blanchet et al. (2008)'s double-stopping criterion was used, and alpha significant level and the adjusted R^2 (R^2_{adj}) of the global analysis were used as forward selection criterion (Blanchet et al., 2008; Astorga et al., 2011), which could choose the explanatory variables that describes the most variation in the species matrix with the lowest possible number of variables (Dray et al., 2006; Borcard et al., 2011). The environmental variables and dbMEMs, selected by the double-stopping criterion, were used for next variation partitioning and RDA analysis.

Variation partitioning analysis was used to reveal the relative contribution of spatial and environmental variables to the bryophyte cover matrix (Borcard et al., 2011). We used partial redundancy analysis (pRDA) with the Monte Carlo permutation test (999 permutations) to explain the total variation of a species matrix by the sources of spatial variables and environmental variables, the combined effect of two or three of these variables, and the unexplained fraction (Peres-Neto et al., 2006). To achieve normality, all environmental variables, except pH, were transformed by $\log(x + 1)$ (Chen et al., 2016). The species matrices were converted by Hellinger transformation to reduce the weight of abundant species (Legendre and Gallagher, 2001).

The relationship between bryophyte cover and environmental variables was analyzed by RDA because detrended correspondence analysis (DCA) showed that the length of the first axis was 3.8, which is less than 4 (Lepš and Šmilauer, 2003). RDA, dbMEM, and variation partitioning analysis were performed in R (version 3.1.1[2]) using the "vegan" package. Detailed statistical analysis methods can be found in the book of Borcard et al. (2011).

The null model of species co-occurrence model (Gotelli, 2000; Arita, 2016) and the niche overlap of niche theory (Pianka, 1974) were used to reveal an overall interaction among bryophytes. We used the common four indices namely the checkerboard score (C-score) (Stone and Roberts, 1990), the number of checkerboard species pairs (Checker), the number of species combinations (Combo), and the variance ratio (V-ratio). In biodiversity studies, C-score is a statistic that determines the randomness of the distribution of two or more species in a biome. The C-score is the average of all possible checkerboard pairs, calculated for species that occur at least once in the matrix. Checker is the number of species pairs that never co-occur in any site. The co-occurrence analysis is sensitive to variation in species occurrence frequencies, so the number of occurrences of each species was preserved as a constraint (Gotelli, 2000; Gao et al., 2014). Additionally, V-ratio was identified by the row and column sums of the matrix, so it was not suitable for fixed–fixed (FF) algorithm (Gotelli, 2000). Therefore, according to the recommendation of Gotelli and Entsminger (2004), FF and fixed-equiprobable (FE) algorithms were used to calculate C-score and Checker; FF, FE, fixed-probability (FP), and probability–probability (PP) were used to calculate Combo; and FE, FP, and PP were used to calculate V-ratio. In a spatially isolated community, the observed

[2]https://www.r-project.org

indexes of C-score and Checker should be larger than the mean of simulated indexes, and the observed Combo and V-ratio should be smaller. The four indicators showed opposite trends in a spatial aggregation community (Gao et al., 2014). To compare our results with other studies (Gotelli and Entsminger, 2004), SES was calculated as follows:

$$\mathrm{SES} = (I_o - I_s)/SD_s \quad (1)$$

where I_o is observed index, I_s is mean of simulated indexes, and SD_s is the standard deviation of simulated indexes (Decaëns et al., 2009). Simulated indices were obtained from 5000 random permutations. The 95% confidence intervals for the SES were between −1.96 and 1.96.

The community-level niche overlap index was calculated by the mean of pairwise species niche overlap (Pianka's O_{jk}). Pianka's O_{jk} (Pianka, 1974) was calculated as follows:

$$O_{jk} = O_{kj} = \sum_{i=1}^{n} p_{ij}p_{ik} \Big/ \sqrt{\sum_{i=1}^{n} p_{ij}^2 \sum_{i=1}^{n} p_{ik}^2} \quad (2)$$

where O_{jk} is the niche overlap of species j and k, p_{ij} is the coverage of species j in class i of one environmental variable.

We also calculated the SES values for niche overlap (Decaëns et al., 2009). Each of the environmental variables was divided into n classes as follows: seven classes for K, eight for WTD, EC, ORP, VPC, SC, and HC, nine for Alt, Mg, Na, 10 for pH, N, Ca, and 11 for P. The co-occurrence model and the niche overlap analyses were performed in Ecosim (version 7.0[3]).

Pearson correlation between the dbMEMs, environmental variables, and bryophyte covers were performed in R (version 3.1.1[4]) using the "stats" package. The environmental variables were taken for spatial interpolation in Surfer 10, where the Kriging interpolation method was used. The resulting spatial distribution maps of environmental variables and bryophyte covers were contour maps.

RESULTS

The dbMEMs

The dbMEM analysis produced 31 variables, and eight dbMEMs (the first, second, third, seventh, 12th, 14th, 17th, and 28th dbMEMs) were selected for spatial variables by the analysis of forward selection with the double-stopping criterion (**Figure 2**). The first dbMEM increased at first and then decreased roughly from north to south, and the second dbMEM decreases roughly from east to west. The value of the third, seventh, 12th, 14th, 17th, and 28th dbMEMs showed spatial fluctuation, and the fluctuation scale gradually decreased. According to the sizes of the eigenvectors, dbMEMs can be divided into two scales: broad (the first, second, third, and seventh dbMEMs) and fine (the 12th, 14th, 17th, and 28th dbMEMs), and represented the global and local spatial structures.

[3]http://garyentsminger.com/ecosim/index.htm

[4]https://www.r-project.org

The Bryophytes and Their Distribution

The frequency and average coverage of bryophyte species in the mire showed in **Table 1**, and the average coverage for all bryophytes was 6.1%. The frequency of *S. subsecundum* and the average coverage of *S. imbricatum* and *S. subsecundum* were the highest. *C. stellatum* showed the lowest both frequency and average coverage.

The eight bryophytes occupy a part in the mire (**Figure 3**). *A. palustre* and *S. imbricatum* were mainly distributed in the northwest part of the mire. *C. stellatum*, *S. flexuosum*, and *S. subsecundum* were roughly distributed in the middle of the mire. *A. undulatum* was mainly distributed in the northeast and southwest part of the mire, *C. cuspidata* in the northeast, and *S. warnstorfii* in the west of the mire (**Figure 3**). At the broad-scale, bryophytes *A. palustre*, *S. flexuosum*, *S. imbricatum*, *S. subsecundum*, and *S. warnstorfii* showed correlation with one or more broad scale dbMEM spatial components (**Table 2**). Of these bryophytes, *S. imbricatum*, *S. subsecundum*, and *S. warnstorfii* correlated with the first dbMEM, which represented *S. imbricatum* and *S. warnstorfii* showed a higher cover toward the north than to the south, and *S. subsecundum* on the contrary. *S. subsecundum* correlated negatively with the second dbMEM, which represented a clear trend of increasing from east to west. At the fine-scale, *C. stellatum*, *S. flexuosum*, *S. imbricatum*, and *S. subsecundum* correlated with the 12th or 28th dbMEM, which indicates that those bryophytes had a local spatial structure.

The Influence of Environmental Variables on Bryophyte Distribution

The environmental water chemistry data in the mire and paddy fields are presented in **Table 3**. In the paddy fields (east of the mire), the concentrations of elements, except N, were higher than those of the mire.

Through the analysis of forward selection with the double-stopping criterion, we found that six environmental variables (Mg, Na, P, and ORP in mire water, SC, and VPC) significantly influenced the distribution of bryophytes in the mire. Environmental variables Na and SC in the mire decreased gradually from north to south (**Figures 4B,F**), and ORP was on the contrary (**Figure 4D**). Pearson correlation analysis showed that Na and SC were negatively correlated with the first dbMEM and ORP was on the contrary (**Table 2**). The concentrations of Mg and P in the mire clearly decreased from east to west (**Figures 4A,C**), and VPC showed a tendency to be higher on all sides than in the middle (**Figure 4E**). Pearson correlation analysis showed that Mg, P, and Na correlated positively with the second dbMEM (**Table 2**). Environmental variables had not only a linear trend but also a periodic variation at different spatial scales (**Figure 4**). In relation to the third dbMEM, ORP and SC were negatively correlated. Mg and Na were positively correlated with the seventh dbMEM, Mg negatively correlated with the 12th dbMEM, and P negatively correlated with the 17th dbMEM (**Table 2**).

In the RDA, the first canonical axis accounted for 24.5% of the variance in the species data, and SC and Na contributed to the most variation in species composition along the first

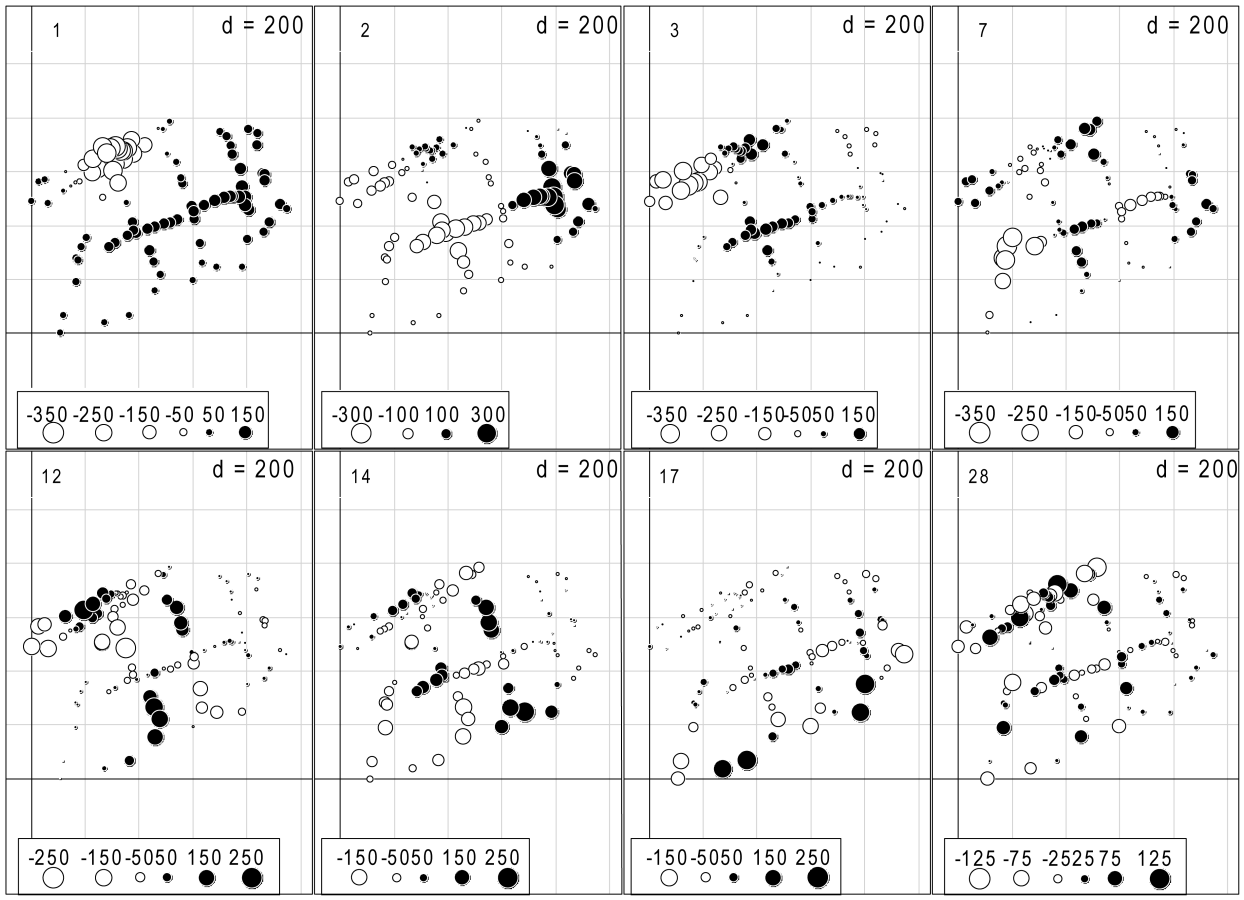

FIGURE 2 | The eight significant dbMEM variables with positive spatial correlation selected by the analysis of forward selection with Blanchet et al. (2008)'s double-stopping criterion, and alpha significant level and the adjusted R^2 (R^2_{adj}) of the global analysis were used as forward selection criterion (Blanchet et al., 2008; Astorga et al., 2011). The dots indicated the position and dbMEM value of each quadrat.

axis (**Figure 5**). The second canonical axis explained 5.6% of the variance in the species data and mainly represented the gradient of P and ORP. The contribution of SC, Na, and P to the bryophyte distribution was relatively large. Most bryophytes followed the first axis, such as *S. imbricatum*, *S. subsecundum*, *S. flexuosum*, and *A. palustre*. *S. imbricatum* and *S. subsecundum* had the maximum score along the first axis, *A. undulatum* and *C. cuspidata* had the maximum score along the second axis, while *S. warnstorfii* had the critical roles along both axes. Pearson correlation analysis showed that all the environmental factors, except ORP, were negative correlation with *S. subsecundum* (**Table 4**). SC was positive correlation with *A. palustre*, *S. imbricatum*, and *S. warnstorfii*, Na positively with *A. undulatum*, *S. imbricatum*, and *S. warnstorfii*, and P positively with *A. undulatum* and *S. warnstorfii*.

TABLE 1 | The frequencies and average coverage of bryophyte species in Jinchuan mire.

Species abbreviations	Species name	Frequencies (%)	Average coverage (%)
Apa	*Aulacomnium palustre*	19	0.50
Aun	*Atrichum undulatum*	28	1.06
Ccu	*Calliergonella cuspidata*	14	0.33
Cst	*Campylium stellatum*	5	0.10
Sfl	*Sphagnum flexuosum*	33	5.16
Sim	*S. imbricatum*	23	15.72
Ssu	*S. subsecundum*	54	15.63
Swa	*S. warnstorfii*	22	6.59

Relative Contribution of Environmental Variables and Spatial Variables

Of the total variation in the cover of bryophyte species, 41.5% could be explained by the spatial and environmental variables (fractions except [h] in **Figure 6**, $p = 0.001$). In this fraction, the environmental variables (upper left-hand circle in **Figure 6**) explained 29.7% of the variation, of which a mere 4.5% was not spatially structured (fraction [a] in **Figure 6**). This fraction represented species-environment relationships associated with local environmental conditions. The proportion explained by ISD (fraction [d], [f], and [g] in **Figure 6**) was 25.2%. That indicated that the spatial structure of environmental factors produced

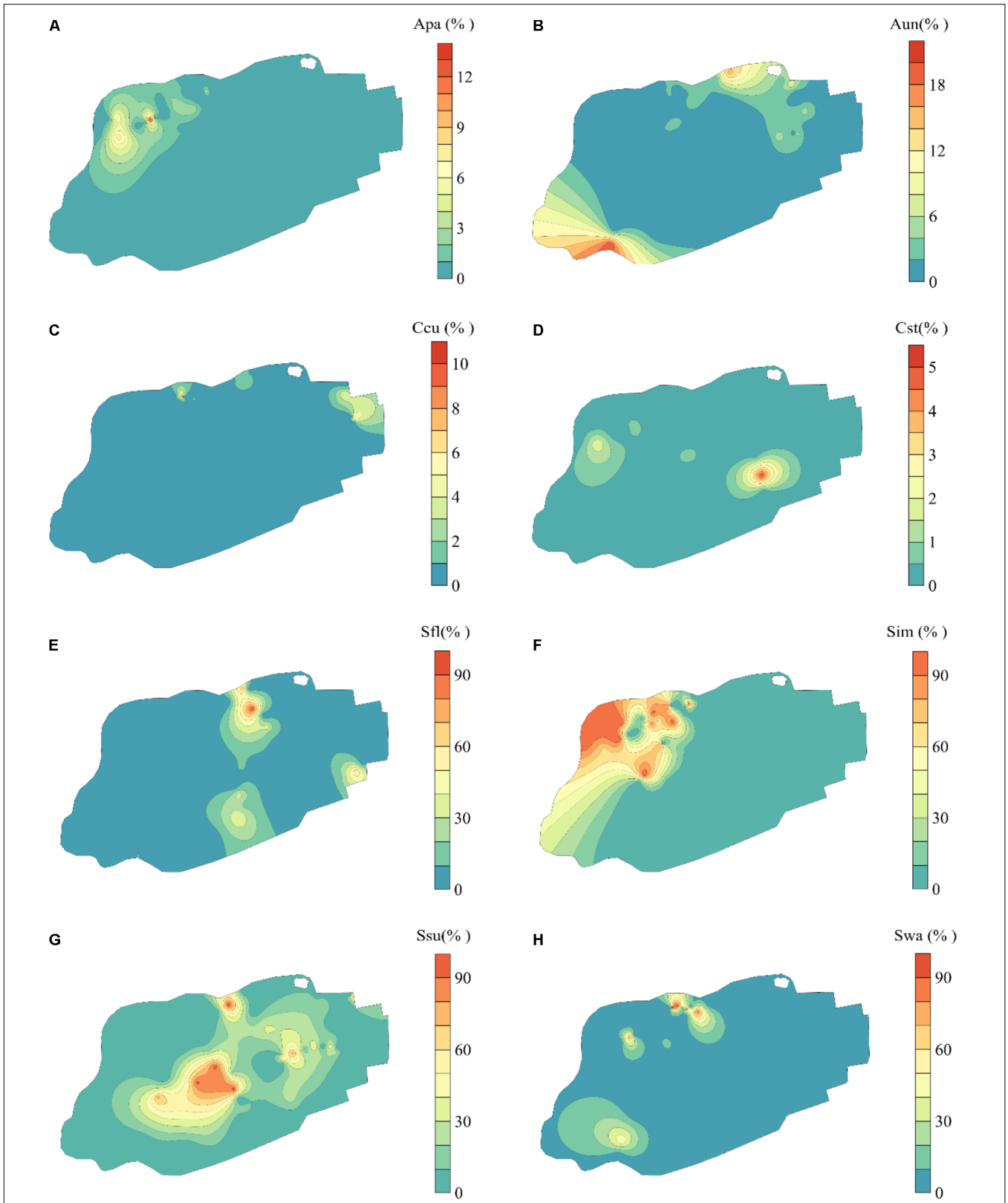

FIGURE 3 | Spatial distribution of bryophytes in Jinchuan mire based on Kriging interpolation. **(A)** *Aulacomnium palustre* (Apa). **(B)** *Atrichum undulatum* (Aun). **(C)** *Calliergonella cuspidata* (Ccu). **(D)** *Campylium stellatum* (Cst). **(E)** *Sphagnum flexuosum* (Sfl). **(F)** *S. imbricatum* (Sim). **(G)** *S. subsecundum* (Ssu). **(H)** *S. warnstorfii* (Swa). The part of bryophyte cover less than 0 fitted by Kriging interpolation has been replaced with 0.

TABLE 2 | The Pearson correlation between the spatial variables and environmental variables and between spatial variables and bryophyte covers.

Spatial variables	Broad scale				Fine scale			
	V1	V2	V3	V7	V12	V14	V17	V28
Environmental variables								
Mg	0.06	0.41**	−0.13	0.28**	−0.22*	0.09	0.03	−0.06
Na	−0.64**	0.27**	−0.10	0.25*	−0.12	0.02	−0.01	−0.05
ORP	0.37**	−0.14	−0.25*	−0.12	−0.01	0.01	0.02	0.06
P	−0.14	0.23*	0.11	0.16	−0.11	−0.08	−0.33**	0.03
SC	−0.67**	0.03	−0.27**	0.07	−0.06	−0.11	−0.07	−0.10
VPC	−0.16	−0.13	−0.18	0.08	−0.08	0.14	0.08	−0.08
Bryophytes								
Apa	−0.15	−0.11	−0.49**	0.09	−0.09	−0.05	−0.01	−0.04
Aun	0	0.16	0.09	0.08	−0.05	−0.15	−0.15	−0.15
Ccu	−0.11	0.16	0.06	0.07	0.01	0.01	0.05	−0.01
Cst	0.05	−0.10	−0.06	0.02	−0.23*	0.12	0.03	0.13
Sfl	0.14	−0.01	0.12	0.24*	0.28**	−0.10	0.07	−0.12
Sim	−0.41**	−0.10	−0.43**	−0.03	−0.12	0.04	0.02	−0.23*
Ssu	0.27**	−0.35**	0.37**	−0.22*	0.01	0.14	−0.13	0.24*
Swa	−0.47**	0.05	0.06	0.02	−0.08	−0.04	−0.06	0.02

*Spatial variables (dbMEM spatial components) were divided into two scales: broad and fine. Environmental variables: magnesium (Mg), sodium (Na), adjusted oxidation–reduction potential (ORP), phosphorus (P), dwarf shrub cover (SC), and vascular plant cover (VPC). Bryophytes: Apa, Aulacomnium palustre; Aun, Atrichum undulatum; Ccu, Calliergonella cuspidata; Cst, Campylium stellatum; Sfl, Sphagnum flexuosum; Sim, S. imbricatum; Ssu, S. subsecundum; Swa, S. warnstorfii. The values of the dbMEMs are shown in **Figure 2**. * indicates $P < 0.05$ and ** indicates $P < 0.01$.*

a similar spatial structure in the response data. Broad scale alone explained 7.5% of the variation (fraction [b] in **Figure 6**, $p = 0.001$), and fine-scale dbMEM alone explained 4.5% only (fraction [c] in **Figure 6**, $p = 0.521$).

Influence of Interspecific Interaction on Bryophytes Distribution

In species co-occurrence analysis, the observed indexes of C-score were larger than the mean of simulated indices, and the observed Combo and V-ratio were smaller. All the co-occurrence models, except the checkerboard species pairs model, showed spatial isolation among all the bryophyte species (**Table 5**). The average niche overlaps of all pairwise combinations of bryophytes were larger than 0.5 for all environmental variables except Na and SC (**Table 6**). Except for Na, N, and VPC, all environmental variables showed larger observed niche overlaps than the mean simulated variances, which indicates that bryophyte communities were competitively structured.

TABLE 3 | The water chemistry in the mire and paddy fields.

Water chemistry	Position	
	Mire (mean ± SE, *n* = 100)	Paddy fields (mean ± SE, *n* = 2)
pH	5.85 ± 0.023	6.28 ± 0.145
EC (μS cm^{-1})	28.9 ± 1.98	115 ± 78.8
ORP (mV)	142 ± 10.4	221 ± 92.0
K (mg L^{-1})	1.34 ± 0.079	1.46 ± 0.432
Ca (mg L^{-1})	3.48 ± 0.224	7.35 ± 4.25
Na (mg L^{-1})	1.26 ± 0.062	1.31 ± 0.562
Mg (mg L^{-1})	1.46 ± 0.112	3.52 ± 2.03
N (mg L^{-1})	0.353 ± 0.0178	0.343 ± 0.109
P (mg L^{-1})	0.0245 ± 0.00263	0.0293 ± 0.0161

EC, electrical conductivity; ORP, adjusted oxidation–reduction potential; Ca, calcium; Mg, magnesium; K, potassium; Na, sodium; N, nitrogen; P, phosphorus.

DISCUSSION

Our research showed that the spatial structure among bryophyte species was partly explained by a combined effect of spatial and environmental variables. ISD played a major role in the spatial structure of the bryophyte community, which supports our first hypothesis, indicating the overlapping and interdependent nature of the structuring forces in the mire (Mikulyuk et al., 2011). The spatial structure of important environmental variables can influence plant distribution and produce a similar spatial structure as for the environmental variables (Borcard et al., 2011; Mikulyuk et al., 2011). In Jinchuan mire, some environmental variables (Na, SC, and ORP) and bryophytes (*S. imbricatum*, *S. subsecundum*, and *S. warnstorfii*) were correlated with the first dbMEM, which represents the influence of the distribution patterns of environmental variables on the distribution of bryophytes. The distribution of *S. subsecundum* with trend of increasing from east to west may result from the influence of the distribution patterns of P and Mg.

In addition to ISD, spatial variables of plant distribution also result from spatial autocorrelation (Dray et al., 2006; Borcard et al., 2011), which in this case could explain 10.6% of the bryophyte distribution (fraction [b], [c], and [g] in

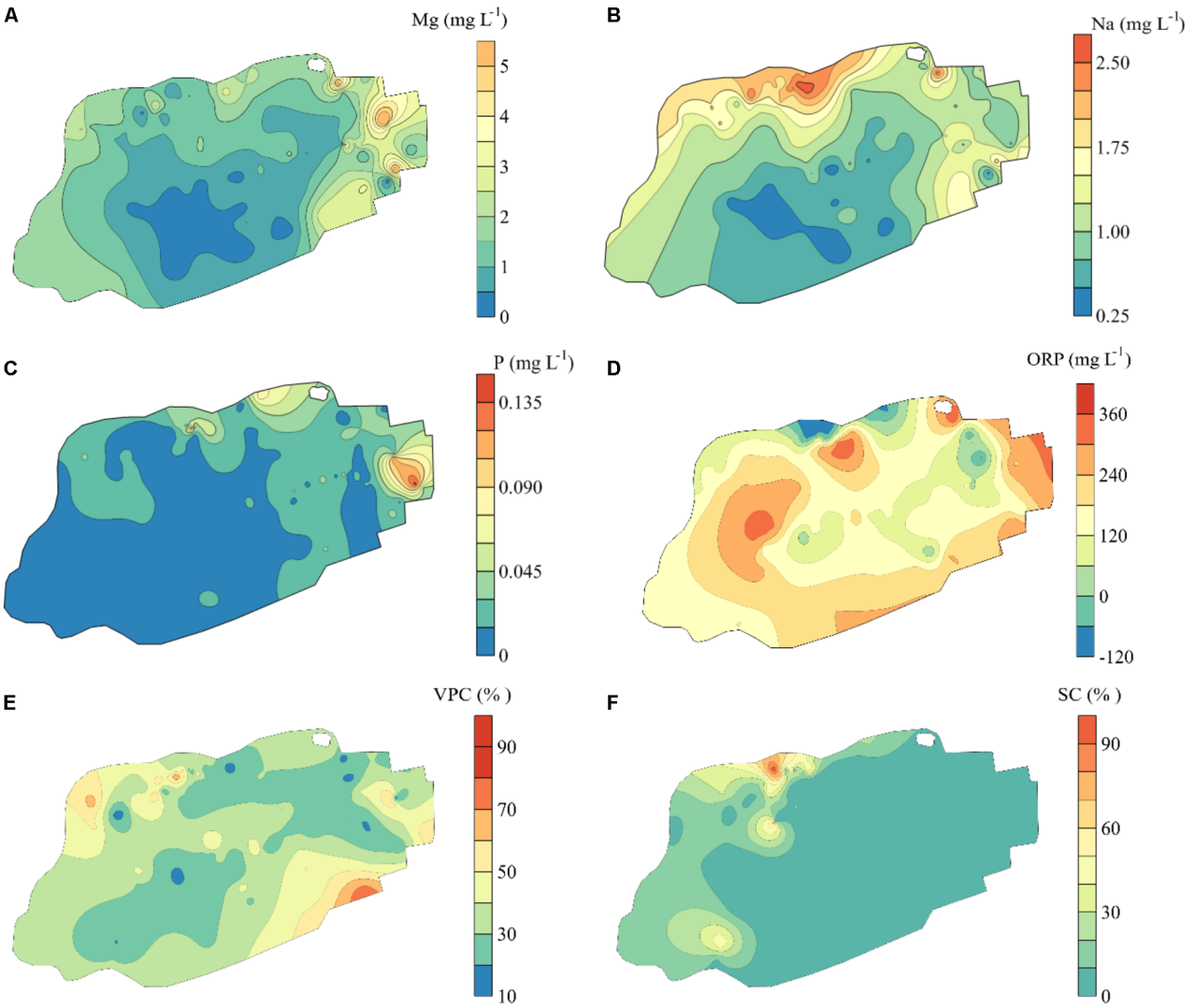

FIGURE 4 | Spatial distribution of environmental variables in Jinchuan mire based on Kriging interpolation. The environmental variables were selected by analysis of forward selection with the double-stopping criterion. **(A)** Magnesium (Mg). **(B)** Sodium (Na). **(C)** Phosphorus (P). **(D)** Adjusted oxidation–reduction potential (ORP). **(E)** Vascular plant cover (VPC). **(F)** Dwarf shrub cover (SC). Vascular plant cover was the ratio of the area of the vertical projection of vascular plants occupying the ground. Dwarf shrub cover was the index of coverage sum of all the dwarf shrubs.

Figure 6). Plant–plant interactions may be a source of spatial autocorrelation (Cottenie and De Meester, 2004). Our co-occurrence analysis (C-score, Combo, and V-ratio) suggests a spatial separation (negative interspecific association) among the bryophytes, which often occurs in a competitively structured community (Gotelli and Entsminger, 2004). Competitive exclusion principle states that two species competing for the same limiting resource cannot coexist at constant population values (Hardin, 1960). We showed that niche overlaps were higher than mean simulated variances of most environmental variables, which indicate that species interactions but not habitat differences resulted in the spatial separations of species in the mire (Schoener, 1983; Decaëns, 2010; Martorell et al., 2015). Such as, a competition was strong between *S. flexuosum* and *S. imbricatum*, which had high niche overlap but negative interspecific association (not shown in the results). Frego and Carleton (1995) found a similar result in a boreal forest, where the obvious spatial separation was associated with large niche overlaps among bryophytes. In shared microhabitats, one bryophyte may have a competitive advantage over other species (Bellamy and Rieley, 1967), and the weaker competitors shift to another location. Because of local competitive advantage, a continuous habitat or a mire is dominated by monodominant bryophyte communities, especially *Sphagnum*. Species interactions exacerbated the spatial separation of bryophytes and formed the local spatial structure of bryophytes in Jinchuan mire.

Jinchuan mire borders a volcanic hill with tephra rich in Na and K (Mao et al., 2009) in the north. Compared to data from North America and Europe (Bourbonniere, 2009), Na

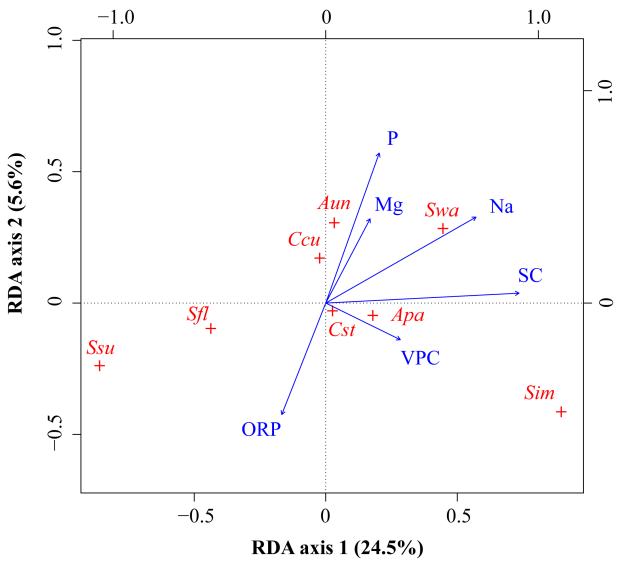

FIGURE 5 | RDA ordinations of bryophyte species with environmental variables. Bryophytes (red +): Apa, *Aulacomnium palustre*; Aun, *Atrichum undulatum*; Ccu, *Calliergonella cuspidata*; Cst, *Campylium stellatum*; Sfl, *Sphagnum flexuosum*; Sim, *S. imbricatum*; Ssu, *S. subsecundum*; Swa, *S. warnstorfii*. Environmental variables (blue arrows): altitude (Alt), calcium (Ca), phosphorus (P), potassium (K), sodium (Na), and water table depth (WTD).

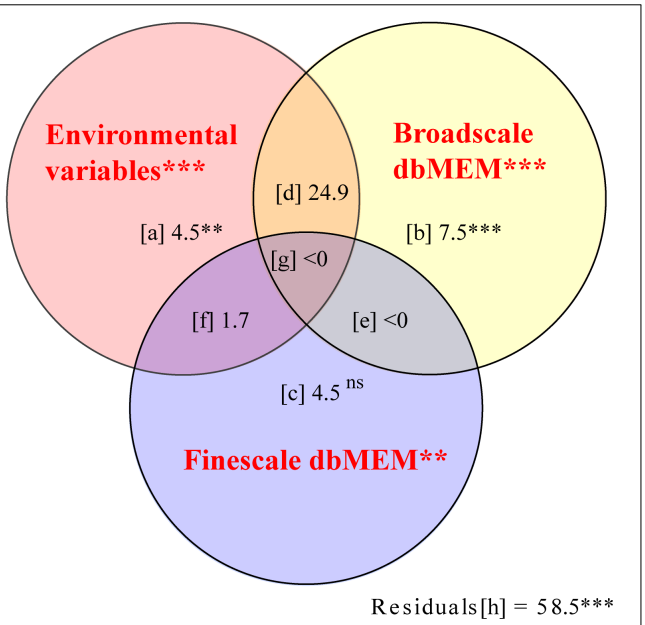

FIGURE 6 | Pure and shared effects of environmental (upper left-hand circle, X1) and spatial variables on the species composition of bryophyte in Jinchuan mire explained by partial redundancy analysis (pRDA) with the Monte Carlo permutation test (Peres-Neto et al., 2006). Spatial variables were separated at two scales: broad scale dbMEM (upper right-hand circle, X2) and fine scale dbMEM (lower circle, X3). When interpreting this variation partitioning diagram, keep in mind that the R^2 adjustment was done for each fraction that can be fitted without resorting to pRDA or multiple regression which included [a], [b], [c], [X1], [X2], [X3], [X1 + X2], [X1 + X3], [X2 + X3], [X1 + X2 + X3], [X1| X2], [X1| X3], [X2| X1], [X2| X3], [X3| X1], [X3| X2], and that the individual fractions [d] to [h] are then computed by subtraction. Fraction [a] represented the variation explained by environment variables alone. Fraction [b], [c], and [e] represented some variation explained by spatial variables independently of the environment. Fraction [d], [f], and [g] represented spatially structured environmental variation. The statistical significance of effects: ns $P > 0.05$, $^{**}P < 0.01$, and $^{***}P < 0.001$.

concentrations were not high in this mire but decreased along the north–south direction. This may be explained by leached Na from the tephra into the mire, with the highest concentrations along the margin. Our RDA analysis suggests that Na played a crucial role in bryophyte distribution. In Jinchuan mire, *A. undulatum*, *S. imbricatum*, *S. subsecundum*, and *S. warnstorfii* showed a strong correlation with Na (**Table 4**). According to Eppinga et al. (2010)'s description on water loss pathway in mires, water loss of Jinchuan mire is mainly due to evaporation, not drainage. Bryophytes, as ectohydric plants (Hayward and Clymo, 1982), are hardly able to regulate internal water (Smith, 1978). Sodium is one of the important chemical components in peatland waters, and can regulate osmosis, turgor pressure, and pH of plant cells (Bourbonniere, 2009). While, excessive intake of sodium is extremely toxic to most plants and detrimental to bryophytes (Sabovljevic and Sabovljevic, 2007). It seems that the last volcanic activity which occurred in the late Holocene not only changed the local climate (Mao et al., 2009) but also influenced plant distribution in this montane mire. Our results clearly suggest that most of the chemical components in the mire water come from the volcanic soil, and effect of historical volcanic activity plays an important role in bryophyte distribution.

Jinchuan mire has become the core area of a nature reserve since 2004, while human activities in the form of rice cultivation continue in the nearby lands, mainly to the east. The surplus of phosphorus is likely originating from fertilizers used in the paddy fields, and the concentrations of P in the mire showed a decreasing trend from east to west. The mire water closest to the paddy fields had the highest concentrations of P (Zeng et al., 2012), where *C. schmidtii* Meinsh dominated the community likely at the expense of bryophytes

TABLE 4 | The Pearson correlation between environmental variables and bryophyte cover.

	Mg	Na	ORP	P	SC	VPC
Apa	0.04	0.18	0.04	0.01	0.36**	0.24*
Aun	0.22*	0.24*	−0.28**	0.21*	0.19	−0.10
Ccu	0.18	0.16	−0.23*	0.11	0.05	−0.11
Cst	−0.07	−0.04	0.05	−0.01	0.10	0.20*
Sfl	−0.17	−0.20	−0.05	−0.12	−0.18	−0.03
Sim	0.04	0.31**	−0.03	−0.09	0.54**	0.21*
Ssu	−0.27**	−0.32**	0.14	−0.21*	−0.30**	−0.28**
Swa	−0.06	0.34**	−0.38**	0.23*	0.31**	0.01

*Environmental variables: magnesium (Mg), sodium (Na), adjusted oxidation–reduction potential (ORP), phosphorus (P), dwarf shrub cover (SC), and vascular plant cover (VPC). Bryophytes: Apa, Aulacomnium palustre; Aun, Atrichum undulatum; Ccu, Calliergonella cuspidata; Cst, Campylium stellatum; Sfl, Sphagnum flexuosum; Sim, S. imbricatum; Ssu, S. subsecundum; Swa, S. warnstorfii. * indicates P < 0.05 and ** indicates P < 0.01.*

TABLE 5 | The species co-occurrence analysis for all investigated bryophytes in Jinchuan mire, northwest China.

Index	Null model	Observed index	Mean of simulated index	SES	*P*
C-score	FF	322.3	295.2	10.2	<0.001
	FE	322.3	278.8	3.21	<0.001
Checker	FF	4.00	1.91	1.84	0.074
	FE	4.00	1.75	2.02	0.064
Combo	FF	36.0	46.5	−5.07	<0.001
	FE	36.0	47.0	−4.92	<0.001
	FP	36.0	47.1	−4.93	<0.001
	PP	36.0	49.3	−4.85	<0.001
V-ratio	FE	0.83	1.00	−1.26	0.11
	FP	0.83	1.50	−4.08	<0.001
	PP	0.83	1.51	−4.18	<0.001

The observed indexes were obtained by the observed matrix. Mean of simulated indexes and the probability of observed values were calculated from the simulated matrices (5000 randomizations). An SES was calculated as Formula 1.

TABLE 6 | Niche overlap analysis for all the environmental variables.

Environmental variables	Mean of observed values	Mean of simulated index	SES	*P*
Alt	0.607	0.442	4.63	0.001
WTD	0.669	0.308	7.64	<0.001
EC	0.587	0.410	4.36	0.001
ORP	0.511	0.443	1.90	0.044
pH	0.612	0.417	5.38	<0.001
Ca	0.665	0.455	6.28	<0.001
Mg	0.653	0.348	7.27	<0.001
K	0.668	0.482	4.85	<0.001
Na	0.481	0.457	0.662	0.223
N	0.551	0.520	1.08	0.138
P	0.547	0.390	4.45	<0.001
VPC	0.520	0.503	0.510	0.263
SC	0.473	0.360	2.52	0.021
HC	0.620	0.542	2.49	0.021

The niche overlaps were the average of all pairwise combinations of bryophytes. Mean of simulated indexes and the probability of observed values were calculated from the simulated matrices (5000 randomizations). An SES was calculated as Formula 1. Environmental variables include altitude (Alt), water table depth (WTD), electrical conductivity (EC), oxidation–reduction potential (ORP), pH, calcium (Ca), magnesium (Mg), potassium (K), sodium (Na), nitrogen (N), phosphorus (P), vascular plant cover (VPC), dwarf shrub cover (SC), and herb cover (HC).

(not shown in the article). Phosphorus input probably increased the competitiveness of vascular plants, thus hampering the distribution of bryophytes. Phosphorus was an important factor affecting the distribution of *A. undulatum*, *S. subsecundum*, and *S. warnstorfii*. Different bryophytes adapt to different phosphorus concentrations. *C. cuspidata* was also positively affected by P too, which conforms well to the observed expansion of *C. cuspidata* in eutrophicated fens of Central Europe (Kooijman, 2012). Although anthropogenic land use in the surrounding landscapes showed a weaker influence than volcanic activity on bryophyte distribution, it has an important influence on bryophytes distribution in the mire.

Vascular plants, especially dwarf shrubs, significantly influenced the distribution of bryophytes in the mire. For example, SC contributed to the most variation in species composition along the first axis. The importance of plant–plant interactions increases with downscaling in vegetation distribution patterns (Hortal et al., 2010). Dwarf shrubs may support the spongy bryophytes (Malmer et al., 1994) to form hummocks thereby facilitating certain bryophytes by providing shade and reducing evaporation (Pedersen et al., 2001; van der Wal et al., 2005), but compete with other bryophytes (Zeng et al., 2012; Ma et al., 2015). Fertilization can improve the productivity of dwarf shrubs, thus enhancing the light competition to bryophytes (Bartsch, 1994). The relationship between vascular plants and bryophytes changed with increased nutrients in a mire, and then may affect the distribution pattern of bryophytes.

Human modification in surrounding landscapes not only affects the bryophyte distribution in the mire but also seriously damages the environment of the nature reserve. Besides nutrients, other harmful substances, such as herbicides and pesticides used in the paddy fields may have entered into the mire. Furthermore, corn has been cultivated in recent years on the hill slopes, bordering the northern part of the mire, and has likely increased nutrient input to the mire and influenced its vegetation pattern and plant biodiversity. Hence, it is necessary to establish a larger buffer zone to block the runoff of nutrient and pesticide-loaded water into the mire to effectively preserve the mire and its ecosystem integrity.

Because of the correlation between environmental variables, the influences of them on bryophyte distribution have some overlap. The analysis of forward selection with Blanchet et al. (2008)'s double-stopping criterion can reduce the explanatory variables and prevent the inflation of the overall type I error. However, it is impossible to determine which of the two related environmental variables is the true cause of species distribution. For example, the spatial distribution of SC and potassium is similar; hence, the analysis of forward selection may mask the significant effect of potassium. Using principal component analysis to reduce environmental variables may lead to different conclusions (Gao et al., 2014).

CONCLUSION

Induced spatial dependence plays a major role in community structuring of bryophytes in Jinchuan mire. Sodium in water mainly from the volcanic hill on the north was a double-edged sword for bryophytes and played an important role in bryophyte distribution. The paddy fields adjacent the east of mire have an important influence on species distribution in the mire due to the influx of P fertilized in rice cultivation. Furthermore, dwarf shrubs affected by nutrient distribution in the mire significantly influenced the distribution of bryophytes in the mire. Competitive interactions exacerbated the spatial separation of bryophytes and formed the local spatial structure of bryophytes in Jinchuan mire. In order to effectively conserve the mire, we suggest to maintain a proper buffer zone around

the mire to prevent influx of nutrient-loaded water from the surrounding landscapes.

DATA AVAILABILITY STATEMENT

The datasets generated for this study are available on request to the corresponding author.

AUTHOR CONTRIBUTIONS

Z-JB conceived and designed the study. J-ZM and XC performed the investigation in the field. J-ZM, M-MZ and S-ZW analyzed the data. J-ZM, AM, SS, and Z-JB wrote the manuscript.

FUNDING

This study was funded by the National Key Research and Development Project (Nos. 2016YFA0602301 and 2016YFC0500407), the National Natural Science Foundation of China (Nos. 41871046, 41471043, 41572343, and 41371103), the Jilin Provincial Science and Technology Development Project (20190101025JH and 20180101002JC), Department of Human Resources and Social Security of Jilin Province and the Program of Introducing Talents of Discipline to Universities (B16011), and Science and Technology projects of Jiangxi Provincial Department of Education (GJJ180781). AM was partially supported by a Chair Professor position at the Institute for Peat and Mire Research, Northeast Normal University.

ACKNOWLEDGMENTS

We thank Jing Zeng, Gao-Lin Zhao, Xing-xing Zheng, Feng Li, Chuan Long, Wei Li, Bing-Jiang Zhang, Qian-Wang Cui, and Li Zhao for their assistance in field vegetation survey and thank Xin-hu Zhou for measurement of environmental variables. We also thank the three reviewers for their comments and suggestions.

REFERENCES

Andrus, R. E. (1986). Some aspects of *Sphagnum* ecology. *Can. J. Bot.* 64, 416–426. doi: 10.1139/b86-057

Arita, H. T. (2016). Species co-occurrence analysis: pairwise versus matrix-level approaches. *Global. Ecol. Biogeogr.* 25, 1397–1400. doi: 10.1111/geb.12418

Astorga, A., Heino, J., Luoto, M., and Muotka, T. (2011). Freshwater biodiversity at regional extent: determinants of macroinvertebrate taxonomic richness in headwater streams. *Ecography* 34, 705–713. doi: 10.1111/j.1600-0587.2010.06427.x

Bartsch, I. (1994). Effects of fertilization on growth and nutrient use by *Chamaedaphne calyculata* in a raised bog. *Can. J. Bot.* 72, 323–329. doi: 10.1139/b94-042

Bates, J. W. (1988). The effect of shoot spacing on the growth and branch development of the moss *Rhytidiadelphus triquetrus*. *New. Phytol.* 109, 499–504. doi: 10.1111/j.1469-8137.1988.tb03726.x

Bellamy, D. J., and Rieley, J. (1967). Some ecological statistics of a "Miniature Bog". *Oikos* 18, 33–40. doi: 10.2307/3564632

Benavides, J., and Vitt, D. (2014). Response curves and the environmental limits for peat-forming species in the northern Andes. *Plant. Ecol.* 215, 937–952. doi: 10.1007/s11258-014-0346-7

Blanchet, F. G., Legendre, P., and Borcard, D. (2008). Forward selection of explanatory variables. *Ecology* 89, 2623–2632. doi: 10.1890/07-0986.1

Borcard, D., Gillet, F., and Legendre, P. (2011). *Numerical Ecology with R*. New York: Springer, 227–292. doi: 10.1007/978-1-4419-7976-6

Bourbonniere, R. A. (2009). Review of water chemistry research in natural and disturbed peatlands. *Can. Water. Resour. J.* 34, 393–414. doi: 10.4296/cwrj3404393

Bragazza, L. (1997). *Sphagnum* niche diversification in two oligotrophic mires in the southern Alps of Italy. *Bryologist* 100, 507–515. doi: 10.2307/3244413

Bragazza, L., and Gerdol, R. (2002). Are nutrient availability and acidity-alkalinity gradients related in *Sphagnum*-dominated peatlands? *J. Veg. Sci.* 13, 473–482. doi: 10.1111/j.1654-1103.2002.tb02074.x

Breeuwer, A., Heijmans, M. P. D., Robroek, B. M., and Berendse, F. (2008). The effect of temperature on growth and competition between *Sphagnum* species. *Oecologia* 156, 155–167. doi: 10.1007/s00442-008-0963-8

Bu, Z., Rydin, H., and Chen, X. (2011). Direct and interaction-mediated effects of environmental changes on peatland bryophytes. *Oecologia* 166, 555–563. doi: 10.1007/s00442-010-1880-1

Bu, Z., Zheng, X., Rydin, H., Moore, T., and Ma, J. (2013). Facilitation vs. competition: does inter-specific interaction affect drought responses in *Sphagnum*?. *Basic. Appl. Ecol.* 14, 574–584. doi: 10.1016/j.baae.2013.08.002

Chambers, F. M., Mauquoy, D., Gent, A., Pearson, F., Daniell, J. R. G., and Jones, P. S. (2007). Palaeoecology of degraded blanket mire in south wales: data to inform conservation management. *Biol. Conserv.* 137, 197–209. doi: 10.1016/j.biocon.2007.02.002

Chen, X., Bu, Z., Stevenson, M. A., Cao, Y., Zeng, L., and Qin, B. (2016). Variations in diatom communities at genus and species levels in peatlands (central China) linked to microhabitats and environmental factors. *Sci. Total Environ.* 568, 137–146. doi: 10.1016/j.scitotenv.2016.06.015

Cottenie, K., and De Meester, L. (2004). Metacommunity structure: synergy of biotic interactions as selective agents and dispersal as fuel. *Ecology* 85, 114–119. doi: 10.1890/03-3004

Decaëns, T. (2010). Macroecological patterns in soil communities. *Global. Ecol. Biogeogr.* 19, 287–302. doi: 10.1111/j.1466-8238.2009.00517.x

Decaëns, T., Jiménez, J. J., and Rossi, J.-P. (2009). A null-model analysis of the spatio-temporal distribution of earthworm species assemblages in Colombian grasslands. *J. Trop. Ecol.* 25, 415–427. doi: 10.1017/S0266467409006075

Dray, S., Legendre, P., and Peres-Neto, P. R. (2006). Spatial modelling: a comprehensive framework for principal coordinate analysis of neighbour matrices (PCNM). *Ecol. Model* 196, 483–493. doi: 10.1016/j.ecolmodel.2006.02.015

Eppinga, M. B., Rietkerk, M., Belyea, L. R., Nilsson, M. B., De Ruiter, P. C., and Wassen, M. J. (2010). Resource contrast in patterned peatlands increases along a climatic gradient. *Ecology* 91, 2344–2355. doi: 10.1890/09-1313.1

Frego, K. A., and Carleton, T. J. (1995). Microsite conditions and spatial pattern in a boreal bryophyte community. *Can. J. Bot.* 73, 544–551. doi: 10.1139/b95-056

Gao, M., He, P., Zhang, X., Liu, D., and Wu, D. (2014). Relative roles of spatial factors, environmental filtering and biotic interactions in fine-scale structuring of a soil mite community. *Soil. Biol. Biochem.* 79, 68–77. doi: 10.1016/j.soilbio.2014.09.003

Gignac, L. D., and Vitt, D. H. (1990). Habitat Limitations of *Sphagnum* along climatic, chemical, and physical gradients in mires of western Canada. *Bryologist* 93, 7–22. doi: 10.2307/3243541

Goffinet, B., and Shaw, A. J. (2009). *Bryophyte Biology*. Cambridge: Cambridge University Press, doi: 10.1017/cbo9780511754807

Gotelli, N. J. (2000). Null model analysis of species co-occurrence patterns. *Ecology* 81, 2606–2621. doi: 10.2307/177478

Gotelli, N. J., and Entsminger, G. L. (2004). *EcoSim: Null Models software for Ecology*, 7 Edn. Jericho: Acquired Intelligence Inc. & Kesey-Bear.

Grimaldo, J. T., Bini, L. M., Landeiro, V. L., O'Hare, M. T., Caffrey, J., Spink, A., et al. (2016). Spatial and environmental drivers of macrophyte diversity and community composition in temperate and tropical calcareous rivers. *Aquat. Bot.* 132, 49–61. doi: 10.1016/j.aquabot.2016.04.006

Hájek, M., Jiroušek, M., Navrátilová, J., Horodyská, E., Peterka, T., Plesková, Z., et al. (2015). Changes in the moss layer in Czech fens indicate early succession triggered by nutrient enrichment. *Preslia* 87, 279–301.

Hájek, M., Roleèek, J., Cottenie, K., Kintrová, K., Horsák, M., Poulíčková, A., et al. (2011). Environmental and spatial controls of biotic assemblages in a discrete semi-terrestrial habitat: comparison of organisms with different dispersal abilities sampled in the same plots. *J. Biogeogr.* 38, 1683–1693. doi: 10.1111/j.1365-2699.2011.02503.x

Hardin, G. (1960). The competitive exclusion principle. *Science* 131, 1292–1297. doi: 10.1126/science.131.3409.1292

Hayward, P. M., and Clymo, R. S. (1982). Profiles of water content and pore size in *Sphagnum* and peat, and their relation to peat bog ecology. *P. Roy. Soc. B-Biol. Sci.* 215, 299–325. doi: 10.1098/rspb.1982.0044

Hortal, J., Roura-Pascual, N., Sanders, N. J., and Rahbek, C. (2010). Understanding (insect) species distributions across spatial scales. *Ecography* 33, 51–53. doi: 10.1111/j.1600-0587.2009.06428.x

Johnson, M. G., Granath, G., Tahvanainen, T., Pouliot, R., Stenøien, H. K., Rochefort, L., et al. (2015). Evolution of niche preference in *Sphagnum* peat mosses. *Evolution* 69, 90–103. doi: 10.1111/evo.12547

Klimkowska, A., Van Diggelen, R., Grootjans, A. P., and Kotowski, W. (2010). Prospects for fen meadow restoration on severely degraded fens. *Perspect. Plant. Ecol.* 12, 245–255. doi: 10.1016/j.ppees.2010.02.004

Kooijman, A. M. (1993). On the ecological amplitude of four mire bryophytes; a reciprocal transplant experiment. *Lindbergia* 18, 19–24.

Kooijman, A. M. (2012). 'Poor rich fen mosses': atmospheric N-deposition and P-eutrophication in base-rich fens. *Lindbergia* 35, 42–52.

Legendre, P., and Gallagher, E. D. (2001). Ecologically meaningful transformations for ordination of species data. *Oecologia* 129, 271–280. doi: 10.1007/s004420100716

Legendre, P., and Gauthier, O. (2014). Statistical methods for temporal and space–time analysis of community composition data. *P. Roy. Soc. B-Biol. Sci.* 281, 1–9. doi: 10.1098/rspb.2013.2728

Lepš, J., and Šmilauer, P. (2003). *Multivariate Analysis of Ecological Data Using CANOCO*. Cambridge: Cambridge University Press. doi: 10.1017/CBO9780511615146

Ma, J., Bu, Z., Zheng, X., Ge, J., and Wang, S. (2015). Effects of shading on relative competitive advantage of three species of *Sphagnum*. *Mires. Peat.* 16, 1–17.

Malmer, N., Svensson, B. M., and Wallén, B. (1994). Interactions between *Sphagnum* mosses and field layer vascular plants in the development of peat-forming systems. *Folia Geobot. Phytotax.* 29, 483–496. doi: 10.1007/bf02883146

Mälson, K., and Rydin, H. (2009). Competitive hierarchy, but no competitive exclusions in experiments with rich fen bryophytes. *J. Bryol.* 31, 41–45. doi: 10.1179/174328209X404916

Mao, X., Cheng, S., Hong, Y., Zhu, Y., and Wang, F. (2009). The influence of volcanism on paleoclimate in the northeast of China: insights from Jinchuan peat. *Jilin Province, China. Chin. J. Geochem.* 28, 212–219. doi: 10.1007/s11631-009-0212-9

Martorell, C., Almanza-Celis, C. A. I., Pérez-García, E. A., and Sánchez-Ken, J. G. (2015). Co-existence in a species-rich grassland: competition, facilitation and niche structure over a soil depth gradient. *J. Veg. Sci.* 26, 674–685. doi: 10.1111/jvs.12283

MEPC, (1989). "*Water Quality-Determination of Total Phosphorus-Ammonium Molybdate Spectrophotometric Method*". China: China Environmental Science Press.

MEPC, (2012). "*Water Quality-Determination of Total Nitrogen-Alkaline Potassium Persulfate Digestion UV Spectrophotometric Method*". China: China Environmental Science Press.

Mikulyuk, A., Sharma, S., Van Egeren, S., Erdmann, E., Nault, M. E., and Hauxwell, J. (2011). The relative role of environmental, spatial, and land-use patterns in explaining aquatic macrophyte community composition. *Can. J. Fish. Aquat. Sci.* 68, 1778–1789. doi: 10.1139/f2011-095

Mitchell, E. A. D., van der Knaap, W. O., van Leeuwen, J. F. N., Buttler, A., Warner, B. G., and Gobat, J. M. (2001). The palaeoecological history of the Praz-Rodet bog (Swiss Jura) based on pollen, plant macrofossils and testate amoebae (Protozoa). *Holocene. Holocene.* 11, 65–80. doi: 10.1191/095968301671777798

Moore, P., and Wilmott, A. (1976). "Prehistoric forest clearance and the development of peatlands in the uplands and lowlands of Britain," in: *Proceedings of the Fifth International Peat Congress, held in Poznan* (Poland), 1–15.

Pedersen, B., Hanslin, H. M., and Bakken, S. (2001). Testing for positive density-dependent performance in four bryophyte species. *Ecology* 82, 70–88. doi: 10.2307/2680087

Peres-Neto, P. R. (2004). Patterns in the co-occurrence of fish species in streams: the role of site suitability, morphology and phylogeny versus species interactions. *Oecologia* 140, 352–360. doi: 10.1007/s00442-004-1578-3

Peres-Neto, P. R., Legendre, P., Dray, S., and Borcard, D. (2006). Variation partitioning of species data matrices: estimation and comparison of fractions. *Ecology* 87, 2614–2625. doi: 10.1890/0012-9658(2006)87%5B2614:vposdm%5D2.0.co;2

Pianka, E. R. (1974). Niche overlap and diffuse competition. *Proc. Nat. Acad. Sci. U.SA.* 71, 2141–2145. doi: 10.1073/pnas.71.5.2141

Plesková, Z., Jiroušek, M., Peterka, T., Hájek, T., Dítě, D., Hájková, P., et al. (2016). Testing inter-regional variation in pH niches of fen mosses. *J. Veg. Sci.* 27, 352–364. doi: 10.1111/jvs.12348

Potvin, L. R., Kane, E. S., Chimner, R. A., Kolka, R. K., and Lilleskov, E. A. (2015). Effects of water table position and plant functional group on plant community, aboveground production, and peat properties in a peatland mesocosm experiment (PEATcosm). *Plant. Soil* 387, 277–294. doi: 10.1007/s11104-014-2301-8

Rydin, H. (1993). Interspecific competition between *Sphagnum* mosses on a raised bog. *Oikos.* 66, 413–423. doi: 10.2307/3544935

Rydin, H., and Jeglum, J. K. (2013). *The Biology of Peatlands*. Oxford: Oxford University Press. doi: 10.1093/acprof:osobl/9780199602995.001.0001

Sabovljevic, M., and Sabovljevic, A. (2007). Contribution to the coastal bryophytes of the northern mediterranean: are there halophytes among bryophytes. *Phytol. Balcan.* 13, 131–135.

Schoener, T. W. (1983). Field experiments on interspecific competition. *Am. Nat.* 122, 240–285. doi: 10.2307/2461233

Sjögren, P., and Lamentowicz, M. (2008). Human and climatic impact on mires: a case study of Les Amburnex mire. *Swiss Jura Mountains. Veg. Hist. Archaeobot.* 17, 185–197. doi: 10.1007/s00334-007-0095-9

Sjörs, H., and Gunnarsson, U. (2002). Calcium and pH in north and central Swedish mire waters. *J. Ecol.* 90, 650–657. doi: 10.1046/j.1365-2745.2002.00701.x

Smith, R. I. L. (1978). Summer and winter concentrations of sodium, potassium and calcium in some maritime Antarctic cryptogams. *J. Ecol.* 66, 891–909. doi: 10.2307/2259302

Stone, L., and Roberts, A. (1990). The checkerboard score and species distributions. *Oecologia.* 85, 74–79. doi: 10.1007/BF00317345

Tahvanainen, T. (2004). Water chemistry of mires in relation to the poor-rich vegetation gradient and contrasting geochemical zones of the north-eastern fennoscandian Shield. *Folia. Geobot.* 39, 353–369. doi: 10.1007/bf02803208

Tahvanainen, T., Sallantaus, T., Heikkilä, R., and Tolonen, K. (2002). Spatial variation of mire surface water chemistry and vegetation in northeastern Finland. *Ann. Bot. Fenn.* 39, 235–251.

van Breemen, N. (1995). How *Sphagnum* bogs down other plants. *Trends. Ecol. Evol.* 10, 270–275. doi: 10.1016/0169-5347(95)90007-1

van der Wal, R., Pearce, I. S. K., and Brooker, R. W. (2005). Mosses and the struggle for light in a nitrogen-polluted world. *Oecologia* 142, 159–168. doi: 10.1007/s00442-004-1706-0

Verleyen, E., Vyverman, W., Sterken, M., Hodgson, D. A., De Wever, A., Juggins, S., et al. (2009). The importance of dispersal related and local factors in shaping the taxonomic structure of diatom metacommunities. *Oikos* 118, 1239–1249. doi: 10.1111/j.1600-0706.2009.17575.x

Vicherová, E., Hájek, M., and Hájek, T. (2015). Calcium intolerance of fen mosses: Physiological evidence, effects of nutrient availability and successional drivers. *Perspect. Plant. Ecol.* 17, 347–359. doi: 10.1016/j.ppees.2015.06.005

Vitt, D. H., Wieder, R. K., Scott, K. D., and Faller, S. (2009). Decomposition and peat accumulation in rich fens of boreal Alberta. *Canada. Ecosystems.* 12, 360–373. doi: 10.1007/s10021-009-9228-6

Wang, Z., Liu, S., Huang, C., Liu, Y., and Bu, Z. (2017). Impact of land use change on profile distributions of organic carbon fractions in peat and mineral soils in Northeast China. *CATENA* 152, 1–8. doi: 10.1016/j.catena.2016.12.022

Zeng, J., Bu, Z., Ma, J., Zhao, G., Long, C., Li, W., et al. (2012). Interspecific correlations among bryophytes and among bryophytes and vascular plants in two scales in jinchuan peatland. *Plant. Sci. J.* 30, 459–467. doi: 10.3724/SP.J.1142.2012.50459

Zhang, M., Bu, Z., Jiang, M., Wang, S., Liu, S., and Jin, Q. (2019). Mid-late Holocene maar lake-mire transition in northeast China triggered by hydroclimatic variability. *Quat.. Sci. Rev.* 220, 215–229. doi: 10.1016/j.quascirev.2019.07.027

Zhao, K. (1999). *Mires of China*. Beijing: Science publishing Company.

Conflict of Interest: The authors declare that the research was conducted in the absence of any commercial or financial relationships that could be construed as a potential conflict of interest.

The handling Editor declared a shared affiliation, though no other collaboration, with one of the authors SS at time of review.

frontiers in Earth Science

ORIGINAL RESEARCH
published: 07 July 2020
doi: 10.3389/feart.2020.00281

Seismic Line Disturbance Alters Soil Physical and Chemical Properties Across Boreal Forest and Peatland Soils

Scott J. Davidson[1], Ellie M. Goud[1,2], Caroline Franklin[3], Scott E. Nielsen[3] and Maria Strack[1]*

[1] Department of Geography and Environmental Management, University of Waterloo, Waterloo, ON, Canada, [2] Department of Ecology and Evolutionary Biology, Cornell University, Ithaca, NY, United States, [3] Department of Renewable Resources, University of Alberta, Edmonton, AB, Canada

Industrial activities for resource extraction have led to a network of seismic lines across Canada's boreal regions where peatlands often make up over 50% of the landscape. These clearings can have a significant influence on ecosystem functioning through vegetation removal, flattening of microtopography, altering hydrological pathways, and impacting biogeochemical processes. Recently, there has been a concerted effort to restore seismic lines to bring back the localized microtopography and encourage ecosystem recovery. A common restoration approach on seismic lines is mounding, which involves using machinery to recreate natural microtopography. Research is scarce on the impact on soil properties following both these disturbances and subsequent restoration on organic soils. The objectives of this study were to: (1) identify differences in soil physical and chemical characteristics between areas disturbed by seismic lines and adjacent natural areas and (2) determine changes to soil physical and chemical properties following the mounding restoration technique. Research was undertaken at two contrasting boreal ecosites (a poor mesic and a treed fen) near Fort McMurray, Alberta, Canada. In July 2018, we collected soil samples at 34 seismic line locations, both on the line and 20 m into the adjacent undisturbed area. Samples were analyzed for bulk density, volumetric water content (VWC), organic matter (OM) content, C:N ratios, and $\delta^{13}C/\delta^{15}N$ isotope analysis. Seismic line disturbances had a significant impact on soil properties, with increased bulk density and VWC on the line at both ecosites. We found an almost 40% reduction in OM on the line compared to natural areas at the poor mesic site, implying changes to carbon cycling, increased mineralization rates, and carbon loss from the system. There was also $\delta^{13}C/\delta^{15}N$ enrichment and narrower C:N ratios on the line, indicating increased decomposition. We found evidence of increased decomposition on the mounds created after restoration at the treed fen. Our results highlight a trade-off between restoration activities that may encourage recovery but also cause increased carbon losses from the system. This research is a first step in gaining a better understanding of these impacts in light of current restoration practices to ensure best management practices for improving ecosystem functioning.

Keywords: linear disturbance, boreal forest, bulk density, decomposition, stable isotopes, restoration, artificial microtopography

OPEN ACCESS

Edited by:
Jianghua Wu,
Memorial University of Newfoundland, Canada

Reviewed by:
David Cooper,
Colorado State University System, United States
Gustaf Granath,
Uppsala University, Sweden

****Correspondence:***
Scott J. Davidson
s7davidson@uwaterloo.ca

Specialty section:
This article was submitted to Biogeoscience, a section of the journal Frontiers in Earth Science

Received: *25 February 2020*
Accepted: *17 June 2020*
Published: *07 July 2020*

Citation:
Davidson SJ, Goud EM, Franklin C, Nielsen SE and Strack M (2020) Seismic Line Disturbance Alters Soil Physical and Chemical Properties Across Boreal Forest and Peatland Soils. Front. Earth Sci. 8:281. doi: 10.3389/feart.2020.00281

INTRODUCTION

Industrial activities for resource extraction have led to an extensive network of exploration lines, known as seismic lines, across Canada's boreal regions (Pasher et al., 2013; Dabros et al., 2018). The construction of these clearings involves vegetation removal and soil compaction, resulting in a network of linear disturbances that have the potential to impair forest cover (Filicetti et al., 2019), alter predator-prey dynamics (DeMars and Boutin, 2018), and increase greenhouse gas emissions (Strack et al., 2019). There is currently no mandate in Canada to restore these seismic line disturbances. According to standard practice in Canada, seismic lines were left for natural regeneration and although some natural tree regeneration does occur (Lieffers et al., 2017), most sites have limited recovery (van Rensen et al., 2015), even after decades (Lee and Boutin, 2006) although this can be dependent on ecosite type. Negative impacts of seismic lines on ecosystem structure, function, and lack of recovery have led to a decline in at-risk species such as woodland caribou (*Rangifer tarandus caribou*) (Dyer et al., 2001, 2002; Filicetti et al., 2019), leading to an increasing interest in restoring inactive seismic lines. In order to address the apparent ecological issues associated with failure to return to forest cover, the energy industry has voluntarily chosen to begin to actively restore seismic lines using a range of techniques including mechanical site preparation, tree planting, and recruitment of coarse woody material. Mounding treatments are a type of mechanical site preparation used to artificially recreate microtopography (Dabros et al., 2018; Filicetti et al., 2019) which is a key functional component of boreal ecosystems. Although application to treed peatlands is not well documented, mechanical site preparation and mounding specifically has a long history in industrial silviculture (Forest Resource Development Agreement [FRDA], 1989). Although it is well established that tree regeneration is largely dependent on soil conditions (Lieffers et al., 2017; Henneb et al., 2019), effects of seismic line disturbance and mounding treatments on organic soil physical and chemical properties are poorly understood. Here, we address this knowledge gap by assessing the effects of these disturbances and restoration techniques on soil physical and chemical properties.

There are two categories of seismic lines; legacy and low impact. Legacy lines (hereinafter referred to as wide lines) are typically 5–10 m wide, are straight and cleared using heavy machinery. Comparatively, low-impact lines (hereinafter referred to as narrow lines) are narrower (∼1–5 m), meandering, and cleared with a goal to limit ground disturbance (Lee and Boutin, 2006). Both of these disturbances result in the removal of vegetation (Filicetti et al., 2019), simplification of microtopography (Stevenson et al., 2019), alterations in microclimate (Stern et al., 2018), and hydrology (Williams et al., 2013; Braverman and Quinton, 2016), as well as changes in biogeochemical processes and soil characteristics (Lee and Boutin, 2006; Strack et al., 2019). Hydrological changes include altered and impeded surface and subsurface water flow (Braverman and Quinton, 2016). Increased compaction can decrease the saturated hydraulic conductivity of peat by 75% (Price et al., 2003). Decreased evapotranspiration can also occur due to the removal of the woody vegetation layer (Lee and Boutin, 2006). The flattening of the typical microtopography (hummocks; Stevenson et al., 2019) and compaction of the soil (Lovitt et al., 2018) leads to changes in soil morphology (Startsev and McNabb, 2009) and a reduction in microsites needed for successful tree germination (Lee and Boutin, 2006).

The compaction of the surface layer during disturbance can be measured by an increase in the bulk density of the soil. As organic particle and pore size decrease with increased decomposition (Boelter, 1969), bulk density can also be a useful indicator of soil decomposition extent. Disturbances can increase rates of mineralization and carbon (C) and nitrogen (N) cycling processes (Walbridge and Lockaby, 1994; Westbrook et al., 2006). C:N ratios have often been used to investigate the amount of soil decomposition (Kuhry and Vitt, 1996). Assuming that organic materials are consistent at the beginning and that volatile loss of N is negligible, this ratio is a measure of mass loss caused by mineralization based on the consumption of C-rich substances in relation to N (Damman, 1988; Drollinger et al., 2019) and subsequent release of carbon dioxide (CO_2) or methane (CH_4) through microbial respiration (Malmer and Holm, 1984). Disturbances such as these can also cause changes in the isotopic composition of the soil, including enrichment of both $\delta^{13}C$ and $\delta^{15}N$. $\delta^{13}C$ in plant litter and soil can be used to differentiate between isotopic effects in the early stages of decomposition (Nadelhoffer and Fry, 1988; Connin et al., 2001). $\delta^{15}N$ can give us an insight into changes in N content within both the plant litter and soil layers (Asada et al., 2005; Goud and Sparks, 2018) and can also be used as an indicator of decomposition extent (Amundson et al., 2003). Nutrient availability may change post-disturbance, linked to warmer, more aerobic, or wetter conditions altering microbial activity that may ultimately change net mineralization rates (Bradford et al., 2008; Li et al., 2012).

Seismic lines can also cause a significant shift in vegetation community composition, altering competitive relationships and making it difficult for trees to recolonize. Dense graminoid cover, especially prevalent after disturbance can shade tree seedlings, whereas dense *Sphagnum* spp. communities can bury small seedlings (Roy et al., 2000; Camill et al., 2010). Furthermore, changes in vegetation community composition and litter inputs can alter microbial communities, changing microbial cycling and potentially enhancing mineralization or overall decomposition extent (Scheffer et al., 2001; Allison and Treseder, 2011).

In order to restore seismic lines and accelerate the recovery of these lines (including regeneration of the tree cover), mounding treatments are used (Dabros et al., 2018; Filicetti et al., 2019). This involved creation of artificial microtopography (hummocks) on which tree seedlings are planted to establish tree growth. The ground surface on the seismic line is often lower than the adjacent forested ecosystem due to compaction (Stevenson et al., 2019) and therefore often has higher soil moisture content. Artificial mounding creates drier conditions that encourage tree seedling establishment and success (Lieffers et al., 2017). Mounding has been successfully shown to enhance tree growth across seismic lines (Filicetti et al., 2019), yet where mounds are formed from well-decomposed soil they can eventually flatten

out (Lieffers et al., 2017), in which case the microsite benefit may be lost. Furthermore, Takyi and Hillman (2000) found little improvement in tree growth on artificial mounding treatments compared to the flat ground in a drained peatland and Pacé et al. (2018) found that nutrient availability could be a limiting factor in tree regrowth. In fact, there is the potential that mounding may have increased rates of decomposition and soil respiration now that the soil is disturbed (Smolander and Heiskanen, 2007). Yet, despite this, the effects of seismic line disturbance and mounding restoration treatments on organic soil characteristics have not been investigated in detail. Therefore, the objectives of this study were: (1) to determine differences in soil physical and chemical characteristics between narrow and wide lines and the adjacent undisturbed areas and (2) document changes to soil physical and chemical characteristics following mounding compared to unmounded lines and adjacent reference sites. We hypothesized that narrow lines and mounded lines would have less compaction and faster rates of nutrient cycling, evidenced by lower bulk density, increased soil moisture, and C and N enrichment compared to wide lines.

MATERIALS AND METHODS

Study Site and Design

This study was undertaken in 2018 across seismic lines at two contrasting ecosites, a poor mesic site (seismic lines cleared in approximately 2006/2007) known as Tiger Sands [**Figure 1A**; defined as a combination of (c1) Laborador tea-mesic Pj-Sb and (g1) Laborador tea-subhygric Sb-Pj (Beckingham and Archibald, 1996) and a treed fen site (lines cleared roughly between 1998 and 2005) known as Kirby (**Figure 1B**; defined as (k1) treed rich fen; Beckingham and Archibald, 1996)] that was subject to a mounding restoration technique in 2015 (**Figure 1C**). The poor mesic site (56°21′11.38.8″ N, 111°35′13.2″ W) and treed fen site (55°22′11.17″ N, 111°09′15.4″ W) are located approximately 1 and 2 h south of the city of Fort McMurray, Alberta, respectively. Mean annual temperature (1981–2018) is 1°C and mean annual precipitation is ∼420 mm (Environment Canada, 2019). Both ecosite types were dominated by *Picea mariana* (Mill.) Britton (black spruce), with *Pinus banksiana* Lamb (jack pine) also present at the poor mesic site. The lines at the treed fen site were dominated by *Carex* spp. and *Sphagnum* spp., and the adjacent undisturbed areas had a much higher coverage of feather mosses.

At the poor mesic site, triplicate soil samples were collected near the center of the line, edge of the line and, 5 and 20 m into the adjacent undisturbed area (hereafter known as reference); this procedure was replicated for 24 lines (12 narrow and 12 wide) to a depth of 10 cm from the ground surface. The narrow lines are approximately 0.25 km apart and the wide lines are approximately 0.5 km apart. At the treed fen site, 10 narrow lines (five mounded and five unmounded) were chosen, with triplicate soil samples collected directly on the line and 20 m into the reference sites, at both high and low microtopographic positions at each sampling location. At the mounded line, the "low" samples were collected in locations as low as possible (lowest point on artificial mound or adjacent flat area) without being underwater. These lines were also approximately 0.25 km apart. A metal can (volume = 415 cm^3) was used to collect the soil samples to a depth of 10 cm, taking care to avoid compaction during collection. Due to the difficulty of defining the transition from living moss to soil in organic soil layers, at both sites, the moss/lichen layer was not removed prior to sample being taken and was assumed to be the top layer of the soil. Although changes to physical and chemical properties may change throughout the soil column, we chose to focus on the near surface conditions as this is the layer in which tree seedlings will establish and the most likely to be disturbed by seismic exploration activities. This also allowed us to conduct a more extensive sampling design across many seismic lines in remote locations.

Soil Analysis

Soil Physical Characteristics

Bulk density (g/cm^3) was determined by drying each sample in an oven at ∼60°C for 2 days or until the sample reached constant weight. Organic matter (OM) content (%) was calculated using the loss on ignition (LOI) method (Rowell, 1995). Approximately 2 g of each dried sample was weighed and then burned in a muffle furnace at 550°C for 3 h. After burning the samples, they were left to cool overnight and weighed post ignition. LOI is calculated as the difference between pre-ignition and post-ignition mass expressed as a percentage of pre-ignition mass. Volumetric water content (VWC) (%) was calculated by taking the wet weight minus the dry weight divided by the volume of the sample. Soil

FIGURE 1 | Example of seismic line disturbance at **(A)** poor mesic site, **(B)** treed fen site, and **(C)** example of the mounding technique.

organic carbon (SOC; kg/m^2) content in the top 10 cm was calculated by first multiplying the bulk density (converted to kg/m^3) by the total carbon content (see next section) and then by 0.1 to account for the depth of the sample.

Soil Chemical Characteristics

Carbon and nitrogen percent element (C, N) and isotope ratios (δ^{13}C, δ^{15}N) were measured using a continuous flow isotope ratio mass spectrometer (Thermo Scientific Delta Plus XL) coupled to an elemental analyzer (Costech ECS 4010). Isotope ratios are expressed as δ values (per mil):

$$\delta^{13}C, \delta^{15}N = (R_{sample}/R_{standard} - 1) \times 1000\ (\%)$$

where R_{sample} and $R_{standard}$ are the ratios of heavy to light isotope of the sample relative to the international standards for C and N, Vienna-Pee-Dee Belemnite and atmospheric nitrogen gas (N_2), respectively. A subset of the samples (approximately 90) was used for this analysis (0.01 mg for C and 0.02 mg for N). Samples were analyzed at the University of Waterloo Environmental Isotope Laboratory, Waterloo, ON, Canada.

Statistical Analyses

To determine potential differences in bulk density, OM content, VWC, C:N ratios, δ^{13}C, and δ^{15}N at the poor mesic site, we conducted a two-way ANOVA (Type III SS) with position (online, edge, 5 m and reference) and location (narrow or wide lines) as fixed factors. We conducted the same analyses for the treed fen site, with position (high or low) and treatment (mounded lines, unmounded lines, or reference) as fixed factors. To account for the nested experimental design, we averaged the measurements (n = 3) taken for bulk density, OM content, and VWC. If significant relationships were found, a Tukey HSD *post hoc* analysis was used (*lsmeans* package; Lenth, 2016). All analyses were performed in R 3.6.2 (R Core Team, 2013).

RESULTS

Soil Physical Characteristics

Wider lines at the poor mesic site (created in approximately 2006/2007) demonstrated significantly greater soil compaction (ANOVA, $F_{2,32}$ = 11.4; p = 0.0001), with a mean (±standard deviation) bulk density of 0.3 ± 0.2 g/cm^3 compared to the narrow lines (0.04 ± 0.1 g/cm^3) (**Figure 2A**). In comparison, the adjacent reference site had a bulk density of 0.05 ± 0.02 g/cm^3 (**Figure 2A**). At the treed fen site (lines created between approximately 1998–2005), the unmounded lines (comparable narrow lines) had similar bulk density at 0.03 ± 0.02 g/cm^3 to the narrower lines at the poor mesic site and the mounded lines had a bulk density of 0.06 ± 0.04 g/cm^3 (**Figure 3A**).

There was significantly higher soil moisture content on the lines compared to the reference sites at the treed fen site (ANOVA, $F_{2,34}$ = 11:00; p = 0.0002) (**Figure 3B**). There was no significant difference between high and low positions at both the

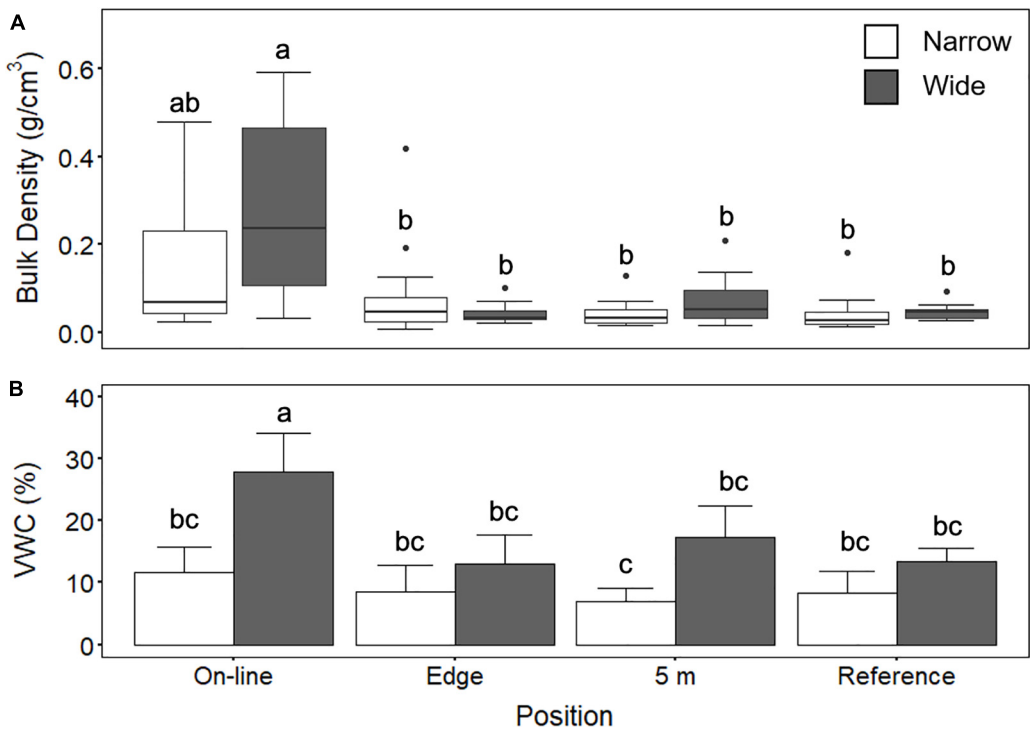

FIGURE 2 | (A) Bulk density (g/cm^3) and **(B)** volumetric water content (VWC; %) on wide and narrow lines at positions Online (wide n = 12, narrow n = 16), Edge (wide n = 16, narrow n = 16), 5 m (wide n = 16, narrow n = 16), and 20 m into the undisturbed site (Reference; wide n = 16, narrow n = 18) at the poor mesic site. Two-way ANOVA followed by a Tukey HSD ($p < 0.05$). Groups sharing a letter are not significantly different.

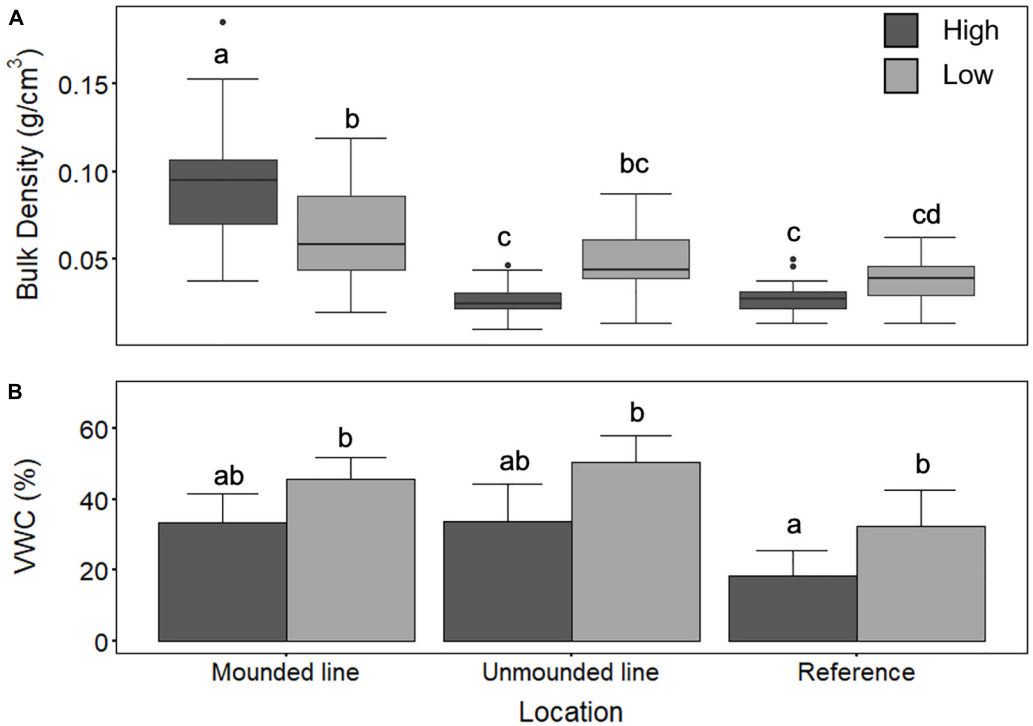

FIGURE 3 | (A) Bulk density (g/cm^3) and **(B)** volumetric water content (VWC; %) for high and low positions at the treed fen site across Mounded line (high n = 16, low n = 15), Unmounded lines (high n = 18, low n = 17), and 20 m into the undisturbed site (Reference; high n = 30, low n = 29). Two-way ANOVA followed by a Tukey HSD ($p < 0.05$). Groups sharing a letter are not significantly different.

mounded and unmounded lines. Wider lines at the poor mesic site also had significantly higher soil moisture content (ANOVA, $F_{3,32} = 3.36$; $p = 0.03$) (∼30%), compared with the adjacent reference site at the poor mesic site (**Figure 2B**).

We found a significant decrease in OM content (between 30 and 40%) from the Reference area and edge to on-line at the poor mesic site (ANOVA, $F_{3,34} = 8.3$, $p = 0.0001$) (**Table 1**). However, there was no significant difference in OM content between the line (both mounded and unmounded) and adjacent undisturbed locations at the treed fen site (**Table 2**). SOC in the top 10 cm was greatest on the wide (3.92 ± 1.6 kg/m^2) and mounded (3.76 ± 1.4 kg/m^2) lines, respectively (**Table 3**), which both had the greatest rates of compaction (**Figures 2A**, **3A**).

Soil Chemical Characteristics

Mean (±SD) C:N ratios ranged from 40.7 ± 7.2 (online) and 63.9 ± 15.5 (reference) at the poor mesic site to 17.1 ± 4.6 (online) and 26.6 ± 0 (reference) at the treed fen site (**Tables 1**, **2**). C:N ratios were significantly narrower on the wide lines at

TABLE 1 | Mean (± standard deviation) organic matter content (OM%), C:N ratio, δ^{13}C and δ^{15}N values for poor mesic site.

Treatment/location	*n*	OM (%)	*n*	C:N ratio
Narrow line				
Online	29	61.8 (34.5)^{ab}	19	58.0 (10.1)^{b}
Edge	28	78.1 (27.1)^{abc}		–
5 m	27	83.9 (22.9)^{abc}		–
Reference	27	90.4 (27.7)^{bc}	24	63.9 (15.5)^{b}
Wide line				
Online	12	47.4 (29.5)^{a}	9	40.7 (7.2)^{a}
Edge	10	84.1 (17.1)^{abc}		–
5 m	12	78.2 (23.6)^{abc}		–
Reference	13	88.7 (9.3)^{bc}	10	55.4 (4.8)^{b}

– denotes no data available. Two-way ANOVA followed by a Tukey HSD ($p < 0.05$). Groups sharing a letter are not significantly different.

TABLE 2 | Mean (±standard deviation) organic matter content (OM%), C:N ratio, δ^{13}C and δ^{15}N values for treed fen site.

Treatment/location	*n*	OM (%)	*n*	C:N ratio
Mounded line				
High	16	94.1 (1.9)	4	17.1 (4.6)^{a}
Low	15	93.5 (1.7)	5	20.2 (2.9)^{ab}
Unmounded line				
High	18	94.8 (2.0)	4	23.4 (2.5)^{ab}
Low	17	92.3 (3.1)	5	21.5 (2.4)^{ab}
Reference				
High	30	97.4 (0.7)	5	26.6 (0)^{b}
Low	29	93.2 (1.6)	8	24.5 (3.8)^{b}

Two-way ANOVA followed by a Tukey HSD ($p < 0.05$). Groups sharing a letter are not significantly different.

TABLE 3 | Mean (±standard deviation) soil organic carbon (SOC; kg/m^2) in the top 10 cm across each location.

Site	Location	*n*	SOC (kg/m^2)
Poor mesic	Narrow line	19	2.07 (1.9)
	Wide line	9	3.92 (1.6)
	Reference	34	1.29 (1)
Treed fen	Mounded line	9	3.76 (1.4)
	Unmounded line	9	1.7 (0.5)
	Reference	13	1.76 (0.8)

the poor mesic site and on the mounded line at the treed fen compared to the adjacent reference areas (**Tables 1**, **2**).

We observed significantly higher δ^{13}C values on the wider lines compared to both the narrow lines and the reference sites (ANOVA, $F_{2,25}$ = 14.73, p = 0.0003) (**Figure 4A**). Similarly, there was significantly higher δ^{15}N enrichment in online samples compared to reference locations (ANOVA, $F_{2,25}$ = 61.02, p < 0.0001) (**Figure 4B**). The mounded lines at the treed fen sites were significantly enriched in both δ^{13}C (ANOVA, $F_{2,24}$ = 7.01, p = 0.004) and δ^{15}N (ANOVA, $F_{2,25}$ = 7.8, p = 0.002) in comparison to the reference sites (**Figure 5**). Overall, δ^{13}C values between both the poor mesic site and the treed fen were similar, but the treed fen was more enriched in δ^{15}N than the poor mesic site.

DISCUSSION

Across Alberta, it is estimated that seismic line disturbances from resource extraction operations account for more than 80% of boreal anthropogenic disturbances (Pasher et al., 2013), covering an area of approximately 1200 km^2 (Strack et al., 2019). Our aim was to investigate the impact of these disturbances and subsequent restoration methods on soil physical and chemical properties across contrasting boreal ecosites. We found a significant effect of seismic line disturbances on soil characteristics at both the poor mesic and treed fen sites. There was a greater impact to soils on the wide lines at the poor mesic site, with greater increases in bulk density and a higher moisture content due to the lowering of the surface (reducing water table depth) following a potential combination of both compaction and loss of OM. Bulk density at the treed fen was similar to an undisturbed boreal peatland by Waddington and Roulet (2000) (between 0.05 and 0.15 g/cm^{-3}) and to a study by Strack et al. (2018) on a boreal peatland impacted by winter road construction (0.04–0.16 g/cm^{-3}), whereas on the wide lines at the poor mesic site, the bulk density was more than five times this. This is due to both higher mineral soil content at this ecosite, but also a combination of increased compaction, mineralization, and decomposition on the line. Soil compaction can cause a decrease in soil aeration, leading to changes in soil morphology and impacting productivity of

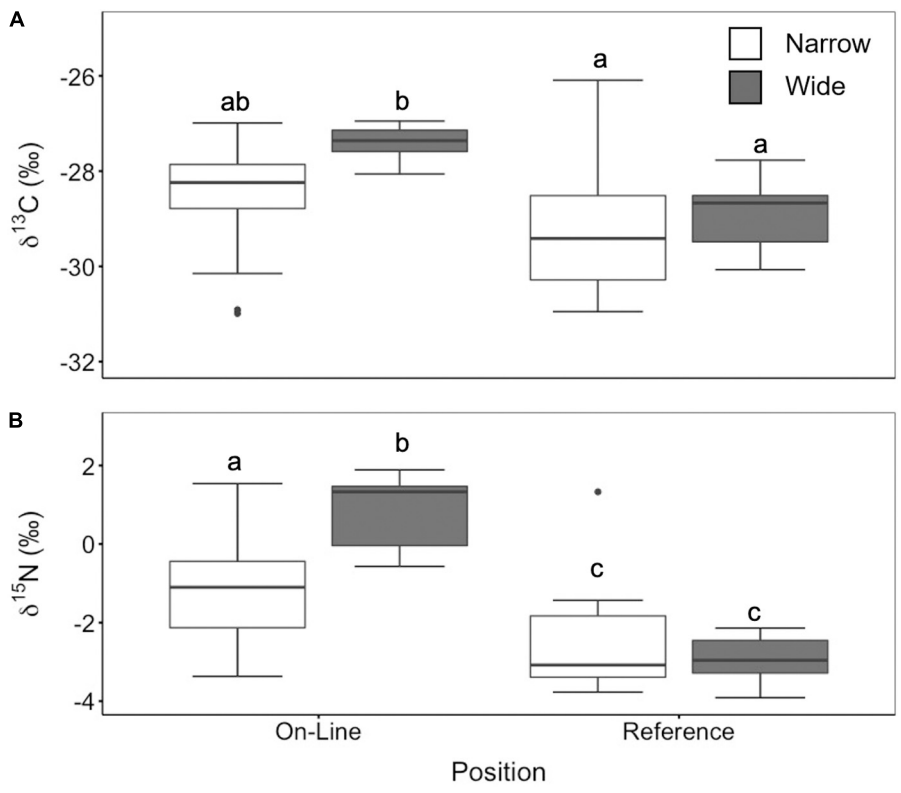

FIGURE 4 | (A) δ^{13}C (‰) and **(B)** δ^{15}N (‰) for online (wide n = 9, narrow n = 19) and reference sites (wide n = 10, narrow = 24) at both narrow and wide lines. Two-way ANOVA followed by a Tukey HSD (p < 0.05). Groups sharing a letter are not significantly different.

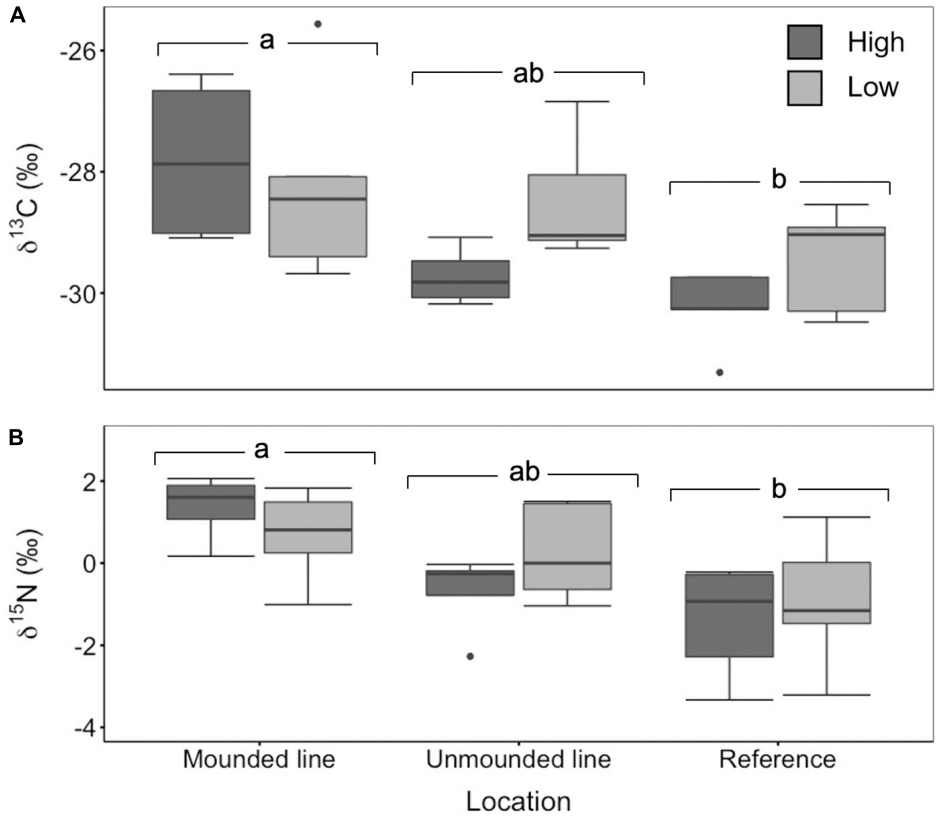

FIGURE 5 | (A) $\delta^{13}C$ (‰) and **(B)** $\delta^{15}N$ (‰) for mounded (high $n = 4$, low $n = 5$) and unmounded lines (high $n = 4$, low $n = 5$) and reference sites (high $n = 5$, low $n = 8$). Two-way ANOVA followed by a Tukey HSD ($p < 0.05$). Groups sharing a letter are not significantly different.

the system (Startsev and McNabb, 2009). A likely cause of this compaction is the use of heavy machinery to clear the wide lines but may also be related to removal of the more porous surface soil layer during the disturbance, or continued mineralization post-disturbance resulting in continued compaction. At both sites, the increased soil compaction on the lines also led to increases in VWC, likely due to the soil surface now being closer to the water table. Higher bulk density may also result in smaller pore sizes that have greater moisture retention, even with a water table drawdown during drier conditions, further contributing to higher soil moisture (Rezanezhad et al., 2016; Golubev and Whittington, 2018). The compaction of the soil and homogenizing of the landscape through the removal of localized microtopographic features may lead to pooling of water near the surface, as water cannot easily infiltrate highly compacted soil (Dabros et al., 2018; Golubev and Whittington, 2018). However, consistent increased moisture levels could also reduce respiration rates through reduction of the aerobic zone, and this will likely lower soil OM decomposition (Ise et al., 2008). Removal of the woody vegetation from the lines can also contribute to increases in soil moisture, through a reduction in water intake and decreased rates of evapotranspiration (Vitt et al., 1975; Dabros et al., 2018).

There was a significant difference in OM content from the reference site to the line in poor mesic sites. This could be attributed to mineralization of OM following disturbance (Mallik and Hu, 1997), either at the time of seismic line construction, or persisting in the new environmental conditions present on the line, or both. It could also result in a change in the net carbon balance of the system due to shifting inputs through lack of tree cover and changing ground layer vegetation. It is possible that seismic line construction and subsequent mounding in the treed fen also caused losses of OM through increased decomposition rates and subsequent respiration. When the soil is disturbed, inverted to create the mound and exposed to the air, higher amounts of decomposition and soil respiration through increased microbial activity would be expected (Mallik and Hu, 1997). Although not significantly different, we did observe consistently lower mean OM content on the line than in the reference ecosystem at the treed fen site. However, given that approximately the entire upper 1 m of the soil column is partially decomposed OM, these losses would likely not be measurable by investigating OM content alone. In fact, the amount of CO_2 lost from the system following this disturbance is poorly known and is the subject of further study.

The poor mesic site had higher C:N ratios, attributed to larger influence of litterfall from adjacent trees and woody vegetation and potentially slower decomposition (Kuhry and Vitt, 1996) compared to the treed fen site. During line clearing, there are a variety of practices for removing tree cover, including removal

from site, creation of windrows, and mulching of woody debris. Given the high C:N ratio of wood, this may have an impact on measured soil C:N values, but this would be difficult to account for, given that specific actions at any given site are difficult to obtain. The low C:N ratios found at the mounded site on the treed fen indicate that decomposition has been enhanced on these artificial hummocks (Kuhry and Vitt, 1996; Drollinger et al., 2019) and support the hypotheses of an increase in respiration rates and lower OM content expected in these areas. This is further supported by the enriched $\delta^{13}C$ values found at these sites. This indicates enhanced decomposition post-disturbance and may be a useful indicator of carbon loss given we cannot easily capture a loss in OM at these wetland sites.

Removal of the woody vegetation would lead to differences in N-inputs between lines and undisturbed areas, resulting from changes in the vegetation and microbial community, and the microclimate/abiotic conditions following disturbance. Enrichment occurs when there are more arbutoid or monotropoid mycorrhizae that give enriched N to their plant partners relative to ericoid or ecto-mycorrhizae that give depleted N (Hobbie and Högberg, 2012; Goud and Sparks, 2018). Higher $\delta^{15}N$ can also be attributed to warmer soils and soils with more ammonium (NH_4^+) relative to nitrate (NO_3^-) (Craine et al., 2015), the latter likely when soil moisture content is high (Macrae et al., 2013; Wood et al., 2016). Perhaps most importantly, and intimately connected to the previous points, are rates of the various N cycling components, especially increasing mineralization and immobilization given the alterations of oxic-anoxic conditions following disturbance (Amundson et al., 2003; Kramer et al., 2003; Asada et al., 2005). Regardless of ecosystem or disturbance type, enrichment of $\delta^{15}N$ in these boreal systems is most likely driven by different N sources, particularly the relative availability of organic vs. mineral/mineralized N (Högberg, 1997) which can have implications for vegetation community change and/or recovery.

The changes in ecohydrological dynamics following disturbance will over time lead to changes in the vegetation composition (Dabros et al., 2018), including increases in graminoid cover (for example, an increase in sedge cover across wetter disturbed peatland areas; van Rensen et al., 2015). The removal of woody vegetation and the opening of the tree canopy allow *Sphagnum* species to rapidly colonize these disturbed sites and outcompete feather moss (Bisbee et al., 2001). This can become an issue where slow growing tree-saplings that are successful in naturally regenerating on the lines are outcompeted by the faster growing moss species (Ohlson and Zackrisson, 1992; Roy et al., 2000). The lines at the treed fen have a substantial cover of *Sphagnum* in comparison to the feather dominated reference areas. We also saw colonization of tree saplings on the artificial mounds at the treed fen site. However, the increase in *Sphagnum* cover could lead to an increase in C uptake and decrease respiration rates as *Sphagnum* is typically highly productive and recalcitrant (Turetsky et al., 2008). In fact, similar carbon exchange function can arise in peatland plant communities despite species turnover (Robroek et al., 2017), suggesting that new communities could offer similar C storage function despite the lack of trees.

CONCLUSION

This work has provided an insight into changes in soil properties following the creation and subsequent restoration of seismic lines across two contrasting ecosites in northern Alberta. Overall, seismic line disturbances significantly impact soil physical and chemical characteristics. Specifically, seismic lines increase bulk density and moisture content, decrease OM content, and enhance decomposition. The large reduction in OM found in poor mesic sites has major implications for carbon cycling across these sites, indicating increased rates of mineralization. This is also highlighted by the increased $\delta^{13}C$ and $\delta^{15}N$ values found on the line, also pointing to increases in decomposition. The mounding technique used for restoration of these lines (Lieffers et al., 2017) also causes some disturbance to soil properties through increased decomposition and higher bulk density. Although seismic lines only make up a relatively small part of the landscape, it has to be questioned whether mounding these lines is a trade-off between disturbing the landscape to encourage tree regeneration and enhancing OM decomposition leading to increased carbon losses from the system. As mounding has been successfully used to improve tree regeneration in other ecosite types, future work should involve investigating alternative mounding techniques to ensure both tree recovery and minimal impact to the surrounding landscape in wetland systems.

AUTHOR'S NOTE

This research was undertaken within the boundaries of Treaty 8, traditional lands of the Dene and Cree, as well as the traditional lands of the Métis of northeastern Alberta. We would also like to acknowledge that the University of Waterloo is on the traditional territory of the Neutral, Anishnaabeg, and Hausenosaunee Peoples. The University of Waterloo is situated on the Haldimand Tract, land promised to Six Nations, which includes six miles on each side of the Grand River.

DATA AVAILABILITY STATEMENT

The datasets generated for this study are available on request to the corresponding author.

AUTHOR CONTRIBUTIONS

All authors contributed to the article and approved the submitted version. SD and MS designed the study. SD and CF performed the research. SD analyzed the data input from EG and MS. SD, EM, CF, SN, and MS wrote the manuscript.

FUNDING

This research is part of the Boreal Ecosystem Recovery and Assessment (BERA) project (www.bera-project.org), and was

supported by a Natural Sciences and Engineering Research Council of Canada Collaborative Research and Development Grant (CRDPJ 469943-14) in conjunction with Alberta-Pacific Forest Industries, Cenovus Energy, ConocoPhillips Canada, and Canadian Natural Resources.

ACKNOWLEDGMENTS

We would like to thank Lucas Schmaus, Duncan Forbes, and Angelo Filicetti for assistance in the field and Matt Coulas and Olivia Trudeau for their help with the soil sample processing. We also thank Sophie Wilkinson for earlier comments on the manuscript and to the two reviewers whose reviews really strengthened this research.

SUPPLEMENTARY MATERIAL

The Supplementary Material for this article can be found online at: https://www.frontiersin.org/articles/10.3389/feart.2020.00281/full#supplementary-material

REFERENCES

Allison, S. D., and Treseder, K. K. (2011). Climate change feedbacks to microbial decomposition in boreal soils. *Fungal Ecol.* 4, 362–374. doi: 10.1016/j.funeco.2011.01.003

Amundson, R., Austin, A. T., Schuur, E. A. G., Yoo, K., Matzek, V., Kendall, C., et al. (2003). Global patterns of isotopic composition of soil and plant nitrogen. *Glob. Biogeochem. Cycles* 17:1031. doi: 10.1029/2002GB001903

Asada, T., Warner, B., and Aravena, R. (2005). Effects of the early stage of decomposition on change in carbon and nitrogen isotopes in *Sphagnum* litter. *J. Plant Interact.* 1, 229–237. doi: 10.1080/17429140601056766

Beckingham, J. D., and Archibald, J. H. (1996). *Field Guide to Ecosites of Northern Alberta. Natural Resources Canada*. Edmonton: Canadian Forest Service.

Bisbee, K. E., Gower, S. T., Norman, J. M., and Nordheim, E. V. (2001). Environmental controls on ground cover species composition and productivity in a boreal black spruce forest. *Oecologia* 129, 261–270. doi: 10.1007/s004420100719

Boelter, D. H. (1969). Physical properties of peats as related to degree of decomposition. *Soil Sci. Soc. Am. J.* 33, 606–609. doi: 10.2136/sssaj1969.03615995003300040033x

Bradford, M. A., Davies, C. A., Frey, S. D., Maddox, T. R., Melillo, J. M., Mohan, J. E., et al. (2008). Thermal adaptation of soil microbial respiration to elevated temperatures. *Ecol. Lett.* 11, 1316–1327. doi: 10.1111/j.1461-0248.2008.01251.x

Braverman, M., and Quinton, W. I. (2016). Hydrological impacts of seismic lines in the wetland-dominated zone of thawing, discontinous permafrost, Northwest Territories, Canada. *Hydrol. Process.* 30, 2617–2627. doi: 10.1002/hyp.10695

Camill, P., Chihara, L., Adams, B., Andreassi, A., Barry, A., Kalim, S., et al. (2010). Early life history transitions and recruitment of *Picea mariana* in thawed boreal permafrost peatlands. *Ecology* 91, 448–459. doi: 10.1890/08-1839.1

Connin, S. L., Feng, X., and Virginia, R. A. (2001). Isotopic discrimination during long term decomposition in an arid land ecosystem. *Soil Biol. Biochem.* 31, 41–51. doi: 10.1016/s0038-0717(00)00113-9

Craine, J. M., Brookshire, E. N. J., Cramer, M. D., Hasselquist, N. J., Koba, K., Marin-spiota, E., et al. (2015). Ecological interpretations of nitrogen isotope ratios of terrestrial plants and soils. *Plant Soil* 396, 1–26. doi: 10.1007/s11104-015-2542-1

Dabros, A., Pyper, M., and Castilla, G. (2018). Seismic lines in the boreal and arctic ecosystems of North America: environmental impacts, challenges, and opportunities. *Environ. Rev.* 26, 214–229. doi: 10.1139/er-2017-0080

Damman, A. W. (1988). Regulation of nitrogen removal and retention in Sphagnum bogs and other peatlands. *Oikos* 51, 291–305.

DeMars, C. A., and Boutin, S. (2018). Nowhere to hide: effects of linear features on predator-prey dynamics in a large mammal system. *J. Anim. Ecol.* 87, 274–284. doi: 10.1111/1365-2656.12760

Drollinger, A., Kuzyakov, Y., and Glatzel, S. (2019). Effects of peat decomposition on δ13C and δ15N depth profiles of Alpine bogs. *Catena* 178, 1–10. doi: 10.1016/j.catena.2019.02.027

Dyer, S. J., O'Neill, J. P., Wasel, S. M., and Boutin, S. (2001). Avoidance of industrial development by woodland caribou. *J. Wildl. Manag.* 65, 531–542.

Dyer, S. J., O'Neill, J. P., Wasel, S. M., and Boutin, S. (2002). Quanitifying barrier effects of roads and seismic lines on movements of female woodland caribou in northeastern Alberta. *Can. J. Zool.* 80, 839–845. doi: 10.1139/z02-060

Environment Canada (2019). *National Climate Data and Information Archive*. Available at: http://www.climate.weatheroffice.ec.gc.ca/climateData/monthlydata_e.html?timeframe=3&Prov=CA&StationID=4977&Year=1951&Month=2&Day=26 (accessed August 1, 2019).

Filicetti, A. T., Cody, M., and Nielsen, S. E. (2019). Caribou conservation: restoring trees in seismic lines in Alberta, Canada. *Forests* 10:185. doi: 10.3390/f10020185

Forest Resource Development Agreement [FRDA] (1989). *Mounding for Site Preparation. FRDA Memo No. 100*. Available online: https://www.for.gov.bc.ca/hfd/pubs/Docs/Frm/Frm100.pdf (accessed November 1, 2019).

Golubev, V., and Whittington, P. (2018). Effects of volume change on the unsaturated hydraulic conductivity of Sphagnum moss. *J. Hydrol.* 559, 884–894. doi: 10.1016/j.jhydrol.2018.02.083

Goud, E. M., and Sparks, J. P. (2018). Leaf stable isotopes suggest shared ancestory is an important driver of functional diversity. *Oecologia* 187, 967–975. doi: 10.1007/s00442-018-4186-3

Henneb, M., Valeria, O., Thiffault, N., Fenton, N. J., and Bergeron, Y. (2019). Effects of mechanical site preparation on microsite availability and growth of planted black spuce in canadian paludified forests. *Forests* 10:670. doi: 10.3390/f10080670

Hobbie, E. A., and Högberg, P. (2012). Tansley review: nitrogen isotopes link mycorrhizal fungi and plants to nitrogen dynamics. *New Phytol.* 196, 367–382. doi: 10.1111/j.1469-8137.2012.04300.x

Högberg, P. (1997). Tansely review No. 96: 15N natural abundance in soil-plant systems. *New Phytol.* 137, 179–203. doi: 10.1046/j.1469-8137.1997.00808.x

Ise, T., Dunn, A. L., Wofsy, S. C., and Moorcroft, P. R. (2008). High sensitivity of peat decomposition to climate change through water table feedback. *Nat. Geosci.* 1, 763–766. doi: 10.1038/ngeo331

Kramer, M. G., Sollins, P., Sletten, R. S., and Swart, P. K. (2003). N isotope fractionation and measures of organic matter alteration during decomposition. *Ecology* 84, 2021–2025. doi: 10.1890/02-3097

Kuhry, P., and Vitt, D. H. (1996). Fossil carbon/nitrogen ratios as a measure of peart decomposition. *Ecology* 77, 271–275. doi: 10.2307/2265676

Lee, P., and Boutin, S. (2006). Persistence and developmental transition of wide seismic lines in the western Boreal Plains of Canada. *J. Environ. Manage.* 78, 240–250. doi: 10.1016/j.jenvman.2005.03.016

Lenth, R. V. (2016). Least-squares means: the R package lsmeans. *J. Stat. Softw.* 69, 1–33. doi: 10.18637/jss.v069.i01

Li, J., Ziegler, S., Lane, C. S., and Billings, S. A. (2012). Warming-enhanced preferential microbial mineralization of humified boreal forest soil organic matter: interpretation of soil profiles along a climate transect using laboratory incubations. *J. Geophys. Res.* 17:G02008. doi: 10.1029/2011JG001769

Lieffers, V. J., Caners, R. T., and Ge, H. (2017). Re-establishment of hummock topography promotes tree regeneration on highly disturbed moderate-rich fens. *J. Environ. Manage.* 197, 258–264. doi: 10.1016/j.jenvman.2017.04.002

Lovitt, J., Rahman, M. M., Saraswati, S., McDermid, G. J., Strack, M., and Xu, B. (2018). UAV remote sensing can reveal the effects of low-impact seismic lines on surface morphology, hydrology and methane (CH4) release in a boreal treed bog. *J. Geophys. Res. Biogeosci.* 123, 1117–1129. doi: 10.1002/2017JG004232

Macrae, M. L., Devito, K. J., Strack, M., and Waddington, J. M. (2013). Effect of water table drawdown on peatland nutrient dynamics: implications for climate change. *Biogeochemistry* 112, 661–676. doi: 10.1007/s10533-012-9730-3

Mallik, A. U., and Hu, D. (1997). Soil respiration following site preparation treatments in boreal mixedwood forest. *For. Ecol. Manag.* 97, 265–275. doi: 10.1016/s0378-1127(97)00067-4

Malmer, N., and Holm, E. (1984). Variation in the C/N-quotient of peat in relaction to decomposition rate and age determination with 210Pb. *Oikos* 43, 171–182.

Nadelhoffer, K., and Fry, B. (1988). Controls on natural nitrogen-15 and carbon-13 abundances in forest soil organic matter. *Soil Sci. Soc. Am. J.* 52, 1633–1640. doi: 10.2136/sssaj1988.03615995005200060024x

Ohlson, M., and Zackrisson, O. (1992). Tree establishment and microhabitat relationships in north Swedish peatlands. *Can. J. For. Res.* 22, 1869–1877. doi: 10.1139/x92-244

Pacé, M., Fenton, N. J., Paré, D., and Bergeron, Y. (2018). Differential effects of feather and *Sphagnum* spp. mosses on black spruce germination and growth. *For. Ecol. Manag.* 415-416, 10–18. doi: 10.1016/j.foreco.2018.02.020

Pasher, J., Seed, E., and Duffe, J. (2013). Development of boreal ecosystem anthropogenic disturbance layers for Canada based on 2008-2010 Landsat imagery. *Can. J. Rem. Sen.* 39, 42–58. doi: 10.5589/m13-007

Price, J. S., Heathwaite, A. L., and Baird, A. J. (2003). Hydrological processes in abandoned and restored peatlands: an overview of management approaches. *Wetlands Ecol. Manag.* 11, 65–83.

R Core Team (2013). *R: A Language and Environment for Statistical Computing*. Vienna: R Foundation for Statistical Computing.

Rezanezhad, F., Price, J. S., Quinton, W. L., Lennartz, B., Milojevic, T., and Van Cappellen, P. (2016). Structure of peat soils and implications for water storage, flow and solute transport: a review update for geochemists. *Chem. Geol.* 429, 75–84. doi: 10.1016/j.chemgeo.2016.03.010

Robroek, B. J. M., Jassey, V. E., Payne, R. J., Marti, M., Bragazza, L., Bleeker, A., et al. (2017). Taxonomic and functional turnover are decoupled in European peat bogs. *Nat. Commun.* 8:1161. doi: 10.1038/s41467-017-01350-5

Rowell, D. L. (1995). *Soil science: Methods and applications*. New York, NY: Wiley.

Roy, V., Ruel, J.-C., and Plamondon, A. P. (2000). Establishment, growth and survival of natural regeneration after clearcutting and drainage on forested wetlands. *For. Ecol. Manag.* 19, 253–267. doi: 10.1016/s0378-1127(99)00170-x

Scheffer, R. A., van Logestijn, R. S. P., and Verhoeven, J. T. A. (2001). Decomposition of *Carex* and *Sphagnum* litter in two mesotrophic fens differing in dominant plant species. *Oikos* 92, 44–54. doi: 10.1034/j.1600-0706.2001.920106.x

Smolander, A., and Heiskanen, J. (2007). Soil N and C transformations in two forest clear-cuts during three year after mounding and inverting. *Can. J. Soil. Sci.* 87, 251–258. doi: 10.4141/s06-028

Startsev, A. D., and McNabb, D. H. (2009). Effects of compaction on aeration and morphology of boreal forest soils in Alberta, Canada. *Can. J. Soil. Sci.* 89, 45–56. doi: 10.4141/cjss06037

Stern, E. R., Riva, F., and Nielsen, S. E. (2018). Effects of narrow linear disturbances on light and wind patterns in fragmented boreal forests in northeastern Alberta. *Forests* 9:486. doi: 10.3390/f9080486

Stevenson, C. J., Fillicetti, A. T., and Nielsen, S. E. (2019). High precision altimeter demonstrates simplification and depression of microtopography on seismic lines in treed peatlands. *Forests* 10:295. doi: 10.3390/f10040295

Strack, M., Hayne, S., Lovitt, S., McDermid, G. J., Rahman, M. M., Saraswati, S., et al. (2019). Petroleum exploration increases methane emissions from northern peatlands. *Nat. Commun.* 10:2804. doi: 10.1038/s41467-019-10762-4

Strack, M., Softa, D., Bird, M., and Xu, B. (2018). Impact of winter roads on boreal peatland carbon exchange. *Glob. Chang. Biol.* 24, 1–12.

Takyi, S. K., and Hillman, G. R. (2000). Growth of coniferous seedlings on a drained and mounded peatland in Central Alberta. *N. J. Appl. For.* 17, 71–79. doi: 10.1093/njaf/17.2.71

Turetsky, M. R., Crow, S. E., Evans, R. J., Vitt, D. H., and Wieder, R. K. (2008). Trade-offs in resource allocation among moss species control decomposition in boreal peatlands. *J. Ecol.* 96, 1297–1305. doi: 10.1111/j.1365-2745.2008.01438.x

van Rensen, C. K., Nielsen, S. E., White, B., Vinge, T., and Lieffers, V. J. (2015). Natural regeneration of forest vegetation on legacy seismic lines in boreal habitats in Alberta's oil sands region. *Biol. Conserv.* 184, 127–135. doi: 10.1016/j.biocon.2015.01.020

Vitt, D. H., Achuff, P., and Andrus, R. E. (1975). The vegetation and chemical properties of patterned fens in the Swan Hills, north central Alberta. *Can. J. Bot.* 53, 2776–2795. doi: 10.1139/b75-306

Waddington, J. M., and Roulet, N. T. (2000). Carbon balance of a boreal patterned peatland. *Glob. Change Biol.* 6, 87–98.

Walbridge, M. R., and Lockaby, B. G. (1994). Effects of forest management on biogeochemical functioning in southern forested wetlands. *Wetlands* 14, 10–17. doi: 10.1007/bf03160617

Westbrook, C. J., Devito, K. J., and Allan, C. J. (2006). Soil N cycling in harvested and pristine Boreal forests and peatlands. *For. Ecol. Manag.* 234, 227–237. doi: 10.1016/j.foreco.2006.07.004

Williams, T. J., Quinton, W. L., and Baltzer, J. L. (2013). Linear disturbances on discontinuous permafrost: implications for thaw-induced changes to land cover and drainage patterns. *Environ. Res. Lett.* 8:025006. doi: 10.1088/1748-9326/8/2/025006

Wood, M. E., Macrae, M. L., Strack, M., Price, J. S., Osko, T. J., and Petrone, R. M. (2016). Spatial Variation in nutrient dynamics among five different peatland types in the Alberta oil sands region. *Ecohydrology* 9, 688–699. doi: 10.1002/eco.1667

Conflict of Interest: The authors declare that the research was conducted in the absence of any commercial or financial relationships that could be construed as a potential conflict of interest.

frontiers in Earth Science

ORIGINAL RESEARCH
published: 25 August 2020
doi: 10.3389/feart.2020.00361

Extrapolation and Uncertainty Evaluation of Carbon Dioxide and Methane Emissions in the Qinghai-Tibetan Plateau Wetlands Since the 1960s

Jiang Zhang[1], Qiuan Zhu[1,2,3], Minshu Yuan[1], Xinwei Liu[4], Huai Chen[4], Changhui Peng[1,5], Meng Wang[6], Zhenan Yang[7], Lin Jiang[1] and Pengxiang Zhao[8]**

[1] Center for Ecological Forecasting and Global Change, College of Forestry, Northwest A&F University, Yangling, China, [2] College of Hydrology and Water Resources, Hohai University, Nanjing, China, [3] National Earth System Science Data Center, National Science & Technology Infrastructure of China, Beijing, China, [4] Chengdu Institute of Biology, Chinese Academy of Sciences, Chengdu, China, [5] Department of Biology Sciences, Institute of Environment Sciences, University of Quebec at Montreal, Montreal, QC, Canada, [6] Key Laboratory of Geographical Processes and Ecological Security in Changbai Mountains, Ministry of Education, School of Geographical Sciences, Northeast Normal University, Changchun, China, [7] Key Laboratory of Southwest China Wildlife Resources Conservation (China West Normal University), Ministry of Education, Nanchong, China, [8] College of Forestry, Northwest A&F University, Yangling, China

OPEN ACCESS

Edited by:
Matthias Peichl, Swedish University of Agricultural Sciences, Sweden

Reviewed by:
Xudong Zhu, Xiamen University, China
Gil Bohrer, The Ohio State University, United States

***Correspondence:**
Qiuan Zhu
zhuq@hhu.edu.cn
Pengxiang Zhao
zhaopengxiang@nwafu.edu.cn

Specialty section:
This article was submitted to Hydrosphere, a section of the journal Frontiers in Earth Science

Received: *30 April 2020*
Accepted: *04 August 2020*
Published: *25 August 2020*

Citation:
Zhang J, Zhu Q, Yuan M, Liu X, Chen H, Peng C, Wang M, Yang Z, Jiang L and Zhao P (2020) Extrapolation and Uncertainty Evaluation of Carbon Dioxide and Methane Emissions in the Qinghai-Tibetan Plateau Wetlands Since the 1960s. Front. Earth Sci. 8:361. doi: 10.3389/feart.2020.00361

Wetlands are important modulators of atmospheric greenhouse gas (GHGs) concentrations. However, little is known about the magnitudes and spatiotemporal patterns of GHGs fluxes in wetlands on the Qinghai-Tibetan Plateau (QTP), the world's largest and highest plateau. In this study, we measured soil temperature and the fluxes of carbon dioxide (CO_2) and methane (CH_4) in an alpine wetland on the QTP from April 2017 to April 2019 by the static chamber method, and from January 2017 to December 2017 by the eddy covariance (EC) method. The CO_2 and CH_4 emission measurements from both methods showed different relationships to soil temperature at different timescales (annual and seasonal). Based on such relationship patterns and soil temperature data (1960–2017), we extrapolated the CO_2 and CH_4 emissions of study site for the past 57 years: the mean CO_2 emission rate was 91.38 mg C m^{-2} h^{-1} on different measurement methods and timescales, with the range of the mean emission rate from 35.10 to 146.25 mg C m^{-2} h^{-1}, while the mean CH_4 emission rate was 2.75 mg C m^{-2} h^{-1}, with the ranges of the mean emission rate from 1.41 to 3.85 mg C m^{-2} h^{-1}. The estimated regional CO_2 and CH_4 emissions from permanent wetlands on the QTP were 94.29 and 2.37 Tg C $year^{-1}$, respectively. These results indicate that uncertainties caused by measuring method and timescale should be fully considered when extrapolating wetland GHGs fluxes from local sites to the regional level. Moreover, the results of global warming potential showed that CO_2 dominates the GHG balance of wetlands on the QTP.

Keywords: climate change, wetlands, greenhouse gas, carbon fluxes, global warming potential

INTRODUCTION

Since the beginning of the Industrial Era, large amounts of greenhouse gases (GHGs) have been released into the atmosphere (Boden et al., 2011). The continuously increasing concentrations of GHGs, particularly carbon dioxide (CO_2), methane (CH_4), and nitrous oxide (N_2O), contribute to the rise of land and ocean surface temperatures globally (IPCC, 2013). The trend of global warming will undoubtedly lead to changes in ecosystem structure, processes and functions in the next decades (Kintisch and Buckheit, 2006).

Although the increasing concentration of GHGs in the atmosphere is due mainly to human activities, about one third derives from natural resources, such as wetland soils (Marin-Muniz et al., 2015). Wetlands are unique in that they are formed by the interaction of terrestrial and aquatic ecosystems (Lewis and Ebrary, 1995). This allows them to serve many important functions, including improving water quality and micro-climate, sequestering carbon, and protecting biodiversity (Costanza et al., 1997; Engelhardt and Ritchie, 2001; Lamers et al., 2014). The wetlands occupy only 5–8% of land areas on Earth, but they store more than 30% of the world's soil carbon (Bridgham et al., 2012; Malone et al., 2013). Especially, in high-latitude wetlands, the combination of high productivity and low decomposition has resulted in significant carbon storage (Whiting and Chanton, 2001). Wetlands are considered as a major source of GHGs emissions (Bridgham et al., 2012; Mitsch et al., 2013). Therefore, quantifying and modeling the emission of GHGs from wetlands is very important for understanding the impacts of climate change on terrestrial ecosystem processes (Liu et al., 2017).

Many studies identified the production of GHGs in wetlands generally depends on soil temperature, water tables and redox conditions (Inglett et al., 2012; Treat et al., 2014). Soil temperature may impact the gaseous diffusivity of surface soils, soil organic matter decomposition, chemical reaction rates and so on, which ultimately impact GHGs emissions in wetlands (Liu et al., 2017; Yu et al., 2017). Although some studies have evaluated the relationships between GHGs fluxes and different environment factors in wetland, they are still uncertain in different wetlands. For example, a strong correlation between GHGs fluxes and soil temperature was found in artificial wetlands (Liu et al., 2013), but weak correlations were found in northern wetlands (Yu et al., 2017). Therefore, more *in situ* observations are still needed in wetlands.

The Qinghai-Tibetan Plateau (QTP), also known as the "Third Pole" of the Earth, is the largest and highest plateau in the world, with an average altitude of about 4 km. About 25% of the plateau's area of 2.5×10^6 km^2 (Chen et al., 2013a) is covered in wetlands (Hirota et al., 2004; Lehner and Doell, 2004; Niu et al., 2012; Chen et al., 2014; Wei and Wang, 2016). Since the 1960s, the QTP has experienced substantial changes due to human activities and natural processes, such as climate warming, water pollution and degradation of grassland and wetland (Piao et al., 2010; Chen et al., 2013b; Gao et al., 2013). The temperature of QTP has increased by 0.2℃ per decade, faster rate than the global average of 0.74℃ over the last century (Chen et al., 2013b; Liu et al., 2017). Climate changes are likely to affect the carbon and nitrogen cycles of alpine wetlands on the QTP (Gao et al., 2009; Tang et al., 2009; Zeng et al., 2017). Therefore, studying the GHGs fluxes in the QTP wetlands is necessary, which will further our understanding of carbon dynamics, as well as provide crucial insight into wetland responses to climate change. Although several studies estimated the dynamic and budget of carbon on the QTP, significant uncertainties of the size and the spatial distribution of carbon still exist when estimating current and future GHGs emissions from wetlands (Chen et al., 2013a; Jin et al., 2015; Wei and Wang, 2016; Cao et al., 2017; Zhang et al., 2020). There is a need for long-term field measurements to quantify carbon dynamics in wetlands under various climatic conditions (Zhao et al., 2006). And to evaluate the differences from different methods at different temporal-spatial scales will contribute to accurately quantify the budget of carbon of wetlands on the QTP.

In the present study, we measured the GHGs (CO_2 and CH_4) exchange between the atmosphere and wetland ecosystem on the QTP by the manual static chamber-gas chromatography method and the eddy covariance (EC) method. We aimed to (1) investigate spatiotemporal variations in CO_2 and CH_4 fluxes between soil and atmosphere and their relationship with soil temperature in the wetlands of the QTP, and (2) assess the uncertainties in extrapolation of CO_2 and CH_4 emissions from wetlands on the QTP.

MATERIALS AND METHODS

Study Site

The study was conducted at the Riganqiao Provincial Wetland Reserve (33°06′25″ N, 102°38′33″ E) located in the National Nature Reserve of Hongyuan county, China (**Figure 1**). The study site lies in the northeastern region of the QTP. The alpine wetland has an annual average temperature of 1.5°C and annual average precipitation of 270 mm (Liu et al., 2016; Zhong et al., 2017). The dominant vegetation is herbaceous plants, including *Carex mulinesis*, *Trollius farreri*, *Gentianan formosa*, and *Caltha palustris* (Yang et al., 2014; Liu et al., 2016; Zhong et al., 2017).

Gas Flux Measurements and Calculations

We performed *in situ* measurements primarily using the manual static chamber-gas chromatography method, already used to study most natural ecosystems (Chen et al., 2013a; Marin-Muniz et al., 2015; Wei and Wang, 2016). The eddy covariance (EC) method, a micrometeorological approach widely was applied to continuously measure carbon exchange between the atmosphere and ecosystems (Yu et al., 2017; Cui et al., 2018).

Chamber Method

GHGs fluxes were measured with static chamber method *in situ* from April 2017 to April 2019. The base of the stainless steel chamber (50 × 50 × 50 cm) was embedded 10 cm into the soil. To begin sampling, the base was filled with water to seal the compartments from outside air. Four

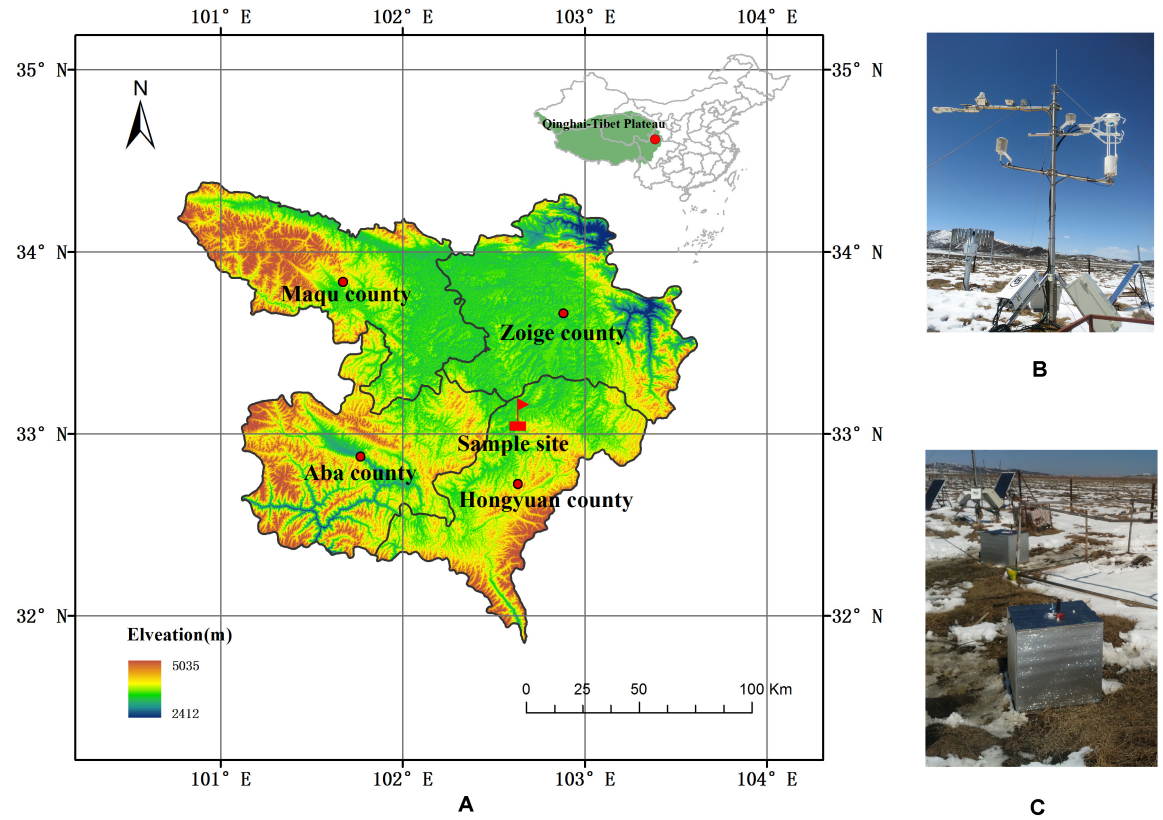

FIGURE 1 | Location of the Riganqiao Provincial Wetland Reserve. **(A)** Elevation map showing the sample site, denoted with a red flag, located on the Qinghai-Tibetan Plateau in the northeast region of Hongyuan county, China. Photographs of the **(B)** eddy covariance system and **(C)** static chamber used in this study.

static chambers were established on the study site. Four air samples were collected per hour from each chamber, which were taken at 10 min intervals after enclosure, stored in 10 ml air-tight vacuum vials. We took eight measurements from 10:00 to 18:00. Eight GHGs fluxes were collected for each chamber and the average value of four chambers was taken as the monthly emission value. No measurements were taken in February because weather conditions blocked access to the sample site. Temperature was recorded during gas sampling by sensors positioned on the inside and outside of the chamber and connected to an electronic thermometer. The GHGs concentrations were analyzed by gas chromatography (7890A GC System, Agilent Technologies, United States) (Chen et al., 2013a).

The fluxes of CO_2 and CH_4 were calculated as:

$$F = H \cdot \frac{M}{V_0} \cdot \frac{P}{P_0} \cdot \frac{T_0}{T} \cdot \frac{dc}{dt} \quad (1)$$

where F is gas flux; H, chamber height above the soil surface; M, molar mass of gas; V_0, standard molar volume (22.4 L mol^{-1}); P, atmospheric pressure at the sampling site; P_0, atmospheric pressure (101,325 Pa); T_0, absolute temperature of 0°C (273.15 K); T, the absolute temperature of the sampling time and dc/dt, change in gas flux rate. Details regarding the calculation of gas fluxes have been described (Chen et al., 2013a; Marin-Muniz et al., 2015).

EC Method

The CH_4 fluxes were measured from January 2017 to December 2017 using the open-path EC method at a height of 2.5 m (**Figure 1**). Flux data were recorded at 10 Hz and logged at 30-min intervals using a data logger (CR3000; Campbell Scientific, United States). The raw CH_4 data were postprocessed and quality controlled by EddyPro v4.2 software[1] to compute the CH_4 fluxes over an half hour interval (Foken et al., 2004). Due to missing and discarded data, in this study, we filled the gaps of CH_4 data by an average diurnal variations based on previous and subsequent days. Details of the CO_2 data processing have been described in previous study (Liu et al., 2019).

Soil Temperature Measurements *in situ*

Soil temperature was automatically recorded at 30-min intervals by sensors (WatchDog-B101, Spectrum, Chicago, United States) placed 5 cm below the soil surface at the sample site. Further investigation was conducted to explore

[1]https://www.licor.com

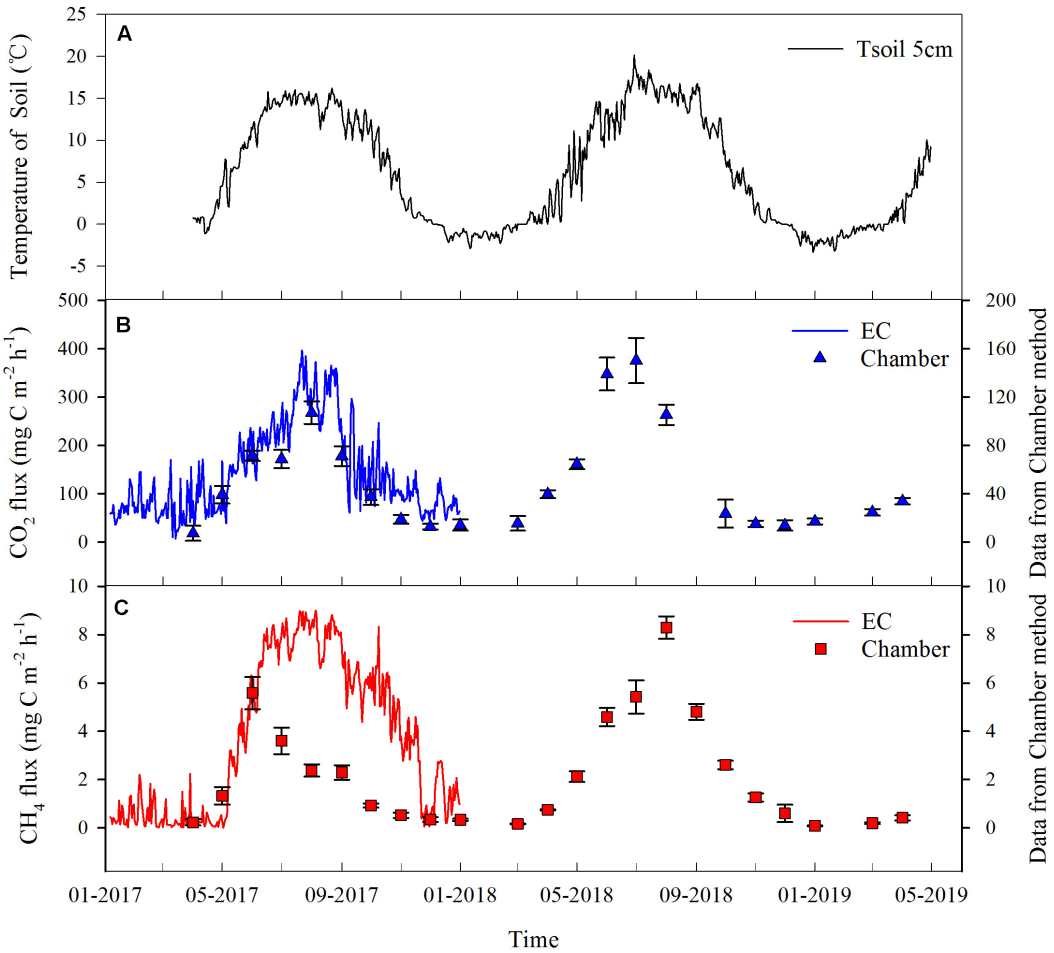

FIGURE 2 | Variations in soil temperature and CO_2 and CH_4 fluxes of the wetland site during the measurement period. Daily mean values of **(A)** soil temperature at 5 cm below ground from April 2017 to April 2019, **(B)** CO_2 flux rates, and **(C)** CH_4 flux rates. Solid blue and red lines indicate data obtained using the eddy covariance (EC) method from January to December 2017. The blue triangles and red squares indicate data collected using the chamber method from April 2017 to April 2019. Standard error is represented by vertical lines on triangles and squares.

the relationships between soil temperature at 5 cm of depth and GHGs emissions.

Additional Data Sources and Preprocessing

Wetland distribution maps (1980, 1990, 2000, and 2008) were acquired from Niu et al. (2009), which had been widely used in wetland classification and ecological regionalization (Liu et al., 2015; Zhu et al., 2016; Wang et al., 2020). In this study, the area overlapping across all four wetland distribution maps was defined as permanent wetland. Grid monthly soil temperatures at a depth of 5 cm (1960–2017) of QTP was extracted form the soil temperature dataset of China, which was constructed by interpolation at a spatial resolution of 5 arc-min using ANUSPLIN based on soil temperature data at a depth of 5 cm of 650 national meteorological stations that obtained from the China Meteorological Data Service Center[2].

[2]http://data.cma.cn/

Statistical Analyses

Mean emissions of CO_2 and CH_4 were calculated by averaging the replicates of sampling data. Soil temperature was calculated by averaging daily data. Linear and non-linear regressions were used to evaluate the relationship between soil temperatures and GHGs fluxes as measured by both methods (static chamber or EC) at different timescales (annual and seasonal). Results from the best fitting regression models are presented. All statistical analyses were performed using the software package R (R Core Team, 2020).

Extrapolation of GHGs Fluxes

The relationship between soil temperature of 5 cm depth and observed CO_2 and CH_4 emissions was explorered at different timescales [annual, non-growing (Jan–Apr and Oct–Dec) or growing season (May–Sep) (NG&G seasonal)]. Then the regression equations were applied to extrapolate the CO_2 and CH_4 emission rates of study site from 1960 to 2017 and the uncertainties were investigated.

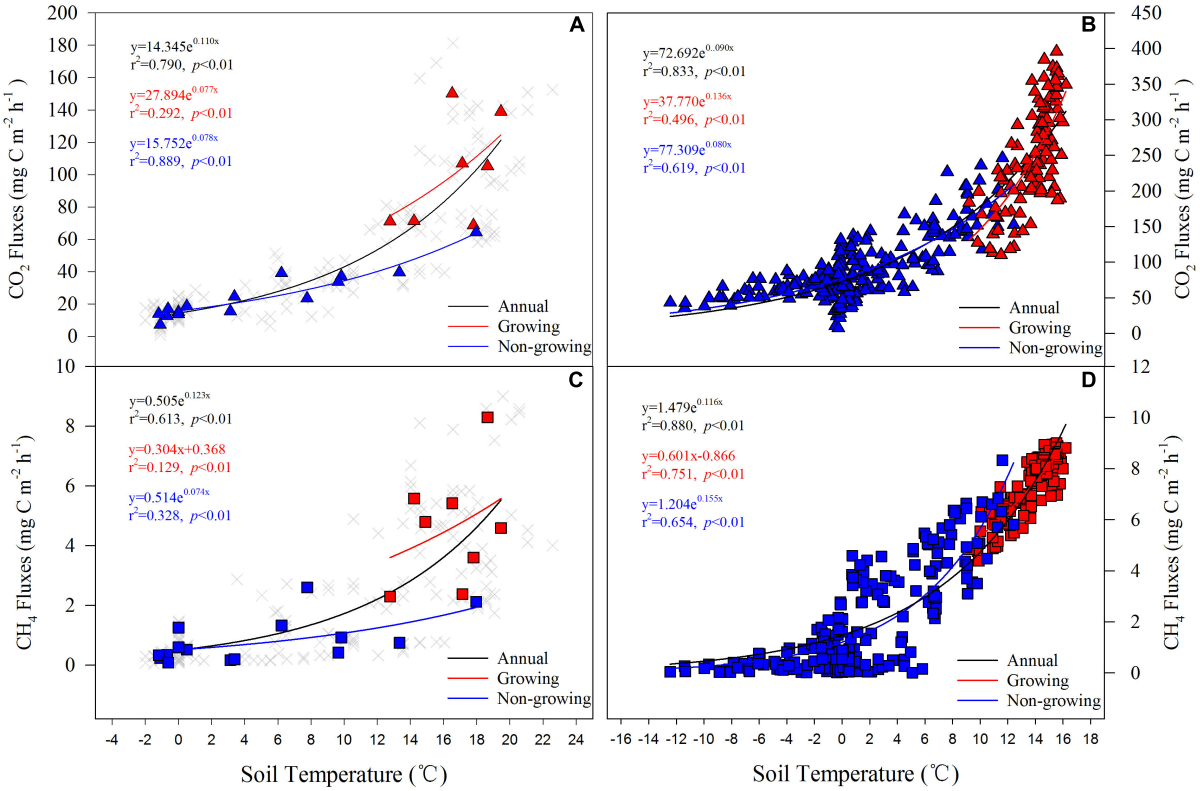

FIGURE 3 | Relationships between GHGs emissions and soil temperatures for annual and growing or non-growing periods, based on linear and non-linear regression. *Annual* refers data throughout the entire year; *Growing*, data in the growing season (May-Sep); *Non-growing*, data in the non-growing season (Jan-Apr and Oct-Dec). Data were collected using thestatic chamber **(A,C)** or eddy covariance (EC) method **(B,D)**.

In addition, the regression equations from EC method at NG&G seasonal timescales was performed for each wetland grid cell in order to roughly evaluate the long-term total and spatial patterns of wetland CO_2 and CH_4 emissions on the whole QTP.

RESULTS

Soil Temperature During Measurements

The daily average soil temperature at a depth of 5 cm ranged from -3.35 to 20.13°C during the entire observation period (April 2017–April 2019) (**Figure 2A**). Soil temperature showed a clear seasonal variation, with higher temperatures recorded during the growing season (from June–September) than during the non-growing season in 2017 and 2018. Daily mean temperatures were often below zero in winter (December–February), when soil layers were frozen.

Seasonal Dynamics of CO_2 and CH_4 Fluxes

The CO_2 fluxes showed a typical seasonal pattern: high fluxes were measured during the plant growing season, and low fluxes during the non-growing season (**Figure 2B**). The EC method showed greater variability in CO_2 fluxes than the chamber method. Measurements by the EC method oscillated between 7.38 and 395.74 mg C m^{-2} h^{-1}. The CO_2 fluxes from the chamber method oscillated between 7.21 ± 6.20 and 150.15 ± 18.73 mg C m^{-2} h^{-1}. Peak CO_2 fluxes were registered in August 2017 by both methods (EC:395.74 mg C m^{-2} h^{-1}; chamber: 106.94 ± 9.29 mg C m^{-2} h^{-1}). However, only the chamber method found another peak flux in July 2018 (150.15 ± 18.73 mg C m^{-2} h^{-1}), as the EC method did not capture data after 2017. Peaks in CO_2 fluxes usually coincided with peaks in soil temperature.

The seasonal dynamics of CH_4 fluxes paralleled those of CO_2 fluxes. The CH_4 emission rate measured by the EC method oscillated between 0.01 and 9.00 mg C m^{-2} h^{-1}, while the rate from the chamber method ranged from 0.08 ± 0.02 to 8.30 ± 0.46 mg C m^{-2} h^{-1} (**Figure 2C**). The EC method measured a higher CH_4 emission rate than the chamber method from May to December 2017. The chamber method captured emission spikes in July 2017 and August 2018. Although CH_4 emission rates exhibited similar dynamics as soil temperature, they slowed down in June 2017 (2.38 ± 0.25 mg C m^{-2} h^{-1}) and August 2017 (2.30 ± 0.30 mg C m^{-2} h^{-1}), despite increasing soil temperature. The winter season also slowed the rate of methane emissions.

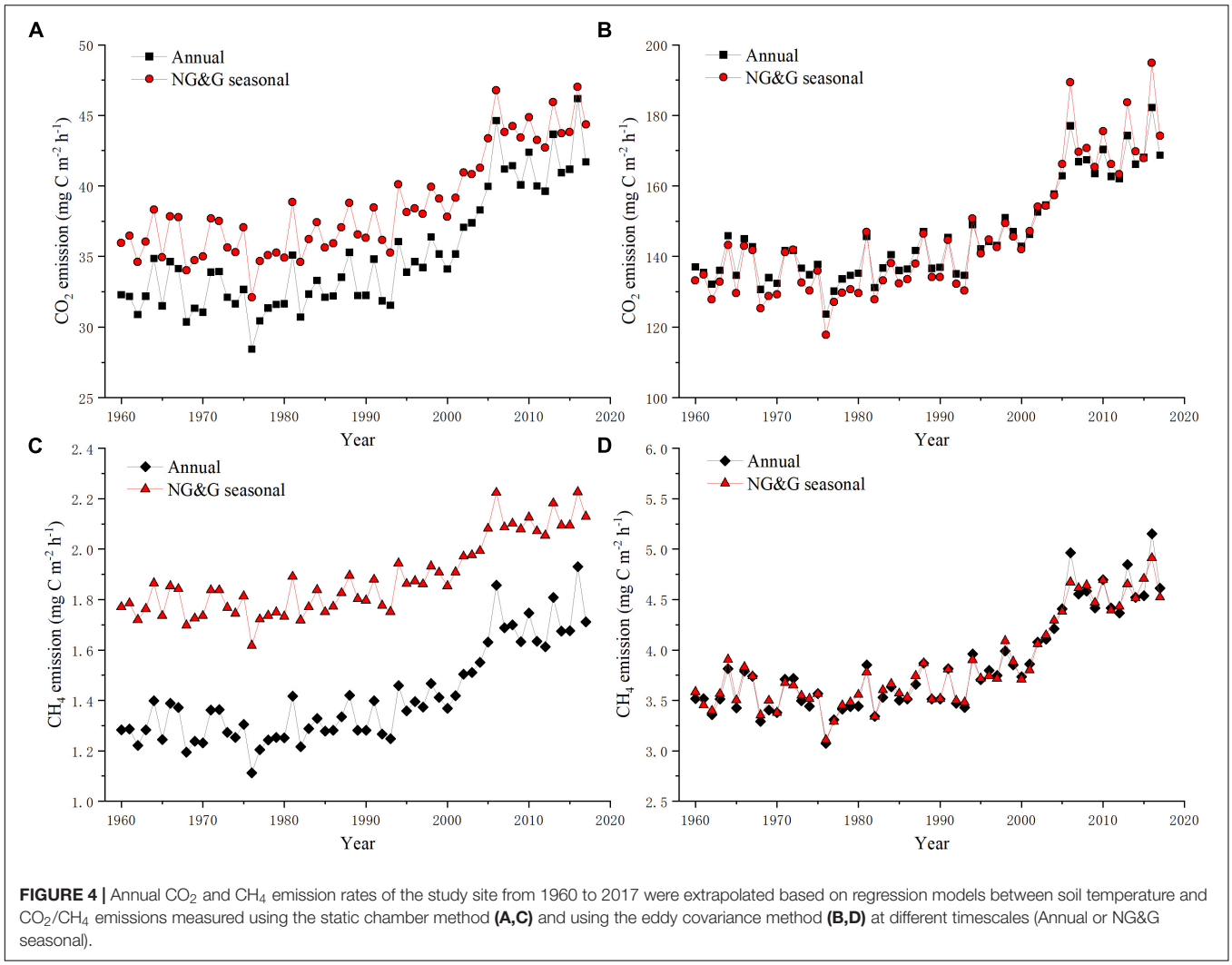

FIGURE 4 | Annual CO_2 and CH_4 emission rates of the study site from 1960 to 2017 were extrapolated based on regression models between soil temperature and CO_2/CH_4 emissions measured using the static chamber method **(A,C)** and using the eddy covariance method **(B,D)** at different timescales (Annual or NG&G seasonal).

TABLE 1 | Extrapolated mean emission rate of CO_2 and CH_4 of study site for the period 1960–2017, based on models derived from data obtained using the chamber or EC method at different timescales*.

Emission rate (mg C m^2 h^{-1})	Measurement method	Annual	NG&G seasonal	Average
CO_2	Chamber	35.10	38.60	91.38
	EC	146.25	145.58	
CH_4	Chamber	1.41	1.88	2.75
	EC	3.85	3.85	

**Timescales were the entire year (Annual), non-growing season and growing season (NG&G seasonal). Abbreviations: Chamber, static chamber; EC, eddy covariance.*

Relationship of CO_2 and CH_4 Fluxes to Soil Temperature

According to regression analyses, CO_2 fluxes increased exponentially with rising soil temperatures based on both EC and chamber measurements. Likewise, positive exponential correlations were found between CO_2 fluxes and soil temperatures during growing season or non-growing season (**Figures 3A,B**). The CH_4 fluxes correlated well with soil temperatures based on both methods. We also found positive relationships between CH_4 fluxes and soil temperatures. The relationship between CH_4 emission and soil temperature was exponential during the non-growing season but linear relationship was found during the growing season (**Figures 3C,D**).

Extrapolation of CO_2 and CH_4 Emission Rates of the Study Site

Based on the soil temperatures of study site and the regression equations, we extrapolated the CO_2 and CH_4 emission rates of the study site for the last 57 years (**Figure 4**). For static chamber method, extrapolated GHGs emission rates were higher for regression equations based

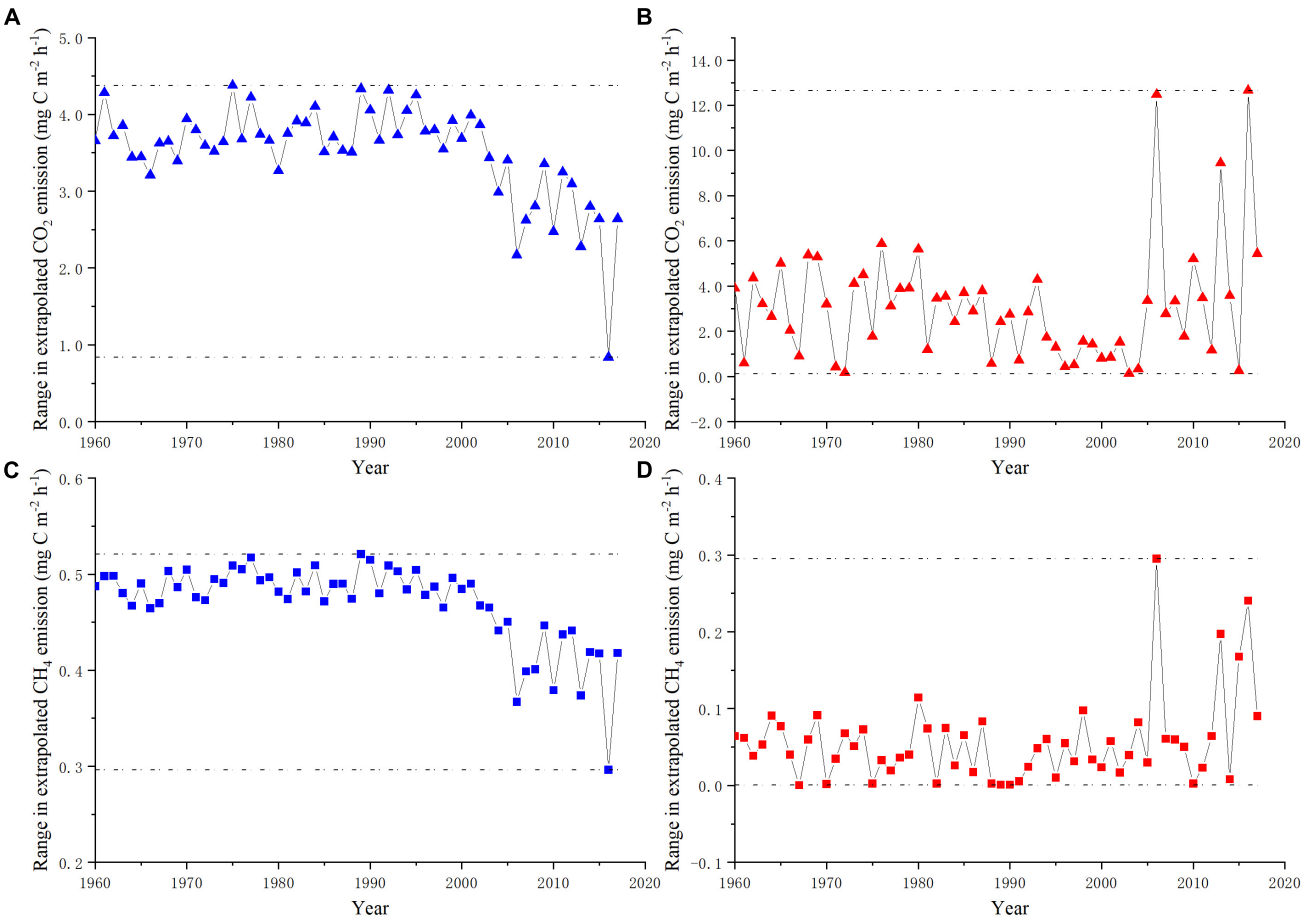

FIGURE 5 | Calculated differences between extrapolated annual greenhouse gas emission rate of study site from 1960 to 2017. CO_2 and CH_4 emission rates were extrapolated by models based on data derived from the static chamber method **(A,C)** or Eddy covariance method **(B,D)** at annual and NG&G seasonal timescales, respectively. The differences between the maximum and minimum extrapolated values of each year were plotted.

on the NG&G seasonal scale than for equations based on the annual scale (**Figures 4A,C**). For the EC method, extrapolated GHGs emission rates are similar at both timescales (**Figures 4B,D**).

Although extrapolated CO_2 emission rate followed similar trends whether based on the static chamber method or the EC method, the two methods gave significantly different magnitudes for the emission rate. the CO_2 emission rate in the static chamber method was far less than that measured by the EC method (**Figures 4A,B**). Extrapolated mean CO_2 emission rate of study site from 1960 to 2017 was calculated to be 91.38 mg C m^{-2} h^{-1}, with the ranges of the mean emission rate from 35.10 to 146.25 mg C m^{-2} h^{-1} on different measurement methods and timescales (**Table 1**). The differences of emission rates between the maximum and minimum values extrapolated for each year reflected uncertainties from the same measurement method at different timescales. Uncertainties in extrapolation of the CO_2 emission rates ranged from 0.84 to 4.38 mg C m^{-2} h^{-1} based on static chamber data, and from 0.13 to 12.67 mg C m^{-2} h^{-1} based on EC data (**Figures 5A,B**).

Extrapolated values for CH_4 emission rate based on EC data were three times larger than extrapolated values based on chamber data (**Figures 4C,D**). Extrapolated mean CH_4 emission rate of the study site was 2.75 mg C m^{-2} h^{-1} from 1960 to 2017, with the ranges of the mean emission rate from 1.41 to 3.85 mg C m^{-2} h^{-1} on different measurement methods and timescales (**Table 1**). Differences in annual average maxima and minima reflected uncertainties from static chamber method data ranging from 0.30 to 0.52 mg C m^{-2} h^{-1} (**Figure 5C**), while uncertainties in data extrapolated from the EC method ranged from 0 to 0.30 mg C m^{-2} h^{-1} (**Figure 5D**).

Regional Extrapolation of CO_2 and CH_4 Emissions From Wetlands on the QTP

Based on spatial soil temperature dataset of wetlands and the regression equations from EC method at NG&G seasonal timescales, total GHGs emissions of permanent wetland on the QTP were roughly extrapolated by performing the model for each wetlands grid cell. The CO_2 and CH_4 emissions of wetlands

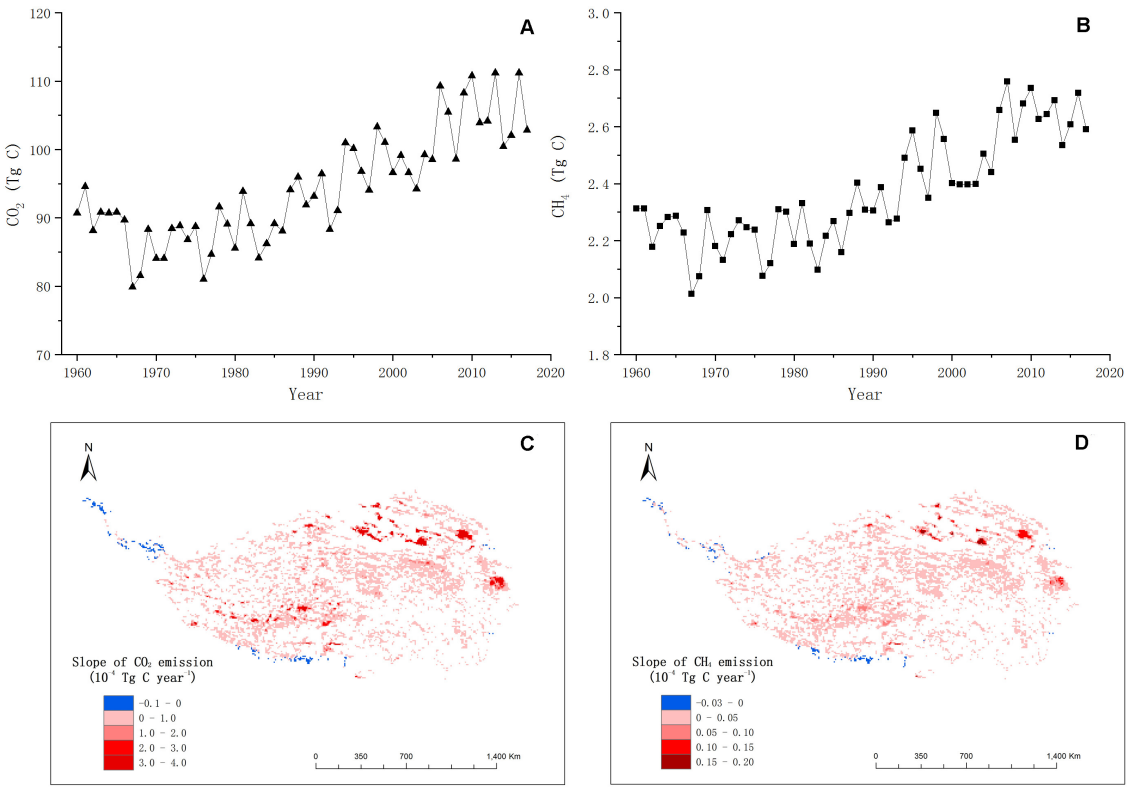

FIGURE 6 | Regional greenhouse gas emissions of wetlands on the Qinghai-Tibetan Plateau from 1960 to 2017. Annual CO_2 **(A)** and CH_4 **(B)** emissions were extrapolated by growing and non-growing seasonal models from the Eddy covariance method. Spatial distribution of **(C)** CO_2 and **(D)** CH_4 emission trends of wetlands on the Qinghai-Tibetan Plateau from 1960 to 2017. Linear regression and the line of best fit were calculated for each grid cell, and the slope of each cell is shown.

TABLE 2 | Estimated greenhouse gas emissions from the Qinghai-Tibetan Plateau wetlands in the literature.

CO_2 Tg C year^{-1}	Method	Period	References	CH_4 Tg C year^{-1}	Method	Period	Wetland Area × 10^4 km^2	References
40.65	Extraploation	2011–2013	Cao et al., 2017	0.53–0.68	Extraploation	1996–1997	18.8	Jin et al., 1999
58.34	Extraploation	2008–2009	Hao et al., 2011	0.42	Extraploation	2001–2002	5.52	Ding et al., 2004
94.29	Regression model	2010–2017	This study	0.17–0.31	Extraploation	2012–2014	6.32	Wei et al., 2015
				1.12	Meta-Analysis	2000		Chen et al., 2013c
				1.85	Model	1995–2005	11.5	Xu et al., 2010
				0.71	Model	2001–2011	13.4	Jin et al., 2015
				0.59–8.55	Model	1980–2010	1.2–9.8	Wei and Wang, 2016
				0.17	Model	2000–2010	3.33	Li et al., 2016
				0.18–0.27	Model	1978–2008	10.0	Zhang et al., 2020
				2.37	Regression model	2010–2017	7.1	This study

displayed pronounced increase on the whole QTP from 1960 to 2017 (**Figures 6A,B**). And the growth tendencies of CO_2 and CH_4 emissions showed no significant spatial heterogeneity on the QTP (**Figures 6C,D**). The northern part of the QTP showed the most obvious increase, while the marginal region displayed a downward trend. Moreover, we examined previously published results on CO_2 and CH_4 emissions from the QTP wetlands and compared them with average values extrapolated from 2010 to 2017 in the present study (**Table 2**). Calculated the regional CO_2 emission (94.29 Tg C year^{-1}) of wetlands on the QTP were higher than the ranges reported in the literature (40.65–58.34 Tg C year^{-1}). And the CH_4 emission (2.37 Tg C year^{-1}) of wetlands

on the QTP in this study fell within the range of previous studies (0.17–8.56 Tg C $year^{-1}$) (**Table 2**).

The GWP was applied to determine the relative and total contributions of CO_2 and CH_4 to the greenhouse effect. CH_4 values were converted to CO_2-equivalents based on published calculations (Kandel et al., 2019). From 1960 to 2017, the CO_2 emissions contributed the largest amount to carbon balance and dominated the atmospheric GHGs balance on the wetlands of the QTP. The CO_2 contributed approximately four times more than CH_4 to the GHGs balance on QTP wetlands (**Figure 7A**). The ratio of CH_4 to CO_2 emissions across all wetlands of the QTP has slightly declined in the past 57 years, despite significant increases in emissions of both gases (**Figure 7B**).

DISCUSSION

Relationships Between GHGs Fluxes and Soil Temperatures *in situ*

The wetland ecosystem of QTP is an important natural emitter of GHGs. The CO_2 and CH_4 fluxes showed similar seasonal emission patterns, with the greatest emissions noted during the plant growing season (Chen et al., 2013b; Liu et al., 2017). In this study, the CO_2 and CH_4 emissions were positively related to soil temperature, as reported for other wetlands (Zhao et al., 2006; Marin-Muniz et al., 2015).

The effects of soil temperature on CO_2 fluxes depend strongly on the availability of oxygen within the soil (Bonnett et al., 2013; Gao et al., 2013). Oxygen is an important factor that regulates organic matter decomposition in soil and the release of CO_2 (Bonnett et al., 2013; Treat et al., 2014; Liu et al., 2017). During the non-growing season on the QTP wetlands, the soil temperature was below freezing, which may inhibit the transport of oxygen from the soil to the rhizosphere zone, resulting in low CO_2 flux. Furthermore, soil temperature may also indirectly affect CO_2 fluxes by influencing rates of substrate supply, transport, and chemical reactions, which ultimately affect the release of CO_2 from wetland soil (Treat et al., 2014; Wei and Wang, 2016).

CH_4 emissions depend on anaerobic (production) and aerobic (oxidation) processes (Liu et al., 2017; Wei and Wang, 2017). Wetlands provide good anaerobic environments, and higher temperatures can promote activity of microbes such as methanogens. Both factors significantly increase CH_4 production in soil (Inglett et al., 2012). Furthermore, changes in soil temperature can also stimulate CH_4 transport from soil into the atmosphere (Yvon-Durocher et al., 2011). This transport slows in winter when soil temperature drops and CH_4 becomes trapped under a layer of ice, allowing only a small portion to be oxidized. As ice thaws during the following growing season, the stored CH_4 gas is released into the atmosphere. This cycle may partly explain the large CH_4 emission from the QTP wetlands during warm seasons. Thus, CH_4 emission appears to depend strongly on seasonal changes in the local environment, especially the influence of soil temperature on gas exchange.

Uncertainties in Extrapolation of GHGs Emission Rates of Study Site

With wetland soil temperatures and regression equations, we extrapolated the CO_2 and CH_4 emission rates of the study site. At different time scales, the GHGs emission rates extrapolated using static chamber measured data had higher uncertain than using EC measured data. The GHGs emission rates extrapolated by EC method were consistent under both time scales (**Figure 4**).

Measurement methods might result in the difference of estimated emission rates. The carbon balance of wetlands located in high latitude regions is strongly related to microtopography (Sullivan et al., 2008; Li et al., 2017). Although the wetland's topography and ecosystem appear to be flat and homogeneous, there is a significant amount of spatial heterogeneity at finer scales (a small chamber) or larger scales (the sample site). GHGs fluxes measured with the static chamber method cover only small patches of soil, which are usually not sufficient to make a full-scale understanding of the carbon exchanges of the heterogeneous ecosystems (Song et al., 2015). The EC method measured the

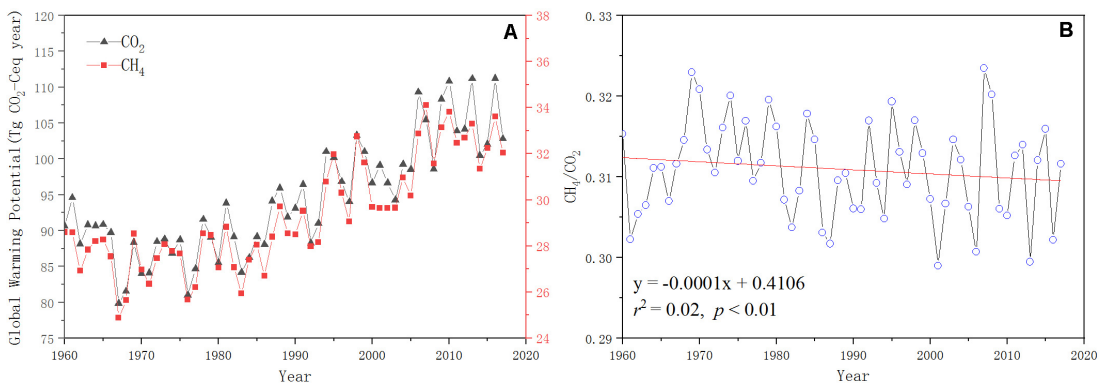

FIGURE 7 | Interannual variation in global warming potential based on CO_2 and CH_4 emissions from the Qinghai-Tibetan Plateau wetlands for the period 1960–2017. **(A)** CH_4 and CO_2 expressed as CO_2-C equivalents according to global warming potential (CH_4:28 and CO_2:1) (Kandel et al., 2019). **(B)** Ratio of extrapolated CH_4–CO_2 emissions over time.

carbon exchange between the atmosphere and ecosystems over a large area. Neglecting the effect of spatial heterogeneity might lead to the difference of GHGs emission rate that resulted in larger variance during extrapolation (Li et al., 2017). In addition, the static chamber method introduces so-called "chamber effects," potentially including modifications of temperature and moisture within the chamber as well as changes in the gas diffusion gradient within the soil profile (Song et al., 2015). The EC method, for its part, is susceptible to intermittent turbulence exchanges, commonly occurring at night, which reduce data quality (Gu et al., 2005; Aubinet et al., 2012; Yu et al., 2017). These limitations may also lead to uncertainties in extrapolated data.

The uncertainties of extrapolated emission rate resulted from the differences of regression models at different timescales. There were linear or non-linear correlations between soil temperature and GHGs fluxes in wetlands in previous studies (Kato et al., 2005; Liu et al., 2013; Song et al., 2015; Yu et al., 2017). Soil temperature has proven to be one of the most important factors affecting GHGs emission, but hydrology, plants, and soil microorganism also have an impact (Bhullar et al., 2013; Marin-Muniz et al., 2015). Particularly in wetlands, GHGs emissions are affected by many complex ecological processes, such as soil carbon and nitrogen cycling and root respiration (Baldock et al., 2012; Liu et al., 2013). All these factors are subject to seasonal and temperature-related changes. For example, during the plant non-growing season, plants begin wilting and gradually lose their ability to transport gas via stomata, and the upper soil and water layers freeze. These seasonal changes alter soil temperature and, consequently, the emission of GHGs (Song et al., 2015). This difference may also reflect the influence of fluctuations in soil temperature and water level. The water level not only limits the oxygen concentration but also influences soil temperature by controlling thermal conductivity (Yu et al., 2017). During the plant growing season, abundant precipitation influences both soil thermal and hydrological conditions, including water table depth, soil temperature and thawing depth. Heat is carried to deeper layers of soil by infiltration, rather than by thermal conduction, due to the low thermal conductance of the wetland and the high efficiency of water infiltration. This heat increases the soil temperature, promoting the thawing of the bottom permafrost. Thus, the rising temperature due to climate change and rising water level due to increased precipitation likely stimulate GHGs emission from wetlands beyond what would occur due to increases in either soil temperature or water level alone (Song et al., 2015). This may explain why, in the present study, the different correlations between soil temperature and the GHGs emission rate were found in different timescales.

Uncertainties in Regional Extrapolation of GHGs Emissions of Wetlands on the QTP

For the whole QTP, we extrapolated regional GHGs emissions from permanent wetlands by the seasonal model calculated EC method. The regional CO_2 emission was higher than the ranges reported in the literature, but the CH_4 emission fell within the ranges of previous studies. The uncertainties of estimation may result from inaccuracies in the wetland area. Jin reported the earliest estimates of CH_4 emissions ranging from 0.53 to 0.68 Tg C $year^{-1}$, based on observations (Jin et al., 1999). Wei made a challenge estimation of CH_4 emissions by integrating a biogeochemical model, which considered the wetland extents, and suggested that previous studies might have underestimated CH_4 emissions, due to bias in wetland extents (Wei and Wang, 2016). Currently, the wetland area on the QTP ranges from 1.2 to 18.8×10^4 km^2 (Jin et al., 1999; Niu et al., 2009, 2012; Zhang et al., 2020). A large discrepancy of wetland extent products largely affects estimations of GHGs emissions from natural wetland (Wei and Wang, 2016). Thus, improving the ability to obtain accurate data on the distribution and extent of wetlands should be a research priority in the future (Li et al., 2016). In addition, the spatial dataset of soil temperature was obtained by the spatial interpolation method, and its uncertainty might also lead to differences of estimated the total GHGs emissions from wetlands on the QTP. Therefore, the impact of these factors should be taken into account when estimating the GHGs emissions from the QTP wetlands, which will improve our understanding of the role of natural wetlands in the GHGs budget.

Spatial Distribution and GWP of GHGs Emissions of Wetlands on the QTP

Since the 1960s, the QTP has experienced universal and significant warming, heating up by 0.2–0.5°C per decade (Piao et al., 2010; Chen et al., 2013b). Projections of the Intergovernmental Panel on Climate Change showed that this warming trend will continue (IPCC, 2013). It is highly likely this will set up a positive feedback loop in the wetlands, in which warmer climate drives release of more GHGs, which in turn will raise the temperature (Song et al., 2015). Although the absolute amounts of CH_4 emitted are small compared to the amounts of CO_2, CH_4 contributes 28 times more than CO_2 to the atmospheric absorption of infrared radiation (Kandel et al., 2019). Previous studies have shown that CO_2 fluxes may mitigate the impact of CH_4 fluxes (Whiting and Chanton, 2001; Mitsch et al., 2013). The ratio of CH_4 fluxes to CO_2 fluxes may serve as an important index for an ecosystem's GHGs exchange balance with the atmosphere (Whiting and Chanton, 2001; Malone et al., 2013). For the entire wetlands of the QTP, the CO_2 emissions dominated the carbon balance in the wetland ecosystem and the GHGs balance in the atmosphere. We calculated a declining ratio of CH_4 to CO_2 for the period 1960–2017, indicating that CO_2 has become the main contributor to total GHGs fluxes. Thus, without human interference, the GHGs exchange balance should remain relatively constant on the wetlands of the QTP in the future.

CONCLUSION

The alpine wetland ecosystem in the QTP is an important source of GHGs. GHGs emissions vary exponentially with soil temperature. The CO_2 dominates the GHGs balance on QTP wetlands. Extrapolating GHGs fluxes from local to regional levels involves substantial uncertainties that depend on the measurement technique, timescale and wetlands extent. These parameters should be taken into consideration to ensure accurate estimation of GHGs fluxes in future research.

DATA AVAILABILITY STATEMENT

Monthly CO_2 and CH_4 flux data and soil temperature data presented in this article will be archived and freely available from figshare, doi: 10.6084/m9.figshare.12703121.v3.

AUTHOR CONTRIBUTIONS

QZ conceived and designed research. JZ, XL, ZY, and LJ collected data and conducted research. JZ and MY wrote the initial manuscript. HC, CP, MW, and PZ revised the manuscript. All authors read and approved the final manuscript.

FUNDING

This study was financially supported by the Second Tibetan Plateau Scientific Expedition (2019QZKK0304), the National Natural Science Foundation of China (41571081), the Fundamental Research Funds for the Central Universities (2019B04714), the National Key R&D Program of China (2016YFC0501804).

REFERENCES

Aubinet, M., Vesala, T., and Papale, D. (2012). *Eddy Covariance: A Practical Guide to Measurement and Data Analysis*. Berlin: Springer, 365–376. doi: 10.1007/978-94-007-2351-1

Baldock, J. A., Wheeler, I., McKenzie, N., and McBrateny, A. (2012). Soils and climate change: potential impacts on carbon stocks and greenhouse gas emissions, and future research for Australian agriculture. *Crop Pasture Sci.* 63, 269–283. doi: 10.1071/CP11170

Bhullar, G., Iravani, M., Edwards, P., and Olde Venterink, H. (2013). Methane transport and emissions from soil as affected by water table and vascular plants. *BMC Ecol.* 13:32. doi: 10.1186/1472-6785-13-32

Boden, T. A., Marland, G., and Andres, R. J. (2011). *Global, Regional, and National Fossil-Fuel CO_2 Emissions*. Bethel, PA: Carbon Dioxide Information Analysis Center.

Bonnett, S. A. F., Blackwell, M. S. A., Leah, R., Cook, V., O'Connor, M., and Maltby, E. (2013). Temperature response of denitrification rate and greenhouse gas production in agricultural river marginal wetland soils. *Geobiology* 11, 252–267. doi: 10.1111/gbi.12032

Bridgham, S., Cadillo-Quiroz, H., Keller, J., and Zhuang, Q. (2012). Methane emissions from wetlands: biogeochemical, microbial, and modeling perspectives from local to global scales. *Glob. Change Biol.* 19, 1325–1346. doi: 10.1111/gcb.12131

Cao, S., Cao, G., Feng, Q., Han, G., Lin, Y., Yuan, J., et al. (2017). Alpine wetland ecosystem carbon sink and its controls at the Qinghai Lake. *Environ. Earth Sci.* 76, 210. doi: 10.1007/s12665-017-6529-5

Chen, H., Wu, N., Wang, Y., Zhu, D., Zhu, Q., Yang, G., et al. (2013a). Inter-Annual variations of methane emission from an open fen on the qinghai-tibetan plateau: a three-year study. *PLoS One* 8:e53878. doi: 10.1371/journal.pone.0053878

Chen, H., Zhu, Q., Peng, C., Wu, N., Wang, Y., Fang, X., et al. (2013b). The impacts of climate change and human activities on biogeochemical cycles on the Qinghai-Tibetan Plateau. *Glob. Change Biol.* 19, 2940–2955. doi: 10.1111/gcb.12277

Chen, H., Zhu, Q., Peng, C., Wu, N., Wang, Y., Fang, X., et al. (2013c). Methane emissions from rice paddies natural wetlands, and lakes in China: synthesis and new estimate. *Glob. Change Biol.* 19, 19–32. doi: 10.1111/gcb.12034

Chen, J., Chen, J., Liao, A., Cao, X., Chen, L., Chen, X., et al. (2014). Global land cover mapping at 30 m resolution: a POK-based operational approach. *ISPRS J. Photogramm. Remote Sens.* 103, 7–27. doi: 10.1016/j.isprsjprs.2014.09.002

Costanza, R., d'Arge, R., de Groot, R., Farber, S., Grasso, M., Hannon, B., et al. (1997). The value of the world's ecosystem services and natural capital. *Nature* 387, 253–260. doi: 10.1038/387253a0

Cui, X., Liang, J., Lu, W., Chen, H., Liu, F., Lin, G., et al. (2018). Stronger ecosystem carbon sequestration potential of mangrove wetlands with respect to terrestrial forests in subtropical China. *Agric. For. Meteorol.* 249, 71–80. doi: 10.1016/j.agrformet.2017.11.019

Ding, W., Cai, Z., and Wang, D. (2004). Preliminary budget of methane emissions from natural wetlands in China. *Atmos. Environ.* 38, 751–759. doi: 10.1016/j.atmosenv.2003.10.016

Engelhardt, K., and Ritchie, M. (2001). Effect of Macrophyte Species Richness on Wetland Ecosystem Functioning and Services. *Nature* 411, 687–689. doi: 10.1038/35079573

Foken, T., Göockede, M., Mauder, M., Mahrt, L., Amiro, B., and Munger, W. (2004). "Post-field data quality control," in *Handbook of Micrometeorology. Atmospheric and Oceanographic Sciences Library*, eds X. Lee, W. Massman, and B. Law, vol. 29 (Dordrecht: Springer), doi: 10.1007/1-4020-2265-4_9

Gao, J., Li, X.-L., Cheng, A., and Yang, Y.-W. (2013). Degradation of wetlands on the qinghai-tibet plateau:a comparison of the effectiveness of three indicators. *J. Mount. Sci.* 10, 658–667. doi: 10.1007/s11629-013-2562-3

Gao, J.-Q., Ouyang, H., Xu, X.-L., Zhou, C.-P., and Zhang, F. (2009). Effects of temperature and water saturation on CO_2 production and nitrogen mineralization in alpine wetland soils. *Pedosphere* 19, 71–77. doi: 10.1016/S1002-0160(08)60085-5

Gu, L., Falge, E., Boden, T., Baldocchi, D., Black, T. A., Saleska, S., et al. (2005). Objective threshold determination for nighttime eddy flux filtering. *Agric. For. Meteorol.* 128, 179–197. doi: 10.1016/j.agrformet.2004.11.006

Hao, Y., Cui, X., Wang, Y., Mei, X., Kang, X., Wu, N., et al. (2011). Predominance of precipitation and temperature controls on ecosystem CO_2 Exchange in Zoige Alpine Wetlands of Southwest China. *Wetlands* 31, 413–422. doi: 10.1007/s13157-011-0151-1

Hirota, M., Tang, Y., Hu, Q., Hirata, S., Kato, T., Kishimoto-Mo, A., et al. (2004). Methane emissions from different vegetation zones in a Qinghai-Tibetan Plateau wetland. *Soil Bio. Biochem.* 36, 737–748. doi: 10.1016/j.soilbio.2003.12.009

Inglett, K. S., Inglett, P. W., Reddy, K. R., and Osborne, T. Z. (2012). Temperature sensitivity of greenhouse gas production in wetland soils of different vegetation. *Biogeochemistry* 108, 77–90. doi: 10.1007/s10533-011-9573-3

IPCC (2013). "Climate Change 2013: the physical science basis. contribution of working group i to the fifth assessment report of the intergovernmental panel on climate change," in *The Intergovernmental Panel on Climate Change*, (Cambridge: Cambridge University Press).

Jin, H., Wu, J., Cheng, G., Nakano, T., and Sun, G. (1999). Methane emissions from wetlands on the Qinghai-Tibet Plateau. *Chin. Scie. Bull.* 44, 2282–2286. doi: 10.1007/BF02885940

Jin, Z., Zhuang, Q., He, J.-S., Zhu, X., and Song, W. (2015). Net exchanges of methane and carbon dioxide on the Qinghai-Tibetan Plateau from 1979 to 2100. *Environ. Res. Lett.* 10:085007. doi: 10.1088/1748-9326/10/8/085007

Kandel, T. P., Lærke, P. E., Hoffmann, C. C., and Elsgaard, L. (2019). Complete annual CO_2, CH_4, and N2O balance of a temperate riparian wetland 12 years after rewetting. *Ecol. Eng.* 127, 527–535. doi: 10.1016/j.ecoleng.2017.12.019

Kato, T., Hirota, M., Tang, Y., Cui, X., Li, Y., Zhao, X., et al. (2005). Strong temperature dependence and no moss photosynthesis in winter CO_2 flux for a Kobresia meadow on the Qinghai-Tibetan plateau. *Soil Biol. Biochem.* 37, 1966–1969. doi: 10.1016/j.soilbio.2005.02.018

Kintisch, E., and Buckheit, K. (2006). Along the road from kyoto: global greenhouse gas emissions keep rising. *Science* 311, 1702–1703. doi: 10.1126/science.311.5768.1702

Lamers, L., Vile, M., Grootjans, A. P., Acreman, M., Diggelen, R., Evans, M., et al. (2014). Ecological restoration of rich fens in Europe and North America: from trial and error to an evidence-based approach. *Biol. Rev.* 90, 182–203. doi: 10.1111/brv.12102

Lehner, B., and Doell, P. (2004). Development and Validation of a Global Database of Lakes. Reservoirs and Wetlands. *J. Hydrol.* 296, 1–22. doi: 10.1016/j.jhydrol.2004.03.028

Lewis, W. M., and Ebrary, I. (1995). *Wetlands : Characteristics and Boundaries. Wetlands Characteristics & Boundaries*. Washington, DC: National Academy Press.

Li, G., Mu, J., Liu, Y., Smith, N., and Sun, S. (2017). Effect of microtopography on soil respiration in an alpine meadow of the Qinghai-Tibetan plateau. *Plant Soil* 421, 1–9. doi: 10.1007/s11104-017-3448-x

Li, T., Zhang, Q., Cheng, Z., Ma, Z., Liu, J., Luo, Y., et al. (2016). Modeling CH_4 emissions from natural wetlands on the tibetan plateau over the past 60 years: influence of climate change and Wetland Loss. *Atmosphere* 7:90. doi: 10.3390/atmos7070090

Liu, L., Chen, H., Zhu, Q., Yang, G., Zhu, E., Hu, J., et al. (2016). Responses of peat carbon at different depths to simulated warming and oxidizing. *Sci. Total Environ.* 548-549, 429–440. doi: 10.1016/j.scitotenv.2015.11.149

Liu, X., Zhu, D., Zhan, W., Chen, H., Zhu, Q., Hao, Y., et al. (2019). Five-year measurements of net ecosystem CO_2 exchange at a fen in the Zoige peatlands on the Qinghai-Tibetan Plateau. *J. Geophys. Res.* 124, 11803–11818. doi: 10.1029/2019JD031429

Liu, Y., Liu, G., Xiong, Z., and Liu, W. (2017). Response of of greenhouse gas emissions from three types of wetland soils to simulated temperature change on the Qinghai-Tibetan Plateau. *Atmos. Environ.* 171, 17–24. doi: 10.1016/j.atmosenv.2017.10.005

Liu, Y., Sheng, L., and Liu, J. (2015). Impact of wetland change on local climate in semi-arid zone of Northeast China. *Chin. Geogr. Sci.* 25, 309–320. doi: 10.1007/s11769-015-0735-4

Liu, Y., Wan, K.-Y., Tao, Y., Li, Z.-G., Zhang, G.-S., Li, S.-L., et al. (2013). Carbon dioxide flux from rice paddy soils in central china: effects of intermittent flooding and draining cycles. *PLoS One* 8:e56562. doi: 10.1371/journal.pone.0056562

Malone, S. L., Gregory, S., Staudhammer, C. L., and Ryan, M. G. (2013). Effects of simulated drought on the carbon balance of Everglades short-hydroperiod marsh. *Glob. Change Biol.* 19, 2511–2523. doi: 10.1111/gcb.12211

Marin-Muniz, J. L., Hernandez, M. E., and Moreno-Casasola, P. (2015). Greenhouse gas emissions from coastal freshwater wetlands in veracruz mexico: effect of plant community and seasonal dynamics. *Atmos. Environ.* 107, 107–117. doi: 10.1016/j.atmosenv.2015.02.036

Mitsch, W. J., Nahlik, A. M., Mander, Ü, Zhang, L., Anderson, C. J., Jørgensen, S. E., et al. (2013). Wetlands, carbon, and climate change. *Landsc. Ecol.* 28, 583–597. doi: 10.1007/s10980-012-9758-8

Niu, Z., Gong, P., Cheng, X., Guo, J., Wang, L., Huang, H., et al. (2009). Geographical characteristics of China's wetlands derived from remotely sensed data. *Sci. China Ser. D* 52, 723–738. doi: 10.1007/s11430-009-0075-2

Niu, Z., Zhang, H., Wang, X., Yao, W., Zhou, D., Zhao, K., et al. (2012). Mapping wetland changes in China between 1978 and 2008. *Chin. Sci. Bull.* 57, 2813–2823. doi: 10.1007/s11434-012-5093-3

Piao, S., Ciais, P., Huang, Y., Shen, Z., Peng, S., Li, J., et al. (2010). The impacts of climate change on water resources and agriculture in China. *Nature* 467, 43–51. doi: 10.1038/nature09364

R Core Team (2020). *R: A Language and Environment for Statistical Computing*. Vienna: R Foundation for Statistical Computing.

Song, W. M., Wang, H., Wang, G. S., Chen, L. T., Jin, Z. N., Zhuang, Q. L., et al. (2015). Methane emissions from an alpine wetland on the Tibetan Plateau: neglected but vital contribution of the nongrowing season. *J. Geophys. Res. Biogeosci.* 120, 1475–1490. doi: 10.1002/2015JG003043

Sullivan, P., Arens, S., Chimner, R., and Welker, J. (2008). Temperature and microtopography interact to control carbon cycling in a high arctic fen. *Ecosystems* 11, 61–76. doi: 10.1007/s10021-007-9107-y

Tang, Y., Wan, S., He, J., and Zhao, X. (2009). Foreword to the special issue: looking into the impacts of global warming from the roof of the world. *J. Plant Ecol.* 2, 169–171. doi: 10.1093/jpe/rtp026

Treat, C. C., Wollheim, W. M., Varner, R. K., Grandy, A. S., Talbot, J., and Frolking, S. (2014). Temperature and peat type control CO_2 and CH_4 production in Alaskan permafrost peats. *Glob. Change Biol.* 20, 2674–2686. doi: 10.1111/gcb.12572

Wang, J., Zhu, Q., Yang, Y., Zhang, X., Zhang, J., Yuan, M., et al. (2020). High uncertainties detected in the wetlands distribution of the Qinghai–Tibet Plateau based on multisource data. *Landsc. Ecol. Eng.* 16, 47–61. doi: 10.1007/s11355-019-00402-w

Wei, D., and Wang, X. (2016). CH_4 exchanges of the natural ecosystems in China during the past three decades: the role of wetland extent and its dynamics. *J. Geophys. Res.* 121, 2445–2463. doi: 10.1002/2016jg003418

Wei, D., and Wang, X. (2017). Uncertainty and dynamics of natural wetland CH_4 release in China. *Atmos. Environ.* 154, 95–105. doi: 10.1016/j.atmosenv.2017.01.038

Wei, D., Xu, R., Tarchen, T., Dai, D., Wang, Y., and Wang, Y. (2015). Revisiting the role of CH_4 emissions from alpine wetlands on the Tibetan Plateau: evidence from two in situ measurements at 4758 and 4320 m above sea level. *J. Geophys. Res.* 120, 1741–1750. doi: 10.1002/2015jg002974

Whiting, G. J., and Chanton, J. P. (2001). Greenhouse carbon balance of wetlands: methane emission versus carbon sequestration. *Tellus B* 53, 521–528. doi: 10.3402/tellusb.v53i5.16628

Xu, K., Kong, C., Liu, J., and Wu, Y. (2010). "Using methane dynamic model to estimate methane emission from natural wetlands in China," in *2010 18th International Conference on Geoinformatics*, Beijing, 1–4.

Yang, G., Chen, H., Wu, N., Tian, J., Peng, C., Zhu, Q., et al. (2014). Effects of soil warming, rainfall reduction and water table level on CH_4 emissions from the Zoige peatland in China. *Soil Biol. Biochem.* 78, 83–89. doi: 10.1016/j.soilbio.2014.07.013

Yu, X., Song, C., Li, S., Wang, X., Shi, F., Qian, C., et al. (2017). Growing season methane emissions from a permafrost peatland of northeast China: observations using open-path eddy covariance method. *Atmos. Environ.* 153, 135–149. doi: 10.1016/j.atmosenv.2017.01.026

Yvon-Durocher, G., Montoya, J., Woodward, G., Jones, J., and Trimmer, M. (2011). Warming increases the proportion of primary production emitted as methane from freshwater mesocosms. *Glob. Change Biol.* 17, 1225–1234. doi: 10.1111/j.1365-2486.2010.02289.x

Zeng, M., Zhu, C., Song, Y., Ma, C., and Yang, Z. (2017). Paleoenvironment change and its impact on carbon and nitrogen accumulation in the Zoige wetland, northeastern Qinghai–Tibetan Plateau over the past 14,000 years. *Geochem. Geophys. Geosyst.* 18, 1775–1792. doi: 10.1002/2016GC006718

Zhang, X., Zhu, Q., Yang, B., Chen, H., and Peng, C. (2020). Evaluating patterns of wetland emission in Qinghai-Tibet plateau based on process model. *Acta Ecol. Sin.* 40, 3060–3071. doi: 10.5846/stxb201904240838

Zhao, L., Li, Y., Xu, S., Zhou, H., Gu, S., Yu, G., et al. (2006). Diurnal, seasonal and annual variation in net ecosystem CO_2 exchange of an alpine shrubland on Qinghai-Tibetan plateau. *Glob. Change Biol.* 12, 1940–1953. doi: 10.1111/j.1365-2486.2006.01197

Zhong, Q., Chen, H., Liu, L., He, Y., Zhu, D., Jiang, L., et al. (2017). Water table drawdown shapes the depth-dependent variations in prokaryotic diversity and structure in Zoige peatlands. *FEMS Microbiol. Ecol.* 93:fix049. doi: 10.1093/femsec/fix049

Zhu, Q., Peng, C., Liu, J., Jiang, H., Fang, X., Chen, H., et al. (2016). Climate-driven increase of natural wetland methane emissions offset by human-induced wetland reduction in China over the past three decades. *Sci. Rep.* 6:38020. doi: 10.1038/srep38020

Conflict of Interest: The authors declare that the research was conducted in the absence of any commercial or financial relationships that could be construed as a potential conflict of interest.

frontiers in Earth Science

CORRECTION
published: 26 March 2021
doi: 10.3389/feart.2021.653753

Corrigendum: Extrapolation and Uncertainty Evaluation of Carbon Dioxide and Methane Emissions in the Qinghai-Tibetan Plateau Wetlands Since the 1960s

Jiang Zhang[1], *Qiuan Zhu*[1,2,3]*, *Minshu Yuan*[1], *Xinwei Liu*[4], *Huai Chen*[4], *Changhui Peng*[1,5], *Meng Wang*[6], *Zhenan Yang*[7], *Lin Jiang*[1] and *Pengxiang Zhao*[8]*

[1] Center for Ecological Forecasting and Global Change, College of Forestry, Northwest A&F University, Yangling, China, [2] College of Hydrology and Water Resources, Hohai University, Nanjing, China, [3] National Earth System Science Data Center, National Science & Technology Infrastructure of China, Beijing, China, [4] Chengdu Institute of Biology, Chinese Academy of Sciences, Chengdu, China, [5] Department of Biology Sciences, Institute of Environment Sciences, University of Quebec at Montreal, Montreal, QC, Canada, [6] Key Laboratory of Geographical Processes and Ecological Security in Changbai Mountains, Ministry of Education, School of Geographical Sciences, Northeast Normal University, Changchun, China, [7] Key Laboratory of Southwest China Wildlife Resources Conservation (China West Normal University), Ministry of Education, Nanchong, China, [8] College of Forestry, Northwest A&F University, Yangling, China

Keywords: climate change, wetlands, greenhouse gas, carbon fluxes, global warming potential

OPEN ACCESS

Edited and reviewed by:
Matthias Peichl, Swedish University of Agricultural Sciences, Sweden

***Correspondence:**
Qiuan Zhu
zhuq@hhu.edu.cn
Pengxiang Zhao
zhaopengxiang@nwafu.edu.cn

Specialty section:
This article was submitted to Hydrosphere, a section of the journal Frontiers in Earth Science

Received: *15 January 2021*
Accepted: *03 March 2021*
Published: *26 March 2021*

Citation:
Zhang J, Zhu Q, Yuan M, Liu X, Chen H, Peng C, Wang M, Yang Z, Jiang L and Zhao P (2021) Corrigendum: Extrapolation and Uncertainty Evaluation of Carbon Dioxide and Methane Emissions in the Qinghai-Tibetan Plateau Wetlands Since the 1960s. Front. Earth Sci. 9:653753. doi: 10.3389/feart.2021.653753

A Corrigendum on

Extrapolation and Uncertainty Evaluation of Carbon Dioxide and Methane Emissions in the Qinghai-Tibetan Plateau Wetlands Since the 1960s
by Zhang, J., Zhu, Q., Yuan, M., Liu, X., Chen, H., Peng, C., et al. (2020). Front. Earth Sci. 8:361. doi: 10.3389/feart.2020.00361

In the original article, we intended to show the annual mean GHG flux rate within **Figures 4**, **5**, and **Table 1**. However, there was an oversight in dividing the number by 12 (months).

Below, you can find the corrected **Figures 4**, **5**, and **Table 1**, as well as the corrections of the numbers cited at various points in the text. The updated section in the **Abstract**, Page 1, Lines 11–14, can be found below. In addition, the updated portion in the **Results**, section 'Extrapolation of CO_2 and CH_4 Emission Rates of the Study Site', Page 7, Lines 1–22, can also be found below.

We apologize for these errors and state that this does not change the scientific conclusions of the article in any way. The original article has been updated.

ABSTRACT

Based on such relationship patterns and soil temperature data (1960–2017), we extrapolated the CO_2 and CH_4 emissions of study site for the past 57 years: the mean CO_2 emission rate was 91.38 mg C m^{-2} h^{-1} on different measurement methods and timescales, with the range of the mean emission rate from 35.10 to 146.25 mg C m^{-2} h^{-1}, while the mean CH_4 emission rate was 2.75 mg C m^{-2} h^{-1}, with the ranges of the mean emission rate from 1.41 to 3.85 mg C m^{-2} h^{-1}.

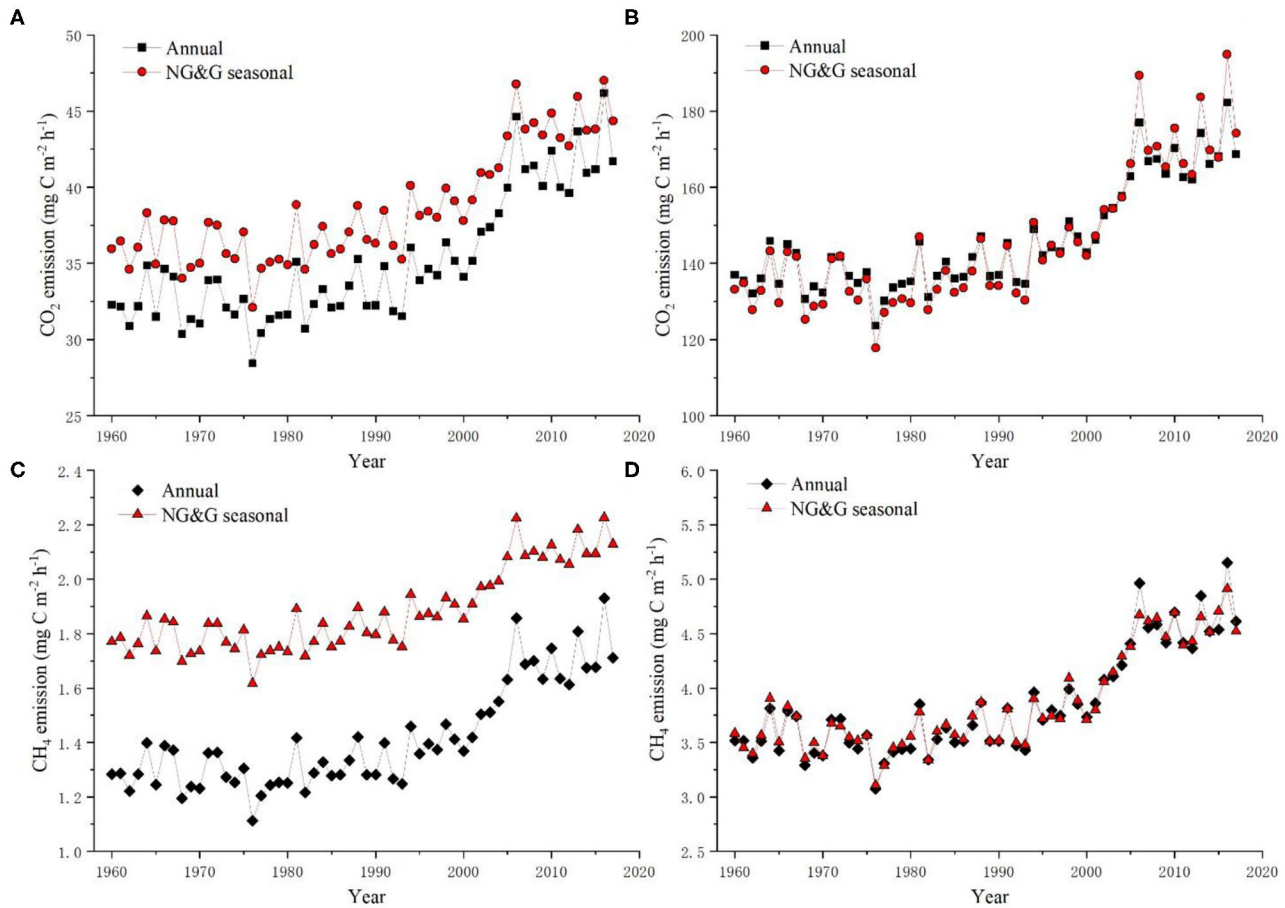

FIGURE 4 | Annual CO_2 and CH_4 emission rates of the study site from 1960 to 2017 were extrapolated based on regression models between soil temperature and CO_2/CH_4 emissions measured using the static chamber method **(A,C)** and using the eddy covariance method **(B,D)** at different timescales (Annual or NG&G seasonal).

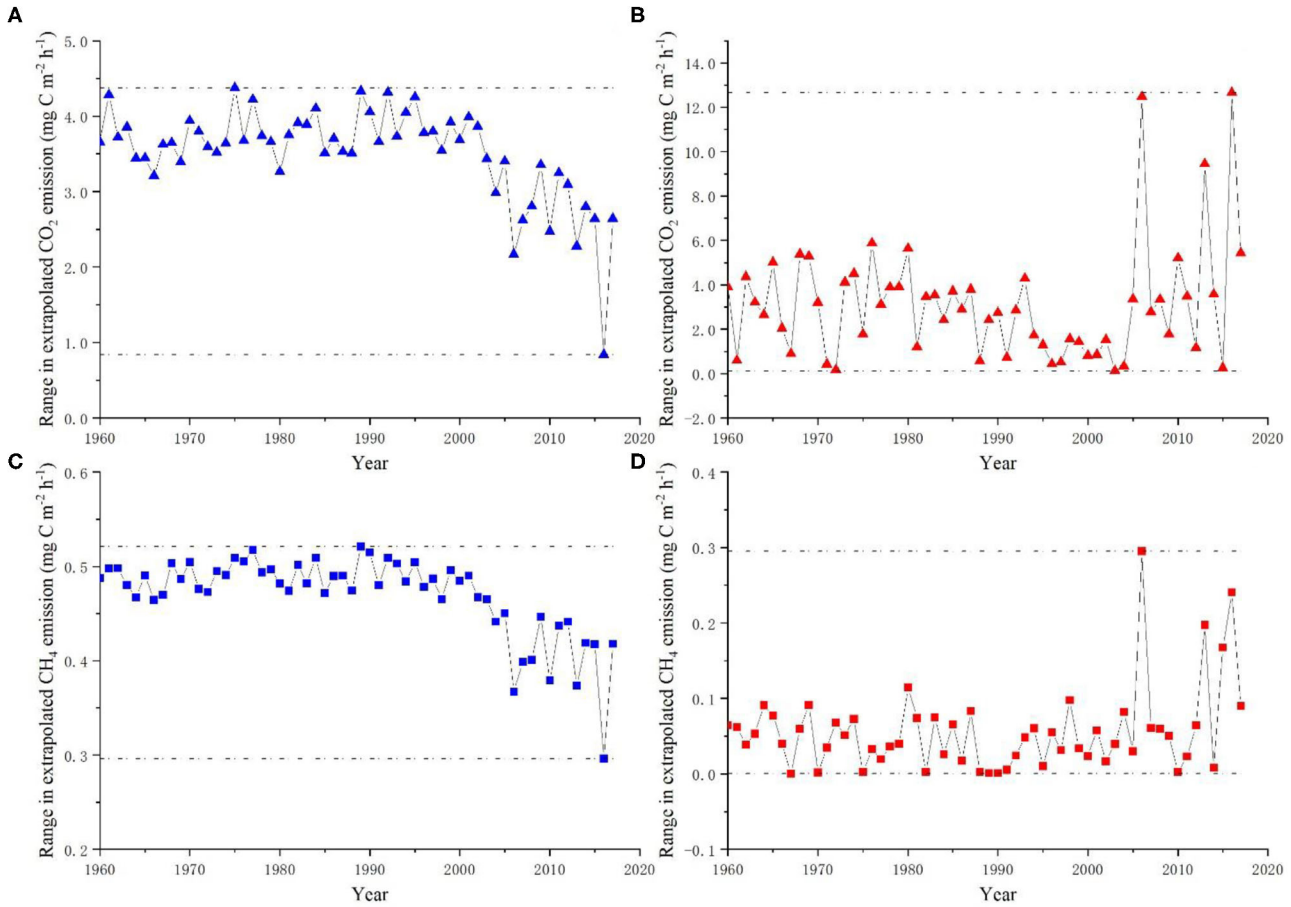

FIGURE 5 | Calculated differences between extrapolated annual greenhouse gas emission rate of study site from 1960 to 2017. CO_2 and CH_4 emission rates were extrapolated by models based on data derived from the static chamber method **(A,C)** or Eddy covariance method **(B,D)** at annual and NG&G seasonal timescales, respectively. The differences between the maximum and minimum extrapolated values of each year were plotted.

TABLE 1 | Extrapolated mean emission rate of CO_2 and CH_4 of study site for the period 1960–2017, based on models derived from data obtained using the chamber or EC method at different timescales*.

Emission rate (mg C m^2 h^{-1})	Measurement method	Annual	NG&G seasonal	Average
CO_2	Chamber	35.10	38.60	91.38
	EC	146.25	145.58	
CH_4	Chamber	1.41	1.88	2.75
	EC	3.85	3.85	

**Timescales were the entire year (Annual), non-growing season and growing season (NG&G seasonal). Abbreviations: Chamber, static chamber; EC, eddy covariance.*

RESULTS

Extrapolation of CO_2 and CH_4 Emission Rates of the Study Site

Extrapolated mean CO_2 emission rate of study site from 1960 to 2017 was calculated to be 91.38 mg C m^{-2} h^{-1}, with the ranges of the mean emission rate from 35.10 to 146.25 mg C m^{-2} h^{-1} on different measurement methods and timescales (**Table 1**). The differences of emission rates between the maximum and minimum values extrapolated for each year reflected uncertainties from the same measurement method at different timescales. Uncertainties in extrapolation of the CO_2 emission rates ranged from 0.84 to 4.38 mg C m^{-2} h^{-1} based on static chamber data, and from 0.13 to 12.67 mg C m^{-2} h^{-1} based on EC data (**Figures 5A,B**).

Extrapolated values for CH_4 emission rate based on EC data were three times larger than extrapolated values based on chamber data (**Figures 4C,D**). Extrapolated mean CH_4 emission rate of the study site was 2.75 mg C m^{-2} h^{-1} from 1960 to 2017, with the ranges of the mean emission rate from 1.41 to 3.85 mg

C m^{-2} h^{-1} on different measurement methods and timescales (**Table 1**). Differences in annual average maxima and minima reflected uncertainties from static chamber method data ranging from 0.30 to 0.52 mg C m^{-2} h^{-1} (**Figure 5C**), while uncertainties in data extrapolated from the EC method ranged from 0 to 0.30 mg C m^{-2} h^{-1} (**Figure 5D**).

frontiers in Earth Science

ORIGINAL RESEARCH
published: 28 September 2020
doi: 10.3389/feart.2020.557961

Controls on Soil Organic Matter Degradation and Subsequent Greenhouse Gas Emissions Across a Permafrost Thaw Gradient in Northern Sweden

*Roya AminiTabrizi[1], Rachel M. Wilson[2], Jane D. Fudyma[1], Suzanne B. Hodgkins[3], Heino M. Heyman[4], Virginia I. Rich[3], Scott R. Saleska[5], Jeffrey P. Chanton[2] and Malak M. Tfaily[1,6]**

[1] Department of Environmental Science, The University of Arizona, Tucson, AZ, United States, [2] Earth, Ocean and Atmospheric Science, Florida State University, Tallahassee, FL, United States, [3] Department of Microbiology, The Ohio State University, Columbus, OH, United States, [4] Bruker Daltonics Inc., Billercia, MA, United States, [5] Ecology and Evolutionary Biology, The University of Arizona, Tucson, AZ, United States, [6] Environmental Molecular Sciences Laboratory, Pacific Northwest National Laboratory, Richland, WA, United States

OPEN ACCESS

Edited by:
Matthias Peichl,
Swedish University of Agricultural Sciences, Sweden

Reviewed by:
Jinyun Tang,
Lawrence Berkeley National Laboratory, United States
Birgit Wild,
Stockholm University, Sweden

***Correspondence:**
Malak M. Tfaily
tfaily@arizona.edu

Specialty section:
This article was submitted to Biogeoscience, a section of the journal Frontiers in Earth Science

Received: 01 May 2020
Accepted: 13 August 2020
Published: 28 September 2020

Citation:
AminiTabrizi R, Wilson RM, Fudyma JD, Hodgkins SB, Heyman HM, Rich VI, Saleska SR, Chanton JP and Tfaily MM (2020) Controls on Soil Organic Matter Degradation and Subsequent Greenhouse Gas Emissions Across a Permafrost Thaw Gradient in Northern Sweden. Front. Earth Sci. 8:557961. doi: 10.3389/feart.2020.557961

Warming-induced permafrost thaw could enhance microbial decomposition of previously stored soil organic matter (SOM) to carbon dioxide (CO_2) and methane (CH_4), one of the most significant potential feedbacks from terrestrial ecosystems to the atmosphere in a changing climate. The environmental parameters regulating microbe-organic matter interactions and greenhouse gas (GHG) emissions in northern permafrost peatlands are however still largely unknown. The objective of this work is to understand controls on SOM degradation and its impact on porewater GHG concentrations across the Stordalen Mire, a thawing peat plateau in Northern Sweden. Here, we applied high-resolution mass spectrometry to characterize SOM molecular composition in peat soil samples from the active layers of a *Sphagnum*-dominated bog and rich fen sites in the Mire. Microbe-organic matter interactions and porewater GHG concentrations across the thaw gradient were controlled by aboveground vegetation and soil pH. An increasingly high abundance of reduced organic compounds experiencing greater humification rates due to enhanced microbial activity were observed with increasing thaw, in parallel with higher CH_4 and CO_2 porewater concentrations. Bog SOM however contained more *Sphagnum*-derived phenolics, simple carbohydrates, and organic- acids. The low degradation of bog SOM by microbial communities, the enhanced SOM transformation by potentially abiotic mechanisms, and the accumulation of simple carbohydrates in the bog sites could be attributed in part to the low pH conditions of the system associated with *Sphagnum* mosses. We show that Gibbs free energy of C half reactions based on C oxidation state for OM can be used as a quantifiable measure for OM decomposability and quality to enhance current biogeochemical models to predict C decomposition rates. We found a direct association between OM chemical diversity and $\delta^{13}C\text{-}CH_4$ in peat porewater; where higher substrate diversity was positively correlated with enriched $\delta^{13}C\text{-}CH_4$ in fen sites. Oxidized sulfur-containing compounds, produced by *Sphagnum*, were

further hypothesized to control GHG emissions by acting as electron acceptors for a sulfate-reducing electron transport chain, inhibiting methanogenesis in peat bogs. These results suggest that warming-induced permafrost thaw might increase organic matter lability, in subset of sites that become wetlands, and shift biogeochemical processes toward faster decomposition with an increasing proportion of carbon released as CH_4.

Keywords: permafrost, peatlands, soil organic matter, fen, bog, mass spectrometry, sphagnum

INTRODUCTION

Permafrost peatlands, characterized by their cold and wet conditions that promote the accumulation of soil organic matter (SOM), contain an estimated 277 Pg of carbon (within the 3 m depth) (Schuur et al., 2008), which represents over one-third of the carbon stock in the atmosphere (ca. 800 Pg) (Schuur et al., 2008; McGuire et al., 2009). In the past 100 years, the mean annual Arctic temperatures have increased at almost twice the rate of the global average (IPCC, 2007; Solomon, 2007), leaving the fate of the previously frozen landscape uncertain. Due to these increasing temperatures coupled with seasonal thawing and freezing, permafrost thaw is changing the thickness of the soil active layer (Fenner et al., 2007), surface vegetation composition (Limpens et al., 2008), carbon accumulation rates in peat profiles (McGuire et al., 2009; Frolking et al., 2011), and microbial communities that govern degradation and transformation of organic C, with direct implications on greenhouse gas (GHG) emissions (de Graaff et al., 2010; Deng et al., 2014).

Absence of oxygen, created by water-logged conditions in thawing permafrost can promote anaerobic oxidation of organic matter (OM) (McLatchey and Reddy, 1998) by microbial communities via multiple anaerobic pathways (e.g., hydrolysis, fermentation, and methanogenesis) (Keller and Bridgham, 2007; Sutton-Grier et al., 2011; Wilson et al., 2017). However accurate prediction of GHG emissions from these systems due to changing environmental conditions is limited by our understanding of substrate quality, heterogeneity, and composition (Bölscher et al., 2017), microbial-organic matter interactions and biotic and abiotic OM degradation pathways (Mikutta et al., 2019). Recently, Zhou et al. (2020) found a positive correlation between the richness and diversity of the microbial communities and the concentration and bioavailability of the dissolved organic matter in pit, headstream, and river samples collected from the northern Qinghai-Tibetan Plateau, as well as physiochemical parameters such as pH and DOC and soluble ion concentrations. While some organisms are affected mainly by the concentration of specific substrates, it was found that the overall diversity of organisms may be affected by substrate quality and heterogeneity (Allison, 2005; Hättenschwiler and Jørgensen, 2010), and these effects in turn depend on the prevalence of resource generalists or resource specialists that shapes the microbial communities (Monard et al., 2016; Muscarella et al., 2019). Recently, (Woodcroft et al., 2018) investigated microbial community composition and function in the active layer of three sites across a thaw gradient at the Stordalen Mire (an intact palsa, a partially thawed bog and a fully thawed fen) and were able to link the Stordalen genome and functionality to the changing habitat. Metagenomics revealed distinct differences in diversity and overall composition of the microbial communities, with fen having the widest range of genes belonging to different phyla and thus higher microbial diversity. Metatranscriptomic data further confirmed the genomic trends, suggesting that in fen, wider range of microorganisms encode more diverse pathways in which organic substrates such as cellulose and xylan are rapidly degraded, providing substrates needed for methanogenesis and a more heterogenous organic matter composition. On the contrary, microbial communities in bog displayed less diverse functionalities in general with the lowest percentage of cellulase- and xylanase-encoding microorganisms. These results were consistent with previous studies at the same site where Hodgkins et al. (2014) and Hodgkins et al. (2016) showed that dissolved organic matter (DOM) becomes more labile with thaw in the Mire as the pH increases from bog to fen, with bog DOM being more recalcitrant, less diverse and contains more oxygen-rich compounds such as phenols and tannin-like compounds with higher oxidation state and overall lower decomposition rate due to the presence of sphagnan and other acidic inhibitors (Stalheim et al., 2009; Hájek et al., 2011). Conversely, fen DOM was more diverse and contained more low molecular weight compounds, more abundant nitrogen-containing compounds (interpreted as evidence of increased microbial activity), and less organic acids (Hodgkins et al., 2014, 2016). Moreover, differences in microbial community composition and function and OM quality were found to alter pathways by which CO_2 and CH_4 are produced. Studies by Svensson and Rosswall (1984), Galand et al. (2005), Lupascu et al. (2012), McCalley et al. (2014), and Singleton et al. (2018) suggested a shift from hydrogenotrophic to acetoclastic methanogenesis along the permafrost thaw gradient from bog to fen in the Stordalen Mire.

Although the ecological roles and properties of resource generalists and specialists in many discontinuous permafrost areas have been examined via extensive metagenomic and metatranscriptomics analysis (Liao et al., 2016; Sriswasdi et al., 2017; Singleton et al., 2018; Woodcroft et al., 2018), highly resolved molecular characterization of the OM is an essential foundation upon which we can understand ecosystem C cycling by both plants and microbes in peatlands for predicting future changes in CO_2 and CH_4 production potential (Qualls and Richardson, 2003). Moreover, current models for estimating permafrost soil carbon loss rates are lacking representations of key microbial processes that control OM transformations, leading to enormous uncertainty in model simulations (Burke et al., 2012; Koven et al., 2015; Chang et al., 2019). At most, such

models only include a quantitative measure of OM concentration (Lucchese et al., 2010) but neglect the fact that the rate of OM degradation is dependent on the abundance and diversity of active microbes and OM quality and diversity. As such, factors accounting for OM transformation (biotically and abiotically) are poorly constrained in most models and are an important area for model improvement. To address this knowledge gap, we used gas chromatography (GC) and Fourier transform ion cyclotron resonance (FT-ICR) mass spectrometry (MS) to characterize SOM chemical composition in bog and fen soil samples collected from the Stordalen Mire. First, we hypothesized that SOM composition and heterogeneity can be used to capture shifts in the functional diversity of microbial communities with thaw gradient. Second, we hypothesized that NOSC and Gibbs free energy of C oxidation can be used to capture C decomposability and changes to the redox conditions of the surroundings (LaRowe and van Cappellen, 2011). Third, we hypothesized that sulfate reduction pathways by sulfate-reducing microorganisms (SRMs) are more active in the bog and are in competition with methanogens, rapidly changing the SOM composition, stimulating CO_2 and suppressing CH_4 emission potentials. Understanding OM energetics and metabolic transformation pathways along the thaw gradient can provide insights on resource heterogeneity and microbial diversity which can then be used to indirectly incorporate microbial processes in different biogeochemistry models and to predict how this ecosystem-level shift will alter GHG emission under a continually changing climate.

MATERIALS AND METHODS

Site Information and Soil Sampling and Preparation

Stordalen Mire (68.35°N, 19.05°E) is a peat plateau in subarctic Sweden underlain by discontinuous permafrost, which is thawing as the region warms. The Mire has three dominant vegetation community types (Johansson et al., 2006): (1) Palsa (intact permafrost) with woody herbaceous vegetation; (2) Ombrotrophic peatland or bog (intermediate thaw) features with *Sphagnum spp*., sedges, and shrubs as the dominant vegetations; and (3) Minerotrophic peatland or fen (fully thawed) dominated by sedges, mainly *Eriophorum spp*. (Bäckstrand et al., 2010). Generally, bogs are fed only by precipitation, have acidic (pH $\sim$ 4) surface waters and *Sphagnum*-dominated vegetation. These *Sphagnum* mosses, are known to inhibit alternate plant growth by acidifying water and creating an environment that is harsh to other plant species (van Breemen, 1995). Fens, on the other hand, are characterized by more mineral-rich water because they are fed by surface water and groundwater, in addition to rainfall. They are usually dominated by grasses and sedges and maintain slightly acidic to alkaline pH. Due to continued warming in the Arctic, the areal extent of intact palsa (Malmer et al., 2005) and *Sphagnum* community (Norby et al., 2019) across the Stordalen Mire has declined significantly since 1970 (Malmer et al., 2005) while at the same time, wetter fen habitats have expanded (Kokfelt et al., 2009; Bäckstrand et al., 2010). The ground's thaw state and consequent relationship to the water table determine the plant community, which in turn determines organic matter composition. In areas where the permafrost is degraded, land subsidence leads to varying degrees of water inundation. In this study, we focused on these inundated sites, and specifically a fen and a bog site with an extensive set of historical gas flux, microbial, and geochemical measurements (previously described by Hodgkins et al., 2014, 2016; McCalley et al., 2014; Woodcroft et al., 2018). In June 2012, peat was collected from both sites with an 11-cm-diameter homemade circular push corer. Both sites were cored in triplicate to capture spatial heterogeneity. Cores were divided into three sections, and the sections were placed into plastic bags and stored frozen until analysis. Eighteen soil samples were collected in total, including nine samples (3 cores $\times$ 3 depths per core) collected from a *Sphagnum*-derived ombrotrophic bog and nine samples collected from a sedge-dominated fen (**Table 1**). Porewater for dissolved organic carbon (DOC) analysis was gathered from the same depths by syringe suction through a 1-m long, 0.5-cm-diameter stainless steel tube with holes drilled along the bottom 3 cm, then filtered through 0.7-μm Whatman GF/F glass microfiber filters into 120-mL brown borosilicate bottles. The pH was measured on-site with an Oakton Waterproof pHTestr 10. The bottles were frozen within 8 hours of collection and stored frozen until analysis. DOC concentrations were measured by high-temperature catalytic oxidation on a Shimadzu Total Organic Carbon analyzer with a non-dispersive infrared detector. Each sample was analyzed in triplicate measurements, which constantly had a coefficient of variance of $<$2%. The concentration was reported as millimolar (mM). Sulfate and nitrate concentrations were measured by ion chromatography on a Dionex ICS-1100 with a 4-mm IonPac AS22 column, with a 4.5 mM carbonate/1.4 mM bicarbonate eluent at a flow rate of 1.2 mL/min. The concentration was reported as micromolar (μM). In this study, we will focus on the overall SOM molecular composition differences observed in the bog vs. the fen and not the depth effect.

Porewater Gas Measurements

Porewater samples for dissolved gas analysis were collected similarly to the DOC samples, with porewater drawn up by syringe suction through perforated stainless-steel tubes that were inserted into the peat at the desired depth. Porewater was immediately filtered in the field using 2.7-μm Whatman GF/D glass-fiber filters, then stored in pre-evacuated glass vials sealed with butyl stoppers. Samples were then processed according to the method described by (Hodgkins et al., 2015). Phosphoric acid (1 mL of 20%) was added to each sample, to convert all dissolved inorganic carbon to CO_2 (thus removing differences in HCO_3^-/CO_2 ratios due to differing pH) and to preserve for shipment to Florida State University. Helium was then added to the sample headspaces to bring them to a constant pressure of 1 atm. Samples were analyzed for CH_4 and CO_2 concentrations and stable isotopic composition ($\delta^{13}C$) on a Thermo Finnigan Delta-V Isotope Ratio Mass Spectrometer. As described in (Corbett et al., 2013, 2015) and (Hodgkins et al., 2014), headspace gas concentrations were then converted to dissolved concentrations (mM) in the original unacidified porewater based

TABLE 1 | Characteristics of the samples gathered for this study.

Sample name	Collection date	Habitat type	Dominant vegetation	Depth	Depth (cm)	Geographical location
S_1_S	2-Jun-12	Bog	*Sphagnum spp.*	Shallow	2.5	68°21.1993'N, 19°02.8511'E
S_1_M	2-Jun-12	Bog	*Sphagnum spp.*	Middle	5.5	68°21.1988'N, 19°02.8546'E
S_1_D	2-Jun-12	Bog	*Sphagnum spp.*	Deep	12.5	68°21.2028'N, 19°02.8554'E
S_2_S	2-Jun-12	Bog	*Sphagnum spp.*	Shallow	2.5	68°21.1993'N, 19°02.8511'E
S_2_M	2-Jun-12	Bog	*Sphagnum spp.*	Middle	6.5	68°21.1988'N, 19°02.8546'E
S_2_D	2-Jun-12	Bog	*Sphagnum spp.*	Deep	10.5	68°21.2028'N, 19°02.8554'E
S_3_S	2-Jun-12	Bog	*Sphagnum spp.*	Shallow	2.5	68°21.1993'N, 19°02.8511'E
S_3_M	2-Jun-12	Bog	*Sphagnum spp.*	Middle	6.5	68°21.1988'N, 19°02.8546'E
S_3_D	2-Jun-12	Bog	*Sphagnum spp.*	Deep	17.5	68°21.2028'N, 19°02.8554'E
E_1_S	2-Jun-12	Fen	*E. angustifolium*	Shallow	2.5	68 21.1941 N, 19 02.8114E
E_1_M	2-Jun-12	Fen	*E. angustifolium*	Middle	6.5	68 21.1986 N, 19 02.7959 E
E_1_D	2-Jun-12	Fen	*E. angustifolium*	Deep	15.5	68 21.2012 N, 19 02.8038 E
E_2_S	2-Jun-12	Fen	*E. angustifolium*	Shallow	2.5	68 21.1941 N, 19 02.8114 E
E_2_M	2-Jun-12	Fen	*E. angustifolium*	Middle	6.5	68 21.1986 N, 19 02.7959 E
E_2_D	2-Jun-12	Fen	*E. angustifolium*	Deep	18.5	68 21.2012 N, 19 02.8038 E
E_3_S	2-Jun-12	Fen	*E. angustifolium*	Shallow	2.5	68 21.1941 N, 19 02.8114 E
E_3_M	2-Jun-12	Fen	*E. angustifolium*	Middle	6.5	68 21.1986 N, 19 02.7959 E
E_3_D	2-Jun-12	Fen	*E. angustifolium*	Deep	17.5	68 21.2012 N, 19 02.8038 E

Letter S indicates bog and letter E indicates fen. Numbers in the sample name indicate the replicate number (Three biological replicates per depth for bog and fen samples). Depths were collected in 3-cm intervals, with numeric depths indicating the middle of each interval.

on previously-determined gas extraction efficiencies (defined as the proportion of formerly-dissolved gas in the headspace after acidification and equilibration between the water and headspace) (**Supplementary Table 1**). Each sample was analyzed twice and the average results for each sample were recorded. Analytical precision of replicate $\delta^{13}C$ measurements was 0.2‰.

Gas Chromatography—Mass Spectrometry (GC-MS)

Organic Matter Extraction

Water was used to extract the labile fraction of SOM from the collected peat (n = 18, 9 fen and 9 bog samples) according to the protocol described by Tfaily et al. (2015) and Tfaily et al. (2017). Briefly, extracts were prepared by adding 1 mL of H_2O to air dried and ground 100 mg bulk soil and shaking in 2 mL capped glass vials for 2 h on an Eppendorf Thermomixer. Samples were then removed from the shaker and left to stand before spinning down and pulling off the supernatant to stop the extraction. All samples were stored at −80°C until analysis. Water extractable organic matter (WEOM; Corvasce et al., 2006) is described as a bioavailable fraction of organic matter that contains mostly polar compounds. Changes in the molecular weight and elemental composition of the WEOM fraction can provide important information regarding ecologically relevant processes in soil.

Around 0.5 ml of water extracted organic matter from nine bog samples and only three fen samples (due to sample limitations) were first freeze dried using a Labconco™ FreeZone Freeze Dryer and then derivatized as described previously (Kim et al., 2015). Briefly, 20 μl of 30 mg/ml methoxyamine hydrochloride in pyridine (Sigma-Aldrich, Saint Louis, MO) was added to each freeze-dried sample for the protection of carbonyl groups. Samples were vortexed for 20s, sonicated for 60s, and were incubated at 37°C for 90 min with generous shaking (1,000 rpm). After the incubation, 80 μL of N-methyl-N-(trimethylsilyl) trifluoroacetamide (MSTFA) (Sigma-Aldrich) with 1% trimethylchlorosilane (TMCS) (Sigma-Aldrich) was added to each sample. The samples were vortexed for 20s, sonicated for 60s, and incubated for 30 min at 37°C with shaking (1000 rpm). After derivatization, the samples were allowed to cool to room temperature.

GC-MS Analysis

Samples were transferred to autosampler vials and analyzed by GC-MS in random order. Blanks and fatty acid methyl ester (FAME) samples (C8-28) were also included in the analysis for the background referencing and retention time calibration, respectively. Metabolites were separated using a HP-5MS column (30 m × 0.25 mm × 0.25 μm; Agilent Technologies, Santa Clara, CA) and analyzed in an Agilent GC 7890A coupled with a single quadrupole MSD 5975C (Agilent Technologies, Santa Clara, CA). For each analysis, 1 μl of sample was injected in splitless mode. The injection port temperature was kept constant at 250°C for the duration of the analysis. The GC analysis started with an initial oven temperature fixed at 60°C for 1 min after injection, and then at a steady rate of 10°C/min, the temperature was increased to 325°C with the analyses finishing with a 5 min hold at 325°C. The GC-MS raw data files were processed with MetaboliteDetector as previously reported by Hiller et al. (2009). Briefly, retention indices (RI) of the detected polar metabolites were calibrated based on the mixture of FAME internal standards, followed by

deconvolution, and subsequent chromatographic alignment of the detected features across all analyses. Identification of the metabolites was carried out by first matching GC-MS spectra and retention indices against a Pacific Northwest National laboratory (PNNL) augmented version (>900 metabolites) of FiehnLib (PMID: 19928838) library containing validated retention indices and spectral information (Kind et al., 2009). Subsequently, unidentified metabolites were screened against the NIST14 GC-MS library by spectral matching alone. To eliminate false identification and reduce the deconvolution errors created during the automated data-processing, all metabolite identifications were individually validated.

Row-wise normalization (by sum) was then performed on the metabolite data using MetaboAnalyst 4.0 to allow for general-purpose adjustment for differences among samples. Data transformation [Generalized log transformation (log_2)] and data scaling [Auto scaling (mean-centered and divided by standard deviation of each variable)] were further performed to make features more comparable using the same platform.

FOURIER-TRANSFORM ION CYCLOTRON RESONANCE MASS SPECTROMETRY (FT-ICR-MS)

Direct Inject FT-ICR-MS Analysis

A 12 Tesla Bruker FT-ICR mass spectrometer located at PNNL was used to collect high resolution mass spectra of the WEOM. A Suwannee River Fulvic Acid standard (SRFA), obtained from the International Humic Substance Society (IHCC), was used as a control to monitor potential carry over from one sample to another and ensure instrument stability in day to day operation. The instrument was flushed between samples using a mixture of Milli-Q water and HPLC grade methanol. The ion accumulation time (IAT) was varied between 0.03 and 0.05 s to account for variations in C concentrations in different samples. For each sample, 144 individual scans were averaged, and an organic matter homologous series separated by 14 Da was used as an internal calibration. The mass measurement accuracy across 100–1,200 m/z range was <1 ppm (accounted for singly charged ions) and the mass resolution at 341 m/z was ∼240 K and the transient was 0.8 s. BrukerDaltonik version 4.2 data analysis software was used to convert raw spectra (obtained from each sample) to a list of m/z values applying FT-MS peak picker module with a signal-to-noise ratio (S/N) threshold of 7 and absolute intensity threshold of 100. Formularity (Tolić et al., 2017) software was used to assign chemical formulae based on the criteria described in Tfaily et al. (2018).

Chemical Compounds Classification and Data Processing

The molecular formulae in each sample were evaluated on van Krevelen diagrams (Van Krevelen, 1950), based on their H:C ratios (y-axis) and O:C ratios (x-axis) (Kim et al., 2003), assigning them to the major biochemical classes (e.g., lipid, protein, lignin, carbohydrate etc.). The H:C and O:C ranges for biochemical classification are provided in **Table 2**.

TABLE 2 | O/C and H/C ranges used to classify the compounds detected via FT-ICR-MS in this study (Adopted from Tfaily et al., 2015, 2017).

Compound class	O/C	H/C range
Amino sugar and carbohydrate	0.5∼0.7	0.8∼2.5
Condensed aromatic	0.0∼0.4	0.2∼0.8
Lignin	0.29∼0.65	0.7∼1.5
Lipid	0.0∼0.3	1.5∼2.5
Protein	0.3∼0.6	1.5∼2.3
Tannin	0.65∼1.00	0.8∼1.5
Unsaturated hydrocarbon	0.0∼0.3	1.0∼1.6

Oxidation state is related to the bioenergetic potential of a specific compound based on its atomic makeup. Oxidation state indicates how a compound may be transformed in biochemical processes without necessarily knowing its structure (LaRowe and van Cappellen, 2011). For each individual compound, the average nominal oxidation state of carbon (NOSC), which represents the number of electrons transferred in C oxidation half reactions, was calculated based on Equation 1 (where C, H, N, O, P, and S represent the numbers of each element, and number coefficients represent typical oxidation states). More negative values for NOSC indicates the presence of more reduced carbon atoms.

$$NOSC = -\left(\frac{4 \times C + H - 3 \times N - 2 \times O + 5 \times P - 2 \times S}{C}\right) + 4 \quad (1)$$

$\Delta G^{\circ}C$-ox (kJ/mol C) indicates the thermodynamic favorability of the compound, with lower values of $\Delta G^{\circ}C$-ox for a compound indicating greater likelihood of degradation (LaRowe and van Cappellen, 2011). $\Delta G^{\circ}C$-ox was estimated from NOSC following Equation (2):

$$\Delta G^{\circ}C - ox = 60.3 - 28.5 * (NOSC) \quad (2)$$

Positive values for $\Delta G^{\circ}C$-ox indicate that the oxidation of the C must be coupled to the reduction of a terminal electron acceptor, which in the TEA-depleted mire can include the soil organic matter itself (Keller and Takagi, 2013; Wilson et al., 2017). Organic matter degradation may become thermodynamically limited depending on the availability of terminal electron acceptors (Boye et al., 2017). Under oxic conditions the availability of high energy yielding O_2 as a terminal electron acceptor couples the decomposition of organic matter of all naturally occurring NOSC values (Keiluweit et al., 2016). However, under the inundated conditions of subsurface peat deposits, oxygen and other terminal electron acceptors become depleted thereby slowing or completely inhibiting the decomposition of organic matter with low NOSC values (Boye et al., 2017). In peat, oxygen is rapidly depleted to below detection limits (20 ppb) within 2–3 cm below the water surface (Lin et al., 2014). At Stordalen Mire, the average annual water table is typically near the peat surface in the fen (Hodgkins et al., 2014) and was 3.5–7 cm above the peat surface during our sampling. Thus, even the shallow fen peat is consistently

under anoxic conditions and subject to depleted TEA availability. In the bog, the mean annual water table depth is around 17 cm (Hodgkins et al., 2014), but was only 2 cm below the peat surface during sampling for this project. Thus, the bog peat is subjected to fluctuating water (and subsequently oxygen) levels throughout the growing season. This could have the effect of enhancing decomposition rates during dry periods and re-oxidizing previously reduced TEAs to support decomposition following subsequent inundation. Relative energy yields associated with the terminal electron acceptors in anoxic conditions also provide insight on the sequences in which organic matter gets decomposed (Grandy and Neff, 2008). Lower ΔG°C-ox is an indication of compounds more thermodynamically favored to undergo metabolic and chemical reactions (Wilson and Tfaily, 2018) (i.e., available for microbial communities), whereas higher ΔG°C-ox reflects microbially degraded and transformed (i.e., recalcitrant) OM.

For each elemental formula, double-bond equivalent (DBE) minus oxygen (DBE-O) was calculated using Equation (3):

$$\mathrm{DBE} - \mathrm{O} = [\mathrm{C}\ (1/2\mathrm{H}) + (1/2\mathrm{N}) + 1] - O \qquad (3)$$

While NOSC and ΔG°C-ox provide information on overall quality of the OM, DBE-O provides more structural information, mostly of carbon-to-carbon double bonds (i.e., lack of hydrogen saturation) without considering the oxygen atoms that mostly exist as carboxyl groups in OM (Bae et al., 2011). Using this formulation, more oxygenated molecules have lower (negative) values for DBE-O while higher values for DBE-O indicate highly unsaturated compounds such as condensed aromatic structures (Herzsprung et al., 2014).

Identification of Metabolic Transformations in Bog and Fen Samples Using Network Analysis

The rich database generated by high resolution mass spectrometry provides accurate mass information, enabling us to infer metabolite composition in complex matrices. We used network analysis to explore metabolic transformations in the bog and fen samples to further understand how two compounds are related to one another and how they might be involved in the same metabolic transformation (via a mass difference between two m/z values demonstrated as an edge in the network, and the initial and final compounds as nodes). Here, we used molecular transformation analysis to identify potential microbial transformation or decomposition pathways using FT-ICR-MS data. For a reaction to be considered and hence counted by this method, both the reactant and the product should be present, hence this approach can provide some information about SOM decomposition, uptake and accumulation (Burgess et al., 2017). We used Cytoscape (Shannon et al., 2003; Kohl et al., 2011) with the MetaNetter plug-in to generate molecular interaction networks. For each sample, the list of m/z values generated by the FT-ICR-MS analysis along with a list of 86 pre-defined m/z values and their subsequent molecular formula and IUPAC names [adopted from (Breitling et al., 2006) (**Supplementary Table 2**)] were imported into Cytoscape. The molecular interaction networks are consisting of nodes (m/z values) and edges (mass difference between two m/z values). Each m/z value inferred from the FT-ICR-MS analysis was defined as a node (described previously in Longnecker and Kujawinski, 2016) connected to other node (s) through the pre-defined m/z values defined as edges, representing a metabolic transformation. For example, gain or loss of CH_2 ($\Delta m = 14.01565007$) between two compounds in the molecular interaction networks is depicted by two nodes and an edge. Nodes represent the two compounds with mass difference of 14.01565007 Da and edge is the mass difference (named CH_2).

In total, 86 metabolic transformations were grouped into four different categories: amino acid-associated transformation (loss/gain of an amino acid and/or involvement of nucleoside or nucleotide), sugar -associated transformation (loss/gain of monomeric or polymeric carbohydrates), carbon transformation (reactions that can occur both biotically or abiotically depending on the environmental conditions), and other transformation that includes heteroatoms (such as loss/gain of a phosphate or an amine group). For this study, we have only focused on the first three categories since similar trends for the bog and fen samples (regardless of depth) were observed in the 'other transformation' category. The output of the Cytoscape is a list with the number of times (count) each transformation occurred between any two peaks in a particular sample as shown in **Supplementary Figure S5**. Normalized values (to the total number of transformations observed in each sample) and subsequently, normalized percentages are then calculated and used for comparison between samples and across sites.

Furthermore, a comprehensive set of topological parameters calculated from these undirected network plots (Assenov et al., 2008) based on transformation data generated by the Cytoscape with the MetaNetter plug-in was used to compare SOM metabolic transformation pathways between the bog and fen samples. For this study, two different parameters were chosen: clustering coefficient and average number of neighbors, all of which can be used to represent the level of population of the transformation network (Barabási and Albert, 1999; Ravasz et al., 2002). The clustering coefficient, C_n, in undirected networks is a ratio of the number of edges (N) between the neighbors of a node n, and the maximum number of edges (M) between the neighbors of n (Barabási and Oltvai, 2004). C_n is calculated as $C_n = 2e_n/(k_n(k_n\text{-}1))$, where k_n is the number (size) of neighbors of n and e_n is the number of connected pairs between all neighbors of n (Watts and Strogatz, 1998). The clustering coefficient of a node is always between 0 and 1(Barabási and Oltvai, 2004). A high clustering coefficient indicates a high number of neighbors for each node and hence represents low selectivity and high diversity since a compound could be produced by multiple reactions. The average number of neighbors therefore is an average of k_n of all nodes in the undirected network (Dong and Horvath, 2007). High number of neighbors indicates low degradation and high selectivity. Values for clustering coefficient and average number of neighbors for each sample are provided in **Supplementary Table 3**. Moreover, the network analysis parameters (clustering coefficient and average number

of neighbors) were used to correlate the overall number and/or density of the metabolic reactions happening in each sample to measured biogeochemical properties in pore water such as pH, $\delta^{13}C$ and DOC.

Statistical Analyses and Data Visualization

GC-MS Data

Univariate (Pearson correlation coefficient, *t*-test significance), multivariate (principal component analysis, PCA) and clustering analysis (heatmap, *t*-test significance) were performed on normalized values to visualize differences between treatments and among samples using MetaboAnalyst 4.0 and plotted using JMP 14.2.0 and R (R Core Team, 2019) package ggplot2 version 3.3.1 (Wickham, 2016).

Porewater Gas, FT-ICR-MS, and Network Analysis Data

Analysis of variance (ANOVA), unpaired t-test, and multivariate (principal component analysis, PCA) analysis were performed using the computing environment R (R Core Team, 2019). Figures were produced using the package ggplot2 version 3.3.1 (Wickham, 2016). Additional software packages (ggpubr, factoextra, ggnewscale, ggrepel, scales, hrbrthemes, and RColorBrewer) were taken from the Bioconductor project (Gentleman et al., 2004).

RESULTS

Changes in SOM Molecular Composition Associated With Permafrost Thaw

Principal component analysis of the relative abundance of different SOM compound classes (as inferred by FT-ICR-MS), biogeochemical properties of peat porewater (TN concentration, DOC, sulfate, nitrate, and ammonia concentration and pH) and peat porewater CO_2 and CH_4 concentrations revealed clear separation between the bog and fen sites along PC1 (which explained 41% of the variance), with higher PC1 scores in rich fens (**Figure 1**). SOM in the *Sphagnum*-dominated bog sites had a higher relative abundance of tannins, lignins, unsaturated, and condensed hydrocarbons (UnSatHC and CondHC, respectively), and lipids compared to the fen sites. In contrast, fen samples were separated from bog samples along PC1 which correlated positively with the abundance of peptide-, carbohydrates (cellulose-)-, and aminosugar-like (AS) compounds. PC2 explained a small proportion of the variance (16%). Higher concentrations (measured in mM) of TN and DOC were observed in the bog porewaters compared to the fen porewater. In contrast, sulfate, nitrate and ammonia concentrations were higher in fen porewater and correlated positively with peat porewater pH. Porewater CO_2 and CH_4 concentrations were higher in the fen sites. Although some depth trends were observed, these trends were generally weak, as they were not consistently observed over the entire depth range and none of the principal components showed significant correlations with depth (**Supplementary Figure 1**).

To better visualize the differences in the bog and fen SOM molecular composition, unique peaks present in each group (bog vs. fen, regardless of the depth) were reported separately on van Krevelen diagrams (**Figures 2A,B**). SOM in bog samples (**Figure 2A**) appeared to be more rich in lignin-like ($0.29 < O/C < 0.65$ and $0.7 < H/C < 1.5$), tannin-like ($0.65 < O/C < 1$ and $0.8 < H/C < 1.5$), and lipid-like ($0 < O/C < 0.3$ and $1.5 < H/C < 2.5$) compounds and fen SOM (**Figure 2B**) was more rich in peptide-like ($0.3 < O/C < 0.6$ and $1.5 < H/C < 2.3$) compounds and amino sugars ($0.5 < O/C < 0.7$ and $0.8 < H/C < 2.5$). Out of 6,906 peaks detected in the bog samples in total, 24% were unique to bog, while only 8% of the peaks (out of 5,973 in total) detected in the fen were unique to fen, suggesting a higher number of unique compounds in bog (potentially not yet degraded) compared to fen samples (Venn diagram in panel B).

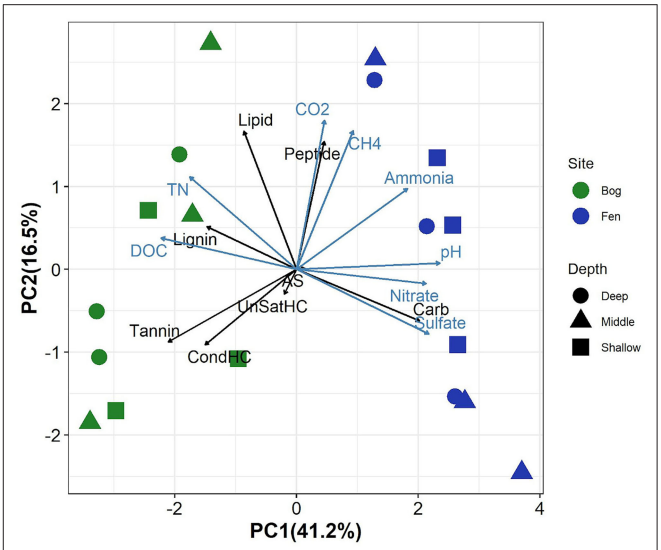

FIGURE 1 | Principal components analysis on elemental composition classes from FT-ICR-MS data (black arrows)and biogeochemical properties including the concentrations of total nitrogen(TN), dissolved organic carbon (DOC), sulfate, nitrate, ammonia, and pH (measured in porewater, indicated by blue arrows) and CO_2 and CH_4 (values for each sample is described in **Supplementary Table 1**). Fen samples are clearly separated from bog along PC2 (which positively correlates with peptides, CO_2, CH_4, sulfate, pH, and nitrate) and bog samples show positive and high correlations with carbohydrates, tannins and condensed hydrocarbon and DOC.

Shifts in Thermodynamics of Carbon Oxidation With Permafrost Thaw

Figure 3A shows $\Delta G^{\circ}C$-ox calculated for 6906 assigned molecular formula in nine bog samples and 5973 assigned molecular formulas in nine fen samples. Lower $\Delta G^{\circ}C$-ox and high NOSC represent thermodynamically more labile organic compounds and vise-versa. For each sample, $\Delta G^{\circ}C$-ox values (**Figure 3A**; **Table 3**) and NOSC values (**Table 3**) were averaged across all formulas and unpaired *t*-test was performed on the averaged values obtained from nine bog samples and nine fen samples. Average $\Delta G^{\circ}C$-ox values in bog samples were lower than fen samples (**Figure 3A**; **Table 3**) and subsequently, average NOSC values were higher in bog samples compared to fen

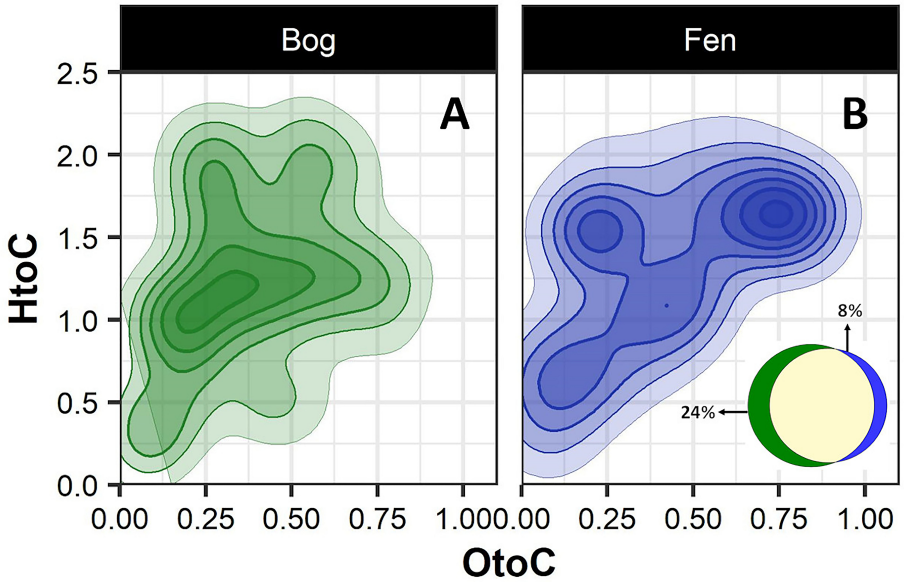

FIGURE 2 | Van Krevelen diagram generated from FT-ICR-MS data comparing the compositional differences in the bog **(A)** and fen **(B)** samples (regardless of depth). Oxygen to carbon (O/C) and hydrogen to carbon (H/C) ratios were calculated for unique peaks in bog (green) and fen (blue) sites. Ven diagram **(B)** indicates that 24% of the peaks (out of 6,906 peaks in total) detected in bog samples are unique to bog and 8% of the peaks (out of 5,973 peaks in total) detected in fen are unique to fen.

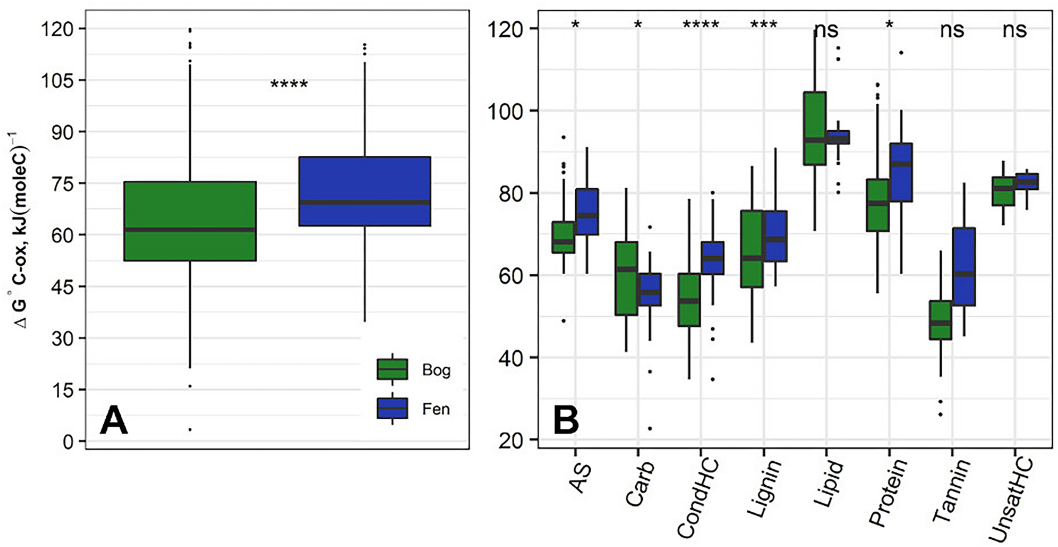

FIGURE 3 | (A) Average ΔG°C-ox (Gibbs free energy of C half reactions based on C oxidation; kJ/mol C) values based on FT-ICR-MS data calculated for the bog (green) and fen (blue) samples (regardless of depth). Low ΔG°C-ox represents thermodynamically favorable organic compounds for microbial degradation. Unpaired *t*-test was performed on the calculated values to determine the significant differences and *P*-values were reported. Additionally, **(B)** ΔG°C-ox values were graphed based on compound classifications for bog and fen samples. Statistical significances were determined by unpaired *t*-test. The "ns" symbol indicates $P > 0.05$. All $P < 0.05$, 0.001, and 0.0001 are summarized with one, three and four asterisks, respectively, indicating ΔG°C-ox values for those classes were significantly different between the bog and fen samples.

samples (**Table 3**). Interestingly, different ΔG°C-ox values were obtained for bog and fen samples within the same class of chemical compounds (**Figure 3B**). While amino sugars were more abundant in the fen sites compared to bog sites, they were characterized with higher average ΔG°C-ox compared to those in the bog sites. On the other hand, while bog sites had an abundance of lignin-like and tannin-like compounds compared to fen, however, they were of lower average ΔG°C-ox compared to those in the fen sites (more oxidized). The lower overall NOSC values of the bog SOM relative to the fen SOM could reflect the influence of oxygen at the bog site. As noted in section Chemical Compounds Classification and Data Processing, the

TABLE 3 | Ratios of O/C, H/C, N/C.

Sample	O/C ratio	H/C ratio	N/C ratio	S/C ratio	Avg MW	NOSC	ΔG°C-ox
S_1_S	0.50	1.16	0.03	0.07	674.29	−0.14	73.24
S_1_M	0.50	1.13	0.03	0.07	373.34	−0.08	48.04
S_1_D	0.48	1.14	0.02	0.08	487.17	−0.12	53.42
S_2_S	0.50	1.13	0.02	0.08	481.55	−0.12	65.04
S_2_M	0.48	1.20	0.03	0.07	480.26	−0.12	73.97
S_2_D	0.49	1.29	0.03	0.07	582.66	−0.17	79.16
S_3_S	0.49	1.28	0.03	0.07	481.23	−0.15	70.54
S_3_M	0.48	1.20	0.03	0.02	480.29	−0.12	62.17
S_3_D	0.40	1.17	0.03	0.05	583.24	−0.13	53.12
Average	0.48	1.18	0.03	0.06	480.20	−0.13	63.87
(SD)	(0.02)	(0.42)	(0.05)	(0.02)	(115.60)	(0.56)	(15.86)
E_1_S	0.50	1.31	0.02	0.04	560.33	−0.40	61.19
E_1_M	0.50	1.31	0.03	0.05	452.25	−0.46	73.23
E_1_D	0.42	1.30	0.02	0.03	450.54	−0.37	86.40
E_2_S	0.42	1.29	0.03	0.05	650.35	−0.48	73.28
E_2_M	0.41	1.39	0.03	0.04	341.02	−0.31	62.92
E_2_D	0.43	1.28	0.02	0.05	452.82	−0.34	72.08
E_3_S	0.39	1.23	0.02	0.05	449.23	−0.44	58.12
E_3_M	0.40	1.21	0.02	0.06	450.14	−0.46	72.14
E_3_D	0.41	1.21	0.02	0.06	450.10	−0.49	72.17
Average	0.4	1.28	0.02	0.05	450.3	−0.42	72.31
(SD)	(0.25)	(0.5)	(0.04)	(0.02)	(111.5)	(0.52)	(14.72)

S/C and values for NOSC and Gibbs free energy (ΔG°C-ox in kJ/mol C) for unique peaks [formulas that were detected in either bog or fen samples but not both (regardless of depth and replicate number)]. For each value, average of nine samples for bog and nine samples for fen as well as standard deviations were calculated.

fen is more consistently inundated (hence anoxic), while the bog habitat experiences alternating periods of oxic and anoxic conditions. These periods of exposure to oxygenation and the potential re-oxidation of organic and inorganic TEAs may facilitate decomposition at the bog site resulting in SOM with an overall lower NOSC value relative to the fen. However, the overall lower NOSC in the bog site may also reflect different starting substrates.

Sulfur and Nitrogen Dynamics With Permafrost Thaw

To further investigate the sulfur and nitrogen dynamics in the Mire, composition of S-containing SOM (regardless of depth) was compared in the bog (A) and fen (B) samples and unique peaks were reported on a van Krevelen diagram (**Figures 4A,B**). Sulfur containing compounds in bog fell in the lipid-like ($0 < O/C < 0.3$ and $1.5 < H/C < 2.5$), peptide-like ($0.3 < O/C < 0.6$ and $1.5 < H/C < 2.3$), and amino sugar-like ($0.5 < O/C < 0.7$ and $0.8 < H/C < 2.5$) regions of the van Krevelen diagram. In contrast, S-containing compounds in fen fell in the condensed hydrocarbon-like ($0 < O/C < 0.4$ and $0.2 < H/C < 0.8$) and lignin-like ($0.29 < O/C < 0.65$ and $0.7 < H/C < 1.5$) regions of the van Krevelen diagram. Overall, a higher abundance of unique S-containing organic compounds was observed in the bog compared to the fen system (∼ 2.6 to ∼1.3% unique S containing compounds, respectively, depicted on Venn diagram in panel A) coincident with lower sulfate concentrations in bog porewater (**Table 1**). Furthermore, molecular weights and nitrogen to carbon ratios (N/C) for unique compounds were calculated, and both were overlaid on the van Krevelen diagram (**Figures 4C,D**). Higher abundance of N-containing compounds (∼5% −345 unique compounds out of 6,906 peaks in total) with molecular weight >400 *m/z* (>400 Da) was observed in bog compared to fen samples. Conversely, fen SOM appeared to have a lower abundance of N-containing compounds (1% −70 unique compounds out of 5,973 peaks in total) and the N-containing compounds in the fen tended to be of lower mass (**Supplementary Figure 2**).

DBE-O was calculated for all unique fen and bog S- and N-containing compounds to better characterize the OM in the bog and fen samples (**Supplementary Figure 3**). Interestingly, for S-containing compounds, average DBE-O value for bogs and fens were significantly different ($p < 0.01$). Average bog DBE-O was 1.36 (±7.03) compared to the fen DBE-O of 4.18 (±8.05), suggesting that S-containing compounds in bog are more oxygenated with potentially higher number of carboxyl groups and fewer C=C double bonds. Average DBE-O values calculated for N-containing compounds were not significantly different between the bog and fen samples.

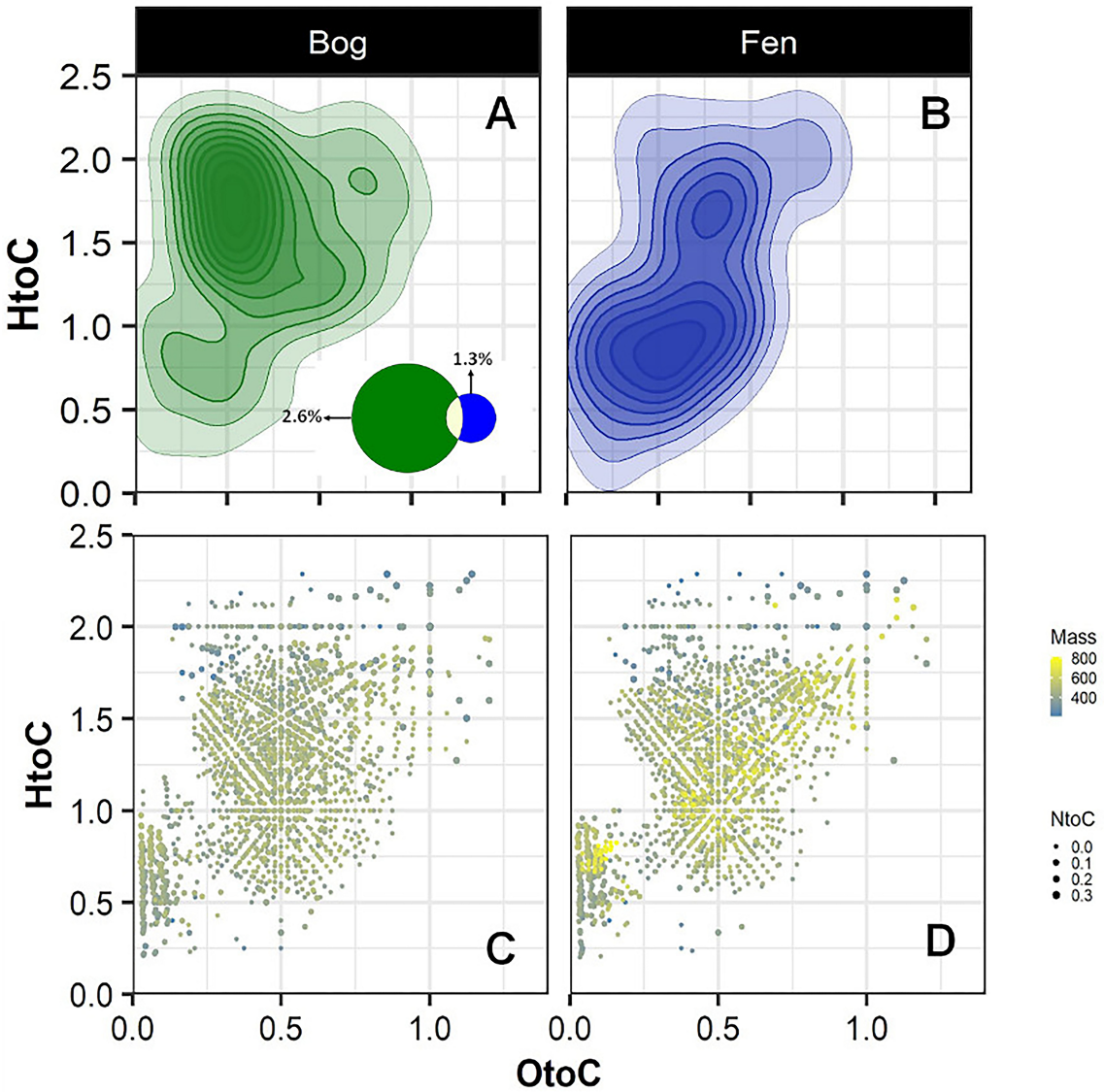

FIGURE 4 | Van Krevelen diagram generated from FT-ICR-MS unique peaks comparing the compositional differences in the bog **(A)** and fen **(B)** samples for sulfur containing compounds (regardless of depth). Venn diagram **(A)** indicates that 177 peaks (out of 6,906 peaks in total) detected in bog samples were unique to bog and 79 peaks of the peaks (out of 5,973 peaks in total) detected in fen were unique to fen. **(C,D)** graphs were generated from graphs **(A,B)** where mass of the unique peaks and nitrogen to carbon (N/C) ratios from unique peaks were overlaid on the van Krevelen diagram separately for the bog and fen. Steel blue to yellow color gradient indicates the mass of the compounds and the size of the points indicates the N/C ratios.

Shifts in Primary Metabolite Metabolism

We used multiple statistical tests to look at changes in SOM primary (central) metabolite composition between bog and fen samples (**Figure 5**; **Table 4**) where we observed statistically significant differences in bog and fen primary metabolite abundance. Principal component analysis (**Figure 5A**) revealed distinct differences in metabolite abundance (explained by PC1, 47.1%) between bog and fen samples. Effect of depth was also explained by PC2 (19.9%). Correlation coefficients of 25 primary metabolite abundances between bog and fen samples (regardless of depth) using Pearson r distance measure were determined at $p < 0.05$ (**Figure 5B**). Sugar acids such as D-galacturonic acid and simple sugars such as D-glucose, melibiose, sucrose, fructose, and D-mannose were significantly upregulated (more abundant) in bog samples (regardless of depth) whereas upregulated metabolites in fen samples were mainly classified as acids such as Erythronic acid, glycolic acid, pyruvic acid and amino acids such as glutamine and isoleucine. Another way to view this data is through the use of heatmaps. A heatmap of the same 25 identified metabolites (*t*-test significance) showed a similar separation (unpregulated sugar acids and simple sugars in bog and organic acid and amino acids in fen) between metabolites identified in different bog and fen samples (**Figure 5D**). **Figure 5C** features the top four upregulated metabolites in bog and fen samples

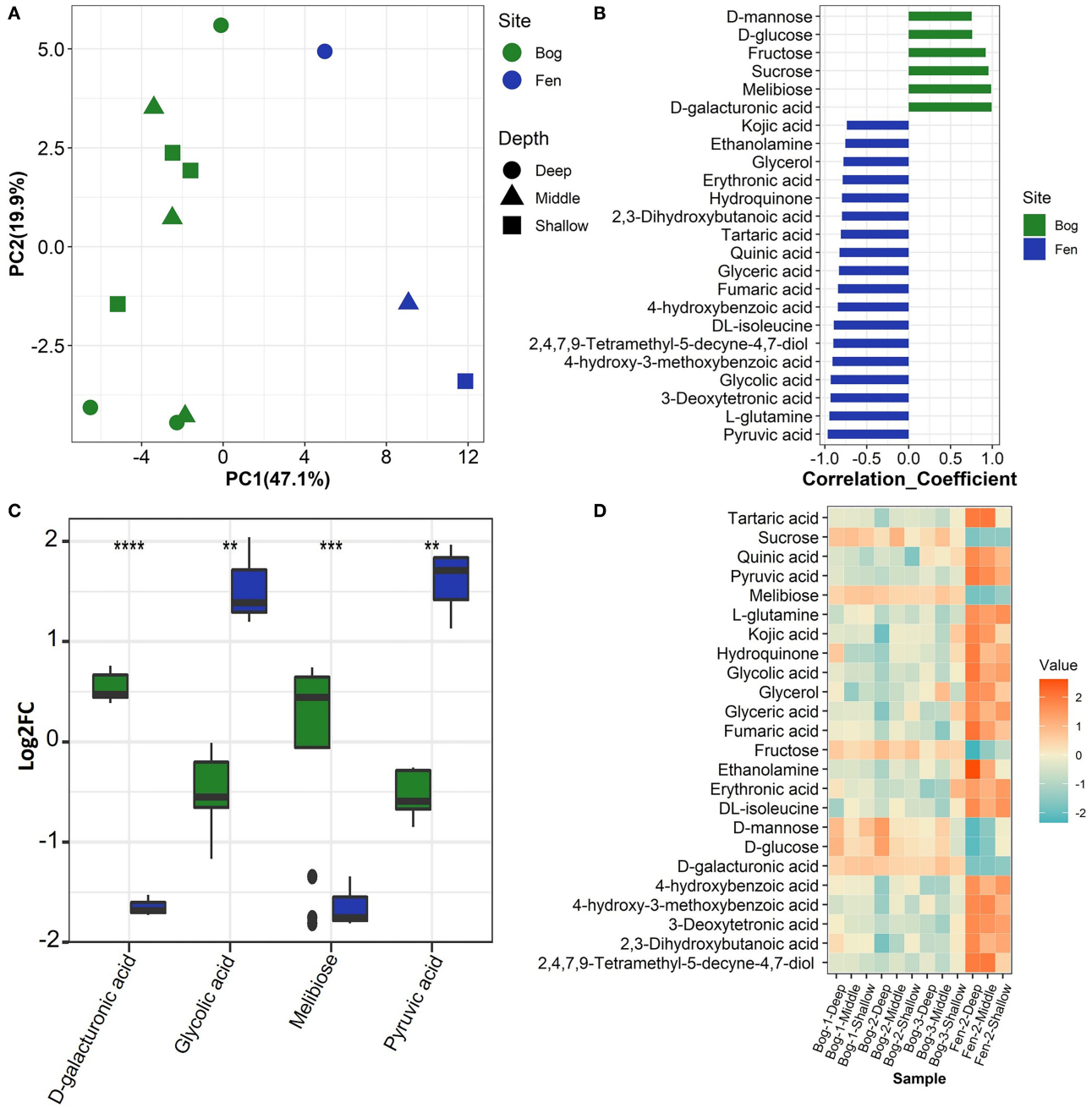

FIGURE 5 | (A) Principal component analysis (PCA) plot derived from GC-MS primary metabolite abundance variation between the bog (green) and fen (blue) groups. **(B)** Correlation analysis performed against Fen-Bog showing the 25 most significant features correlated with the pattern with $p < 0.05$. Distance measure used: Pearson r. **(C)** Box plots visualizing distribution of a subset of metabolites that are significantly changing (pairwise *t*-test, $p < 0.05$) between the two treatments. All *P* values less than 0.01, 0.001, and 0.0001 are summarized with two, three and four asterisks, respectively. **(D)** Heatmap of the significant metabolites (pairwise t-test) upregulated (orange) and downregulated (blue) between the bog and fen groups at different time points.

created via fold change (FC) analysis and *t*-test on absolute value changes between metabolites identified in bog and fen samples.

Shifts in C Transformations With Thaw

Consistent with changes in SOM and primary metabolite composition, transformation analysis indicated that the biochemical processes associated with the SOM degradation were significantly different between the bog and fen sites (**Figure 6A**). We observed higher abundances of sugar-associated transformations for the bog sites compared to the fen sites, which generally correlated with carbon transformations (**Figure 6A**). These data are consistent with **Figures 2**, **4B** where bog sites had

TABLE 4 | Metabolites that display both large magnitude fold-changes (fold change threshold >2 and $p < 0.05$); comparison type" Bog/Fen) and high statistical significance (*P*-value threshold = 0.05).

Metabolite name	Fold change	Log_2(FC)	*P* value	Chemical class
4-hydroxyphenylacetic acid	0.0001875	−12.381	0.0014809	Phenol derivative
Pyruvic acid	0.054091	−4.2085	1.97E-05	α-keto acid
3-Deoxytetronic acid	0.076363	−3.711	0.0001358	Fatty acid
Glycolic acid	0.09286	−3.4288	8.35E-05	α-hydroxy acid
4-hydroxy-3-methoxybenzoic acid	0.10877	−3.2007	0.0006269	dihydroxybenzoic acid
2,4,7,9-Tetramethyl-5-decyne-4,7-diol	0.1119	−3.1598	0.0052057	glycol
2,3-Dihydroxybutanoic acid, tristrimethylsilyl	0.13987	−2.8379	0.0067571	Organic acid
L-glutamine	0.14716	−2.7646	0.0001358	α-amino acid
D L-isoleucine	0.15699	−2.6712	0.0002079	α-amino acid
4-hydroxybenzoic acid	0.18953	−2.3995	0.0016227	Phenol derivative
Fumaric acid	0.22224	−2.1698	0.0071197	Organic acid
Tartaric acid	0.22292	−2.1654	0.049424	Organic acid
N,9-bisTrimethylsilyl-6-trimethylsilyloxy-9H-purin-2-amine	0.23355	−2.0982	0.0052057	Nitrogenous base derivative
Glyceric acid	0.26547	−1.9134	0.0020432	Sugar acid
Erythronic acid	0.32836	−1.6067	0.012038	Organic acid
Glycerol	0.33471	−1.579	0.037481	Polyol
Succinic acid	0.35168	−1.5077	0.037481	Dicarboxylic acid
Adenine	0.41888	−1.2554	0.030045	Amino acid
Hydroquinone	0.48962	−1.0303	0.046572	Phenol derivative
D-mannose	2.9914	1.5808	0.014911	Simple sugar
D-glucose	3.4837	1.8006	0.014452	Monosaccharide
lactobionic acid	4.1415	2.0502	0.019697	Sugar acid
L- sorbose	4.2542	2.0889	0.026852	Monosaccharide
D-malic acid	6.6396	2.7311	0.038903	Dicarboxylic acid
Citric acid	8.8833	3.1511	0.0071197	Organic acid
Fructose	21.452	4.423	0.0001953	Monosaccharide
Sucrose	22.465	4.4896	8.35E-05	Disaccharide
D-galactouronic acid	206.25	7.6882	0.049424	Sugar acid
Melibiose	256.46	8.0026	1.54E-05	Disaccharide

If the fold change threshold is >1, the metabolite is more prevalent in the bog, and if <1, it's more prevalent in the fen.

TABLE 5 | Concentrations of porewater CO_2 and CH_4 (reported in mM) and CO_2/CH_4 ratio measured in site for bog and fen (averaged).

		CO_2	CH_4	CO_2/CH_4
Bog	Average	1.35	0.12	11.16
	(SD)	(0.88)	(0.14)	(0.52)
Fen	Average	1.46	0.35	4.12
	(SD)	(0.61)	(0.34)	(0.19)
	P-value	0.003	0.001	0.0001

a lower abundance of carbohydrate molecules with mass >400 Da but a higher abundance of mono and disaccharides, reflective of decomposition of complex carbohydrates into mono, and disaccharides. However, based on their higher relative abundance in the porewater (**Figure 5**), these sugars are likely being slowly utilized by microbial communities and/or undergoing slow decomposition. In contrast, fen samples had a higher abundance of complex carbohydrate molecules, but lower abundance of simple, mono, and disaccharides. Despite the higher abundance of complex carbohydrate compounds in the fen site and the higher abundance of sugar - associated transformations in the bog compared to the fen, principal component analysis on specific sugar -associated metabolic transformations on all elemental formulas detected in the bog and fen samples (**Figure 6B**) indicated similar sugar transformations, suggesting that microbes at both sites have the capability of degrading simple and complex sugar molecules. These data suggest that simple sugars are being utilized at a higher rate in the fen sites compared to the bog sites. The slow decomposition at the bog sites and/or slow uptake of glucose by microbial communities for fermentation or anaerobic cellular respiration suggest additional controls (e.g., thermodynamic, abiotic processes) on SOM decomposition in the bog sites. The high amino acid-associated transformations in the fen samples (**Figure 6A**) is consistent with a higher abundance of amino acid compounds at the fen sites, reflective of protein degradation and /or release of amino acids by fen vegetation through roots.

CO_2 and CH_4 Emissions Associated With SOM Chemical Composition

Figure 7 and **Supplementary Figure 4** show the correlation between network analysis parameters to pH, DOC (mM), and $\delta^{13}C$ -CH_4 of bog and fen porewater samples. Significant correlations were observed between clustering coefficient and

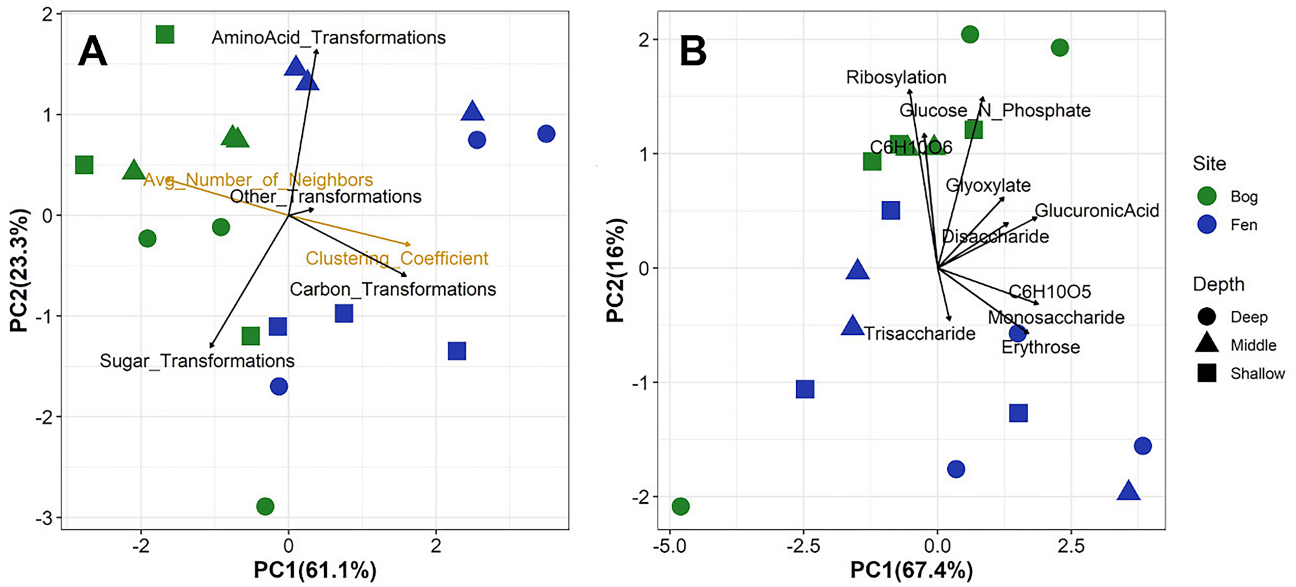

FIGURE 6 | Principal component analysis of **(A)** overall metabolic transformations and network analysis parameters and **(B)** specific sugar-associated metabolic transformation for all formulas detected in the bog and fen samples. Fen samples are separated by higher correlation to clustering coefficient whereas bog samples are highly correlated to average number of neighbors. Higher correlation between bog samples and sugar-associated transformation indicates preservation of these compounds in the bog. However, **(B)** indicates similar specific sugar-associated metabolic transformation in both the bog and fen samples.

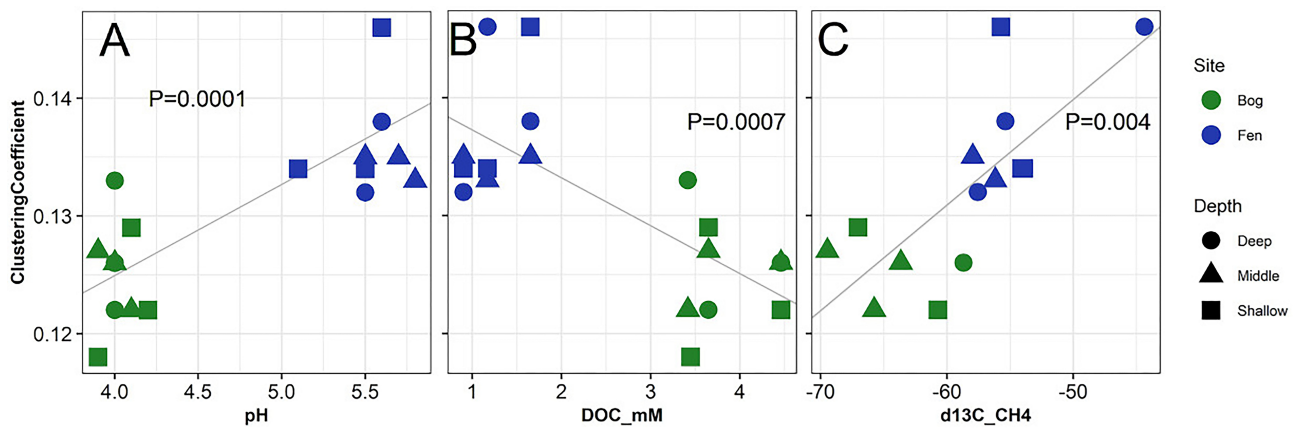

FIGURE 7 | Correlation of network analysis parameter (clustering coefficient) with **(A)** pH, **(B)** dissolved organic carbon and **(C)** $\delta^{13}C$ for CH_4 measured from the porewater of the bog (green) and fen (blue) samples. One-Way ANOVA (at $p < 0.05$) was performed on the calculated values to determine the significant differences and *P*-values were reported to be 0.0001, 0.0007, and 0.004, respectively.

average number of neighbors for SOM molecules to porewater pH, DOC (mM) and $\delta^{13}C$ -CH_4 values. SOM clustering coefficient increased with increasing pH (**Figure 7A**), decreasing DOC (**Figure 7B**), and enriched $\delta^{13}C$ -CH_4 (**Figure 7C**) values as in the case of fen and decreased with decreasing pH (**Figure 7A**) and depleted $\delta^{13}C$ -CH_4 values (**Figure 7C**) as in the case of bog. On the other hand, SOM average number of neighbors had an opposite trend to the clustering coefficient (**Supplementary Figure 4**). Significant correlations ($p < 0.05$) were also observed between different biogeochemical properties including concentrations of DOC, TN, DIC (CO_2), CH_4, ammonia, nitrate, sulfate, $\delta^{13}C$pw-DIC, $\delta^{13}C$pw-CH_4 (**Supplementary Table 4**), revealing clear coupling between different biogeochemical properties and GHG emissions.

DISCUSSION

Based on our advanced analytical characterization of peat SOM along a permafrost thaw gradient, organic matter compositional differences were clear between the bog and fen sites. Fen SOM appeared to be more degraded (regardless of the depth), transformed, and reduced as evident by the more negative NOSC and higher $\Delta G^{\circ}C$-ox values. This data is consistent with

previous studies comparing bog and rich fen samples from different locations across the Stordalen Mire from different years (Hodgkins et al., 2014, 2016). Phenol oxidase is an important enzyme in peatlands, as it is one of the few that can decompose recalcitrant phenolic compounds generally produced by *Sphagnum spp.* (McLatchey and Reddy, 1998; Freeman et al., 2004). Degradation of these phenolic compounds by microbes without the aid of phenol oxidase is challenging due to the high resonance energy that stabilizes the C-C bonds in aromatic rings (Harwood and Parales, 1996). Our data indicated that the bog SOM was more oxidized, dominated by tannin-like (polyphenolic) and organic acids, all with large number of carboxyl, aromatic, and methoxylated phenol groups (higher MWs). Previous reports have shown inhibition of microorganisms and the extracellular enzymes by these large polymers via crossbridged hydrogen bonds with proteins (enzymes) as well as penetration to the sensitive sites within microorganisms, hence altering their physiology (Wang et al., 1991; Field and Lettinga, 1992). These findings suggest that the high abundance of phenolic compounds in peat bogs could have a toxic effect on microorganisms in addition to lower decomposition rates by extracellular enzymes (Freeman et al., 2004). The activity of phenol oxidase is also dependent on various factors such as bimolecular oxygen availability, extent of waterlogging, and plant communities, which in the peat bog are factors controlled by *Sphagnum spp.* (Freeman et al., 2004). *Sphagnum spp.* creates waterlogged conditions, acidifies its environment using high cation exchange rates (Rudolph and Samland, 1985; Rasmussen et al., 1995; Thormann, 2006), produces lignin-like polymeric phenols that inhibit enzymatic activity (such as 5-keto-D-mannuronic acid, p-hydroxy-b[carboxymethyl]-cinnamic acid) (Stalheim et al., 2009; Fudyma et al., 2019), and has highly recalcitrant cell walls (Stalheim et al., 2009; Hájek et al., 2011). *Sphagnum* moss is also known to decay more slowly than vascular plants (Hodgkins et al., 2014; Tfaily et al., 2014). The preservation of labile compounds in the peat bog observed in our data is likely due to the anoxic, acidic, and nutrient sequestration traits intrinsic to *Sphagnum spp.* and likely impedes phenol oxidase activity and subsequent organic matter decay by microbial communities (Williams et al., 2000; Freeman et al., 2004).

Diversity in microbial communities is important to the function and stability of many microbial ecosystems, such as animal- and plant-associated microbiomes (Worm et al., 2002; Muscarella et al., 2019). Uncovering mechanisms to maintain microbial diversity in these environments is important in understanding belowground metabolic transformations and subsequent GHG emissions (Muscarella et al., 2019). Substrate generalists vs. specialists can interact with different available substrates and depending upon the substrates that are used, we can partly understand microbial preferences and predict gas flux changes (Chen et al., 2020; Zhou et al., 2020). Based on our data, bog SOM exhibited higher DOC porewater concentrations, lower microbial diversity (inferred from Shannon diversity; Singleton et al., 2018; Woodcroft et al., 2018), and activity (inferred from the high average number of neighbors and lower clustering coefficient in the bog metabolic transformations analysis—**Supplementary Table 3**), suggesting that bog microbial communities are comprised of substrate specialists that are only capable of performing a limited set of specific functions (Monard et al., 2016; Muscarella et al., 2019) under anoxic and acidic conditions mainly created by *Sphagnum* spp. (Williams et al., 2000; Freeman et al., 2004). On the other hand, fen SOM was characterized by increased substrate heterogeneity (higher clustering coefficient), suggesting fen microbial communities are substrate generalists and are able to use and transform same substrates through different metabolic pathways. This observation is again consistent with Woodcroft et al. (2018) that showed microbial diversity (Shannon index) in the bog to be significantly lower than that in the fen. GC-MS data showed that the majority of upregulated metabolites in the bog were mono and disaccharides and sugar acids, in particular galacturonic acid, while the fen had higher abundances of amino acids and polyphenols (**Figures 5**, **6B**), suggesting that in the fen, mono and disaccharides are consumed by microbial communities as soon as they are degraded by various biotic and abiotic metabolic pathways and the high abundances of amino acids and polyphenols reflect microbial byproducts and thus an active microbial community (Whiting and Chanton, 1992; Chanton et al., 1995, 2008; Hodgkins et al., 2014).

Recently, Fudyma et al. (2019) showed that *Sphagum fallax* metabolite profile is composed of flavonoid glycoside compounds (a compound formed from a simple sugar and a phenol), that could be acting as potent antimicrobial compounds. Thus, the quality of bog SOM (i.e., high abundance of lignin-like and polyphenolics and simple sugars, recalcitrant dead *Sphagnum* litter, and the low phenol oxidase enzymes activity) all suggest limited OM degradation by biotic factors. Here we hypothesize that the accumulation of simple sugars is either due to low rates of biotic decomposition and consumption, leading to its accumulation or that the release of simple sugars is occurring abiotically through acid catalyzed hydrolysis of lignocellulose and cellulose (BeMiller, 1967; Timell, 1967; Hopkinson, 1969; Girisuta et al., 2007; Ahmad and Pant, 2018) (**Figures 2A**, **5B–D**). Therefore, we further postulate that low pH could be aiding the acid catalyzed hydrolysis of carbohydrates and sugar acids (glycosides) in bog systems (Ahmad and Pant, 2018) leading to the release of mono and disaccharides with lower average $\Delta G^{\circ}C$-ox. However, accumulation of these compounds in the peat with time probably due to low pH and high abundance of galacturonic acids produced by *Sphagnum*, further shed light on the limited microbial activities in respiring these compounds (**Figures 1**, **3**, **5**) (Rasmussen et al., 1995; Thormann, 2006). Metabolic transformation analysis and FT-ICR-MS data confirm this trend, with higher abundance of sugar transformations present in bog samples. Because both reactant and product of the metabolic transformation are present in the bog samples, we believe in the bog biotic degradation of organic matter happens more slowly than at fen sites, and that possible byproducts of *Sphagnum* OM degradation in the bog (i.e., upregulated galacturonic acid—which is a by-product of pectin degradation known to have antimicrobial effects—Hájek et al., 2011) could be limiting the biotic complex carbohydrate degradation pathways, resulting in the accumulation of both complex and labile

sugars. Observed correlations between the pH and the SOM clustering coefficient (positive correlation; $p < 0.0001$) and the average number of neighbors (negative correlation; $p = 0.0002$) potentially indicates the impact of pH on substrate quality and concentration. Lower pH values promote carbon accumulation and low substrate diversity whereas higher pH values are correlated with higher substrate quality and diversity. The bog porewater DOC concentration correlated positively ($p = 0.0008$) with the average number of neighbors, reflecting accumulation of OM in the bog sites consistent with lower decomposition rates (**Supplementary Figure 3**) and acidic conditions (low pH). Moreover, in fens, vascular plant roots may transport oxygen into the soil, where it activates phenol oxidase and thereby decreases the concentration of decomposition-inhibiting phenolics and organic acids (Joabsson and Christensen, 2001; Estop-Aragonés et al., 2012). However, further experiments are required to validate these assumptions.

Depleted $\delta^{13}C$ -CH_4 in the bog porewater samples suggest that hydrogenotrophic rather than acetcolastic methanogenesis is likely the preferred pathway for methane production. This is consistent with low degradation potential of the bog SOM and higher DOC concentrations (Hodgkins et al., 2014; McCalley et al., 2014; Tfaily et al., 2014). More enriched $\delta^{13}C$ -CH_4 in fen porewater, on the other hand, suggests that acetoclastic methanogenesis is the dominant pathway for CH_4 production and that methanogenisis substrates are produced by OM fermentation leading to low DOC concentration (Chanton et al., 1995; Chasar et al., 2000). Observed correlation between the clustering coefficients and the $\delta^{13}C$ -CH_4 for the bog and fen samples potentially suggests that the network analysis parameters indicating the substrate diversity and heterogeneity can be used as an indication of pathways by which microbial communities are utilizing the OM and ultimately producing GHG and they indirectly provide information on the microbial diversity. However, further studies should aim to replicate these findings in a larger experimental setup.

Pathways underlying CO_2 and CH_4 productions in peatlands are also dependent on S and N cycling and the microorganisms that interact with these compounds (Granberg et al., 2001; Limpens et al., 2008; Pester et al., 2012). Sulfate (SO_4^{2-}) and nitrate (NO_3^-) can act as terminal electron acceptors in anoxic conditions, allowing microorganisms to couple the oxidization of substrates (e.g., H_2, organosulfur and organonitrogen compounds) and reduction of TEAs to produce CO_2 and CH_4 (Muyzer and Stams, 2008). Hence sulfate reducing microorganisms (SRM) and methanogens can co-exist or compete for substrates within these oxygen-limited environments (Raskin et al., 1996; Schink, 1997). Recently, Woodcroft et al. (2018) identified the presence and activation of high diversity deep-branching lineages of the dsrAB genes (dissimilatory sulfate reduction genes) belonging to sulfate-reducing microorganisms (SRMs) in *Sphagnum*-dominated bog in the Mire. SRMs utilize sulfur containing compounds and produce CO_2. In peatlands, H_2 is generated from fermentation of carbohydrates (especially the ones with aromatic rings), while oxidized S-containing compounds come from plant matter (Rawat et al., 2012). Peat bogs generally have larger amounts of oxidized organosulfur compounds due to high S uptake potential by *Sphagnum* and therefore dead *Sphagnum* is rich in organic S compounds, which can drive sulfate reduction (Urban et al., 1989; Novák and Wieder, 1992; Fritz et al., 2014). Our data suggests that hydrogenotrophic reduction by SRM and nitrate reduction is occurring in the peat bog due to the following factors: (1) increased organosulfur compounds, potentially acting as TEAs for SRMs and suggesting that sulfate reduction is not limited by S availability (Baena et al., 1998); (2) low porewater mM concentrations of SO_4^{2-} and NO_3^-, suggesting rapid turnover of TEAs; (3) low pH, which is likely inhibiting methanogen activities (Tang et al., 2018); and (4) high abundance of mono and disaccharides, suggesting degradation of large carbohydrates by fermentative bacteria in addition to acid-catalyzed dissociations. Fermentation byproducts such as CO_2, and H_2, are then further consumed in hydrogenotrophic reduction (Conrad et al., 1987; Goodwin et al., 1991). CO_2 and CH_4 porewater concentrations measured in the bog samples were lower compared to the fen samples (**Table 4**), however, CO_2:CH_4 production ratios (**Table 4**) were higher in the bog compared to the fen, suggesting likely consumption of fermentation and acid-catalyzed dissociation byproducts by SRMs, leading to suppressed methanogenesis potentials by methanogens in the bog (Ward et al., 2009; Rawat et al., 2012; Hausmann et al., 2018). Similarly, SRMs can oxidize CH_4 coupled with sulfate reduction, which is also likely driving the lower CH_4 production rates in bogs (Cord-Ruwisch and Ollivier, 1986; Ward et al., 2009; Rawat et al., 2012). Higher CO_2 and CH_4 porewater concentrations in the fen are likely due to a decrease in *Sphagnum*-derived inhibitory organic acids (**Figure 5**) driven by changing plant inputs and increasing pH (**Table 1** and **Supplementary Table 1**) from bog to fen systems. Lower C/N ratios in the fen, driven by lower C/N of plant inputs from sedges compared to *Sphagnum*, may also lead to greater organic matter decomposition in the fen by alleviating N limitation for decomposers (Hodgkins et al., 2014; Khadka et al., 2016).

CONCLUSION

Due to the contribution from aboveground vegetation and belowground metabolic transformations under various redox conditions, microbial processes both affect and are being affected by the chemical composition and quality of SOM. In order to gain better insight on the overall metabolic transformations in bog and fen and to link substrate diversity and quality with microbial activity and GHG production, we calculated the Gibbs free energy of C half reactions based on C oxidation state for OM, a quantifiable measure for OM decomposability and quality, which can be incorporated into current biogeochemical models to represent OM lability and microbial diversity. We further correlated clustering coefficients and average number of neighbors, two network analysis parameters, with different biogeochemical properties of bog and fen samples. Our data revealed that pH is a main driver of SOM decomposition. We hypothesized that the low pH of the bog, driven by *Sphagnum*-derived organic acids, along with phenolics, could

potentially impact substrate quality and concentration and microbial diversity thereby promoting carbon accumulation and low substrate diversity. We further hypothesized that abiotic degradations such as acid catalyzed hydrolysis reactions (i.e., hydrolysis of Lignocellulose, complex carbohydrates, and sugar acids) are happening at a greater rate in bog, freeing bioavailable compounds for microbial utilization and further biotic metabolic pathways. In the fen, the presence of lower molecular weight compounds with higher Gibbs free energy, low DOC, more populated and diverse metabolic transformations, and higher net CH_4 and CO_2 fluxes and higher pH is indicative of more diverse substrate composition and higher microbial diversity than the bog, suggesting a more active system where biotic pathways are largely upregulated. The correlation observed between the clustering coefficient and the average number of neighbors with $\delta^{13}C$ -CH_4 values further reflects that organic matter quality and composition has an impact on microbial activity (as revealed by FT-ICR-MS and GC-MS data) measured indirectly through CH_4 fluxes.

While many microbial pathways can be inhibited by acidic and anoxic conditions, as observed in the bog, we found evidence of activity of sulfur reducing bacteria. Lower concentrations of sulfate in the bog porewater suggest a rapid turnover of organosulfur compounds acting as TEAs. This is also confirmed by lower CH_4 production rates and lower pH in the bog, with low pH likely inhibiting methanogenesis, as well as SRM either consuming H_2 and producing CO_2 or consuming CH_4 and producing CO_2 ($CH_4 + SO_4^{2-} \rightarrow HCO_3^- + HS^- + H_2O$). Due to these results, fen ecosystems that are composed of more diverse and active microbial communities should be more stable with changing environmental conditions (e.g., similar GHG fluxes) whereas bog microbial populations may be more easily affected by a changing climate. It is expected that thaw progression in northern peatlands will rapidly change the water table level, plant communities and nutrient input sources, all contributing to a decline of *Sphagnum* moss (Norby et al., 2019). This could result in shifts in decomposition, as well as altered contributions from biotic and abiotic pathways of OC toward higher CH_4 and CO_2 emission which ultimately creates positive climate feedbacks. Therefore, insights into how metabolite diversity and resource heterogeneity relate to the taxonomic and functional diversity of microbial communities allows for aspects of ecosystem stability and functional redundancy to be studied and provides a unique opportunity to understand how microbial communities will respond to climate perturbations.

DATA AVAILABILITY STATEMENT

The original contributions generated for the study are included in the article/**Supplementary Materials**. The data sets generated from this study are currently available online at https://doi.org/10.17605/OSF.IO/GS2UT.

AUTHOR CONTRIBUTIONS

RW, SH, and MT designed and performed the experiment and data acquisition. RA and MT did the analysis and interpretation of data for the work. RA, MT, and RW drafted and revised the manuscript with contribution from SH, JF, JC, VR, and SS. All authors contributed to the article and approved the submitted version.

FUNDING

This study was funded by the Genomic Science Program of the United States Department of Energy (DOE) Office of Biological and Environmental Research (BER), grants DE-SC0004632, DE-SC0010580, and DE-SC0016440. A portion of the research was performed using Environmental Molecular Sciences Laboratory (EMSL), a DOE Office of Science User Facility under proposal number 48467.

ACKNOWLEDGMENTS

We thank the Abisko Scientific Research Station for providing infrastructure for sampling. We thank the IsoGenie 1, 2, and 3 Project Teams (https://isogenie.osu.edu) and the 2012 IsoGenie sampling team for sample collection, particularly Carrie McCalley, and Tyler Logan, as well as the Abisko Scientific Research Station for sampling infrastructure and support.

SUPPLEMENTARY MATERIAL

The Supplementary Material for this article can be found online at: https://www.frontiersin.org/articles/10.3389/feart.2020.557961/full#supplementary-material

REFERENCES

Ahmad, E., and Pant, K. K. (2018). "Lignin conversion: a key to the concept of lignocellulosic biomass-based integrated biorefinery," in *Waste Biorefinery* (Elsevier), 409–444. doi: 10.1016/B978-0-444-63992-9.00014-8

Allison, S. D. (2005). Cheaters, diffusion and nutrients constrain decomposition by microbial enzymes in spatially structured environments. *Ecol. Lett.* 8, 626–635. doi: 10.1111/j.1461-0248.2005.00756.x

Assenov, Y., Ramírez, F., Schelhorn, S.-E., Lengauer, T., and Albrecht, M. (2008). Computing topological parameters of biological networks. *Bioinformatics* 24, 282–284. doi: 10.1093/bioinformatics/btm554

Bäckstrand, K., Crill, P., Jackowicz-Korczyński, M., Mastepanov, M., Christensen, T., and Bastviken, D. (2010). Annual carbon gas budget for a subarctic peatland, northern Sweden. *Biogeosciences* 7, 95–108. doi: 10.5194/bg-7-95-2010

Bae, E., Yeo, I. J., Jeong, B., Shin, Y., Shin, K.-H., and Kim, S. (2011). Study of double bond equivalents and the numbers of carbon and oxygen atom distribution of dissolved organic matter with negative-mode FT-ICR MS. *Anal. Chem.* 83, 4193–4199. doi: 10.1021/ac200464q

Baena, S., Fardeau, M.-L., Labat, M., Ollivier, B., Garcia, J.-L., and Patel, B. K. C. (1998). Desulfovibrio aminophilus sp. nov., a novel amino acid degrading and sulfate reducing bacterium from an anaerobic dairy wastewater lagoon. *Syst. Appl. Microbiol.* 21, 498–504. doi: 10.1016/S0723-2020(98)80061-1

Barabási, A.-L., and Albert, R. (1999). Emergence of scaling in random networks. *Science* 286, 509–512. doi: 10.1126/science.286.5439.509

Barabási, A.-L., and Oltvai, Z. N. (2004). Network biology: understanding the cell's functional organization. *Nat. Rev. Genet.* 5, 101–113. doi: 10.1038/nrg1272

BeMiller, J. N. (1967). "Acid-catalyzed hydrolysis of glycosides," in *Advances in Carbohydrate Chemistry, Vol. 22* (Academic Press), 22, 25–108. doi: 10.1016/S0096-5332(08)60151-4

Bölscher, T., Paterson, E., Freitag, T., Thornton, B., and Herrmann, A. M. (2017). Temperature sensitivity of substrate-use efficiency can result from altered microbial physiology without change to community composition. *Soil Biol. Biochem.* 109, 59–69. doi: 10.1016/j.soilbio.2017.02.005

Boye, K., Noël, V., Tfaily, M. M., Bone, S. E., Williams, K. H., Bargar, J. R., and Fendorf, S. (2017). Thermodynamically controlled preservation of organic carbon in floodplains. *Nat. Geosci.* 10, 415–419. doi: 10.1038/ngeo2940

Breitling, R., Ritchie, S., Goodenowe, D., Stewart, M. L., and Barrett, M. P. (2006). Ab initio prediction of metabolic networks using fourier transform mass spectrometry data. *Metabolomics* 2, 155–164. doi: 10.1007/s11306-006-0029-z

Burgess, K. E. V., Borutzki, Y., Rankin, N., Daly, R., and Jourdan, F. (2017). MetaNetter 2: a Cytoscape plugin for ab initio network analysis and metabolite feature classification. *J. Chromatogr. B*, 1071, 68–74. doi: 10.1016/j.jchromb.2017.08.015

Burke, E. J., Jones, C. D., and Koven, C. D. (2012). Estimating the permafrost-carbon climate response in the CMIP5 climate models using a simplified approach. *J. Clim.*, 26, 4897–4909. doi: 10.1175/JCLI-D-12-00550.1

Chang, K.-Y., Riley, W. J., Brodie, E. L., McCalley, C. K., Crill, P. M., and Grant, R. F. (2019). Methane production pathway regulated proximally by substrate availability and distally by temperature in a high-latitude mire complex. *J. Geophys. Res. Biogeosci.* 124, 3057–3074. doi: 10.1029/2019JG005355

Chanton, J. P., Bauer, J. E., Glaser, P. A., Siegel, D. I., Kelley, C. A., Tyler, S. C., et al. (1995). Radiocarbon evidence for the substrates supporting methane formation within northern Minnesota peatlands. *Geochim. Cosmochim. Acta* 59, 3663–3668. doi: 10.1016/0016-7037(95)00240-Z

Chanton, J. P., Glaser, P. H., Chasar, L. S., Burdige, D. J., Hines, M. E., Siegel, D. I., et al. (2008). Radiocarbon evidence for the importance of surface vegetation on fermentation and methanogenesis in contrasting types of boreal peatlands. *Glob. Biogeochem. Cycles* 22, 1–11. doi: 10.1029/2008GB003274

Chasar, L. S., Chanton, J. P., Glaser, P. H., Siegel, D. I., and Rivers, J. S. (2000). Radiocarbon and stable carbon isotopic evidence for transport and transformation of dissolved organic carbon, dissolved inorganic carbon, and CH4 in a northern Minnesota peatland. *Glob. Biogeochem. Cycles* 14, 1095–1108. doi: 10.1029/1999GB001221

Chen, J., Elsgaard, L., van Groenigen, K. J., Olesen, J. E., Liang, Z., Jiang, Y., et al. (2020). Soil carbon loss with warming: new evidence from carbon-degrading enzymes. *Glob. Chang. Biol.* 26, 1944–1952. doi: 10.1111/gcb.14986

Conrad, R., Schütz, H., and Babbel, M. (1987). Temperature limitation of hydrogen turnover and methanogenesis in anoxic paddy soil. *FEMS Microbiol. Ecol.* 3, 281–289. doi: 10.1111/j.1574-6968.1987.tb02378.x

Corbett, J. E., Burdige, D. J., Tfaily, M. M., Dial, A. R., Cooper, W. T., Glaser, P. H., et al. (2013). Surface production fuels deep heterotrophic respiration in northern peatlands. *Glob. Biogeochem. Cycles* 27, 1163–1174. doi: 10.1002/2013GB004677

Corbett, J. E., Tfaily, M. M., Burdige, D. J., Glaser, P. H., and Chanton, J. P. (2015). The relative importance of methanogenesis in the decomposition of organic matter in northern peatlands. *J. Geophys. Res. Biogeosci.* 120, 280–293. doi: 10.1002/2014JG002797

Cord-Ruwisch, R., and Ollivier, B. (1986). Interspecific hydrogen transfer during methanol degradation by Sporomusa acidovorans and hydrogenophilic anaerobes. *Arch. Microbiol.* 144, 163–165. doi: 10.1007/BF00414728

Corvasce, M., Zsolnay, A., D'Orazio, V., Lopez, R., and Miano, T. M. (2006). Characterization of water extractable organic matter in a deep soil profile. *Chemosphere* 62, 1583–1590. doi: 10.1016/j.chemosphere.2005.07.065

de Graaff, M.-A., Classen, A. T., Castro, H. F., and Schadt, C. W. (2010). Labile soil carbon inputs mediate the soil microbial community composition and plant residue decomposition rates. *New Phytol.* 188, 1055–1064. doi: 10.1111/j.1469-8137.2010.03427.x

Deng, J., Li, C., Frolking, S., Zhang, Y., Backstrand, K., and Crill, P. (2014). Assessing effects of permafrost thaw on C fluxes based on multiyear modeling across a permafrost thaw gradient at Stordalen, Sweden. *Biogeosciences* 4753–4770. doi: 10.5194/bg-11-4753-2014

Dong, J., and Horvath, S. (2007). Understanding network concepts in modules. *BMC Syst. Biol.* 1:24. doi: 10.1186/1752-0509-1-24

Estop-Aragonés, C., Knorr, K.-H., and Blodau, C. (2012). Controls on *in situ* oxygen and dissolved inorganic carbon dynamics in peats of a temperate fen. *J. Geophys. Res. Biogeosci.* 117:1–14. doi: 10.1029/2011JG001888

Fenner, N., Freeman, C., Lock, M. A., Harmens, H., Reynolds, B., and Sparks, T. (2007). Interactions between elevated CO2 and warming could amplify DOC exports from peatland catchments. *Environ. Sci. Technol.* 41, 3146–3152. doi: 10.1021/es061765v

Field J.A., and Lettinga G. (1992). "Toxicity of tannic compounds to microorganisms," in *Plant Polyphenols. Basic Life Sciences,* Vol. 59, eds R. W. Hemingway and P. E. Laks (Boston, MA: Springer). doi: 10.1007/978-1-4615-3476-1_39

Freeman, C., Ostle, N. J., Fenner, N., and Kang, H. (2004). A regulatory role for phenol oxidase during decomposition in peatlands. *Soil Biol. Biochem.* 36, 1663–1667. doi: 10.1016/j.soilbio.2004.07.012

Fritz, C., Lamers, L. P. M., Riaz, M., van den Berg, L. J. L., and Elzenga, T. J. T. M. (2014). Sphagnum mosses—masters of efficient N-uptake while avoiding intoxication. *PLoS One* 9:e79991. doi: 10.1371/journal.pone.0079991

Frolking, S., Talbot, J., Jones, M. C., Treat, C. C., Kauffman, J. B., Tuittila, E.-S., et al. (2011). Peatlands in the Earth's 21st century climate system. *Environ. Rev.* 19, 371–396. doi: 10.1139/a11-014

Fudyma, J., Lyon, J., AminiTabrizi, R., Gieschen, H., Chu, R. K., Hoyt, D. W., et al. (2019). *Untargeted Metabolic Profiling of Sphagnum fallax from Boreal Peatlands Identifies Antimicrobial Compounds and Novel Metabolites. AGU Fall Meeting Abstracts* 13. Available online at: http://adsabs.harvard.edu/abs/2019AGUFM.B13G2584F

Galand, P. E., Fritze, H., Conrad, R., and Yrjälä, K. (2005). Pathways for methanogenesis and diversity of methanogenic archaea in three boreal peatland ecosystems. *Appl. Environ. Microbiol.* 71, 2195–2198. doi: 10.1128/AEM.71.4.2195-2198.2005

Gentleman, R. C., Carey, V. J., Bates, D. M., Bolstad, B., Dudoit, S., Ellis, B. C., et al. (2004). Bioconductor: open software development for computational biology and bioinformatics. *Genome Biol.* 5:R80. doi: 10.1186/gb-2004-5-10-r80

Girisuta, B., Janssen, L. P. B. M., and Heeres, H. J. (2007). Kinetic study on the acid-catalyzed hydrolysis of cellulose to levulinic acid. *Ind. Eng. Chem. Res.* 46, 1696–1708. doi: 10.1021/ie061186z

Goodwin, S., Giraldo-Gomez, E., Mobarry, B., and Switzenbaum, M. S. (1991). Comparison of diffusion and reaction rates in anaerobic microbial aggregates. *Microb. Ecol.* 22, 161–174. doi: 10.1007/BF02540221

Granberg, G., Sundh, I., Svensson, B. H., and Nilsson, M. (2001). Effects of temperature, and nitrogen and sulfur deposition, on methane emission from a boreal mire. *Ecology*, 82, 1982–1998. doi: 10.1890/0012-9658(2001)082[1982:EOTANA]2.0.CO;2

Grandy, A. S., and Neff, J. C. (2008). Molecular C dynamics downstream: the biochemical decomposition sequence and its impact on soil organic matter structure and function. *Sci. Total Environ.* 404, 297–307. doi: 10.1016/j.scitotenv.2007.11.013

Hájek, T., Ballance, S., Limpens, J., Zijlstra, M., and Verhoeven, J. T. A. (2011). Cell-wall polysaccharides play an important role in decay resistance of Sphagnum and actively depressed decomposition *in vitro. Biogeochemistry* 103, 45–57. doi: 10.1007/s10533-010-9444-3

Harwood, C. S., and Parales, R. E. (1996). The β-ketoadipate pathway and the biology of self-identity. *Annu. Rev. Microbiol.* 50, 553–590. doi: 10.1146/annurev.micro.50.1.553

Hättenschwiler, S., and Jørgensen, H. B. (2010). Carbon quality rather than stoichiometry controls litter decomposition in a tropical rain forest. *J. Ecol.* 98, 754–763. doi: 10.1111/j.1365-2745.2010.01671.x

Hausmann, B., Pelikan, C., Herbold, C. W., Köstlbacher, S., Albertsen, M., Eichorst, S. A., et al. (2018). Peatland Acidobacteria with a dissimilatory sulfur metabolism. *ISME J.* 12, 1729–1742. doi: 10.1038/s41396-018-0077-1

Herzsprung, P., Hertkorn, N., von Tümpling, W., Harir, M., Friese, K., and Schmitt-Kopplin, P. (2014). Understanding molecular formula assignment of fourier transform ion cyclotron resonance mass spectrometry data of natural organic matter from a chemical point of view. *Anal. Bioanal. Chem.* 406, 7977–7987. doi: 10.1007/s00216-014-8249-y

Hiller, K., Hangebrauk, J., Jäger, C., Spura, J., Schreiber, K., and Schomburg, D. (2009). *Metabolite* detector: comprehensive analysis tool for targeted and nontargeted GC/MS based metabolome analysis. *Anal. Chem.* 81, 3429–3439. doi: 10.1021/ac802689c

Hodgkins, S. B., Chanton, J. P., Langford, L. C., McCalley, C. K., Saleska, S. R., Rich, V. I., et al. (2015). Soil incubations reproduce field methane dynamics in a subarctic wetland. *Biogeochemistry* 126, 241–249. doi: 10.1007/s10533-015-0142-z

Hodgkins, S. B., Tfaily, M. M., McCalley, C. K., Logan, T. A., Crill, P. M., Saleska, S. R., et al. (2014). Changes in peat chemistry associated with permafrost thaw increase greenhouse gas production. *Proc. Natl. Acad. Sci.* 111, 5819–5824. doi: 10.1073/pnas.1314641111

Hodgkins, S. B., Tfaily, M. M., Podgorski, D. C., McCalley, C. K., Saleska, S. R., Crill, P. M., et al. (2016). Elemental composition and optical properties reveal changes in dissolved organic matter along a permafrost thaw chronosequence in a subarctic peatland. *Geochim. Cosmochim. Acta* 187, 123–140. doi: 10.1016/j.gca.2016.05.015

Hopkinson, A. C. (1969). Acid-catalysed hydrolysis of alkyl benzoates. *J. Chem. Soc. B Phys. Organic* 203–205. doi: 10.1039/j29690000203

IPCC (2007). "Climate change 2007: the physical science basis," in *Contribution of Working Group I to the Fourth Assessment Report of the Intergovernmental Panel on Climate Change,* eds S. Solomon, D. Qin, M. Manning, Z. Chen, M. Marquis, K. B. Averyt, M. Tignor and H. L. Miller (Cambridge, New York, NY: Cambridge University Press).

Joabsson, A., and Christensen, T. R. (2001). Methane emissions from wetlands and their relationship with vascular plants: an arctic example. *Glob. Chang. Biol.* 7, 919–932. doi: 10.1046/j.1354-1013.2001.00044.x

Johansson, T., Malmer, N., Crill, P. M., Friborg, T., Åkerman, J. H., Mastepanov, M., et al. (2006). Decadal vegetation changes in a northern peatland, greenhouse gas fluxes and net radiative forcing. *Glob. Chang. Biol.* 12, 2352–2369. doi: 10.1111/j.1365-2486.2006.01267.x

Keiluweit, M., Nico, P.S., Kleber, M., and Fendorf, S. (2016). Are oxygen limitations under recognized regulators of organic carbon turnover in upland soils?. *Biogeochemistry* 127, 157–171. doi: 10.1007/s10533-015-0180-6

Keller, J. K., and Bridgham, S. D. (2007). Pathways of anaerobic carbon cycling across an ombrotrophic-minerotrophic peatland gradient. *Limnol. Oceanogr.* 52, 96–107. doi: 10.4319/lo.2007.52.1.0096

Keller, J. K., and Takagi, K. K. (2013). Solid-phase organic matter reduction regulates anaerobic decomposition in bog soil. *Ecosphere* 4:art54. doi: 10.1890/ES12-00382.1

Khadka, B., Munir, T. M., and Strack, M. (2016). Dissolved organic carbon in a constructed and natural fens in the Athabasca oil sands region, Alberta, Canada. *Sci. Total Environ. 557–558*, 579–589. doi: 10.1016/j.scitotenv.2016.03.081

Kim, S., Kramer, R. W., and Hatcher, P. G. (2003). Graphical method for analysis of ultrahigh-resolution broadband mass spectra of natural organic matter, the van krevelen diagram. *Anal. Chem.* 75, 5336–5344. doi: 10.1021/ac034415p

Kim, Y.-M., Nowack, S., Olsen, M. T., Becraft, E. D., Wood, J. M., Thiel, V., et al. (2015). Diel metabolomics analysis of a hot spring chlorophototrophic microbial mat leads to new hypotheses of community member metabolisms. *Front. Microbiol.* 6:209. doi: 10.3389/fmicb.2015.00209

Kind, T., Wohlgemuth, G., Lee, D. Y., Lu, Y., Palazoglu, M., Shahbaz, S., et al. (2009). FiehnLib: Mass spectral and retention index libraries for metabolomics based on quadrupole and time-of-flight gas chromatography/mass spectrometry. *Anal. Chem.* 81, 10038–10048. doi: 10.1021/ac9019522

Kohl, M., Wiese, S., and Warscheid, B. (2011). "Cytoscape: software for visualization and analysis of biological networks," in *Data Mining in Proteomics. Methods in Molecular Biology (Methods and Protocols)*, Vol. 696, eds M. Hamacher, M. Eisenacher, and C. Stephan (Humana Press). doi: 10.1007/978-1-60761-987-1_18

Kokfelt, U., Rosén, P., Schoning, K., Christensen, T. R., Förster, J., Karlsson, J., et al. (2009). Ecosystem responses to increased precipitation and permafrost decay in subarctic Sweden inferred from peat and lake sediments. *Glob. Chang. Biol.* 15, 1652–1663. doi: 10.1111/j.1365-2486.2009.01880.x

Koven, C. D., Schuur, E. A. G., Schädel, C., Bohn, T. J., Burke, E. J., Chen, X., et al. (2015). A simplified, data-constrained approach to estimate the permafrost carbon–climate feedback. *Philos. Trans. R Soc. A Math. Phys. Eng. Sci.* 373:20140423. doi: 10.1098/rsta.2014.0423

LaRowe, D. E., and van Cappellen, P. (2011). Degradation of natural organic matter: a thermodynamic analysis. *Geochim. Cosmochim. Acta* 75, 2030–2042. doi: 10.1016/j.gca.2011.01.020

Liao, J., Cao, X., Zhao, L., Wang, J., Gao, Z., Wang, M. C., et al. (2016). The importance of neutral and niche processes for bacterial community assembly differs between habitat generalists and specialists. *FEMS Microbiol. Ecol.* 92:fiw174. doi: 10.1093/femsec/fiw174

Limpens, J., Berendse, F., Blodau, C., Canadell, J. G., Freeman, C., Holden, J., et al. (2008). Peatlands and the carbon cycle: From local processes to global implications? *A synthesis. Biogeosci. Discussions* 5, 1379–1419. doi: 10.5194/bgd-5-1379-2008

Lin, X., Tfaily, M. M., Steinweg, J. M., Chanton, P., Esson, K., Yang, Z. K., et al. (2014). Microbial community stratification linked to utilization of carbohydrates and phosphorus limitation in a boreal peatland at Marcell experimental forest, Minnesota, USA. *Appl. Environ. Microbiol.* 80, 3518–3530. doi: 10.1128/AEM.00205-14

Longnecker, K., and Kujawinski, E. B. (2016). Using network analysis to discern compositional patterns in ultrahigh-resolution mass spectrometry data of dissolved organic matter. *Rapid Commun. Mass Spectrometry* 30, 2388–2394. doi: 10.1002/rcm.7719

Lucchese, M., Waddington, J. M., Poulin, M., Pouliot, R., Rochefort, L., and Strack, M. (2010). Organic matter accumulation in a restored peatland: evaluating restoration success. *Ecol. Eng.* 36, 482–488. doi: 10.1016/j.ecoleng.2009.11.017

Lupascu, M., Wadham, J. L., Hornibrook, E. R. C., and Pancost, R. D. (2012). Temperature sensitivity of methane production in the permafrost active layer at stordalen, Sweden: a comparison with non-permafrost Northern Wetlands. *Arct. Antarct. Alp. Res.* 44, 469–482. doi: 10.1657/1938-4246-44.4.469

Malmer, N., Johansson, T., Olsrud, M., and Christensen, T. R. (2005). Vegetation, climatic changes and net carbon sequestration in a North-Scandinavian subarctic mire over 30 years. *Glob. Chang. Biol.* 11, 1895–1909. doi: 10.1111/j.1365-2486.2005.01042.x

McCalley, C. K., Woodcroft, B. J., Hodgkins, S. B., Wehr, R. A., Kim, E.-H., Mondav, R., et al. (2014). Methane dynamics regulated by microbial community response to permafrost thaw. *Nature* 514, 478–481. doi: 10.1038/nature13798

McGuire, A. D., Anderson, L. G., Christensen, T. R., Dallimore, S., Guo, L., Hayes, D. J., et al. (2009). Sensitivity of the carbon cycle in the Arctic to climate change. *Ecol. Monogr.* 79, 523–555. doi: 10.1890/08-2025.1

McLatchey, G. P., and Reddy, K. R. (1998). Regulation of organic matter decomposition and nutrient release in a wetland soil. *J. Environ. Qual.* 27, 1268–1274. doi: 10.2134/jeq1998.00472425002700050036x

Mikutta, R., Turner, S., Schippers, A., Gentsch, N., Meyer-Stüve, S., Condron, L. M., et al. (2019). Microbial and abiotic controls on mineral-associated organic matter in soil profiles along an ecosystem gradient. *Sci. Rep.* 9:10294. doi: 10.1038/s41598-019-46501-4

Monard, C., Gantner, S., Bertilsson, S., Hallin, S., and Stenlid, J. (2016). Habitat generalists and specialists in microbial communities across a terrestrial-freshwater gradient. *Sci. Rep.* 6:37719. doi: 10.1038/srep37719

Muscarella, M. E., Boot, C. M., Broeckling, C. D., and Lennon, J. T. (2019). Resource heterogeneity structures aquatic bacterial communities. *ISME J.* 13, 2183–2195. doi: 10.1038/s41396-019-0427-7

Muyzer, G., and Stams, A. J. M. (2008). The ecology and biotechnology of sulphate-reducing bacteria. *Nat. Rev. Microbiol.* 6, 441–454. doi: 10.1038/nrmicro1892

Norby, R. J., Childs, J., Hanson, P. J., and Warren, J. M. (2019). Rapid loss of an ecosystem engineer: sphagnum decline in an experimentally warmed bog. *Ecol. Evol.* 9, 12571–12585. doi: 10.1002/ece3.5722

Novák, M., and Wieder, R. K. (1992). Inorganic and organic sulfur profiles in nine Sphagnum peat bogs in the United States and Czechoslovakia. *Water Air Soil Pollut.* 65, 353–369. doi: 10.1007/BF00479898

Pester, M., Knorr, K.-H., Friedrich, M. W., Wagner, M., and Loy, A. (2012). Sulfate-reducing microorganisms in wetlands – fameless actors in carbon cycling and climate change. *Front. Microbiol.* 3:72. doi: 10.3389/fmicb.2012.00072

Qualls, R. G., and Richardson, C. J. (2003). Factors controlling concentration, export, and decomposition of dissolved organic nutrients in the Everglades of Florida. *Biogeochemistry* 62, 197–229. doi: 10.1023/A:1021150503664

R Core Team (2019). *R: A Language and Environment for Statistical Computing.* Vienna: R Foundation for Statistical Computing. Available online at: http://www.R-project.org/

Raskin, L., Rittmann, B. E., and Stahl, D. A. (1996). Competition and coexistence of sulfate-reducing and methanogenic populations in anaerobic biofilms. *Appl. Environ. Microbiol.* 62, 3847–3857. doi: 10.1128/AEM.62.10.3847-3857.1996

Rasmussen, S., Wolff, C., and Rudolph, H. (1995). Compartmentalization of phenolic constituents in sphagnum. *Phytochemistry* 38, 35–39. doi: 10.1016/0031-9422(94)00650-I

Ravasz, E., Somera, A. L., Mongru, D. A., Oltvai, Z. N., and Barabási, A.-L. (2002). Hierarchical organization of modularity in metabolic networks. *Science* 297, 1551–1555. doi: 10.1126/science.1073374

Rawat, S. R., Männist,ö, M. K., Bromberg, Y., and Häggblom, M. M. (2012). Comparative genomic and physiological analysis provides insights into the role of Acidobacteria in organic carbon utilization in Arctic tundra soils. *FEMS Microbiol. Ecol.* 82, 341–355. doi: 10.1111/j.1574-6941.2012.01381.x

Rudolph, H., and Samland, J. (1985). Occurrence and metabolism of sphagnum acid in the cell walls of bryophytes. *Phytochemistry* 24, 745–749. doi: 10.1016/S0031-9422(00)84888-8

Schink, B. (1997). Energetics of syntrophic cooperation in methanogenic degradation. *Microbiol. Mol. Biol. Rev.* 61, 262–280. doi: 10.1128/.61.2.262-280.1997

Schuur, E. A. G., Bockheim, J., Canadell, J. G., Euskirchen, E., Field, C. B., Goryachkin, S. V., et al. (2008). Vulnerability of permafrost carbon to climate change: implications for the global carbon cycle. *Bioscience* 58, 701–714. doi: 10.1641/B580807

Shannon, P., Markiel, A., Ozier, O., Baliga, N. S., Wang, J. T., Ramage, D., et al. (2003). Cytoscape: a software environment for integrated models of biomolecular interaction networks. *Genome Res.* 13, 2498–2504. doi: 10.1101/gr.1239303

Singleton, C. M., McCalley, C. K., Woodcroft, B. J., Boyd, J. A., Evans, P. N., Hodgkins, S. B., et al. (2018). Methanotrophy across a natural permafrost thaw environment. *ISME J.* 12, 2544–2558. doi: 10.1038/s41396-018-0065-5

Solomon, S. (2007). Intergovernmental Panel on Climate Change and Intergovernmental Panel on Climate Change. *Climate Change 2007: The Physical Science Basis: Contribution of Working Group I To The Fourth Assessment Report of the Intergovernmental Panel on Climate Change.* Cambridge University Press.

Sriswasdi, S., Yang, C., and Iwasaki, W. (2017). Generalist species drive microbial dispersion and evolution. *Nat. Commun.*, 8, 1–8. doi: 10.1038/s41467-017-01265-1

Stalheim, T., Ballance, S., Christensen, B. E., and Granum, P. E. (2009). Sphagnan – a pectin-like polymer isolated from Sphagnum moss can inhibit the growth of some typical food spoilage and food poisoning bacteria by lowering the pH. *J. Appl. Microbiol.* 106, 967–976. doi: 10.1111/j.1365-2672.2008.04057.x

Sutton-Grier, A. E., Keller, J. K., Koch, R., Gilmour, C., and Megonigal, J. P. (2011). Electron donors and acceptors influence anaerobic soil organic matter mineralization in tidal marshes. *Soil Biol. Biochem.* 43, 1576–1583. doi: 10.1016/j.soilbio.2011.04.008

Svensson, B. H., and Rosswall, T. (1984). *In situ* methane production from acid peat in plant communities with different moisture regimes in a subarctic mire. *Oikos* 43, 341–350. doi: 10.2307/3544151

Tang, J., Yurova, A. Y., Schurgers, G., Miller, P. A., Olin, S., Smith, B., et al. (2018). Drivers of dissolved organic carbon export in a subarctic catchment: importance of microbial decomposition, sorption-desorption, peatland and lateral flow. *Sci. Total Environ. 622–623*, 260–274. doi: 10.1016/j.scitotenv.2017.11.252

Tfaily, M. M., Chu, R. K., Tolić, N., Roscioli, K. M., Anderton, C. R., Paša-Tolić, L., et al. (2015). Advanced solvent based methods for molecular characterization of soil organic matter by high-resolution mass spectrometry. *Anal. Chem.* 87, 5206–5215. doi: 10.1021/acs.analchem.5b00116

Tfaily, M. M., Chu, R. K., Toyoda, J., Tolić, N., Robinson, E. W., Paša-Tolić, L., et al. (2017). Sequential extraction protocol for organic matter from soils and sediments using high resolution mass spectrometry. *Anal. Chim. Acta* 972, 54–61. doi: 10.1016/j.aca.2017.03.031

Tfaily, M. M., Cooper, W. T., Kostka, J. E., Chanton, P. R., Schadt, C. W., Hanson, P. J., et al. (2014). Organic matter transformation in the peat column at Marcell experimental forest: humification and vertical stratification. *J. Geophys. Res. Biogeosci.* 119, 661–675. doi: 10.1002/2013JG002492

Tfaily, M. M., Wilson, R. M., Cooper, W. T., Kostka, J. E., Hanson, P., and Chanton, J. P. (2018). Vertical stratification of peat pore water dissolved organic matter composition in a peat bog in Northern Minnesota. *J. Geophys. Res. Biogeosci.* 123, 479–494. doi: 10.1002/2017JG004007

Thormann, M. N. (2006). Diversity and function of fungi in peatlands: a carbon cycling perspective. *Can. J. Soil Sci. 86*, 281–293. doi: 10.4141/S05-082

Timell, T. E. (1967). Recent progress in the chemistry of wood hemicelluloses. *Wood Sci. Technol.* 1, 45–70. doi: 10.1007/BF00592255

Tolić, N., Liu, Y., Liyu, A., Shen, Y., Tfaily, M. M., Kujawinski, E. B., et al. (2017). Formularity: software for automated formula assignment of natural and other organic matter from ultrahigh-resolution mass spectra. *Anal. Chem.* 89, 12659–12665. doi: 10.1021/acs.analchem.7b03318

Urban, N. R., Eisenreich, S. J., and Grigal, D. F. (1989). Sulfur cycling in a forested Sphagnum bog in northern Minnesota. *Biogeochemistry* 7, 81–109. doi: 10.1007/BF00004123

van Breemen, N. (1995). How Sphagnum bogs down other plants. *Trends Ecol. Evol. (Amst).* 10, 270–275. doi: 10.1016/0169-5347(95)90007-1

Van Krevelen, D. W. (1950). Graphical-statistical method for the study of structure and reaction processes of coal. *Fuel* 29, 269–284.

Wang, Y., Gabbard, H.D., and Pai, P. (1991). Inhibition of acetate methanogenesis by phenols. *J. Environ. Eng.* 117. doi: 10.1061/(ASCE)0733-9372(1991)117:4(487)

Ward, S. E., Bardgett, R. D., McNamara, N. P., and Ostle, N. J. (2009). Plant functional group identity influences short-term peatland ecosystem carbon flux: Evidence from a plant removal experiment. *Funct. Ecol.* 23, 454–462. doi: 10.1111/j.1365-2435.2008.01521.x

Watts, D. J., and Strogatz, S. H. (1998). Collective dynamics of 'small-world' networks. *Nature* 393, 440–442. doi: 10.1038/30918

Whiting and Chanton (1992). *Plant-Dependent CH4 Emission In A Subarctic Canadian Fen—Whiting—1992—Global Biogeochemical Cycles—Wiley Online Library.* (n.d.). Available online at: https://agupubs.onlinelibrary.wiley.com/doi/abs/10.1029/92GB00710 (accessed April 30, 2020).

Wickham, H. (2016). *ggplot2: Elegant Graphics for Data Analysis*. New York, NY: Springer-Verlag. doi: 10.1007/978-3-319-24277-4

Williams, C. J., Shingara, E. A., and Yavitt, J. B. (2000). Phenol oxidase activity in peatlands in New York state: response to summer drought and peat type. *Wetlands* 20, 416–421. doi: 10.1672/0277-5212(2000)020[0416:POAIPI]2.0.CO;2

Wilson, R. M., and Tfaily, M. M. (2018). Advanced molecular techniques provide new rigorous tools for characterizing organic matter quality in complex systems. *Rev. Geophys.* 1790–1795. doi: 10.1029/2018JG004525

Wilson, R. M., Tfaily, M. M., Rich, V. I., Keller, J. K., Bridgham, S. D., Zalman, C. M., et al. (2017). Hydrogenation of organic matter as a terminal electron sink sustains high CO2:CH4 production ratios during anaerobic decomposition. *Org. Geochem.* 112, 22–32. doi: 10.1016/j.orggeochem.2017.06.011

Woodcroft, B. J., Singleton, C. M., Boyd, J. A., Evans, P. N., Emerson, J. B., Zayed, A. A. F., et al. (2018). Genome-centric view of carbon processing in thawing permafrost. *Nature* 560, 49–54. doi: 10.1038/s41586-018-0338-1

Worm, B., Lotze, H. K., Hillebrand, H., and Sommer, U. (2002). Consumer versus resource control of species diversity and ecosystem functioning. *Nature* 417, 848–851. doi: 10.1038/nature00830

Zhou, L., Zhou, Y., Yao, X., Cai, J., Liu, X., Tang, X., et al. (2020). Decreasing diversity of rare bacterial subcommunities relates to dissolved organic matter along permafrost thawing gradients. *Environ. Int.* 134:105330. doi: 10.1016/j.envint.2019.105330

Conflict of Interest: HH was employed by the company Bruker Daltonics Inc. after the data was collected and while the manuscript was written.

The remaining authors declare that the research was conducted in the absence of any commercial or financial relationships that could be construed as a potential conflict of interest.

frontiers in Earth Science

ORIGINAL RESEARCH
published: 09 October 2020
doi: 10.3389/feart.2020.576510

Selection Cuttings as a Tool to Control Water Table Level in Boreal Drained Peatland Forests

Kersti Leppä[1], Hannu Hökkä[2], Raija Laiho[1], Samuli Launiainen[1], Aleksi Lehtonen[1], Raisa Mäkipää[1], Mikko Peltoniemi[1], Markku Saarinen[3], Sakari Sarkkola[1] and Mika Nieminen[1]*

[1]Natural Resources Institute Finland, Helsinki, Finland, [2]Natural Resources Institute Finland, Oulu, Finland, [3]Natural Resources Institute Finland, Tampere, Finland

Continuous cover management on peatland forests has gained interest in recent years, in part because the tree biomass with significant evapotranspiration capacity retained in selection cuttings could be used as a tool to optimize the site water table level (WTL) from both tree growth and environmental perspectives. This study reports WTL responses from six field trials established on fertile Norway spruce–dominated drained peatland forests across Finland. At each site, replicates of different intensity selection cuttings (removing 17–74% of the stand basal area) or clear-cut in parallel with intact control stands were established and monitored for the WTL for 2–5 postharvest years. The observed WTL rose after selection cuttings, and the response increased with harvest intensity and depended on the reference WTL; that is, larger responses were found during dry summers or in more southern location. Selection cuttings removing about 50% of the stand basal area raised the WTL typically by 15–40%. Using a process-based ecohydrological model, tested against data from the field trials, we show that the role of tree stand in controlling the WTL clearly decreases along the latitudinal climate gradient in Finland. This suggests that the potential of controlling WTL using selection cuttings is more prominent in southern than in northern Finland. Predictions with future climate (2070–2099) further indicated a general decrease of the WTL and that the importance of the tree stand in controlling the WTL will increase, especially in northern Finland. The results overall thus suggest that selection cuttings can be used as a tool to control the WTL in boreal drained peatland forests, and the potential is likely to increase in future climate.

Keywords: continuous cover forestry, drainage, hydrology, partial harvesting, peatland forestry, selection cutting, water table level

OPEN ACCESS

Edited by:
Matthias Peichl, Swedish University of Agricultural Sciences, Sweden

Reviewed by:
Zhenming Ge, East China Normal University, China
Hongkai Gao, East China Normal University, China

****Correspondence:***
Kersti Leppä
kersti.leppa@luke.fi

Specialty section:
This article was submitted to Hydrosphere, a section of the journal Frontiers in Earth Science

Received: *29 June 2020*
Accepted: *04 September 2020*
Published: *09 October 2020*

Citation:
Leppä K, Hökkä H, Laiho R, Launiainen S, Lehtonen A, Mäkipää R, Peltoniemi M, Saarinen M, Sarkkola S and Nieminen M (2020) Selection Cuttings as a Tool to Control Water Table Level in Boreal Drained Peatland Forests. Front. Earth Sci. 8:576510. doi: 10.3389/feart.2020.576510

INTRODUCTION

About 15 Mha of peatlands and wetlands have been drained for forestry purposes in the temperate and boreal zones (Paavilainen and Päivänen, 1995). The water table level (WTL) in peat soil is the key to their environmentally and economically feasible management. Too high WTL is detrimental to tree growth and vitality, making WTL lowering by drainage a necessary forest operation on the majority of peatlands. At the same time, drainage and ditch cleaning are substantial sources of sediments and particulate nutrients to receiving water courses (Joensuu et al., 1999; Nieminen et al., 2010; Stenberg et al., 2015; Nieminen et al., 2017a). In fact, ditch cleaning is currently regarded as the most harmful forestry operation affecting surface water quality in Finland (Finér et al., 2010).

Compared with mineral soil forests, maintenance of ditch networks is also a significant extra cost which impacts the overall economic profitability of peatland forestry (Ahtikoski et al., 2008; Ahtikoski et al., 2012). However, Sarkkola et al. (2010), Sarkkola et al. (2012), and Sarkkola et al. (2013) suggest that ditch cleaning is unnecessary in high-volume peatland stands, which has given rise to the idea of growing peatland forests according to the principles of continuous cover forestry (CCF) instead of rotation-based management with clear-cuts (Nieminen et al., 2018a).

CCF, which relies on regular partial harvests, could also address other environmental consequences that rotation-based management on peatlands induces. After clear-cutting, the rise of WTL to near the soil surface results in anoxic redox reactions, enhancing the mobilization and outflow of redox-sensitive compounds, such as phosphate, iron, and dissolved organic nitrogen and carbon (Kaila et al., 2014; Kaila et al., 2015; Nieminen et al., 2015). High WTL after clear-cutting may also increase methane (CH_4) emissions, particularly when the WTL rises higher than 30 cm below the soil surface (Ojanen et al., 2010; Ojanen et al., 2013; Korkiakoski et al., 2019). Also, very low WTL, prevailing in densely stocked stands, may be environmentally unfavorable. Ojanen et al. (2010), Ojanen et al. (2013), and Ojanen and Minkkinen (2019) showed high carbon dioxide (CO_2) and nitrous oxide (N_2O) emissions from drained peatland forests with a low WTL, presumably because of enhanced peat decomposition of deep peat layers. Lowering of the WTL and consequent diffusion of oxygen into deep peat layers are also thought to explain why nitrogen and phosphorus exports have been shown to increase from drained peatland forests across Finland (Nieminen et al., 2017b; Nieminen et al., 2018b).

To summarize, the aim of CCF would be to manage peatland forests in such a way that i) WTL does not rise near the soil surface (reduced tree growth, enhanced CH_4 emissions, export of redox-sensitive nutrients, and need for drainage) and ii) WTL does not drop very deep, causing enhanced decomposition of deep peat layers (CO_2 and N_2O emissions and exports of mineralized nitrogen and phosphorus). According to Nieminen et al. (2018a), this not only would be beneficial from environmental perspectives but could also present economical savings by avoiding ditch cleaning and site preparation. They hypothesize that executing partial harvests, such as selection or gap cuttings, instead of clear-cutting would raise the WTL only marginally. Also, as the average stand volumes maintained in CCF forests would be lower than those in mature forests approaching clear-cut, the WTL would not drop as deep as in rotation-based management.

The feasibility of CCF thus comes down to the relationship between tree stand characteristics and WTL, which are linked through the water balance of the peatland strip. The stand intercepts and evaporates (E_c) part of the incoming precipitation (P), and takes up water from the soil by transpiration (T), while WTL dynamics reflect the changes in soil water storage (dS/dt). Additionally, the water balance is affected by forest floor evaporation (E_f) and runoff (Q):

$$\frac{dS}{dt} = P - \left(T + E_c + E_f \right) - Q, \quad (1)$$

where $T + E_c + E_f$ form total evapotranspiration (ET). Stand interception evaporation has been suggested to scale almost linearly with stand density (Mazza et al., 2011), whereas transpiration responds in a nonlinear manner as light availability decreases in more dense canopies (Bréda et al., 1995; Lagergren and Lindroth, 2004; Launiainen et al., 2016). Forest floor evaporation depends on the amount of throughfall and radiation reaching the forest floor; thus, it is generally higher the more open the canopy (Boczoń et al., 2016; Launiainen et al., 2019). Last, the role of runoff depends on ditching parameters, peat properties, WTL, and rainfall amount and frequency, meaning that it is more pronounced during wet years and sites with low ET (Sarkkola et al., 2013).

The relationship between mean growing season WTL and stand properties on drained peatland forests is commonly acknowledged (Ahti and Hökkä, 2006; Hökkä et al., 2008b; Sarkkola et al., 2010), but the shape and strength of the relationship vary with climatic conditions, site type, and drainage configuration (Hökkä et al., 2008a; Sarkkola et al., 2010). To date, this relationship has typically been studied by comparing WTLs across sites of varying stand density (e.g., Hökkä et al., 2008a; Sarkkola et al., 2010) and only seldom by implementing harvests of different intensities and monitoring responses to WTL (Heikurainen and Päivänen, 1970; Päivänen, 1982; Päivänen and Sarkkola, 2000). As CCF would rely on such harvests, it is important to study the stand properties to WTL relationship in such setup and to understand how the relationship is affected by varying stand and drainage characteristics across climatic regions. This has been mostly omitted in earlier studies as they were limited to single sites (Heikurainen and Päivänen, 1970; Päivänen and Sarkkola, 2000), with the exception of Päivänen (1982) who studied harvest responses in spruce- and pine-dominated stands, however, in close proximity to each other.

In this work, we quantify and predict the effects of selection cuttings and the role of tree stand on the WTL in drained peatland forests. Specifically, we address the following research questions:

(1) How does growing season WTL respond to selection cuttings?
(2) How does the role of the tree stand vary along the climatic gradient in Finland?
(3) How will climate change affect WTL and its response to stand characteristics?

To find answers to these questions, six field trials were established on fertile Norway spruce-dominated drained peatland forests in Finland. At each site, replicated study plots with different intensity selection cuttings (removing 17–74% of the stand basal area) or clear-cutting in parallel with intact control stands were monitored for WTL for 2–5 postharvest years. The empirical results were complemented with predictions by a process-based ecohydrological model, which we validate against the field observations. The model is further used to generalize the WTL responses of selection cuttings of various

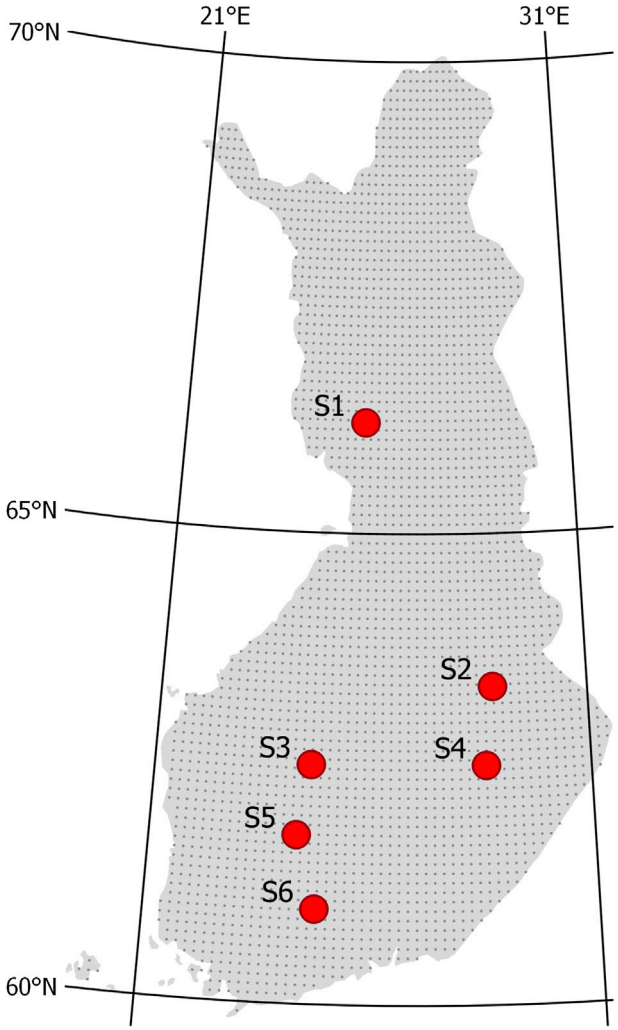

FIGURE 1 | Location of study sites S1–S6 in Finland. Gray dots indicate resolution used in generalizing climate simulations (see section *Scenario Simulations for Current and Future Climate*).

intensities over the climate gradient in Finland in current and future climate.

STUDY SITES

General Descriptions

The six study sites covered a latitude gradient from 61.0 to 66.2°N in Finland (**Figure 1**; **Table 1**). The sites represented a range of drained Norway spruce (*Picea abies*)–dominated peatland forests with varying mixture of downy birch (*Betula pubescens*) and Scots pine (*Pinus sylvestris*). Sites S1, S4, and S6 represented the highest fertility level of drained peatland forests, classified as herb-rich type according to Laine (1989). S2 and most of S3 represented the *Vaccinium myrtillus* type, and part of S3 and S5 the *Vaccinium vitis-idaea* type. The peat layer was more than 1 m thick in other sites, except S1 and parts of S3. Peat in S2, S4, and S6 was characterized by sedge (*Carex*) remains, and in other sites, a mixture of *Sphagnum* mosses and decomposed wood. The sites were drained for forestry in 1940–1960s and managed at least once by ditch network maintenance. At present, the ditch networks are in poor or moderate condition with large variation in depth (**Table 1**). The stands approached maturity before selection harvestings, and Norway spruce occurred in the understory below the stand canopy. According to the tree diameter distribution, all the stands had structural inequalities and can be regarded as uneven-aged having J-shaped, skewed, or two-storied size distribution before harvesting.

Harvesting Treatments and Field Measurements

Each site had 4–16 permanent sample plots (**Figure 2**), whose area varied between 970 and 2,000 m^2. The plots were treated either with selection cutting or clear-cutting, or left intact as control plots (no harvest) each having two to five replicates. The setup assumes neighboring plots on same strip are independent, that is, that the WTL rise in one plot does not affect that of the neighboring plot. This may not always be true (cf. Koivusalo et al., 2008), but here this concern is addressed by having replicates of each treatments and control plots at each site unlike in earlier studies (Heikurainen and Päivänen, 1970; Päivänen, 1982; Päivänen and Sarkkola, 2000).

Selection cuttings were performed at different intensities with the target postharvest stand basal area varying from 6 to 17 $m^2\ ha^{-1}$. The emphasis of the harvest removal was on the upper half of the stand diameter at breast height (DBH) distribution within each plot, retaining the suppressed and understory trees and also some of the largest trees. Harvestings were carried out during winter in 2015–2018 (**Table 1**). For details of all experimental plots, see **Supplementary Table 3**.

Before harvest, stand measurements were performed at each experimental plot recording species and DBH of all trees taller than 1.3 m. Additionally, on average, 45 sample trees per plot representing the whole diameter distribution of that plot were measured for tree height and crown base height. Except for site S5, all the trees to be removed were measured and marked before harvesting. At S5, stand measurements were conducted after harvest, and the DBH of harvested trees (d, cm) was derived from stump diameter of felled trees (d_s, cm):

$$d = \frac{1}{1.25}(d_s - 2). \quad (2)$$

WTL (level of the water table relative to the soil surface) was monitored manually from nine ground water tubes (32 mm diameter) installed in each experimental plot in a form of a regular grid (3 × 3). The tubes were perforated (3 mm holes) from the bottom to a height about 10 cm below peat surface and were installed down to 1 m depth or, in thinner peated sites, down to the subsoil below peat. Measurements were taken during growing seasons at 1- to 2-week intervals during 2015–2019, except for site S1 where monitoring started already in September 2014.

TABLE 1 | Site characteristics of the studied experimental stands on drained peatland forests in Finland.

Site	Location	Precipitation (mm y^{-1})[a]	Temperature sum (degree-days C)[a]	Preharvest basal area (m^{-2} ha^{-1})	Species shares of basal area (S:P:B)	Site type[b]	Peat type	Peat thickness (m)	Ditch spacing (m)	Ditch depth (m)	Time of harvest
S1	66.18°N, 25.67°E	610	1,080	21–32	74:0:26	Rhtkg	*Sphagnum*	0.4–0.6	40–60	0.3–0.8	March 2015
S2	63.38°N, 28.78°E	730	1,180	19–29	70:5:25	Mtkg	*Carex*	>1.0	25–60	0.4	February 2017
S3	62.54°N, 24.58°E	660	1,200	26–31	70:16:14	Mtkg-ptkg	*Sphagnum*	0.3–1.0	30–40	0.3	March 2016
S4	62.54°N, 28.59°E	700	1,410	21–24	65:16:19	Rhtkg	*Carex*	>1.0	40–75	0.4	February 2017
S5	61.79°N, 24.30°E	680	1,320	21–38	31:45:23	Ptkg	*Sphagnum*	>1.0	50	0.9–1.05	February 2018
S6	61.01°N, 24.75°E	590	1,460	22–31	98:0:2	Rhtkg	*Carex*	>1.5	65–70	0.55–0.7	February 2017

[a]*Mean values for period 2006–2019.*
[b]*Classification according to Laine (1989).*

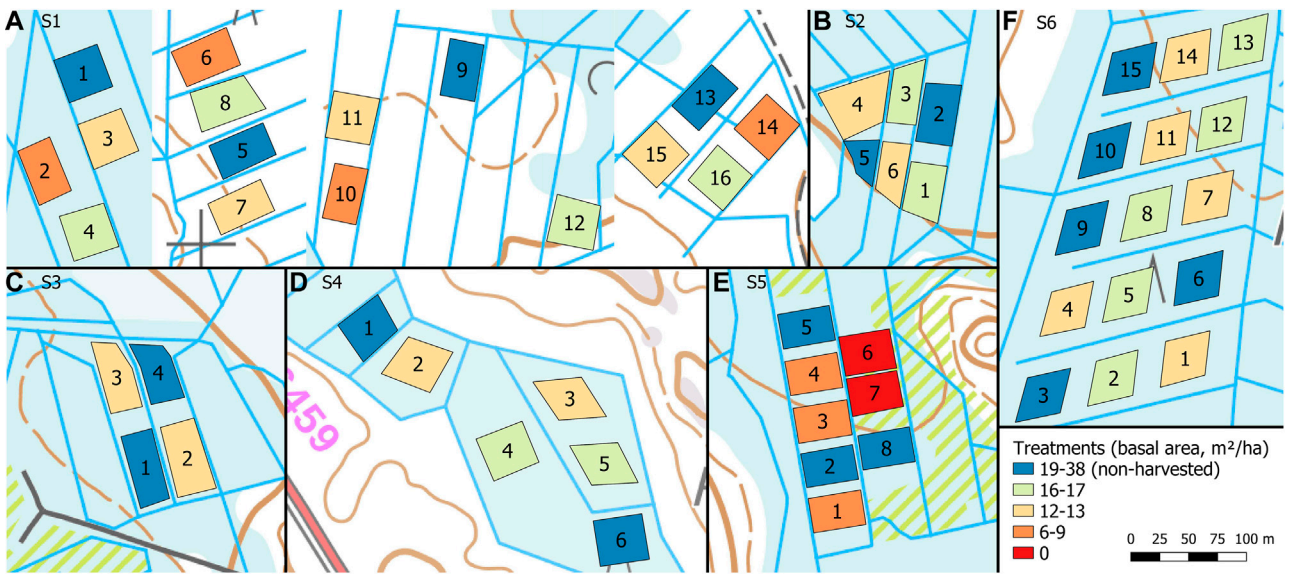

FIGURE 2 | Experimental plots in the study sites S1–S6 **(A–F)** categorized by the postharvest stand basal area. Site S1 **(A)** was composed of four blocks located 0.2–2.5 km apart. Background map: basic map raster © National Land Survey of Finland March 2020.

METHODS

Water Table Level Data Analysis

The nine WTL observations for each plot j of site i at the observation time t were aggregated as median values:

$$WTL_{i,j}(t) = \underset{k=1\ldots9}{\text{med}}\left\{WTL_{i,j,k}(t)\right\}, \quad (3)$$

where k stands for the tube number. Occasionally, the number of observations from plot j at time t was less than nine due to dry or frozen tubes. Medians (**Eq. 3**) were not derived if there were less than four observations at time t.

In order to predict the WTL response to harvest, we applied the paired catchment approach (e.g., Kaila et al., 2014) within each site (subscript i omitted from **Eqs 4–6**). First, ordinary least square linear regressions were fitted between WTL of each plot (j) and control plots (j_{ctrl}) for the preharvest period.

$$WTL_j(t) = a_{j,j_{ctrl}} WTL_{j_{ctrl}}(t) + b_{j,j_{ctrl}} + \varepsilon. \quad (4)$$

Second, these linear models were applied to predict reference WTL (corresponding to non-harvested conditions) for each plot for the postharvest period as the arithmetic mean of the predictions based on individual parallel control plots.

$$WTL_j^{ref}(t) = \underset{j_{ctrl}}{\text{mean}}\left\{a_{j_{tr},j_{ctrl}} WTL_{j_{ctrl}}(t) + b_{j_{tr},j_{ctrl}}\right\}. \quad (5)$$

Comparing the predicted reference WTL to the observed postharvest WTL gives the WTL response to harvest at plot j:

$$\Delta WTL_j(t) = WTL_j(t) - WTL_j^{ref}(t). \quad (6)$$

To analyze the dependence of the WTL response on harvest intensity at each site i, we explored the fit of the following ordinary least square regression model:

$$WTL_{i,j,year} = \left(c_i + d_i \cdot f_{BA_{i,j}}\right) WTL_{i,j,year}^{ref} + \varepsilon, \quad (7)$$

where WTL and WTL^{ref} are given as yearly mean values during June–October, and f_{BA} is the fraction of the removed basal area compared to the preharvest conditions.

Yearly (June–October) values for $WTL_{i,j}$ and $\Delta WTL_{i,j}$ were further used to analyze the performance of the applied ecohydrological model (sections *Model Description* and *Application to Study Sites*).

Modeling Water Table Level

Model Description

In order to simulate WTL dynamics, we combined the aboveground modules from the SpaFHy-model (Launiainen et al., 2019) with a simple hydrological description of the peat profile and lateral ditch drainage. The adopted SpaFHy modules describe rainfall and snow interception by the canopy and a moss/litter layer, snow accumulation and melt, infiltration to soil profile, and ET components. SpaFHy runs on a daily time step applying daily precipitation, air temperature, global radiation, photosynthetically active radiation, mixing ratios of H_2O and CO_2, and wind speed as meteorological forcing. SpaFHy accounts for leaf area index (LAI) dynamics of deciduous species and their different photosynthetic capacity compared to conifers. Thus, model parameters include LAI (one-sided) separately for conifers and deciduous trees. Further stand characteristics required by the model are canopy closure and dominant tree height.

The only modifications compared to Launiainen et al. (2019) was made to the soil moisture limit on canopy stomatal conductance. We described it following Koivusalo et al. (2008), but excluding the restriction of stomatal conductance during wet conditions:

$$f_w = \begin{cases} \min\left(0.5\left(1 + \dfrac{\theta - \theta_{r1}}{\theta_{r0} - \theta_{r1}}\right), 1.0\right), & \theta > \theta_{r1} \\ \max\left(0.5\left(\dfrac{\theta - \theta_{wp}}{\theta_{r1} - \theta_{wp}}\right), 0.0\right), & \theta < \theta_{r1} \end{cases} \quad (8)$$

where f_w (unitless) is the moisture limit, θ ($m^3\ m^{-3}$) is the mean moisture content in the rooting zone, and θ_{r0}, θ_{r1}, and θ_{wp} ($m^3\ m^{-3}$) are the root zone moisture contents corresponding to the pressure heads of −0.7, −1.2, and −150 m, respectively. Root zone depth was defined as 0.2 m (Koivusalo et al., 2008).

The below ground hydrology is described by a 2-m-deep peat profile that stores infiltrated water and loses water due to transpiration, ditch drainage, and, in case of full saturation, surface runoff. WTL in the profile is computed based on the amount of water stored in the profile assuming hydraulic equilibrium (constant hydraulic head in vertical dimension, Skaggs, 1980). The function between water storage and WTL depends on peat water retention characteristics (van Genuchten) defined for the peat profile (see section *Application to Study Sites*). The function was obtained from tabulated values of water storage and WTL computed at 1mm intervals prior to simulations. The root zone moisture content (needed in **Eq. 8**) is computed using the same assumption of hydraulic equilibrium.

Drainage from the peat profile to the ditches follows Hooghoudt (1940) equation, but neglecting drainage from below the ditches which was considered minor:

$$Q = 4\,K_{sat}\left(\frac{WTL + D_d}{L}\right)^2, \quad (9)$$

where Q ($m\ d^{-1}$) is the drainage, D_d (m) is the depth of the ditches, K_{sat} ($m\ d^{-1}$) is the hydraulic conductivity of the saturated layer above the ditch bottom, and L (m) is the distance between the ditches. The hydraulic conductivity of the profile is defined by 0.1 m layers; thus, K_{sat} is a function of WTL.

Summary from the free-air CO_2 enrichment (FACE) studies (Ainsworth and Rogers, 2007) and theoretical arguments (Katul et al., 2010; Medlyn et al., 2011) both suggest leaf and canopy stomatal conductance decrease with increasing atmospheric CO_2 concentrations, leading to reduced transpiration rates in future climates. We account the effect of CO_2 (ppm) concentration on canopy stomatal conductance through a modifier function (unitless):

$$f_{CO_2} = 1.0 - 0.387 \ln\left(\frac{CO_2}{380}\right), \quad (10)$$

where 380 ppm is the reference CO_2 concentration. **Equation 10** is based on predictions of a multilayer ecosystem model, parameterized for boreal coniferous forests (Launiainen et al., 2015; Launiainen et al., 2016), run using various atmospheric CO_2 mixing ratios. It results into about 15% reduction in canopy stomatal conductance for 1.5-fold rise in atmospheric CO_2 concentration from reference 380 ppm, in line with FACE experiments (Ainsworth and Rogers, 2007).

Application to Study Sites

The model was run for the unharvested and harvested stands of each plot on each site resulting in 55 (non-harvested stands) + 38 (harvested stands) = 93 modeling cases. The simulation period was 2010–2019 to ensure appropriate model spin-up before the monitoring period. Simulated WTL and WTL responses to harvests were evaluated against the observations. We evaluated the model performance using site average mean absolute error (MAE):

$$MAE = \underset{i}{\text{mean}}\left\{\underset{j,year}{\text{mean}}\left\{\left|X_{i,j,year} - X_{i,j,year}^{mod}\right|\right\}\right\}, \quad (11)$$

where X is either WTL or ΔWTL (m), and superscript *mod* stands for modeled. In the case of ΔWTL, *MAE* includes only treated plots and postharvest years.

For forcing data, we used spatially averaged (10 km^2 × 10 km^2 resolution or 1 km^2 × 1 km^2 since July 2016) daily meteorological data obtained from the Finnish Meteorological Institute (FMI) weather stations and provided by the FMI (Aalto et al., 2013). Additionally, we checked if there were FMI precipitation stations closer by our sites than the weather stations. That was true for one site (S4), for which we used precipitation data from that station instead of the gridded weather station data. Unavailable forcing variables were defined as follows: photosynthetically active radiation as 45% of global radiation, wind speed as constant 2.0 m s^{-1}, and CO_2 mixing ratio as 400 ppm.

Stand parameters for the pre- and postharvest stand of each plot were derived from tree stand measurements (see **Supplementary Material**). First, species-specific equations for tree height and crown base height were fitted to the sample trees, and then the fitted models were used to predict tree height and crown base height for all measured trees. This allowed us to determine dominant tree height for each plot. Because tree heights and crown base heights from the same site were correlated, we applied nonlinear mixed-effects models to account for the correlation. We assumed that the relationships between diameters and tree heights and crown heights of the same species follow similar functional form and applied model formulation named "Curtis" provided by *lmfor* R package (Mehtätalo et al., 2015; Mehtätalo, 2019). Application of mixed models by tree species allowed us to use the random part of the model to estimate calibrated heights and crown base heights for each tree by site ensuring more precise estimates for each tree (Lappi, 1991). Second, one-sided LAI was derived separately for conifers and deciduous species based on DBH, crown base height, and tree height using foliage biomass functions (Tupek et al., 2015; Lehtonen et al., 2020) and specific leaf area values (Härkönen et al., 2015). When estimating LAI, we assumed that 50% of needle mass were sunlit leaves and 50% shaded leaves; this assumption was made due to relative high basal area within these stands. Canopy closure was estimated based on the basal area (model fitted to data presented by Korhonen et al. (2007)):

$$f_c = \frac{0.1939 * BA}{0.1939 * BA + 1.69}, \quad (12)$$

where f_c (unitless) is the canopy closure and BA (m^{-2} ha^{-1}) is the basal area. For clear-cut sites, LAI was set 0.5 m^2 m^{-2}, height of the vegetation to 0.5 m, and canopy closure to 0.1.

For each plot, ditch spacing was determined from maps, and ditch depth was either measured in the field (sites S1, S5, and S6) or estimated from 2 m^2 × 2 m^2 digital elevation model provided by the National Land Survey of Finland. These as well as the stand parameters for each plot are listed in the **Supplementary Table 3**.

The water retention characteristics and saturated hydraulic conductivities of the soil profiles were defined based on the peat type at the site (**Table 1**). Typical profiles for *Sphagnum* and *Carex* peat were derived from the datasets collected by Päivänen (1973). Below 0.1 m from the soil surface, the water retention characteristics were based on the fit to all peat type–specific (*Carex*/*Sphagnum*) data presented by Päivänen (1973), while the water retention parameters of the topmost 0.1 m were set based on the *Carex*/*Sphagnum* sample with the poorest water retention capacity (**Figure 3**). Saturated hydraulic conductivity for each 0.1 m layer was defined in relation to depth with the peat type–specific functions presented by Päivänen (1973), restricting it to a minimum 0.01 m d^{-1}. Conductivities of the 0–0.1, 0.1–0.2, and 0.2–0.3 m layers from the soil surface were multiplied by 30, 20, and 10, respectively, to represent anisotropy which results in the surface peat having a much larger horizontal conductivity than the deeper peat layer (Koivusalo et al., 2008; Haahti et al., 2016).

Scenario Simulations for Current and Future Climate

To explore to the potential of selection cuttings in controlling WTL in current and future climate, we run scenario simulations at a 0.1-grid resolution for entire Finland (**Figure 1**). As forcing, we used reference period (1981–2010) and future (2070–2099) climate scenario data. The climate scenario dataset consisted of bias-corrected predictions of weather parameters from the five global climate models (CanESM2, CNRM, GFDL, HadGEM2, and MIROC5) (Lehtonen et al., 2016) for three representative concentration pathways RCP2.6 (low emission scenario), RCP4.5 (moderate emission scenario), and RCP8.5 (high emission scenario). Bias correction in the dataset used gridded weather data from the reference period (Aalto et al., 2013), and applied methods are described in Räisänen and Räty (2013) and Räty et al. (2014). The simulations were run both with and without the CO_2 effect on canopy stomatal conductance described by **Eq. 10**.

The scenario simulations were run with the stand basal area varying from 6 to 30 m^{-2} ha^{-1} (at 6 m^{-2} ha^{-1} intervals, i.e., 5 levels). LAI corresponding to these values was estimated based on the LAI to basal area relationship obtained using a linear regression and the data from the study sites (excluding stands with high share of pines which have low LAI to basal area ratio). This resulted in LAI ranging from 1.4 to 6.7 m^2 m^{-2}. Canopy closure was estimated using **Eq. 12**. Other model parameters were set to the mean values of study sites and peat type as *Carex* (**Table 2**).

RESULTS

Observed Water Table Level Responses at Study Sites

The mean preharvest WTL varied typically by 0.1–0.2 m between parallel plots of the same site, except for site S1 where the difference was up to 0.4 m (**Figure 4**). Control plot WTL during pre- and postharvest periods further indicates that meteorological conditions of these periods were different. For example, at site S5 (**Figure 4E**), the mean WTL at the control plots before harvest was about 0.1 m higher than that after harvest during 2018–2019, which were both dry and warm summers. Thus, comparing postharvest WTL of treated plots directly to that

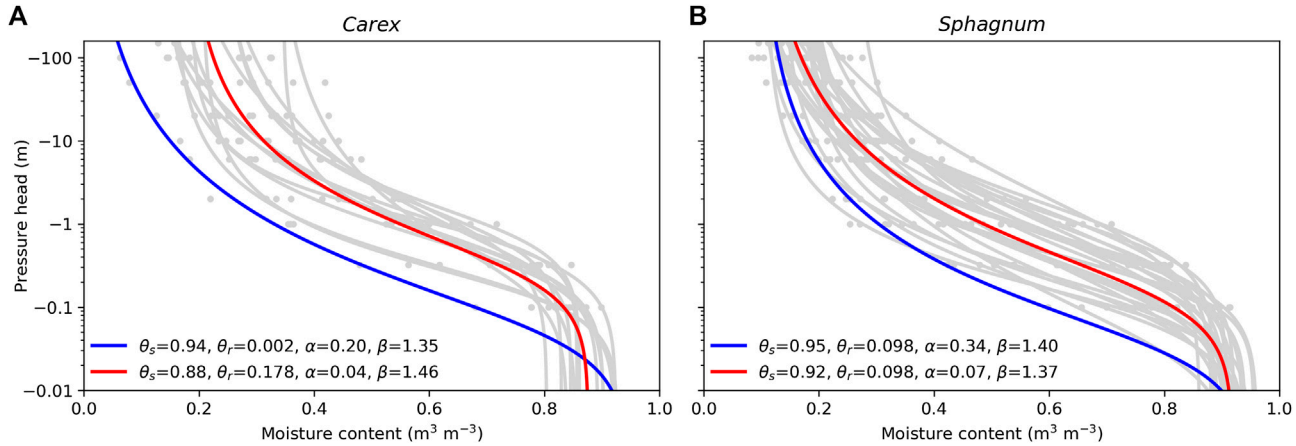

FIGURE 3 | Water retention of *Carex* **(A)** and *Sphagnum* **(B)** samples published by Päivänen (1973): water retention curves for individual samples in gray, for whole data in red, and for sample with poorest water retention capacity in blue. θ_s = soil porosity; θ_r = residual water content; α, β = van Genuchten water retention curve parameters.

TABLE 2 | Parameter values applied in scenario simulations.

Parameter	Value
Ditch spacing (m)	50
Ditch depth (m)	0.5
Peat type	*Carex*
Fraction of decidious species leaf area index (–)	0.15
Dominant height (m)	21

of control plots or to the preharvest WTL could be misleading, and therefore we used the paired catchment approach (see section *Water Table Level Data Analysis*).

Generally, WTL of harvested plots rose compared to the reference WTL predicted for each plot based on their parallel control plots (**Table 3**). At site S1 and for the less intensive harvest at site S2, the responses were less than 0.05 m (**Table 3**). The response of WTL was the stronger the more intense the harvest and the deeper the reference WTL (**Figure 5**). This is particularly evident at sites S4 and S6 where **Eq. 7** produces a good fit (**Figures 5D,F**). The explanatory variable describing the influence of harvest intensity (f_{BA}) was significant (p-value < 0.01) for all sites, except S1. **Figure 5** also indicates how well WTL at control plots ($f_{BA} = 0$) was predicted based on their parallel control plots. Especially at site S1, the variability around the 1:1 line is large, which probably was caused by the short monitoring period before harvest, causing uncertainty to the fit of **Eq. 4**. Consequently, also the reference WTL of the treated plots contains uncertainty. On the other hand, **Figure 4A** and **Table 3** also suggest that there might not be a clear response to WTL caused by harvest at site S1. The coefficients of the fitted regression model for sites S3, S5, and S6 (**Figures 5C,E,F**) were similar, suggesting that harvesting X% of the basal area would result in a WTL increase of about 0.55X%, where X is between 0 (i.e., no harvest) and 100 (i.e., clear-cut). The WTL responses were more pronounced at site S4, which on average had the smallest preharvest stand basal area (**Figure 5D**). At site S2, where only the higher intensity harvest showed a clear increase in WTL (**Table 3**), it is suggested that the response between WTL and stand basal area is not linear as assumed by **Eq. 7**.

Simulating Water Table Level at Study Sites

The years 2018 and 2019, coinciding with the postharvest periods, were dryer and warmer than long-term averages (Pirinen et al., 2012) in many parts of Finland. The annual mean WTL was well reproduced by the model during preharvest at all sites (**Figure 6A**), but after harvest, WTL was underestimated for the dry years, especially 2018 (**Figure 6B**). Nevertheless, the site mean WTL responses to harvests (see **Eq. 6**) do not show systematic bias during the dry years (**Figure 6B**), excluding S5 where the WTL response was overestimated by about 0.1 m. **Figures 6D–F** further illustrate how the variability between plots at each site is captured by the model. Before harvest, observations show larger variability between plots of the same site than the model results (**Figure 6D**). The between-plot variability increases after harvest, which is generally well captured (**Figure 6E**). **Figure 6F** indicates that plot-level WTL responses are well reproduced, except for sites S1 and S5. At site S1, the poor correspondence between the model results and the observation was expected based on **Figure 5A**. For S1, only the site annual mean WTL could be predicted by the model (**Figures 6A,B**), while the between-plot variability both before and after harvest remained unresolved (**Figures 6D,E**).

The site average MAE (see **Eq. 11**) was 0.099 m for WTL and 0.062 m for the WTL response. To assess the impact of site- and plot-specific parameters (ditch spacing, ditch depth, peat type, stand LAI, and fraction of deciduous species LAI) and meteorology on the model performance, we run the simulations by setting each of these constant one by one. The constant value applied for the parameters corresponded to the mean of all sites, whereas the effect of meteorology was tested by setting it to that of S3 for all sites, and the peat type was set in turns to *Carex* and *Sphagnum*. The change caused to model performance (MAE for WTL) in each case is visualized in **Figure 7**. Meteorology had an obvious effect on model

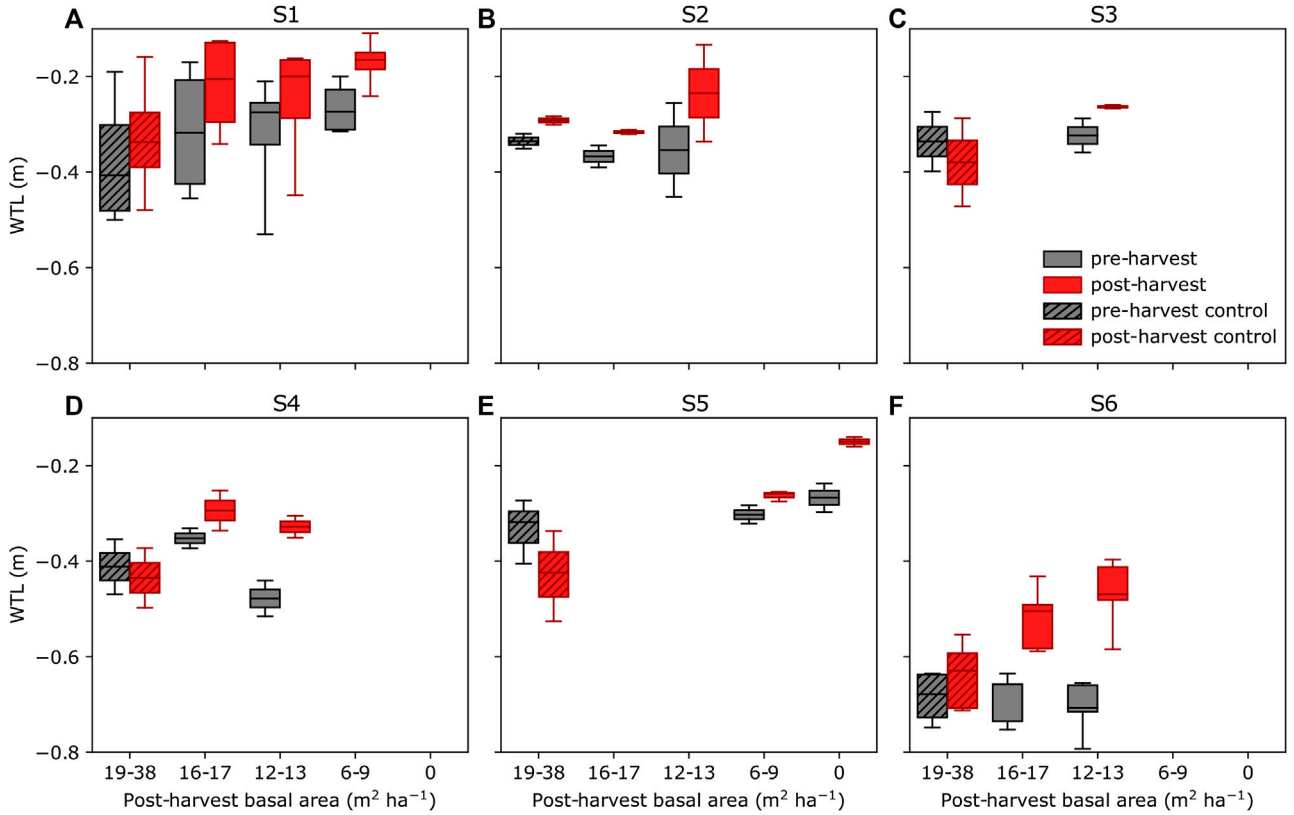

FIGURE 4 | Mean water table level (WTL) before harvest (gray) and after harvest (red) at sites S1–S6 **(A–F)** grouped by treatments (see **Figure 2**) during June–October. Data from non-harvested control plots are indicated by hatching. The boxplots indicate the median, the 25–75% percentile, and the min–max range.

TABLE 3 | Mean water table response to harvest (see **Eq. 6**) at sites S1–S6 grouped by treatments (i.e., postharvest stand basal area, $m^2\ ha^{-1}$) during June–October.

Site\treatment	Water table level response (m)[a]			
	16–17 $m^2\ ha^{-1}$	**12–13 $m^2\ ha^{-1}$**	**6–9 $m^2\ ha^{-1}$**	**0 $m^2\ ha^{-1}$**
S1	0.04 (±0.012)	0.02 (±0.006)	0.05 (±0.031)	—
S2	0.01 (±0.015)	0.09 (±0.01)	—	—
S3	—	0.10 (±0.032)	—	—
S4	0.08 (±0.02)	0.18 (±0.016)	—	—
S5	—	—	0.13 (±0.019)	0.20 (±0.023)
S6	0.12 (±0.005)	0.18 (±0.014)	—	—

[a]*SE in parenthesis, with number of replicates 2–5 (see **Figure 2**).*

performance, increasing the MAE by 60%. Specifying stand LAI for each plot instead of a constant also had a clear impact on model performance, especially at the more southern sites. On the other hand, applying a constant LAI fraction for deciduous trees only marginally decreased model performance. The model runs with a standardized peat type (*Carex*/*Sphagnum*) show that sites S2 and S6 differ from the sites characterized by *Sphagnum* peat, while for S4, the effect of peat type was minor (**Figure 7B**). Finally, standardizing ditch spacing decreased model performance, while standardizing ditch depth slightly increased the performance (**Figure 7A**). This was caused especially by the improving effect ditch depth of 0.5 m had on the WTL predictions at site S5, which was characterized by the deepest ditches (see **Table 1**).

The role of site characteristics and meteorology as controls of WTL depends on the stand LAI (**Figure 8**). Overall, decreasing stand LAI raises the WTL, as was seen at the study sites (**Figures 4, 5**), but the effect is nonlinear, with a stronger impact when LAI is less than about $3.5\ m^2\ m^{-2}$. Increasing ditch spacing and decreasing ditch depth are predicted to raise WTL independent of stand LAI (**Figures 8A,B**). Closer inspection showed that WTL variation caused by ditch spacing and depth was slightly stronger at stands with low LAI, suggesting that harvesting on a site with wide ditch spacing or shallow ditches leads to a slightly stronger WTL response than harvesting on a site with narrow ditch spacing or deep ditches. The other factors (**Figures 8C–E**) showed the opposite behavior as their effect on WTL decreased with decreasing stand LAI. This suggests that WTL responses to harvests would be more pronounced on sites with *Carex* compared to *Sphagnum* peat, with higher fraction of deciduous trees, or in southern compared to northern location. In addition to stand LAI, harvest can also alter the fraction of deciduous trees in the stand (**Figure 8D**). The WTL response to harvest from a stand with deciduous trees accounting for 50% of preharvest LAI may thus be higher or lower than that shown in **Figure 8D** if deciduous or coniferous trees, respectively, are harvested first.

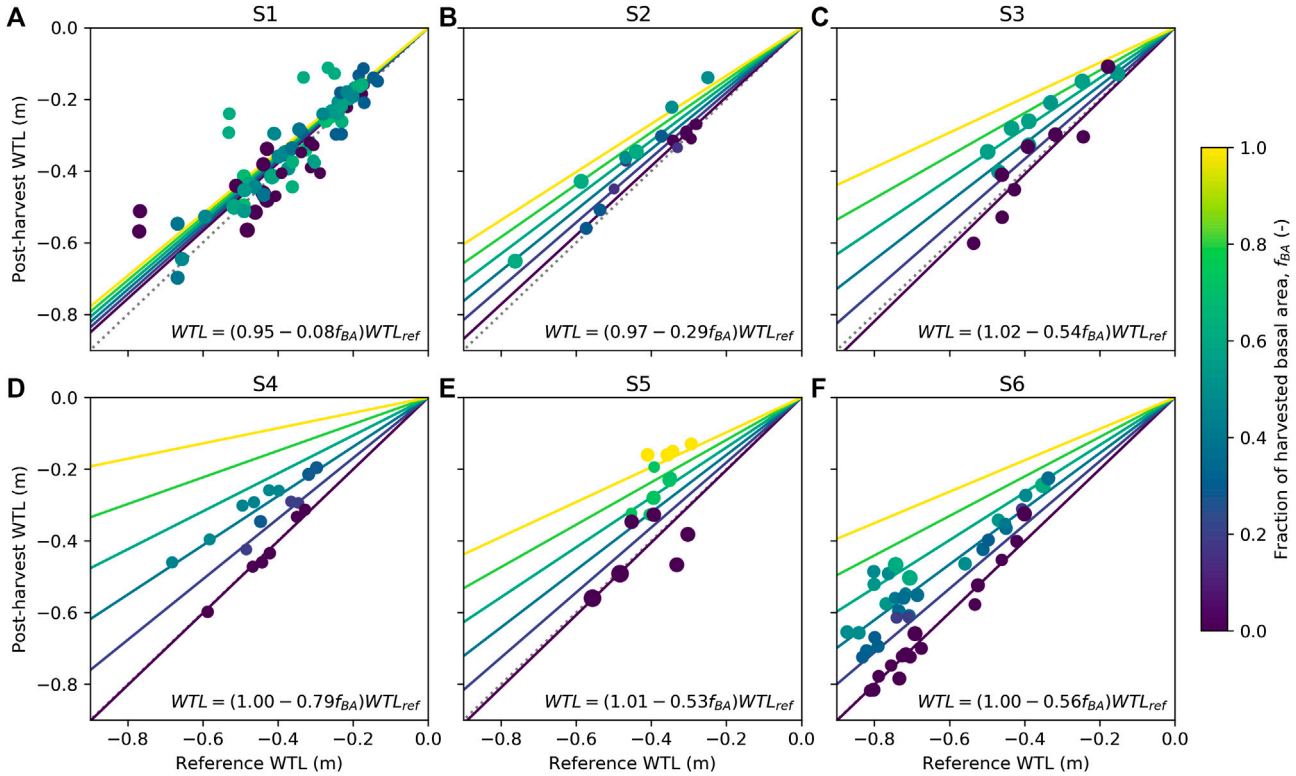

FIGURE 5 | Dependency of postharvest water table level (WTL) on reference WTL (see **Eqs 4 and 5**) for sites S1–S6 **(A–F)**. The colors indicate the harvest intensity and symbol size the preharvest stand basal area. Data are presented as mean yearly values for June–October separately for each plot within a site. WTL predicted by the linear regression model (see **Eq. 7**) is shown for six different harvest intensities (line colors correspond to harvest intensities) and the 1:1 line is shown as dotted.

Water Table Level in Current and Future Climate

Simulations with weather forcing from global climate models for the extent of Finland during 1981–2010 showed a strong influence of latitude on WTL (**Figure 9**), which is caused by the strong latitudinal gradient in air temperature and global radiation (**Figures 10B,C**) that drive ET demand. The results further suggest that altering the stand basal area by harvests in southern Finland has larger impacts on growing season WTL than corresponding alterations in northern Finland (**Figure 9**), as shown also by the two-site comparison in **Figure 8E**. The same is predicted to hold in future climate; however, the response of WTL to stand basal area is likely to increase and the absolute WTL to decrease, especially with RCP4.5 and RCP8.5 emission scenarios (**Figure 11**).

On average, WTL lowered by 0.02 m for RCP2.6 and by 0.06 m for both RCP4.5 and RCP8.5 compared to the current climate (**Figures 11A–C**). Compared to the current conditions, the ET demand increases in all RCPs (**Figures 10B,C**) driving WTL lower, while the increase in precipitation (**Figure 10A**), especially in RCP2.6, counteracts this impact. In fact, **Figure 11A** suggests that RCP2.6 WTL in some areas, especially in stands with a low basal area, in northern Finland may even rise due to increased precipitation. The change in WTL was generally stronger the higher the stand basal area, especially for RCP4.5 and RCP8.5 at northern latitudes (**Figures 11B,C**). Compared to the current climate, atmospheric CO_2 is predicted to increase by 18, 47, and 120% for RCP2.6, RCP4.5, and RCP8.5 by the end of the century, respectively. Omitting the effect of CO_2 effect on canopy stomatal conductance results into larger changes in WTL; it lowered on average by 0.03, 0.10, and 0.19 m for RCP2.6, RCP4.5, and RCP8.5, respectively (**Figures 11D–F**). Despite the differences in magnitudes, results in both cases indicate that the impact of the stand basal area on mean growing season WTL increases in future climate, especially in northern Finland and for RCP4.5 and RCP8.5.

Figures 9, 11 only consider the WTL produced as average from the simulations, with weather forcing from different climate models. It is worth noting that also climate models, not only different RCPs, caused large variability to the WTL predictions in future climate. The average standard deviation caused by climate models was 0.05 m for RCP2.6 and RCP4.5, while for RCP8.5 it was 0.08 m. In current climate, WTL predictions using data from different climate models had an average standard deviation of 0.02 m. The WTL variability increased with the stand basal area and was generally higher in the south than in the north.

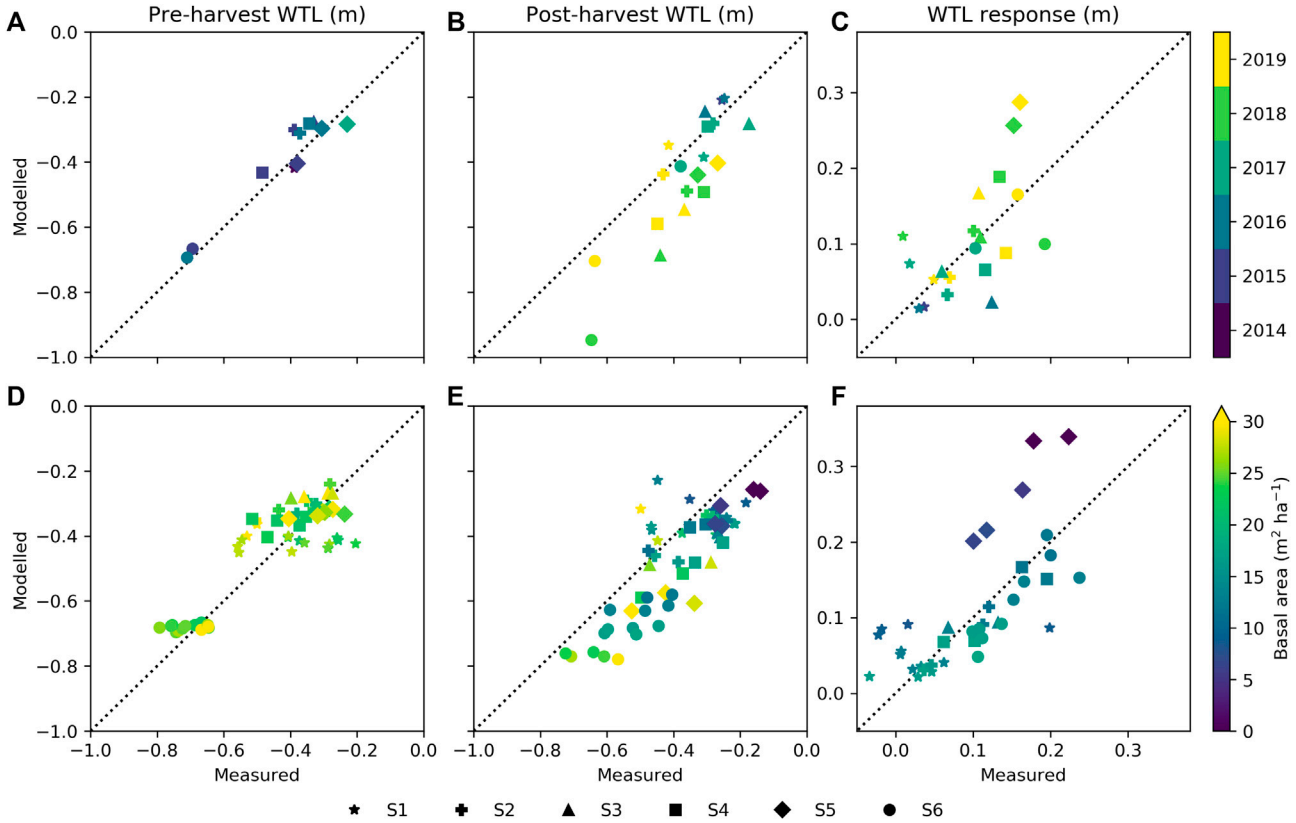

FIGURE 6 | Modeled against measured water table level (WTL) for pre- and postharvest periods and WTL response to harvesting as **(A–C)** yearly site mean, and **(D–F)** plot mean with colors showing stand basal area and symbols indicating study sites. Data from period June to October are included.

DISCUSSION

Model Performance and Future Use

The model–data comparison (**Figure 6**) and the analysis of model performance (**Figure 7**) implied that the model represents the hydrological behavior of drained peatland forests well and showed WTL differences (between sites and plots) are mostly driven by meteorology and stand LAI (or basal area), but that peat type and drainage characteristics also play important roles. Describing peat type either as *Carex* or *Sphagnum* peat, which differ in water retention properties and hydraulic conductivity (Päivänen, 1973), was well founded as *Carex* peat sites S2 and S6 differed from other sites in their behavior (**Figure 7**). Ditch spacing, which varied from 25 to 75 m, had a clear impact on WTL (**Figure 8A**) and improved the WTL predictions at the plot and site levels (**Figure 7**). Increasing ditch depth from 0.3 to 1.0 m was predicted to have a larger effect on WTL than decreasing ditch spacing from 75 to 25 m (**Figures 8A,B**). However, the effect of ditch depth did not necessarily improve model performance, but this might be caused by the difficulty to define ditch depth in the sense the model requires it. If ditches are poorly designed with not enough slope, or vegetation ingrowth has been excessive, some section may pond water almost constantly and that decreases the gradient between the WTL and ditch water level. Also, part of the ditch depths was measured in the field, while others were extracted from the digital elevation model, and thus likely includes more uncertainties than other plot-specific parameters.

Considering that spatially interpolated instead of onsite measured weather data were used in model simulations, WTL and its response to harvests were well reproduced. Especially summertime precipitation, which can be locally extremely variable, probably caused some of the inconsistencies between modeled and measured WTL during individual years. However, the rather systematic inconsistency in the estimation of WTL during dry summers (especially 2018, see **Figure 6B**) was most likely caused by model structure. At most of the sites, May of 2018 was exceptionally warm and dry with high radiation intensity. The model predicted high stand transpiration rates for this period, but in reality, transpiration may have been more limited by, for example, spring recovery or soil frost. Also, the model assumption that water in the peat profile instantaneously sets to hydraulic equilibrium is likely violated during long dry periods when the capillary rise to the root zone may be cut off.

The correspondence between modeled and measured WTL of individual sites may also be affected by their special characteristics, which were not accounted for in the model, for example, thin peat layers (S1 and S3), sloping area (S1), ponding effects caused by shallow bedrock (S3), or possible inflow from surrounding areas (S5). However, such special characteristics

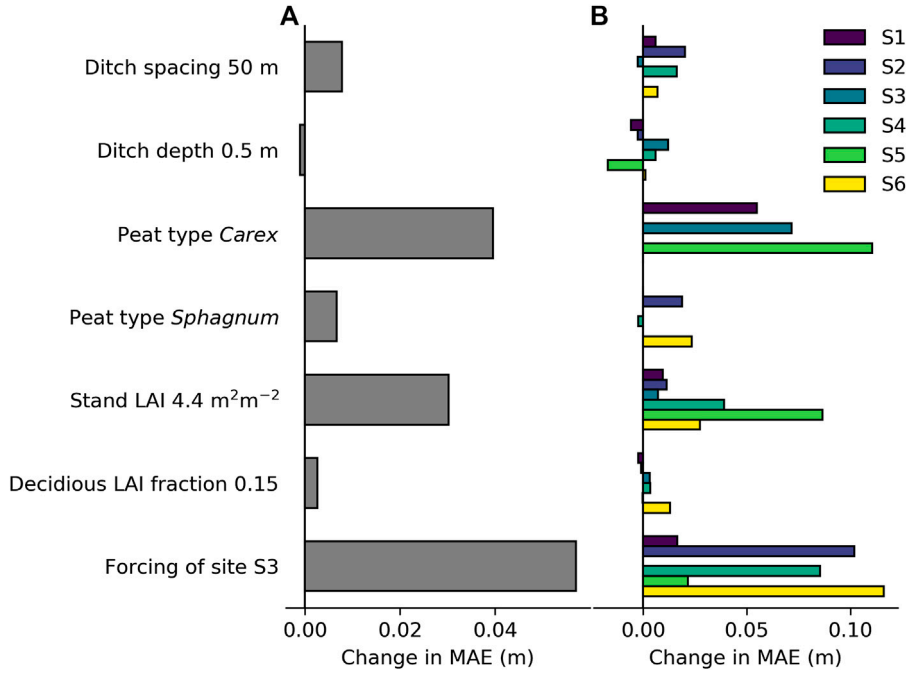

FIGURE 7 | Effect of standardizing model parameters and model forcing one by one on model performance in predicted water table level: **(A)** Effect on site average mean absolute error (MAE; see **Eq. 10**) and **(B)** effect on MAE of sites individually. A positive change in MAE indicates impaired model performance compared to model simulations where none of the factors are standardized.

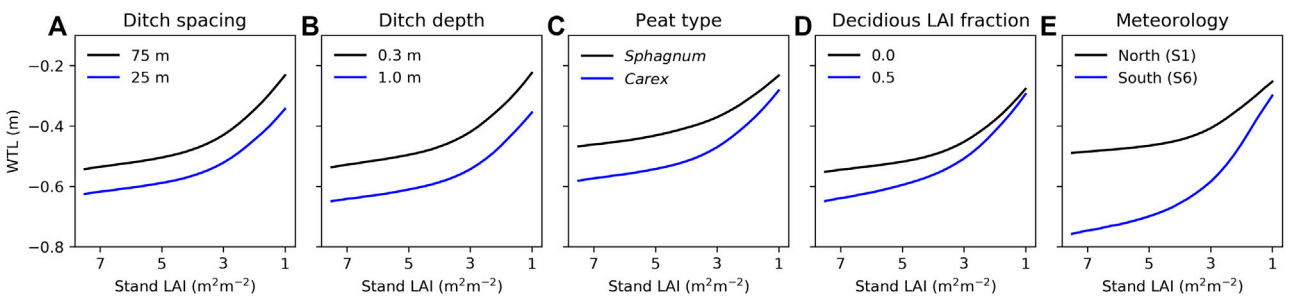

FIGURE 8 | Model predicted impact of **(A)** ditch spacing, **(B)** ditch depth, **(C)** peat type, **(D)** deciduous trees fraction of stand leaf area index (LAI), and **(E)** meteorology on water table level (WTL) in relation to stand LAI. The ranges of the varied parameters **(A–D)** are set based on their variability in sites S1–S6, while other parameters correspond to the values presented in **Table 2** and forcing is from site S3, except in **(E)** where forcing is varied from the northernmost to the southernmost site. WTL is the mean value for July–October during 2014–2019. Note that stand LAI decreases along the x-axis, describing increasing cutting intensity.

were not our focus as we aimed to keep the model simple and easily applicable with the purpose of using it for regional analysis and as a decision support tool in practical forestry in the future. In this respect, the results were satisfactory and suggest the model can produce WTL in different meteorological locations and account for the effect of harvests, ditching parameters, and peat type with reasonable accuracy. For Finland, the parameters needed by the model can be derived from open data, such as multisource National Forest Inventory of Finland (Mäkisara et al., 2016), and map products of the National Land Survey of Finland. Future model work will aim to improve the estimation of country-level greenhouse gas fluxes from peatlands by accounting for WTL (Ojanen et al., 2010) and to estimate the potential CCF in controlling WTL and greenhouse gas exchange of these soils on the country level.

Water Table Level Responses to Harvests and Practical Implications

The study showed that selection cuttings on peatland forest sites generally decreased WTL and that the responses were larger the more intense the harvests, as shown earlier by Päivänen (1982), Heikurainen and Päivänen (1970). No harvest responses could be detected at the northernmost site S1, and only the most intensive harvest affected WTL at S2. At site S1, the short preharvest

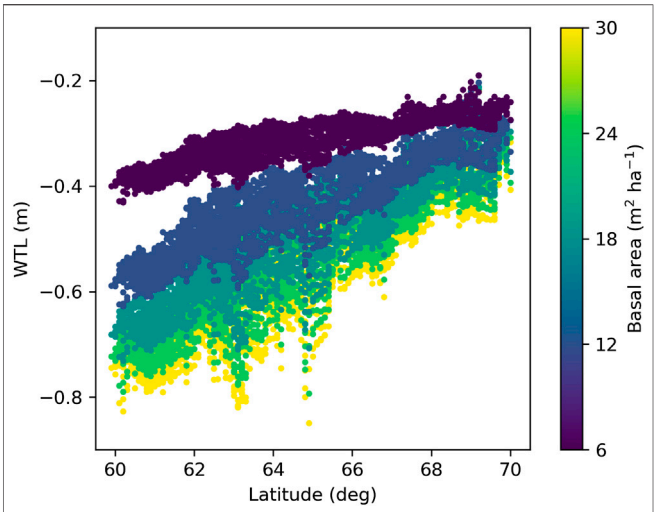

FIGURE 9 | Mean June–October water table level (WTL) predicted with weather data produced by climate models for Finland under current climate (1981–2010). WTL was simulated at five different levels of the stand basal area while other parameters were fixed to values in **Table 2**.

monitoring period, the thin peat layer, and the slope of some of the plots may have masked the effect of harvest on WTL. However, also according to the model, WTL responses were expected to be small at this site due to low ET demand in northern climate. The magnitude of harvest response at the more southern sites (S3–S6) was similar to Päivänen (1982), who reported an about 15, 30, and 60% increase in WTL in response to harvesting 20, 35, and 100% of the basal area, respectively, on a spruce-dominated site in southern Finland. Heikurainen and Päivänen (1970), on the other hand, showed weaker responses in a pine-dominated forest in southern Finland: harvesting 60% of stand volume resulted in a 15% rise of WTL, while removing 20% or 40% both led to an about 5% rise. In line with this, Päivänen and Sarkkola (2000) concluded that thinnings of up to 28% caused an ecologically insignificant rise in the WTL at their studied pine stand in southern Finland.

The model results showed that the relationship between tree stand and WTL is nonlinear, which has also been proposed by empirical studies (Hökkä et al., 2008b; Sarkkola et al., 2010). This is caused by the nonlinear response of ET to LAI, and is predominantly attributed to light limitations of transpiration in dense canopies (Launiainen et al., 2016). This nonlinearity may explain some of the phenomena seen at the study sites. At site S2, the less intense harvest, which had almost no effect on WTL, decreased tree stand LAI from 4.9 to 3.7 $m^2\ m^{-2}$, which is in the LAI range where responses to WTL are much smaller than when LAI decreases below 3.5 $m^2\ m^{-2}$, especially in the north (**Figure 8E**). On the other hand, at site S4, where harvest led to largest WTL responses (**Figure 5D**), the preharvest LAI was 3.9–4.3 $m^2\ m^{-2}$ and after harvest 2.3–3.4 $m^2\ m^{-2}$, that is, within the range where WTL responses to LAI are the most pronounced (**Figure 8E**). Thus, not only the amount of removed basal area dictate the WTL response but also the size of the preharvest stand. Additionally, the LAI to basal area ratio varies strongly between species, which implicates that conducting similar basal area–based harvests in pure pine stands would lead to different responses compared to spruce-dominated stands. However, this cannot be concluded based on our data.

In line with earlier harvest studies (Heikurainen and Päivänen, 1970; Päivänen, 1982; Päivänen and Sarkkola, 2000), we show that the WTL response to harvest is the greater the deeper the reference WTL (**Figure 5**), meaning that during wet summers, the effect of the tree stand is less significant than during dry summers (cf. Sarkkola et al., 2010). This effect is analogous with the changes in WTL to LAI responses in south *vs.* north (**Figures 8E, 9A**). During wet summers or in northern locations, the effect of the stand on WTL is smaller because of lower ET demand and the increased role of runoff as WTL more commonly increases close to the soil surface (Sarkkola et al., 2013). Our results suggest

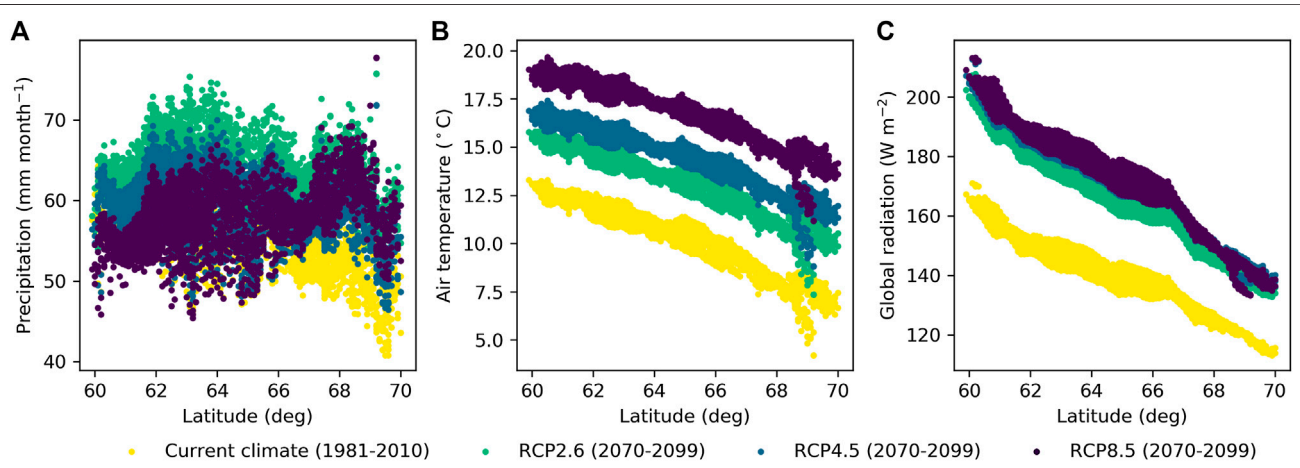

FIGURE 10 | Mean June–October **(A)** precipitation, **(B)** air temperature, and **(C)** global radiation along latitudinal gradient in Finland derived from global climate models for current climate and future climate with representative concentration pathways RCP2.6, RCP4.5, and RCP8.5.

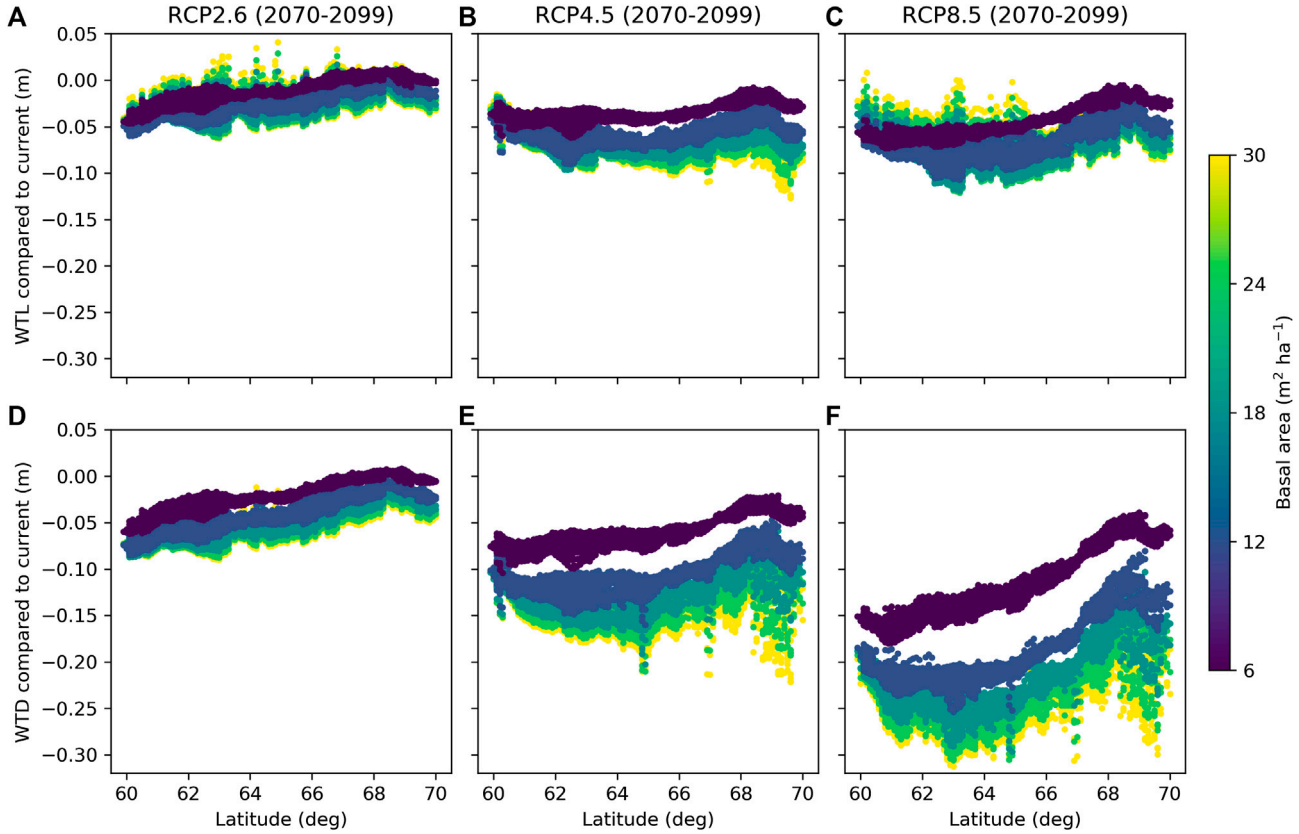

FIGURE 11 | Difference between mean June and October water table level (WTL) in future and current climate predicted for RCP2.6 **(A,D)**, RCP4.5 **(B,E)**, and RCP8.5 **(C,F)**, when accounting for the effect of atmospheric CO_2 on canopy stomatal conductance (see **Eq. 10**) **(A,B)** or when neglecting that effect **(C,D)**. Colors indicate five different levels of the stand basal area, while other parameters were fixed to values in **Table 2**.

that in southern Finland, selection cuttings could limit WTL from dropping too deep and enhancing peat decomposition, while in the northern Finland, keeping large stands would be less concerning from climatic perspectives. Then again regarding high WTL, smaller stands are required in the south than in the north, which is in line with Sarkkola et al. (2010) and Sarkkola et al. (2013).

Model simulations with scenarios for future climate (RCP2.6, RCP4.5, and RCP8.5, 2070–2099) indicated that the atmospheric ET demand will increase and, in most cases, lead to a WTL decrease despite the predicted increase in precipitation. The WTL decrease was, however, constrained to about half (**Figure 11**) when the effect of increasing atmospheric CO_2 concentration was accounted for (**Eq. 10**). Although the magnitude of the CO_2 effect on leaf, plant, and stand-scale water use is still under debate (Katul et al., 2012; Keenan et al., 2013; Hasper et al., 2016; Jaramillo et al., 2018), our results indicate that this uncertainty does not affect our conclusion that growing season WTL will become deeper and the role of tree stand in controlling WTL more pronounced in future climates, especially in northern Finland and for RCP4.5 and RCP8.5. This implies that the potential of using selection cutting to control WTL will become stronger in the future also in northern Finland. Managing stand density could also provide means to avoid drought stress in trees (Bréda et al., 1995), which may become more topical in the boreal region in future climate.

CONCLUSIONS

This study quantified the effect of selection cuttings and the role of tree stand on growing season WTL in drained peatland forests. Such information is important for the proposed transition toward CCF that aims to optimize WTL for multiple ecosystem services on drained peatlands. To this end, WTL responses to various intensity harvests were monitored at six fertile Norway spruce–dominated drained peatland forests across Finland for 1–3 pretreatment and 2–5 postharvest years. The data analysis was accompanied with WTL predictions by a process-based ecohydrological model, which is proposed suitable for predicting WTL in different meteorological locations and based on relatively easily available parameters. This is beneficial for assessing the potential of CCF as tool for WTL regulation and, for example, improving estimates of country-level greenhouse gas fluxes from peatlands. Regarding the three

research questions framed in the introduction, our conclusions are as follows:

(1) WTL increased after harvests at most of the studied plots. The WTL response increased with harvest intensity and depended on the meteorological conditions (wet vs. dry summer, north vs. south). Generally, selection cuttings removing about 50% of the stand basal area raised WTL by 15–40%. The nonlinear relationship between tree stand and WTL explained differences between sites, emphasizing the role of the preharvest stand basal area (or LAI).
(2) Because of lower ET in northern compared to southern Finland, the role of tree stand on WTL decreases with latitude. An identical harvest in the south compared to the north can result to an even two times larger WTL rise. This suggests the potential of CCF in avoiding high and low WTL using selection cuttings is currently more prominent in southern Finland.
(3) WTL was predicted to decrease in future climate (2070–2099) with representative concentration pathways RCP2.6, RCP4.5, and RCP8.5. The magnitude of the WTL decrease was sensitive to the way atmospheric CO_2 rise is described to affect tree stomatal conductance. Especially in northern Finland and for RCP4.5 and RCP8.5, the role of tree stand on WTL was predicted to increase, which implicates that the potential for CCF is likely to increase in future climate.

DATA AVAILABILITY STATEMENT

The datasets generated for this study and the model source code are available on request from the corresponding author.

AUTHOR CONTRIBUTIONS

SS, HH, MS, RL, RM, and MN designed, established and were responsible of monitoring the harvesting experiments on the study sites. KL analyzed the WTL data and performed the modeling with assistance from SL. AL generated the stand parameters from the tree stand measurements. MP provided the weather data for the study sites and the scenario simulations. All authors participated in conceptualizing the study, analyzing the results, and writing the manuscript in the lead of KL.

FUNDING

This work was supported by the Academy of Finland projects CCFPeat (no. 310203), CLIMOSS (no. 296116), and SOMPA, which was funded by the Strategic Research Council at the Academy of Finland (no. 312912).

ACKNOWLEDGMENTS

The authors wish to acknowledge CSC—IT Center for Science, Finland, for computational resources. The Finnish Meteorological Institute is acknowledged for the meteorological data.

SUPPLEMENTARY MATERIAL

The Supplementary Material for this article can be found online at: https://www.frontiersin.org/articles/10.3389/feart.2020.576510/full#supplementary–material

REFERENCES

Aalto, J., Pirinen, P., Heikkinen, J., and Venäläinen, A. (2013). Spatial interpolation of monthly climate data for Finland: comparing the performance of kriging and generalized additive models. *Theor. Appl. Climatol.* 112, 99–111. doi:10.1007/s00704-012-0716-9

Ahti, E., and Hökkä, H. (2006). "Effects of the growth and volume of Scots pine stands on the level of the water table on peat in central Finland," in Proceedings of an international conference of hydrology and management of forested wetlands, New Bern, NC, April 8–12, 2006. (American Society of Agricultural and Biological Engineers), 37.

Ahtikoski, A., Kojola, S., Hökkä, H., and Penttilä, T. (2008). Ditch network maintenance in peatland forest as a private investment: short- and long-term effects on financial performance at stand level. *Mires Peat.* 3, 1–11.

Ahtikoski, A., Salminen, H., Hökkä, H., Kojola, S., and Penttilä, T. (2012). Optimising stand management on peatlands: the case of northern Finland. *Can. J. For. Res.* 42, 247–259. doi:10.1139/x11-174

Ainsworth, E. A., and Rogers, A. (2007). The response of photosynthesis and stomatal conductance to rising [CO2]: mechanisms and environmental interactions. *Plant Cell Environ.* 30, 258–270. doi:10.1111/j.1365-3040.2007.01641.x

Boczoń, A., Dudzińska, M., and Kowalska, A. (2016). Effect of thinning on evaporation of Scots pine forest. *Appl. Ecol. Environ. Res.* 14, 367–379. doi:10.15666/aeer/1402_367379

Bréda, N., Granier, A., and Aussenac, G. (1995). Effects of thinning on soil and tree water relations, transpiration and growth in an oak forest (*Quercus petraea* (Matt.) Liebl.). *Tree Physiol.* 15, 295–306. doi:10.1093/treephys/15.5.295

Finér, L., Mattsson, T., Joensuu, S., Koivusalo, H., Laurén, A., Makkonen, T., et al. (2010). *A method for calculating nitrogen, phosphorus and sediment load from forest catchments*. Helsinki, Finland: Finnish Environmental Institute. . Available at: http://hdl.handle.net/10138/37973 (Accessed June 1, 2020).

Haahti, K., Marttila, H., Warsta, L., Kokkonen, T., Finér, L., and Koivusalo, H. (2016). Modeling sediment transport after ditch network maintenance of a forested peatland. *Water Resour. Res.* 52, 9001–9019. doi:10.1002/2016WR019442

Härkönen, S., Lehtonen, A., Manninen, T., Tuominen, S., and Peltoniemi, M. (2015). Estimating forest leaf area index using satellite images: comparison of k-NN based Landsat-NFI LAI with MODIS-RSR based LAI product for Finland. *Boreal Environ. Res.* 20, 181–195.

Hasper, T. B., Wallin, G., Lamba, S., Hall, M., Jaramillo, F., Laudon, H., et al. (2016). Water use by Swedish boreal forests in a changing climate. *Funct. Ecol.* 30, 690–699. doi:10.1111/1365-2435.12546

Heikurainen, L., and Päivänen, J. (1970). The effect of thinning, clear cutting, and fertilization on the hydrology of peatland drained for forestry. *Acta For. Fenn.* 104, 1–24. doi:10.14214/aff.7538

Hökkä, H., Koivusalo, H., Ahti, E., Nieminen, M., Laine, J., Saarinen, M., et al. (2008a). "Effects of tree stand transpiration and interception on site water balance in drained peatlands: experimental design and measurements." in *After*

wise use - the future of peatlands. Editors C. Farrell and J. Feehan (Tullamore, Ireland: International Peat Society), 169–171.

Hökkä, H., Repola, J., and Laine, J. (2008b). Quantifying the interrelationship between tree stand growth rate and water table level in drained peatland sites within Central Finland. *Can. J. For. Res.* 38, 1775–1783. doi:10.1139/X08-028

Hooghoudt, S. B. (1940). "General consideration of the problem of field drainage by parallel drains, ditches, watercourses, and channels," in *Publication No.7 in the series contribution to the knowledge of some physical parameters of the soil*. Groningen, Netherlands: Bodemkundig Insitituut.

Jaramillo, F., Cory, N., Arheimer, B., Laudon, H., van der Velde, Y., Hasper, T. B., et al. (2018). Dominant effect of increasing forest biomass on evapotranspiration: interpretations of movement in Budyko space. *Hydrol. Earth Syst. Sci.* 22, 567–580. doi:10.5194/hess-22-567-2018

Joensuu, S., Ahti, E., and Vuollekoski, M. (1999). The effects of peatland forest ditch maintenance on suspended solids in runoff. *Boreal Environ. Res.* 4: 343–355.

Kaila, A., Laurén, A., Sarkkola, S., Koivusalo, H., Ukonmaanaho, L., O'Driscoll, C., et al. (2015). Effect of clear-felling and harvest residue removal on nitrogen and phosphorus export from drained Norway spruce mires in southern Finland. *Boreal Environ. Res.* 20: 693–706.

Kaila, A., Sarkkola, S., Laurén, A., Ukonmaanaho, L., Koivusalo, H., Xiao, L., et al. (2014). Phosphorus export from drained Scots pine mires after clear-felling and bioenergy harvesting. *For. Ecol. Manag.* 325, 99–107. doi:10.1016/j.foreco.2014.03.025

Katul, G. G., Oren, R., Manzoni, S., Higgins, C., and Parlange, M. B. (2012). Evapotranspiration: a process driving mass transport and energy exchange in the soil-plant-atmosphere-climate system. *Rev. Geophys.* 50, RG3002. doi:10.1029/2011RG000366

Katul, G., Manzoni, S., Palmroth, S., and Oren, R. (2010). A stomatal optimization theory to describe the effects of atmospheric CO_2 on leaf photosynthesis and transpiration. *Ann. Bot.* 105, 431–442. doi:10.1093/aob/mcp292

Keenan, T. F., Hollinger, D. Y., Bohrer, G., Dragoni, D., Munger, J. W., Schmid, H. P., et al. (2013). Increase in forest water-use efficiency as atmospheric carbon dioxide concentrations rise. *Nature* 499, 324–327. doi:10.1038/nature12291

Koivusalo, H., Ahti, E., Laurén, A., Kokkonen, T., Karvonen, T., Nevalainen, R., et al. (2008). Impacts of ditch cleaning on hydrological processes in a drained peatland forest. *Hydrol. Earth Syst. Sci.* 12, 1211–1227. doi:10.5194/hess-12-1211-2008

Korhonen, L., Korhonen, K. T., Stenberg, P., Maltamo, M., and Rautiainen, M. (2007). Local models for forest canopy cover with beta regression. *Silva Fenn.* 41, 671–685. doi:10.14214/sf.275

Korkiakoski, M., Tuovinen, J.-P., Penttilä, T., Sarkkola, S., Ojanen, P., Minkkinen, K., et al. (2019). Greenhouse gas and energy fluxes in a boreal peatland forest after clear-cutting. *Biogeosciences* 16, 3703–3723. doi:10.5194/bg-16-3703-2019

Lagergren, F., and Lindroth, A. (2004). Variation in sapflow and stem growth in relation to tree size, competition and thinning in a mixed forest of pine and spruce in Sweden. *For. Ecol. Manag.* 188, 51–63. doi:10.1016/j.foreco.2003.07.018

Laine, J. (1989). Classification of peatlands drained for forestry. *Suo* 40, 37–51.

Lappi, J. (1991). Calibration of height and volume equations with random parameters. *For. Sci.* 37, 781–801. doi:10.1093/forestscience/37.3.781

Launiainen, S., Guan, M., Salmivaara, A., and Kieloaho, A.-J. (2019). Modeling boreal forest evapotranspiration and water balance at stand and catchment scales: a spatial approach. *Hydrol. Earth Syst. Sci.* 23, 3457–3480. doi:10.5194/hess-23-3457-2019

Launiainen, S., Katul, G. G., Kolari, P., Lindroth, A., Lohila, A., Aurela, M., et al. (2016). Do the energy fluxes and surface conductance of boreal coniferous forests in Europe scale with leaf area? *Global Change Biol.* 22, 4096–4113. doi:10.1111/gcb.13497

Launiainen, S., Katul, G. G., Lauren, A., and Kolari, P. (2015). Coupling boreal forest CO2, H2O and energy flows by a vertically structured forest canopy - soil model with separate bryophyte layer. *Ecol. Model.* 312, 385–405. doi:10.1016/j.ecolmodel.2015.06.007

Lehtonen, A., Heikkinen, J., Petersson, H., Ťupek, B., Liski, E., and Mäkelä, A. (2020). Scots pine and Norway spruce foliage biomass in Finland and Sweden - testing traditional models vs. the pipe model theory. *Can. J. For. Res.* 50, 146–154. doi:10.1139/cjfr-2019-0211

Lehtonen, I., Kämäräinen, M., Gregow, H., Venäläinen, A., and Peltola, H. (2016). Heavy snow loads in Finnish forests respond regionally asymmetrically to projected climate change. *Nat. Hazards Earth Syst. Sci.* 16, 2259–2271. doi:10.5194/nhess-16-2259-2016

Mäkisara, K., Katila, M., Peräsaari, J., and Tomppo, E. (2016). *The multi-source national forest inventory of Finland – methods and results 2013*. Luke, Finland: Natural Resources Institute Finland. Available at: http://urn.fi/URN (Accessed June 24, 2020).

Mazza, G., Amorini, E., Cutini, A., and Manetti, M. C. (2011). The influence of thinning on rainfall interception by Pinus pinea L. in Mediterranean coastal stands (Castel Fusano-Rome). *Ann. For. Sci.* 68, 1323–1332. doi:10.1007/s13595-011-0142-7

Medlyn, B. E., Duursma, R. A., Eamus, D., Ellsworth, D. S., Prentice, I. C., Barton, C. V. M., et al. (2011). Reconciling the optimal and empirical approaches to modelling stomatal conductance. *Global Change Biol.* 17, 2134–2144. doi:10.1111/j.1365-2486.2010.02375.x

Mehtätalo, L., de-Miguel, S., and Gregoire, T. G. (2015). Modeling height-diameter curves for prediction. *Can. J. For. Res.* 45, 826–837. doi:10.1139/cjfr-2015-0054

Mehtätalo, L. (2019). Lmfor: functions for forest biometrics. Available at: https://CRAN.R-project.org/package=lmfor (Accessed November 1, 2019).

Nieminen, M., Ahti, E., Koivusalo, H., Mattsson, T., Sarkkola, S., and Laurén, A. (2010). Export of suspended solids and dissolved elements from peatland areas after ditch network maintenance in south-central Finland. *Silva Fenn.* 44, 39–49. doi:10.14214/sf.161

Nieminen, M., Hökkä, H., Laiho, R., Juutinen, A., Ahtikoski, A., Pearson, M., et al. (2018a). Could continuous cover forestry be an economically and environmentally feasible management option on drained boreal peatlands? *For. Ecol. Manag.* 424, 78–84. doi:10.1016/j.foreco.2018.04.046

Nieminen, M., Koskinen, M., Sarkkola, S., Laurén, A., Kaila, A., Kiikkilä, O., et al. (2015). Dissolved organic carbon export from harvested peatland forests with differing site characteristics. *Water Air Soil Pollut.* 226, 181. doi:10.1007/s11270-015-2444-0

Nieminen, M., Palviainen, M., Sarkkola, S., Laurén, A., Marttila, H., and Finér, L. (2017a). A synthesis of the impacts of ditch network maintenance on the quantity and quality of runoff from drained boreal peatland forests. *Ambio* 47, 523–534. doi:10.1007/s13280-017-0966-y

Nieminen, M., Sallantaus, T., Ukonmaanaho, L., Nieminen, T. M., and Sarkkola, S. (2017b). Nitrogen and phosphorus concentrations in discharge from drained peatland forests are increasing. *Sci. Total Environ.* 609, 974–981. doi:10.1016/j.scitotenv.2017.07.210

Nieminen, M., Sarkkola, S., Hellsten, S., Marttila, H., Piirainen, S., Sallantaus, T., et al. (2018b). Increasing and decreasing nitrogen and phosphorus trends in runoff from drained peatland forests-is there a legacy effect of drainage or not? *Water Air Soil Pollut.* 229, 286. doi:10.1007/s11270-018-3945-4

Ojanen, P., Minkkinen, K., Alm, J., and Penttilä, T. (2010). Soil-atmosphere CO2, CH4 and N2O fluxes in boreal forestry-drained peatlands. *For. Ecol. Manag.* 260, 411–421. doi:10.1016/j.foreco.2010.04.036

Ojanen, P., Minkkinen, K., and Penttilä, T. (2013). The current greenhouse gas impact of forestry-drained boreal peatlands. *For. Ecol. Manag.* 289, 201–208. doi:10.1016/j.foreco.2012.10.008

Ojanen, P., and Minkkinen, K. (2019). The dependence of net soil CO_2 emissions on water table depth in boreal peatlands drained for forestry. *Mires Peat.* 24, 1–8. doi:10.19189/MaP.2019.OMB.StA.1751

Paavilainen, E., and Päivänen, J. (1995). *Peatland forestry: ecology and principles*. Berlin, Germany: Springer.

Päivänen, J. (1973). Hydraulic conductivity and water retention in peat soils. *Acta For. Fenn.* 129, 1–70. doi:10.14214/aff.7563

Päivänen, J., and Sarkkola, S. (2000). The effect of thinning and ditch network maintenance on the water table level in a Scots pine stand on peat soil. *Suo* 51, 131–138.

Päivänen, J. (1982). The effect of cutting and fertilization on the hydrology of an old forest drainage area (in Finnish). *Folia For.* 516, 1–19.

Pirinen, P., Simola, H., Aalto, J., Kaukoranta, J.-P., Karlsson, P., and Ruuhela, R. (2012). *Tilastoja Suomen ilmastosta 1981–2010 (climatological statistics of Finland 1981–2010)*. Helsinki, Finland: Finnish Meteorological Institute. Available at: http://hdl.handle.net/10138/35880 (Accessed May 24, 2020).

Räisänen, J., and Räty, O. (2013). Projections of daily mean temperature variability in the future: cross-validation tests with ENSEMBLES regional climate simulations. *Clim. Dynam.* 41, 1553–1568. doi:10.1007/s00382-012-1515-9

Räty, O., Räisänen, J., and Ylhäisi, J. S. (2014). Evaluation of delta change and bias correction methods for future daily precipitation: intermodel cross-validation using ENSEMBLES simulations. *Clim. Dynam.* 42, 2287–2303. doi:10.1007/s00382-014-2130-8

Sarkkola, S., Hökkä, H., Ahti, E., Koivusalo, H., and Nieminen, M. (2012). Depth of water table prior to ditch network maintenance is a key factor for tree growth response. *Scand. J. For. Res.* 27, 649–658. doi:10.1080/02827581.2012.689004

Sarkkola, S., Hökkä, H., Koivusalo, H., Nieminen, M., Ahti, E., Päivänen, J., et al. (2010). Role of tree stand evapotranspiration in maintaining satisfactory drainage conditions in drained peatlands. *Can. J. For. Res.* 40, 1485–1496. doi:10.1139/X10-084

Sarkkola, S., Nieminen, M., Koivusalo, H., Laurén, A., Ahti, E., Launiainen, S., et al. (2013). Domination of growing-season evapotranspiration over runoff makes ditch network maintenance in mature peatland forests questionable. *Mires Peat.* 11, 1–11.

Skaggs, R. W. (1980). "A water management model for artificially drained soils," in *Technical bulletin*. Raleigh, NC: North Carolina Agricultural Research Service, 54.

Stenberg, L., Tuukkanen, T., Finér, L., Marttila, H., Piirainen, S., Kløve, B., et al. (2015). Ditch erosion processes and sediment transport in a drained peatland forest. *Ecol. Eng.* 75, 421–433. doi:10.1016/j.ecoleng.2014.11.046

Tupek, B., Mäkipää, R., Heikkinen, J., Peltoniemi, M., Ukonmaanaho, L., Hokkanen, T., et al. (2015). Foliar turnover rates in Finland-comparing estimates from needle-cohort and litterfall-biomass methods. *Boreal Environ. Res.* 22, 283–304.

Conflict of Interest: The authors declare that the research was conducted in the absence of any commercial or financial relationships that could be construed as a potential conflict of interest.

frontiers in Environmental Science

ORIGINAL RESEARCH
published: 17 November 2020
doi: 10.3389/fenvs.2020.576307

The Operation of the Three Gorges Dam Alters Wetlands in the Middle and Lower Reaches of the Yangtze River

Gongqi Sun[1], Guangchun Lei[1], Yi Qu[2], Chengxiang Zhang[1] and Ke He[1]*

[1] School of Ecology and Nature Conservation, Beijing Forestry University, Beijing, China, [2] Nature and Ecology Institute of Heilongjiang Academy of Sciences, Harbin, China

The operation of the Three Gorges Dam (TGD) has significantly impact on downstream wetland ecosystems. This study applied 3S technology, landscape ecology, and computational models to investigate impact of the TGD on downstream spatial dynamics of floodplains in future. Results revealed the relationship between siltation patterns and wetland types transformation after the operation of the TGD, which are critically important to understand ecological characters dynamics in new environmental setting, and provide science-based conservation and restoration recommendation. After the operation of the TGD, changes between water surface and floodplains areas were spatial heterogeneity. With the increase of distance to the TGD, floodplain erosion force declining gradually. The most important finding is the asymmetric erosion between main river course and its associated floodplain lakes, e.g., Dongting lake.This has significant implications for dam operation in autumn and habitat management. After the operation of the TGD, floodplain in the estuary is driven by both the Yangtze river and ocean currents. The strong hydrological force and reduced sediments of Yangtze river drive erosion of the southern river course in the estuary, whereas, the weakened hydrological force in the northern river course attracts sedimentation.

Keywords: floodplains, water surface, three gorges dam, Yangtze River, landscape fragmentation, CA-Markov

OPEN ACCESS

Edited by:
Ligang Xu,
Nanjing Institute of Geography and Limnology (CAS), China

Reviewed by:
Yuankun Wang,
Nanjing University, China
Mei Xuefei,
East China Normal University, China

****Correspondence:***
Guangchun Lei
guangchun.lei@foxmail.com

Specialty section:
This article was submitted to Freshwater Science, a section of the journal Frontiers in Environmental Science

Received: *26 June 2020*
Accepted: *14 October 2020*
Published: *17 November 2020*

Citation:
Sun G, Lei G, Qu Y, Zhang C and He K (2020) The Operation of the Three Gorges Dam Alters Wetlands in the Middle and Lower Reaches of the Yangtze River. Front. Environ. Sci. 8:576307. doi: 10.3389/fenvs.2020.576307

INTRODUCTION

Global wetland changes are affected by climate change and human activities (Vörösmarty et al., 2000; Ramsar Convention on Wetlands, 2018), in particularly, river diversion or damming (Postel et al., 1996; United Nations Department of Economic and Social Affairs, 2015; Jean-François et al., 2016), which have been identified as global aquatic stressors (Etienne et al., 2020), or regional level, such as the Curuai floodplain in the lower Amazon River (Park et al., 2020), West Bengal (India) (Das et al., 2020). Human activities have altered the flow regimes of many rivers, with negative impacts on biodiversity, water quality, and ecological processes (Margaret and Albert, 2019).

The Yangtze River is the third-largest river in the world, and it supports a great amount of biodiversity from 6300 meters above sea level in the Tibetan Plateau to the Eastern China Sea in Shanghai. Its upstream reaches have been identified as global biodiversity hotspots, namely, the Himalayan Mountains and River Valley of the Yangtze River, the Global 200

Ecoregion (Zhao et al., 2000; Barter et al., 2006), the Ecoregion of the Central Yangtze River and Lakes, as well as the Yellow River Ecoregion (including the Yangtze River delta and estuary) (Oslon and Dinerstein, 2002).

Since the Three Gorges Dam (TGD) became operational in 2003, worldwide attention has been focused on dam's impact on environment in the middle-lower Yangtze River (Wang, 2010; Pan and Hu, 2015; Zhang et al., 2020). The operation of the TGD changed hydrological regime downstream (Zhang et al., 2016; Tian et al., 2019), through storing water in autumn, and releasing of clear water that disturb balance between riverbed erosion and siltation (Li, 2009; Jiang et al., 2014; Han and Huang, 2018), leading to asymmetric erosion on riverbed and lake (Lu et al., 2018). Such disturbance has significant impact on waterbird habitat (Cao et al., 2008; Guan et al., 2014; Liu et al., 2015), as well as fish populations (Xie et al., 2016).

To date, major research efforts have focused on impact of the TGD on hydrology, or biodiversity based on data from a limited number of hydrological stations (Jiang et al., 2014; Yang et al., 2017; Liu et al., 2018); few studies have focused on hydrological changes and their relationship with siltation patterns and habitat transformation, which are critically important to understand ecological characters dynamics in new environmental setting after the operation of the TGD, and provide science-based conservation and restoration recommendation. This study applied 3S technology, landscape ecology, and computational models to investigate impact of the TGD on downstream spatial dynamics of floodplains in future.

MATERIALS AND METHODS

Study Area

Study area covers main river course and its floodplains along the Yangtze River between the TGD in Yichang City and estuary in Shanghai, with a total length of 1771 km (**Figure 1**). On basis of hydrological station data and impact of river flow downstream, study area was divided into four sections, i.e., Yichang Station-Chenglingji Station (Y-C), Chenglingji Station-Hukou Station (C-H), Hukou Station-Nantong Station (H-N), and Nantong Station-Estuary (N-E).

Data Collection

Wetland datasets in 1990, 2000, 2005, 2010, and 2015 were produced by extracting floodplain areas from land-use maps obtained from the Resource and Environment Data Cloud Platform[1]. Land-use maps were generated by human-computer interactive software, using Landsat TM/ETM remote sensing images of each period as main data source. Images in early March or late October when water level is stable were selected to avoid influence of water level fluctuation on image interpretation. All selected images were projected in the Conical Projection of Albers Orthogonal Axis with Equal Area and Double Standard Latitude Lines. The reliability of these datasets and monitoring data was verified and firmly quality controlled before their release. The locations of stations are shown in **Figure 1**.

Data Analysis

According to ecological characteristics of the study area, we applied CNLUCC method to generate maps based on a unified land-use and plant classification system and to connect individual remote images. All data analysis was conducted with interactive QGIS software. We first constructed maps within laboratory and then verified them on-site to minimize errors in computer interpretation. Remote sensing data analysis included data collection, false color composite generation, image data correction, image data cutting, and establishment of info-source of remote database.

For standard false color composites, the TM images used bands 4, 3, and 2; MSS4-5 used bands 4, 2, and 1; and MSS1-3 used bands 7, 5, and 4[2]. Since the TGD began operations in 2003, remote sensing data from 1990, 2000, 2005, 2010, and 2015 were used for the interpretation. According to characteristics of wetlands in the middle and lower reaches of the Yangtze River, we divided wetlands into two types, i.e., water surface and floodplains.

Transition matrix were built to characterize impact of the TGD on spatial distribution of wetlands using four periods of remote sensing data and dividing them into time before (1990–2000) and after (2005–2015) TGD operations.

Firstly, we applied transition matrix analysis to identify how wetlands changed after the TGD operation. Then, we conducted a comparative analysis to determine the differences in transition periods and analyze impact of the TGD operation on spatial distribution of wetlands. We calculated two kinds of transition rates, P_{S-F} and P_{F-S}:

$$\mathbf{P_{S-F} = A_{W-TF}/A_W}, \quad (1)$$

where $\mathbf{A_{S-TF}}$ is total area of water surface that is converted into floodplains, and $\mathbf{A_S}$ is area covered in water surface;

$$\mathbf{P_{F-W} = A_{F-TW}/A_F}, \quad (2)$$

where $\mathbf{A_{F-TS}}$ is total area of floodplain that is converted into all types of water surface, and $\mathbf{A_F}$ is area classified as floodplains.

According to characteristics of different parameters, we chose class and landscape metrics as main parameters to analyze impacts of the TGD on landscape, and we utilized land-use data from 2000 and 2015 for data before and after the operation of the TGD, respectively. We used FRAGSTATS to calculate Percentage of Landscape (PLAND), Number of Patches (NP), Patch Density (PD), and Mean Patch Areas (AREA_MN) to analyze impacts of the TGD operation on wetland fragmentation.

To predict impact of the TGD operation on spatial distribution of wetlands in the middle and lower reaches of the Yangtze River, we applied a Cellular Automata_Markov chain (CA_Markov) model to predict trend of floodplain changes caused by operation of the TGD. This model is a long-term forecasting method based on a Markov chain procedure, which

[1]http://www.resdc.cn/

[2]http://www.resdc.cn

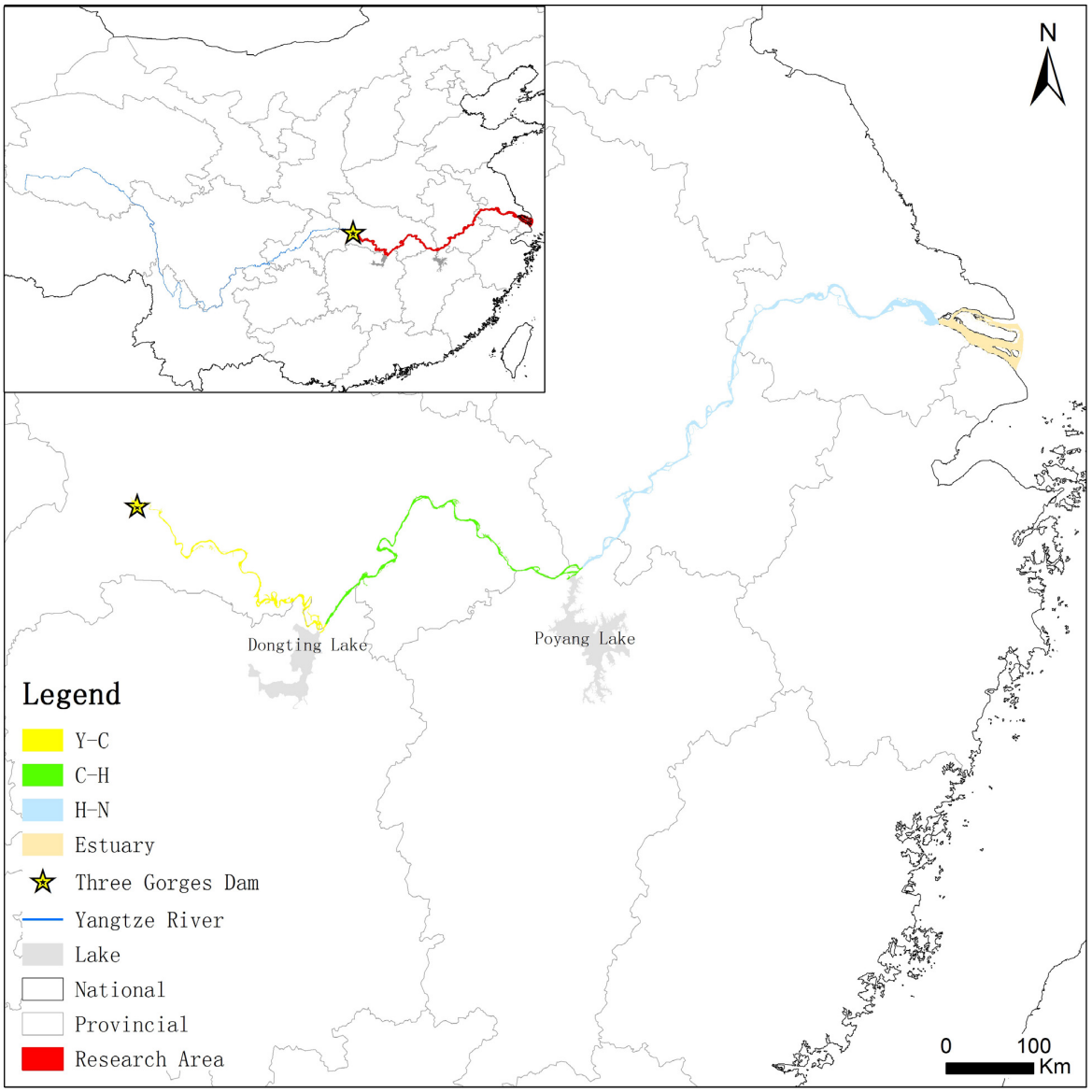

FIGURE 1 | Study area.

predicts change in every future moment (or period), according to situation and probability of an event at a certain time. Key is to determine probability of event occurrence and transitions (Anderson and Goodman, 1957). CA is a grid dynamic model with discrete time, space, and state variables that has ability to simulate spatiotemporal evolution process of complex systems. The CA_Markov model is a combination of the Markov chain and CA models in IDRISI software. It makes full use of advantages of the Markov chain to make long-term predictions and ability of CA to simulate spatial variations in complex systems, thereby forecasting future changes based on existing land-use patterns.

Test of predictive power of CA-Markov model: We used cross tabulation method to calculate Kappa index for model test, using 1990 and 1995 data in N-E to predict spatial distribution of wetlands in 2000. Then we did cross tabulation between predictive and real spatial distribution of the N-E wetlands in 2000, with the Kappa index 0.97 which confirm model is reliable (Li et al., 2020; Lu et al., 2020; Wang et al., 2020). **Figure 2** shows comparison results of predictive and real spatial distribution of wetlands in 2000.

1990 and 2000 interpretation data were used to predict spatial distribution of wetlands in 2010 and 2030 under assumption of no TGD. We also used 2005 and 2015 data to predict distribution of wetlands in 2030 under assumption of the TGD operation.

We calculated areas of floodplains and compared distribution of wetlands in simulated and actual 2010 scenarios. We then

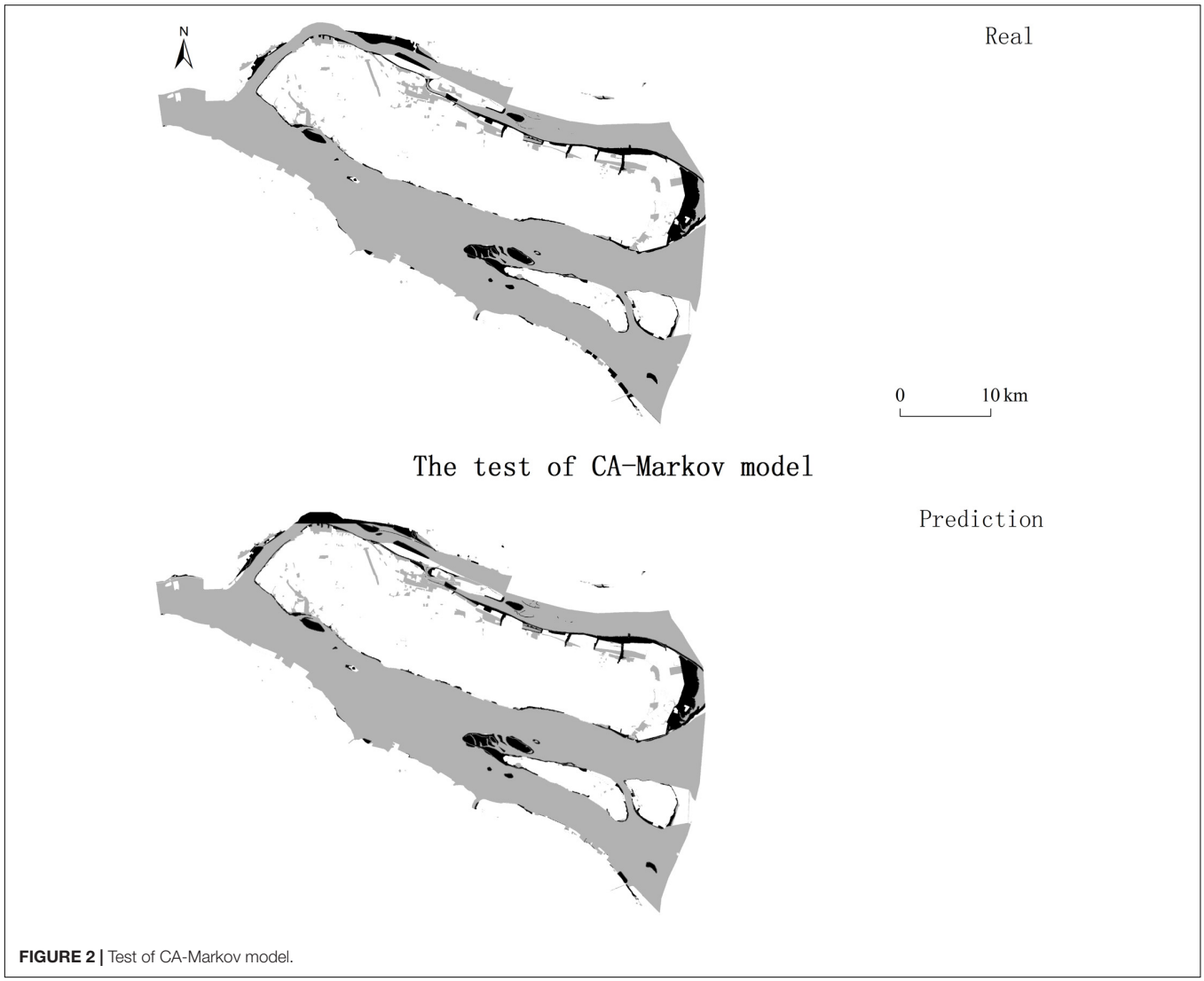

FIGURE 2 | Test of CA-Markov model.

calculated floodplain area in 2030 under both scenarios and siltation rate (P_s) difference from 2010 to 2030:

$$\mathbf{P_s} = (\mathbf{A_{2030}} - \mathbf{A_{2010}})/\mathbf{A_{2010}}, \quad (3)$$

where $\mathbf{P_s}$ is siltation rate, $\mathbf{A_{2030}}$ is area of floodplain in 2030, and $\mathbf{A_{2010}}$ is area of floodplain in 2010.

RESULTS

Changes in Wetland Spatial Structure After the TGD Operation

Yichang-Chenglingji Section

In Yichang-Chenglingji section (Y-C), before the operation of the TGD, the floodplain areas increased by 1613.86 ha from 1990 to 2000, due to increased transition rate from water surface to floodplains (W-F), and reduced transition rate from floodplains to water surface (F-W) (**Table 1**). However, after the operation of the TGD, floodplain area decreased by 1,738.2 ha, due to increased transition rate from floodplains to water surface (**Table 1**). We performed spatial overlay analysis on change in spatial structure between water surface and floodplains during (1990–2000) and (2005–2015). Results showed that floodplain areas decreased in upstream section of Y-C and increased with more red-color areas in downstream region of Y-C (**Figure 3**).

Chenglingji-Hhukou Section

In Chenglingji-Hhukou section (C-H), transition rate from water surface to floodplains maintained as same (1.67%) both before and after the operation of the TGD, whereas transition rate from floodplains to water surface showed increase from 1.38 to 3.77% (**Table 2**). However, overlay analysis between 2000 and 2015 indicated no clear pattern of spatial transition from floodplains to water surface (**Figure 4**).

Hukou-Nantong Section

In Hukou-Nantong section (H-N), the floodplain areas increased by 4,547.97 ha transition rate from water surface to floodplains

TABLE 1 | Wetland transition in the Yichang-Chenglingji section between 1990–2000 and 2005–2015 (area unit: ha).

Wetland type	Floodplains 2000	Water surface 2000	Transition rate (%)
Floodplains 1990	16, 310.80	407.30	2.44
Water surface 1990	2, 021.16	52, 519.80	3.71
Wetland type	**Floodplains 2015**	**Water surface 2015**	**Transition rate (%)**
Floodplains 2005	16, 846.90	1, 861.40	9.95
Water surface 2005	123.20	54, 675.80	0.22

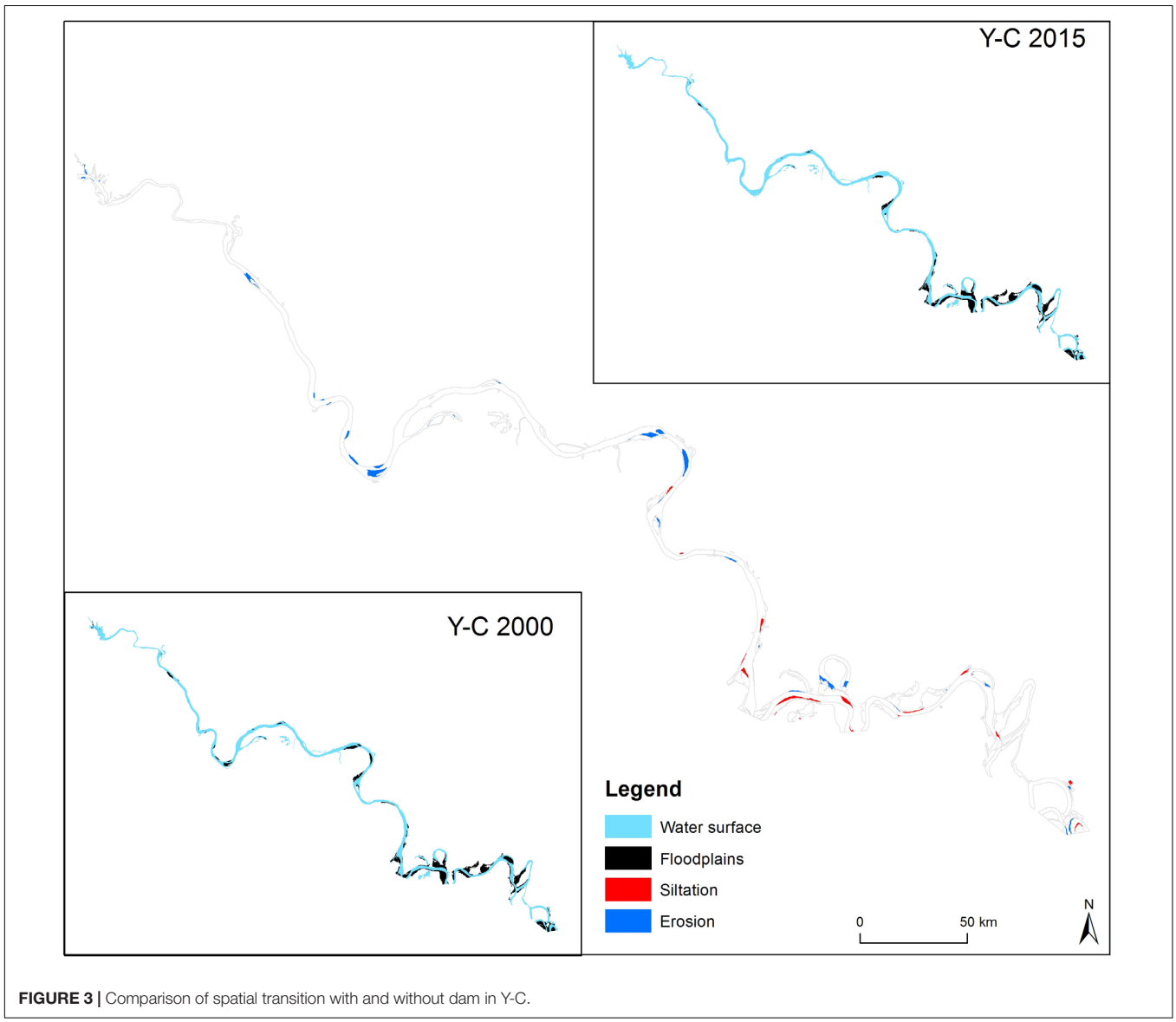

FIGURE 3 | Comparison of spatial transition with and without dam in Y-C.

was 0.33% before and it increased to 2.72% after. Transition of water surface to floodplain were 635.85 ha before the operation of the TGD and increased to 5,183.82 ha afterward (**Table 3**). Based on spatial overlay analysis of water surface and floodplains in H-N section, the added floodplain area extended around original floodplain patches, and they were mainly distributed in downstream region of H-N section, close to estuary (**Figure 5**).

Impact of the TGD on Wetland Landscapes in the Middle and Lower Reaches of the Yangtze River

Yichang-Chenglingji Section

After the operation of the TGD, fragmentation of the water surface and floodplain reduced. Results of FRAGSTATS

TABLE 2 | Wetland transition in the Chenglingji-Hukou section between 1990–2000 and 2005–2015 (area unit: ha).

Wetland type	Floodplains 2000	Water surface 2000	Transition rate (%)
Floodplains 1990	17, 640.90	246.15	1.38
Water surface 1990	1, 506.27	88, 895.30	1.67
Wetland type	**Floodplains 2015**	**Water surface 2015**	**Transition rate (%)**
Floodplains 2005	18, 340.50	718.27	3.77
Water surface 2005	1, 510.13	89, 047.10	1.67

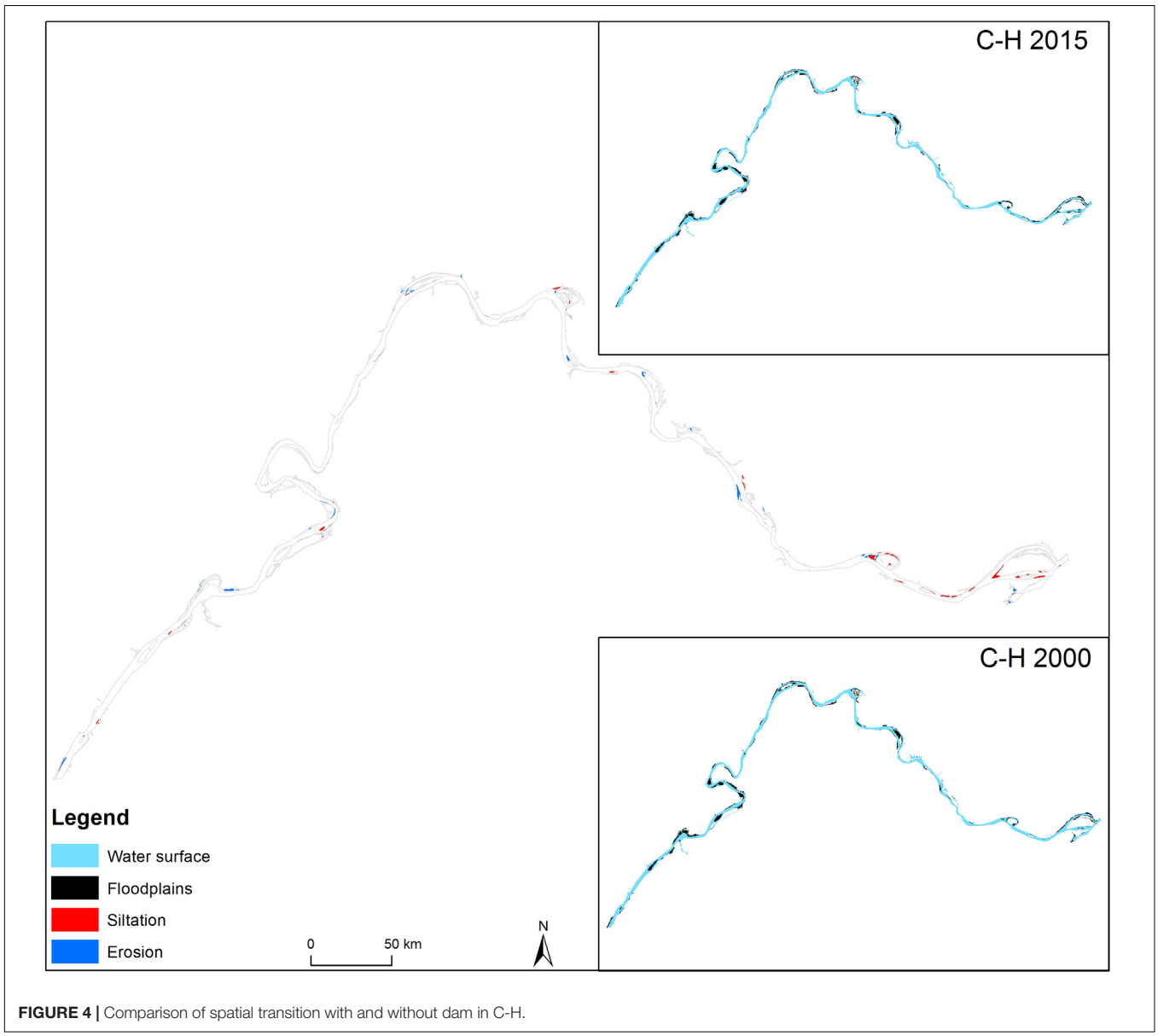

FIGURE 4 | Comparison of spatial transition with and without dam in C-H.

analysis showed that number of patches (NP) and patch density (PD) indexes of water surface and floodplains decreased in Y-C. Further, percentage of landscape (PLAND) index of water surface increased and that of the floodplain decreased. Mean patch areas (AREA_MN) index of water surface increased from 138.05 to 404.72 ha, while floodplain increased from 57.69 to 137.99 ha (**Table 4**).

Chenglingji-Hukou Section

After the operation of the TGD, fragmentation of water surface and floodplain reduced, siltation was not significant

TABLE 3 | Wetland transition in Hukou-Nantong section between 1990–2000 and 2005–2015 (area unit: ha).

Wetland type	Floodplains 2000	Water surface 2000	Transition rate (%)
Floodplains 1990	55, 259.10	291.74	0.53
Water surface 1990	635.85	190, 006.00	0.33
Wetland type	**Floodplains 2015**	**Water surface 2015**	**Transition rate (%)**
Floodplains 2005	5, 5726.10	175.33	0.31
Water surface 2005	5, 183.82	185, 404.00	2.72

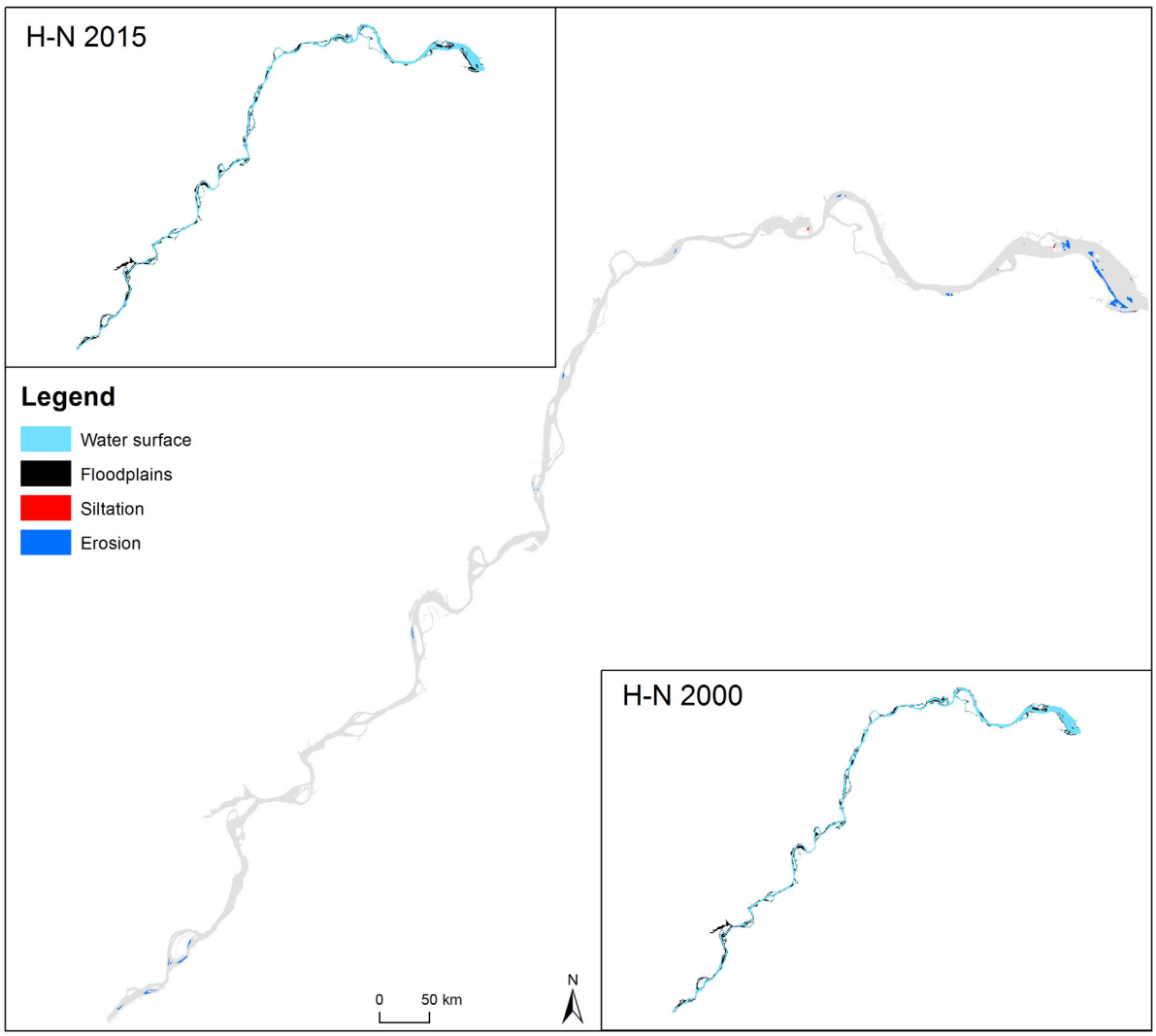

FIGURE 5 | Comparison of spatial transition with and without dam in H-N.

TABLE 4 | Wetland landscape of Yibin-Chenglingji section in 2000 and 2015.

TYPE	PLAND		NP		PD		AREA_MN	
	2000	2015	2000	2015	2000	2015	2000	2015
Water surface	74.42	76.95	389.00	140.00	0.54	0.19	138.05	404.72
Floodplains	25.58	23.05	320.00	123.00	0.44	0.17	57.69	137.99

TABLE 5 | Wetland landscape of the Chenglingji-Hukou in 2000 and 2015.

TYPE	PLAND		NP		PD		AREA_MN	
	2000	2015	2000	2015	2000	2015	2000	2015
Water surface	82.19	81.88	517.00	130.00	0.48	0.12	173.04	690.98
Floodplains	17.81	18.12	565.00	251.00	0.52	0.23	34.30	79.18

TABLE 6 | Wetland landscape of the Hukou-Nantong in 2000 and 2015.

TYPE	PLAND		NP		PD		AREA_MN	
	2000	2015	2000	2015	2000	2015	2000	2015
Water surface	77.31	75.24	286	346	0.12	0.14	665.90	537.72
Floodplains	22.69	24.76	511	435	0.21	0.18	109.39	140.78

TABLE 7 | No dam and dam siltation areas and rate in the middle and lower reaches of the Yangtze river.

Section	Types	No Dam			Dam		
		2010(ha)	2030(ha)	Siltation rate	2010(ha)	2030(ha)	Siltation rate
Y-C	Floodplains	190.78	190.38	−0.0021	123.87	101.70	−0.1790
	Water surface	455.45	455.65		543.26	520.44	
C-H	Floodplains	178.09	202.28	0.1358	163.28	181.95	0.1144
	Water surface	855.80	830.35		868.66	853.10	
H-N	Floodplains	256.32	268.40	0.0471	257.10	296.11	0.1517
	Water surface	1, 848.12	1836.20		1, 847.48	1658.94	
N-E	Floodplains	366.11	365.96	−0.0004	161.65	370.40	1.2914
	Water surface	1, 336.01	1336.01		1, 606.54	1210.27	

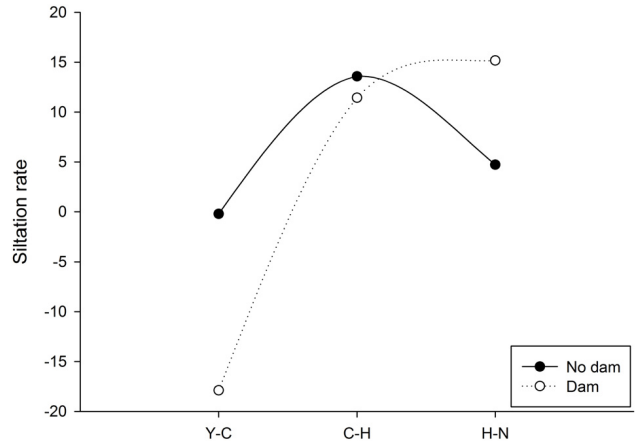

FIGURE 6 | Siltation index trends with and without dam.

in Chenglingji-Hukou section. Results show that NP index of water surface decrease from 517 to 130, the index of floodplains decreased from 565 to 251. PLAND index of water surface decreased, and that of floodplains increased. AREA_MN index of floodplains and water surface increased, but increasing was relatively small from 34.3 to 79.18 ha (**Table 5**).

Hukou-Nantong Section

After the operation of the TGD, fragmentation of water surface area increased and floodplains decreased. NP index of surface water increased from 286 to 346, and PD index of the water surface increased from 0.12 to 0.14. NP index of floodplains decreased from 511 to 435, and PD index decreased from 0.21 to 0.18. PLAND index of water surface decreased, and that of floodplain increased. AREA_MN index of water surface decreased from 665.9 to 537.72 ha, meanwhile floodplain increased from 109.39 to 140.78 ha, after the operation of the TGD (**Table 6**).

Predictions of Wetland Changes Along Main Stream of the Yangtze River

CA_Markov model prediction for 2030 indicates (**Figure 6**), under the operation of the TGD, immediate downstream, Yichang-Chenglingji section will become more eroded (from 0.0021 to 0.1790), in Chenglingji-Hukou section, siltation rate will be lowered from 0.14 to 0.11, whereas in Hukou-Nantong section, siltation rate will be increased from 0.05 to 0.15 (**Table 7**).

Estuary Wetland Spatial Distribution and Landscape Pattern Changes

Estuary Wetland Spatial Structure Changes

Before the operation of the TGD, estuary experienced erosion, as transition rate from floodplains to water surface was 12.91%,

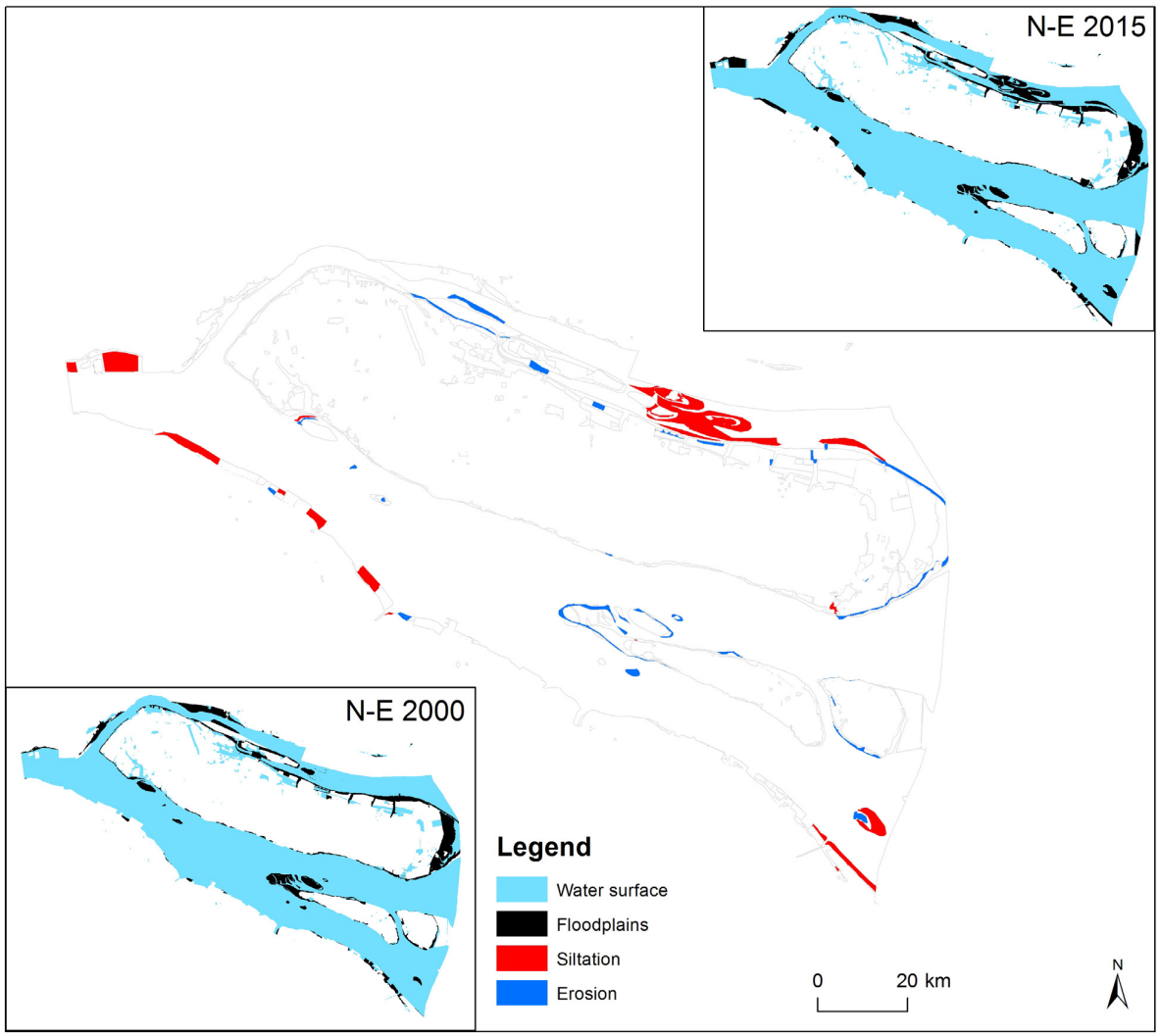

FIGURE 7 | Comparison of spatial transition with and without dam in N-E.

and rate of water surface to floodplains was 0.74%. After the operation of the TGD, transition rate from floodplains to water surface decreased to 12.77%, and water surface to floodplains transition rate increased to 3.83%. Overlay analysis indicated that change in floodplains displayed greater spatial heterogeneity, with the floodplains increased in the north but decreased in the south of Chongming Island. On the other hand, water surface areas increased around edges of floodplains and islands (**Figure 7**). Under no dam scenario, floodplains and water surface areas reached balance in 2010, and the floodplain areas reached 36,611 ha in 2010, and 36,596 ha in 2030. However, with the operation of the TGD, floodplains will increase from 16,165 ha in 2010 to 37,040 ha (**Table 7**).

Estuary Wetland Landscape Changes

After the operation of the TGD, NP index of water surface decreased slightly from 537 to 523, NP index of floodplain increased from 359 to 520, and PD index of water surface and floodplain showed the same trend. AREA_MN index of water surface increased from 317.20 to 319.28 ha, and index of floodplains decreased from 57.28 to 47.31 ha.

DISCUSSION

Spatial Heterogeneity of Wetland Changes and Driver

After the operation of the TGD, changes of wetland in the middle and lower reaches of the Yantze river displayed typical spatial heterogeneity, e.g., erosion at the immediate section downstream (Y-C section), relative stable river section between Dongting Lake and Poyang Lake (C-H section), siltation river section at the lower reaches of Yangtze river. The estuary displayed a complex pattern featured by erosion. Main driver was clear water releasing from the TGD which led to Y-C section erosion, confirms Yang et al. (2017) and Yuan (2014) findings, as well as the turning point

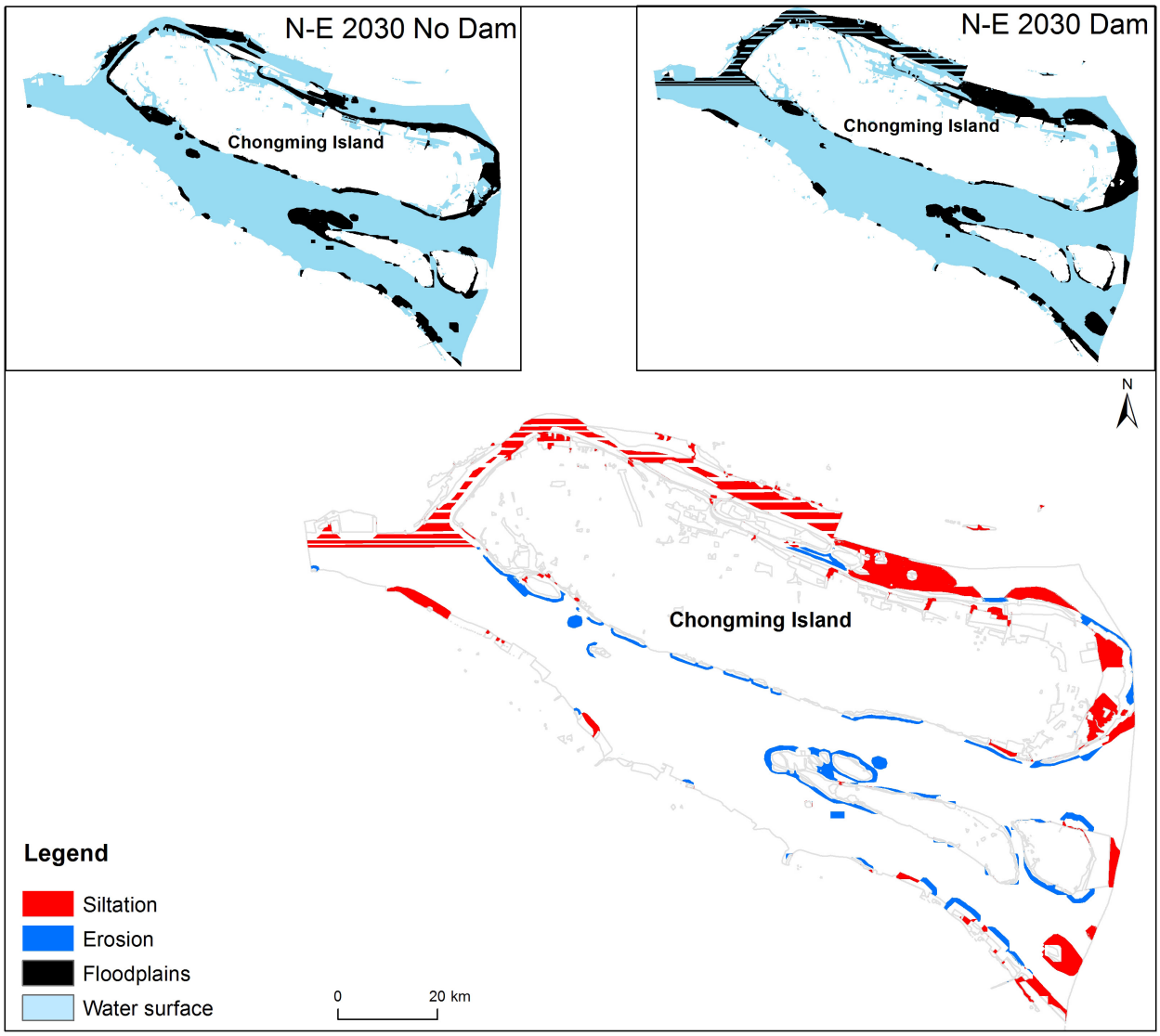

FIGURE 8 | Comparison of estuarine wetland landscape with and without dam.

between Dongting Lake and Jingjiang River in hydrological regim shift (Lu et al., 2018). The relative stable status in floodplains and water surface areas between Chenglingji and Hukou may be the consequences of water and sediments dynamics of mainstream Yangtze and Dongting Lake, such stable status may continue for a period of time depending the speed of river bed erosion of the lower part of Y-C section. Siltation at H-N section remains similar to the period before the operation of the TGD, which is a continue processes and combination of Poyang Lake (Duan, 1993; Li, 2009; Su et al., 2019).

Asymmetric Erosion Between Mainstream and Two Lakes

Dongting Lake is one of the largest freshwater lakes in China, and has been listed as one of the most important wetland biodiversity region. It has been fed by four rivers and three major waterways from Yichang-Chenglingji section of Yangtze River (which is also called Jingjiang River), among which water inflow from Jingjiang River accounts for 50%. However, since the operation of the TGD, clear water released from the dam scoures river bed at Yichang-Chenglingji section, led to decrease of river water level, and shifted permanent river channels to seasonal rivers between Yangtze River and Dongting Lake. Thus causes asymmetric erosion between mainsteam and its associated floodplain lakes, in particular, Dongting Lake (Lu et al., 2018). After the operation of the TGD, distribution of siltation and erosion along river changed from "bed scouring and beach building" to "erosion of both river bed and banks" (Xu et al., 2010; Dai and Liu, 2013). Asymetric erosion between river and two lakes (Dongting and Poyang), also drives water level recession faster than before, and floodplains exposed when

TGD start fill in water, floodplain vegetation, e.g., Carex grow quickly in autumn before wintering geese ariving and caused food shortage (Guan et al., 2014, 2016). Shift of river channels between Jingjiang and Dongting Lake has significant impact on migration of fishes and Yangtze finless porpoises (Nabi et al., 2018). With the operation of the TGD in the future, combined with climate change effect, such asymmetric erosion in Jingjiang-Dongting Lake wetland complex may become even worse, and thus urgent mitigation measures are needed.

Why Esturay Floodplain Areas Increase

Due to dam effect, the estuary lost 80% of the sediments (Cao and Wang, 2015), which should lead to erosion of the floodplains in the estuary, however, our model suggested the opposite. It is important to note that, the increased floodplain areas are mainly in the north river course, whereas, floodplain areas in the south river course are eroding as most studies suggested (**Figure 8**; Li, 2012). The reason why the estuary floodplains areas increase in the north, may not be linked to the operation of the TGD. Instead, such increase may cause by other two facts. Firstly, the morphological change in Chongming Island drives the northern river cause much less influence by hydrological forces of Yangtze river, and thus the water flow slows down and leads to siltation. Secondly, the sediments deposite in northern river course maybe transport by ocean currents.

CONCLUSION

The operation of the TGD has significantly impact on downstream wetland ecosystems. Our study revealed the relationship with siltation patterns and wetland types transformation after the operation of the TGD, which are critically important to understand ecological characters dynamics in new environmental setting, and provide science-based conservation and restoration recommendation.

After the operation of the TGD, changes between water surface and floodplains areas were spatial heterogeneity. With the increase of distance to the TGD, floodplain erosion force declining gradually. The most important finding is the asymmetric erosion between main river course and its associated floodplain lakes, e.g., Dongting lake. This has significant implications for dam operation in autumn and habitat management.

After the operation of the TGD, floodplain in the estuary is driven by both the Yangtze river and ocean currents. The strong hydrological force and reduced sediments of Yangtze river drive erosion of the southern river course in the estuary, whereas, the weakened hydrological force in the northern river course attracts sedimentation.

DATA AVAILABILITY STATEMENT

The raw data supporting the conclusions of this article will be made available by the authors, without undue reservation.

AUTHOR CONTRIBUTIONS

All authors contribute equally and agreed to be accountable for the content of the work.

FUNDING

This work is supported by the National Key Research and Development Program of China (2017YFC0405303).

REFERENCES

Anderson, T. W., and Goodman, L. A. (1957). Statistical inference about markov chains[J]. *Ann. Mathemat. Stat.* 28, 89–110.

Barter, M., Chen, L. W., Cao, L., and Lei, G. (2004). *Waterbird Survey of the Middle and Lower Yangtze River Floodplain in Late January and Early February*. Beijing: China Forestry Pulishing House.

Barter, M., Lei, G., and Cao, L. (2006). *Waterbird Survey of the Middle and Lower Yangtze River Floodplain (February2005)*. Beijing: World Wildlife Fund-China and Chinese Forestry Publishing House.

Cao, G. C., and Wang, J. (2015). *Observation and Study on Hydrology and Sediment of Three Gorges Project*. Beijing: Science Press.

Cao, L., Barter, M., and Lei, G. (2008). New Anatidae population estimates for eastern China: implications for current flyway estimates. *Biol. Conserv.* 141, 2301–2309. doi: 10.1016/j.biocon.2008.06.022

Chen, Y. (2019). *Connectivity Mechhhanism and Prediction Evaluation Model of Alluvial River System*. Ph.D dissertation, China Iinstitute of Water Resources and Hydropower Research, Beijiing.

Chen, Y. S., Qu, X., Xiong, F. Y., Lu, Y., Wang, L. Z., and Hughes, R. M. (2020). Challenges to saving China's freshwater biodiversity: fishery exploitation and landscape pressures. *Ambio* 49, 926–938. doi: 10.1007/s13280-019-01246-2

Dai, Z., and Liu, J. T. (2013). Impacts of large dams on downstream fluvial sedimentation: an example of the Three Gorges Dam (TGD) on the Changjiang (Yangtze River). *J. Hydrol.* 480, 10–18. doi: 10.1016/j.jhydrol.2012.12.003

Das, S., Pradhan, B., Shit, P. K., and Alamri, A. M. (2020). Assessment of wetland ecosystem health using the pressure-state-response (PSR) model: a case study of Mursidabad district of West Bengal (India). *Sustainability* 12:5932. doi: 10.3390/su12155932

Duan, W. Z. (1993). The relation between cut-offs in lower Jingjiang river and water level at Chenglingji. *J. Sediment Res.* 1, 39–50.

Etienne, F. C., Ben, S. K., Nick, D. C., Max, F., and Peter, B. M. (2020). Reciprocal insights from global aquatic stressor maps and local reporting across the Ramsar wetland network. *Ecol. Indic.* 109:105772. doi: 10.1016/j.ecolind.2019.105772

Fu, C. C., Wu, J. H., Chen, J. K., Wu, Q. H., and Lei, G. C. (2003).) Freshwater fish biodiversity in the Yangtze river basin of China: patterns, threats and conservation. *Biodivers. Conserv.* 12, 1649–1685.

Gao, B., Yang, D. W., and Yang, H. B. (2013). Impact of the three Gorges Dam on flow regime in the middle and lower Yangtze River. *Quat. Int.* 304, 43–50. doi: 10.1016/j.quaint.2012.11.023

Guan, L., Lei, J. L., Zuo, A. J., Wen, L., and Lei, G. C. (2016). Optimizing the timing of water level recession for conservation of wintering geese in dongting lake, China. *Ecol. Eng.* 88, 90–98. doi: 10.1016/j.ecoleng.2015.12.009

Guan, L., Wen, L., Feng, D. D., Zhang, H., and Lei, G. C. (2014). Delayed flood recession in central Yangtze floodplains can cause significant food shortages for wintering geese: results of inundation experiment. *Environ. Manage.* 54, 1331–1341. doi: 10.1007/s00267-014-0350-7

Han, J. Q., and Huang, L. B. (2018). Numerical experiments on stagnation points influenced by the Three Gorges Dam in the Yangtze Estuary. *Water Sci. Technol. Water Supply* 18, 1032–1040. doi: 10.2166/ws.2017.173

Jean-François. P., Andrew, C., Noel, G., and Alan, S. B. (2016). High-resolution mapping of Global surface Water and Its Long-Term changes. *Nature* 540, 418–422. doi: 10.1038/nature20584

Jiang, L., Ban, X., Wang, X., and Cai, X. (2014). Assessment of hydrologic alterations caused by the Three Gorges Dam in the middle and lower reaches of Yangtze River, China. *Water* 6, 1419–1434. doi: 10.3390/w6051419

Lai, X. H. (2018). *The Process and Mechanism of River Channel Erosion Below Three Gorges Dam its Effect and Prediction to Sedimemt Load into the Sea*. PhD dissertation, The East China Normal University, Shanghai.

Li, L. L. (2009). *Hydrodynamics of Jingjiang River and Dongting Lake as a Coupled System*. PhD dissertation, Tsinghua University, Beijiing.

Li, P. (2012). *Variations in Estuarine and Coastal Suspended Sediment Concentration and Delta Accretion/Erosion in Response to Decline in Sediment Supply From the Yangtze River*. PhD dissertation, The East China Normal University, Shanghai.

Li, Y. Y., Chang, J. X., Wang, Y. M., Liu, Q., Fan, J. J., and Ye, D. Y. (2020). Land use simulation and prediction in the yellow river basin based on CA-Markov model. *J. Northwest A F Univ. Nat. Sci.* 48, 1–10.

Liu, J., Niu, J. Y., Zou, Y. A., Lu, S., and Wang, T. H. (2015). Changes in the waterbird community of the ecological Restoored Wetlands in Pudong Dongtan, Shanghai. *Resour. Environ. Yangtze Basin* 24, 219–226.

Liu, W. B., Yang, T., Du, M. Y., Sun, F. B., and Liu, C. M. (2018). Impact of the Three Gorges Dam on the hydrology mechanism of typical hydrologic stations in the middle and lower reaches of the Yangtze River. *Ecol. Environ. Monit. Three Gorges* 3, 8–15.

Lu, C., Jia, Y. F., Jing, L., Zeng, Q., Lei, J., Zhang, S., et al. (2018). Shifts in river floodplain relationship reveal the impacts of river regulation: a case study of Dongting Lake in China. *J. Hydrol.* 559, 932–941. doi: 10.1016/j.jhydrol.2018.03.004

Lu, H. Y., Guo, C., Zhang, T., Hu, C., and Xie, T. (2020). Study on land use change of Panzhou city based on CA- Markov. *J. Guangxi Univ. Nat. Sci.* 45, 550–557.

Margaret, P., and Albert, R. (2019). Linkages between flow regime, biota, and ecosystem processes: implications for river restoration. *Science* 365:aaw2087. doi: 10.1126/science.aaw2087

Mei, Z. G., Chen, M., Li, Y. T., Huang, S. L., Haung, J., Wang, D., et al. (2016). Habitat preference of the Yangtze finless porpoise in a minimally disturbed environment. *Ecol. Model.* 353, 47–53. doi: 10.1016/j.ecolmodel.2016.12.020

Nabi, G., Hao, Y. J., Robeck, T. R., Zheng, J. S., and Wang, D. (2018). Physiological consequences of biologic state and habitat dynamics on the critically endangered Yangtze finless porpoises (*Neophocaena Asiaeorientalis ssp. Asiaeorientalis*) dwelling in the wild and semi-natural environment. *Conserv. Physiol.* 6:coy072. doi: 10.1093/conphys/coy072

Oslon, D., and Dinerstein, E. (2002). The Global 200: priority ecoregions for global conservation. *Ann. Mo. Bot. Gard.* 89, 199–224. doi: 10.2307/3298564

Pan, Q. X., and Hu, X. Y. (2015). Review of 60 years' river channel harnessing of Jingjiang reach in Yangtze River. *Yangtze River* 46, 1–6.

Pan, T., Wang, H., Duan, S. L., Ali, I., Yan, P., and Wu, X. B. (2019). Historical population decline and habitat loss in a critically endangered species, the Chinese Alligator (*Alligator Sinensis*). *Glob. Ecol. Conserv.* 20:e00692. doi: 10.1016/j.gecco.2019.e00692

Park, E., Emadzadeh, A., Alcantara, E., Yang, X. K., and Ho, H. L. (2020). Inferring floodplain bathymetry using inundation frequency. *J. Environ. Manage.* 273:111138. doi: 10.1016/j.jenvman.2020.111138

Postel, S. L., Daily, G. C., and Ehrlich, P. R. (1996). Human appropriation of renewable fresh water. *Science* 271, 785–788. doi: 10.1126/science.271.5250.785

Ramsar Convention on Wetlands (2018). *Global Wetland Outlook: State of the World's Wetlands and their Services to People*. Gland: Ramsar Convention Secretariat.

Su, Z. K., Ho, M., Hao, Z. C., Lall, U., Sun, X., Chen, X., et al. (2019). The impact of the Three Gorges Dam on summer streamflow in the Yangtze River Basin. *Hydrol. Processes* 34, 705–717. doi: 10.1002/hyp.13619

Tian, J. X., Chang, J., Zhang, Z. X., Wang, Y. J., Wu, Y. F., and Jiang, T. (2019). Influence of Three Gorges Dam on downstream low flow. *Water* 11:65. doi: 10.3390/w11010065

United Nations Department of Economic and Social Affairs (2015). . *WorldPopulation Prospects: The 2015 Revision, Key Findings and Advance Tables. Working Paper No. ESA/P/WP.241*. Available online at: https://esa.un.org/unpd/wpp/publications/files/key_findings_wpp_2015.pdf (accessed June 15, 2020).

Vörösmarty, C. J., Green, P., Salisbury, J., and Lammers, R. B. (2000). Global water resources: vulnerability from climate change and population growth. *Science* 289, 284–288. doi: 10.1126/science.289.5477.284

Wang, D. (2010). Last stand on the Yangtze. *Science* 329:378. doi: 10.1126/science.329.5990.378

Wang, J. D., Sheng, Y. W., Gleason, C. J., and Wada, Y. (2013). Downstream Yangtze River levels impacted by Three Gorges Dam. *Environ. Res. Lett.* 8:044012. doi: 10.1088/1748-9326/8/4/044012

Wang, L. X., Zhang, J. W., Meng, N. N., Zhang, S. C., and Liu, Z. (2020). Simulation and prediction of temporal and spatial changes of NDVI in Weihe river basin based on Ca-Markov. *Res. Soil Water Conserv.* 27, 206–212.

Wang, Y. Y., Kao, Y. C., Zhou, Y. M., Zhang, H., Yu, X. B., and Lei, G. C. (2019). Can water level management, stock enhancement, and fishery restriction offset negative effects of hydrological changes on the four major Chinese Carps in China's largest freshwater Lake? *Ecol. Model.* 403, 1–10. doi: 10.1016/j.ecolmodel.2019.03.020

Xie, P., Wu, J. G., Huang, J. H., and Han, X. G. (2016). Three-Gorges Dam:risk to ancient fish. *Science* 302, 1149–1151.

Xu, X. J., Yang, S. L., and Zhang, Z. (2010). Variation in grain size of sedimentin middle and lower changjiang river since impoundment of three gorges reservoir. *Sci. Geol. Sin.* 30, 103–107.

Yang, Y. P., Zhang, M. J., Sun, Z. H., Han, J. Q., Li, H. G., and You, X. Y. (2017). The relationship between water level change and river channel geometry adjustment in the downstream of the Three Gorges Dam (TGD). *Acta Geographica Sinica* 72, 776–789. doi: 10.11821/dlxb201705002

Yuan, W. H. (2014). *The Fluvial Dynamic Process of River-Channel Erosion in the Middle Yangtze River after 3-Gorges Dam Closure-A Prediction of New Sediment Source to Estuary*. PhD dissertation, East China Normal University, Shanghai.

Zhang, H., Kang, M., Shen, L., Wu, J. M., Li, J. Y., Du, H., et al. (2020). Rapid change in Yangtze Fisheries and its implications for global freshwater ecosystem management. *Fish. Fish.* 21, 601–620. doi: 10.1111/faf.12449

Zhang, X., Dong, Z. C., Gupta, H., Wu, G. D., and Li, D. Y. (2016). Impact of the Three Gorges Dam on the hydrology and ecology of the Yangtze River. *Water* 8:590. doi: 10.3390/w8120590

Zhao, S. Q., Fang, J. Y., and Lei, G. C. (2000). Global 200: an approach to setting large_scale biodiversity conservation priorities. *Chin. Biodivers.* 8:435–440.

Conflict of Interest: The authors declare that the research was conducted in the absence of any commercial or financial relationships that could be construed as a potential conflict of interest.

frontiers in Earth Science

ORIGINAL RESEARCH
published: 30 November 2020
doi: 10.3389/feart.2020.557943

Greenhouse Gas Emissions Dynamics in Restored Fens After *In-Situ* Oil Sands Well Pad Disturbances of Canadian Boreal Peatlands

Meike Lemmer[1]*, *Line Rochefort*[1] and *Maria Strack*[1,2]

[1]Department of Plant Sciences, Centre for Northern Studies, University Laval, Quebec, QC, Canada, [2]Department of Geography and Environmental Management, Wetland Soils and Greenhouse Gas Exchange Lab, University of Waterloo, Kitchener, ON, Canada

In-situ oil extraction activities impact the vast mosaic of boreal wetlands and uplands. Peatland restoration in these regions aims at reestablishing crucial peatland functions, such as peat accumulation and carbon (C) sequestration. In order to assess the success of fen restoration, we evaluated the biogeochemical conditions, the seasonal carbon balances via carbon dioxide (CO_2) fluxes and methane (CH_4) emissions, and addressed the global warming potential following different restoration techniques at two restored *in-situ* oil sands well pads, during two consecutive growing seasons. Restoration work involved: 1) the partial or complete removal of introduced well pad construction materials, and spontaneous revegetation, or 2) the partial removal of foreign clay, in addition to reintroduction of typical fen plant species such as *Larix laricina*, *Salix lutea* and *Carex aquatilis*. Comparisons were done with regional reference ecosystems (REF) consisting of three peatlands: a wooded bog, a wooded rich fen and a wooded extreme-rich fen. While the average electric conductivity of restored sectors (946 $\mu S\ cm^{-1}$) was higher compared to REF (360 $\mu S\ cm^{-1}$), the pH was quite similar (pH 5.8 REF, pH 6 restored). Dissolved organic carbon concentration was lower in all restored sectors (5–11 $mg\ L^{-1}$ restored sectors, 15–35 $mg\ L^{-1}$ REF), presumably due to the still incomplete recovery of vegetation and lower organic matter content associated with remnant well pad material. Re-establishment of shrub and brown moss species improved significantly the C uptake. However, the active introduction of plant species was no crucial restoration step, in order to return species beneficial for C uptake. Restoration treatments that were leveled closest to the surrounding REF showed the most similar seasonal C balance to REF. In shallow open water areas resulting from the complete removal of all construction materials, we measured the highest methane emissions making these flooded sites net C sources to the atmosphere with elevated global warming potential. The partial removal of the well pad's mineral soil to near the water table level and the surface elevation of the surrounding ecosystem seems to be the most effective site management method to sequester carbon efficiently. However, further research is needed to evaluate the suitability of this restoration method for the recovery of biodiversity and possible impacts of residual foreign materials on fen ecosystems.

Keywords: fen restoration, oil sands disturbances, mineral wetlands, seasonal net ecosystem exchange modeling, fluxes of carbon dioxide and methane

OPEN ACCESS

Edited by:
Jianghua Wu,
Memorial University of Newfoundland, Canada

Reviewed by:
Ronny Lauerwald,
Université Paris-Saclay, France
Gerald Jurasinski,
University of Rostock, Germany

***Correspondence:**
Meike Lemmer
meike.lemmer.1@ulaval.ca

Specialty section:
This article was submitted to Biogeoscience, a section of the journal Frontiers in Earth Science

Received: *30 April 2020*
Accepted: *22 October 2020*
Published: *30 November 2020*

Citation:
Lemmer M, Rochefort L and Strack M (2020) Greenhouse Gas Emissions Dynamics in Restored Fens After In-Situ Oil Sands Well Pad Disturbances of Canadian Boreal Peatlands. Front. Earth Sci. 8:557943. doi: 10.3389/feart.2020.557943

INTRODUCTION

In the boreal biomes of the northern countries, industrial activities are constantly increasing within the last decades, including the sector of oil sands mining, crude oil and gas extraction. The location of the development of this fast-growing industry coincides with the main distribution of the world's peatlands. Here we investigate the carbon (C) dynamics of disturbed northern peatlands impacted by oil and gas extraction infrastructure, following restoration with a variety of different techniques after in-place (*in-situ*) bitumen extraction has ended. The goal is to evaluate the impact of fen restoration on different ecosystem attributes, such as greenhouse gas emissions and the return of the carbon sequestration function, compared with conditions prior to disturbances.

Undisturbed peatlands are recognized as the most effective C storing ecosystems on earth, which, globally, cover an area of more than 3 million km^2 and store an estimated 644 to 1,105 Pg C (Leifeld and Menichetti 2018; Nichols and Peteet 2019). At the same time, they continuously take up approximately 0.37 Pg carbon dioxide (CO_2) from the atmosphere per year IUCN (International Union for Conservation of Nature) (2017), making them a substantial ally in the fight to reverse global warming. Nevertheless, approximately 1.91 Pg CO_2-e are emitted annually by drained and degrading peatlands (Leifeld and Menichetti 2018). Restoration and rewetting of disturbed peatlands is therefore recognized as a natural climate solution and allows countries to improve their C emission balance according to the national climate action plan under the UN Framework Convention on Climate Change (UNFCCC 2009).

Peatland disturbances by the oil and gas industry in the boreal region of northern Alberta are caused by open-pit oil sands mining activities up to 75 m depth (3% of the deposits), and the deep drilling *in-situ* bitumen extraction infrastructure for oil deposits at ~200 m depth (97% of the deposits; Government of Alberta 2020). The *in-situ* oil sands extraction process involves the construction of thousands of oil extraction well pads scattered across the landscape, associated steam, power, and water treatment plants, processing and storage facilities, and exploration and access roads. While an average oil sands well pad is ~1 ha in size, the total area disturbed, including more than 180,000 well pads and associated facilities installed to date, added up to >149,000 km^2 by 2009 (Lee and Cheng 2009; Natural Resources Canada 2015). These developments occur in the boreal region's vast mosaic of forest and wetlands, and affect the ecosystems' hydrology, biodiversity, and biogeochemistry by ground compaction and introduction of foreign mineral substrates (Price, Heathwaite, and Baird 2003; Graf 2009). In order to stabilize the oil pumps and other processing facilities within a peatland ecosystem, an *in-situ* oil sands well pad needs to be well-drained and firm. The construction process involves the clearing of larger trees and shrubs if necessary and placing of a geotextile over the then leveled original peatland surface, followed by the installation of a 1–2 m thick layer of compacted mineral substrate, prior the installation of pumping equipment and related oil extraction infrastructure. When the oil reserves are exhausted and the well pad will no longer be used, oil sands operators are required to reclaim these disturbed peatlands according to the Alberta Environmental Protection and Enhancement Act (Alberta Queen's Printer 1994). Specifically targeted peatland restoration outcomes anticipating an "equivalent land capability" were defined in 2015, where criteria for restoration assessment are based on the vegetation species composition of bryophytes and vascular plants, biogeochemical soil conditions, such as nutrient supply rate, hydrology and soil organic matter content, as well as landscape quality (Environment and Parks 2017). Environment and Parks (2017) defined the long-term goals of peatland restoration after well pad disturbances to be the return of the interdependent ecosystem functions present prior to disturbance, including water storage and filtration, wildlife habitat, peat accumulation, and carbon sequestration.

Restoring peatland functions after *in-situ* oil sands well site disturbances in Alberta is a fairly new process that has started in 2007. All available trials have stressed the importance of restoring hydrological conditions (Vitt et al., 2011; Vitt, Hayes, and Wieder 2012a; Sobze, Schoonmaker, and Rochefort 2012; Caners and Lieffers 2014). Although few studies have investigated ecological functions returning to restored peatlands after oil sands well site disturbances, the importance of restoring proper hydrologic conditions in peatlands affected by drainage and peat extraction has been broadly studied (Price et al., 2003; Large et al., 2007; Price, McLaren, and Rudolph 2010; Cooper et al., 2017; Ahmad et al., 2020; Saraswati et al., 2020). If oxygen levels rise in the upper peat layer called "acrotelm", which is periodically saturated and aerated according to the changing water table level, microbial activity and aerobic oxidation are enhanced (Price et al., 2003). In the case of disturbed peatlands due to peat extraction, vascular plant cover is often higher following restoration than in comparable undisturbed peatlands (Strack et al., 2016). The higher the vascular plant cover, the higher the ecosystem respiration (R_{eco}) but they also uptake significant amounts of CO_2 at the same time, generally leading to net CO_2 storage (Strack et al., 2006; Nwaishi et al., 2016; Strack et al., 2016; Nugent et al., 2018). Vascular plant species of boreal peatlands in Northern Alberta include shrub species, such as *Betula* sp., *Larix laricina*, *Salix* sp., *Picea mariana*, and ericaceous shrubs like *Rhododendron groenlandicum* and *Vaccinium* sp., as well as herbaceous species, namely *Caltha palustris*, *Comarum palustre*, *Equisetum* sp., *Maianthemum* sp., and a large variety of sedges, such as *Carex aquatilis*, *Carex diandra, Carex bebbii, Carex lasiocarpa, Carex utriculata, Eleocharis* sp., *Eriophorum* sp (Alberta Environment and Sustainable Resource Development (ESRD) 2015). However, vascular peatland plant species, in particular graminoid species such as sedges, rushes, and grasses, are considered to enhance methane (CH_4) emissions due to their large aerenchyma (Green and Baird 2012; Lazcano et al., 2018), while Strack et al. (2017) have found brown mosses to effectively decrease CH_4 emissions. Following a hydrological restoration after peat extraction for example, an increase in the water table level and vascular plant and moss cover result in the return to uptake of CO_2, while CH_4 emissions rise due to enhanced methanogenesis, but do not reach the emission rates of natural peatlands (Sundh et al., 1995; Evans, Renou-Wilson, and Strack 2016; Strack et al., 2016; Hemes et al., 2018).

As mentioned above, very few well pad to peatland restoration projects have been attempted to date. In 2012, the moss layer transfer technique (Quinty and Rochefort 2003) was successfully applied on a restored well pad within a wooded bog, in the Carmon Creek division of the Peace River, Alberta. The inversion of the mineral pad and underlying peat layers proved to be a successful base for the introduction of bog moss propagules (Sobze, Schoonmaker, and Rochefort 2012). Shunina et al. (2016) conclude from their bog restoration trial in the Cold Lake region, Alberta, that different microtopographic conditions prove to be favorable for different vascular plant and moss species, while they observed a higher resilience toward interannual moisture variation due to changes in water table level. On the other hand, to restore fens on former *in-situ* oil sands well pads, only few attempts have been made during the last 12 years, and our understanding of fen restoration method's abilities to return ecosystem functions remains limited. In this study, we evaluate the effect of different fen restoration techniques on two research sites, located in the oil sands regions of Peace River and Cold Lake, Alberta where a series of different restoration strategies were tested, including the complete and partial removal of the former well pad's mineral soil and clay layers, as well as re-introduction of specific plant species or natural re-vegetation. While the complete removal of a well pad favors the development of shallow open water sectors with aquatic vegetation, the partial removal of the mineral soil promised to achieve a well-adjusted leveling of the residual well pad with the surrounding fen ecosystems, and obtain an optimal water table level to stimulate natural fen revegetation Imperial Oil Resources. (2007). In 2007, Vitt et al. (2011) attempted to imitate fen initiation via paludification, by restoring peatlands directly on the mineral substrate of the well pad. Pioneer plant species were introduced and the water table level was well managed, in order to promote plant succession for the development of organic matter accumulation over time (Vitt et al., 2011; Koropchak et al., 2012). The introduction of sedge species known to colonize early stage fens proved successful, if hydrological conditions were maintained (Wieder and Vitt 2006; Vitt et al., 2011; Vitt et al., 2012; Koropchak et al., 2012). Another peatland initiation technique was tested in 2009, focusing on the transfer of moss propagules (*Sphagnum* sp.) in addition to the introduction of vascular plant species (Gauthier 2014; Gauthier et al., 2018). This study clearly illustrated the importance of choosing characteristic fen moss species over bog moss species for mineral wetland restoration after well pad disturbances (Gauthier 2014).

The investigated fen restoration techniques in this study represent some first trials to restore Canadian *in-situ* oil sands well pads in the boreal region, hence, the outcomes have not been studied before and no best practice has been established to restore former *in-situ* oil sands well sites. Since the restoration of characteristic peatland functions such as C sequestration and peat accumulation is targeted, our aim was to evaluate the impact of fen restoration techniques on different ecosystem attributes, such as greenhouse gas emission rates and primary production. In this paper we will focus especially on the net ecosystem exchange (NEE) of CO_2 and CH_4 flux dynamics of spontaneously emerged vegetation communities and of communities with intentionally re-introduced species, in restored fens impacted by mineral substrate. Comparisons will be made to regional peatland reference ecosystems. We hypothesize that the net C uptake will be most similar to the rate of reference ecosystems when 1) characteristic fen vegetation species are present, and also when 2) biogeochemical conditions, such as nutrient rates, pH and electric conductivity, are most similar to reference peatlands. We further hypothesize that 3) CH_4 emissions are enhanced through the complete well pad removal, as in the process created depressions and permanently saturated conditions enhance methanogenesis.

METHODS

Study Sites

This study was conducted in two different research areas in the Peace River and Cold Lake oil sands regions in northern Alberta, Canada (**Figure 1**). Two decommissioned *in-situ* oil sands well pads and three adjacent reference ecosystems served as study sites. Both well pads were about 100 m by 100 m in size and were constructed in the following manner: first, trees and taller shrubs were cut, then a geotextile was placed over the remaining vegetation upon the original peatland, and then 1–2 m compacted clay was laid down on the top of it to stabilize the "swampy" ground before the oil extraction equipment and infrastructure were installed.

Well Pad in the Peace River Oil Sands

Located 35 km northeast of the city of Peace River, Alberta, one well pad was constructed within a wooded bog ecosystem (56°23'0.95"N, 116°46'43.43"W). In the adjacent bog, a natural undisturbed sector was chosen as one REF for this study (see Reference sites; **Figure 2**). Peace River, the well pad's name from here on, is located in the Dry Mixedwood natural region of Alberta's boreal region (Beckingham and Archibald 1996), with 70% of its annual precipitation falling between April and August, while the annual average precipitation reaches 386 mm (Government of Canada 2019). The average frost free period is 112 days with average daily temperatures of 13°C between May and September (Government of Canada 2019). Wooded and shrubby fens dominate in this region, while sedge fens and bogs are rather seldomly encountered (Natural Regions Committee 2006).

Peace River was decommissioned in 2000, 20 years post construction. The unaltered original well pad was reclaimed with herb seedings of *Melilotus alba* and *M. officinalis*, which were spread atop of the compacted clay surface. In 2007, the site was offered to a research group for a restoration experiment based on the principles of ecological restoration, to assist the return of a peatland. On the east side, a band of the well pad (30 by 100 m) was used to trial treatments to initiate fen development on mineral soil (Vitt et al., 2011; Koropchak et al., 2012). The experimental area was divided into two sectors (**Figure 2**). Within one sector, the clay fill was partially removed in order to create a surface profile sitting on average 4–6 cm above the water table level of the adjacent bog.

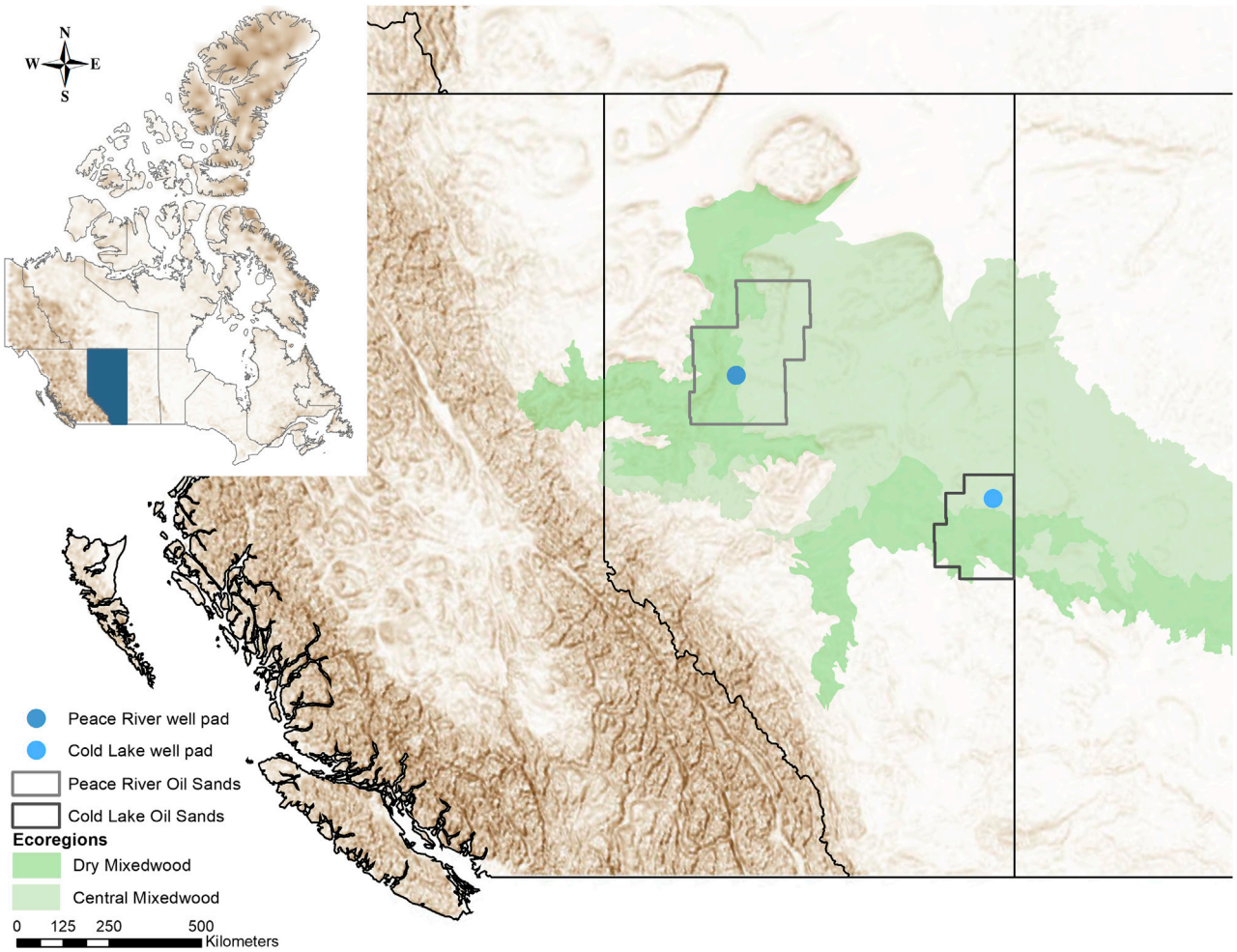

FIGURE 1 | The study sites, two restored *in-situ* oil sands well pads, situated within the oil sands regions of Peace River and Cold Lake. Both sites are located in the Boreal Mixedwood ecoregion of boreal Northern Alberta.

In this study, we refer to this treatment as partial removal with water table at 5 cm (PR-5). Within the second sector, less clay was removed so that the grading would create a surface profile being on average 15 cm above the bog's water level (PR-15). In both sectors, different soil and fertilization amendments were then applied (see Vitt et al., 2011 for details), while *Larix laricina*, *Salix lutea* and *Carex aquatilis* were planted. Ten years following this study, we observe in PR-5 some *S. planifolia* and *S. exigua* present among the very dominant *C. aquatilis*, while in PR-15 *L. laricina*, *S. planifolia* and *S. pyrifolia* were well developed among the mix of dominating *Calamagrostis inexpansa* and *C. aquatilis.* To minimize possible effects of the type of soil amendments on the greenhouse gas dynamics, the measurement plots installed in the present study were chosen within amendments as natural as possible, such as commercial peat, slough hay and control plots without any amendment (Vitt et al., 2011; Koropchak et al., 2012).

Well Pad in the Cold Lake Oil Sands

The second well pad in this study is located 33 km northwest of the city of Cold Lake, Alberta (54°41'10.82"N, 110°30'59.75"W). Cold Lake, what this second well pad will be named from here on, was partially constructed on upland, partially in a wooded rich fen characterized by tall trees and partially in a wooded extreme-rich fen, characterized by shrub-sized tree species (see Reference sites; **Figure 3**). Within each of these two fens adjacent to the well pad, at least 10 m away from any disturbance, a sector was chosen as REF: 1. treed rich fen (*TRF*) and 2. shrubby extreme-rich fen (*SRF*). Cold Lake lies in the moist Central Mixedwood ecoregion of boreal Alberta (Beckingham and Archibald 1996), with an annual average of 421 mm precipitation, an average frost free period of 116 days and a daily average temperatures of 13.9°C during the summer months (Government of Canada 2019).

Cold Lake was decommissioned in 2003, only one year after its construction, due to drilling problems caused by underlying shale. The well pad was subject to different restoration techniques between 2008 and 2009. The central part of the well pad was kept intact in order to continue operating a monitoring well (unrestored study sector, UNR hereafter, **Figure 3**). For another part, a complete removal of all

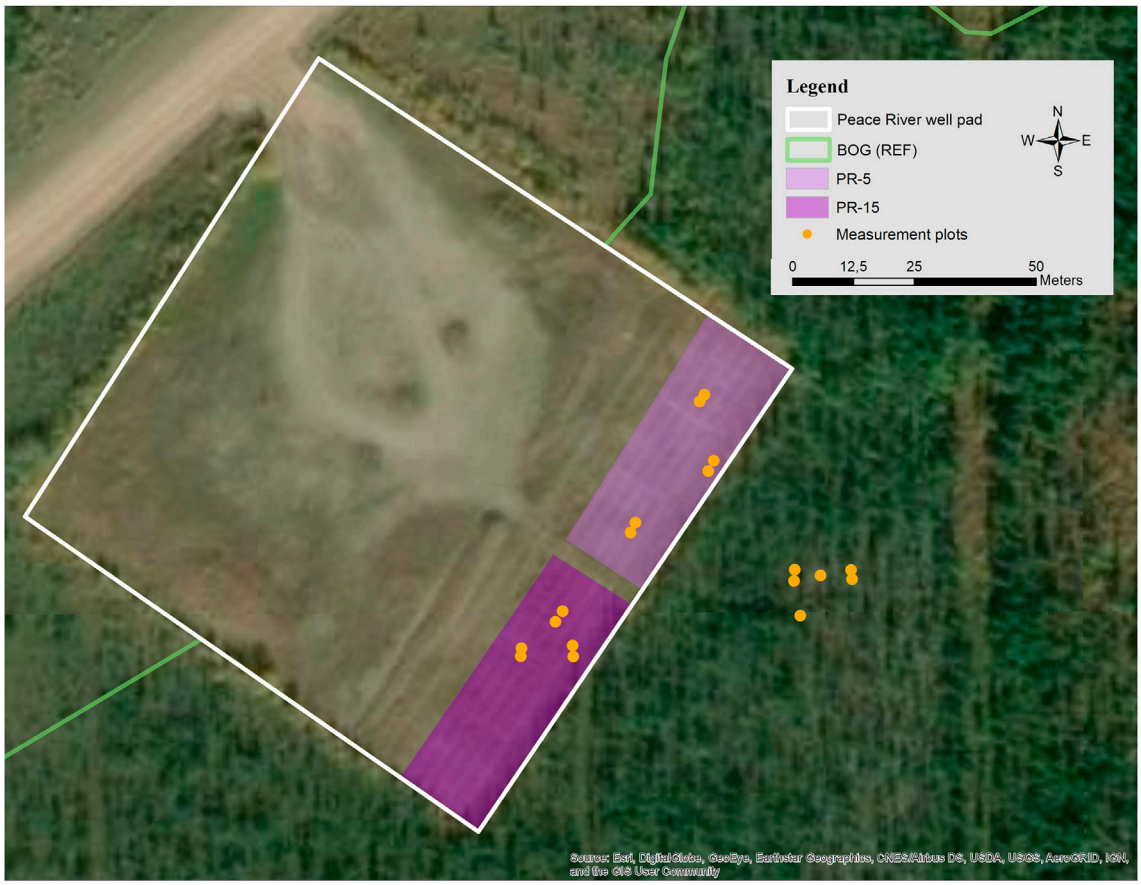

FIGURE 2 | The Peace River well pad (white outline) is located within a wooded bog ecosystem, which serves as reference ecosystem (BOG) in this study. In two restored sectors of the well pad, the mineral soil was partially removed (PR) to 15 cm (PR-15) and to 5 cm (PR-5) above the water table of the adjacent peatland. Yellow dots indicate measurement plots.

introduced building materials (mineral substrate and geotextile) was achieved in spring 2008 (complete removal, CR). In this complete removal sector, a shallow open water area established due to compaction of the underlying peat by the weight of the mineral material. For a third part of the pad, a partial removal of the mineral substrate was carried out successively during 2008 and 2009, as done at Peace River. The goal was to obtain a surface elevation similar to that of the surrounding fens, where water table is close to surface elevation (PR-0). All restored sectors of Cold Lake were left to revegetate spontaneously, with the reasoning that the surrounding wetlands could provide a natural source of diaspores by dispersion. By 2017, emergent aquatic vegetation and a floating moss carpet with sedges and emergent *Salix* sp. and *Betula* sp. had formed in the CR sector. We separated the PR-0 sector into two areas with diverse ground relief, where different marsh-like vegetation communities had established. One part is characterized by an uneven relief forming drier and wetter microhabitats, where dominant *Typha latifolia*, *Salix* sp., and sedge communities formed (named PR-0-D/W, D for dry and W for wet). The other sector's ground relief is even, and a diverse moss layer formed between abundant *Equisetum* spp. and *T. latifolia* (named PR-0-E, E standing for even).

Reference Sites

Three peatland REF served as monitoring sites for comparison: *BOG* (56°22'59.50"N, 116°46'38.60"W; **Figure 2**), a wooded bog, had a characteristic tree and shrub vegetation composition of *Picea mariana*, *Rhododendron groenlandicum*, *Chamaedaphne calyculata* and *Vaccinium vitis-idaea*, as well as a dense moss layer with *Sphagnum fuscum*, *S. rubellum* and *Ptychostomum pseudotriquetrum*. *TRF* (54°41'8.88"N, 110°31'4.06"W; **Figure 3**), a wooded rich fen, had a distinct tree layer with *P. mariana* and *Larix laricina*, a shrub layer with *R. groenlandicum* and a ground layer with *Equisetum hyemale*, *Menyanthes trifoliata* and moss species, such as *Aulacomnium palustre*, *Helodium blandowii* and *Tomentypnum nitens*. *SRF* (54°41'14.80"N, 110°31'0.54"W; **Figure 3**) was a wooded extreme-rich fen with abundant *Betula pumila*, *Salix* sp. and *L. laricina* that formed a shrub mosaic with abundant herbaceous vegetation like *Equisetum* sp., *M. trifoliata*, *Triglochin maritima*, and sedges, such as *Carex lasiocarpa, C. interior, and C. sartwellii*.

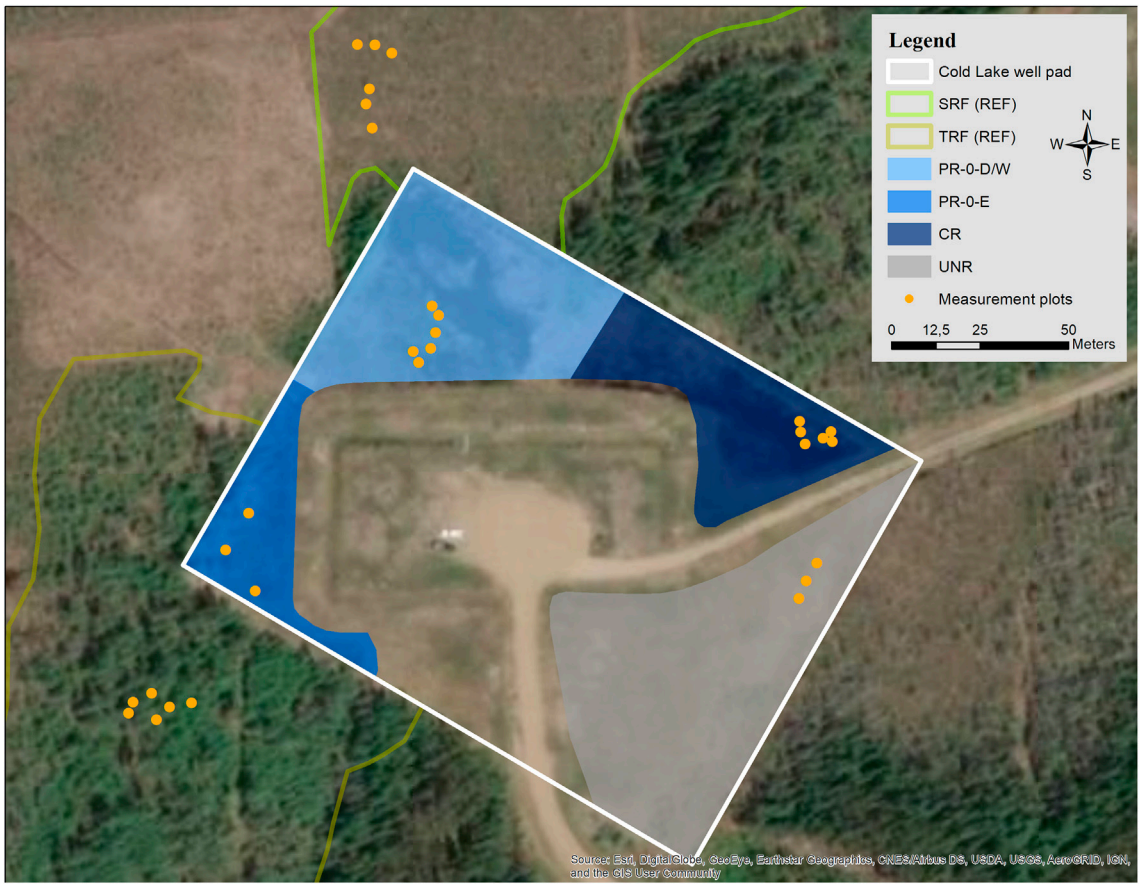

FIGURE 3 | The Cold Lake well pad (white outline) is located within a mosaic of uplands and wetlands, which serve as reference ecosystems (TRF = treed rich fen, SRF = shrubby extreme-rich fen). Blue shaded sectors are restored areas where different restoration techniques of complete and partial mineral soil removal were tested (CR = complete removal, PR-0-D/W and PR-0-E = partial removal of mineral soil to near the adjacent fen ecosystems, with high/dry (D) and low/wet (W) microforms, and with even ground (E)). The gray shaded unrestored sector (UNR) serves as a control sector on the former well pad's residual mineral soil. Yellow dots indicate measurement plots.

Measurement Plots

Within all study sites (Supplementary Figure 1A–I)., monitoring sectors were selected according to the restoration technique applied (see Well pad in the Peace River Oil Sands and Well pad in the Cold Lake Oil Sands) and according to the most representative natural state of the reference sites (see Reference sites). Special focus was placed on the vegetation development resulting from differing microforms (**Table 1**). Microforms were considered either for different elevation, such as hummock/hollow (i.e., in BOG), or for different moisture gradients, such as dry/wet/even (i.e., high lawn with shrubs/low lawn with sedges and mosses/even lawn with mosses). Triplicate measurement plots were selected in each microform within each of the eight study sectors (n = 48) where measurements of CO_2, CH_4, and abiotic data took place (**Figures 2**, **3**). Each measurement plots was defined by a metal collar of 60 × 60 × 20 cm size that was inserted approximately 17 cm deep into the ground, and which served as a base for the gas flux chamber. All plots were accessible via boardwalks in order to mitigate ground disturbance around the installed collars, during measurements. At each plot, data was collected biweekly during the regional vegetation period from May to September of both monitoring years, 2017 and 2018. The large distance between the sites, as well as weather and industry related constraints made a higher sampling frequency impossible to achieve. This data collection corresponded to 10–11 years post-restoration for Peace River and 8–10 years for Cold Lake.

Carbon Dioxide Exchange

Measurements of carbon dioxide fluxes were assessed between May 17 and September 28 in 2017 and between May 14 and August 14 in 2018. Fluxes were measured using a dynamic closed chamber technique with a portable infrared gas analyzer (EGM-4) fitted with a PAR Quantum sensor (both PP Systems, Amesbury, MA, USA) that was placed on top of the chamber during measurements. The 60 × 60 × 30 cm large clear polyethylene chamber was equipped with two standard computer fans connected to an external 12 V battery for air

TABLE 1 | Site characteristics for the unrestored and restored sectors on two former *in-situ* oil sands well sites in Peace River and Cold Lake and three reference sites (SRF, TRF, BOG). Monitoring sectors were selected according to the representativity of the natural state, restoration and re-vegetation technique.

Monitoring sector		Restoration			Microform/moisture gradient	Re-vegetation	
Microform	Site	Substrate removal	Surface elevation	Year		Technique	Dominant plant group
UNR	Cold lake	Unrestored	N. a	2002	Lawn	Spontaneous	Mosses, herbaceous
CR-D	Cold lake	Complete removal	Below surrounding References ecosystems	2008	Floating carpet	Spontaneous	Mosses, herbaceous, small shrubs
CR-W	Cold lake	Complete removal	Below surrounding References ecosystems	2008	Shallow open water	Spontaneous	Floating aquatics
PR-15	Peace river	Partial removal	15 cm above water table	2007	High, dry lawn	Spontaneous	Shrubs, sedges
PR-15-P	Peace river	Partial removal	15 cm above water table	2007	High, dry lawn	Re-introduced	Shrubs, sedges
PR-5	Peace river	Partial removal	4–6 cm above water table	2007	Wet, low lawn	Spontaneous	Sedges
PR-5-P	Peace river	Partial removal	4–6 cm above water table	2007	Wet, low lawn	Re-introduced	Sedges
PR-0-D	Cold lake	Partial removal	Adjusted to surrounding References ecosystem	2009	Dry, high	Spontaneous	Shrubs, herbaceous, mosses
PR-0-W	Cold lake	Partial removal	Adjusted to surrounding natural ecosystem	2009	Wet, low	Spontaneous	Sedges, aquatics
PR-0-E	Cold lake	Partial removal	Equal to surrounding natural ecosystem	2009	Lawn	Spontaneous	Herbaceous, mosses
SRF-D	Shrubby extreme-rich fen	N. a	N. a	N. a	Dry, high lawn	Natural	Shrubs, mosses
SRF-W	Shrubby extreme-rich fen	N. a	N. a	N. a	Wet depression	Natural	Herbaceous
TRF-D	Treed rich fen	N. a	N. a	N. a	Hummock	Natural	Mosses, ericaceous
TRF-W	Treed rich fen	N. a	N. a	N. a	Hollow	Natural	Herbaceous
BOG-D	Wooded bog	N. a	N. a	N. a	Hummock	Natural	Mosses, ericaceous
BOG-W	Wooded bog	N. a	N. a	N. a	Hollow	Natural	Ericaceous, sedges

circulation, a thermocouple wire to connect to an external type K thermometer (Sper scientific, Scottsdale, AZ, USA), and two tube adapters to connect the IRGA, in order to exchange the sampled air in a circular flow. During measurements, the chamber was fit into the collar's u-profile rim, which we then filled with water in order to create an airtight seal. In sample plots, where water levels were too high to install collars (CR-W) or collars were submerged (PR-0-W) at certain times, the chamber was fitted with a Styrofoam collar, enabling it to float on the surface. In plots, where shrubby vegetation was too large to fit in the 30 cm high chamber, a 60 cm tall extension made likewise from clear polyethylene, with a u-profile collar at the upper edge, was stacked under the chamber. To account for the enlarged chamber volume, calculations for the flux analysis were accordingly adjusted. Readings of CO_2 concentration (ppm), PAR (μmol m^{-2} s^{-1}) and temperature in the chamber (°C) were recorded in a 15 s interval during 105–120 s. Measurements of net ecosystem exchange (NEE) were repeated under full light conditions and imitating different light conditions through shading of the chamber and the PAR sensor with a mesh material. One mesh cover created 25% shading and a second cover imitated up to 48% covered conditions. Ecosystem respiration (R_{eco}) was determined 8–10 min after full light conditions were captured, by blocking all incoming PAR with an opaque tarp covering both the chamber and PAR sensor. Between each measurement imitating different light conditions, the chamber headspace was vented to adjust to ambient conditions.

Methane Emissions

Methane fluxes were measured bi-weekly eight times each year between May 17 and September 28 in 2017 and between May 14 and August 24 in 2018. CH_4 concentration was determined using a closed static chamber technique with opaque polyethylene chambers of the same dimensions as for CO_2 measurements. Chambers were darkened with standard spray-paint, aluminum-colored to reduce heating during the flux measurement. Chamber equipment included one standard computer fan for air circulation connected to an external 12 V battery, a thermocouple connected to an external thermometer and one tube with a three-way-valve in order to extract gas samples. All wires and tubes exited the chamber via a rubber plug that fills a hole (5 cm diameter) in the chamber top. At the same time, the rubber plug served as a regulator for possible build-up of air pressure inside the chamber when fitting the chamber to the collar. Again, water poured into the u-profile rim of the collar created an airtight seal of the chamber headspace. Gas samples were taken at 7, 15, 25, and 35 min after chamber closure using a standard 20 ml disposable syringe connected to the three-way-valve. A 20 ml gas sample from the chamber headspace was stored in a 12 ml round bottom Exetainer vial with a septum lid (Labco Limited, Lampeter, Wales, United Kingdom). The created overpressure was necessary in order to prevent any ambient air leaking in. Also, septum lids were discarded after the third use, in order to prevent any leakage due to repeated piercing. Gas samples were sent to the Wetland Soils and Greenhouse Gas Exchange Laboratory at the University of Waterloo, ON for analysis. Analysis for CH_4 concentrations was done with a Shimadzu GC2014 gas chromatograph equipped with a flame ionization detector (Shimadzu Scientific Instruments, Kyoto, Japan).

Environmental Parameters, Soil and Water Chemistry

At each plot, manual measurements of water table level and soil temperature (ST) were taken biweekly at the same time as flux measurements. Water level was measured at each spot in perforated pipes, serving as well tubes, that were covered with nylon mesh to prevent silting. These were inserted about 50–100 cm deep into the ground. ST was measured at 2, 5, 10, 15, 20, 25, and 30 cm with a thermocouple probe temperature sensor and reader (Digital thermometer, VWR, Radnor, PA, USA). Water chemistry (pH and electrical conductivity) was measured in August of both 2017 and 2018 with an Orion Versastar Advanced Electrochemistry Meter (Thermo Fisher Scientific Inc., Chelmsford, MA, USA).

Soil samples were collected in August 2018 at each measurement spot and were analyzed for plant available nutrient concentrations of ammonium ($N\text{-}NH_4^+$), iron (Fe), phosphate ($P\text{-}PO_4^{3-}$), and sulfate ($S\text{-}SO_4^{2-}$) as well as for DOC, as these elements were considered indicators of nutrient status and redox state. Analysis for $P\text{-}PO_4$, and $S\text{-}SO_4^{2-}$ were done using a FIA Quikchem 8,500 Series 2 (Lachat Instruments, Milwaukee, WI, USA). Fe and $N\text{-}NH_4^+$ were analyzed via an ICP Agilent 5110 SVDV (Agilent Technologies Inc., Santa Clara, CA, USA). Solutions for DOC analysis were produced via 1:3 soil to water mixtures from soil samples taken within the top 10 cm at each plot. Filtration was done the following day through a 0.45 μm glass fiber filter and stored at 4°C until being analyzed at the Physical Geography Laboratory at the University of Calgary with a TOC-L analyzer (Shimadzu Scientific Instruments Inc., Columbia, MD, USA).

Environmental data of soil temperature (GS3 sensor) and water temperature (CTD-10 sensor) was continuously recorded via EM 50 data loggers (Meter Group Inc., Pullman, WA, USA) from May to September 2017 and May to August 2018. Water tables were also continuously measured with a levelogger (Solinst Canada Ltd., Georgetown, ON) inside a well tube, while the atmospheric pressure for calculating corrected water table level was measured with barologgers (Solinst Canada Ltd., Georgetown, ON) at each site. Additionally, continuous meteorological data of air temperature, precipitation (ECRN-100 sensor), and photosynthetically active radiation (PAR; PYR sensor) was recorded. At Cold Lake, the data recording station was installed directly on the well pad, whereas at Peace River, only environmental data was recorded on site, while the weather station was set up at a nearby restored well pad (approximately 7 km).

Vegetation

The vegetation survey was done within the different sectors during the peak of the vegetation period, in August of both monitoring years. The cover percentage of each vegetation stratum, as well as the percentage of water, bare peat and litter present, was surveyed in all survey quadrats. For each stratum, an additional focus was put on important plant groups, i.e., *Ericaceae* in the shrub strata, sedges in the herbaceous strata, and *Sphagnum* sp. in the moss stratum. Within each sector, five vascular plant surveys were done using a 1 m^2 survey quadrat and 20 Bryophyte surveys were done using a 625 cm^2 survey quadrats. According to the survey type, all plant species were identified to species level while their respective percentage cover and height (in cm) were noted. We determined if a given species, including vascular and moss species likewise, was characteristic of the different fen types found in Alberta, following (Environment and Parks 2017). From here on we refer to these species as fen typical plant species.

Data Analysis

Instantaneous CO_2 and CH_4 fluxes

NEE ($g\,CO_2\,m^{-2}\,d^{-1}$) was calculated according to the linear change of measured CO_2 concentration over time, considering collar surface area, chamber volume and air temperature. Gross ecosystem productivity (GEP) was then calculated according to **Eq. 1**, considering measured NEE and R_{eco},

$$GEP = NEE - R_{eco} \quad (1)$$

Following the atmospheric sign convention, we use negative values to indicate uptake by the ecosystem from the atmosphere, while positive values indicate the release of carbon dioxide and methane. During data cleaning 1% of the data was discarded, including fluxes without a linear change in concentration over time and negative values of R_{eco}.

Methane fluxes ($mg\,CH_4\,m^{-2}\,d^{-1}$) were calculated according to the linear change of CH_4 concentration over time, in consideration of collar surface area, chamber volume and air temperature inside the chamber. When concentration was low (<3 ppm) and changed less than 0.5 ppm (precision of the sampling and analysis method), respective fluxes were set to 0. In cases where no obvious trend was recognized and where no linearity was achievable, the flux data was rejected. Rejection occurred also in cases of a negative curve following high starting values (>5 ppm). These fluxes are considered as evidence of ebullition caused by ground disturbance during chamber placement and do not represent regular CH_4 fluxes. Following this data cleaning procedure, 5% of the data were discarded.

Statistical analyses were done in R 3.6.0 (R Core Team 2019). The package "ggplot2" was used to create figures (Wickham 2016). Analysis of histograms, residuals and the Shapiro-Wilk test for normality indicated that data was not normally distributed in all cases, but no transformations were able to improve the distribution to normality. Despite the non-normally distributed data, we are confident in reporting on one-way ANOVA results, because of the ANOVA's robustness, where we fit linear models with "microform" as fixed factor and "plot" as random factor. We achieved additional validation by comparison with the results of a non-parametric Kruskal-Wallis test. The Kruskal-Wallis test was validated with a Conover-Iman post-hoc test after Bonferroni adjustment using the package "conover.test" (Dinno 2017), and results were consistent with the ANOVA output. Furthermore, we performed pairwise comparisons using the "emmeans" package and a Tukey Honest Significant Differences (HSD) post hoc analysis with 95% confidence interval (Lenth 2019). We further performed multiple comparisons of treatments between groups with the "agricolae" package (DeMendiburu 2019), in order to complete figures with letters for groups with statistical significant differences. All ANOVAs for NEE and GEP included PAR values >1,000 $\mu mol\,m^{-2}\,s^{-1}$ to obtain rates for CO_2 uptake that were not limited by light availability (Bubier et al., 2003). A statistical significance was accepted when $p < 0.05$.

Environmental Influence on Greenhouse Gas Fluxes

Linear regressions were used to further investigate the effect of vascular plant and moss cover, especially of FTP, and water present in the measurement plots, using the lme function (linear mixed effects) in the "nlme" package (Pinheiro et al., 2019). Regressions were calculated between mean seasonal fluxes of CO_2 and CH_4, and nine independent variables including water table level (WTL), soil temperature at 5 cm depth (ST_5), cover of fen typical plant species (FTP), and of all plant functional types (trees, shrubs, ericaceous, herbaceous, sedges, mosses, Sphagnum) and surface available water, litter and bare soil, while plot functioned as a random factor to account for repeated measures over the two years. Package "MuMIn" was used to determine the marginal and conditional R^2 (Bartoń 2020). We used a principal component analysis (PCA) to examine the variation among measurement plots considering biotic and abiotic data, and furthermore to explain the variables' contribution to the observed differences among the plots.

Seasonal Carbon Balance

The seasonal carbon balance was estimated according to **Eq. 2**, where the seasonal GEP ($g\,CO_2\,m^{-2}\,h^{-1}$) modeling was done following Baird et al. (2019), fitting a two-parameter model with PAR values in a non-linear regression:

$$GEP = \frac{\alpha \times PAR \times GP_{max}}{(\alpha \times PAR + GP_{max})}. \quad (2)$$

The model parameters are given physical meaning as α represents the slope of a rectangular hyperbola, Q, and gross photosynthesis GP_{max} is the asymptotic limit theoretical maximum (Baird et al., 2019).

Modeling R_{eco} ($g\,CO_2\,m^{2}\,h^{1}$) was done following Renou-Wilson et al. (2014), who considered water table level (WT) and soil temperature in order to factor in the different microforms' diverse moisture regimes, using the **Eq. 3**:

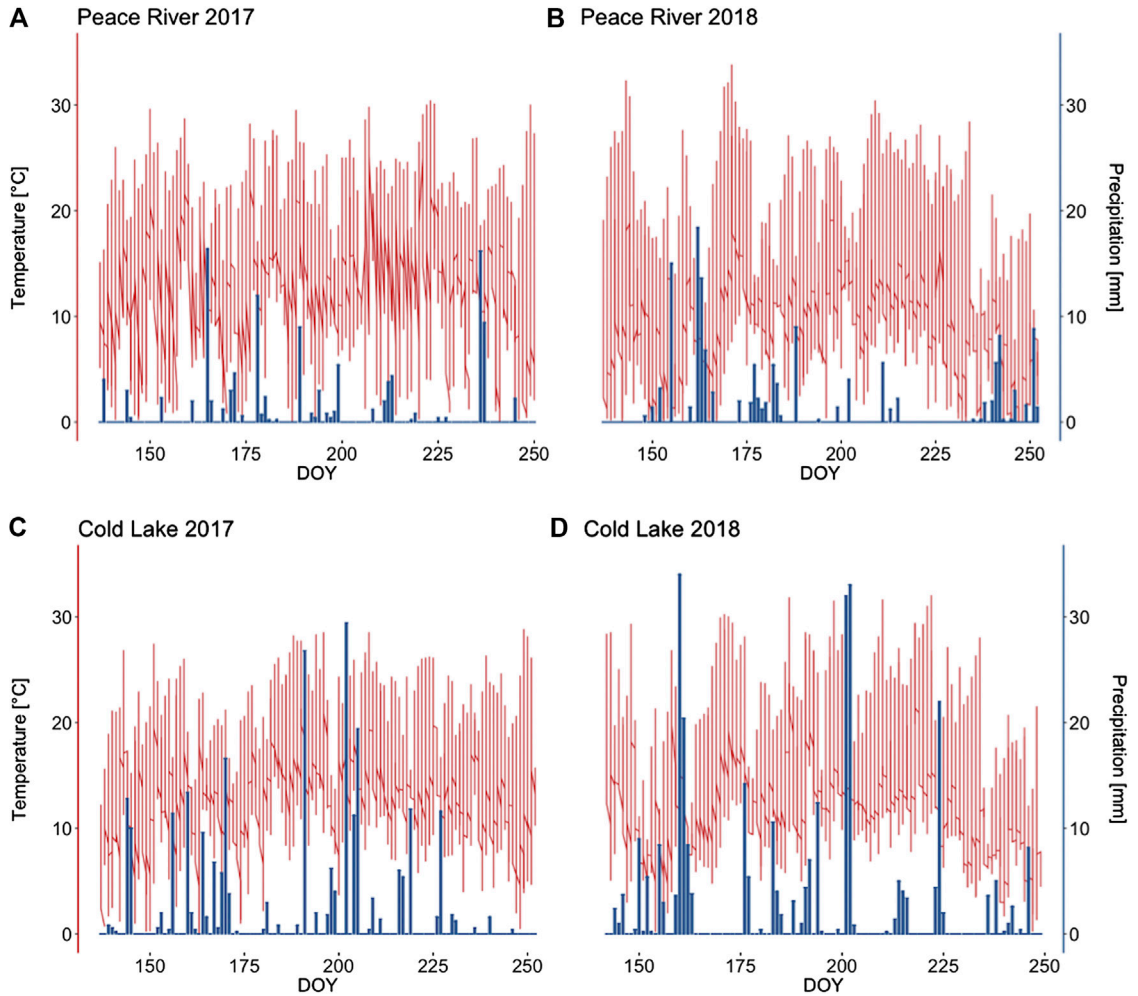

FIGURE 4 | Precipitation (mm) and air temperature (°C) measured at a meteorological station on restored *in-situ* oil sands well pads in the Peace River and Cold Lake Oil Sands, during the monitoring period (May 17 until September 9) in the years 2017 **(A+C)** and 2018 **(B+D)**.

$$R_{eco} = (a + (b \times WT)) \times \left[\exp\left(c \times \left(\frac{1}{T_{Ref} - T_0} - \frac{1}{T_{Soil} - T_0} \right) \right) \right], \quad (3)$$

where a, b, and c are model parameters, T_{Ref} is the reference temperature of 283.15 K, T_0 is the temperature at biological activation (227.13 K), and T_{Soil} is the measured soil temperature at 5 cm depth (Lloyd and Taylor 1994). Model parameters a, b, and c for the seasonal carbon models of GEP and R_{eco} were calculated using the nonlinear least squares (nls) function in R. GEP and R_{eco} were estimated in half-hourly intervals, averaged and summed for the growing season between May 17 to August 31 in 2017 and between May 22 to September 5 in 2018.

The models' form was evaluated considering statistically significant parameters and the highest possible correlation coefficient between measured and modeled values.

For each collar we fitted an individual model per year, after exploration of the data suggested that models fits were improved by dividing the data. Due to smaller GEP values caused by springtime conditions such as low temperatures and less photosynthesizing vegetation cover in the early season in 2018, we additionally divided the season into early season (May 22 until June 5, 2018) and late season measurements (June 6 to September 6, 2018) for each sector and fit separate models for each collar per season.

Seasonal CH_4 fluxes were estimated by multiplying the measured mean flux values with the number of days for each growing season, following Baird et al. (2019).

RESULTS

Environmental Parameters, Soil and Water Chemistry

The climatic conditions observed during the time of the study were well within the range of the Dry Mixedwood ecoregion's dry

TABLE 2 | Mean ± SD water table level (in cm), pH and electric conductivity (EC in µS cm^{-1}) in all different restoration sectors[a] on two well pads *PRIV* and *CLAK* and three reference ecosystems. Negative values signify a water table below the soil surface, and positive values signify a water table above the soil surface.

Sector[a]	2017			2018		
	WTL	$pH_{(W)}$	$EC_{(W)}$	WTL	$pH_{(W)}$	$EC_{(W)}$
UNR	−26.2 ± 17	6.7 ± 0	1,015.3 ± 194.9	−27.4 ± 11.6	3.6 ± 0.2	604.7 ± 39
CR	29.2 ± 19.7	6.7 ± 0.2	305 ± 9.5	41.6 ± 38.4	6 ± 0.2	245.3 ± 110.2
PR-15	−36.9 ± 19.2	5.8 ± 0.2	2,456 ± 282.4	−15.2 ± 9.5	3.4 ± 0.3	461.3 ± 793
PR-5	−24.1 ± 20.1	6 ± 0.5	1,452.6 ± 1,329.9	1.4 ± 5.2	3.6 ± 0.2	2,573.7 ± 515.9
PR-0-D/W	18.4 ± 10.9	7.3 ± 0.4	458.7 ± 55	20.2 ± 11.3	7.4 ± 0.1	341.5 ± 13.2
PR-0-E	−1.7 ± 3.8	6.9 ± 0.4	687 ± 450.6	-1.9 ± 2.6	7.3 ± 0.1	476.3 ± 232.7
REF-SRF	16 ± 3.9	7.1 ± 0.4	452.3 ± 18.7	15.1 ± 4.7	7.3 ± 0.3	284.9 ± 23.6
REF-TRF	3.1 ± 9.3	6.8 ± 0.2	478.8 ± 9.5	5.5 ± 10.6	5.3 ± 0.1	329.8 ± 4.9
REF-BOG	−25.7 ± 13.3	4.8 ± 0.3	512.9 ± 1,058	−10.4 ± 9.6	3.5 ± 1.4	102.1 ± 54.5

[a]*UNR: Unrestored; CR: Complete removal of mineral soil (MS); PR-15: Partial removal MS to 15 cm above seasonal water table; PR-5: Partial removal of MS to 4–6 cm above seasonal water table; PR-0-D/W: Partial removal of MS to surface elevation of surrounding fen reference ecosystem (uneven ground relief); PR-0-E: Partial removal of MS to near the surrounding fen reference ecosystem (even ground relief); REF-BOG: a wooded bog; REF-TRF: a treed rich fen; REF-SRF: a shrubby extreme-rich fen.*

TABLE 3 | Mean ± SD soil pH and electric conductivity (EC in µS cm^{-1}), as well as mean dissolved organic carbon (DOC in mg 1^{-1}) and plant available soil nutrient supply rates (in mg 1^{-1}) of ammonium ($N\text{-}NH_4^+$), iron (Fe), phosphorus ($P\text{-}PO_4$) and sulfur ($S\text{-}SO_4^{2-}$), in all monitoring sectors[a] in 2018. BDL stands for values below detection limit (detection limit for Fe 0.12 µg L^{-1}).

Sector[a]	$pH_{(S)}$	$EC_{(S)}$	DOC	Fe	$N\text{-}NH_4^+$	$P\text{-}PO_4$	$S\text{-}SO_4^{2-}$
UNR	8 ± 0.2	290 ± 27.6	n.a	BDL	14.4	44.5	24.8
CR-D	4.8 ± 0.3	106.3 ± 13.3	8.6	0.55	168.6	267.5	32.5
PR-15	4.8 ± 0.2	1,109.8 ± 870.8	5	BDL	33.6	85.6	5,608.2
PR-5	4.2 ± 0.3	1,442 ± 753.3	6.3	BDL	21	113.7	1,638.2
PR-0-D	3.2 ± 0.4	378.7 ± 17.2	5.8	2.43	15.9	58.2	12.2
PR-0-W	3.3 ± 0.4	344.3 ± 26.9	6.5	BDL	28.8	88.6	80.8
PR-0-E	5 ± 2.1	348.7 ± 11.5	10.8	BDL	11	76.4	9.7
REF-ERF-D	4.9 ± 0.3	122.5 ± 27.8	24.5	5.43	364.9	330.6	95.7
REF-ERF-W	4.6 ± 0.2	76.1 ± 32.9	15.5	2.97	332.7	296.5	69.2
REF-PF-D	5 ± 0.1	86.7 ± 58.5	n.a	1.76	213	182.2	88.9
REF-PF-W	4.9 ± 0.2	68.7 ± 20.2	n.a	1.47	356.6	355.7	81.5
REF-BOG-D	4 ± 0.2	34.7 ± 10.9	35	2.19	109	117.1	100.2
REF-BOG-W	2.9 ± 0.6	38.9 ± 3.6	28.8	0.90	126.8	85.2	95.2

[a]*UNR: Unrestored; CR: Complete removal of mineral soil (MS); PR-15: Partial removal MS to 15 cm above seasonal water table; PR-5: Partial removal of MS to 4–6 cm above seasonal water table; PR-0-D/W: Partial removal of MS to surface elevation of surrounding fen reference ecosystem (uneven ground relief); PR-0-E: Partial removal of MS to near the surrounding fen reference ecosystem (even ground relief); REF-BOG: a wooded bog; REF-TRF: a treed rich fen; REF-SRF: a shrubby extreme-rich fen.*

climate in Peace River, and the Moist Mixedwood ecoregion's humid climate in Cold Lake (**Figure 4**). During both years of data recording, Cold Lake was characterized by about twice as many rain days as the region of Peace River and even shows consistently higher precipitation data as compared to the 1981–2010 climate normal average of ~213 and ~246 mm (Environment and Climate Change Canada 2019). In both regions, the year 2018 was characterized by much wetter conditions than 2017 (Supplementary Table 1). Due to the higher precipitation in 2018's field season, water table level in the restored and reference sectors were accordingly higher especially in the Peace River region (**Table 2**). We observed an average rise in water table level of 10.4 cm in the restored sectors, compared to an average rise of 5.6 cm in the reference sectors.

The restored sectors PR-5 and PR-15 at Peace River, that were restored by partial removal of the former well pad mineral soil, showed higher values of water pH and electric conductivity in 2017, compared to the water chemistry conditions of wooded fens at SRF and TRF adjacent to Cold Lake, which had lightly more acidic but brackish milieu, with moderate salinity and elevated electric conductivity (**Table 2**). In 2018, the pH of PR-5 and PR-15 were lower and comparable to the conditions of the adjacent acidic BOG. Here, the values were consistently characteristic for ombrotrophic bogs throughout both years, with highly acidic and oligotrophic conditions (Alberta Environment and Sustainable Resource Development (ESRD) 2015). In all other restored sectors, PR-0 and CR at Cold Lake, fen conditions were maintained throughout both years, where the electric conductivity of water declined in the second year on average by 129 µS cm^{-1} compared to the previous year, and pH stayed quite stable throughout both years. The same trend in the drop of electric conductivity and water pH can be seen in the unrestored sector UNR. TRF and SRF water chemistry remained quite consistent during both study seasons, with high pH and slightly brackish conditions typical for fens.

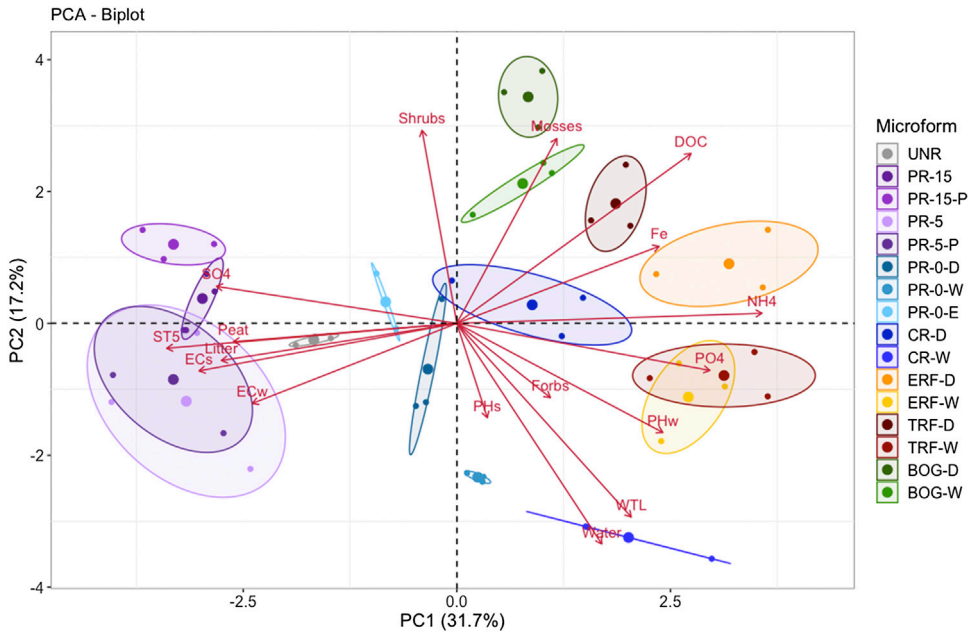

FIGURE 5 | Principle component analysis (PCA) of microforms, according to environmental controls of water table level (WTL), soil temperature at 5 cm depth (ST_5), soil pH (pH_S) and electric conductivity (EC_S), water pH (pH_W) and electric conductivity (EC_W), dissolved organic carbon (DOC), vegetation survey strata (shrubs, forbs, mosses, water, litter, peat), and plant available soil nutrient supply rates (Fe, NH_4, PO_4, SO_4). Strong clustering of monitoring sectors* can be observed.* Restored sectors: UNR = unrestored, PR-15 = partial removal of mineral soil (MS) to 15 cm above seasonal water table, PR-5 = partial removal of MS to 4–6 cm above seasonal water table, PR-0-D/W = partial removal of MS to surface elevation of surrounding fen reference ecosystem (uneven ground relief with microforms dry (D) and wet (W), PR-0-E = partial removal of MS to near the surrounding fen reference ecosystem (even ground relief), CR = complete removal of mineral soil (MS). Reference ecosystem (REF): SRF = shrubby extreme-rich fen; TRF = treed rich fen, BOG = wooded bog.

Acidic soil conditions were maintained in all restored sectors and BOG throughout 2018 (**Table 3**). The only outlier with a slight alkaline pH 8 was observed at UNR. EC of the soil remained notably higher in all unrestored and restored sectors, compared to the REF sectors. Dissolved organic carbon (DOC) in the REF was on average 19 mg L^{-1} higher than in the restored sectors. Comparisons of the average plant available nutrient concentrations of iron, ammonium, phosphorus and sulfur reveal mean concentrations found in the restored sectors were below values found in REF. Only the shallow open water sector CR-D showed REF-equivalent concentrations. In PR-15 and PR-5 we noted exceptionally high sulfur concentrations (5,608 and 1,638 mg S-SO_4^{2-} l^{-1}, respectively). Highest sulfur concentration found in the REF, was measured in BOG-D.

According to the principal component analysis (PCA), the first two components explain 48,9% of the variation in biogeochemistry among study plots (**Figure 5**). Chemical differences are represented in PC1, while PC2 depicts mostly the impact of vegetation and hydrology. The Kaiser-Meyer-Olkin test for sampling adequacy of variables reached 0.57 (Dziuban and Shirkey 1974). Six of the 17 components showed an eigenvalue larger than 1, accounting for more than 81% of the variation. The two variables with the highest loadings are DOC and Fe concentration. A strong clustering according to microforms, especially distinctive between the restored and REF sectors, can be seen (**Figure 5**). Restored and reference sectors are clearly separated along PC1 with REF sites having higher N-NH_4^+, and lower S-SO_4^{2-} and electric conductivity. REF sites were further separated along PC2 depending on differences in vegetation cover, hydrology and pH. Restored sites where fill was removed or scraped to near surface level (PR-0) were closer to the REF sites along PC1 than those sites with thicker fill remaining. CR-W was separated from other sites along PC2 due to deep inundation.

Vegetation

The total vegetation cover in restored sectors ranges from 37% (PR-5) to 80% (PR-0-E), compared to 68–95% in REF (**Table 4**). The high cover in PR-0-E is due to bryophytes covering 54%, which represents the highest moss cover in all sectors. The other restored sectors had similar mix of forbs and mosses, while no especially dominant vegetation strata developed, ranging from a lowest 9% forb-cover in PR-5–45% moss-cover in PR-0-D/W. The shrub-cover of 16% in PR-15 was nearly three times higher than in the neighboring sector PR-5 (4%), while shrub species were planted in both sectors equally during the restoration process. Yet PR-5 is characterized by standing surface water of 40% cover, while PR-15 remains dry. On the other hand, an even higher rate of flooding of 93% water cover in PR-0-D/W does not seem to prevent a natural establishment of plants (67% total vegetation cover) in this sector, of which 7% were shrubs. Considering the fen typical plant species cover, natural fens TRF (74%) and SRF (77%) have more than double the cover compared to the restored sectors PR-15 (31%), PR-5 (34%) and

TABLE 4 | Mean cover (±SD) in % for plant functional types, water, litter and bare soil (mineral soil or peat), as surveyed in August 2017 and 2018 in all monitoring sectors.

Sector[a]	Total	Fen typical plant species	Vascular plants Ligneous		Herbaceous			Bryophytes		Water	Litter	Bare soil
			Trees	Shrubs	Ericaceous	Forbs	Sedges	Brown mosses	Sphagnum			
UNR	68 ± 19	31 ± 46	4 ± 6	4 ± 6		51 ± 24	5 ± 12	16 ± 12			45	7
PR-15	50 ± 19	32 ± 26	16 ± 24	16 ± 24		22 ± 17	18 ± 10	16 ± 19			63	21
PR-5	37 ± 20	35 ± 22	6 ± 9	6 ± 9		9 ± 9	22 ± 9	17 ± 28		14	63	29
PR-0-D/W	70 ± 18	35 ± 25	7 ± 9	7 ± 8	2 ± 6	33 ± 14	22 ± 14	45 ± 27	2 ± 6	57	19	8
PR-0-E	80 ± 24	64 ± 30	3 ± 6	1 ± 3		38 ± 24	24 ± 20	54 ± 27		45	21	8
CR	48 ± 35	32 ± 34	1 ± 1	1 ± 2		13 ± 6	16 ± 15	29 ± 43		67	16	10
SRF	68 ± 25	70 ± 37	32 ± 21	28 ± 20	4 ± 8	31 ± 14	16 ± 8	21 ± 22		50	8	12
TRF	79 ± 29	71 ± 44	75 ± 14	16 ± 17	7 ± 13	31 ± 22	19 ± 22	33 ± 40	15 ± 31	42	5	
BOG	95 ± 3	80 ± 32	15 ± 9	10 ± 10	51 ± 18	7 ± 7	2 ± 2	12 ± 12	47 ± 34		17	4

[a]*UNR: Unrestored; CR: Complete removal of mineral soil (MS); PR-15: Partial removal MS to 15 cm above seasonal water table; PR-5: Partial removal of MS to 4–6 cm above seasonal water table; PR-0-D/W: Partial removal of MS to surface elevation of surrounding fen reference ecosystem (uneven ground relief); PR-0-E: Partial removal of MS to near the surrounding fen reference ecosystem (even ground relief); REF-BOG: a wooded bog; REF-TRF: a treed rich fen; REF-SRF: a shrubby extreme-rich fen.*

PR-0-D/W (31%). Only for PR-0-E, we can report a fen typical plant species cover (64%) comparable to REF.

Greenhouse Gas Exchange and Seasonal Carbon Balance

GEP fluxes in 2017 were between –104.4 g CO_2 m^{-2} d^{-1} at PR-15-P, and –0.1 g CO_2 m^{-2} d^{-1} in SRF-D (**Figure 6A**). In 2018 on the other hand, lowest GEP fluxes were measured in SRF-W (–89.6 g CO_2 m^{-2} d^{-1}), while CR-W showed highest fluxes with –0.2 g CO_2 m^{-2} d^{-1} (**Figure 6D**). NEE in 2017 ranged from –55.9 g CO_2 m^{-2} d^{-1} in PR-15-P to 34.6 CO_2 m^{-2} d^{-1} in ERF-W (**Figure 6B**), and in 2018 from –56.6 g CO_2 m^{-2} d^{-1} in ERF-W to 20.6 CO_2 m^{-2} d^{-1} in CR-W (**Figure 6E**). ANOVA results reveal a significant effect of soil temperature on GEP and R_{eco} in 2017, which is repeated only for R_{eco} in 2018 (**Table 5**). Microform on the other hand has a consistent significant effect on all fluxes, whereas water table level only has a significant effect on all fluxes 2018. We notice that the wetter the microform, the higher the R_{eco} fluxes (**Figure 6**)C+F and CH_4 fluxes (**Figure 7**).

Methane emissions were especially high at all submerged and regularly flooded measurement plots that occurred at CR, SRF, TRF-W (**Figure 7**). The same trend can be noted for extremely wet plots close to the water table level, like PR-0 and PR-5. Microform showed a significant effect on CH_4 fluxes (**Figure 7**). Microforms with highest water table level showed significant effects on CH_4 fluxes, where highest averaged methane fluxes of 417 ± 476 mg CH_4 m^{-2} d^{-1}) in TRF-W, 398 ± 711 mg CH_4 m^{-2} d^{-1} in CR-W, 354 ± 608 mg CH_4 m^{-2} d^{-1} in SRF-W, and 199 ± 294 mg CH_4 m^{-2} d^{-1} in SRF-D were observed. The lowest fluxes on the other hand were recorded at the driest sites with 7 ± 20 mg CH_4 m^{-2} d^{-1} in BOG-D, 1 ± 5 mg CH_4 m^{-2} d^{-1} in BOG-W, 2 ± 8 mg CH_4 m^{-2} d^{-1} in PR-15-P, and 7 ± 19 mg CH_4 m^{-2} d^{-1} in PR-5-P.

In particular CR-W was not comparable with the other restored sectors and behaved in a completely opposite manner, where specifically NEE and GEP in CR-W differed significantly from all other sectors. CH4 fluxes in CR-W and the reference fens showed similarities, whereas all other restored and unrestored sectors were comparable to the reference bog.

Both linear regression analyses to evaluate spatial variation in NEE and CH_4 fluxes based on environmental variables, such as vegetation strata, water table level and soil temperature at 5 cm depth were found to be significant (**Table 6**). While for NEE the significant variables were soil temperature, shrub cover, and forb cover, the significant variables to predict CH_4 fluxes were soil temperature at 5 cm, water table level, cover of ericaceous, and cover of sedges. The higher the cover of these plant functional types, the higher the emission rates observed in the respective sectors. Despite wetter and colder weather conditions in 2018, we did not observe a significant effect of climate on CH_4 emissions. Compared to the first year, methane fluxes actually decreased by almost 45% in 2018. Furthermore, we cannot confirm any significant relation between NEE or CH_4 fluxes and fen typical plant species.

Modeled seasonal net ecosystem exchange revealed restored and REF sectors to be greater C sources in 2017 than in 2018 (**Table 7**). A cumulative two-year total C balance shows that C sinks have established in the restored sectors closest to the water table level, in PR-5, PR-0-D and PR-0-E, and CR-D, ranging from –625 to –67 g C m^{-2} (**Table 8**). On the contrary, very wet sectors with inundated conditions, such as PR-0-W, CR-W, and SRF acted as C sources with C emission up to 1,039 g C m^{-2}. Very dry sectors, such as PR-15 and UNR also act as C sources.

DISCUSSION

Reestablishing hydrological conditions has become the main goal in peatland restoration (Bonn et al., 2016). However, several studies report an increase of CH_4 rates during the first years of rewetting of sites previously drained and used for peat extraction, due to higher methanogenesis activity (Jordan et al., 2016; Nugent 2019). Reported greenhouse gas fluxes of restored peatlands range from –90 to –30 g CO_2-C m^{-2} $d^{-1}$and 3.7–4.2 g CH_4-C m^{-2} d^{-1} (Strack, Keith, and Xu 2014; Abdalla et al., 2016; Nugent et al.,

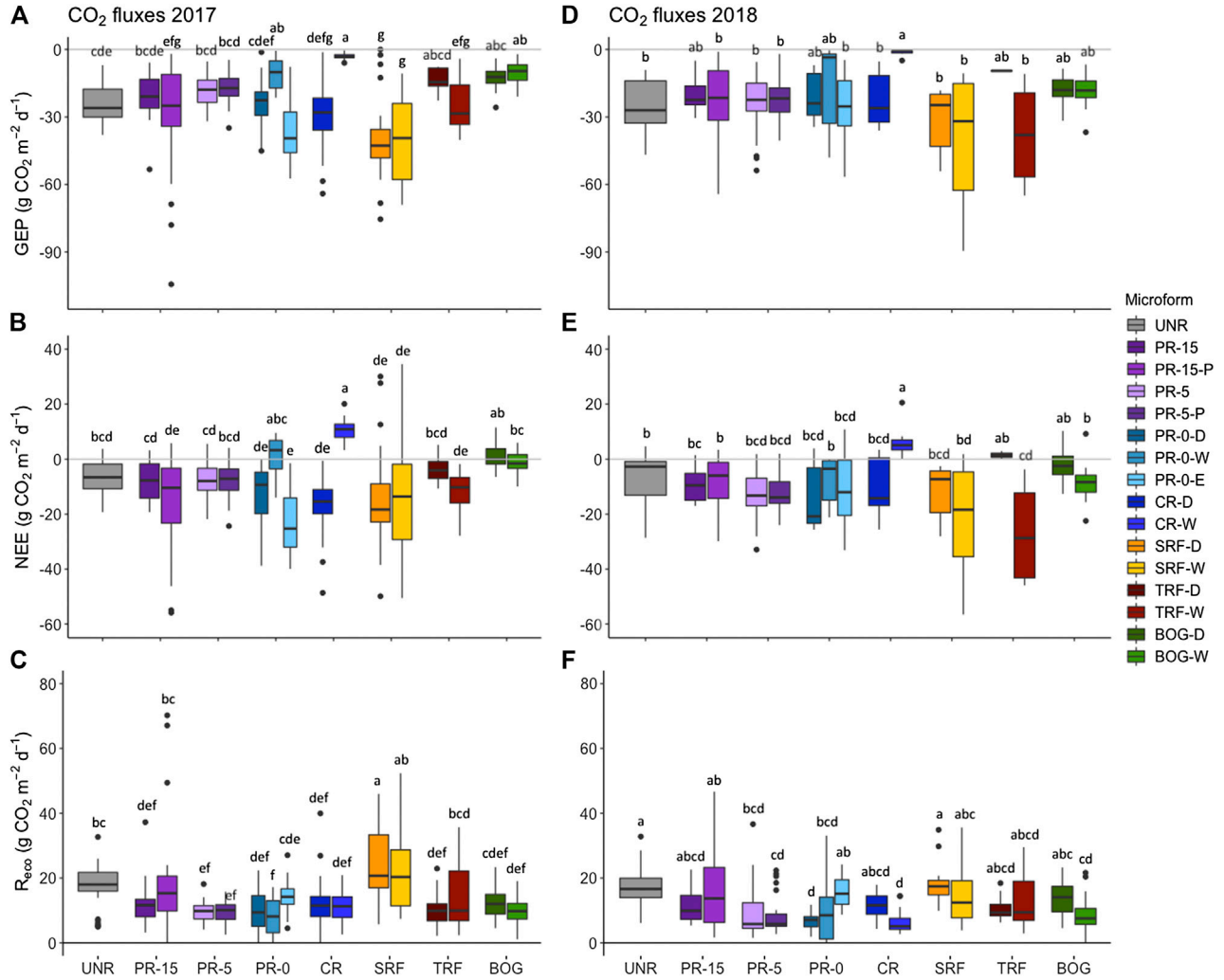

FIGURE 6 | Measurements in all monitoring sectors* during the monitoring season of 2017 **(A–C)** and the season of 2018 (D–F) show the mean gross ecosystem production (GEP in g CO_2 m^{-2} d^{-1}) at a photosynthetically active radiation (PAR) photon flux density ≥1,000 μmol m^{-2} s^{-1} (A+D), the mean net ecosystem exchange (NEE in g CO_2 m^{-2} d^{-1}, B+ E), and the mean ecosystem respiration (R_{eco} in g CO_2 m^{-2} d^{-1}, C + F). Groups with the same letters are not significantly different. Statistical results of the ANOVAs for 2017 show GEP: $F_{(17, 359)} = 16.43$, $p < 0.001$, adj. $R^2 = 0.41$; NEE: $F_{(17, 376)} = 14$, $p < 0.001$, adj. $R^2 = 0.36$; R_{eco}: $F_{(17, 550)} = 19.16$, $p < 0.001$, adj. $R^2 = 0.35$. For flux recordings in 2018 the ANOVA results reveal GEP: $F_{(17, 212)} = 4.38$, $p < 0.001$, adj. $R^2 = 0.2$; NEE: $F_{(17, 220)} = 7.29$, $p < 0.001$, adj. $R^2 = 0.31$; R_{eco}: $F_{(17, 329)} = 6.77$, $p < 0.001$, adj. $R^2 = 0.22$.* Restored sectors: UNR = unrestored, PR-15 = partial removal of mineral soil (MS) to 15 cm above seasonal water table, PR-5 = partial removal of MS to 4–6 cm above seasonal water table, PR-0-D/W = partial removal of MS to surface elevation of surrounding fen reference ecosystem (uneven ground relief with microforms dry (D) and wet (W), PR-0-E = partial removal of MS to near the surrounding fen reference ecosystem (even ground relief), CR = complete removal of mineral soil (MS). Reference ecosystem (REF): SRF = shrubby extreme-rich fen; TRF = treed rich fen, BOG = wooded bog.

2018). On the contrary, rates of NEE and CH_4 for undisturbed peatlands in the Mixedwood region of the Canadian boreal forest range from −7.6 to −3.1 g CO_2 m^{-2} d^{-1} and 3–65.8 mg CH_4 m^{-2} d^{-1} (Webster et al., 2018).

Since complete removal of introduced oil sands well pad construction materials creates open water areas that are not representative of pre-disturbance conditions, we hypothesize that this technique would not be beneficial for peatland restoration efforts and would likely increase carbon emission rates. We further hypothesized that the emergence and a high abundance of fen typical plant species post-restoration, as well as biogeochemical attributes comparable to reference peatlands, would enable the return of net C uptake in restored sectors at rates similar to nearby reference peatlands.

Fen Typical Vegetation Not Improving C Uptake, Whilst Need for Shrub Species

Biogeochemical conditions, specifically nutrient rates, differed greatly between reference and restored sectors. Reference sectors were characterized by high ammonium, phosphate and iron concentrations and did not compare to any restored sector. The sulfur concentration of only one restored sector, PR-0-W, was comparable to the reference fen sectors, while sulfur concentration of all remaining restored sectors were very

TABLE 5 | Statistical results of ANOVAs for fluxes in 2017 and 2018.

Year	Component	Effect	F Statistics	*p*-value	Adjusted R^2
2017	GEP		$F_{(17, 359)} = 16.43$	<0.001	0.41
		Microform	$F_{(15, 359)} = 17$	<0.001	
		Soil temperature 5 cm	$F_{(1, 359)} = 24.18$	0.000	
		Water table level	$F_{(1, 359)} = 0.21$	0.65	
	NEE		$F_{(17, 376)} = 14$	<0.001	0.36
		Microform	$F_{(15, 376)} = 15.7$	<0.001	
		Soil temperature 5 cm	$F_{(1, 376)} = 2.41$	0.12	
		Water table level	$F_{(1, 376)} = 0.01$	0.91	
	R_{eco}		$F_{(17, 550)} = 19.16$	<0.001	0.35
		Microform	$F_{(15, 550)} = 15.62$	<0.001	
		Soil temperature 5 cm	$F_{(1, 550)} = 91.15$	<0.001	
		Water table level	$F_{(1, 550)} = 0.23$	0.63	
	CH_4	Microform	$F_{(15, 292)} = 6.75$	<0.001	0.22
2018	GEP		$F_{(17, 212)} = 4.38$	<0.001	0.2
		Microform	$F_{(15, 212)} = 4.05$	0.000	
		Soil temperature 5 cm	$F_{(1, 212)} = 2.04$	0.155	
		Water table level	$F_{(1, 212)} = 11.75$	0.001	
	NEE		$F_{(17, 220)} = 7.29$	<0.001	0.31
		Microform	$F_{(15, 220)} = 6.86$	0.000	
		Soil temperature 5 cm	$F_{(1, 220)} = 0.26$	0.609	
		Water table level	$F_{(1, 220)} = 20.74$	0.000	
	R_{eco}		$F_{(17, 329)} = 6.77$	<0.001	0.22
		Microform	$F_{(15, 329)} = 6.41$	<0.001	
		Soil temperature 5 cm	$F_{(1, 329)} = 15.52$	<0.001	
		Water table level	$F_{(1, 329)} = 3.47$	0.063	
	CH_4	Microform	$F_{(15, 283)} = 7.54$	<0.001	0.25

different than reference sectors. It is likely that the extremely high sulfur concentrations in PR-15 and PR-5 to sulfur compounds in the well-pad materials leaching through the root zone and being held in place by the clay layer (Himes 1998), used for infilling the well pad, which does not allow an exchange between the mineral clay and the peat layer underneath. This effect might be enhanced through decomposing organic matter at the surface, considering the high cover percentage of plant litter (63%) and the low water table level in both sectors. These processes would also explain the low pH in the same sectors despite the residual mineral soil (pH 3.4 in PR-15, pH 3.6 in PR-5) in the second drier year 2018. Indeed during drier conditions, H^+ ions might have been produced and dissolved, acidifying the milieu (DeVries and Breeuwsma 1987).

Soil chemistry post-restoration is comparable to characteristic poor fen (pH <5.5 and EC <100 $\mu S\,cm^{-1}$) and moderate-rich fen (pH 5.5–7 and EC 100–250 $\mu S\,cm^{-1}$) conditions (Alberta Environment and Sustainable Resource Development (ESRD) 2015) that come with the acidic and moist environment. The exceptional high EC_{Soil} values in PR-5 and PR-15 might be due to the remnants of various soil amendments, i.e., the application of commercial peat, field peat, slough hay, or woodchips, applied during the restoration work in 2007 (Vitt et al., 2011). We note, that the chemical conditions depicted for CR depicts conditions found in CR-D and no represent well CR-W, because soil sampling was not possible in deep water.

Despite the chemical differences at the restored well-pads, vegetation re-established among all restored sites. We observed a fen-like vegetation recovery in sectors that were most closely leveled with the water table level of the surrounding ecosystem. This effect was especially true of the moss layer. However, we could not confirm a higher abundance of fen typical plant species the closer the restored sectors are leveled to the water table level. We had expected to observe a gradient of low abundance of fen typical plant species in the sectors with a highest distance to the water table level, PR-15, to a high abundance of fen typical species in the sectors with the shortest distance and most even level to the water table level, PR-0-E. Indeed, the highest cover of fen typical species in restored sectors (64%) was observed in PR-0-E, but among the remaining sectors with partially and completely removed mineral soil, and even the unrestored sector, there was no difference in the fen typical species cover. Water table level is an important driver of vegetation re-establishment on residual mineral soil (Vitt et al., 2011; Howie et al., 2016), but it does not appear to be a crucial factor for fen typical plant species to distribute. While Halsey et al. (1998) consider the mineral soil's larger grain size (i.e., glaciofluvial and eolian deposits) with high hydraulic conductivity to be an important driver for peatland development, our findings indicate that achieving an elevation similar to the surrounding peatland is likely sufficient for the establishment of typical fen plant communities.

Furthermore, we cannot confirm that the cover of fen typical plants improved the C sink function considerably. In fact, we found no significant relationship between the cover of fen typical plant and either CO_2 or CH_4 exchange. While the species composition in PR-0-E was most comparable to a reference fen ecosystem and the C sink function seems to have returned to this sector, CH_4 fluxes were not drastically decreased. This might be due to the high cover of sedges (24%), such as *Carex* sp. and *Typha latifolia,* with their large aerenchymatic systems and

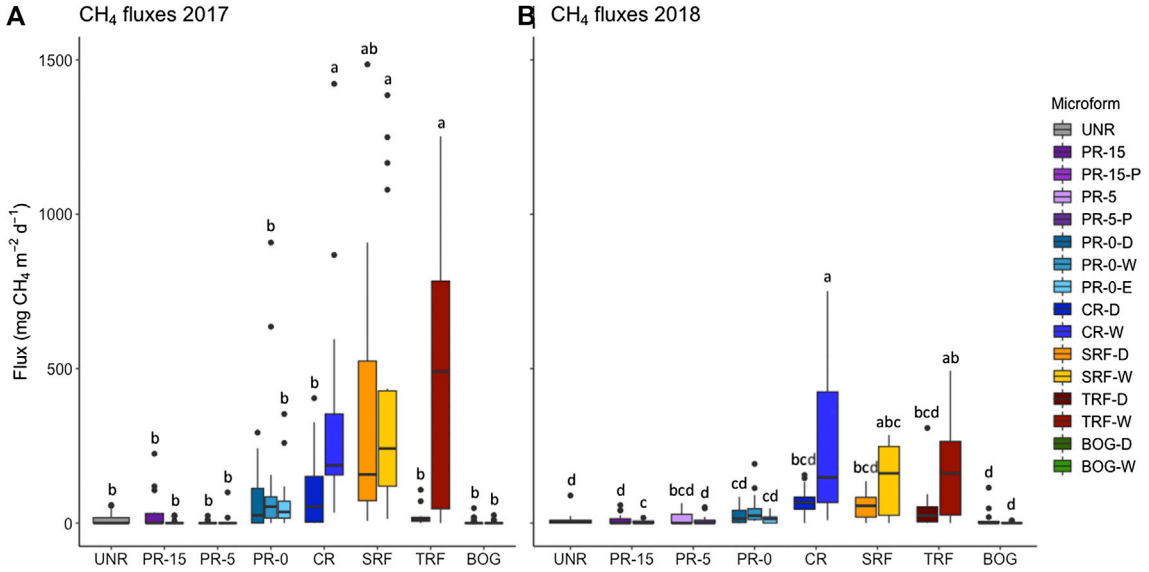

FIGURE 7 | Measurements of mean methane fluxes (mg CH_4 m^{-2} d^{-1}) during the 107-days-monitoring seasons in 2017 **(A)** and in 2018 **(B)**. Groups with the same letters (in separate years) are not significantly different. Microform showed a significant effect on CH_4 fluxes in both monitoring years, 2017 ($F_{(15, 292)} = 6.75$, $p < 0.001$, adj. $R^2 = 0.2$) and 2018 ($F_{(15, 283)} = 7.54$, $p < 0.001$, adj. $R^2 = 0.3$).* Restored sectors: UNR = unrestored, PR-15 = partial removal of mineral soil (MS) to 15 cm above seasonal water table, PR-5 = partial removal of MS to 4–6 cm above seasonal water table, PR-0-D/W = partial removal of MS to surface elevation of surrounding fen reference ecosystem (uneven ground relief with microforms dry (D) and wet (W), PR-0-E = partial removal of MS to near the surrounding fen reference ecosystem (even ground relief), CR = complete removal of mineral soil (MS). Reference ecosystem (REF): SRF = shrubby extreme-rich fen; TRF = treed rich fen, BOG = wooded bog.

TABLE 6 | Statistical results of multiple linear regressions to predict NEE and CH_4 fluxes in 2017 and 2018, based on soil temperature (at 5 cm depth), cover of vegetation strata, and water table level. Marginal $R^2_{(m)}$ shows the proportion of variance explained by the fixed factors alone, while the conditional $R^2_{(c)}$ describes the proportion of variance explained by fixed factors and the random factor "plot".

Component	Effect	F-value	*p*-value	SE	$R^2_{(m)}$	$R^2_{(c)}$
NEE	Intercept	$F_{(1,46)} = 69.64$	<0.0001	5.84	0.22	0.67
	Soil temperature	$F_{(1,42)} = 2.24$	0.142	0.29		
	Shrub cover	$F_{(1,42)} = 15.46$	<0.001	0.09		
	Forb cover	$F_{(1,42)} = 8.64$	0.005	0.06		
CH4	Intercept	$F_{(1, 47)} = 56.26$	<0.0001	108.83	0.44	0.46
	Soil temperature	$F_{(1, 44)} = 24.47$	<0.0001	6.84		
	Water table level	$F_{(1,42)} = 39.22$	<0.0001	0.58		
	Ericaceous cover	$F_{(1,42)} = 6.69$	0.013	1.07		
	Sedge cover	$F_{(1,42)} = 4.74$	0.035	1.58		

abundant root biomass that are known to promote CO_2 emissions and are more likely to enhance C emissions to the atmosphere rather than C uptake (Bellisario et al., 1999; Strack et al., 2016; Rupp et al., 2019). These species were also well-established in the sectors with partially removed mineral soil, PR-15, PR-5 and PR-0. Overall, it appeared that the presence of plant cover in general and the position of the water table level were the drivers of the net carbon balance observed in each restoration treatment.

On the contrary, other studies show that species identity, and especially the presence of *Carex aquatilis* was important for C sequestration at restored fens, specifically in combination with moss species (Hassanpour Fard et al., 2019; Murray et al., 2019). The floating moss carpet CR-D displays very well the positive effect of this combination of fen typical vegetation on C accumulation and greenhouse gas fluxes, where the total carbon emission rates of the emerging floating moss carpet in CR-D (>7.2 g C m^{-2} d^{-1}) are almost 85% lower than in the open water sector CR-W. The development of the floating moss carpet in this sector was favored by proximity to the adjacent peatland with moss able to grow out from the edge of the open water area, but this result cannot be applied in case of the removal of an entire well pad of 1 ha where much of the area would be far from the edge. In that case, the development of vast shallow open water will cause wave development and too rough water movements for a moss carpet to establish (Blievernicht et al., 2007; Gaudig et al., 2013). At the same time the vegetation that developed in CR-D accommodated the second highest cover rate of fen typical plant species (7%), including species such as *Carex aquatilis*, *C. diandra*, *Drepanocladus aduncus*, *D. polygamus*, and *Menyanthes trifoliata*.

The highest C sink was found in PR-0-D, a sector defined by a vegetation community including shrub and sedge species. Fen typical plant species in this sector included *Andromeda polifolia*, *Betula pumila*, *C. limosa*, *C. utriculata*, *Comarum palustre*, *Ptychostomum pseudotriquetrum*. Opposed to herbaceous species, shrub species store C in their woody structures and in combination with their smaller root structure, emit lower rates of CO_2 to the atmosphere (Rupp et al., 2019). Furthermore, because of their overwintering photosynthesizing leaves, shrubby and moss species have the advantage to begin C uptake early in

TABLE 7 | Cumulative seasonal carbon fluxes of methane (CH_4), and net ecosystem exchange (NEE) as a product of gross ecosystem production (GEP) and ecosystem respiration (R_{eco}), for all monitoring sectors[a] in 2017 and 2018. Both seasonal calculations were done for a time period of 107 days (17.5.2017–31.8.2017 and 22.5.2018–5.9.2018).

Sector[a] microform	May—September 2017					May—August 2018				
	GEP	R_{eco}	NEE	CH_4	$Total_{2017}$	GEP	R_{eco}	NEE	CH_4	$Total_{2018}$
			(g C m^{-2})					(g C m^{-2})		
UNR	−394	506	112	0.7	225	−487	574	87	0.8	175
PR-15	−322	368	47	1.4	95	−348	368	21	0.7	42
PR-15-P	−525	559	34	0.2	69	−512	499	−13	0.2	−26
PR-5	−339	285	−54	3.5	−105	−416	346	−70	6.1	−133
PR-5-P	−329	282	−47	0.6	−94	−342	224	−118	0.7	−235
PR-0-D	−417	314	−103	3.9	−202	−323	110	−213	1.8	−423
PR-0-W	−160	206	46	6.6	99	−216	580	365	3.3	732
PR-0-E	−421	420	−2	3.3	0	−443	409	−34	1.1	−67
CR-D	−475	348	−127	7.2	−246	−375	284	−91	5.8	−177
CR-W	−39	333	294	31.9	621	−27	225	198	21.7	418
REF-SRF-D	−606	715	109	16	234	−407	638	231	4.6	466
REF-SRF-W	−652	671	19	28.4	66	−606	561	−45	11.9	−79
REF-TRF-D	−219	299	81	2.7	164	−150	334	184	3.7	371
REF-TRF-W	−578	418	−160	33.4	−286	−454	283	−171	14.3	−328
REF-BOG-D	−204	358	155	0.6	310	−283	377	94	0.8	190
REF-BOG-W	−184	262	77	0.1	155	−337	248	−88	0	−177

[a]*UNR: Unrestored; CR: Complete removal of mineral soil (MS); PR-15: Partial removal MS to 15 cm above seasonal water table; PR-5: Partial removal of MS to 4–6 cm above seasonal water table; PR-0-D/W: Partial removal of MS to surface elevation of surrounding fen reference ecosystem (uneven ground relief); PR-0-E: Partial removal of MS to near the surrounding fen reference ecosystem (even ground relief); REF-BOG: a wooded bog; REF-TRF: a treed rich fen; REF-SRF: a shrubby extreme-rich fen.*

the growing season before herbaceous plants species (Arndal et al., 2009). The regression analysis also indicated that shrubby plant species had an effect on NEE and CH_4 fluxes. In sectors PR-0-D, CR-D, and PR-5-P, we observed the same trend of highest C uptake, compared to the other restored sectors that act as a source of C. Especially in these three sectors similar plant species composition had established, with high cover of *C. aquatilis* in combination with various shrub (PR-0-D) and moss (CR-D) species. However, we note that both REF fens TRF and SRF, despite a high cover of shrub species (31% and 32% shrub cover, respectively) in combination with high water table level (32% and 37% water cover respectively), were carbon sources. We note, however, that the tall overstory trees of both wooded reference sectors TRF and BOG were not included in our C flux measurements, which would contribute additional C uptake to the system. Furthermore, tree root respiration rates in TRF and BOG were not considered in our measurements and likely contributed to the R_{eco} measured indicating that actual NEE needs to be adjusted according to previous research (Munir et al., 2017; Munir et al., 2015). report on tree root respiration rates in an ombrotrophic bog in Alberta ranging from 2 ± 0 g CO_2-C m^{-2} in ambient hollows to 70 ± 6 g CO_2-C m^{-2} in warmed hummocks. Several studies describe a strong relation between tree productivity and hydrology, where belowground production and root respiration rates were enhanced in drained conditions (Hanson et al., 2000; Hermle et al., 2010; Munir et al., 2017).

Despite the apparently importance of shrubs, the introduction of plant species in some sectors, even including *Salix* shrub species, does not seem to have specifically improved the C sequestration at the respective sectors. Considering the high percentage of bare soil in both PR-5 (22%) and PR-15 (16%), as compared to a maximum of 3% bare soil in PR-D/W, the re-vegetation effort does not seem to be more successful than natural revegetation (Prach and Hobbs 2008), which is favorable if landscape factors, such as water table and a nearby abundant

TABLE 8 | Cumulative two-year total C balance and global warming potential (GWP) for two 107-days-research seasons in two consecutive years (17.5.2017–31.8.2017 and 22.5.2018–5.9.2018). Calculations of the total C balance include C fluxes of methane (CH_4), and net ecosystem exchange (NEE) as a sum of gross ecosystem production (GEP) and ecosystem respiration (R_{eco}).

Status	Sector[a]	Total C balance	GWP
		(g C m^{-2})	(g CO_2-e)
Well pad	UNR	400	788
Restored 2009	PR-15	137	326
	PR-15-P	43	92
Restored 2009	PR-5	−238	−94
	PR-5-P	−329	−556
Restored 2008	PR-0-D	−625	−942
	PR-0-W	831	1875
	PR-0-E	−67	34
Restored 2007	CR-D	−423	−315
	CR-W	1,039	3,807
REF	SRF-D	700	2013
	SRF-W	−13	1,408
REF	TRF-D	535	1,210
	TRF-W	−614	571
REF	BOG-D	500	964
	BOG-W	−22	−37

[a]*UNR: Unrestored; CR: Complete removal of mineral soil (MS); PR-15: Partial removal MS to 15 cm above seasonal water table; PR-5: Partial removal of MS to 4–6 cm above seasonal water table; PR-0-D/W: Partial removal of MS to surface elevation of surrounding fen reference ecosystem (uneven ground relief); PR-0-E: Partial removal of MS to near the surrounding fen reference ecosystem (even ground relief); REF-BOG: a wooded bog; REF-TRF: a treed rich fen; REF-SRF: a shrubby extreme-rich fen*

species pool, are considered during the restoration process (Konvalinková and Prach 2014). This effect can be seen in the mean cover of fen typical species, such as *Betula pumila*, *C. aquatilis*, *C. diandra*, *Comarum palustre*, *Campylium stellatum*, *Sphagnum warnstorfii*, *Tomentypnum nitens*, being almost twice as high in PR-0 (43%) where no plants were introduced compared to PR-5 (24%) and PR-15 (22%) where planting occurred. The combination of shrub species and a stable water table at the soil surface, as can be found in PR-0-D, seems to provide best results in returning a C sink function to restored sectors, as well as establishing biogeochemical conditions comparable with REF fen sectors. This effect seems to have greater impact on C exchange, rather than the variable climatic conditions, since despite wetter and colder conditions during the second year, GEP rates were higher than in the previous year with lower precipitation rates and warmer temperatures (Strack et al., 2016).

Enhanced CH_4 Emissions After Complete Well Pad Removal

Our third hypothesis that a complete well pad removal would enhance CH_4 emissions was confirmed through highest emission rates observed in the permanent open water sector CR-W (21.7–31.9 g C m^{-2} d^{-1}). Sectors PR-0-W, TRF-W and SRF, with water table level above ground surface, show comparable emissions rates of 11.9–33.4 g C m^{-2} d^{-1}. While such high CH_4 emission rates are normal in undisturbed fens with high water table (Waddington and Roulet 2000; Strack et al., 2006; Bienida et al., 2020), adjusted management practices are available to avoid unnecessary high emission rates in restored wetlands (Strack, Keith, and Xu 2014), just as it has been done in the drier managed microforms PR-0 (<3.9 g C m^{-2} d^{-1}), PR-5 (<6.1 g C m^{-2} d^{-1}), PR-15 (<1.4 g C m^{-2} d^{-1}), which low emission rates endorse this argument. Considering the enormous global warming potential (GWP; Myhre et al., 2013) of the wet sectors of up to 3,807 g CO_2-e in CR-W (**Table 8**), the drier managed sites ranging between –556 g CO_2-e and 326 g CO_2-e prove to be a powerful argument to pay attention to proper site management and hydrological adjustments. Furthermore, Günther et al. (2020) show that rewetting of drained peatlands should not be feared or avoided, because the positive effects of rewetting for restoration purposes outweighs the rather short-lived radiative forcing of CH_4, as opposed to the long-lived impacts of CO_2 emissions, when sites remain too dry, and the long-term benefits of recreating net carbon accumulating ecosystem through restoration.

CONCLUSION

After eight to eleven years following restoration, the rates of C exchange in the restored sectors were comparable with the rates of long-time established reference wetlands, although the soil and water chemistry still remained quite different due to the residual mineral soil layer. Regarding our results, we conclude that the C uptake in restored mineral wetlands is most similar to reference peatlands, when vegetation has established and particularly when regional wetland typical shrub species have colonized. The crucial base for vegetation communities to emerge is the proper hydrological management of the site, where the surface elevation should be evenly adjusted to the surrounding ecosystem and as close to the landscape surrounding water table level as possible. It appears that in order to have appropriate chemical fen conditions establish post-restoration, available plant organic matter needs to remain in anaerobic conditions and therefore the water table level is crucial to remain near the surface. However, the development of deep open water sectors is to be avoided at all times. As was observed in flooded conditions in PR-0-W where the water table is >30 cm above surface, and in the shallow open water sector CR-W, with a water table >77 cm above surface, hydrological conditions appeared to be less beneficial to fen plant establishment while driving carbon emissions, resulting in high rates of R_{eco} and CH_4 emissions. It is therefore crucial during future restoration work, to level any residual layers of remaining mineral soil with the adjacent peatland ecosystem, in order to obtain a seamless connection and create optimal hydrological conditions in the restored area. Re-introduction of (shrub) species can be neglected, if appropriate hydrological conditions are achieved and a source of peatland species is available in adjacent ecosystems.

The assessment of the biogeochemical conditions in these sectors should continue on a regular, long-term basis in order to monitor the effect of the developing fen vegetation and associated peat accumulation on the soil chemistry. Long-term monitoring is important to maintain in the context of peatland development, as these ecosystems may take several decades to centuries to establish. We again stress the importance of individual management adjustment of *in-situ* oil mining well pads.

DATA AVAILABILITY STATEMENT

The raw data supporting the conclusions of this article will be made available by the authors, without undue reservation.

AUTHOR CONTRIBUTIONS

MS and LR developed the experimental sampling design. ML performed the practical field research and prepared this manuscript. Statistical analysis were done by ML with support from MS. Supervision and critical feedback were provided by MS and LR at all times.

FUNDING

This research was funded by the Natural Sciences and Engineering Research Council of Canada Industrial Research

Chair for Colleges Grant (CRDPJ 501619- 16) to LR, MS and B. Xu in collaboration with Imperial Oil Resources Ltd.

ACKNOWLEDGMENTS

We thank Bin Xu and his team at the NAIT Boreal Research Center in Peace River, Alberta, for their great technical support during field work, and especially Melanie Bird, whose smiles, motivation and organization were greatly appreciated. Special thanks to Brittany Whiteman and Aaron Gomes for keeping up the spirits and fun during long hours in the field and on the road, as well as to my supervisors and colleagues for their constant support, critical thinking and motivation. Many thanks to the two reviewers for much appreciated feedback on a previous version of the manuscript.

SUPPLEMENTARY MATERIAL

The Supplementary Material for this article can be found online at: https://www.frontiersin.org/articles/10.3389/feart.2020.557943/full#supplementary-material

REFERENCES

Abdalla, M. Hastings, A. Truu, J. Espenberg, M. Mander, Ü. and Smith, P. (2016). "Emissions of methane from northern peatlands: a review of management impacts and implications for future management options," in *Ecology and evolution*. Hoboken, NY: John Wiley and Sons.

Ahmad, S., Liu, H., Günther, A., Couwenberg, J., and Lennartz, B. (2020). Long-term rewetting of degraded peatlands restores hydrological buffer function. *Sci. Total Environ.* 749 (December), 141571. doi:10.1016/j.scitotenv.2020.141571

Alberta Environment and Sustainable Resource Development (ESRD) (2015). *Alberta wetland classification system*. Edmonton, AB: Water Policy Branch, Policy and Planning Division.

Alberta Queen's Printer (1994). *Environmental protection and enhancement act*. Edmonton, AB: Alberta Queen's Printer.

Arndal, M. F., Illeris, L., Michelsen, A., Albert, K., Tamstorf, M., and Hansen, B. U. (2009). Seasonal variation in gross ecosystem production, plant biomass, and carbon and nitrogen pools in five high arctic vegetation types. *Arctic Antarct. Alpine Res.* 41 (2), 164–173. doi:10.1657/1938-4246-41.2.164

Baird, A. J., Green, S. M., Brown, E., and Dooling, G. P. (2019). Modelling time-integrated fluxes of CO2 and CH4 in peatlands: a review. *Mires Peat* 24, 1–15. doi:10.19189/MaP.2019.DW.395

Bartoń, K. (2020). Version 1.43.17. MuMIn: multi-model inference. Available at: https://cran.r-project.org/package=MuMIn (Accessed April 15, 2020).

Beckingham, J. D., and Archibald, J. H. (1996). *Field guide to ecosites of northern Alberta*. Edmonton, AB: Northern Forestry Centre.

Bellisario, L. M., Bubier, J. L., Moore, T. R., and Chanton, J. P. (1999). Controls on CH_4 emissions from a northern peatland. *Global Biogeochem. Cycles* 13 (1), 81–91. doi:10.1029/1998gb900021

Bienida, A., Daté, V., Andersen, R., Nwaishi, F., Price, J., Mahmood, M. S., et al. (2020). Methane emissions from fens in Alberta's boreal region: reference data for functional evaluation of restoration outcomes. *Wetl. Ecol. Manag.* 28 (4), 559–575. doi:10.1007/s11273-020-09715-2

Blievernicht, A. Feuerhahn, B. Grüneberg, H. Zander, M. and Ulrichs, C. (2007). "Torfmooskul- tivierung auf schwimmfähigen vegetationsträgern zur entwicklung eines nachhaltigen torfsubstitutes als substratrohstoff im erwerbsgartenbau." in *45 Gartenbauwissenschaftliche Tagung*. Vol. 26, Bundesverband der Hochschul-Absolventen/Ingenieure Gartenbau und Landschaftsarchitektur.

Bonn, A., Tim, A., Evans, M., Joosten, H., and Stoneman, R. (2016). "Peatland restoration and ecosystem services: an introduction," in *Peatland Restoration and ecosystem services: science, Policy and prcatice*. Editors A. Bonne, T. Allott, M. Evans, H. Joosten, and R. Stoneman (Cambridge: British Ecological Society), 1–16.

Bubier, J., Crill, P., Mosedale, A., Steve, F., and Linder, E. (2003). Peatland responses to varying interannual moisture conditions as measured by automatic CO2 chambers. *Global Biogeochem. Cycles* 17 (2). doi:10.1029/2002gb001946

Caners, R. T., and Lieffers, V. J. (2014). Divergent pathways of successional recovery for in situ oil sands exploration drilling pads on wooded moderate-rich fens in Alberta, Canada. *Restor. Ecol.* 22 (5), 657–667. doi:10.1111/rec.12123

Cooper, D. J., Kaczynski, K. M., Sueltenfuss, J., Gaucherand, S., and Hazen, C. (2017). Mountain wetland restoration: the role of hydrologic regime and plant introductions after 15 years in the Colorado Rocky Mountains, U.S.A. *Ecol. Eng.* 101 (April), 46–59. doi:10.1016/j.ecoleng.2017.01.017

De Vries, W. and Breeuwsma, A. (1987). The relation between soil acidification and element cycling. *Water Air Soil Pollut.* 35 (3–4), 293–310. doi:10.1007/bf00290937

DeMendiburu, F. (2019). Version 1.3-3. Agricolae: statistical procedures for agricultural research. Available at: https://cran.r-project.org/package=agricolae (Accessed June 7, 2020).

Dinno, A. (2017). Version 1.1.5. Conover.test: conover-iman test of multiple comparisons using rank sums. Available at: https://cran.r-project.org/web/packages/conover.test/conover.test.pdf (Accessed October 30, 2017).

Dziuban, C. D., and Shirkey, E. C. (1974). When Is a Correlation Matrix Appropriate for Factor Analysis? Some Decision Rules. *Psychol. Bull.* 81 (6), 358–361. doi:10.1037/h0036316

Environment and Climate Change Canada (2019). Historical data—climate—environment and climate change Canada. Available at: https://climate.weather.gc.ca/historical_data/search_historic_data_e.html (Accessed November 2, 2019).

Environment and Parks (2017). *Reclamation criteria for wellsites and associated facilities for peatlands*. Edmonton, AB: Environment and Parks, 147.

Evans, C. D., Renou-Wilson, F., and Strack, M. (2016). The Role of Waterborne Carbon in the Greenhouse Gas Balance of Drained and Re-Wetted Peatlands. *Aquat. Sci.* 78 (3), 573–590. doi:10.1007/s00027-015-0447-y

Gaudig, G., Fengler, F., Ma, K., Prager, A., Schulz, J., Wichmann, S., et al. (2013). Sphagnum Farming in Germany—a Review of Progress. *Sphagnum Growing* 13 (08), 1–11.

Gauthier, M.-E., Rochefort, L., Nadeau, L., Hugron, S., and Xu, B. (2018). Testing the Moss Layer Transfer Technique on Mineral Well Pads Constructed in Peatlands. *Wetl. Ecol. Manag.* 26 (4), 475–487. doi:10.1007/s11273-017-9532-4

Gauthier, M.-E. (2014). *Restoring peatland plant communities on mineral well pads*. Québec, Canada: Université Laval.

Government of Alberta (2020). Oil sands facts and statistics. Available at: https://www.alberta.ca/oil-sands-facts-and-statistics.aspx (Accessed February 2020).

Government of Canada (2019). Canadian climate normals 1981–2010 station data—climate—environment and climate change Canada. Available at: https://climate.weather.gc.ca/climate_normals/results_1981_2010_e.html?stnID=2770&autofwd=1 (Accessed November 2019).

Graf, M. D. (2009). *Literature review on the restoration of Alberta's boreal wetlands affected by oil, gas and in situ oil sands development*. Available at: http://www.biology.ualberta.ca/faculty/stan_boutin/ilm/uploads/footprint/Graf.20Wetland_Restoration_Review.20FINAL-Small.20File.pdf (Accessed July 2009).

Green, S. M., and Baird, A. J. (2012). A mesocosm study of the role of the sedge Eriophorum angustifolium in the efflux of methane-including that due to episodic ebullition-from peatlands. *Plant Soil* 351 (1–2), 207–218. doi:10.1007/s11104-011-0945-1

Günther, A., Barthelmes, A., Huth, V., Joosten, H., Jurasinski, G., Koebsch, F., et al. (2020). Prompt Rewetting of Drained Peatlands Reduces Climate Warming despite Methane Emissions. *Nat. Commun.* 11 (1), 1644. doi:10.1038/s41467-020-15499-z

Halsey, L. A., Vitt, D. H., and Bauer, I. E. (1998). Peatland Initiation during the Holocene in Continental Western Canada. *Climatic Change* 40, 315–342. doi:10.1023/a:1005425124749

Hanson, P. J., Edwards, N. T., Garten, C. T., and Andrews, J. A. (2000). Separating Root and Soil Microbial Contributions to Soil Respiration: A Review of Methods and Observations. *Biogeochemistry* 48, 115–146. doi:10.1023/a:1006244819642

Hassanpour Fard, G. Elena, F. Bérubé, V. Rochefort, L. and Maria, S. (2019). Key species superpose the effect of species richness and species interaction on carbon fluxes in a restored minerotrophic peatland. *Wetlands* 40, 333–349. doi:10.1007/s13157-019-01176-5

Hemes, K. S., Chamberlain, S. D., Eichelmann, E., Knox, S. H., and Baldocchi, D. D. (2018). A biogeochemical compromise: the high methane cost of sequestering carbon in restored wetlands. *Geophys. Res. Lett.* 45 (12), 6081–6091. doi:10.1029/2018gl077747

Hermle, S., Lavigne, M. B., Bernier, P. Y., Bergeron, O., and Paré, D. (2010). Component Respiration, Ecosystem Respiration and Net Primary Production of a Mature Black Spruce Forest in Northern Quebec. *Tree Physiol.* 30 (4), 527–540. doi:10.1093/treephys/tpq002

Himes, F. L. (1998). "Nitrogen, Sulfur, and Phosphorus and the Sequestering of Carbon," in *Soil processes and the carbon cycle*. Editors R. Lal, J. M. Kimble, R. F. Follett, and B. A. Stewart (Boca Raton: CRC Press), 315–320.

Howie, S. A. van Meerveld, H. J., and Hebda, R. J. (2016). Regional patterns and controlling factors in plant species composition and diversity in Canadian lowland coastal bogs and laggs. *Mires Peat* 18, 1–23. doi:10.19189/MaP.2016.OMB.242

Imperial Oil Resources. (2007). Cold Lake operations wetlands reclamation trial program. Site specific reclamation plamn for Mahihkan H38 field pad (15-3-66-4W4M). Edmonton, Alberta: Alberta Environment

IUCN (International Union for Conservation of Nature 2017). Peatlands and climate change. Issues brief. Available at: https://www.iucn.org/sites/dev/files/peatlands_and_climate_change_issues_brief_final.pdf

Jordan, S., Stromgren, M., Fiedler, J., Lundin, L., Lode, E., and Nilsson, T. (2016). Ecosystem respiration, methane and nitrous oxide fluxes from ecotopes in a rewetted extracted peatland in Sweden. *Mires Peat* 17 (SI), 1–23. doi:10.19189/MaP.2016.OMB.224

Konvalinková, P., and Prach, K. (2014). Environmental factors determining spontaneous recovery of industrially mined peat bogs: a multi-site analysis. *Ecol. Eng.* 69, 38–45. doi:10.1016/j.ecoleng.2014.03.090

Koropchak, S., Vitt, D. H., Bloise, R., and Kelman Wieder, R. (2012). "Fundamental paradigms, foundation species selection, and early plant responses to peatland initiation on mineral soils," in *Restoration and reclamation of boreal ecosystems: attaining sustainable development*. Editors D. H. Vitt and J. Bhatti (Cambridge University Press), 76–100.

Large, A. R. G., Mayes, W. M., Newson, M. D., and Parkin, G. (2007). Using long-term monitoring of fen hydrology and vegetation to underpin wetland restoration strategies. *Appl. Veg. Sci.* 10 (3), 417–428. doi:10.1111/j.1654-109x.2007.tb00441.x

Lazcano, C., Robinson, C., Hassanpour, G., and Strack, M. (2018). Short-term effects of fen peatland restoration through the moss layer transfer technique on the soil CO_2 and CH_4 Efflux. *Ecol. Eng.* 125 (December), 149–158. doi:10.1016/j.ecoleng.2018.10.018

Lee, P., and Cheng, R. (2009). *Bitumen and biocarbon land use conversions and loss of biological carbon due to bitumen operations in the boreal forests of Alberta, Canada*. Edmonton, AB: Global Forest Watch Canada.

Leifeld, J., and Menichetti, L. (2018). The Underappreciated Potential of Peatlands in Global Climate Change Mitigation Strategies. *Nat. Commun.* 9 (1), 1071. doi:10.1038/s41467-018-03406-6

Lenth, R. (2019). Emmeans: estimated marginal means, aka least-squares means. Available at: https://cran.r-project.org/web/packages/emmeans/emmeans.pdf (Accessed October 25, 2020).

Lloyd, J., and Taylor, J. A. (1994). On the temperature dependence of soil respiration. *Funct. Ecol.* 8 (3), 315–323. doi:10.2307/2389824

Munir, T., Khadka, B., Xu, B., and Strack, M. (2017). Partitioning forest-floor respiration into source based emissions in a boreal forested bog: responses to experimental drought. *Forests* 8 (3), 75. doi:10.3390/f8030075

Munir, T. M., Perkins, M., Kaing, E., and Strack, M. (2015). Carbon dioxide flux and net primary production of a boreal treed bog: responses to warming and water-table-lowering simulations of climate change. *Biogeosciences* 12 (4), 1091–1111. doi:10.5194/bg-12-1091-2015

Murray, K. R., Yi, M., Brummell, M. E., and Strack, M. (2019). The influence of Carex Aquatilis and Juncus Balticus on methane dynamics: a comparison with water sourced from a natural and a constructed fen. *Ecol. Eng.* 139 (August), 105585. doi:10.1016/j.ecoleng.2019.105585

Myhre, G., Drew, S., François-Marie, B., Collins, W., Jan, F., Huang, J., Koch, D., et al. (2013). "Anthropogenic and natural radiative forcing," in *climate change 2013: the physical science basis. Contribution of working group I to the fifth assessment Report of the intergovernmental Panel on climate change*. Editors T. F. Stockner, D. Qin, G.-K. Plattner, M. Tignor, S. K. Allen, J. Boschung, et al. (Cambridge, UK: Cambridge University Press), 82.

Natural Regions Committee (2006). T/852. Natural regions and subregions of Alberta. Editors D. J. Downing and W. W. Pettapiece (Edmonton, AB: Government of Alberta).

Natural Resources Canada (2015). Alberta's shale and tight resources. Canada: Natural Resources Canada. . Available at: https://www.nrcan.gc.ca/our-natural-resources/energy-sources-distribution/clean-fossil-fuels/natural-gas/shale-and-tight-resources-canada/albertas-shale-and-tight-resources/17679 (Accessed July 15, 2015).

Nichols, J. E., and Peteet, D. M. (2019). Rapid expansion of Northern Peatlands and doubled estimate of carbon storage. *Nat. Geosci.* 12 (11), 917–921. doi:10.1038/s41561-019-0454-z

Nugent, K. A., Strachan, I. B., Strack, M., Roulet, N. T., and Rochefort, L. (2018). Multi-Year Net Ecosystem Carbon Balance of a Restored Peatland Reveals a Return to Carbon Sink. *Global Change Biol.* 24 (12), 5751–5768. doi:10.1111/gcb.14449

Nugent, Kelly. A. (2019). *Carbon cycling at a post-extraction restored peatland: small-scale processes to global climate impacts*. Quebec, Canada: McGill University.

Nwaishi, F., Petrone, R. M., Macrae, M. L., Price, J. S., Strack, M., and Andersen, R. (2016). Preliminary Assessment of Greenhouse Gas Emissions from a Constructed Fen on Post-Mining Landscape in the Athabasca Oil Sands Region, Alberta, Canada. *Ecol. Eng.* 95 (October), 119–128. doi:10.1016/j.ecoleng.2016.06.061

Pinheiro, J., Douglas, B., DebRoy, S., and Sarkar, D., and R Core Team (2019). Nlme: Linear and Nonlinear Mixed Effects Models. Available at: https://cran.r-project.org/package=nlme (Accessed October 24, 2019).

Prach, K., and Hobbs, R. J. (2008). Spontaneous Succession versus Technical Reclamation in the Restoration of Disturbed Sites. *Restor. Ecol.* 16 (3), 363–366. doi:10.1111/j.1526-100x.2008.00412.x

Price, J. S., Heathwaite, A. L., and Baird, A. J. (2003). Hydrological Processes in Abandoned and Restored Peatlands: An Overview of Management Approaches. *Wetl. Ecol. Manag.* 11, 65–83. doi:10.1023/a:1022046409485

Price, J. S., McLaren, R. G., and Rudolph, D. L. (2010). Landscape Restoration after Oil Sands Mining: Conceptual Design and Hydrological Modelling for Fen Reconstruction. *Int. J. Min. Reclamat. Environ.* 24 (2), 109–123. doi:10.1080/17480930902955724

Quinty, F., and Rochefort, L. (2003). *Peatland restoration guide*. 2nd Edn. Québec, Canada: Canadian Sphagnum Peat Moss Association, New Brunswick Department of Natural Resources and Energy.

R Core Team (2019). *R: a language and environment for statistical computing*. Vienna, Austria: R Foundation for Statistical Computing.

Rahman, A., Osko, T. J., Foote, L., and Bork, E. W. (2016). Comparison of site preparation and revegetation strategies within a sphagnum-dominated Peatland following removal of an oil well pad. *Ecol. Restor.* 34 (3), 225–235. doi:10.3368/er.34.3.225

Renou-Wilson, F., Barry, C., Müller, C., and Wilson, D. (2014). The impacts of drainage, nutrient status and management practice on the full carbon balance of grasslands on organic soils in a maritime temperate zone. *Biogeosciences* 11 (16), 4361–4379. doi:10.5194/bg-11-4361-2014

R. K. Wieder and Vitt (Editors) (2006). "Boreal Peatland ecosystems: with 73 figures, 6 in color, and 22 tables," in *Ecological studies*. Berlin: Springer, 188.

Rochefort, M., Waddington, J. M., Rochefort, L., and Tuittila, E.-S. (2006). Response of vegetation and net ecosystem carbon dioxide exchange at different Peatland microforms following water table drawdown. *J. Geophys. Res. Biogeosci.* 111 (G2), 10. doi:10.1029/2005jg000145

Rupp, D., Kane, E. S., Dieleman, C., Keller, J. K., and Turetsky, M. (2019). Plant functional group effects on peat carbon cycling in a boreal rich fen. *Biogeochemistry* 144 (3), 305–327. doi:10.1007/s10533-019-00590-5

Saraswati, S., Petrone, R. M., Rahman, M. M., McDermid, G. J., Xu, B., and Strack, M. (2020). Hydrological effects of resource-access road crossings on boreal forested peatlands. *J. Hydrol.* 584 (May), 124748. doi:10.1016/j.jhydrol.2020.124748

Sobze, J.-M., Schoonmaker, A., and Rochefort, L. (2012). Wellsite pad removal and inversion: a peatland restoration pilot project. *Canadian Reclamation* 12 (1), 10–13.

Strack, M., Cagampan, J., Fard, G. H., Keith, A. M., Nugent, K. A., Rankin, T., Robinson, C., Strachan, I. B., et al. (2016). Controls on plot-scale growing season CO_2 and CH_4 fluxes in restored peatlands: do they differ from unrestored and natural sites? *Mires Peat* 17, 1–18. doi:10.19189/MaP.2015.OMB.216

Strack, M., Keith, A. M., and Xu, B. (2014). Growing season carbon dioxide and methane exchange at a restored peatland on the western boreal plain. *Ecol. Eng.* 64, 231–239. doi:10.1016/j.ecoleng.2013.12.013

Strack, M., Mwakanyamale, K., Fard, G. H., Bird, M., Bérubé, V., and Rochefort, L. (2017). Effect of plant functional type on methane dynamics in a restored minerotrophic peatland. *Plant Soil* 410 (1–2), 231–246. doi:10.1007/s11104-016-2999-6

Sundh, I., Mikkelä, C., Nilsson, M., and Svensson, B. H. (1995). Potential aerobic methane oxidation in a sphagnum-dominated peatland—controlling factors and relation to methane emission. *Soil Bid. Biochem.* 27, 829–837. doi:10.1016/0038-0717(94)00222-m

UNFCCC, UN Framwork Convention on Climate Change (2009). Kyoto protocol reference manual on accounting of emissions and assigned amount. *Work. Pap.* Available at: https://unfccc.int/resource/docs/publications/08_unfccc_kp_ref_manual.pdf (Accessed January 2020).

Vitt, Dale. H., Hayes, Ciara., and Kelman, Wieder. (2012). Reclamation of Decomissioned Oil and Gas Pads Constructed in Boreal Peatlands. *Canadian Reclamation* 2 (12), 12–18.

Vitt, D. H., Wieder, R. K., Xu, B., Kaskie, M., and Koropchak, S. (2011). Peatland establishment on mineral soils: effects of water level, amendments, and species after two growing seasons. *Ecol. Eng.* 37 (2), 354–363. doi:10.1016/j.ecoleng.2010.11.029

Waddington, J. M., and Roulet, N. T. (2000). Carbon balance of a boreal patterned peatland. *Global Change Biol.* 6 (1), 87–97. doi:10.1046/j.1365-2486.2000.00283.x

Webster, K. L., Bhatti, J. S., Thompson, D. K., Nelson, S. A., Shaw, C. H., Bona, K. A., et al. (2018). Spatially-integrated estimates of net ecosystem exchange and methane fluxes from Canadian Peatlands. *Carbon Bal. Manag.* 13 (1), 16. doi:10.1186/s13021-018-0105-5

Wickham, H. (2016). *Ggplot2: elegant graphics for data analysis*. New York: Springer-Verlag.

Conflict of Interest: Part of this research funding is from a NSERC-industrial partnership program, with Esso Imperial Ltd who leased and operated the research sites. The company provided PPE, access and safety guidelines and measures on site, but did not have any contribution in the decision-making for experimental set-up and measurements, unless there were safety concerns interfering with the researcher's plan of action. Further, the company did not have any contribution in the preparation of the manuscript or the opinions and statements made in it.

frontiers in Earth Science

ORIGINAL RESEARCH
published: 21 January 2021
doi: 10.3389/feart.2020.562401

Carbon Dioxide and Methane Flux Response and Recovery From Drought in a Hemiboreal Ombrotrophic Fen

J. B Keane[1,2], S. Toet[2], P. Ineson[3], P. Weslien[4], J. E. Stockdale[2] and L. Klemedtsson[4]*

[1]Department of Animal and Plant Sciences, The University of Sheffield, Sheffield, United Kingdom, [2]Department of Environment and Geography, University of York, York, United Kingdom, [3]Department of Biology, University of York, York, United Kingdom, [4]Department of Earth Sciences, University of Gothenburg, Gothenburg, Sweden

Globally peatlands store 500 Gt carbon (C), with northern blanket bogs accumulating 23 g C m^{-2} y^{-1} due to cool wet conditions. As a sink of carbon dioxide (CO_2) peat bogs slow anthropogenic climate change, but warming climate increases the likelihood of drought which may reduce net ecosystem exchange (NEE) and increase soil respiration, tipping C sinks to sources. High water tables make bogs a globally important source of methane (CH_4), another greenhouse gas (GHG) with a global warming potential (GWP) 34 times that of CO_2. Warming may increase CH_4 emissions, but drying may cause a reduction. Predicted species composition changes may also influence GHG balance, due to different traits such as erenchyma, e.g., *Eriophorum vaginatum* (eriophorum) and non-aerenchymatous species, e.g., *Calluna vulgaris* (heather). To understand how these ecosystems will respond to climate change, it is vital to measure GHG responses to drought at the species level. An automated chamber system, SkyLine2D, measured NEE and CH_4 fluxes near-continuously from an ombrotrophic fen from August 2017 to September 2019. Four ecotypes were identified: sphagnum (*Sphagnum spp*), eriophorum, heather and water, hypothesizing that fluxes would significantly differ between ecotypes. The 2018 drought allowed comparison of fluxes between drought and non-drought years (May to September), and their recovery the following year. Methane emissions differed between ecotypes ($p < 0.02$), ordered high to low: eriophorum > sphagnum > water > heather, ranging from 23 to 8 mg CH_4-C m^{-2} d^{-1}. Daily NEE was similar between ecotypes ($p > 0.7$), but under 2018 drought conditions all ecotypes were greater sources of CO_2 compared to 2019, losing 1.14 g and 0.24 g CO_2-C m^{-2} d^{-1} respectively ($p < 0.001$). CH_4 emissions were ca. 40% higher during 2018 than 2019, 17 mg compared to 12 mg CH_4-C m^{-2} d^{-1} ($p < 0.0001$), and fluxes exhibited hysteresis with water table depth. A lag of 84–88 days was observed between rising water table and increased CH_4 emissions. A significant interaction between ecotype and year showed fluxes from open water did not return to pre-drought levels. Our findings suggest that short-term drought may lead to a net increase in C emissions from northern wetlands.

Keywords: drought, blanket bog (peatland), carbon, methane, CO_2, greenhouse gas, climate change

OPEN ACCESS

Edited by:
Ligang Xu,
Nanjing Institute of Geography and Limnology (CAS), China

Reviewed by:
Annalea Lohila,
University of Helsinki, Finland
Xudong Zhu,
Xiamen University, China

****Correspondence:***
J. B Keane
ben.keane@sheffield.ac.uk

Specialty section:
This article was submitted to Biogeoscience, a section of the journal Frontiers in Earth Science

Received: *15 May 2020*
Accepted: *16 December 2020*
Published: *21 January 2021*

Citation:
Keane JB, Toet S, Ineson P, Weslien P, Stockdale JE and Klemedtsson L (2021) Carbon Dioxide and Methane Flux Response and Recovery From Drought in a Hemiboreal Ombrotrophic Fen. Front. Earth Sci. 8:562401. doi: 10.3389/feart.2020.562401

INTRODUCTION

Peatlands are found across the northern hemisphere and are a globally important store of approximately 500 Gt carbon (C) (Yu, 2012). These ecosystems have accumulated ca. 23 g C m^{-2} y^{-1} following the last ice age through peat formation from undecomposed organic material due to the prevailing cool wet conditions (Billett et al., 2010). As a sink of carbon dioxide (CO_2) they act as an important brake on anthropogenic climate change (Strack and Waddington, 2008). Due to the anaerobic conditions caused by high water tables, these bogs are also a major source of methane (CH_4) (IPCC, 2014), an important greenhouse gas (GHG) with a global warming potential (GWP) 34 times that of CO_2 (IPCC, 2014).

In the warming climate, rainfall is predicted to become more variable, increasing the likelihood of drought in these landscapes (Arneth et al., 2019). Simulated drought has been shown to decrease the productivity of the common blanket bog species, sphagnum mosses (*Sphagnum spp.*) (Lees et al., 2019), eriophorum (*Eriophorum vaginatum*) (Buttler et al., 2015) and heather (*Calluna vulgaris*) (Ritson et al., 2017). Such a reduction in primary productivity, alongside increased soil respiration (R_s) due to warming (Bond-Lamberty et al., 2004) will, by definition, lead to reduced net ecosystem exchange (NEE) of CO_2 (reduced C uptake) and might cause these important C sinks to become sources.

It is further expected that the changing climate will alter the species composition of northern wetlands (Robroek et al., 2017), which may also have an influence on the GHG balance of these systems. A key functional trait of some blanket bog species, including eriophorum, is erenchyma which have been shown to increase (Greenup et al., 2000) and decrease CH_4 emissions (Dinsmore et al., 2009). Additionally, pools of water within wetlands are known to be 'hotspots' of CH_4 emissions (Cooper et al., 2014) and the depth of water table within blanket bog has been shown to have a significant effect on GHG emissions (Dinsmore et al., 2009). Thus, in order to understand how northern peatlands will respond to climate change it is vital to understand how drought will affect the GHG balance at the species-ecotype level. Measuring GHG fluxes at a spatial resolution suitable to achieve this has often been conducted using manual chambers (e.g., Kutzbach et al., 2004; Juszczak and Augustin 2013; Rigney et al., 2018; Rey-Sanchez et al., 2019), but it has been demonstrated that GHGs may exhibit unusual diurnal variation (Keane and Ineson, 2017; Jarveoja et al., 2020), and particularly CH_4, may be released in rapid pulses following changes to water table depth (Dinsmore et al., 2009). Since such pulses may contribute a large proportion of the annual GHG flux, it is essential to monitor at a suitable frequency to detect rapid changes in flux dynamics. We therefore used an automated chamber system, SkyLine2D, to measure CO_2 and CH_4 fluxes quasi-continuously from an ombrotrophic blanket peat bog.

The peatland had been surveyed prior to the study period, and had identified four general ecotypes present, consisting of different functional types: sphagnum, eriophorum, heather and open water. Water depth of the pools was up to ca. 20 cm over sediment and some moss. During the drought period the substrate was exposed when the water table dropped. We followed the fluxes of CO_2 and CH_4 within the fen over the course of 27 months, starting in August 2017, to investigate how GHG fluxes differed between areas dominated by different ecotypes. Since peatland pools are known to be important sources of CH_4 (Waddington and Roulet, 1996; Pelletier et al., 2014), we hypothesized that CH_4 fluxes would be highest from the open water and, due to erenchymatous tissue, eriophorum (Greenup et al., 2000; McNamara et al., 2008), and would be lowest from the heather, which prefers drier tussocks. A second hypothesis was that we would detect differences in NEE between ecotypes: faster growth rates of eriophorum and heather (Milne et al., 2002) compared to sphagnum (Bengtsson et al., 2016) would suggest that photosynthesis would be greater in these two ecotypes, though their preference for drier conditions could also lead to greater R_s, countering C uptake. By measuring NEE, we were able to determine the net C balance of these two GHGs, and to investigate their relative contribution toward a net sink or source in this landscape. The study period included the two full growing seasons of 2018 and 2019, very distinct years in which a prolonged drought period (2018) was followed by a year of more typical conditions, enabling observation of response and recovery of the ecosystem GHG balance to the very dry and warm summer conditions that are predicted to occur more often over the coming decades.

MATERIALS AND METHODS

Site Description

All work was undertaken at Mycklemossen, an ombrotrophic mire ca. 100 km north of Gothenburg, Sweden (58.36732626 N, 12.16856373 E, ca. 75 m asl). The site is part of the Skogaryd research catchment, which has been monitored since 2013. Mycklemossen is a hemi-boreal bog-like fen, vegetated predominantly by heather (*Calluna vulgaris*), sphagnum moss (*Sphagnum* spp.) and sedges (*Eriophorum vaginatum*) and during typical conditions the water table is high enough so that there are areas of open water within the mire year-round. In 2018 the mire experienced drought conditions, receiving less rainfall, higher temperatures and more solar radiation than in 2019 (**Table 1**).

Experimental Design

In January 2017 a transect within the mire, comprising all the vegetation types, was selected and marked out. Spatial blocks were defined along the transect, and within each block replicate points were identified at random and classified as either sedge (**eriophorum n = 6**), heather (**calluna n = 6**), sphagnum (**sphagnum n = 6**) or open water (**water n = 6**). At each of the 24 measurement points a PVC collar (inner diameter 20 cm, height 10 cm) was inserted ~2 cm below the soil surface, or into the sediment at the water positions.

GHG Flux Measurements

Surface GHG fluxes were measured along the transect using SkyLine2D, an automated chamber system designed and built

TABLE 1 | Summary of meteorological conditions at Mycklemossen in 2017, 2018, 2019, and 1990–2019. Values are annual means unless otherwise stated.

Year	Total rain (mm)	Total par (mol m^{-2})	Temperature (°C)	Par (µmol m^{-2} s^{-1})	RH (%)	Pressure (mbar)
2017	681	–	7.02	–	80.8	1002.20
2018	705	4.48	8.10	255.60	75.45	1005.80
2019	1,083	4.13	7.69	235.76	78.24	1002.39
30-years avg[a]	1,021	–	6.72	–	83.2	–

[a]*SMHI, Kroppefjäll 1990–2019.*

FIGURE 1 | The SkyLine2D system used for GHG measurements at the Mycklemossen field site.

at the University of York. For a full description of the SkyLine2D system, see Keane et al. (2018). Briefly, the equipment comprised a single, clear cylindrical chamber (Perspex, inner diameter 20 cm, height 40 cm), suspended from a motorized trolley, programmed to traverse on parallel ropes *ca.* 2 m above the transect. The ropes were anchored from a vertical aluminum mast at one end and a tree at the other (**Figure 1**). The system was programmed to repeatedly visit the pre-selected positions on the transect, where the chamber was lowered to sit on a collar to complete a gas flux measurement over a period of 4 min. Upon completion of the programmed chamber closure, the system raised the chamber and moved to the next position to repeat the process. The time taken to complete a full cycle was approximately 2.5 h, which allowed each chamber to be measured ca. 10 times per day.

The headspace gas from within the chamber was circulated in series through a Licor infrared gas analyser (IRGA, LI-8100, Licor, NE, United States) to measure CO_2 and a cavity ringdown laser (CRD, LGR U-GGA-91, Los Gatos Research, CA United States) to measure both CO_2 and CH_4. The chamber design does not include a fan for mixing based upon previous tests: a comparison of fluxes measured with and without a fan and sampling the headspace from the full height profile of the chamber detected no significant differences (Keane et al., 2018), indicating that the flow of the analyser was sufficient to achieve complete mixing of the chamber (see **Supplementary Material**). Data from both analysers were recorded on a data logger (CR1000x, Campbell Scientific, UT USA). Fluxes of CO_2 and CH_4 were calculated using linear regression to determine the rate of change of gas concentrations; a deadband of at least 20 s was allowed for the chamber headspace to mix and a window of 90 s was used for CO_2 and 240 s used for CH_4. Fluxes were adjusted for area, air temperature and gas volume (Mosier, 1989). Further adjustment was made to the CO_2 fluxes during daylight hours based upon the light response curve to account for attenuation of light by the chamber material, after Heinemeyer et al. (2013).

Environmental Variables

Air temperature and relative humidity were measured by a HC2S3 sensor (Rotronic, Switzerland) mounted in a ventilated radiation shield at 1.5 m height. Incoming and reflected short- and longwave radiation were measured by a NR01 net radiometer (Hukseflux, the Netherlands) at 3 m height. Precipitation was measured by a tipping bucket rain gauge (SBS500H, Campbell Scientific, United Kingdom). Soil variables including soil temperature (107 thermistors, Campbell Scientific, United Kingdom) and ground water level (CS450, Campbell Scientific, UT United States) were measured at three different locations, representing dry, wet and intermediate conditions, characterized by heather, sphagnum and intermediate vegetation respectively. Soil temperatures were measured at 2, 6, 12, 18, 30, and 60 cm depth at each profile. All meteorological variables were measured at 1 Hz and recorded as 30United Statesmin averages on a data logger (CR1000, Campbell Scientific, UT United States).

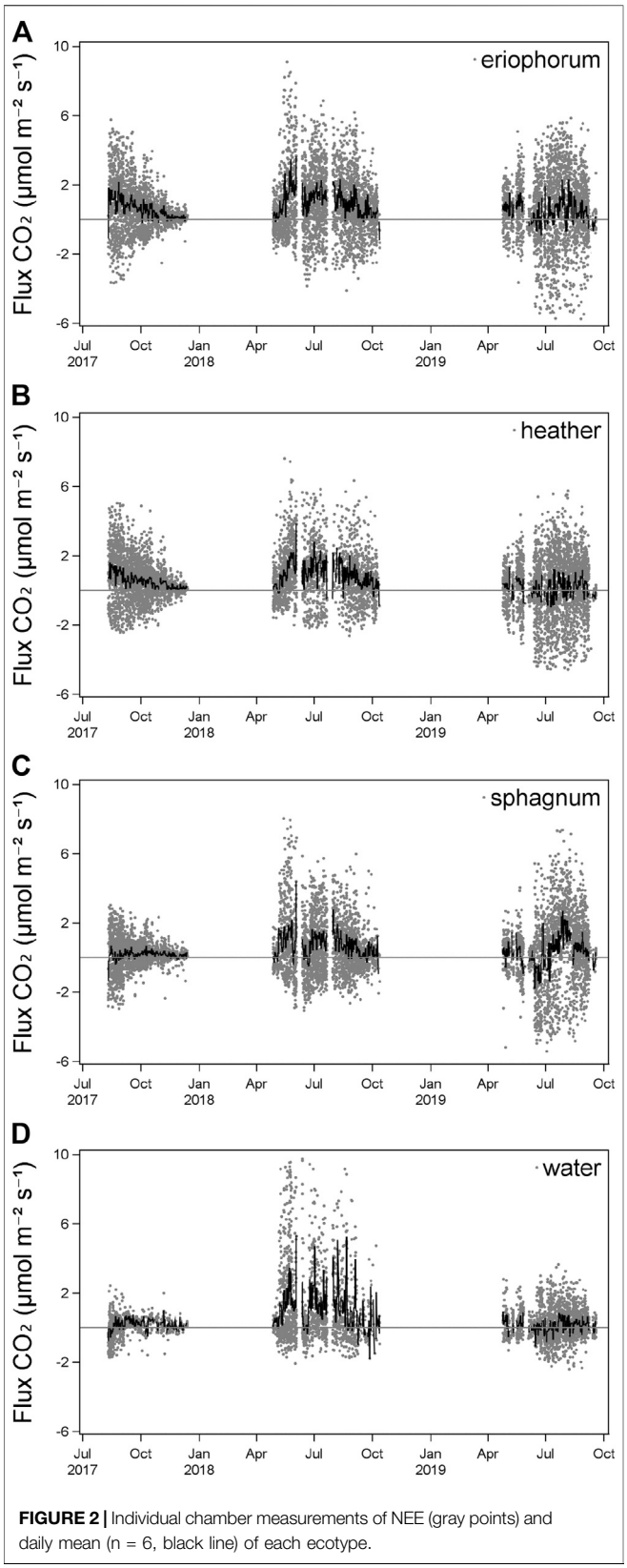

FIGURE 2 | Individual chamber measurements of NEE (gray points) and daily mean (n = 6, black line) of each ecotype.

Data Processing

All data manipulation, analyses and figures were produced using SAS 9.4 (SAS Institute, CA United States). GHG flux data (for both CO_2 and CH_4) were quality controlled in the first instance using the R^2 statistic of the CO_2 flux measurement, with values < 0.9 discarded. Measurements passing this threshold were then assessed using the output statistics from the regression calculation of CH_4 fluxes, where regressions with a p value < 0.05 were accepted, while those that did not were treated as zero flux. Data outliers were defined as those ±1.96 standard errors of the mean flux value for each collar and were excluded from the analyses. Data were further filtered to account for overestimation of fluxes during still atmospheric nighttime conditions (Lai et al., 2012; Koskinen et al., 2014). Using the procedure outlined in Jarveoja et al. (2020), fluxes where the mean CO_2 concentration for the 20 s period before and after chamber closure dropped by more than 25 ppm where discounted. This led to 329 fluxes being excluded. Differences of NEE and CH_4 fluxes between ecotypes and years were investigated using linear mixed effects models, using the differences of least square means as post hoc tests on significant effects. Cumulative fluxes were calculated using trapezoidal integration. Regression models were constructed for the daily means of fluxes and environmental measurements, first testing drivers of individual years, then pooling the data from all years. Further analysis of CH_4 fluxes was undertaken by construction of forward stepwise multiple regression models of daily mean flux and daily means of environmental variables.

RESULTS

CO_2 Fluxes

NEE of CO_2 was characterized by positive and negative (net uptake from the atmosphere) fluxes of CO_2 across all ecotypes (**Figure 2**). The largest range of fluxes was seen during July and August of all 3 years, where photosynthesis was strongest during the daytime and ecosystem respiration during the night-time (**Figure 2**). A seasonal trend was seen across all years, with fluxes increasing through the spring and decreasing again during autumn. In August 2017, daily mean NEE was negative in both sphagnum and water ecotypes but positive in both August 2018 and 2019. From October 2017 until the end of that year, NEE reduced in daily range and tended toward a daily mean of zero. 2018 was characterized by a reduction in negative CO_2 fluxes (**Figure 2**). Daily mean NEE was almost exclusively positive for all ecotypes in 2018, and by October was again tending toward a net zero flux. The following year NEE was more typical, with daily mean negative fluxes seen across all ecotypes during late April and May 2019. NEE was much more strongly negative during July and August 2019 than in 2018, although the daily mean flux for all ecotypes was positive during this period, most clearly in sphagnum and intermediate ecotypes. Fluxes reduced and trended toward zero by October 2019.

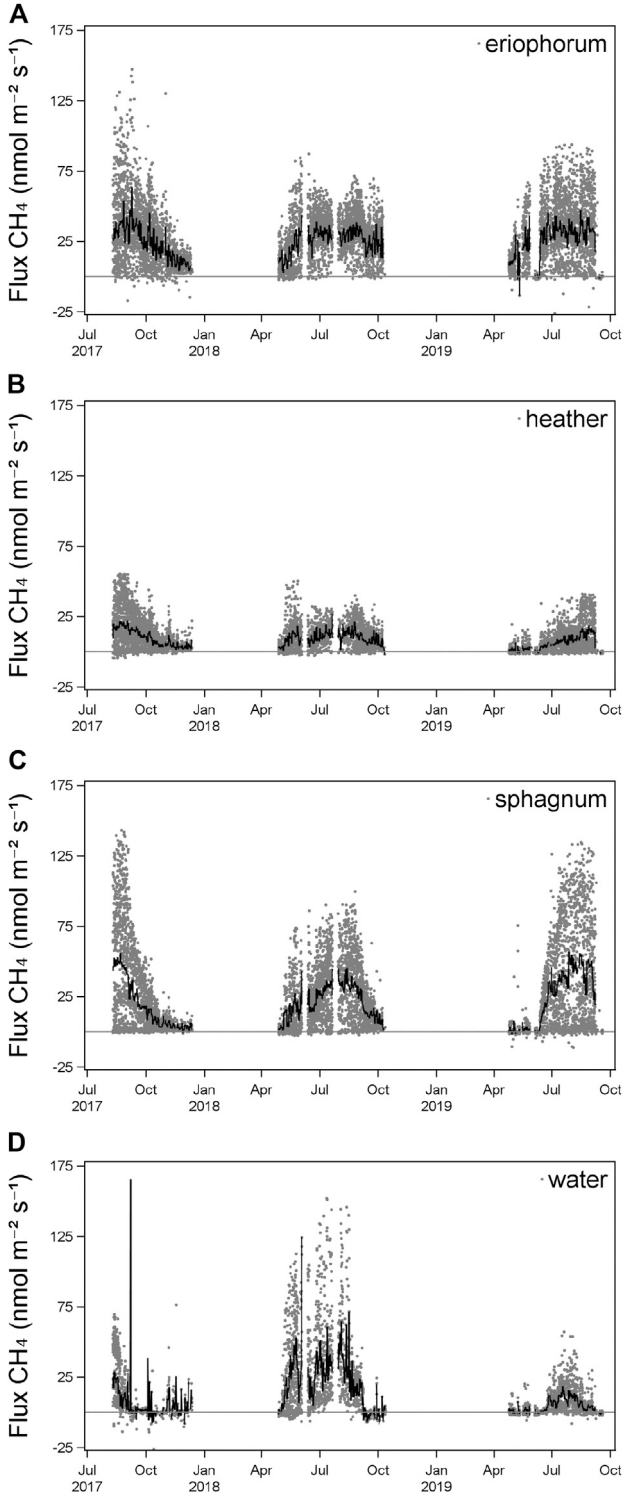

FIGURE 3 | Individual chamber measurements of CH_4 (gray points) and daily mean (n = 6, black line) of each ecotype.

CH_4 Fluxes

All fluxes of CH_4 recorded were positive at this site, indicating net release to the atmosphere. A strong seasonal pattern of CH_4 fluxes was observed across all years, with highest fluxes occurring during July and August, for all ecotypes (**Figure 3**), where fluxes in excess of 100 nmol m^{-2} s^{-1} were seen from the open water and sphagnum.

Cumulative Fluxes

Flux measurements began in autumn 2017 toward the end of that year's growing season. This is reflected in the positive cumulative flux of CO_2 (**Figure 4**) for all ecotypes that year. In 2018, from the start of April, the accumulated flux of CO_2 was positive and never dropped below zero for any ecotype, indicating a loss of carbon from the mire that year. This was in contrast with 2019, when the cumulative NEE was negative until day 200 for sphagnum, and net zero was also within the measurement uncertainty for heather, water and eriophorum (**Figure 4**). All ecotypes proceeded to be a source of CO_2 in the second half of the year in 2019, with the most positive flux observed in the eriophorum and the intermediate, with heather, sphagnum and water all remaining close to carbon neutral. There were no significant differences in the daily total CO_2 flux between ecotypes, $F = 0.19$, $p > 0.9$ (**Figure 5**). Across all ecotypes, there was a net loss of 1.13 g CO_2-C m^{-2} d^{-1} in 2018 which was significantly greater than C losses of 0.24 g CO_2-C m^{-2} d^{-1} in 2019, $F = 112.24$, $p < 0.001$.

Over the entire study period, there was a significant effect of ecotype on the daily CH_4 fluxes, $F = 3.05$, $p = 0.03$, with the highest mean emissions of 23 mg CH_4-C m^{-2} d^{-1} observed in the eriophorum (**Figure 6**), differing from all other ecotypes except sphagnum (16 mg CH_4-C m^{-2} d^{-1}); the next highest flux was seen from the water (10 mg CH_4-C m^{-2} d^{-1}), then heather (8 mg CH_4-C m^{-2} d^{-1}). Emissions of CH_4 were ca. 40% higher during the drought of 2018 (17 mg CH_4-C m^{-2} d^{-1}) than in 2019 (12 mg CH_4-C m^{-2} d^{-1}), $F = 34.93$, $p < 0.0001$, however, there were significant interactions between year and month ($F = 4.50$, $p < 0.001$), ecotype and year ($F = 6.74$, $p < 0.001$) and ecotype, year and month ($F = 2.12$, $p < 0.02$). Post hoc tests reveal that, despite CH_4 emissions being higher during spring of 2018, in the late summer, fluxes declined and were lower than in 2019, especially in the high flux ecotypes of eriophorum and sphagnum (**Figures 6A,C**).

Net Greenhouse Gas Balance

The total global warming potential (GWP) was calculated at the end of the summer (defined as day 240) for both 2018 and 2019. Annual GWP did not significantly differ between ecotypes, $F = 0.51$ $p < 0.7$, in 2018 ranging from a high of 823 g CO_2-eq m^{-2} in eriophorum and a low of 649 g CO_2-eq m^{-2} in the heather; this was in contrast with 2019, where the range of 370 g CO_2-eq m^{-2} in the eriophorum to 74 g CO_2-eq m^{-2} in the water (**Figure 4**, right hand column) was significantly higher than in 2018, $F = 47.66$, $p < 0.001$. This difference was driven by the change in the proportion of net CO_2 fluxes to the CH_4 emissions, with non-significant increases in the contribution of CH_4 fluxes to the total GWP seen from 2018 to 2019 from 31% in 2018 to 81% in eriophorum, and in sphagnum from 26 to 150%.

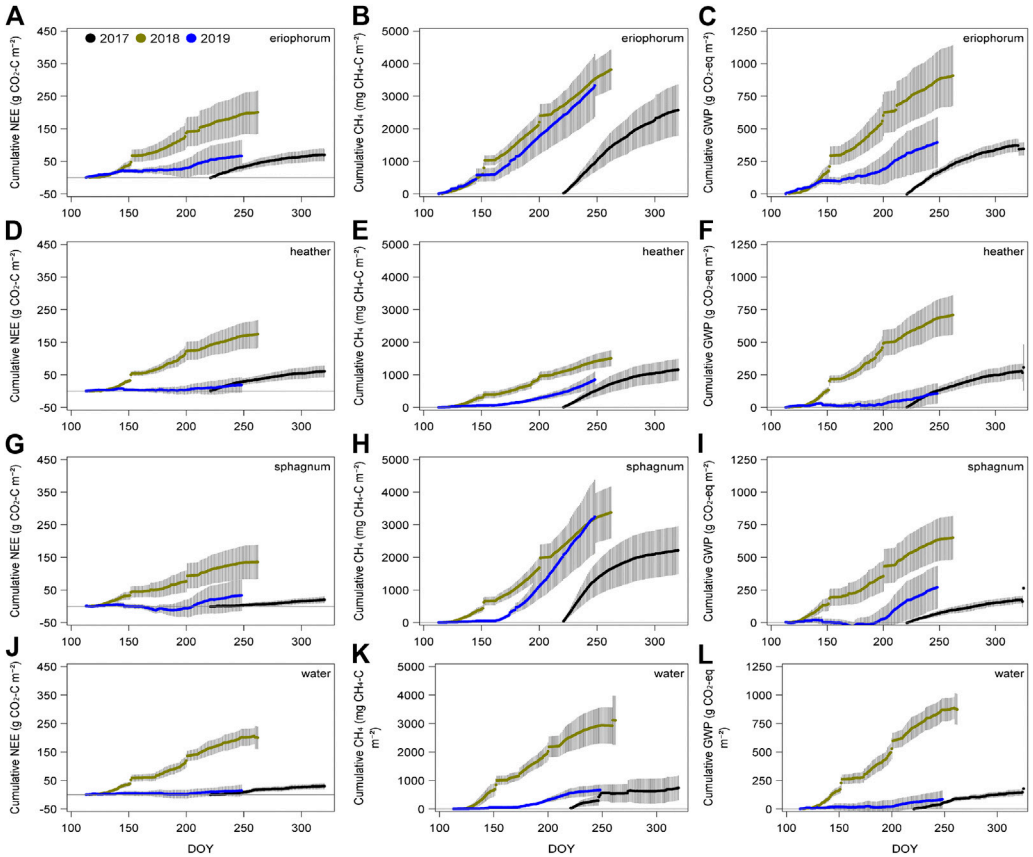

FIGURE 4 | Mean daily cumulative fluxes of CO2 **(A,D,G,J)**, CH4 **(B,E,H,K)** and aggregated CO2 and CH4 in terms of global warming potential (IPCC, 2013, **C,F,I,L**) for each ecotype (n 6, ± 1 SE) for 2017 (black line), 2018 (olive line) and 2019 (blue line).

Environmental Controls

A warm dry spring in 2018 was characterized by high temperatures during May, with air temperature frequently approaching 30°C, which in turn saw a sharp rise in soil temperature from close to zero at the end of April to 15°C a couple of weeks later (**Figure 7**). This continued throughout June and July, which alongside periods of weeks without rain caused the water table to drop below 40 cm (**Figure 7**). These drought conditions started in the second half of 2017 and persisted for 18 months. Relative to the thirty-year average, air temperature was + 1.38°C, rainfall – 378 mm (ca. 35%) and relative humidity was 8% (**Table 1**). In contrast, rainfall was much more evenly spread during 2019, with 62 mm more rain than the thirty-year average, and the water table remained closer to the surface, except for a few weeks during August.

Sub-diel variation of NEE was best explained by radiation (**Supplementary Figure S2**), but daily fluxes displayed positive relationships with air temperature in all ecotypes except water, ranging from $R^2 = 0.16$ (sphagnum) to $R^2 = 0.08$ (heather); daily variation from water ecotypes was positively related to relative humidity ($R^2 = 0.12$).

Relationships between daily CH_4 fluxes and environmental variables were also closely related to soil temperature, ranging from strong relationships in sphagnum ($R^2 = 0.69$), eriophorum ($R^2 = 0.37$), and heather ($R^2 = 0.38$), with much weaker, but significant relationships in water ($R^2 = 0.11$) (**Figure 8A**). The depth at which soil temperature had the strongest effect differed between ecotypes, with temperature at 12 cm controlling sphagnum fluxes, 18 cm in eriophorum and heather and 60 cm in mix and water ecotypes.

Concurrent measurements of water table depth displayed negative relationships with CH_4 emissions from all ecotypes (**Figure 8B**), with the strongest effect seen in the water ecotype ($R^2 = 0.53$), and the weakest seen in eriophorum ($R^2 = 0.09$). It might be expected to see relationships of CH_4 emission with water table, since methanogenesis would be expected to take place in anaerobic conditions. Only by looking at delayed responses of fluxes to water table did a positive effect become apparent, in all ecotypes with the exception of water, which remained a negative relationship (**Figure 8C**). The delay of the response of CH_4 flux to water table depth, i.e. the lag at which the strongest relationship was seen, was around three months for all ecotypes, eriophorum (84 days, $R^2 = 0.42$), heather (86 days, $R^2 = 0.42$), sphagnum (86 days, $R^2 = 0.51$) except water (zero days, $R^2 = 0.30$).

Using the all the measured environmental variables, multiple regression analyses revealed that soil temperature and lagged

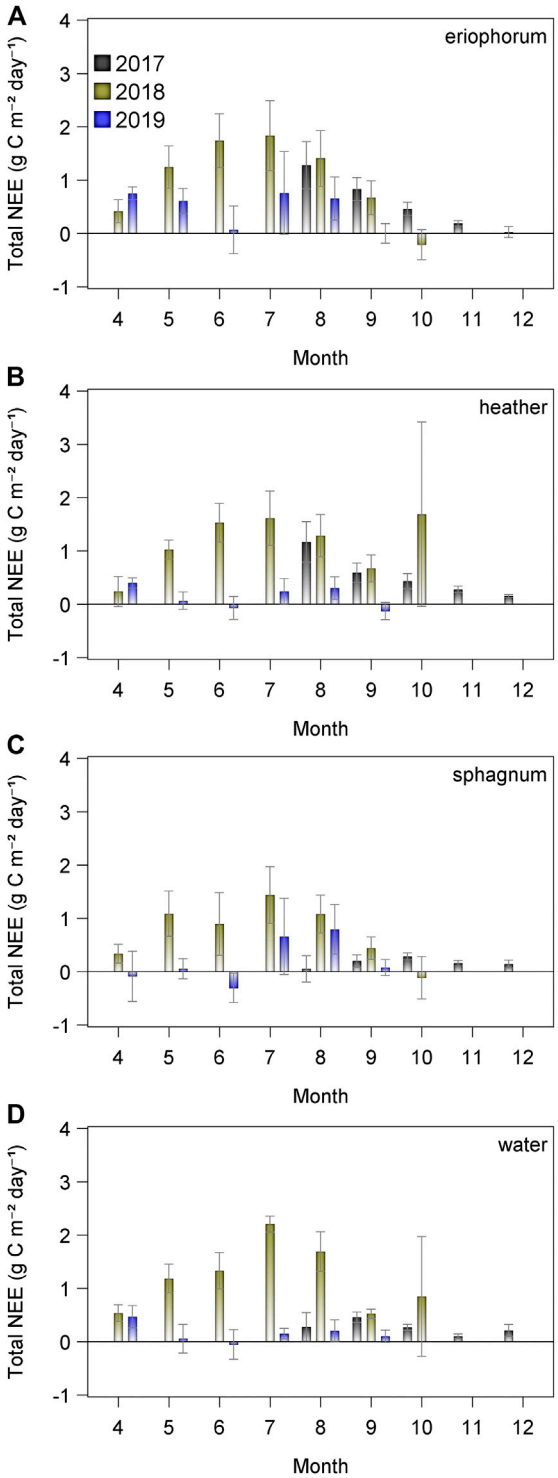

FIGURE 5 | Total monthly flux of CO_2 from each ecotype (n = 6, ± 1SE) for 2017 (black), 2018 (olive) and 2019 (blue).

water table depth were the two most important drivers of CH_4 fluxes from eriophorum (R^2 = 0.37), heather (R^2 = 0.46) and sphagnum (R^2 = 0.73), but the story was less clear in water, where concurrent water table depth and relative humidity were important drivers (R^2 = 0.60) (**Table 2**).

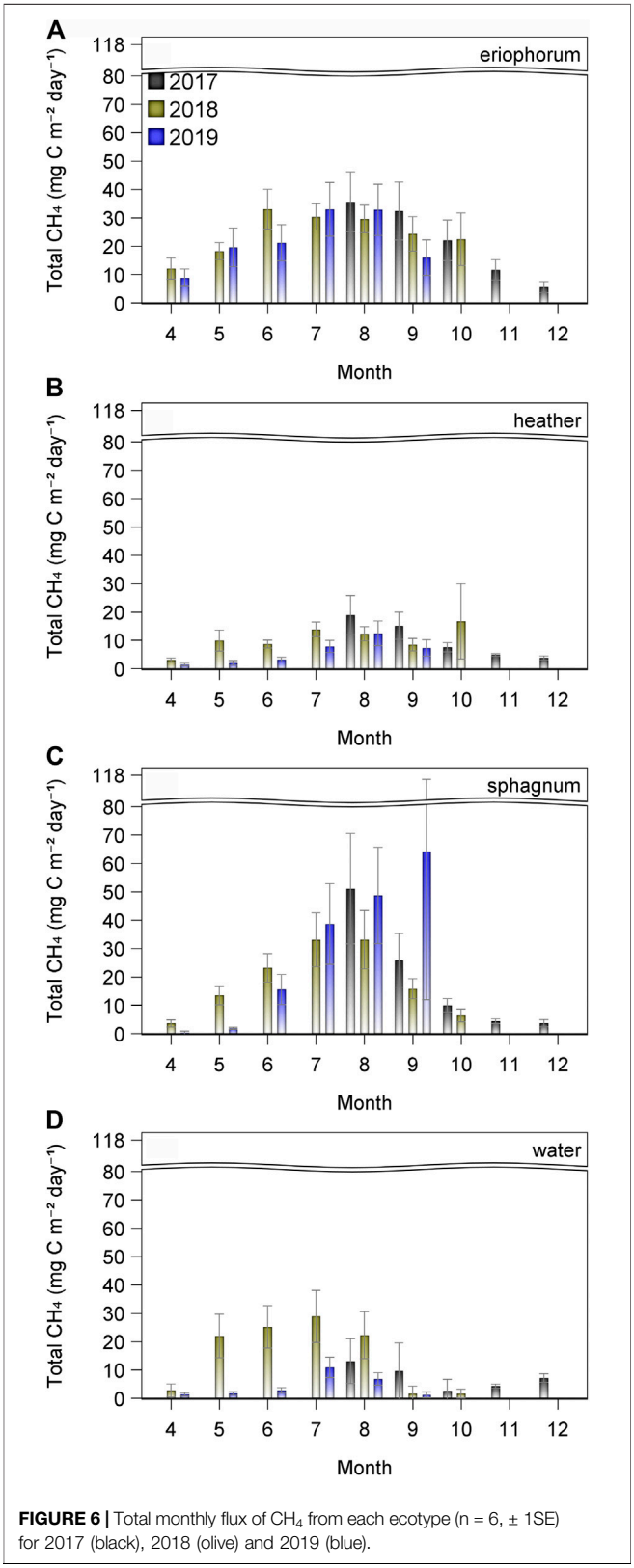

FIGURE 6 | Total monthly flux of CH_4 from each ecotype (n = 6, ± 1SE) for 2017 (black), 2018 (olive) and 2019 (blue).

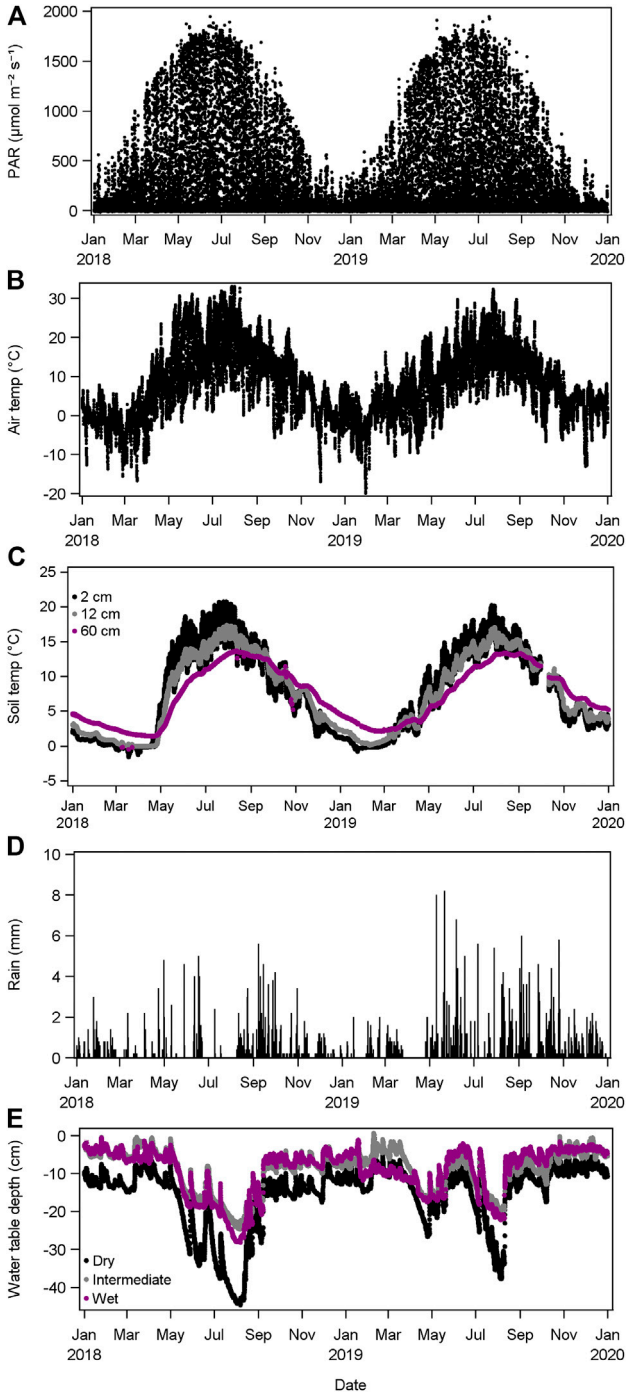

FIGURE 7 | Environmental variables measured at the study site during 2018–2019. **(A)** Photosynthetically active radiation; **(B)** air temperature; **(C)** Soil temperature at 2 cm, 12 cm and 60 cm; **(D)** rainfall; **(E)** water table depth measured at three locations.

DISCUSSION

Drought conditions in 2018 saw GHG emissions from a hemiboreal bog increase, ensuring that this important landscape was a greater net C source that year. The GHG increase was driven largely by a decline in photosynthesis, with NEE remaining positive during 2018 compared to 2019. This decline in C uptake by the vegetation might have been expected to be offset by a decline in CH_4 emissions under drier conditions. However, due to a delayed response to water table depth, CH_4 fluxes did not fall until the second half of summer 2018, ensuring that the GHG balance was higher than in 2019, under more typical conditions. In fact, the rapid warming of soil during May 2018 drove a pulse of CH_4 not seen the subsequent year. The annual fluxes reported here of 3,000–4,000 mg CH_4-C

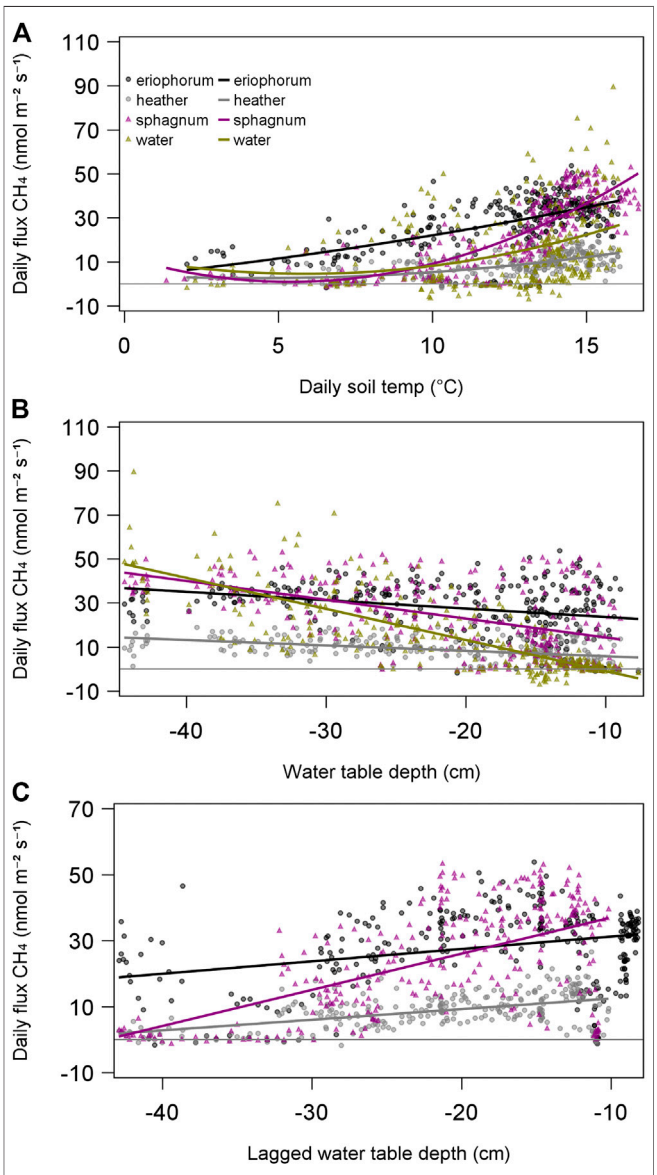

FIGURE 8 | Effect of soil temperature **(A)** and water table **(B)** on daily mean CH_4 flux from each ecotype. Hysteresis of CH_4 flux response to water is illustrated by the negative relationship of fluxes to concurrent measurements of water table depth. A delayed response is apparent when fluxes are regressed against a lagged running average of water table depth (except in the open water ecotype), with the lag varying between 84 days (eriophorum) and 86 days (sphagnum) **(C)**.

TABLE 2 | Multiple regression models of significant ($p < 0.05$) environmental variables on CH_4 fluxes. Subscripts for soil temperature indicate depth and for water table number of lagged days.

Ecotype	Variable	Estimate	Partial r^2	Model r^2
Eriophorum	Soil $temp_{18}$	2.35	0.37	0.37
	WT_{84}	0.14	0.01	0.38
	Intercept			
Heather	Soil $temp_{18}$	1.00	0.35	0.35
	WT_{84}	0.21	0.11	0.46
	Intercept			
Sphagnum	Soil $temp_{12}$	3.32	0.60	0.60
	WT_{84}	0.68	0.12	0.72
	Max PAR	0.01	0.01	0.73
	Intercept			
Water	WT_0	−1.25	0.38	0.38
	RH	−0.40	0.17	0.55
	Air temp	1.11	0.03	0.58
	Soil $temp_{60}$	−0.85	0.01	0.59
	Air pressure	0.27	0.01	0.60
	Intercept			

from eriophorum, sphagnum and water (in 2018) approximate closely to the median emissions reported across all northern peatlands of 3,300–6,300 mg CH_4-C (Abdalla et al., 2016), and the monthly averages from sphagnum and eriophorum were similar to the growing season fluxes reported elsewhere (Roulet et al., 1992; Grondahl et al., 2008; Dinsmore et al., 2017). Mean summertime emissions of five times the magnitude that we report have been observed from sphagnum lawns (Kettunen et al., 1996) where the water table was consistently above 5 cm year-round.

Effect of Ecotype on GHG Fluxes

As we hypothesized, the lowest average CH_4 emissions were seen from heather, and the greatest from eriophorum, which is known to be erenchymatous (Smirnoff and Crawford, 1983; Camill, 1999) and develop deep rooting systems to the full depth of the active layer (Wein, 1973). This physiology facilitates the transport of CH_4 formed at depth in the peat to be transported directly to the atmosphere, by-passing erobic upper layers of the soil in which CH_4 oxidizing microbes can reduce net CH_4 emissions (Raghoebarsing et al., 2005; Kip et al., 2010; Rahman et al., 2011). Our finding is consistent with previous studies which have shown that eriophorum cover is directly correlated to the magnitude of CH_4 fluxes (McNamara et al., 2008; Cooper et al.,2014). In this current study, sphagnum and water ecotypes were also associated with high CH_4 emissions, which were the wettest of the ecotypes and indicative of conditions favoring CH_4 production. Sphagnum cover is associated with areas of CH_4 emission in peat soils (Roura-Carol and Freeman, 1999; Dinsmore et al., 2017), often forming floating mats on ground water surface. The ecotype with the lowest CH_4 emissions was heather, consistent with previous work (Grondahl et al., 2008); heather dominated the driest areas of the bog, where it would be expected to see a combination of lowest CH_4 formation and highest CH_4 oxidation, due to the erobic conditions.

Effect of Drought on GHG Fluxes and Balance

The biggest effect of the drought in 2018 was an increase in net CO_2 emissions. Although photosynthesis is controlled by radiation, the warmer, drier conditions of 2018 stimulated increased respiration so that CO_2 losses exceeded uptake. Light response curves indicated that photosynthesis was lower during the drought of 2018 (**Supplementary Figure S2**) and that it saturated at lower light levels than under the more usual conditions of 2019. A lower water table in 2018 increased the oxygenation of the soil profile, exposing much of the accumulated organic matter to erobic decomposition. The extent of the water table drop was such that, for most of 2018, the areas which were covered by open water during the establishment of the study dried out and exposed the underlying peat and vegetation. Under more typical conditions of 2019, most ecotypes reverted to C sinks until late in the year when photosynthesis declined due to reduced hours of daylight. With the exception of eriophorum, at the end of the growing season net zero CO_2 flux was within the error term of the cumulative NEE. However, once the winter CO_2 and CH_4 fluxes have been considered, the site was still a net C source under more typical conditions. While this may be unusual for other similar wetlands, which are commonly seen to be C sinks (Campbell et al., 2019; Mazzola et al., 2020; Mehtatalo et al., 2020; Rinne et al., 2020), it is not unusual for this site under 30-years average climatic conditions (Rinne et al., 2020).

The most important driver of CH_4 fluxes at this site was soil temperature, with the warmer spring of 2018 driving an increase in fluxes. While water table was also significantly related to CH_4 emissions, it appeared to be a delayed effect rather than an instantaneous one, with contemporaneous water table depth appearing to have a negative effect on CH_4 emissions. Superficially this was a surprise, since CH_4 emissions are greatest in wetter organic soil ecosystems (e.g., Roulet et al., 1992; Levy et al., 2012), and the wettest areas within such ecosystems (Macdonald et al., 1996; Dinsmore et al., 2017). However, a negative relationship between water table depth and CH_4 emission has been reported several times from ecosystems similar to the current study site (Kettunen et al., 1996; McNamara et al., 2008; Dinsmore et al., 2009), though the reasons for such a relationship appear to be poorly understood. However, an explanation may lie in a lag between CH_4 emissions and increasing water table, which has been described previously, though the lag is generally less than two weeks (Goodrich et al., 2015; Chamberlain et al., 2016). Several factors may contribute to such a lag: drying of the peat profile will reduce the methanogen population (Tian et al., 2012) and the severity of dieback is related to the strength of drought conditions (Estop-Aragones et al., 2013); during drought, the C substrates for methanogenesis are exposed to erobic conditions, leading to rapid decomposition (Goodrich et al., 2015), thus it can take time to replenish substrate once the water table rises; another consequence of erobic drought conditions is that alternative electron acceptors can build up in the peat (Knorr et al., 2009) and the preferential use of these over acetate and CO_2 following rewetting slows the rate of CH_4 production (Yavitt and Seidmann-Zager, 2006). While the lag described in the present study is larger than commonly reported, it is not inconceivable that a

combination of depleted substrate, reduced methanogen population and alternative electron acceptors persisted for the lag period we report. A theoretical explanation for such a negative effect of water table on CH_4 flux was provided by Stockdale et al. (2012) in which the author proposes a delay between water table depth and emission, which has further been supported experimentally in manipulated microcosms where a four-month delay was seen before CH_4 emissions increased (Stockdale et al., 2014). This timescale is similar to the delay of 84–88 days between water table and CH_4 fluxes observed from the terrestrial ecotypes at the current study site.

A further possible explanation for the delayed response of fluxes to water table is that the effect of temperature was a much stronger influence. It is clear that soil temperature was the most important factor controlling CH_4 emissions. In wetlands, under anaerobic conditions, methanogenesis is known to be directly dependent on temperature and substrate availability (Segers, 1998), and microcosm experiments have shown CH_4 emissions to increase from sphagnum under elevated temperatures (van Winden et al., 2012). Given that CH_4 flux is the balance between microbial production and oxidation of CH_4, identifying a single driver is challenging and perhaps misguided. Hotspots of CH_4 production are known to occur at suitable microsites within peat soil profiles (Laing et al., 2010) and we suggest that our data indicate that, despite water table dropping as low as 40 cm below the vegetation-air interface, there remained sufficient anaerobic microsites within the soil profile to sustain methanogenesis at all times. This would be further supported by the highest fluxes from eriophorum, whose deep roots (Bliss, 2000) will likely have remained below the water table even during the driest periods. The rapidly warming soil temperatures of May 2018 increased the rate of microbial activity at such sites within the peat and also coincided with increasing photosynthetic activity of the aboveground vegetation and the resultant supply of substrate for CH_4 production. If the rate of CH_4 production was greater than oxidation, this would result in increased emissions. In the low flux ecotypes, the effect of water table was less important.

Implications for Hemiboreal Wetlands Under Future Climate

The significant interaction of CH_4 emissions between ecotype and year demonstrated how common bog species differed in their response to drought conditions. Recovery of CH_4 fluxes from sphagnum and eriophorum late in 2019 contrasted with the suppressed emissions from heather and in particular, open water. Under predicted changes to climate, it is likely that precipitation patterns in the northern hemisphere will alter, so that periods without rain are interspersed by more intense rainfall events, in a drought-deluge pattern (Arneth et al., 2019). It has been known for 25 years that sphagnum-dominated wetland C sinks are at risk from drought (Alm et al., 1999) and the current study has shown that, through the influence of both temperature and water table, drought increased net CO_2 emissions while warm temperatures maintain high CH_4 fluxes across all ecotypes in such ecosystems. What will be critical for the carbon balance is the duration of drought periods. If intermittent deluges of rain are enough to maintain a water table within the rooting zone of vegetation such as eriophorum, it is likely that CH_4 emissions will remain high. The desiccation of aboveground biomass will reduce CO_2 uptake which will inevitably reduce the build-up of organic material. If the water table drops for more prolonged periods, then CH_4 emissions would be expected to decline due to a combination of factors: increased eration of the soil profile will halt methanogenesis and increase methane oxidation; erobic respiration of existing organic material will reduce the substrate available for methanogenesis; reduced primary productivity will slow the delivery of new organic material. Persistence of drought conditions over several growing seasons may alter the species composition of the ecosystem, which in turn may influence the C balance of the system. For example, it is known that permanent water table lowering will kill *Eriophorum vaginatum* (Wein, 1973) and sphagnum species, the ecotypes associated with the highest CH_4 fluxes in this study. However, although temperature and precipitation are the key drivers of species turnover in these ecosystems, wetlands may be resilient to climate change as individual species are replaced with others possessing similar traits (Robroek et al., 2017; Jassey and Signarbieux, 2019; Lamentowicz et al., 2019). Such functional redundancy may buffer wetlands as a C sink, and there are instances of southern hemisphere wetlands persisting as C sinks despite undergoing drought (Goodrich et al., 2017). Inevitably, there will be a tipping point beyond which a succession is seen from wetland C sink to a drier landscape with increased vascular plant abundance (Swindles et al., 2019). A GWP approach to assessing the C balance of peatlands may be oversimplistic, since an annual account of GHG emissions does not consider the previous cooling effect of centuries of C sequestration following peat formation (Frolking et al., 2006; Frolking and Roulet, 2007). However, it is useful to consider the future consequences of a sustained shift in C dynamics, particularly a transition from a net CO_2 sink, or an increased C source in the case of the current study site. Our study has shown that a 0.5°C rise in annual temperature, and a 35% reduction in annual rainfall led to C losses of up to 1 kg CO_2-eq m^{-2} y^{-1}, and with 10–12 million ha of blanket bog globally (O'Brien et al., 2007), vast stores of C within these landscapes may well act as a climate feedback, before a new equilibrium is reached as a grass dominated landscape.

CONCLUSION

Anthropogenic climate change is likely to create conditions under which hemiboreal blanket bogs increase their C emissions, creating a positive feedback, ultimately exhausting the C stored in these ecosystems. Achieving net zero emissions may well maintain peatlands as a C sink helping to mitigate climate change. However, under a 'business as usual' scenario, years like 2018 will become more prevalent and if we fail to keep global heating to 2°C, northern wetlands will be a key driver of future climate change.

DATA AVAILABILITY STATEMENT

The raw data supporting the conclusions of this article will be made available by the authors, without undue reservation.

AUTHOR CONTRIBUTIONS

JK, PI, LK, and PW designed the experiment set up the study. PW and LK had responsibility of the study site and JK and ST also contributed to maintenance of the experiment. PW and JK processed the data and conducted the analyses, and all authors contributed to the writing and editing of the manuscript.

FUNDING

This work was funded by an EU Cost Action (COST-STSM-ECOST-STSM-ES1308–080216–068955), Swedish Infrastructure for Ecosystem Science (SITES), who provided access to the Skogaryd Research Catchment and the Natural and Environmental Research Council (NE/P008690/1).

ACKNOWLEDGMENTS

We thank David Allbrand, Johanna Pihlblad, Steve Howarth, and Mark Bentley for their technical support.

SUPPLEMENTARY MATERIAL

The Supplementary Material for this article can be found online at: https://www.frontiersin.org/articles/10.3389/feart.2020.562401/full#supplementary-material.

REFERENCES

Abdalla, M., Hastings, A., Truu, J., Espenberg, M., Mander, Ü., and Smith, P. (2016). Emissions of methane from Northern Peatlands: a review of management impacts and implications for future management options. *Ecol. Evol.* 6, 7080–7102. doi:10.1002/ece3.2469

Alm, J., Schulman, L., Walden, J., Nykanen, H., Martikainen, P. J., and Silvola, J. (1999). Carbon balance of a boreal bog during a year with an exceptionally dry summer. *Ecology.* 80, 161–174. doi:10.2307/176987

Arneth, A., Barbosa, H., Benton, T., Calvin, K., Calvo, E., Connors, S., et al. (2019). *Technical report, intergovernmental panel on climate change. IPCC special report on climate change, desertification, land degradation, sustainable land management, food security, and greenhouse gas fluxes in terrestrial ecosystems.*

Bengtsson, F., Granath, G., and Rydin, H. (2016). Photosynthesis, growth, and decay traits in Sphagnum - a multispecies comparison. *Ecol. Evol.* 6, 3325–3341. doi:10.1002/ece3.2119

Billett, M. F., Charman, D. J., Clark, J. M., Evans, C. D., Evans, M. G., Ostle, N. J., et al. (2010). Carbon balance of UK Peatlands: current state of knowledge and future research challenges. *Clim. Res.* 45, 13–29. doi:10.3354/cr00903

Bliss, L. C. (1998). *Arctic tundra and polar desert biome*. In North American Terrestrial Vegetation. Editors M. G. Barbour and W. D. Billings (Cambridge, United Kingdom).

Bond-Lamberty, B., Wang, C. K., and Gower, S. T. (2004). A global relationship between the heterotrophic and autotrophic components of soil respiration?. *Global Change Biol.* 10, 1756–1766. doi:10.1111/j.1365-2486.2004.00816.x

Buttler, A., Robroek, B. J. M., Laggoun-Defarge, F., Jassey, V. E. J., Pochelon, C., Bernard, G., et al. (2015). Experimental warming interacts with soil moisture to discriminate plant responses in an ombrotrophic Peatland. *J. Veg. Sci.* 26, 964–974. doi:10.1111/jvs.12296

Camill, P. (1999). Patterns of boreal permafrost Peatland vegetation across environmental gradients sensitive to climate warming. *Can. J. Bot. -Revue Canadienne De Botanique.* 77, 721–733. doi:10.1139/b99-008

Campbell, D. I., Clarkson, B. R., Wall, A. M., Schipper, L. A., and Ratcliffe, J. L. (2019). Water table fluctuations control CO_2 exchange in wet and dry bogs through different mechanisms. *Sci. Total Environ.* 655, 1037–1046. doi:10.1016/j.scitotenv.2018.11.151

Chamberlain, S. D., Gomez-Casanovas, N., Walter, M. T., Boughton, E. H., Bernacchi, C. J., DeLucia, E. H., et al. (2016). Influence of transient flooding on methane fluxes from subtropical pastures. *J. Geophys. Res. Biogeosci.* 121, 965–977. doi:10.1002/2015JG003283

Cooper, M. D. A., Evans, C. D., Zielinski, P., Levy, P. E., Gray, A., Peacock, M., et al. (2014). Infilled ditches are hotspots of landscape methane flux following Peatland Re-wetting. *Ecosystems.* 17, 1227–1241. doi:10.1007/s10021-014-9791-3

Dinsmore, K. J., Drewer, J., Levy, P. E., George, C., Lohila, A., Aurela, M., et al. (2017). Growing season CH_4 and N_2O fluxes from a subarctic landscape in northern Finland; from chamber to landscape scale. *Biogeosciences.* 14, 799–815. doi:10.5194/bg-14-799-2017

Dinsmore, K. J., Skiba, U. M., Billett, M. F., and Rees, R. M. (2009). Effect of water table on greenhouse gas emissions from Peatland mesocosms. *Plant Soil.* 318, 229–242. doi:10.1007/s11104-008-9832-9

Estop-Aragones, C., Knorr, K. H., and Blodau, C. (2013). Belowground *in situ* redox dynamics and methanogenesis recovery in a degraded fen during dry-wet cycles and flooding. *Biogeosciences.* 10, 421–436. doi:10.5194/bg-10-421-2013

Frolking, S., and Roulet, N. T. (2007). Holocene radiative forcing impact of Northern Peatland carbon accumulation and methane emissions. *Global Change Biol.* 13, 1079–1088. doi:10.1111/j.1365-2486.2007.01339.x

Frolking, S., Roulet, N., and Fuglestvedt, J. (2006). How Northern Peatlands influence the Earth's radiative budget: sustained methane emission versus sustained carbon sequestration. *J. Geophys. Res. Biogeosci.* 111, G01008. doi:10.1029/2005JG000091

Goodrich, J. P., Campbell, D. I., Roulet, N. T., Clearwater, M. J., and Schipper, L. A. (2015). Overriding control of methane flux temporal variability by water table dynamics in a Southern Hemisphere, raised bog. *J. Geophys. Res. Biogeosci.* 120, 819–831. doi:10.1002/2014JG002844

Goodrich, J. P., Campbell, D. I., and Schipper, L. A. (2017). Southern Hemisphere bog persists as a strong carbon sink during droughts. *Biogeosciences.* 14, 4563–4576. doi:10.5194/bg-14-4563-2017

Greenup, A. L., Bradford, M. A., McNamara, N. P., Ineson, P., and Lee, J. A. (2000). The role of *Eriophorum vaginatum* in CH_4 flux from an ombrotrophic peatland. *Plant Soil.* 227, 265–272. doi:10.1023/a:1026573727311

Grondahl, L., Friborg, T., Christensen, T. R., Ekberg, A., Elberling, B., Illeris, L., et al. (2008). Spatial and inter-annual variability of trace gas fluxes in a heterogeneous high-arctic landscape. *Adv. Ecol. Res.* 40 (40), 473–498. doi:10.1016/s0065-2504(07)00020-7

Heinemeyer, A., Gornall, J., Baxter, R., Huntley, B., and Ineson, P. (2013). Evaluating the carbon balance estimate from an automated ground-level flux chamber system in artificial grass mesocosms. *Ecol. Evol.* 3, 4998–5010. doi:10.1002/ece3.879

IPCC (2014). *Climate change 2014: synthesis report. Contribution of working groups I, II and III to the fifth assessment report of the intergovernmental panel on climate change [core writing team*. Editors R. K. Pachauri and L. A. Meyer (Geneva, Switzerland: IPCC), 151.

Jarveoja, J., Nilsson, M. B., Crill, P. M., and Peichl, M. (2020). Bimodal diel pattern in peatland ecosystem respiration rebuts uniform temperature response. *Nat. Commun.* 11, 4255. doi:10.1038/s41467-020-18027-1

Jassey, V. E. J., and Signarbieux, C. (2019). Effects of climate warming on Sphagnum photosynthesis in peatlands depend on peat moisture and species-specific anatomical traits. *Global Change Biol.* 25, 3859–3870. doi:10.1111/gcb.14788

Juszczak, R., and Augustin, J. (2013). Exchange of the greenhouse gases methane and nitrous oxide between the atmosphere and a temperate Peatland in Central Europe. *Wetlands.* 33, 895–907. doi:10.1007/s13157-013-0448-3

Keane, J. B., and Ineson, P. (2017). Technical note: differences in the diurnal pattern of soil respiration under adjacent *Miscanthus x giganteus* and barley

crops reveal potential flaws in accepted sampling strategies. *Biogeosciences.* 14, 1181–1187. doi:10.5194/bg-14-1181-2017

Keane, J. B., Ineson, P., Vallack, H. W., Blei, E., Bentley, M., Howarth, S., et al. (2018). Greenhouse gas emissions from the energy crop oilseed rape (*Brassica napus*); the role of photosynthetically active radiation in diurnal N_2O flux variation. *Global Change Biol. Bioenergy.* 10, 306–319. doi:10.1111/gcbb.12491

Kettunen, A., Kaitala, V., Alm, J., Silvola, J., Nykanen, H., and Martikainen, P. J. (1996). Cross-correlation analysis of the dynamics of methane emissions from a boreal Peatland. *Global Biogeochem. Cycles.* 10, 457–471. doi:10.1029/96gb01609

Kip, N., van Winden, J. F., Pan, Y., Bodrossy, L., Reichart, G. J., Smolders, A. J. P., et al. (2010). Global prevalence of methane oxidation by symbiotic bacteria in peat-moss ecosystems. *Nat. Geosci.* 3, 617–621. doi:10.1038/ngeo939

Knorr, K. H., Lischeid, G., and Blodau, C. (2009). Dynamics of redox processes in a minerotrophic fen exposed to a water table manipulation. *Geoderma.* 153, 379–392. doi:10.1016/j.geoderma.2009.08.023

Koskinen, M., Minkkinen, K., Ojanen, P., Kamarainen, M., Laurila, T., and Lohila, A. (2014). Measurements of CO_2 exchange with an automated chamber system throughout the year: challenges in measuring night-time respiration on porous peat soil. *Biogeosciences.* 11, 347–363. doi:10.5194/bg-11-347-2014

Kutzbach, L., Wagner, D., and Pfeiffer, E. M. (2004). Effect of microrelief and vegetation on methane emission from wet polygonal tundra, Lena Delta, Northern Siberia. *Biogeochemistry.* 3, 341–362. doi:10.1023/B:BIOG.0000031053.81520

Lai, D. Y. F., Roulet, N. T., Humphreys, E. R., Moore, T. R., and Dalva, M. (2012). The effect of atmospheric turbulence and chamber deployment period on autochamber CO_2 and CH_4 flux measurements in an ombrotrophic peatland. *Biogeosciences.* 9, 3305–3322. 10.5194/bgd-9-1439-2012

Laing, C. G., Shreeve, T. G., and Pearce, D. M. E. (2010). The fine scale variability of dissolved methane in surface peat cores. *Soil Biol. Biochem.* 42, 1320–1328. doi:10.1016/j.soilbio.2010.03.015

Lamentowicz, M., Gałka, M., Marcisz, K., Słowiński, M., Kajukało-Drygalska, K., Dayras, M. D., et al. (2019). Unveiling tipping points in long-term ecological records from Sphagnum-dominated Peatlands. *Biol. Lett.* 15, 20190043. doi:10.1098/rsbl.2019.0043

Lees, K. J., Clark, J. M., Quaife, T., Khomik, M., and Artz, R. R. E. (2019). Changes in carbon flux and spectral reflectance of Sphagnum mosses as a result of simulated drought. *Ecohydrology.* 12, e2123. doi:10.1002/eco.2123

Levy, P. E., Burden, A., Cooper, M. D. A., Dinsmore, K. J., Drewer, J., Evans, C., et al. (2012). Methane emissions from soils: synthesis and analysis of a large UK data set. *Global Change Biol.* 18, 1657–1669. doi:10.1111/j.1365-2486.2011.02616.x

Macdonald, J. A., Skiba, U., Sheppard, L. J., Hargreaves, K. J., Smith, K. A., and Fowler, D. (1996). Soil environmental variables affecting the flux of methane from a range of forest, moorland and agricultural soils. *Biogeochemistry.* 34, 113–132. doi:10.1007/BF00000898

Mazzola, V., Perks, M. P., Smith, J., Yeluripati, J., and Xenakis, G. (2020). Seasonal patterns of greenhouse gas emissions from a forest-to-bog restored site in northern Scotland: influence of microtopography and vegetation on carbon dioxide and methane dynamics. *Eur. J. Soil Sci.* doi:10.1111/ejss.13050

McNamara, N. P., Plant, T., Oakley, S., Ward, S., Wood, C., and Ostle, N. (2008). Gully hotspot contribution to landscape methane (CH_4) and carbon dioxide (CO_2) fluxes in a Northern Peatland. *Sci. Total Environ.* 404, 354–360. doi:10.1016/j.scitotenv.2008.03.015

Mehtatalo, L., Alekseychik, P., Uljas, S., Mammarella, I., Korrensalo, A., Mehtätalo, L., et al. (2020). Varying vegetation composition, respiration and photosynthesis decrease temporal variability of the CO_2 sink in a boreal bog. *Ecosystems.* 23, 842–858. doi:10.1007/s10021-019-00434-1

Milne, J. A., Pakeman, R. J., Kirkham, F. W., Jones, I. P., and Hossell, J. E. (2002). Biomass production of upland vegetation types in England and Wales. *Grass Forage Sci.* 57, 373–388. doi:10.1046/j.1365-2494.2002.00339.x

Mosier, A. R. (1989). Chamber and isotope techniques. In exchange of trace gases between terrestrial ecosystems and the atmosphere. Life sciences research report 47. Editors G. P. Robertson, D. S Schimel, and M. O. Andreae (Berlin, Germany) 175–187.

O'Brien, H., Labadz, J. C., and Butcher, D. P. (2007). *Review of blanket bog management and restoration*. London: Nottingham Trent University research rep.(BD1241Defra.

Pelletier, L., Strachan, I. B., Garneau, M., and Roulet, N. T. (2014). Carbon release from boreal peatland open water pools: implication for the contemporary C exchange. *J. Geophys. Res. Biogeosci.* 119, 207–222. doi:10.1002/2013JG002423

Raghoebarsing, A. A., Smolders, A. J., Schmid, M. C., Rijpstra, W. I., Wolters-Arts, M., Derksen, J., et al. (2005). Methanotrophic symbionts provide carbon for photosynthesis in peat bogs. *Nature.* 436, 1153–1156. doi:10.1038/nature03802

Rahman, M. T., Crombie, A., Chen, Y., Stralis-Pavese, N., Bodrossy, L., Meir, P., et al. (2011). Environmental distribution and abundance of the facultative methanotroph Methylocella. *ISME J.* 5, 1061–1066. doi:10.1038/ismej.2010.190

Rey-Sanchez, C., Bohrer, G., Slater, J., Li, Y. F., Grau-Andres, R., Hao, Y. S., et al. (2019). The ratio of methanogens to methanotrophs and water-level dynamics drive methane transfer velocity in a temperate kettle-hole peat bog. *Biogeosciences.* 16, 3207–3231. doi:10.5194/bg-16-3207-2019

Rigney, C., Wilson, D., Renou-Wilson, F., Muller, C., Moser, G., and Byrne, K. A. (2018). Greenhouse gas emissions from two rewetted peatlands previously managed for forestry. *Mires Peat.* 21, 23. doi:10.19189/MaP.2017.OMB.314

Rinne, J., Tuovinen, J. P., Klemedtsson, L., Aurela, M., Holst, J., Lohila, A., et al. (2020). Effect of the 2018 European drought on methane and carbon dioxide exchange of northern mire ecosystems. *Philos. Trans. R. Soc. B.* 375, 20190517. 10.1098/rstb.2019.0517

Ritson, J. P., Brazier, R. E., Graham, N. J. D., Freeman, C., Templeton, M. R., and Clark, J. M. (2017). The effect of drought on dissolved organic carbon (DOC) release from peatland soil and vegetation sources. *Biogeosciences.* 14, 2891–2902. doi:10.5194/bg-14-2891-2017

Robroek, B. J. M., Jassey, V. E. J., Payne, R. J., Martí, M., Bragazza, L., Bleeker, A., et al. (2017). Taxonomic and functional turnover are decoupled in European peat bogs. *Nat. Commun.* 8, 1161. doi:10.1038/s41467-017-01350-5

Roulet, N. T., Ash, R., and Moore, T. R. (1992). Low boreal wetlands as a source of atmospheric methane. *J. Geophys. Res. Atmos.* 94, 3739–3749. doi:10.1029/91jd03109

Roura-Carol, M., and Freeman, C. (1999). Methane release from peat soils: effects of Sphagnum and Juncus. *Soil Biol. Biochem.* 31, 323–325. doi:10.1016/s0038-0717(98)00125-4

Segers, R. (1998). Methane production and methane consumption: a review of processes underlying wetland methane fluxes. *Biogeochemistry.* 41 (1), 23–51. doi:10.1023/a:1005929032764

Smirnoff, N., and Crawford, R. M. M. (1983). Variation in the structure and response to flooding of root aerenchyma in some wetland plants. *Ann. Bot.* 51, 237–249. doi:10.1093/oxfordjournals.aob.a086462

Stockdale, J. E., Stockdale, J., Toet, S., Lukac, M., Milcu, A., and Ineson, P. (2012). Scaling up of methane flux: a case study in the UK uplands. PhD Thesis, UK: University of York.

Stockdale, J. E., Toet, S., Lukac, M., Milcu, A., and Ineson, P. (2014). The hysteretic response 620 of peatland methane fluxes: an improved approch to identify the factors controlling methane 621 flux. Paper presented at the EGU General Assembly Conference Abstracts.

Strack, M., and Waddington, J. M. (2008). Spatiotemporal variability in peatland subsurface methane dynamics. *J. Geophys. Res. Biogeosci.* 113, 12. doi:10.1029/2007jg000472

Swindles, G. T., Morris, P. J., Mullan, D. J., Payne, R. J., Roland, T. P., Amesbury, M. J., et al. (2019). Widespread drying of European peatlands in recent centuries. *Nat. Geosci.* 12, 922–928. doi:10.1038/s41561-019-0462-z

Tian, J. Q., Zhu, Y. B., Kang, X. M., Dong, X. Z., Li, W., Chen, H., et al. (2012). Effects of drought on the archaeal community in soil of the Zoige wetlands of the Qinghai-Tibetan plateau. *Eur. J. Soil Biol.* 52, 84–90. doi:10.1016/j.ejsobi.2012.07.003

van Winden, J. F., Reichart, G. J., McNamara, N. P., Benthien, A., and Damsté, J. S. (2012). Temperature-induced increase in methane release from peat bogs: a mesocosm experiment. *Plos One.* 7, e39614. doi:10.1371/journal.pone.0039614

Waddington, J. M., and Roulet, N. T. (1996). Atmosphere-wetland carbon exchanges: scale dependency of CO_2 and CH_4 exchange on the developmental topography of a Peatland. *Global Biogeochem. Cycles.* 10, 233–245. doi:10.1029/95GB03871

Wein, R. W. (1973). Biological flora of the British Isles- Eriophorum vaginatum L. *J. Ecol.* 61, 601–615. doi:10.2307/2259047

Yavitt, J. B., and Seidmann-Zager, M. (2006). Methanogenic conditions in northern peat soils. *Geomicrobiol. J.* 23, 119–127. doi:10.1080/01490450500533957

Yu, Z. C. (2012). Northern peatland carbon stocks and dynamics: a review. *Biogeosciences.* 9, 4071–4085. doi:10.5194/bg-9-4071-2012

Conflict of Interest: The authors declare that the research was conducted in the absence of any commercial or financial relationships that could be construed as a potential conflict of interest.

frontiers in Earth Science

ORIGINAL RESEARCH
published: 28 January 2021
doi: 10.3389/feart.2020.542391

Seasonal Variation in Biomass and Production of the Macrophytobenthos in two Lagoons in the Southern Baltic Sea

Martin Paar[1*†], *Maximilian Berthold*[2], *Rhena Schumann*[2], *Sven Dahlke*[1] *and Irmgard Blindow*[1]

[1]*Biological Station of Hiddensee, University of Greifswald, Greifswald, Germany,* [2]*Biological Station Zingst, University Rostock, Rostock, Germany*

Baltic coastal lagoons are severely threatened by eutrophication. To evaluate the impact of eutrophication on macrophytobenthos, we compared the seasonal development in macrophytobenthic composition, biomass and production, water column parameters (light, nutrients), phytoplankton biomass and production in one mesotrophic and one eutrophic German coastal lagoon. We hypothesized that light availability is the main driver for primary production, and that net primary production is lower at a higher eutrophication level. In the mesotrophic lagoon, macrophytobenthic biomass was much higher with distinct seasonal succession in species composition. Filamentous algae dominated in spring and late summer and probably caused reduced macrophytobenthic biomass and growth during early summer, thus decreasing vegetation stability. Light attenuation was far higher in the eutrophic lagoon, due to high phytoplankton densities, explaining the low macrophytobenthic biomass and species diversity in every season. Areal net primary production was far lower in the eutrophic lagoon. The "paradox of enrichment" hypothesis predicts lower production at higher trophic levels with increased nutrient concentrations. Our results prove for the first time that this hypothesis may be valid already at the primary producer level in coastal lagoons.

Keywords: eutrophication, photosynthesis, submerged vegetation, drivers, transitional waters

OPEN ACCESS

Edited by:
Jianghua Wu,
Memorial University of Newfoundland, Canada

Reviewed by:
Martin Snickars,
Åbo Akademi University, Finland
Jan Köhler,
Leibniz-Institute of Freshwater Ecology and Inland Fisheries (IGB), Germany

****Correspondence:***
Martin Paar
martin.paar@uni-rostock.de

[†]Present address:
Martin Paar
Aquatic Ecology, Universität Rostock, Rostock, Germany

Specialty section:
This article was submitted to Biogeoscience, a section of the journal Frontiers in Earth Science.

Received: *12 March 2020*
Accepted: *14 December 2020*
Published: *28 January 2021*

Citation:
Paar M, Berthold M, Schumann R, Dahlke S and Blindow I (2021) Seasonal Variation in Biomass and Production of the Macrophytobenthos in two Lagoons in the Southern Baltic Sea. Front. Earth Sci. 8:542391. doi: 10.3389/feart.2020.542391

INTRODUCTION

At the southern Baltic Sea coast, an intricate system of coastal lagoons connects terrestrial ecosystems with the open Baltic Sea, acting as a filter for nutrients and dissolved organic substances originating from their catchment areas. These lagoons differ in their connectivity with the open sea and size of there catchment areas, whichinfluence the lagoons ecosystem response to eutrophication (Cloern, 2001). Lagoons of the Baltic Sea can be classified either as estuarine, with direct river discharge, or marine, without direct river discharge (sensu Tagliapietra et al., 2009). Especially in estuarine lagoons of the southern Baltic Sea, high nutrient supplies from their catchment area have accelerated pelagic primary production and caused high water turbidity and a massive reduction of the macrophytobenthos (Schiewer, 1998; Munkes, 2005). The macrophytobenthos has up to now not recovered (Schiewer, 1998; Munkes, 2005) though nutrient discharges have considerably decreased since the 1980ies in accordance with national and European water framework directives (Berthold et al., 2018a), Macrophytobenthos increases the structural and functional complexity of shallow waters including coastal lagoons (e.g. Duffy et al., 2001) and is therefore a

key component of shallow aquatic ecosystems. Macrophytobenthos consists of "rooted canopy forming" tracheophyte species, rooted "bottom-dwellers", loosely attached macroalgae, and filamentous algae growing as epiphyton. The complex structure of the macrophytobenthos can slow down hydrodynamic movements (Gregg and Rose, 1982), store and immobilize nutrients (Pederson and Borum, 1997), elevate sedimentation rates and, thus, redirect resources from the pelagic to the benthic system (Kennedy et al., 2010). Macrophytobenthos improves habitat diversity and fosters a rich and diverse associated fauna by providing structural support, shelter from predation and food to higher trophic levels (Hansen et al., 2011; Wlodarska-Kowalczuk et al., 2014). The influence of the macrophytobenthos on its environment depends strongly on the seasonal development of the vegetation canopy and the length of the growing period (Sayer et al., 2010), which is determined by the number of seasonal strategies and, thus, the species richness of the community.

Generally, the macrophytobenthic growing period starts in spring with the growth of rooted species, often fueled by storage metabolites (Middelboe and Markager, 1997) resulting in a macrophytobenthic biomass maximum in summer (Jankowska et al., 2014). Macrophytobenthic primary production is limited mainly by light (Pärnoja et al., 2014; Piepho, 2017) and nutrient availability (Granéli and Solander, 1988). New growing leaves are substrate for fast growing filamentous algae. Fast growing filamentous algae have the ability to take up 30% of occurring dissolved inorganic phosphorus pulses (Howard-Williams and Allanson, 1981). It leads to high production and growth of this group of macrophytes under elevated nutrient concentrations. Proliferating filamentous algae growing on macrophytes prevent leaf uptake, shade and outcompete their host for carbon and nutrients, resulting in an overall reduced production of the overgrown macrophytes (Madsen and Brix, 1997; Apostolaki et al., 2011).

During progressive eutrophication, light availability decreases in the water column because of increasing phytoplankton densities, causing a breakdown of the macrophytobenthos at a certain critical turbidity and a sudden shift to an alternate, phytoplankton-dominated turbid state. The existence of such alternative stable states has not only been shown for freshwater lakes (Scheffer et al., 1993), but also been assumed for brackish water ecosystems such as Baltic Sea coastal lagoons. In a eutrophication gradient in coastal waters of the Baltic Sea (Dahlgren and Kautsky, 2004), observed a change from slow-growing rooted macrophytes to filamentous sheet-like, fast growing species to phytoplankton dominance, similar to changes in freshwater ecosystem, where tall macrophytes with a short vegetation period form an instable "crashing" state between an stable clearwater and a stable turbid state (Sayer et al., 2010).

High self-shading within the phytoplankton assemblage decreases the euphotic zone and phytoplankton gross primary production, and can explain why nutrient enrichment does not further increase pelagic NPP in coastal ecosystems, once a certain threshold is exceeded (Oviatt et al., 1986; Schiewer, 1998). In lakes, higher pelagic NPP has consequently been found under lower nutrient concentrations. Higher total system primary production at lower nutrient and higher light conditions is further explained by the fact that submerged vegetation, together with its epiphyton, is highly productive and the main contributor to total production under these conditions (Lopez-Archilla et al., 1992; Blindow et al., 2006). This pattern supports the "paradox of enrichment" hypothesis originally described by Rosenzweig (1971), which predicts lower production with increasing nutrient availability. While Rosenzweig (1971) described this decrease in production for higher trophic levels due to increasingly instable predator-prey relationships, a corresponding decrease has thus been observed in shallow lakes already evident on the primary production level. For coastal lagoons, Schiewer (1998) and Kemp et al. (2001) assumed lower production of higher trophic levels after eutrophication, caused by reduced trophic efficiencies, but empirical evidence is scarce. Also for coastal lagoons, we assume that a paradox of enrichment already may occur at the primary producer level.

Here, we compare the seasonal development in macrophytobenthic species composition, biomass and net primary production (NPP) in two lagoons of the southern Baltic Sea under different eutrophication pressures: the mesotrophic marine Westrügensche lagoon, and the outermost part of the eutrophic estuarine Darß-Zingst lagoon system. We discuss the seasonal variation of the macrophytobenthos in relation to pelagic NPP, underwater light climate, nutrients and lagoon system attributes. We predict that one-the underwater light availability is the main driver of seasonal development of the macrophytobenthic community in the mesotrophic lagoon two-the macrophytobenthic species numbers are lower, the vegetation period is shorter and the NPP reduced in the eutrophic lagoon and three-the total areal NPP is lower in the eutrophic than in the mesotrophic lagoon. Increased knowledge of drivers and mechanisms of the macrophytobenthos and the changes affecting this community during eutrophication is essential to improve management strategies for the recovery the macrophytobenthos in lagoons of the southern Baltic Sea.

MATERIALS AND METHODS

Investigation Areas

The mesotrophic, marine Westrügensche lagoon is approximately 170 km^2 with an average depth of 1.9 m. It is connected to the Baltic Sea in the northeast and in the south, resulting in a strong water exchange. Its catchment area is relatively small, and only a slight increase in nutrient concentrations was detected in the 1980–1990 (Blindow and Meyer, 2015). The extension and cover of the macrophytobenthos did not change over the last 90 years, but changes in macrophytobenthic species composition and vegetation architecture were observed in the last decades (Blindow et al., 2016). In the Westrügensche lagoon, the samples were taken in the Vitter Bodden, between the island of Rügen and Hiddensee (**Figure 1**). The shallow coast south of

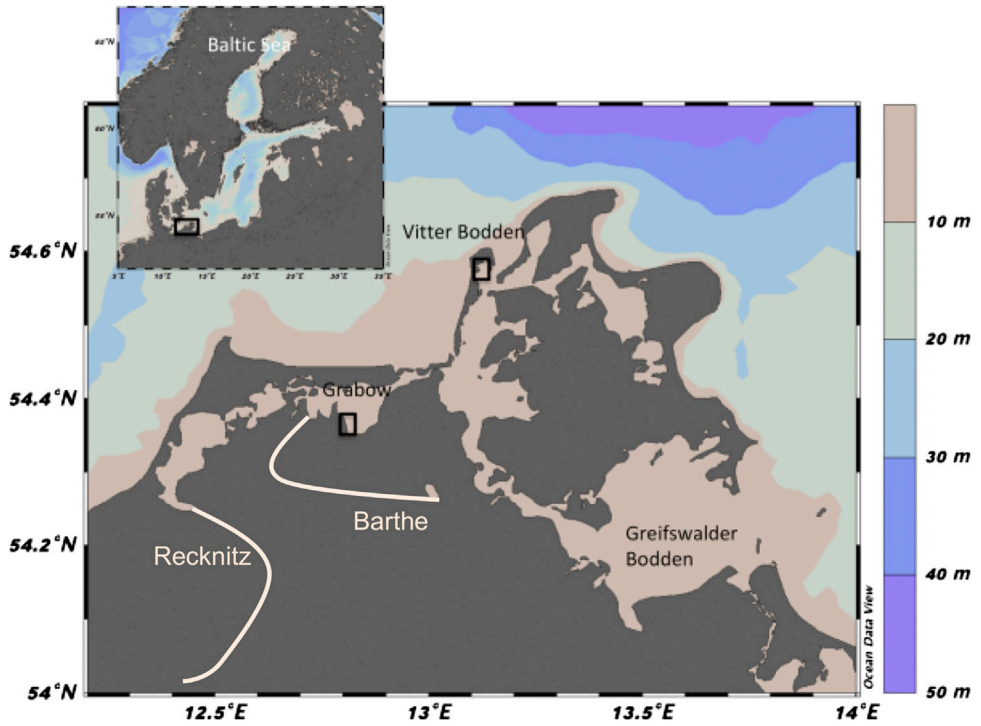

FIGURE 1 | Map of sampling sites at Grabow (Darß-Zingst Bodden chain) and Vitter Bodden (Westrügensche Bodden), southern coast of the Baltic Sea. Colors indicate water depths. White lines denote main riverine inflow of the rivers Recknitz and Barthe in this area. Maps were created with Ocean Data View (Schlitzer, 2018).

Kloster in the north of Hiddensee was chosen as the sampling location at 54°34.810′N and 13°6.913′E. Here, the macrophytobenthos density increases with depth, from 1 m down to 2.8 m water (the maximum depth of the Vitter Bodden), where it reaches up to 70% coverage. At water depths below 1 m, *Ruppia* spp. dominates the vegetation with patches of *Chara* spp. Between one and 1.5 m water depths, *Stuckenia pectinata* is dominating, and *Fucus vesiculosus* can build extensive patches. *Zostera marina* dominates below 1.5 m (Blindow et al., 2016; Bühler, 2016).

The eutrophic, estuarine Darß-Zingst Bodden Chain (DZBC) consists of four linked lagoons, which receive different freshwater (and nutrient) influxes, have different nutrient cycling, planktonic community structure and NPP. This lagoon system has been monitored since 1969 with eutrophication documented until the middle of the 1990s (Schiewer, 2007). The DZBC shows almost no recovery from eutrophication over the last 30 years. Freshwater and nutrients are flowing into the DZBC from two rivers, the Recknitz and the Barthe (**Figure 1**). Here, we focus on the outermost lagoon of the DZBC, the Grabow, which represents 21% of the total area of the four lagoons (**Figure 1**, Correns, 1976). The Grabow is the only lagoon of the system with a direct connection to the Baltic Sea. The total nitrogen (TN) and total phosphorus (TP) concentrations in the Grabow (100 and 2 mol L^{-1}, respectively) are about 50% lower than the innermost part of the DZBC (Berthold et al., 2018a). The shallow coast east of Dabitz was chosen as the sampling location (54°21.976′N and 12°48.418′E), where the macrophytobenthos reaches high cover down to water depths of 1.2 m and is dominated by *S. pectinata* (Blindow and Meyer, 2015).

Water Column Parameters

Physical Parameters and Nutrients, Pigment and Seston Concentrations

The Vitter Bodden was monitored biweekly from March 2017 to april 2018. The Grabow was monitored once a month at a central cite (Buoy B53, 54°23.483′N, 12°51.146′E). Temperature and salinity were measured using a WTW Cond 1970i, probe Tetracon 325. Secchi depth was additionally determined. Water samples for determination of nutrients, pigments and seston were taken using a 1.5 m long acrylic glass tube with a diameter of 10 cm to ensure sampling of the entire water column in Vitter Bodden. A Limnos water sampler was used to sample surface water in Grabow. Here, complete mixing of water column can be assumed for most days of the year (Schubert and Foster, 1997).

Seston concentrations were determined after filtering a known volume of water through pre-weighed GF/F (Vitter Bodden, Co. Whatman) and GF6 filters (Grabow, Co. Whatman), which were dried at 60°C until constant weight was achieved. GF6 filters were used to prevent clogging of the filter by a high cyanobacterial biomass with large mucuous envelopes (Schumann et al., 2001). In an investigation performed during 2014, about 1.2 µg L^{-1} Chl a were lost through GF6-filters (mean value, $n = 21$), equivalent to 2.6% of the Chl a concentrations obtained after GF/F-filtration (unpublished results).

For pigment analyses, water samples were filtered on same types of filters in triplicates and stored frozen. Pigments were extracted with 96% ethanol and analyzed spectrophotometrically (HELCOM 2014; LUNG SOP-Nr: 640-Chlorophyll-KG). Chlorophyll *a* values were converted into biomass assuming a C:Chl a^{-1} weight ratio of 31 (Schumann et al., 2009. Despite the large variation of this ratio (10–130) in coastal waters the annual average was choosen to allow comparison between studied lagoons. Subsamples for nutrient analyses were frozen immediately after sampling for total nutrients and after filtration through cellulose acetate (0.45 µm) for dissolved nutrients. TP, TN, dissolved inorganic phosphorus (DIP) and dissolved inorganic nitrogen (DIN) were analyzed at the Biological Station Zingst (University of Rostock, Germany). TP and TN (10–15 ml per analysis) were digested with an adapted alkaline persulphate procedure (Huang and Zhang, 2009; Berthold et al., 2015) to phosphate and nitrate, respectively. A continuous flow analyser (Alliance Instruments, 5 cm cuvette) was used to determine TP and DIP (Murphy and Riley, 1962; Malcolm-Lawes and Wong, 1990). The determination limit was 0.05 µmol L^{-1} and the combined standard uncertainty 4.2% for DIP as well as 0.22 µmol L^{-1} and 8.7% for TP. Nitrate was measured after conversion to nitrite at a cadmium reductor column and nitrite by the same method without the catalyzed reduction step as an azodye (Hansen and Koroleff, 1999). Nitrate was corrected by nitrite. Samples were diluted for nitrate and TN with ultrapure water (Purelab Flex, Elga) by 2–20 times. The samples were measured in a segmented flow analyser (FlowSys, Alliance Instruments) equipped with a 5 cm cuvette (Armstrong et al., 1967). Determination limit for nitrate was 0.32 µmol L^{-1} and 3 µmol L^{-1} for TN. Ammonium was measured as an indophenol blue dye photometrically (Hansen and Koroleff, 1999). Samples had to be diluted by up to five times. The samples were measured in a photometer (Hach, 5 cm cuvette). Determination limit is 0.7 µmol L^{-1} and the combined standard uncertainty 6.3%.

Underwater Light Climate

The solar irradiance data were provided from the German Meteorological Service measured at Arkona station (St.-Nr. 00183) near the two sampling locations. The solar irradiance was recorded as the sum of solar radiation in J cm^{-2} s^{-1} in 10 min intervals and transformed into photosynthetic active radiation (PAR) in µmol m^{-2} s^{-1} by using a conversion factor of 2.04 (Meek et al., 1984). Underwater irradiance (PAR0) was calculated from solar irradiance, Sun elevation and water attenuation (Walsby, 1997). The light attenuation coefficient (K_d) is the slope of log PAR0 with increasing water depth. The variation of K_d for both lagoons depends on several turbidity parameters and was calculated employing the formula by Xu et al. (2005):

$$K_d = 1.17 + 0.024\ \text{Chl}\ a + 0.006\ \text{seston} - 0.0225\,\text{salinity}$$

where Chl *a* is the chlorophyll *a* concentration in µg L^{-1}, seston the seston concentration in mg L^{-1}, and salinity. The data for the calculation were taken from one biweekly recording of the parameters in Vitter Bodden and from a monthly monitoring of Grabow. At both locations, measurements of light attenuation at the sampling location (K_{par}) were additionally recorded with three underwater quantum sensors (LI-192, LICOR Biosciences, Lincoln, United States) attached to a bar at intervals of 50 cm using a LI-1400 (LICOR Biosciences, Lincoln, United States) during the macrophytobenthic biomass determination in the lagoons (see below). Measurements were taken for 5 min every second at mid day during each of the sampling occasions. If available, measured K_{par} was used for estimating PAR_z above the macrophytobenthic canopy.

The underwater irradiance above the macrophytobenthic canopy at 0.75 m water depth (PAR_z) was derived from the underwater irradiance (PAR0) by applying the Lambert-Beer law:

$$PAR_z = PAR0 \times exp^{(-(K_d \times z))}$$

The self-shading of macrophytobenthos was taken into consideration by estimating the available irradiance within the macrophytobenthic canopy in µmol m^{-2} s^{-1} using the equation of Cerco and Moore (2001):

$$PAR_{mc} = \frac{PAR_z}{K_{mc} \times MPB}\left(1 - e^{-K_{mc} \times MPB}\right)$$

where PAR_z is the irradiance above the macrophytobenthic canopy at 0.75 m water depth, K_{mc} the attenuation by the macrophytobenthos (Cerco and Moore, 2001), and MPB the total macrophytobenthic dry mass in mg C m^{-2}.

Biomass and Species Composition of the Macrophytobenthos

In both lagoons, the macrophytobenthos was sampled in 2017 in five replicates in spring (March/April) and winter (November/December) and in 10 replicates in summer (June/July) and late summer (August/September). All replicates were collected randomly at a distance of at least 10 m and within three days during the sampling occasions. The samples were taken at 1 m water depth using a drop trap consisting of a 1.2 m high aluminum frame with a bottom area of 0.25 m^2. The trap was lowered from the side of a small boat into the water. The enclosed macrophytobenthos was removed using a metal bow rake. The samples were taken to the laboratory and sorted. The macrophytobenthos was identified to the lowest taxonomical level possible (**Table 1**). All samples were blotted dry, and wet mass for the entire macrophytobenthos was determined. If filamentous algae were present, a subsample was analyzed for species composition. Afterward, the samples were dried at 60°C until constant weight was reached. Organic carbon content of each sample was determined using an elemental analyser (Flash EA 1112, Thermo Scientific, Milan, Italy) at the LIENSs stable isotope facility of the University of La Rochelle, France (**Table 2**).

Net Primary Production of the Macrophytobenthos

Hourly oxygen evolution rates were calculated of the single macrophytobenthic taxa per gram dry mass (mg O_2 g DM^{-1}

TABLE 1 | Complete list of macrophytobenthic species sampled in Vitter Bodden and Grabow from March to December 2017.

Phyla	Class/Order	Dominant taxa	Growth form	Live cycle	Growth period	Sources
Rhodophyta	Ceramiales	*Ceramium* spp.	filamentous	Annual	May-August	Kiirikki and Lehvo (2012)
	Gigartinales	*Furcellaria lumbricalis*	Loosely attached	Annual	March-May	King and Schramm (1976)
Ochrophyta	Laminariales	*Chorda filum*	Attached thallus	Annual	May-September	
	Ectocarpales	*Ectocarpus* spp.	filamentous	Annual	April-August	Kiirikki and Lehvo (2012)
		Sytosiphon lomentaria	Attached thallus	Perennial	May-June	
	Fucales	*Fucus vesiculosus*	Loosely attached	Perennial	May-September	King and Schramm (1976)
Chlorophyta	Ulvophyceae	*Ulva* sp	Attached thallus	Annual	na	
		Chaetomorpha linum	filamentous	Perennial	na	
Charophyta	Charophyceae	*Chara baltica*	Rooted thallus	Annual - perennial	May-September	Blümel (2004)
Tracheophyta	Saxifragales	*Myriophyllum spicatum*	Rooted plant	Perennial	June-August	
	Alismatales	*Stuckenia pectinata*	Rooted plant	Perennial	May-September	
		Zannichellia sp	Rooted plant	Annual	May-September	Blindow et al. (2016)
		Ruppia spp.	Rooted plant	Perennial	May-September	
		Zostera marina	Rooted plant	Perennial	n.a	Apostolaki et al. (2011)

TABLE 2 | Ratios and equations used to calculate biomass and production of the model.

Taxa sampled	g DM/ g FM	g AFDM/ g DM	gC/g DM	mgChl *a*/ g DM	Sources Chl *a*	P_{max}	Q_{10} P_{max}	α	β	R_d	Model	Sources photosynthesis
Ceramium spp.	0.099*	0.651*	0.301	2.26	7	10.21	1.04	0.104		-1.926	Jasby and Platt (1976)	4, 5
Furcellaria fastigata	0.197*	0.699*	0.329	2.38	6	2.765	0.78	0.023		-0.244	Jasby and Platt (1976)	5
Chorda filum	0.138*	0.709*	0.248	6.50	7	2.045	0.95	0.011		-0.35	Jasby and Platt (1976)	4, 12
Ectocarpus sp.	0.101*	0.658*	0.342	1.55*		9.949*	0.97	0.077*	-0.0007*	-0.936	Walsby (1997)	4, 5
Sytosiphon lomentaria	0.101*	0.695*	0.277	1.55*		9.949*	0.97	0.077*	-0.0011*	-0.936	Walsby (1997)	3, 5
Fucus vesiculosus	0.211*	0.757*	0.346	4.74	13	5.852	1.13	0.030		-0.758	Jasby and Platt (1976)	5
Ulva sp	0.079	0.616*	0.215	6.50	5	13.377	1.49	0.162		-2.007	Jasby and Platt (1976)	12
Chaetomorpha linum	0.07*	0.575*	0.1915	1.07	10	10.634	1.02	0.087		-0.467	Jasby and Platt (1976)	12
Chara baltica	0.225	0.460*	0.177	1.80		2.212	1.73	0.011		-0.36	Walsby (1997)	11
Myriophyllum spicatum	0.165	0.705*	0.349	1.84	9	3.699	1.54	0.0280		-0.551	Walsby (1997)	2, 14
Stuckenia pectinata	0.153	0.844*	0.343	3.47	11	2.788	1.64	0.030		-0.504	Walsby (1997)	11
Zannichellia sp	0.114	0.844*	0.33	1.22	1	1.308	1.64	0.0071		-0.582	Walsby (1997)	2, 11
Ruppia spp.	0.180	0.873*	0.315	4.46	11	2.871	1.64	0.0096		-0.385	Walsby (1997)	11
Zostera marina	0.199*	0.767*	0.303	7.05	6	3.115	1.25	0.045		-0.875	Jasby and Platt (1976)	12

*α slope of the photosynthesis-irradiance curve where irradiance is limited (mg O_2 g DM^{-1} h^{-1} [µmol photons m^{-2} s^{-1}]$^{-1}$), AFDW ash free dry mass, β coefficient of photoinhibition, CC carbon content, Chl a Chlorophyll a, DM dry mass, P_{max} maximum photosysnthesis (mg O_2 g DM^{-1} h^{-1}), Rd dark respiration (mg O_2 g DM^{-1} h^{-1}), Q_{10} temperature coefficient. All photosynthetic parameters are temperature corrected and given at 9°C. *indicates when factors where taken from own measurements. 1 Angradi (1993); 2 Blümel (2004); 3 Evans et al. (1986); 4 Johansson and Snoeijs (2002); 5 King and Schramm (1976); 6 Lapointe and Tenore (1981); 7 Leskinen et al. (1992); 8 Madsen and Brix (1997); 9 Marcus (1980); 10 Menendez et al. (2002); 11 Piepho (2017); 12 Plus et al. (2005); 13 Russell et al. (2012); 14 Stanley and Naylor (1972).*

h^{-1}) in relation to the available irradiance within the macrophytobenthic canopy. Single species approach was chosen to incorporate seasonal variability in macrophytobenthic species composition, which differ considerably in their photosynthetic parameters. The following steps were repeated for the available irradiance within the macrophytobenthic canopy for each of the seven days during each sampling occasion to access daily variation of hourly oxygen evolution rates. Two different equations were used based on the models given for the single macrophytobenthic taxa in the literature (**Table 2**). The equation of Walsby (1997) was employed:

$$P = P_{max}\left(1 - e^{\frac{-\alpha \times PAR_{mc}}{P_{max}}}\right) + \beta \times PAR_{mc} + R_d$$

where P_{max} is the maximum oxygen evolution rate in mg O_2 g DM^{-1} h^{-1}, α the initial slope of the photosynthetic irradiance curve in mg O_2 g DM^{-1} h^{-1} (µmol photons m^{-2} s^{-1})$^{-1}$, PAR_{mc}

irradiance within the macrophytobenthic canopy in μmol m^{-2} s^{-1}, β the factor of photoinhibition and R_d the dark respiration in mg O_2 g DM^{-1} h^{-1}. The second equation employed to calculate hourly oxygen evolution rates of single macrophytobenthic species was taken from Jasby and Platt (1976):

$$P = P_{max} \times \tan h\left(\frac{\alpha \times PAR_{mc}}{P_{max}}\right)$$

All photosynthetic parameters, either taken from own measurements or from the literature (**Table 2**), were corrected for temperature. Own photosynthetic parameters were fitted to photosynthesis-irradiance measurements for *Ectocarpus* sp. and *Syctosiphon lomentaria*. As described in Piepho (2017), dark adapted apical shoots of plants were incubated in a 2.5 ml cuvette within a photosynthetic light suspension system. Oxygen evolution rates were measured in triplicates at nine light intensities from 13 to 2,000 μmol m^{-2} s^{-1} at constant temperature. The seasonal photosynthetic parameters were calculated with the following equation (Prosser, 1961):

$$P_{smax} = P_{max} \times Q10^{(T2-T1)/10}$$

where P_{max} is the maximum photosynthetic rate in mg O_2 g DM^{-1} h^{-1} at T1 9°C, P_{smax} the seasonal maximum photosynthetic rate in mg O_2 g DM^{-1} h^{-1} at the seasonal mean water temperature T2 in either of the two sampled lagoons. Species-specific Q_{10} values were calculated for P_{max} and used to temperature-correct the initial slope of the photosynthetic irradiance curve (α) and the factor of photoinhibition (β). For the dark respiration a fixed Q_{10} of 1.94 was assumed (Rasmusson 2015).

The species-specific hourly productivity (mg C DM^{-1} h^{-1}) was calculated from positive hourly oxygen evolution rates assuming a photosynthetic quotient of 1.2 during daytime (Oviatt et al., 1986). Negative hourly oxygen evolution rates were transformed into hourly respiration (mg C DM^{-1} h^{-1}) during night-time assuming a respiration quotient of 1.1 (Oviatt et al., 1986). The species-specific hourly productivity and night-time respiration were multiplied with species-specific DM to calculate the species-specific daytime hourly net primary production (NPP) and respiration (mg C m^{-2} h^{-1}). Daytime hourly NPP refers to primary production exceeding respiration during hours of daylight. Daily NPP was calculated from the sum of species-specific hourly production and respiration within each sample representing the amount of oxygen produced by each macrophytobenthic species during the hours of sunlight, which is not lost by respiration during the night. The sum of all species-specific daily NPP within a sample was regarded as the total daily macrophytobenthic community NPP. The described steps were repeated for all samples at both locations. For seven days covering each sampling occasion at both lagoons hourly daytime productivity, daytime hourly NPP, daily NPP, and total community daily NPP are reported as sampling occasion averages and were calculated by non-parametric bootstrapping.

Pelagic NPP

The hourly daytime pelagic NPP was measured at both locations in parallel to the quantitative sampling of the macrophytobenthos in 2017. Each of ten bottles was filled with prefiltered ambient water (<55 μm) from the sampling location to remove larger zooplankton. Thus, pelagic NPP consisted of phytoplankton gross primary production and community (bacteria, phytoplankton and microzooplankton) respiration. Four bottles were covered with aluminum foil (dark bottles) and used to determine the respiration. Six bottles (light bottles) were placed pairwise in the water column at the surface, half and total average annual Secchi depth. In Vitter Bodden the light bottles were deployed at 0, 0.8 and 1.6 m water depths, in Grabow at 0, 0.25 and 0.5 m water depths. Oxygen concentrations were measured (HQ40days, LDO, Hach-Lange) before the incubation and in the light bottles after incubation over 4 h (11 am–3 pm). For light bottles, hourly oxygen evolution rates were calculated from concentration differences between before and after incubation divided by the hours of deployment. Pelagic NPP was measured at each location on an average sunny day during the sampling occasion. Significant differences in ambient irradiance between sampling locations were only detected during the spring deployment between lagoons. The dark bottles were kept deployed for 24 h in a closed box within the water before measuring the final oxygen concentration. Percentages of oxygen saturation measured were converted into mg O_2 L^{-1} using solubility values to correct for water salinity and temperature (Benson and Krause, 1984). Water column oxygen evolution rates in light bottles were depth-integrated for a water column of 1 m by extrapolating oxygen evolution rates between deployment depths of light bottles in 1 cm steps. The hourly daytime pelagic NPP (mg C m^{-2} h^{-1}) was calculated from hourly oxygen evolution rates assuming a photosynthetic quotient of 1.2 (Oviatt et al., 1986).

Statistical Analyses

To assess the uncertainty, error propagation was calculated as the partial derivation of each of the formula used to calculate the underwater light climate and NPP (**Supplementary Table S1**, Taylor, 1997). Standard errors of solar radiation, attenuation, temperature and biomass were used as input variability in the error propagation.

Water column parameters were compared using Wilcoxon Rank sum test between the lagoons. The same test was used for the comparison between calculated and measured light attenuation. Pearson correlation test was used to analyze the relationship between photosynthetic parameters. Total biomass and production of the macrophytobenthos were compared by a two-way analysis of variance with the independent variables season (March/April, June/July, August/September and November/December) and location (Vitter Bodden, Grabow) followed by a pairwise *t*-test. To achieve normality and homogeneity of variances, the data were log+1 transformed. Due to their small sample size and lack of normal distribution, the standard error and confidence intervals of the mean values of species-specific biomass and production data were calculated by non-parametric bootstrapping using the R package boot (Davison and Hinkley, 1997; Canty and Ripley, 2017). The non-parametric bootstrapping routine of the confidence intervals of the mean used the biased percentile method (Wang, 2001). We considered the differences

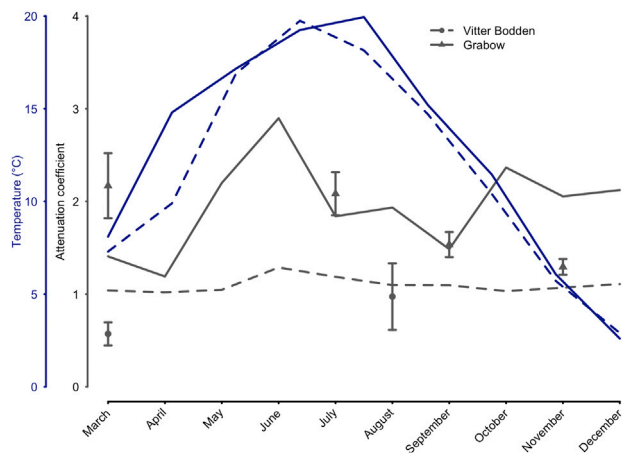

FIGURE 2 | Attenuation coefficient and water temperature in 2017. Temperature (°C), salinity, Chlorophyll *a* (μg L^{-1}) and seston (mg L^{-1}) were monitored biweekly (Vitter Bodden–VB) and monthly (Grabow–GB). Blue dashed (VB), and solid lines (GB) show the temperature development for both sampling locations (March to September). The attenuation coefficient (m^{-1}) was calculated based on Chlorophyll, seston, and salinity (Xu et al., 2005), and additionally measured with Li-Cor sensors simultaneously to macrophyte sampling. Circles (VB) and triangles (GW) show the measured attenuation coefficients during the sampling occasions (mean values + standard deviations).

significant when 95% confidence intervals of the mean were not overlapping. Seasonal patterns in floral biomass of non-filamentous macroalgal species were examined using canonical correspondence analysis (CCA). Water column parameters included in the CCA were PAR_{mc}, the DIN:TP ratio and water column Chl *a* concentration. Trends in biomass related to environmental gradients were analyzed by canonical permutation tests (number of permutations = 999) using the R package vegan. All statistical analyses were conducted with R version 3.5.3 (R Core Team, 2019).

RESULTS

Water Column Parameters

The water temperature in both lagoons was similar and increased from 4 °C in March to maximum values in July/August (**Fig. 2**; **Supplementary Table S2, S3**). The lowest values were recorded in both lagoons in December. The highest water temperature was measured in Vitter Bodden in July reaching 19.8°C, while in Grabow the highest water temperature of 20.0°C was measured in August. The salinity ranged from 8.8 to 9.9 PSU in Vitter Bodden and from 7.8 to 9.5 PSU in Grabow. Seston and Chl *a* concentration were markedly higher in Grabow. Thus, the average monthly calculated light attenuation (K_d) was significantly lower in Vitter Bodden (n = 24, Z = 3.2, p < 0.01) and showed less variability. The measured attenuation (K_{par}) showed the same difference between the lagoons and was in agreement only with the K_d in summer and autumn in both lagoons. Based on measured K_{par}, the water depth penetrated by at least 1% of the surface irradiance (i.e. euphotic zone) was on average 60% lower in Grabow than in Vitter Bodden. TP concentrations were about 50% lower in Vitter Bodden than in Grabow in all seasons. Mean TN concentrations were three times higher in Grabow than in Vitter Bodden, while the average DIN:TP ratio was three times higher in Vitter Bodden than in Grabow.

Seasonal Development of Macrophyte Community Structure and Biomass

Vitter Bodden

The macrophytobenthic total biomass was on average 27 times higher in Vitter Bodden than in Grabow, due to higher biomasses of filamentous algae. Filamentous algae such as *Ectocarpus* sp., *Ceramium* sp. and *Chaetomorpha linum* dominated the vegetation and represented on average 41% of its total biomass throughout the season (**Figure 3**). The ratio between rooted and non-rooted species was lowest in spring (0.5) and highest in winter (1.0). In spring, *Ectocarpus* sp. dominated the filamentous biomass representing 78% of its total biomass, while *Chaetomorpha linum* was the dominant filamentous alga in autumn contributing to 58% to its total biomass. *Ceramium* spp. represented up to 28% of the filamentous algae biomass in winter. *S. pectinata* and *Ruppia* ssp. were the most common tracheophyta and represented together on average 39% of the total floral biomass. Filamentous algae grew mostly as epiphyton on these two tracheophyta.

Maximum biomasses of filamentous algae, *Fucus vesiculosus* and *S. pectinata* were recorded in spring. Biomass composition was highly variable among samples and either dominated by

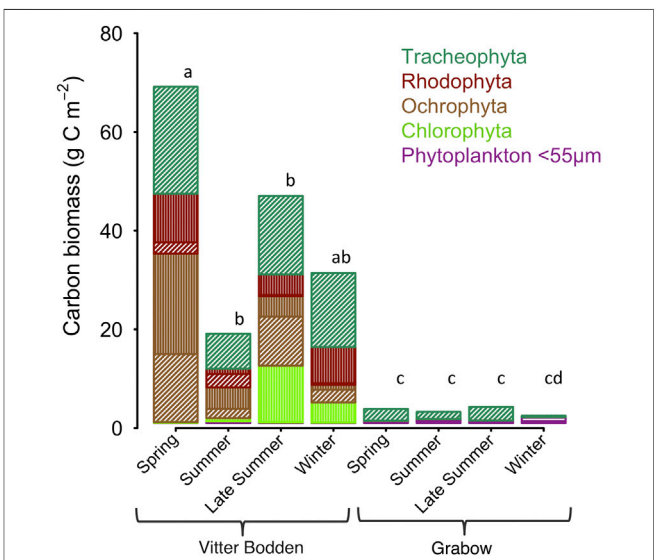

FIGURE 3 | Average biomass in carbon (g C m^{-2}) shown for each macrophytobenthic phylum in Vitter Bodden and Grabow. Filamentous macroalgal biomass is highlighted in vertical lines, non-filamentous macrophyte biomass in dashed lines, and phytoplankton in horizontal lines. Letters indicate significant differences between total biomasses (pairwise comparison, F = 3.16, p < 0.05).

TABLE 3 | Macrophytobenthic biomass in Vitter Bodden and Grabow sampled by drop trap.

	Vitter Bodden				Grabow			
Taxa sampled	April (n = 5) g C m^{-2}	July (n = 10) g C m^{-2}	September (n = 10) g C m^{-2}	December (n = 5) g C m^{-2}	April (n = 5) g C m^{-2}	July (n = 10) g C m^{-2}	September (n = 10) g C m^{-2}	December (n = 5) g C m^{-2}
Ceramium spp.	9.88 ± 2.37 (4.36–13.88)	1.06 ± 0.31 (0.53–1.72)	4.2 ± 1.82 (1.31–8.47)	7.38 ± 1.1 (4.51–8.98)	0	0	0	0
Furcellaria fastigiata	2.27 ± 1.75 (0.17–8.11)	2.7 ± 1.5 (0.33–6.3)	0.24 ± 0.1 (0.1–0.52)	0.3 ± 0.24 (0–0.97)	0	0	0	0
Chorda filum	0	0.05 ± 0.02 (0.01–0.11)	0.34 ± 0.11 (0.16–0.64)	0.12 ± 0.05 (0.02–0.23)	0	0	0	0
Ectocarpus sp.	20.37 ± 4.64 (10.29–27.97)	4.34 ± 1.27 (2.17–7.01)	4.13 ± 1.81 (1.34–8.98)	0.98 ± 0.8 (0.06–3.68)	0	0	0	0
Scytosiphon lomentaria	0.21 ± 0.19 (0–0.42)	0.02 ± 0.02 (0–0.06)	0.11 ± 0.1 (0–0.34)	0.06 ± 0.03 (0–0.12)	0	0	0	0
Fucus vesiculosus	13.54 ± 10.76 (1.15–48.47)	1.82 ± 0.76 (0.66–4.03)	9.51 ± 3.22 (4.15–17.21)	2.41 ± 1.75 (0.31–8.07)	0.06 ± 0.05 (0–0.18)	0.0008 ± 0.0008 (0–0.0024)	0	0
Ulva sp	0.18 ± 0.08 (0.04–0.37)	0	0.05 ± 0.03 (0.01–0.16)	0.01 ± 0.01 (0–0.02)	0.01 ± 0.01 (0–0.02)	0	0	0
Chaetomorpa halinum	0	0.7 ± 0.19 (0.35–1.15)	11.44 ± 4.93 (4.44–25.51)	4.08 ± 3.1 (0.25–15.07)	0	0	0	0
Chara baltica	0	0.0001 ± 0 (0–0.0004)	0	0	0	0	0	0
Myriophyllum spicatum	0.8 ± 0.63 (0.01–2.34)	0.04 ± 0.04 (0–0.15)	0.07 ± 0.06 (0–0.26)	0.01 ± 0.01 (0–0.02)	0.05 ± 0.05 (0–0.1)	0	0	0
Stuckenia pectinata	20.09 ± 7.97 (5.97–37.67)	3.71 ± 0.94 (1.92–5.77)	10.6 ± 2.45 (5.81–14.89)	12.16 ± 2.94 (6.93–19.45)	2.24 ± 0.56 (1.42–3.71)	1.45 ± 0.51 (0.79–3.31)	2.77 ± 0.71 (1.58–4.41)	0.27 ± 0.11 (0.09–0.53)
Zannichellia sp	0	0.01 ± 0 (0–0.02)	0	0	0	0	0	0
Ruppia ssp	0	3.31 ± 1.34 (1.19–7.06)	4.13 ± 1.64 (1.66–8.64)	2.59 ± 1.94 (0.31–7.13)	0	0	0	0
Zostera marina	0.78 ± 0.42 (0.03–1.55)	0.04 ± 0.02 (0.01–0.1)	0.05 ± 0.02 (0.02–0.12)	0.21 ± 0.15 (0–0.6)	0.08 ± 0.06 (0.01–0.24)	0	0	0
Sum	68.12 ± 19.74 (33.79–111.94)	17.8 ± 3.67 (9.52–24.62)	44.87 ± 13.6 (24.44–78.55)	30.31 ± 5.1 (23.0–44.13)	2.44 ± 0.60 (1.49–4.18)	1.45 ± 0.50 (0.77–3.15)	2.77 ± 0.72 (1.57–4.65)	0.27 ± 0.11 (0.1–0.48)

Macrophytobenthic biomass is given in g C per square meter ± bootstrapped standard error and 95% confidence intervals of the mean.

TABLE 4 | Macrophytobenthic hourly daytime productivity (HDP) in Vitter Bodden and Grabow.

	Vitter Bodden				Grabow			
Taxa sampled	April mg C gDM^{-1} m^{-2} h^{-1}	July mg C gDM^{-1} m^{-2} h^{-1}	September mg C gDM^{-1} m^{-2} h^{-1}	November mg C gDM^{-1} m^{-2} h^{-1}	April mg C gDM^{-1} m^{-2} h^{-1}	July mg C gDM^{-1} m^{-2} h^{-12}	September mg C gDM^{-1} m^{-2} h^{-1}	December mg C gDM^{-1} m^{-2} h^{-1}
Ceramium spp.	4.11 ± 0.56 (3.2–4.82)	3.94 ± 0.48 (2.4–4.76)	4.26 ± 0.34 (3.87–4.52)	1.35 ± 0.67 (0–0)	0	0	0	0
Furcellaria fastigata	1.03 ± 0.14 (0.79–1.22)	0.89 ± 0.12 (0.56–1.08)	1 ± 0.08 (0.84–1.06)	0.11 ± 0.17 (0–0.27)	0	0	0	0
Chorda filum	0	0.59 ± 0.07 (0.43–0.7)	0.54 ± 0.08 (0.43–0.61)	0	0	0	0	0
Sytosiphon lomentaria	3.11 ± 0.47 (2.41–3.78)	3.06 ± 0.46 (1.85–3.82)	3.52 ± 0.33 (3.05–3.95)	1.21 ± 0.41 (0–0)	0	0	0	0
Ectocarpus spp.	3.15 ± 0.46 (2.37–3.81)	3.1 ± 0.47 (1.9–3.86)	3.58 ± 0.33 (3.06–3.96)	1.23 ± 0.41 (0–0)	0	0	0	0
Fucus vesiculosus	1.85 ± 0.35 (1.19–2.38)	2.08 ± 0.3 (1.26–2.65)	2.22 ± 0.28 (1.82–2.53)	0.51 ± 0.1 (0–0)	1.74 ± 0.34 (1.13–2.29)	2.54 ± 0.29 (2.13–2.84)	0	0
Ulva sp	7.27 ± 0.82 (6.03–8.48)	0	10.36 ± 0.83 (9.33–11.21)	0.95 ± 1.83 (0.03–2.81)	7.06 ± 0.83 (5.85–8.31)	0	0	0
Chaetomorpha linum	0	4.95 ± 0.59 (3.29–5.94)	5.67 ± 0.48 (5.1–6.13)	0.52 ± 0.4 (0.28–1.17)	0	0	0	0
Chara baltica	0	0.9 ± 0.14 (0.54–1.16)	0	0	0	0	0	0
Myriophyllum spicatum	1.39 ± 0.22 (0.99–1.67)	1.67 ± 0.26 (1–2.06)	2.12 ± 0.22 (1.75–2.49)	0.51 ± 0.21 (0–0)	1.33 ± 0.22 (0.9–1.62)	0	0	0
Stuckenia pectinata	1.26 ± 0.17 (0.93–1.5)	1.51 ± 0.21 (0.99–1.85)	1.93 ± 0.19 (1.61–2.21)*	0.59 ± 0.2 (0–0)	1.19 ± 0.18 (0.85–1.43)	2.03 ± 0.18 (1.57–2.22)	0.96 ± 0.2 (0.73–1.51)	0.26 ± 0.07 (0.16–0.4)
Zannichellia sp	0	0.28 ± 0.04 (0.23–0.34)	0	0	0	0	0	0
Ruppia spp.	0	0.93 ± 0.13 (0.65–1.12)	0.96 ± 0.16 (0.73–1.15)	0.07 ± 0.04 (0–0)	0	0	0	0
Zostera marina	1.36 ± 0.15 (1.12–1.54)	1.28 ± 0.15 (0.85–1.52)	1.52 ± 0.09 (1.44–1.61)	0.6 ± 0.27 (0–0)	1.33 ± 0.16 (1.06–1.52)	0	0	0

*Macrophytobenthic productivity is given in mgC DM^{-1} h^{-1} per square meter ± bootstrapped standard error and 95% confidence intervals of the mean. HDP was calculated from the available irradiance under the macrophytobenthic canopy (PAR_{mc}) and species-specific photosynthetic parameters taken from the literature (**Table 2**). In winter, for some species bootstrap confidence intervals could not be calculated due to reduced sample size. An asterisk indicates a significant difference between the lagoons within one season.*

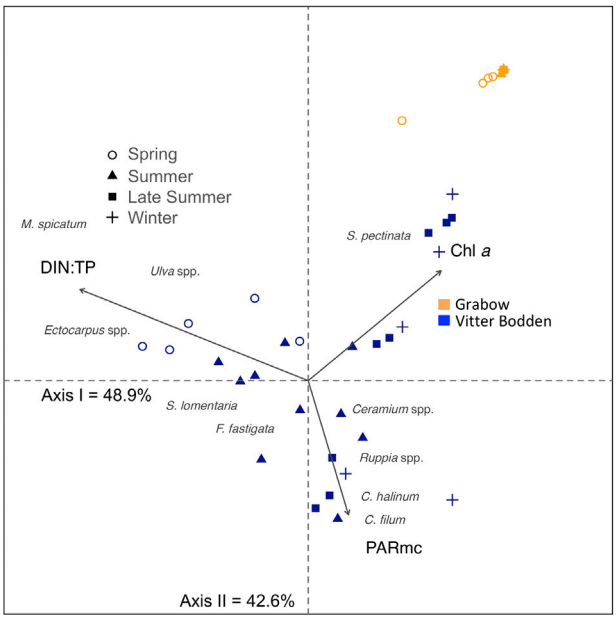

FIGURE 4 | Canonical correspondence analysis plot for the macrophytobenthic biomass sampled in spring (March/April, circle), summer (June/July, triangle), late summer (August/September, square), and winter (November/December, cross) in Vitter Bodden (blue) and Grabow (orange). Shown macrophytobenthic species are *Ceramium* spp, *Chaetomorpha linum*, *Chorda filum*, *Ectocarpus* spp, *Furcellaria fastigata*, *Myriophyllum spicatum*, *Ruppia* spp, *Stuckenia pectinata*, *Sytosiphon lomentaria*, *Ulva* spp.. Environmental factors (arrows) are calculated underwater irradiances within the macrophyte canopy (PARmc), dissolved inorganic nitrogen to total phosphorus ratio (DIN:TP), and Chlorophyll *a* concentration (Chl *a*). Positions of macrophytes show their probable occurrence based on the explanatory variables (PARmc, DIN:TP, Chl *a*). Only environmental factors significantly correlated to the ordination ($p < 0.01$) are shown.

filamentous algae plus tracheophyta or *F. vesiculosus* plus *Furcellaria fastigiata*. The macrophytobenthic biomass was lower at the beginning of summer, most pronounced in filamentous algae, which were reduced to 20% of their spring biomass, while tracheophyta were reduced to 33% of their spring biomass (**Table 3**). Species numbers increased from 10 to 14 from spring to summer. At the end of the summer, macrophyte biomasses recovered, and tracheophyta reached 70% of their spring biomass. The biomass of tracheophyta in November was about the same as in August, while filamentous algae and some phaeophytes had lost biomass.

Grabow

The total macrophytobenthic biomass was significantly lower in Grabow than in Vitter Bodden at each sampling occasion (df = 3, F = 3.16, $p < 0.05$). The most significant difference of total macrophytobenthic biomass between the lagoons was observed in spring ($p < 0.001$). Apart from some drifting *Zostera marina* specimens, only four macrophytobenthic species were found (**Table 3**). *S. pectinata* dominated in all seasons representing on average more than 98% of the total biomass (**Table 3**). As observed in Vitter Bodden, the average total macrophytobenthic biomass in Grabow was reduced to 1.5 g C m^{-2} at the beginning of summer, and tracheophyta lost 39% of the biomass present in spring. The species number decreased to two from spring to summer. In September, macrophyte biomass recovered and tracheophyta reached their maximum biomass (2.8 g C m^{-2}). In winter, the macrophytobenthos was lowest (0.3 g Cm^{-2}).

Drivers of the Seasonal Development

The seasonal changes in macrophytobenthic community structure in relation to water column parameters were visualized by multivariate correspondence analysis (**Figure 4**). Along the first axis, only samples from Vitter Bodden were separated. Sample separation reflected the differences in biomass contribution to the total macrophytobenthos community between species with an early and late growth period. In spring, the relative biomass contributions of *Myriophyllum spicatum*, *Enteromorpha* sp., and *Ectocarpus* sp. were the highest. *Ruppia* spp, *C. linum* and *Chorda filum* were observed in the samples from June onwards, corresponding with highest available irradiance within the macrophytobenthic canopy. This seasonal change in species composition was correlated to DIN:TP ratio, which decreased over the season in Vitter Bodden. The second axis refers to the dominance of *S. pectinata* in the biomass composition of samples. At the positive end of the second axis all samples from Grabow are grouped and clearly separated from all Vitter Bodden samples. The positive end of the second axis was characterized by the lowest available irradiance within the macrophytobenthic canopy but the highest Chl *a* concentration.

Photosynthetic Parameters of Dominating Macrophyte Species

Overall there was a strong negative correlation between maximum oxygen evolution and respiration rates ($p < 0.01$, $R^2 = 0.87$). The highest variability of photosynthetic parameters was found within the attached macroalgae (**Table 2**), with the highest maximum oxygen evolution and respiration rates in *Ulva* sp. and the lowest in *Fucus vesiculosus*. The highest maximum oxygen evolution and respiration rates of filamentous algae were found in *Chaetomorpha linum*, while the lowest values of these two parameters were found for *Ectocarpus* sp. Tracheophyta showed the lowest variability in maximum oxygen evolution rates with the lowest values in *Zannichellia* sp. and the highest in *M. spicatum*. The initial slope of the photosynthesis-irradiance curve was the highest in *Ulva* sp. and the lowest in *Zannichellia* sp. The Q_{10} coefficient for the maximum oxygen evolution rate was the lowest in *Furcellaria fastigata* and the highest in *Chara baltica*. On average, tracheophyta had a considerably higher Q10 than all other macrophytobenthos.

Seasonal Development of Macrophytobenthic Production

The mean macrophytobenthic hourly daytime NPP was 3.5 mg C m^{-2} h^{-1} in Grabow compared to 383.3 mg C m^{-2} h^{-1} in Vitter

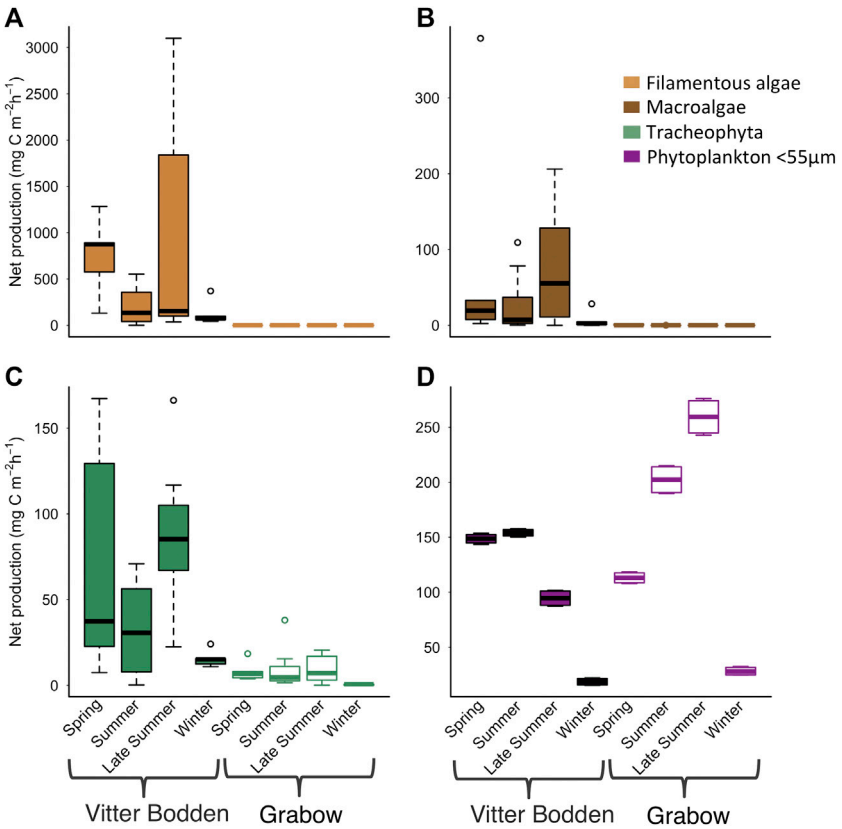

FIGURE 5 | Average hourly daytime primary production for **(A)** filamentous algae **(B)** macroalgae **(C)** tracheophyte **(D)** phytoplankton in Vitter Bodden (filled) and Grabow (open) at sampling occasions. Phytoplankton production was experimentally determined by oxygen evolution in light and dark bottles. The benthic production from filamentous algae, tracheophyte and macrophytes was calculated using species specific photosynthesis parameters from the literature combined with own biomass data. Note the different scales.

Bodden (**Figure 5**). In Vitter Bodden, the average hourly daytime NPP of filamentous algae was highest in March and lowest in June with highest variability in August (**Figure 5**). The average daytime hourly NPP of tracheophyta and macroalgae increased between March and August in Vitter Bodden. For each individual species, average hourly daytime productivity was similar in Grabow and Vitter Bodden except for *S. pectinata* that had significantly lower values in September in Grabow (**Table 4**).

In Vitter Bodden, all macrophytobenthos groups had a positive daily NPP from spring to autumn. The mean value of daily macrophytobenthos NPP was about two orders of magnitudes lower in Grabow (39.2 mg C m^{-2} d^{-1}; range based on error propagation: 25.7 and 52.8 mg C m^{-2} d^{-1}) than in Vitter Bodden (4.1 g C m^{-2} d^{-1}; range based on error propagation: 2.9–5.2 g C m^{-2} d^{-1}; **Figure 6**; **Supplementary Table S3**). In Vitter Bodden, filamentous algae were the main primary producers contributing to 83% of the total community daily NPP (mean of all sample occasions), followed by tracheophyta (11%) and macroalgae (6%). In Grabow, *S. pectinata* was the dominant primary producer representing about 98% of the mean annual daily community NPP. In Grabow, only tracheophyta and macroalgae had a positive daily NPP from april until September.

Seasonal Comparison of Pelagic Producer Biomass and NPP

The mean biomass of pelagic producers was about one order of magnitude lower in Vitter Bodden (0.1 g C m^{-2}) than in Grabow (0.9 g C m^{-2}) (**Figure. 3**). In Vitter Bodden, the mean pelagic hourly NPP was 104.0 mg C m^{-2} h^{-1} with the highest values in March and June and the lowest values in November (**Figure 5**). Here, the hourly NPP was significantly higher in spring than in late summer. In Vitter Bodden, the hourly macrophytobenthic NPP was higher than the pelagic NPP in spring, equal in summer and five times higher in autumn. The mean total hourly NPP per square meter of both macrophytobenthos and pelagic producers was three times higher in Vitter Bodden than in Grabow.

In Grabow, pelagic producers represented 50% of macrophytobenthic biomass in summer and had four-times higher biomasses than the macrophytobenthos in winter. Mean pelagic hourly production of phytoplankton was 150.8 mg C m^{-2} h^{-1} with the highest values in September and

the lowest in December. Phytoplankton contributed 98% of total primary production per square meter in comparison to 2% of the macrophytobenthos with highest contributions in summer and lowest in autumn.

DISCUSSION

Seasonal Development of the Macrophytobenthic Community in Vitter Bodden

Macrophytobenthic species composition in Vitter Bodden was similar to earlier observations (Blindow et al., 2016; Meyer et al., 2019). The main growing period of the macrophyte community occurred between March and September with maximum biomass reached in summer.

Species-specific differences in onset and duration of the growing period could be influenced by the specific needs of individual species for light and nutrients. In spring, high values of TN:TP and DIN:TP suggested P limitation with high availability of N, while low values of these ratios suggested N limitation in summer, which is supported by previous studies in Baltic coastal areas (Kronvang et al., 2005; Schumann et al., 2009; Berthold et al., 2018a). The filamentous alga *Ectocarpus* sp. which usually starts growing at the beginning of the season (Wennberg, 1992), contributed most to macrophytobenthic biomass and may have benefitted from highly available N in spring. The higher surface to volume ratio of filamentous algae allows higher P and N uptake rates from the water column compared to thick leathery tracheophytes (Raven and Taylor, 2003), which may contribute to the high spring production and biomass accumulation of this filamentous alga in spring. At similar TN and TP concentrations, proliferating filamentous algae were found also in other coastal areas of the Baltic Sea during spring (Dahlgren and Kautsky, 2004). The strong decrease of about 75% of the biomasses of macrophytes and epiphyton in early summer is probably linked to this high spring production of filamentous algae, which is assumed to have resulted in a severe decrease in light availability within the macrophytes canopy. As rooted macrophytes can use sediment nutrients (Granéli and Solander, 1988), any nutrient competition with epiphyton is assumed to be of minor importance. High grazing pressure by macrozoobenthos species may have added up to this reduction of biomass. In fact, high biomasses of macrozoobenthic grazers were observed within the vegetation (personal observation) similarly as in other vegetated Baltic lagoons (Hansen et al., 2011; Wlodarska-Kowalczuk et al., 2014). Our results suggest synergetic effects of epiphyton shading and herbivore grazing triggering macrophytobenthic biomass loss as assumed by (Hidding et al., 2016). A second bloom of the green filamentous alga *C. linum* was observed in late summer, probably related to the higher availability of P in the water column in this season. Proliferation of *C. linum* was observed under similar P concentrations (Menendez et al., 2002). The reduction in macrophytes total biomass at the end of the season was most probably caused by autumnal senescence and increasing hydrodynamic disturbances.

Apart from the temporary biomass decrease in early summer, the macrophytobenthic biomass was high throughout the vegetation period in the Vitter Bodden. High species numbers including different life strategies and species-specific growth periods may explain the high level of calculated macrophytobenthic NPP throughout the vegetation season. Spatial (e.g., distribution, growth forms) as well as temporal (e.g., seasonal strategies, length of growing season) variation in the macrophytobenthic community probably had a positive and stabilizing effect on its NPP. Small, low light adapted species such as *F. fastigiata* and *F. vesiculosus* grow in patches between and below higher vegetation, mainly consisting of *S. pectinata*, which creates a dense macrophytobenthic cover during the summer months (personal observations). High NPP was observed in other multi-species macrophytobenthic communities explained by the averaging species-specific photosynthetic performance and exposing constantly new tissue to irradiance in dense canopies (Middelboe and Binzer, 2004). Despite uncertainty in our estimations of available irradiance within the macrophytes canopy and macrophytobenthic NPP, calculated macrophytobenthic NPP in Vitter Bodden was within the range of temperate seagrass beds (Duarte, 1989) and macrophyte assemblages in freshwater lakes (Vadeboncoeur et al., 2001). The seasonal development of the macrophytobenthos in this mesotrophic lagoon indicates that reduced light availability within the macrophytobenthos is the most limiting factor with co-occurring nutrient limitation of epiphyton in spring and late summer. The underwater light climate has been shown to be the most relevant limiting factor for primary production of the macrophytobenthos in coastal waters of the southern Baltic Sea (Pärnoja et al., 2014; Piepho 2017).

Low Light Availability in Grabow Efficiently Suppresses Seasonal Development in the Macrophytobenthos

During 2017, high concentrations of seston and pigments caused a constantly low light availability in Grabow with a decreased euphotic zone of 60% in comparison to Vitter Bodden. The phytoplankton in the whole lagoon system of the DZBC is dominated by small-celled cyanobacteria of the *Cyanobium* clade (Albrecht et al., 2017), which are able to take up available nutrients very efficiently in this system (Berthold and Schumann, 2020), due to their high surface to volume ratio (Friebele and Fasut, 1978; Grillo and Gibson, 1979) resulting in high biomasses and low underwater light availability. Only *S. pectinata* persisted throughout the year. High abundances in clear water have been observed at somewhat elevated nutrient conditions and are explained by a competitive advantage of this fast-growing species under such conditions (Hilt et al., 2013; Blindow et al., 2016).

Biomass and primary production in the Grabow in 2017 were similar to what was described in the mid-1980s after the shift from clearwater to turbid water (Schiewer, 2001). In the early 1980ies, eutrophication caused a collapse of the macrophytobenthos in the entire DZBC which became dominated by the pelagic producers (Schiewer, 1998). Lagoons of the Baltic Sea receive nutrients from

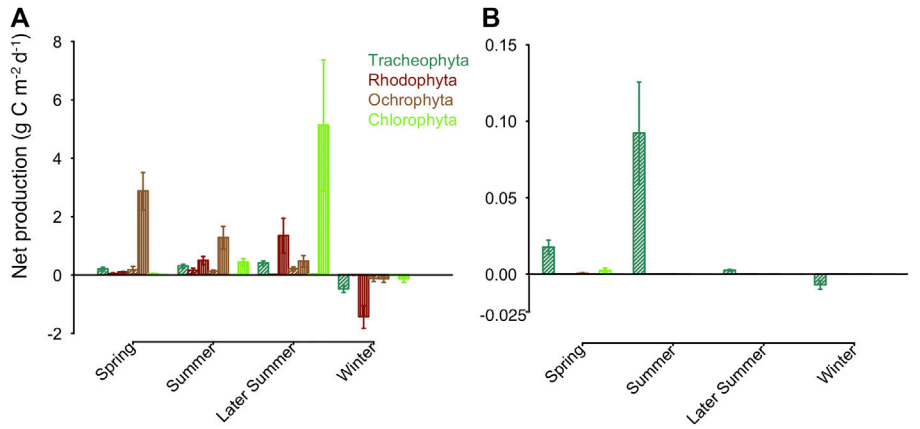

FIGURE 6 | Average daily net primary production for each macrophytobenthic phylum in **(A)** in g $Cm^{-2}d^{-1}$ for Vitter Bodden and **(B)** in g $Cm^{-2}d^{-1}$ for Grabow. Filamentous growth is shown in vertical lines, all other growth forms in dashed lines. Bars are representing standard error of the mean.

diffuse run-offs (Berthold et al., 2018b), atmospheric wet and dry deposition (Berthold et al., 2019) and from sediment (Bitschofsky, 2016; Berthold et al., 2018c). In 1990, new wastewater treatment plants reduced the discharge of P and N in the lagoons of the German Baltic Sea by over 89% (Nausch et al., 2011). Despite an 80% decline in nitrogen and phosphate discharge from the direct river sources, water column nutrient concentrations in the single lagoons of the DZBC have not decreased in the same magnitude (Berthold et al., 2018a), and the macrophytobenthos did not recover in the last 3 decades (Schiewer, 2001; Blindow and Meyer, 2015), which may be explained by long water retention times within this lagoon system and low exchange with the Baltic Sea.

Importance of Macrophytobenthos for the Lagoons' Ecosystem Functioning

The moderate eutrophication of the Westrügensche lagoon still allows for a dense and species-rich macrophytobenthos, but with seasonal dominance of fast growing epiphyton which causes lower NPP and growth in the overgrown rooted tracheophyta and, combined with probably high grazing pressure, causes temporarily biomass decreases. Such seasonally fluctuating biomass indicates a reduction of vegetation stability, and are interpreted as an early warning signal of eutrophication, similarly to former observations in the Vitter Bodden that "bottom-dwellers" such as charophytes were replaced by taller macrophytes such as *S. pectinata* (Blindow et al., 2016). In the long-term, these changes may cause a decline of macrophytobenthic species richness and shortening of the vegetation period, described as a "crashing state" of freshwater ecosystems (Sayer et al., 2010). Proliferating filamentous algae have caused a decline of rooted vegetation in response to nutrient enrichment in other lagoons of the Baltic Sea over the last decades (Dahlgren and Kautsky, 2004).

Decreases in macrophytobenthic biomass weaken the habitat-stabilizing effects of the complex vegetation structure by reduction of water movements, sediment stabilization, immobilization of nutrients and accumulation of floral biomass (Gregg and Rose, 1982; Pedersen and Borum, 1997; Middelboe and Binzer, 2004) and has far reaching consequences for a lagoon's food web. In the Vitter Bodden, the effect of the vegetation on water column parameters such as nutrients, phytoplankton densities and suspended material was found to be negligible, probably due to high water exchange rates with the open Baltic Sea and a low vegetation height. However, a distinct refuge effect of this vegetation was found for zooplankton and assumed to contribute to the temporarily high grazing pressure on phytoplankton (Meyer et al., 2019). In the more eutrophic Grabow, macrophytobenthos had low contributes to total system primary production and a reduced accumulation of biomass, which indicates severe light limitation.

Phytoplankton biomasses were roughly one order of magnitude higher in the Grabow than in the Vitter Bodden, but measured daytime hourly NPP rates were rather similar in both lagoons. These findings suggest that also phytoplankton was severely light-limited in the Grabow. The dominating alpha picocyanobacteria are of low food value for zooplankton, as their mucous envelopes may obstruct the filtering organs or lead to a rejection of the colonies (Schumann et al., 2009), and low phytoplankton mortality may therefore explain the maintenance of high densities in spite of low NPP rates. Earlier investigations from the same lagoon system showed that high water turbidity, caused by high phytoplankton biomass, can cause negative depth-integrated net primary production in winter and spring (Schumann et al., 2005). In addition, high microbial respiration rates may occur in summer months (Schiewer 1998). High self-shading and high community respiration rates can explain why nutrient enrichment does not further increase pelagic NPP in aquatic ecosystems, once a certain threshold is exceeded (Oviatt et al., 1986; Schiewer 1998; Blindow et al., 2006). Despite uncertainty in our estimates, we can show that total community areal NPP was far lower in the eutrophic lagoon than in the mesotrophic lagoon. We suggest that like shallow freshwater ecosystems (Lopez-Archilla et al., 1992; Blindow et al., 2006), also coastal lagoons can show a "paradox of enrichment" phenomenon already on the primary

production level. According to our knowledge, this is the first empirical evidence of this phenomenon for coastal lagoons. As primary producers form the basis of the food web, we predict that the same pattern may be reflected by higher trophic levels.

Macrophytobenthos Response to Eutrophication and Management Recommendation

Macrophytobenthos, which is the most important contributor to total ecosystem primary production in the Vitter Bodden, has severely declined in the DZBC. Restoration efforts have to focus on stabilizing or–when lost–trying to restore this community. Thereby, it has to be considered that the steps leading to macrophytobenthic re-colonization may deviate from a simple reversion of the causes, which were responsible for the former loss (Duarte et al., 2008), and that, once lost, considerable efforts are necessary to restore this community (Scheffer et al., 1993). In the two studied coastal lagoons, the macrophytobenthos showed a complex response to different eutrophication pressures. Moderate eutrophication in the marine lagoon still allowed for a typical seasonal succession of the macrophytobenthic community, but the heavy overgrowth of rooted macrophytobenthos by filamentous algae in spring and autumn indicates that the nutrient levels were critical. During 2017, the macrophytobenthos main growth period and species succession was squeezed between the turbid spring and late summer condition, where proliferation of filamentous algae reduced the light available under the macrophytobenthic canopy. Additionally, a species shift from small bottom-dwellers, especially charophytes, to tall canopy-formers has occurred since the 1930s (Blindow et al., 2016). As a restoration measurement, exogenous nutrient flows into the lagoon should be reduced to prevent further decline in species diversity and thereby its habitat and food web stabilising effect. To control the success of this restoration effort, new macrophytobenthic health indicators sensitive to nutrient loads need to be developed, as already proposed for Danish coastal waters (Carstensen et al., 2014). For example, sensitive species with a later growing period such as *F. vesiculosus* and *F. fastigiata* need to be included into the macrophytobenthic health assessment and their biomass and cover regularly monitored in coastal lagoons (Carstensen et al., 2014).

High eutrophication pressure in the estuarine lagoon reduced macrophytobenthic species number, lowered biomass and production and shortened its growing period (Piepho, 2017). Only the pondweed *S. pectinata* was present during the complete observation period of 2017 and could start its growing period before the high phytoplankton biomasses limiting underwater light availability during the rest of the year. Exogenous nutrient load reductions for the DZBC over the last 40 years have not led to the recovery of the macrophytobenthic species diversity and biomasses in Grabow. Strong feedback mechanisms are assumed to stabilise the phytoplankton dominance (Schiewer, 1998). Additional internal restoration measurements have to be considered to reduce the endogenous nutrient burden and phytoplankton biomass and improve the under water light availability, but are hard to apply because of the large catchment area of this lagoon system and its connection to surrounding lagoons. Planting of submerged macrophytes in spring, when light conditions are most favourable for plant growth should be considered, to recreate lost vegetated areas (van Keulen et al., 2003).

DATA AVAILABILITY STATEMENT

The datasets generated for this study are available on request to the corresponding author.

AUTHOR CONTRIBUTIONS

All authors were involved in the conception and design of the study as well as the provision of study material. MP, MB, and RS analyzed and interpreted the nutrient data. MP and IB analyzed the macrophytobenthos data set. SD monitored water column parameter in Vitter Bodden. MP wrote the manuscript with extensive inputs from MB, RS, SD and IB. All authors read and approved the manuscript.

FUNDING

This research was funded by the Federal Ministry of Education and Research, Germany, project BACOSA (03F0737C). We acknowledge support for the Article Processing Charge from the DFG (German Research Foundation, 393148499) and the Open Access Publication Fund of the University of Greifswald.

ACKNOWLEDGMENTS

This work was done with the permission of the State Office for Agriculture, Food Safety and Fisheries Mecklenburg-Vorpommern and the National Park Authority Vorpommern. The authors thank the German Meteorological Service for providing the irradiance and wind data sets. This study would not have been possible without the logistic and analytic support by the employees of the Biologische Station Zingst, namely R. Wulff and V. Reiff, and the Biologische Station of Hiddensee, namely I. Kreuzer, G. Zenke and T. Kreuzer. We like to thank the field assistance by B. Anderson, M. Steinmüller, R. Liebetrau, F. Blaffert, L. Sniehotte, J. Reiche, T. Wagner, A. Brauer, K. Steinfurth, B. Heeren, I. Petersen, and D. Auch. Thanks to H. Radtke for his help with calculating the error propagation. The manuscript improved considerably due to the valid comments of both reviewers.

SUPPLEMENTARY MATERIAL

The Supplementary Material for this article can be found online at: https://www.frontiersin.org/articles/10.3389/feart.2020.542391/full#supplementary-material.

REFERENCES

Albrecht, M., Pröschold, T., and Schumann, R. (2017). Identification of cyanobacteria in a eutrophic coastal lagoon on the southern Baltic coast. *Front. Microbiol.* 8, 923. doi:10.3389/fmicb.2017.00923

Angradi, T. R. (1993). Chlorophyll a content of seston in a regulated Rocky Mountain river, Idaho, USA. *Hydrobiologia*. 259, 39–46. doi:10.1007/BF00005963

Apostolaki, E. T., Holmer, M., Marbà, N., and Karakassis, I. (2011). Epiphyte dynamics and carbon metabolism in a nutrient enriched Mediterranean seagrass (*Posidonia oceanica*) ecosystem. *J. Sea Res.* 66, 135–142. doi:10.1016/j.seares.2011.05.007

Armstrong, F. A., Stearns, C. R., and Strickland, J. D. (1967). Measurement of upwelling and subsequent biological processes by means of Technicon autoanalyzer and associated equipment. *Deep-Sea Res.* 14, 381–389. doi:10.1016/0011-7471(67)90082-4

Benson, B. B., and Krause, J. C. (1984). The concentration and isotopic fractionation of oxygen dissolved in freshwater and seawater in equilibrium with the atmosphere. *Limnol. Oceanogr.* 29, 620–632. doi:10.4319/lo.1984.29.3.0620

Berthold, M., Karsten, U., von Weber, M., Bachor, A., and Schumann, R. (2018a). Phytoplankton can bypass nutrient reductions in eutrophic coastal water bodies. *Ambio*. 47, 146–158. doi:10.1007/s13280-017-0980-0

Berthold, M., Karstens, S., Buczko, U., and Schumann, R. (2018b). Potential export of soluble reactive phosphorus from a coastal wetland in a cold-temperate lagoon system: buffer capacities of macrophytes and impact on phytoplankton. *Sci. Total Environ.* 616-617, 46–54. doi:10.1016/j.scitotenv.2017.10.244

Berthold, M., and Schumann, R. (2020). Phosphorus dynamics in a eutrophic lagoon: uptake and Utilization of nutrient pulses by phytoplankton. *Front Mar Sci.* 7, 281. doi:10.3389/fmars.2020.00281

Berthold, M., Wulff, R., Reiff, V., Karsten, U., Nausch, G., and Schumann, R. (2019). Magnitude and influence of atmospheric phosphorus deposition on the southern Baltic Sea coast over 23 years: implications for coastal waters. *Environ. Sci. Eur.* 31, 27. doi:10.1186/s12302-019-0208-y

Berthold, M., Zimmer, D., Reiff, V., and Schumann, R. (2018c). Phosphorus contents re-visited after 40 years in muddy and sandy sediments of a temperate lagoon system. *Front Mar Sci.* 5, 305. doi:10.3389/fmars.2018.00305

Berthold, M., Zimmer, D., and Schumann, R. (2015). A simplified method for total phosphorus digestion with potassium persulphate at sub-boiling temperatures in different environmental samples. *Rostocker Meeresbiol Beitr.* 25, 7–25.

Bitschofsky, F. (2016). "Phosphorus dynamics in sediments of Darß-Zingst Bodden chain, a eutrophic estuary in the southern Baltic Sea." Available at: http://rosdok.uni-rostock.de/file/rosdok_disshab_0000001782/rosdok_derivate_0000037768/Dissertation_Bitschofsky_2017.pdf.

Blindow, I., Dahlke, S., Dewart, A., Flügge, S., Hendreschke, M., Kerkow, A., et al. (2016). Long-term and interannual changes of submerged macrophytes and their associated diaspore reservoir in a shallow southern Baltic Sea bay: influence of eutrophication and climate. *Hydrobiologia*. 778 (1), 121–136. doi:10.1007/s10750-016-2655-4

Blindow, I., Hargeby, A., Meyercordt, J., and Schubert, H. (2006). Primary production in two shallow lakes with contrasting plant form dominance: a paradox of enrichment?. *Limnol. Oceanogr.* 51, 2711–2721. doi:10.4319/LO.2006.51.6.2711

Blindow, I., and Meyer, J. (2015). Submerse Makrophyten während Eutrophierung und Remesotrophierung – ein Vergleich von inneren und äußeren Boddengewässern. *Rostocker Meeresbiol Beitr.* 25, 105–118.

Blümel, C. (2004). "Chara baltica," in *Charophytes of the Baltic Sea*. Editors H. Schubert and I. Blindow (Ruggell, Liechtenstein: Gantner), 53–56.

Bühler, A. (2016). *Distribution of* Zostera marina *in the coastal waters of the Baltic Sea - a case study at the German island HiddenseeMaster thesis*. Germany: University of Rostock.

Canty, A. S., and Ripley, B. (2016). Boot: bootstrap R (S-plus) functions. *R package version1*., 3–18.

Carstensen, J., Krause-Jensen, D., and Josefson, A. (2014). *Development and testing of tools for intercalibration of phytoplankton, macrovegetation and benthic fauna in Danish coastal areas*. Aarhus: Aarhus University, DCE – Danish Centre for Environment and Energy, 85. Available at:http://dce2.au.dk/pub/SR93.pdf.

Cerco, C. F., and Moore, K. (2001). System-wide submerged aquatic vegetation model for Chesapeake Bay. *Estuar. Coast.* 24, 622–634. doi:10.2307/1353254

Cloern, J. E. (2001). Our evolving conceptual model of the coastal eutrophication problem. *Mar. Ecol. Prog. Ser.* 210, 223–253. doi:10.3354/meps210223

Correns, M. (1979). *Der Wasserhaushalt der Bodden- und Haffgewässer der DDR als Grundlage für die weitere Erforschung ihrer Nutzungsfähigkeit zu Trink- und Brauchwasserzwecken*. Berlin, Germany: Dissertation, Humboldt-Universität.

Dahlgren, S., and Kautsky, L. (2004). Can different vegetative states in shallow coastal bays of the Baltic Sea be linked to internal nutrient levels and external nutrient load?. *Hydrobiologia*. 514, 249–258.

Davison, A. C., and Hinkley, D. V. (1997). *Bootstrap methods and their applications*. Cambridge, UK: Cambridge University Press.

Duarte, C. M., Conley, D. J., Carstensen, J., and Sánchez-Camacho, M. (2008). Return to neverland: shifting baselines affect eutrophication restoration targets. *Estuar. Coast.* 32, 29–36. doi:10.1007/s12237-008-9111-2

Duarte, C. M. (1989). Temporal biomass variability and production/biomass relationships of seagrass communities. *Mar. Ecol. Prog. Ser.* 51, 269–276. doi:10.3354/meps051269

Duffy, J. E., Macdonald, K. S., Rhode, J. M., and Parker, J. D. (2001). Grazer diversity, functional, redundancy, and productivity in seagrass beds: an experimental test. *Ecology*. 82, 2417–2434. doi:10.1890/0012-9658(2001)082[2417:GDFRAP]2.0.CO;2

Evans, A. S., Kenneth, L. W., and Penhale, P. A. (1986). Photosynthetic temperature acclimation in two coexisting seagrasses, *Zostera marina* L. and *Ruppia maritima* L. *Aquat. Bot.* 24, 185–197. doi:10.1016/0304-3770(86)90095-1

Friebele, E. S., and Fasut, M. A. (1978). Relationship between phytoplankton cell size and the rate of orthophosphate uptake: *in situ* observations of an estuarine population. *Mar. Biol.* 45, 39–52. doi:10.1007/BF00388976

Granéli, W., and Solander, D. (1988). Influence of aquatic macrophytes on phosphorus cycling in lakes. *Hydrobiologia*. 170, 245–266. doi:10.1007/BF00024908

Gregg, W. W., and Rose, F. L. (1982). The effects of aquatic macrophytes on the stream microenvironment. *Aquat. Bot.* 14, 309–324. doi:10.1016/0304-3770(82)90105-X

Grillo, J. F., and Gibson, J. (1979). Regulation of phosphate accumulation in the unicellular cyanobacterium Synechococcus. *J. Bacteriol.* 140, 508–517.

Hansen, H. P., and Koroleff, F. (1999). "Chapter 10 determination of nutrients," in *Methods of seawater analysis*. Editors K. Grasshoff, K. Kremling, and M. Erhardt. 3rd ed. (Wiley VCH), 159–228.

Hansen, J. P., Wikström, S. A., Axemar, H., and Kautsky, L. (2011). Distribution differences and active habitate choices of invertebrates between macrophytes of different morphological complexity. *Aquat. Ecol.* 45, 11–22. doi:10.1007/s10452-010-9319-7

Hidding, B., Bakker, E. S., Hootsmans, M. J. M., and Hilt, S. (2016). Synergy between shading and herbivory triggers macrophytes loss and regime shift in aquatic systems. *Oikos*. 125, 1489–1495. doi:10.1111/oik.03104

Hilt, S., Köhler, J., Adrian, R., Monaghan, M. T., and Sayer, C. D. (2013). Clear, crashing, turbid and back – long-term changes in macrophyte assemblages in a shallow lake. *Freshw. Biol.* 58, 2027–2036. doi:10.1111/fwb.12188

Howard-Williams, C., and Allanson, B. R. (1981). Phosphorus cycling in a dense *Potamogeton pectinatus* L. bed. *Oecologia*. 49, 56–66. doi:10.1007/BF00376898

Huang, X. L., and Zhang, J. Z. (2009). Neutral persulfate digestion at sub-boiling temperature in an oven for total dissolved phosphorus determination in natural waters. *Talanta*. 78, 1129–1135. doi:10.1016/j.talanta.2009.01.029

Jankowska, E., Wlodarska-Kowalczuk, M., Kotwicki, L., Balazy, P., and Kuliński, K. (2014). Seasonality in vegetation biometrics and its effects on sediment characteristics and meiofauna in Baltic seagrass meadows. *Estuar. Coast Shelf Sci.* 1139, 159–170. doi:10.1016/j.ecss.2014.01.003

Jasby, S. W., and Platt, T. (1976). Mathematical formulation of the relationship between photosynthesis and light for phytoplankton. *Limnol. Oceanogr.* 21, 540–547. doi:10.4319/lo.1976.21.4.0540

Johansson, G., and Snoeijs, P. (2002). Macroalgal photosynthetic responses to light in relation to thallus morphology and depth zonation. *Mar. Ecol. Prog. Ser.* 244, 63–72. doi:10.3354/meps244063

Kemp, W. M., Brooks, M. T., and Hood, R. R. (2001). Nutrient enrichment, habitat variability and trophic transfer efficiency in simple models of pelagic ecosystems. *Mar. Ecol. Prog. Ser.* 223, 83–87. doi:10.3354/MEPS223073

Kennedy, H., Beggins, J., Duarte, C. M., Fourqurean, J. W., Holmer, M., Marbà, N., et al. (2010). Seagrass sediments as a global carbon sink: isotopic constraints. *Global Biogeochem. Cycles*. 24, GB4026. doi:10.1029/2010GB003848

Kiirikki, M., and Lehvo, A. (2012). Life strategies of filamentous algae in the northern Baltic proper. *Sarsia*. 82, 259–267. doi:10.1080/00364827.1997.10413653

King, R. J., and Schramm, W. (1976). Photosynthetic rates of benthic marine algae in relation to light intensity and seasonal variations. *Mar. Biol.* 37, 215–222. doi:10.1007/BF00387606

Kronvang, B., Jeppesen, E., Conley, D. J., Søndergaard, M., Larsen, S. E., Ovesen, N. B., et al. (2005). Nutrient pressures and ecological responses to nutrient loading reductions in Danish streams, lakes and coastal waters. *J. Hydrol.* 304, 274–288. doi:10.1016/j.jhydrol.2004.07.03

Lapointe, B. E., and Tenore, K. R. (1981). Experimental outdoor studies with *Ulva fasciata* Delile. I. Interaction of light and nitrogen on nutrient uptake, growth, and biochemical composition. *J. Exp. Mar. Biol. Ecol.* 53, 135–152. doi:10.1016/0022-0981(81)90015-0

Leskinen, E., Miikinen, A., Fortelius, W., Lindström, M., and Salemaa, H. (1992). "Primary production of macroalgae in relation to the spectral range and sublittoral light conditions in the Tvärminne archipelago, northern Baltic Sea," in *Algological studies of nordic coastal waters*. (Uppsala, Sweden: Acte Phytogeographica Suecica), 85–94.

López-Archilla, A. I., Mollá, S., Coleto, M. C., Guerrero, M. C., and Montes, C. (1992). Ecosystem metabolism in a mediterranean shallow lake (laguna de Santa olallan, doñana national Park, SW Spain). *Wetlands*. 24, 848–858. doi:10.1672/0277-5212(2004)024[0848:emiams]2.0.co;2

Madsen, T. V., and Brix, H. (1997). Growth, photosynthesis and acclimation by two submerged macrophytes in relation to temperature. *Oecologia*. 110, 320–327. doi:10.1007/s004420050165

Malcolm-Lawes, D. J., and Wong, K. H. (1990). Determination of orthophosphate in water and soil using a flow analyzer. *Analyst*. 15, 65–67. doi:10.1039/AN9901500065

Marcus, B. M. (1980). Relationship between light intensity and chlorophyll content in *Myriophyllum spicatum* L. in Canadice Lake (New York, U.S.A.). *Aquat. Bot.* 9, 169–172. doi:10.1016/0304-3770(80)90017-0

Meek, D., Hatfield, J., Howell, T., Idso, S., and Reginato, R. J. (1984). A generalized relationship between photosynthetically active radiation and solar radiation. *Argonomy J.* 76, 939–945.

Menendez, M., Herrera, J., and Comín, F. A. (2002). Effect of nitrogen and phosphorus supply on growth, chlorophyll content and tissue composition of the macroalga *Chaetomorpha linum* (O.F. Müll.) Kütz in a Mediterranean coastal lagoon. *Sci. Mar.* 66, 355–364.

Meyer, J., Dahlke, S., Kafka, M., Kerkow, A., Lindner, C., Kube, S., et al. (2019). Submerged vegetation in a shallow brackish lagoon does not enhance water clarity but offers substantial refuge for zooplankton. *Aquat. Bot.* 154, 1–10. doi:10.1016/j.aquabot.2018.12.002

Middelboe, A. L., and Blinzer, T. (2004). Importance of canopy structure on photosynthesis in single- and multi-species assemblages of marine macroalgae. *Oikos*. 107, 422–432. doi:10.1111/j.0030-1299.2004.13345.x

Middelboe, A. L., and Markager, S. (1997). Depth limits and minimum light requirements of freshwater macrophytes. *Freshw. Biol.* 37, 553–568.

Munkes, B. (2005). Eutrophication, phase shift, the delay and the potential return in the Greifswalder Bodden, Baltic Sea. *Aquat. Sci.* 67, 372–381. doi:10.1007/s00027-005-0761-x

Murphy, J., and Riley, J. P. (1962). A modified single solution method for the determination of phosphate in natural waters. *Anal. Chim. Acta*. 27, 31–36. doi:10.1016/S0003-2670(00)88444-5

Nausch, G., Bachor, A., Petenati, T., Voss, J., and Von Weber, M. (2011). Nutrients in the German coastal waters of the Baltic Sea and adjacent areas. *Meeresumwelt Aktuell Nord Ostsee*. 1, 1–16.

Oviatt, C. A., Rudnick, D. T., Keller, A. A., Sampou, P. A., and Almqvist, G. T. (1986). A comparison of system (O_2 and CO_2) and C-14 measurements of metabolism in estuarine mesocosms. *Mar. Ecol. Prog. Ser.* 28, 57–68.

Pärnoja, M., Kotta, J., Orav-Kotta, H., and Paalme, T. (2014). Comparisons of individual and community photosynthetic production indicate light limitation in the shallow water macroalgal communities of the Northern Baltic Sea. *Mar. Ecol.* 35, 19–27. doi:10.1111/maec.12074

Pedersen, M. F., and Borum, J. (1997). Nutrient control of estuarine macroalgae growth: Growth strategy and balance between nitrogen requirements and uptake. *Mar. Ecol. Prog. Ser.* 161, 155–163. doi:10.3354/meps161155

Piepho, M. (2017). Assessing maximum depth distribution, vegetated area, and production of submerged macrophytes in shallow, turbid coastal lagoons of the southern Baltic Sea. *Hydrobiologia*. 788, 1–14. doi:10.1007/s10750-017-3107-5

Plus, M., Auby, I., Verlaque, M., and Levavasseur, G. (2005). Seasonal variations in photosynthetic irradiance response curves of macrophytes from a Mediterranean coastal lagoon. *Aquat. Bot.* 81, 157–173. doi:10.1016/j.aquabot.2004.10.004

Prosser, C. L. (1961). "Oxygen: respiration and metabolism," in *Comparative anidal physiology*. Editors C. L. Prosser, F. A. Brown, and B. Saunders. 2nd ed. (Philadelphia, PA: W.B. Saunders), 165–211.

R Core Team (2019). *R: a language and environment for statistical computing*. Vienna, Austria: R Foundation for Statistical Computing. Available at:https://www.R-project.org/.

Rasmusson, L. (2015). *Seagrass respiration. An assessment of oxygen consumption patterns of temperate marine macrophytes*. Stockholm, Sweden: Stockholm University.

Raven, J. A., and Taylor, R. (2003). Macroalgae growth in nutrient-enriched estuaries: a biogeochemical and evolutionary approach. Water. *Air Soil Pollut*. 3, 7–26. doi:10.1023/A:1022167722654

Rosenzweig, M. L. (1971). Paradox of enrichment: destabilization of exploitation ecosystems in ecological time. *Science* 171, 385–387. doi:10.1126/science.171.3969.385

Russell, G., Ruuskanen, A., Kiirikki, M., and Høisæter, T. (2012). Sunlight, shade and tidal night: Photoadaptation in *Fucus vesiculosus* L. *Sarsia*. 83, 381–386. doi:10.1080/00364827.1998.10413697

Sayer, C. D., Burgess, A., Karl, K., Davidson, T. A., Peglar, S., Yang, H., et al. (2010). Long-term dynamics of submerged macrophytes and algae in a small and shallow, eutrophic lake: implications for the stability of macrophyte-dominance. *Freshw. Biol.* 55, 565–583. doi:10.1111/j.1365-2427.2009.02353.x

Scheffer, M., Hosper, S. H., Meijer, M. L., Moss, B., and Jeppesen, E. (1993). Alternative equilibria in shallow lakes. *Trends Ecol. Evol.* 8, 275–279. doi:10.1016/0169-5347(93)90254-M

Schiewer, U. (1998). 30 years' eutrophication in shallow brackish waters – lessons to be learned. *Hydrobiologia*. 363, 73–79. doi:10.1023/A:1003194226294

Schiewer, U. (2007). "Darß-Zingst Boddens, Northern Rügener Boddens and Schlei," in *Ecology of Baltic coastal waters*. Editors U. Schiewer, M. M. Caldwell, G. Heldmaier, R. B. Jackson, O. L. Lange, H. A. Mooney, et al. (Berlin-Heidelberg: Springer), 35–86.

Schiewer, U. (2001). Salzhaff, Greifswalder Bodden, Darß-Zingster Boddenkette: Gewässereutrophierung und Pufferkapazität – ein Vergleich. *Rostocker Meeresbiol Beitr*. 9, 5–19.

Schlitzer, R. (2018). Ocean Data View. Available at:https://odv.awi.de.

Schubert, H., and Foster, M. (1997). Sources of variability in the factors used for modelling primary productivity in eutrophic waters. *Hydrobiologia*. 349, 75–85. doi:10.1023/A:1003097512651

Schumann, R., Hammer, A., Görs, S., and Schubert, H. (2005). Winter and spring phytoplankton composition and production in a shallow eutrophic Baltic lagoon. *Estuar. Coast Shelf Sci.* 62, 169–181. doi:10.1016/j.ecss.2004.08.015

Schumann, R., Rentsch, D., Görs, S., and Schiewer, U. (2001). Seston particles along a eutrophication gradient in coastal waters of the Southern Baltic Sea: Significance of detritus and transparent mucoid material. *Mar. Ecol. Prog. Ser.* 218, 17–31. doi:10.3354/meps218017

Schumann, R., Schoor, A., and Schubert, H. (2009). Fine resolution of primary production and its limitation in phytoplankton communities of the Darß-Zingst Bodden Chain, a coastal lagoon of the Southern Baltic Sea Baltic. *Coast. Zone*. 13, 97–125.

Stanley, R. A., and Naylor, A. W. (1972). Photosynthesis in Eurasian Watermilfoil (*Myriophyllum spicatum* L.). *Plant Physiol.* 50, 149–151. doi:10.1104/pp.50.1.149

Tagliapietra, D., Sigovini, M., and Chiradini, A. V. (2009). A review of terms and definititons to categorise estuaries, lagoons and associated environments. *Mar. Freshw. Res.* 60, 497–509. doi:10.1071/MF08088

Taylor, J. R. (1997). *An introduction to error analysis*. Sausalito, CA: University Science Books.

Vadeboncoeur, Y., Lodge, D. M., and Carpenter, S. R. (2001). Whole lake detilization effects on distribution of primary production between benthic and pelagic habitats. *Ecology*. 82, 1065–1077. doi:10.1890/0012-9658(2001)082[1065:WLFEOD]2.0.CO;2

van Keulen, M., Paling, E. I., and Walker, C. J. (2003). Effect of planting unit size and sediment stabilization on seagrass transplants in Western Australia. *Restor. Ecol.* 11, 1–6. doi:10.1046/j.1526-100X.2003.00036.x

Walsby, A. E. (1997). Numerical integration of phytoplankton photosynthesis through time and depth in a water column. *New Phytol*. 136, 189–209. doi:10.1046/j.1469-8137.1997.00736.x

Wang, F. K. (2001). Confidence interval for the mean of non-normal data. *Qual. Reliab. Eng. Int*. 17, 257–267. doi:10.1002/qre400

Wennberg, T. (1992). "Colonization and succession of macroalgae on a breakwater in Laholm Bay, a eutrophicated brackish water area (SW Sweden)," in *Algological studies of nordic coastal waters*. (Uppsala, Sweden: Acte Phytogeographica Suecica), 49–65.

Włodarska-Kowalczuk, M., Jankowska, E., Kotwicki, L., and Balazy, P. (2014). Evidence of season-dependency in vegetation effects on macrofauna in temperate seagrass meadows (Baltic Sea). *PloS One*. 9, e100788. doi:10.1371/journal.pone.0100788

Xu, J., Hood, R. R., and Chao, S. Y. (2005). A simple empirical optical model for simulating light attenuation variability in a partially mixed estuary. *Estuar. Coast*. 28, 572–580. doi:10.1007/BF02696068

Conflict of Interest: The authors declare that the research was conducted in the absence of any commercial or financial relationships that could be construed as a potential conflict of interest.

frontiers in Earth Science

ORIGINAL RESEARCH
published: 03 February 2021
doi: 10.3389/feart.2020.577746

Consequences of Increased Variation in Peatland Hydrology for Carbon Storage: Legacy Effects of Drought and Flood in a Boreal Fen Ecosystem

Evan S. Kane[1,2*†], *Catherine M. Dieleman*[3*†], *Danielle Rupp*[1], *Kevin H. Wyatt*[4], *Allison R. Rober*[4] *and Merritt R. Turetsky*[5]

[1]College of Forest Resources and Environmental Sciences, Michigan Technological University, Houghton, MI, United States, [2]Northern Research Station, USDA Forest Service, Houghton, MI, United States, [3]College of Biological Science, University of Guelph, Guelph, ON, Canada, [4]Department of Biology, Ball State University, Muncie, IN, United States, [5]Institute of Arctic and Alpine Research, University of Colorado Boulder, Boulder, CO, United States

OPEN ACCESS

Edited by:
Jianghua Wu,
Memorial University of Newfoundland, Canada

Reviewed by:
Jason Fellman,
University of Alaska Southeast, United States
Benjamin N. Sulman,
Oak Ridge National Laboratory (DOE), United States

***Correspondence:**
Evan S. Kane
eskane@mtu.edu
Catherine M. Dieleman
cdielema@uoguelph.ca

[†]*These authors contributed equally to this manuscript*

Specialty section:
This article was submitted to Biogeoscience, a section of the journal Frontiers in Earth Science

Received: *29 June 2020*
Accepted: *07 December 2020*
Published: *03 February 2021*

Citation:
Kane ES, Dieleman CM, Rupp D, Wyatt KH, Rober AR and Turetsky MR (2021) Consequences of Increased Variation in Peatland Hydrology for Carbon Storage: Legacy Effects of Drought and Flood in a Boreal Fen Ecosystem. Front. Earth Sci. 8:577746. doi: 10.3389/feart.2020.577746

Globally important carbon (C) stores in boreal peatlands are vulnerable to altered hydrology through changes in precipitation and runoff patterns, groundwater inputs, and a changing cryosphere. These changes can affect the extent of boreal wetlands and their ability to sequester and transform C and other nutrients. Variation in precipitation patterns has also been increasing, with greater occurrences of both flooding and drought periods. Recent work has pointed to the increasing role of algal production in regulating C cycling during flooded periods in fen peatlands, but exactly how this affects the C sink-strength of these ecosystems is poorly understood. We evaluated temporal trends in algal biomass, ecosystem C uptake and respiration (using static and floating chamber techniques), and spectroscopic indicators of DOM quality (absorbance and fluorescence) in a boreal rich-fen peatland in which water table position had been experimentally manipulated for 13 years. Superimposed on the water table treatments were natural variations in hydrology, including periods of flooding, which allowed us to examine the legacy effects of flooding on C cycling dynamics. We had a particular focus on understanding the role of algae in regulating C cycling, as the relative contribution of algal production was observed to significantly increase with flooding. Ecosystem measures of gross primary production (GPP) increased with algal biomass, with higher algal biomass and GPP measured in the lowered water table treatment two years after persistent flooding. Prior to flooding the lowered treatment was the weakest C sink (as CO_2), but this treatment became the strongest sink after flooding. The lower degree of humification (lower humification index, HIX) and yet lower bioavailability (higher spectral slope ratio, Sr) of DOM observed in the raised treatment prior to flooding persisted after two years of flooding. An index of free or bound proteins (tyrosine index, TI) increased with algal biomass across all plots during flooding, and was lowest in the raised treatment. As such, antecedent drainage conditions determined the sink-strength of this rich fen—which was also reflected in DOM characteristics. These findings indicate that monitoring flooding history and its effects on algal production could become important to estimates of C balance in northern wetlands.

Keywords: boreal, peat, climate change, carbon dioxide, dissolved organic matter, DOM, spectroscopy, algae

INTRODUCTION

Northern peatlands are a globally important reservoir of carbon (C), representing a large magnitude of C vulnerable to loss in a changing climate (Goldstein et al., 2020). Rich fens are one of the most common boreal peatland types in western North America (Vitt et al., 2000), and open peatlands and mineral wetlands comprise about 85% of wetland area in Alaska (Kolka et al., 2018) — an area of land nearly twice that of all wetland area in the contiguous United States (Ford and Bedford, 1987). Moreover, the extent of fens in interior Alaska has been increasing owing to permafrost degradation and changing ground water and runoff patterns in recent decades (Jorgenson et al., 2001; Lara et al., 2016). Observed regional climate trends and modelling efforts also suggest increased precipitation with overall higher variation (anomalies) in total amounts in Alaska's boreal region (Stewart et al., 2013; Euskirchen et al., 2016). These patterns suggest prolonged or more variable periods of inundation in the future, with yet uncertain consequences for the C storage capacity of Alaska's vast fen ecosystem complexes.

The carbon balance of peatlands has shown varied responses to changes in the water table position occurring with periods of flooding or drought. While high water tables are generally associated with higher fluxes of methane (e.g., Turetsky et al., 2014), the balance between ecosystem respiration (ER) and gross primary production (GPP) can vary with changes in water table position (Belyea, 2009; Strack et al., 2009). For example, a decade of research in an interior Alaskan fen has shown that drought conditions generally reduced GPP, but had muted effects on ER, which switched from increased autotrophic respiration in wet years to increased heterotrophic respiration in dry years (Olefeldt et al., 2017). However with flooding, variation in respiration in this fen complex changed with the timing and sources of inundation, with persistent flooding late into the growing season resulting in lower GPP relative to ER (Euskirchen et al., 2020). Exactly how constituent autotrophic and heterotrophic respiration components are likely to change with different regimes of flooding are not yet well understood.

A key difference in the active mode of primary production during flooded conditions, which affords a photic zone within the water column, is the relative activity of algae (Goldsborough and Robinson, 1996). While little is still known about algal production in boreal fens, recent work highlights the importance of algae as a component of the photosynthetic community during flooded conditions in interior Alaskan peatlands (Wyatt and Turetsky, 2015; DeColibus et al., 2017). Moreover, antecedent drainage conditions prior to flooding have been shown to exert strong controls over algal production. Experimental drainage in an Alaskan fen peatland resulted in increased pore water nutrient concentrations which fostered algal production upon flooding due to high rainfall (Wyatt et al., 2012). However, exactly how long this "ecosystem memory" of antecedent dry conditions can affect algal production, and how this in turn affects net C balance with persistent flooding is not clear (DeColibus et al., 2017). For example, observed increases in the exudates (dissolved organic matter, DOM) concomitant with increased algal production are very bioavailable (Bertilsson and Jones, 2003; Wyatt et al., 2012; Wyatt and Rober 2020) and could increase ER with persistent flooding. As such, component fluxes of ecosystem respiration along with algal production need to be measured together during periods of persistent flooding to ascertain the net consequences of flooding history on C balance in fens.

We investigated trace gas production, algal biomass, and DOM quality in an experimental manipulation of water table positions that simulate both drought (lowered water table treatment) and flooding (raised water table treatment) conditions relative to a control treatment without manipulation in an Alaskan boreal rich fen. We conducted our measurements prior to flooding across all experimental treatments and after two years of consecutive flooding. Our over-arching hypothesis was that hydrologic variation affects the balance between GPP and ER (**Figure 1**). With flooding, we expected algal production to offset carbon losses through ER, increasing the C sink-strength of the ecosystem. As such, we hypothesized the lowered water table treatment would be a stronger sink of C when reflooded owing to greater algal biomass associated with elevated nutrient availability, whereas the previously raised water table treatment would be a weaker sink of C when flooded, owing to reduced GPP from vascular plants. On the other hand, increased water-soluble organic carbon, algae-derived DOM and nutrients from the lowered water table treatment could increase heterotrophic respiration, and hence drive higher ER relative to GPP in the flooded environment. However, exactly how antecedent changes in DOM quality persist with prolonged flooding periods are not well understood. Therefore, we specifically ask: 1) How does the legacy of flooding history influence peatland C balance? 2) What is the role of DOM quality in driving ecosystem C fluxes and how does algal biomass relate to DOM quality?

MATERIALS AND METHODS

Study Site and Experimental Design

The rich fen (surface pH ~6) is in the boreal peatland lowlands of the Tanana Flats of interior Alaska (cf. Hopkins et al., 1955) approximately 30 km southeast of Fairbanks, Alaska United States. The vegetation and climate characteristics of this site have been previously described in detail (Churchill et al., 2015; Olefeldt et al., 2017; Euskirchen et al., 2020), but briefly, emergent vascular species (*Equisetum, Carex,* and *Comarum* (*Potentilla*) genera) and some brown mosses and *Sphagnum* dominate the site. The fen complex lacks permafrost but is within the region of discontinuous permafrost in Alaska's interior. There is little microtopography at the rich fen, which has accumulated peat to a depth of approximately 1–1.5 m. The site is associated with the Bonanza Creek Long Term Ecological Research Program (lter.uaf.edu).

The Alaska Peatland Experiment (APEX) was established in 2005 to investigate the effects of altered hydrologic regimes on C cycling processes in a controlled experiment. Three plots (approximately 20 × 20 m) were assigned each to one of three water table (WT) treatments (raised, lowered, and a control

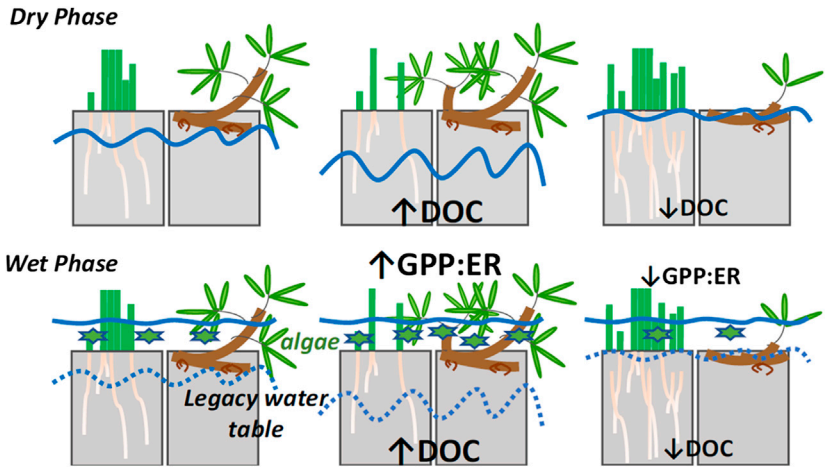

FIGURE 1 | Conceptual model of how our experimental water table treatments (control, lowered and raised) have affected the pool size of nutrients, dissolved organic carbon [DOC] and its quality, and how these factors have affected algal production during flooding (wet phase). We hypothesize that these factors affect the balance between gross primary production and ecosystem respiration (GPP:ER). The solid blue lines indicate water table position by treatment, and the dashed lines indicate legacy water table position during flooding. The green stars indicate the relative abundance of algae. The plants indicate relative abundances of sedges and shrubs (see Rupp et al., 2019).

reference plot, each approximately 25 m apart), as previously described in detail (see Turetsky et al., 2008 and Chivers et al., 2009 for experiment details). Briefly, in the winter of 2005 channels were dug to facilitate water drainage from the lowered water table plot. This water in turn was pumped into the raised water table treatment with solar-powered bilge pumps, throughout the growing season (approximately June-September). There were no significant differences in water table position or vegetation composition among plots prior to treatment initiation. The goal of the experiment was to maintain lowered (drained) and raised water table positions relative to the control while allowing for the natural seasonal variability in water table position at this site. However, it was impossible to experimentally manipulate the water table position during periods of natural flooding, including years when flooding (water table > 40 cm above peat surface) persisted for the entire growing season (2014, 2017 and 2018; see Euskirchen et al., 2020 for hydrograph data). In this current study, we measured trace gas flux, algal biomass, and DOM quality within the APEX plots prior to a natural flooding event in 2016, which persisted through 2017 and 2018. We remeasured the experimental plots after continuous flooding during the growing season of 2018 to test our hypotheses regarding persistent flooding effects on C cycle dynamics.

Gas Flux Measurements

We used the static chamber technique for gas flux measurements during non-flooded years as previously described in detail (Chivers et al., 2009). Briefly, six collars (60 × 60 cm) were inserted to a depth of 10 cm in 2005 within each WT treatment. A clear lexan chamber (0.227 m^3) with closed-cell foam sealed the chamber with the collar. Two computer CPU fans mixed the air within the chamber during measurements. The change in chamber CO_2 concentrations was measured for approximately 4 min using a portable infrared gas analyzer (IRGA; PP Systems EGM 4, Amesbury, Massachusetts, United States). ER was measured by shading chambers with an opaque shroud and net ecosystem exchange (NEE) was measured without a shroud. Temperature, relative humidity, and photosynthetically active radiation (PAR) were logged continuously within the chamber during each flux measurement with a PP Systems TRP-1 sensor. Measurements occurred approximately bi-weekly.

A floating chamber was employed for gas flux measurements in flooded conditions during the growing season of 2018. This static chamber was constructed from a clear polycarbonate plastic bucket (18.9 L) with Styrofoam floatation around the base and one CPU fan inside for air circulation. This design allows for the measure of CO_2 flux in the airspace above the water. The floating chamber was equipped with an airlock to equilibrate pressure. The clear chamber was covered with an opaque shroud during ER measurements and NEE was measured without a shroud. Temperature, relative humidity, and PAR were logged continuously with a PP Systems TRP-1 sensor mounted within the clear floating chamber. The change in chamber CO_2 concentrations was measured with an IRGA as previously described. Floating chamber measurements were conducted within water table manipulation plots (within plot n = 3) from a small inflatable boat and by wading along the established boardwalk network.

Algal Biomass

Algal material was collected biweekly during the 2018 growing season for estimates of algal biomass measured as chlorophyll a (mg cm^{-2}). Owing to shallow water with a well-lit photic zone, algae within this fen complex grow primarily affixed to submersed substrata (DeColibus et al., 2017). Attached algal material was collected from four senesced *Carex utriculata* stems (10 cm length) cut below the water surface within each

of three randomly selected 1 m^2 areas per water table treatment using methods modified from DeColibus et al. (2017). There was no floating or loosely attached algae (i.e. metaphyton) observed during the study. Each composite sample was placed into a clean 15 ml polyethylene tube and kept on ice until returning to the lab where samples were frozen at −20°C until subsequent processing. Algal chlorophyll a was extracted with 90% ethanol in the dark for 24 h and the resulting pigment extracts were analyzed with an Agilent Cary 60 UV-Vis spectrophotometer (Agilent Technologies, Santa Clara, CA, United States) at 665 and 750 nm after acidification to correct for phaeophytin (APHA, 1998).

Dissolved Organic Matter Quality

When the water table was below the peat surface in 2016, a stainless steel "sipper" (0.52 cm diameter tubing with 2 cm slotted region at the end) was carefully inserted into the peat to a depth of 20 cm. Pore water was drawn up through the sipper into a syringe that was rinsed first with deionized (DI) water, then with sample prior to collection. When conditions were flooded in 2018, surface waters from the photic zone were collected in addition to pore water. Specifically, a clean, sample rinsed 60 ml syringe was used to sample the water column 10 cm below the surface of the water. After collection, the sample was injected into a 125 ml dinitrogen gas flushed and evacuated Wheaton glass vial capped with a butyl rubber septa via a 0.45 μm Whatman syringe filter and needle and then refrigerated prior to analysis, following Rupp et al. (2019). Samples were collected at three locations, spaced approximately 3 m apart, in each WT treatment throughout the growing seasons of 2016 (prior to flooding) and 2018 (during sustained flooding). Dissolved organic carbon (DOC) and total dissolved nitrogen (TDN) were determined on samples within 10 days on an TOCV Analyzer with TDN module (Shimadzu Scientific Instruments, Columbia, MD, United States).

Pore water was extracted from each of the Wheaton vials and run on a fluorometer (Horiba–Jobin–Yvon Aqualog C; Horiba Co., Edison, NJ) to simultaneously collect UV–Vis absorbance and florescence spectra. Run parameters were excitation: 240–600 nm in 3 nm increments; emission: 212–608 nm by 3 nm bandpass; integration time = 0.25 s. Samples with absorbance greater than 0.6 at λ = 254 were diluted to satisfy the assumption of detector linearity required by modeling (Stedmon and Bro 2008; Lawaetz and Stedmon 2009). Data post-processing and correction for inner filter effects were as described in detail by Veverica et al. (2016), following Stedmon and Bro (2008) and Lawaetz and Stedmon (2009).

Fluorescence and absorbance spectroscopic indices were calculated to characterize dissolved organic matter in all samples as previously described (Veverica et al., 2016; Rupp et al., 2019). Fluorometric indices considered in this study included an index of DOM humification (humification index; HIX; Zsolnay et al., 1999; Ohno, 2002; cf. Zsolnay, 2002). Higher HIX values can generally be considered as more biologically recalcitrant or aromatic in boreal systems (Chen et al., 2011; Frey et al., 2016; Herzsprung et al., 2017). We calculated an index of free or bound proteins (tyrosine or tryptophan index; TI; Fellman et al., 2010; cf. Chen et al., 2003). Higher TI values are considered relatively labile in comparison to the humified products associated with HIX (cf. Cory and Kaplan, 2012). We also calculated the Spectral slope ratio (Sr), an absorbance index of photodegradation, molecular weight (Helms et al., 2008) and source (Chen et al., 2011). The Sr is also an inverse indicator of relatively labile carbon compounds, with lower values associated with more bioavailable DOM (Frey et al., 2016).

Statistics and Analyses

We examined WT treatment effects, flooding, and their interaction (WT treatment x flooded or not flooded state) on CO_2 flux data (ER, GPP, NEE), algal biomass, and DOM composition variables (HIX, Sr, TI). We collected these data throughout the growing seasons of 2016 (pre-flood; four campaigns) and 2018 (after continuous flooding; five campaigns). We used a generalized linear mixed model approach to examine differences in CO_2 flux and DOM composition data prior to flooding and in the flooded state; this approach enables statistical models to be fit to data where the response is not necessarily normally distributed (PROC GLIMMIX; SAS version 9.4, SAS Institute, Cary, North Carolina, United States). Sampling campaign was treated as a random effect to account for repeated measures. The distributions of response variables were evaluated in Kolmogorov-Smirnov tests using the UNIVARIATE procedure, and were assigned as gaussian or lognormal as appropriate. Differences in DOC and TDN concentrations were explored using a mixed effects model via the "nlme" package in R statistical software version 3.4.2 (R Core Development Team, 2017). The WT treatment was used as a fixed effect, while sampling date was a random effect to account for repeated measures. The TDN values were transformed using the power-based Tukey Ladder of Powers transformation via the "rcompanion" package (Mangiafico, 2018; TDN 10 cm below water surface lambda = 2.2; TDN 20 cm below peat surface lambda = 1.5). We explored relationships with algal biomass (chlorophyll a) and ER, Sr, and TI with linear regression. Type-III tests of fixed effects and post hoc comparisons of least squared means tests across treatments were considered significant at $\alpha = 0.05$. All data used in these analyses are available in the public domain via the Bonanza Creek Data Catalog (https://www.lter.uaf.edu/data/data-catalog).

RESULTS

Change in Carbon Balance

Across all treatments, there were changes in ER and GPP in response to flooding that resulted in interactions between drainage history and flooding for net C balance (**Table 1**). Prior to flooding, the raised water table (WT) treatment had marginally lower ER (2.79 ± 0.14 CO_2 μmol m^{-2} s^{-1}) than the lowered (3.25 ± 0.30 CO_2 μmol m^{-2} s^{-1}) or control (4.10 ± 0.54 CO_2 μmol m^{-2} s^{-1}) treatments ($F = 3.31$, $p = 0.08$), though there were no differences in ER among treatments after flooding (mean of 3.28 ± 0.63 CO_2 μmol m^{-2} s^{-1}; $F = 0.75$, $p = 0.60$; cf. **Figure 2**).

TABLE 1 | Results of mixed effects models testing the effects of experimental water table treatment, flooding, and their interaction on ecosystem respiration (ER), gross primary production (GPP) and net ecosystem exchange (NEE). Model numerator (Num.) and Denominator (Den.) degrees of freedom (DF) are provided.

Model	Effect	Num. DF	Den. DF	F	*p*
ER	Treatment plot	2	14	5.330	0.019
	Flooded state	1	18	9.090	0.008
	Plot x flooded state	2	14	1.080	0.365
GPP	Treatment plot	2	10	1.900	0.200
	Flooded state	1	5	6.310	0.054
	Plot x flooded state	2	10	4.280	0.045
NEE	Treatment plot	2	10	0.250	0.786
	Flooded state	1	5	9.340	0.028
	Plot x flooded state	2	10	4.090	0.050

In contrast, GPP was reduced (less uptake, less negative) following flooding in both the control (−8.22 ± 0.65 vs. −5.33 ± 0.99 CO_2 μmol m^{-2} s^{-1}) and raised (−7.19 ± 0.33 vs. −4.18 ± 0.99 CO_2 μmol m^{-2} s^{-1}) treatments, whereas in the lowered treatment GPP did not decrease with flooding (−6.36 ± 0.82 vs. −6.07 ± 0.34 CO_2 μmol m^{-2} s^{-1}), resulting in an interaction between WT treatment and flooding (**Table 1**; F = 4.28, p = 0.045). As a result of these processes the site was a stronger sink of C prior to flooding (mean NEE −3.88 ± 0.67 CO_2 μmol m^{-2} s^{-1}) than after flooding (−1.18 ± 0.87 CO_2 μmol m^{-2} s^{-1}), with the lowered treatment becoming a stronger sink, and the raised treatment being a source of C on one measurement day with flooded conditions (**Figure 2B**). The change in the C sink-strength with flooding in the raised treatment contributed to a weak interaction between water table treatment and flooding in explaining variation in NEE (**Table 1**; F = 4.09, p = 0.05).

In 2018, mean [DOC] obtained from 10 cm beneath the surface of the water table was significantly lower in the raised WT treatment (32 ± 1.4 mg L^{-1}) than in both the lowered (36 ± 0.4 mg L^{-1}) or control (39 ± 0.5 mg L^{-1}) treatments (F = 16.53, p < 0.001). Mean [DOC] obtained from 20 cm beneath the surface of the peat was also lower in the raised WT treatment (56 ± 3 mg L^{-1}) than in both the lowered (93 ± 7 mg L^{-1}) or control (80 ± 2 mg L^{-1}) treatments (F = 29.88, p < 0.001). There were no WT treatment effects on mean [TDN] obtained from 10 cm beneath the surface of the water table (0.5 ± 0.1 mg L^{-1}; F = 0.73, p = 0.49). Mean [TDN] obtained from 20 cm beneath the surface of the peat was lower in the raised WT treatment (1.1 ± 0.1 mg L^{-1}) than in both the lowered (2.8 ± 0.2 mg L^{-1}) or control (2.1 ± 0.2 mg L^{-1}) treatments (F = 20.61, p < 0.001).

Algal Biomass and Carbon Quality

Algal biomass (chlorophyll a) was significantly higher in the control (mean ± standard error; 2.61 mg m^{-2} ± 0.46) and lowered (2.57 mg m^{-2} ± 0.38) treatment plots compared with the raised (1.55 mg m^{-2} ± 0.22) treatment (F = 4.24, p = 0.04). Ecosystem respiration and the index of free or bound-in proteins (TI) increased with algal biomass, while the degree of DOM photodegradation or molecular weight (Sr, or inversely related to humification, or HIX) declined with algal biomass (**Figure 3**). After accounting for changes in chlorophyll a content in mixed models (Type III tests of fixed effects), WT treatment also had significant effects on Sr (F = 6.50, p = 0.03), and marginally significant treatment effects on ER and TI (F = 3.12, p = 0.09 and F = 3.50, p = 0.08, respectively).

DOM Quality Before and After Flooding

Indices of DOM quality changed as a function of WT treatment and flooding. Prior to flooding (2016), DOM humification (HIX) at 20 cm in the peat was greater in the lowered water table treatment than in the raised WT treatment (F = 8.09, p = 0.004; **Figure 4A**). Following flooding, humification was much more variable at the lowered WT treatment, and was only significantly different (lower value) in the raised treatment

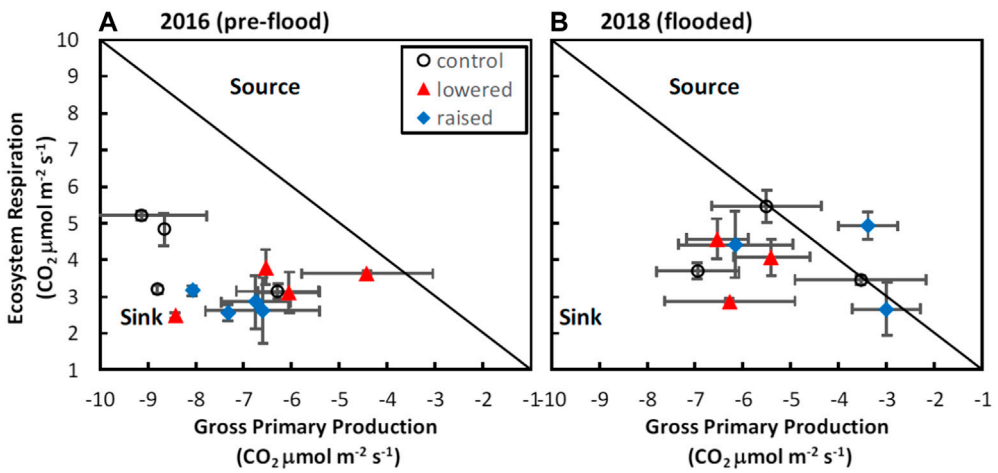

FIGURE 2 | Changes in ecosystem carbon balance prior to flooding, and after two years of continuous flooding. Depicted are means for a given campaign by water table treatment plot. Error bars represent standard errors of the mean values.

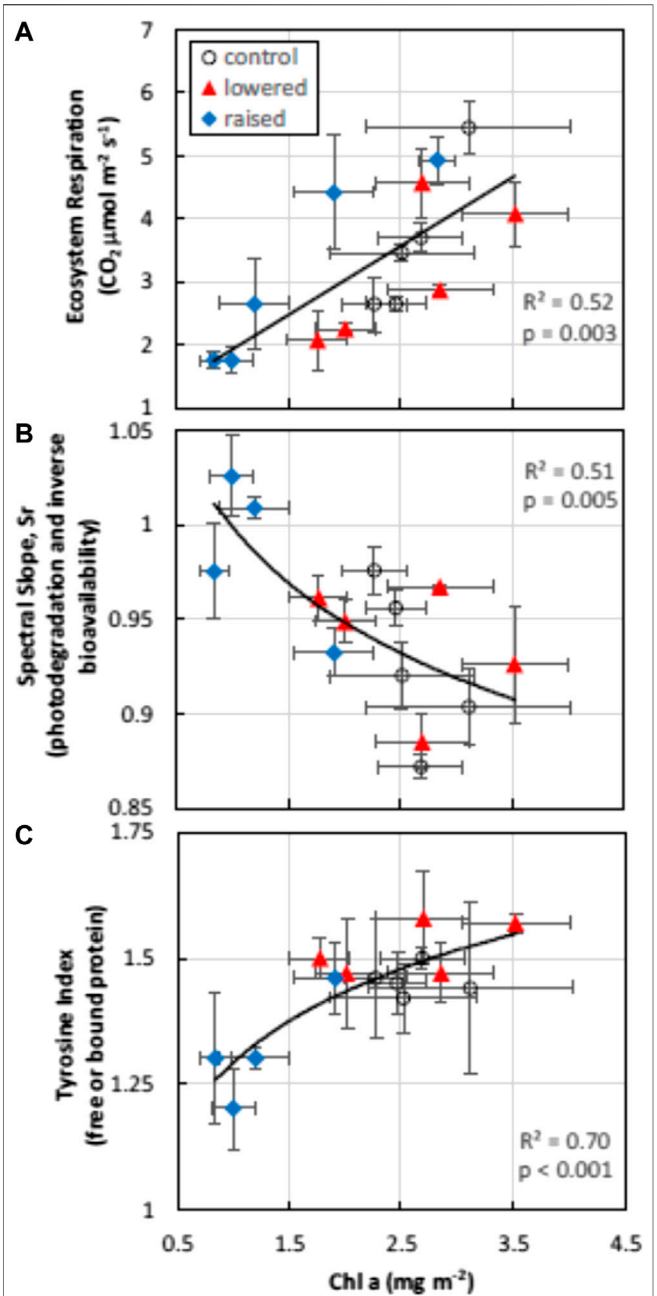

FIGURE 3 | Algal biomass (chlorophyll a content) was strongly related to changes in ecosystem respiration (top pane) measured with floating chambers during flooding, the bioavailability of DOM (inversely related to spectral slope ratio, Sr, middle pane) and the content of free or bound protein (TI, bottom pane). Depicted are daily means by water table treatment plot in the flooded year (2018). Error bars represent standard errors of the mean values.

(**Figure 4B**; $p < 0.001$). Overall, the degree of humification was higher, in the flooded year, in the control and lowered plots (year x WT treatment interaction, F = 9.84, $p < 0.001$). In contrast, Sr, an indicator of photodegradation and an inverse indicator of molecular weight and bioavailability, was higher in the raised WT treatment than in the other treatments (**Figures 4C, D**), and there was no difference between the flooded and non-flooded years (p = 0.70). The index of free or bound-in proteins (TI) did not vary by WT treatment prior to flooding (**Figure 4E**; p = 0.17), but was significantly greater in the lowered WT treatment, and less in the raised treatment following flooding (**Figure 4F**; $p < 0.001$). Moreover, TI was greater overall in the flooded year than prior to flooding (F = 17.67, $p < 0.001$) and there was a marginal year x WT treatment interaction (F = 2.92, p = 0.06). These changes in DOM quality measured at 20 cm within the peat pore water were maintained in DOM collected within the water column two years after persistent flooding (10 cm from water table surface), with the raised plot being different from the other treatments (**Figure 5**). With flooding, DOM in the water column of the raised WT treatment exhibited less bioavailability or increased photodegradation (Sr; F = 6.17, p = 0.005), a lower degree of humification (HIX; F = 11.29, $p <$ 0.001) and less proteinaceous compounds (TI; F = 8.12, p = 0.001).

DISCUSSION

Carbon Balance With Drainage History and Flooding

In conditions of variable hydrology, lowering the water table generally promotes an increase in both ER and GPP, which has made it difficult to ascribe single mechanisms for the sign of net C balance with hydrologic change (Weltzin et al., 2003; Strack and Waddington, 2007; Ballantyne et al., 2014). A major difference between previous studies and this current work, and fens in general, was the prolonged period of saturation where water table remained above the peat surface. Prior work at this site had shown no significant WT treatment effects on ER (Chivers et al., 2009; Olefeldt et al., 2017), but was not able to investigate WT treatment effects on C cycling when the site was flooded. More recent work has shown that the site as a whole exhibited higher ER in years when flooding occurred from the spring season onward (Euskirchen et al., 2020). This work showed that with persistent flooding, the previously raised WT treatment exhibited higher ER relative to GPP, with the most parsimonious explanation being limitations to the production of algal biomass (cf. **Figure 3**). While prior work had also shown the ability of algae to capitalize on the nutrients released from increased decomposition in the lowered WT treatments when flooded (DeColibus et al., 2017), this current work demonstrated that algae also affected ecosystem C balance. Interestingly, the increase in labile C supply in response to algal production (e.g., higher TI) did not result in a significant increase in the relative amount of heterotrophic respiration (cf. Wyatt et al., 2019), which certainly warrants further investigation as to the limiting factors of ER when the ecosystem is flooded. For example, the protein-like fluorescence in this study may not be reflecting the pool of bioavailable DOM (Maie et al., 2007). These findings refine our prior hypothesis (Olefeldt et al., 2017) that the lack of a response in ER to WT treatments reflects a shift in the component flux contributions to ER, from autotrophic respiration in wet years to heterotrophic respiration in dry

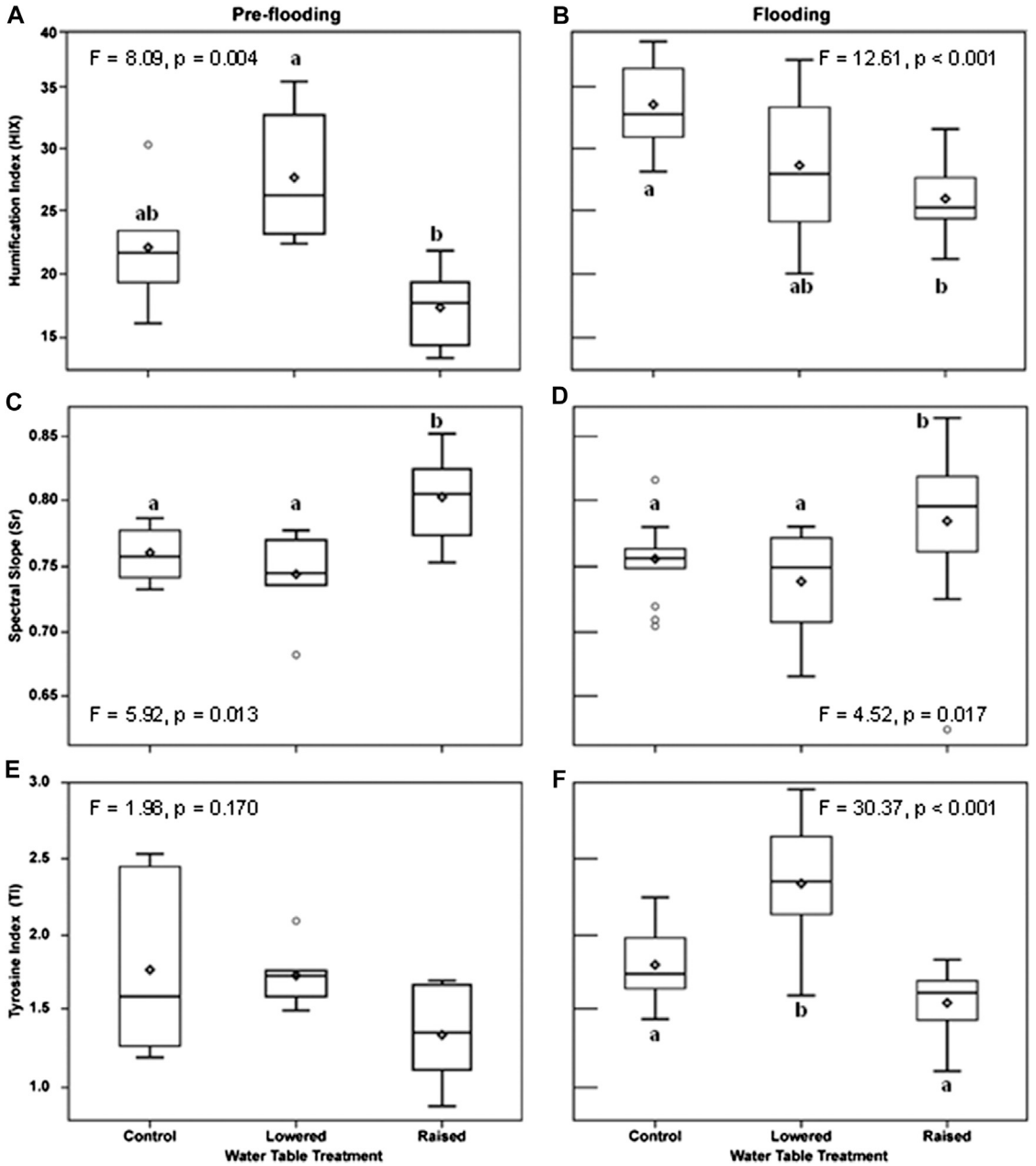

FIGURE 4 | Indexes of peat pore water (20 cm into the peat) character before flooding in 2016 **(A,C,E)** and after continuous flooding, measured in 2018 **(B,D,F)**. Depicted are seasonal means by water table treatment plot. An index of DOM humification (HIX) was higher in the flooded year (b, $F = 44.09$, $p < 0.001$), and there was a year × treatment interaction ($F = 8.84$, $p < 0.001$). An inverse index of DOM bioavailabilty and molecular size (Spectral Slope Ratio, Sr) did not vary by year ($F = 0.15$, $p = 0.70$), but was higher in the raised treatment **(C,D)**. An index of peat pore water free or bound protein (TI) was higher in the flooded year ($F = 17.67$, $p < 0.001$), and the lowered treatment was higher than the raised treatment **(F)**. Letters indicate significant differences in post-hoc comparisons of means within a treatment year (flood state).

years, and demonstrate that an algal-mediated increase in GPP in the lowered WT treatments can attenuate net C losses during flooding.

Insights Gained From DOM Composition

The DOM absorbance and fluorescence spectroscopy provided insights into C cycle processes within the peat prior to and after two years of flooding. Prior to flooding, pore water was more humified in the lowered WT treatment, which is consistent with the accumulation of water-soluble products of increased decomposition in a broader, more aerobic region above the water table, or acrotelm (Strack et al., 2008; Tfaily et al., 2018). HIX remained higher (and yet more variable) in the lowered WT treatment upon being flooded, which is consistent with prior work demonstrating that a sustained HIX upon rewetting drained peatland soil represents an increased amount of oxygen-rich and relatively unsaturated (O/C >

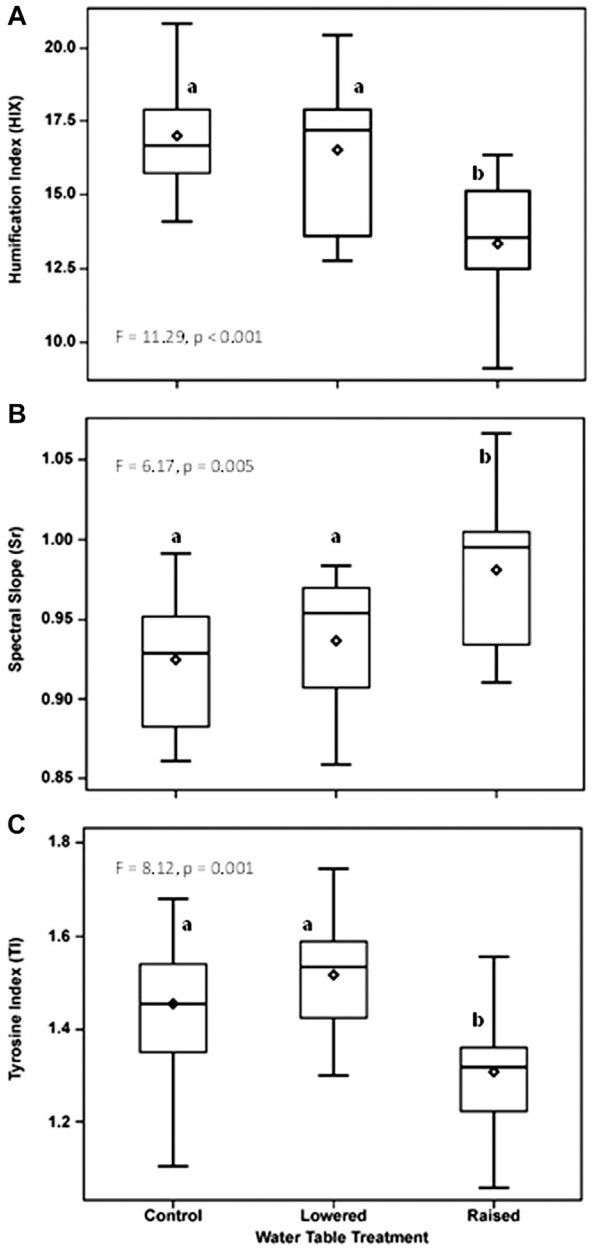

FIGURE 5 | Water table treatment differences in an index of humification (HIX, **(A)**, an index of photodegradation or an inverse index of bioavailability (Sr, **(B)**, and an index of free or bound protein (TI, **(C)** of water taken 10 cm below the surface of the water during flooding throughout the 2018 growing season. Depicted are seasonal means by water table treatment plot. Letters indicate significant differences in post-hoc comparisons of means.

0.5; H/C < 1.0) DOM (Herzsprung et al., 2017). The lower HIX values in the raised WT treatment, regardless of flooding history, suggest less accumulation of the products of peat mineralization. Lower HIX is consistent with the increased Sr (Chen et al., 2011) observed at the raised WT treatment, and could also be reflecting increased photodegradation of the DOM as opposed to biological degradation of the DOM (Helms et al., 2008; Wilske et al., 2020). Increased photodegradation would be facilitated by the water table being at or slightly above the peat surface in the raised WT treatment. The potential for DOM photodegradation to CO_2 could be contributing to the lower C sink strength in the raised WT treatment. In turn, DOM with relatively high Sr exhibits low bioavailability (Frey et al., 2016). In contrast, TI—an index of free or bound proteins, is generally thought to be highly bioavailable (Cory and Kaplan, 2012). There were no WT treatment effects on soil TI values prior to flooding, but significant increases in the lowered WT treatment and decreases in the raised WT treatments were measured when flooded (**Figure 4E, F**; **Figure 5**). Taken together, these indices indicate that the raised WT treatment had less bioavailable DOM within the peat (higher Sr, low TI) than the lowered WT treatment, even though the lowered WT treatment also had a fraction of more humified DOM (higher HIX). A parsimonious explanation for increased HIX and decreased Sr with increasing TI is the increase in algal production and algal exudation in response to the increased nutrients released in the lowered WT treatment relative to the raised WT treatment (Wyatt et al., 2012), while also having more water-soluble products from increased decomposition in the lowered WT treatment prior to flooding (Kane et al., 2010). Moreover, it could be that the protein-like fluorescence in this case reflects higher molecular weight lignin polyphenols (Herns et al., 2009; Stubbins et al., 2014), and more detailed analysis of the presence of aromatic amino acids in this system is certainly warranted.

These results are consistent with prior work demonstrating the ability of algae to capitalize on the "legacy effect" of prior drainage and nutrient release (Wyatt et al., 2012; DeColibus et al., 2017), and further demonstrate that the elevated nutrient legacy effects on algal production can persist after two consecutive years of flooding. While vascular plants are a significant component of NEE (Rupp et al., 2019), photosynthetic capacity (NDVI) has been shown to be lower in the lowered WT treatment during flooded conditions (McPartland et al., 2019), which further suggests a different mode of primary production to be driving C uptake when flooded. The duration of flooding is an important consideration for C cycling and algal production. For example, relatively short-term (<40 days) wet events did not generate lag effects in C cycling, and the lowered WT treatment in wet years exhibited similar GPP and NEE to that of the raised WT treatment in dry years (Olefeldt et al., 2017). After persistent flooding, however, the lowered WT treatment became the strongest C sink, whereas the raised WT treatment became a source (e.g., **Table 1**; **Figure 2**). However, it is not clear how long the "legacy effect of drought" can continue to fuel increased algal production. For example, nutrient co-limitations or competition with vascular plants may override any nutrient legacy effect on algal production over the span of decades (Lougheed et al., 2011; Lougheed et al., 2015). Flooding events at this rich fen site have been increasing over time, commensurate with the study region becoming a greater source of C to the atmosphere (Euskirchen et al., 2020). If periods of inundation increase in duration (i.e., become more lake-like), as has been observed in other regions of interior Alaska (Jorgenson et al., 2001), these data suggest rich fens could become a weaker sink for C, with

reduced algal production likely being a contributing factor. These findings indicate that incorporating an understanding of flooding history and its effects on algal production are important in assessments of C storage in boreal fen peatlands.

DATA AVAILABILITY STATEMENT

The datasets presented in this study can be found in online repositories. The names of the repository/repositories and accession number can be found below: All data used in these analyses are available in the public domain via the Bonanza Creek Data Catalog (https://www.lter.uaf.edu/data/data-catalog).

AUTHOR CONTRIBUTIONS

All authors contributed to the conception of this study. EK lead the analyses and writing, with input from all authors. CD lead field activities during flooding (2018), with input from all authors. KW and AR lead algal biomass methods and analyses.

FUNDING

This project was funded by National Science Foundation grants DEB LTREB-1354370 (to EK and MT) and DEB-1651195 (to KW and AR). The APEX site has been supported by National Science Foundation Grants DEB-0425328, DEB-0724514 and DEB-0830997 (to MT). The Bonanza Creek Long-Term Ecological Research program was funded jointly by NSF Grant DEB-0620579 and an USDA Forest Service Pacific Northwest Research Grant PNW01-JV11261952-231. The project received in-kind support from the U.S.D.A. Forest Service, Northern Research Station (Houghton, MI, United States). Jamie Hollingsworth and the Bonanza Creek LTER site provided tremendous support for this project.

ACKNOWLEDGMENTS

We thank Morgan Brown, Evan Schijns, Mara McPartland, Lucas Albano, and Natalie Zwanenburg for their help in the field and Karl Meingast for his expertise in spectroscopy.

REFERENCES

APHA (1998). *Standard methods for the examination of water and wastewater*. 20th edition. Washington, DC: American Public Health Association.

Ballantyne, D. M., Hribljan, J. A., Pypker, T. G., and Chimner, R. A. (2014). Long-term water table manipulations alter peatland gaseous carbon fluxes in Northern Michigan. *Wetl. Ecol. Manag.* 22 (1), 35–47. doi:10.1007/s11273-013-9320-8

Belyea, L. R. (2009). "Nonlinear dynamics of peatlands and potential feedbacks on the climate system," in *Carbon cycling in northern peatlands*. Editors A. J. Baird, L. R. Belyea, X. Comas, A. S. Reeve, and L. D. Slater (Washington, DC: American Geophysical Union Geophysical Monograph), 184, 5. doi:10.1029/2008GM000829

Bertilsson, S., and Jones, J. B. (2003). "Supply of dissolved organic matter to aquatic ecosystems: autochthonous sources," in *Aquatic ecosystems: interactivity of dissolved organic matter*. Editors S. E. G. Findlay and R. L. Sinsabaugh (San Diego, CA: Academic Press), 3–25.

Chen, H., Zheng, B., Song, Y., and Qin, Y. (2011). Correlation between molecular absorption spectral slope ratios and fluorescence humification indices in characterizing CDOM. *Aquat. Sci.* 73, 103–112. doi:10.1007/s00027-010-0164-5

Chen, W., Westerhoff, P., Leenheer, J. A., and Booksh, K. (2003). Fluorescence excitation-emission matrix regional integration to quantify spectra for dissolved organic matter. *Environ. Sci. Technol.* 37, 5701–5710. doi:10.1021/es034354c

Chivers, M. R., Turetsky, M. R., Waddington, J. M., Harden, J. W., and McGuire, A. D. (2009). Effects of experimental water table and temperature manipulations on ecosystem CO2 fluxes in an Alaskan rich fen. *Ecosystems* 12, 1329–1342. doi:10.1007/s10021-009-9292-y

Churchill, A. C., Turetsky, M. R., McGuire, A. D., and Hollingsworth, T. N. (2015). Response of plant community structure and primary productivity to experimental drought and flooding in an Alaskan fen. *Can. J. For. Res.* 45, 185–193. doi:10.1139/cjfr-2014-0100

Cory, R. M., and Kaplan, L. A. (2012). Biological lability of streamwater fluorescent dissolved organic matter. *Limnol. Oceanogr.* 57 (5), 1347–1360. doi:10.4319/lo.2012.57.5.1347

DeColibus, D. T., Rober, A. R., Sampson, A. M., Shurzinske, A., Walls, J. T., Turetsky, M. R., et al. (2017). Legacy effects of drought alters the aquatic food web of a northern boreal peatland. *Freshw. Biol.* 62, 1377–1388. doi:10.1111/fwb.12950

Euskirchen, E. S., Bennett, A., Breen, A. L., Genet, H., Lindgren, M., Kurkowski, T., et al. (2016). Consequences of changes in vegetation and snow cover for climate feedbacks in Alaska and northwest Canada. *Environ. Res. Lett.* 11 (10, 105003. doi:10.1088/1748-9326/11/10/105003

Euskirchen, E. S., Kane, E. S., Edgar, C. W., and Turetsky, M. R. (2020). When the source of flooding matters: divergent responses in carbon fluxes in an alaskan rich fen to two types of inundation. *Ecosystems* 23, 1138–1153. doi:10.1007/s10021-019-00460-z

Fellman, J. B., Hood, E., and Spencer, R. G. M. (2010). Fluorescence spectroscopy opens new windows into dissolved organic matter dynamics in freshwater ecosystems: a review. *Limnol. Oceanogr.* 55 (6), 2452–2462. doi:10.4319/lo.2010.55.6.2452

Ford, J., and Bedford, B. L. (1987). The hydrology of Alaskan wetlands, United States: a review. *Arctic Antarct. Alpine Res.* 19 (3), 209–229. doi:10.1080/00040851.1987.12002596

Frey, K. E., Sobczak, W. V., Mann, P. J., and Holmes, R. M. (2016). Optical properties and bioavailability of dissolved organic matter along a flow-path continuum from soil pore waters to the Kolyma River mainstem, East Siberia. *Biogeosciences* 13, 2279–2290. doi:10.5194/bg-13-2279-2016

Goldsborough, L. G., and Robinson, G. G. C. (1996). "Pattern in wetlands," in *Algal Ecology: freshwater benthic ecosystems*. Editors R. J. Stevenson, M. L. Bothwell, and R. L. Lowe (New York, NY: Academic Press), 77–117.

Goldstein, A., Turner, W. R., Spawn, S. A., Anderson-Teixeira, K. J., Cook-Patton, S., Fargione, J., et al. (2020). Protecting irrecoverable carbon in Earth's ecosystems, *Nat. Cli. Change* 10, 287–295. doi:10.1038/s41558-020-0738-8

Helms, J. R., Stubbins, A., Ritchie, J. D., Minor, E. C., Kieber, D. J., and Mopper, K. (2008). Absorption spectral slopes and slope ratios as indicators of molecular weight, source, and photobleaching of chromophoric dissolved organic matter. *Limnol. Oceanogr.* 53 (3), 955–969. doi:10.4319/lo.2008.53.3.0955

Herns, P. J., Bergamaschi, B. A., Eckard, R. S., and Spencer, R. G. M. (2009). Fluorescence-based proxies for lignin in freshwater dissolved organic matter. *J. Geophys. Res.* 114, G00F03. doi:10.1029/2009JG000938

Herzsprung, P., Osterloh, K., von Tümpling, W., Harir, M., Hertkorn, N., Schmitt-Kopplin, P., et al. (2017). Differences in DOM of rewetted and natural peatlands—Results from high-field FT-ICR-MS and bulk optical parameters. *Sci. Total Environ.* 586, 770–781. doi:10.1016/j.scitotenv.2017.02.054

Hopkins, D. M., Karlstrom, T. N. V., Black, R. F., Williams, J. R., Pewe, T. L., Fernold, A. T., et al. (1955). Permafrost and ground water in Alaska. *U. S. Geol. Surv. Prof. Pap.* 264-F, 113–130.

Jorgenson, M. T., Racine, C. H., Walters, J. C., and Osterkamp, T. E. (2001). Permafrost degradation and ecological changes associated with a warming climate in central Alaska. *Climatic Change* 48, 551–579. doi:10.1023/A:1005667424292

Kane, E. S., Turetsky, M. R., Harden, J. W., McGuire, A. D., and Waddington, J. M. (2010). Seasonal ice and hydrologic controls on dissolved organic carbon and nitrogen concentrations in a boreal-rich fen. *J. Geophys. Res.* 115, G04012. doi:10.1029/2010JG001366

Kolka, R., Trettin, C., Tang, W., Krauss, K., Bansal, S., Drexler, J., et al. (2018). "Chapter 13: Terrestrial wetlands," in *Second state of the carbon cycle report (SOCCR2): a sustained assessment report*. Editors N. Cavallaro, G. Shrestha, R. Birdsey, M. A. Mayes, R. G. Najjar, S. C. Reed, et al. (Washington, DC: Z. U.S. Global Change Research Program), 507–567. doi:10.7930/SOCCR2.2018.Ch13

Lara, M. J., Genet, H., McGuire, A. D., Euskirchen, E. S., Zhang, Y., Brown, D., et al. (2016). Thermokarst rates intensify due to climate change and forest fragmentation in an Alaskan boreal forest lowland. *Global Change Biol.* 22, 816–829. doi:10.1111/gcb.13124

Lawaetz, A. J., and Stedmon, C. (2009). Fluorescence intensity calibration using the Raman scatter peak of water. *Appl. Spectrosc.* 63 (8), 936–940. doi:10.1366/000370209788964548

Lougheed, V. L., Butler, M. G., McEwen, D. C., and Hobbie, J. E. (2011). Changes in Tundra pond limnology: re-sampling Alaskan ponds after 40 years. *Ambio* 40 (6), 589–599. doi:10.1007/s13280-011-0165-1

Lougheed, V. L., Hernandez, C., Andresen, C. G., Miller, N. A., Alexander, V., and Prentki, R. (2015). Contrasting responses of phytoplankton and benthic algae to recent nutrient enrichment in Arctic tundra ponds. *Freshw. Biol.* 60, 2169–2186. doi:10.1111/fwb.12644

Maie, N., Scully, N. M., Pisani, O., and Jaffé, R. (2007). Composition of a protein-like fluorophore of dissolved organic matter in coastal wetland and estuarine ecosystems. *Water Res.* 41, 563–570. doi:10.1016/j.watres.2006.11.006

Mangiafico, S. (2018). *Package "rcompanion": functions to support extension education program evaluation*. CRAN R Project. . Available at:

McPartland, M. Y., Kane, E. S., Falkowski, M. J., Kolka, R., Turetsky, M. R., Palik, B., et al. (2019). The response of boreal peatland community composition and NDVI to hydrologic change, warming, and elevated carbon dioxide. *Global Change Biol.* 25, 93–107. doi:10.1111/gcb.14465

Ohno, T. (2002). Comment on "Fluorescence inner-filtering correction for determining the humification index of dissolved organic matter". *Environ. Sci. Technol.* 36 (4), 4195–4196. doi:10.1021/es0155276

Olefeldt, D., Euskirchen, E. S., Harden, J., Kane, E., McGuire, A. D., Waldrop, M., et al. (2017). Greenhouse gas fluxes and their cumulative response to inter-annual variability and experimental manipulation of the water table position in a boreal fen. *Global Change Biol.* 23, 2428–2440. doi:10.1111/gcb.13612

R Core Development Team (2017). *R: a language and environment for statistical computing*. Vienna, Austria: R Foundation for Statistical Computing.

Rupp, D. R., Kane, E. S., Dieleman, C., Keller, J. K., and Turetsky, M. R. (2019). Plant functional group effects on peat carbon cycling in a boreal rich fen. *Biogeochemistry* 144, 305–327. doi:10.1007/s10533-019-00590-5

Stedmon, C. A., and Bro, R. (2008). Characterizing dissolved organic matter fluorescence with parallel factor analysis: a tutorial. *Limnol. Oceanogr.* 6 (11), 572–579. doi:10.4319/lom.2008.6.572

Stewart, B. C., Kunkel, K. E., Stevens, L. E., Sun, L., and Walsch, J. E. (2013). NOAA technical report NESDIS 142-4. Regional climate trends and scenarios for the United States national climate assessment. Available at: www.nesdis.noaa.gov/content/technical-reports (Accessed January, 2021).

Strack, M., Waddington, J. M., Bourbonniere, R. A., Buckton, E. L., Shaw, K., Whittington, P., et al. (2008). Effect of water table drawdown on peatland dissolved organic carbon export and dynamics. *Hydrol. Process.* 22, 3373–3385. doi:10.1002/hyp.6931

Strack, M., Waddington, J. M., Lucchese, M. C., and Cagampan, J. P. (2009). Moisture controls on CO2 exchange in a Sphagnum-dominated peatland: results from an extreme drought field Experiment. *Ecohydrology* 2, 454–461. doi:10.1002/eco.68

Strack, M., and Waddington, J. M. (2007). Response of peatland carbon dioxide and methane fluxes to a water table drawdown experiment. *Global Biogeochem. Cycles* 21, GB1007. doi:10.1029/2006GB002715

Stubbins, A., Lapierre, J. F., Berggren, M., Prairie, Y. T., Dittmar, T., and del Giorgio, P. A. (2014). What's in an EEM? Molecular signatures associated with dissolved organic fluorescence in boreal Canada. *Environ. Sci. Technol.* 48, 10598–10606. doi:10.1021/es502086e

Tfaily, M. M., Wilson, R. M., Cooper, W. T., Kostka, J. E., Hanson, P., and Chanton, J. P. (2018). Vertical stratification of peat pore water dissolved organic matter composition in a peat bog in northern Minnesota. *J. Geophys. Res.: Biogeosciences* 123, 479–494. doi:10.1002/2017JG004007

Turetsky, M. R., Kotowska, A., Bubier, J., Dise, N. B., Crill, P., Hornibrook, E. R., et al. (2014). A synthesis of methane emissions from 71 northern, temperate, and subtropical wetlands. *Global Change Biol.* 20 (7), 2183–2197. doi:10.1111/gcb.12580

Turetsky, M. R., Treat, C. C., Waldrop, M. P., Waddington, J. M., Harden, J. W., and McGuire, A. D. (2008). Short-term response of methane fluxes and methanogen activity to water table and soil warming manipulations in an Alaskan peatland. *J. Geophys. Res.* 113, G00A10. doi:10.1029/2007jg000496

Veverica, T. J., Kane, E. S., Marcarelli, A. M., and Green, S. A. (2016). Ionic liquid extraction unveils previously occluded humic-bound iron in peat soil pore water. *Soil Sci. Soc. Am. J.* 80 (3), 771–782. doi:10.2136/sssaj2015.10.0377

Vitt, D. H., Halsey, L. A., Bauer, I. E., and Campbell, C. (2000). Spatial and temporal trends of carbon sequestration in peatlands of continental western Canada through the Holocene, *Can. J. Earth Sci.* 37, 683–693. doi:10.1139/cjes-37-5-683

Weltzin, J., Bridgham, S., Pastor, J., Chen, J. M., and Harth, C. (2003). Potential effects of warming and drying on peatland plant community composition. *Global Change Biol.* 9 (2), 141–151. doi:10.1046/j.1365-2486.2003.00571.x

Wilske, C., Herzsprung, P., Lechtenfeld, O. J., Kamjunke, N., and von Tumpling, W. (2020). Photochemically induced changes of dissolved organic matter in a humic-rich and forested stream. *Water* 12 (2), 331. doi:10.3390/w12020331

Wyatt, K. H., Turetsky, M. R., Rober, A. R., Giroldo, D., Kane, E. S., and Stevenson, R. J. (2012). Contributions of algae to GPP and DOC production in an Alaskan fen: Effects of historical water table manipulations on ecosystem responses to a natural flood. *Oecologia* 169 (3), 821–832. doi:10.1007/s00442-011-2233-4

Wyatt, K. H., and Rober, A. R. (2020). Warming enhances the stimulatory effect of algal exudates on dissolved organic carbon decomposition. *Freshw. Biol.* 65, 1288–1297. doi:10.1111/fwb.13390

Wyatt, K. H., Seballos, R. C., Shoemaker, M. N., Brown, S. P., Chandra, S., Kuehn, K. A., et al. (2019). Resource constraints highlight complex microbial interactions during lake biofilm development. *J. Ecol.* 107, 2737–2746. doi:10.1111/1365-2745.13223

Wyatt, K. H., and Turetsky, M. R. (2015). Algae alleviate carbon limitation of heterotrophic bacteria in a boreal peatland. *J. Ecol.* 103, 1165–1171. doi:10.1111/1365-2745.12455

Zsolnay, A., Baigar, E., Jimenez, M., Steinweg, B., and Saccomandi, F. (1999). Differentiating with fluorescence spectroscopy the sources of dissolved organic matter in soils subjected to drying. *Chemosphere* 38, 45–50. doi:10.1016/s0045-6535(98)00166-0

Zsolnay, A. (2002). Comment on "Fluorescence inner-filtering correction for determining the humification index of dissolved organic matter". *Environ. Sci. Technol.* 36 (19), 4195–4195.

Conflict of Interest: The authors declare that the research was conducted in the absence of any commercial or financial relationships that could be construed as a potential conflict of interest.

frontiers in Earth Science

ORIGINAL RESEARCH
published: 08 February 2021
doi: 10.3389/feart.2021.590103

Soil Organic Matter, Soil Structure, and Bacterial Community Structure in a Post-Agricultural Landscape

Joseph B. Yavitt[1], Gwendolyn T. Pipes[1], Emily C. Olmos[1], Jiangbo Zhang[2] and James P. Shapleigh[3]*

[1]Department of Natural Resources, Cornell University, Ithaca, NY, United States, [2]College of Life Science, Northwest A and F University, Yangling, China, [3]Department of Microbiology, Cornell University, Ithaca, NY, United States

Converting forest and wetland landscapes to agriculture has shown to result in a loss of organic matter, structure, and microbial diversity in the converted soil but recovery of post-agricultural soils remains poorly understood. Here we coupled landscape-scale surveys of soil 1) carbon and nitrogen levels, 2) aggregation, and 3) bacterial metagenomes to investigate soil recovery after 30 years in sites with soils ranging from well drained to poorly drained. Sites with no evidence of past agriculture (Reference) served as recovery endpoints. A secondary aim evaluated the role of nitrogen-fixing symbiosis, here associated with alder (*Alnus incana*) trees, in soil restoration. Soil carbon levels in restored sites (3.5%) were comparable to levels in a present-day farm (3.4%) but much lower than in Reference sites (>7.3%). The same trend occurred with soil nitrogen levels. Sites with alder trees had more acidic soil pH values. Alder trees promoted soil structure with macroaggregates being the largest fraction of bulk soil (75%). Natural abundance of stable nitrogen isotopes suggested extensive decay of organic matter within aggregates. Comparison of total reads from the soil metagenomes indicated the bacterial community in restored sites were more comparable to the present-day farm than Reference sites, except for a well-drained soil with alder. Dissimilarity among sites in terms of gene abundances in soil bacterial community occurred in carbon metabolism, membrane transport, and genetic repair pathways. Soil recovery in post-agricultural landscapes is slow when agriculture caused a large loss of soil organic matter, as is the case in our study, and when the soil bacterial community structure changed markedly, as it did in our study. However, fairly rapid recovery of soil structure, as we noted in our study, is promising, and now we need a better understanding of plant species that improve soil structure for restoration of both well-drained and poorly drained soils.

Keywords: natural abundance stable isotopes, New York State, restoration, shotgun metagenomics, soil aggregates, wetlands

KEY POINTS

- Bulk soils in both well-drained and poorly drained (wetland) sites showed no increase in organic matter with 30 years post-agricultural recovery.
- Soil structure, measured by aggregation, was promoted by alder trees established in both restored and natural sites.

OPEN ACCESS

Edited by:
Matthias Peichl, Swedish University of Agricultural Sciences, Sweden

Reviewed by:
Ember Morrissey, West Virginia University, United States
Christopher Craft, Indiana University, United States
Manqiang Liu, Nanjing Agricultural University, China

****Correspondence:***
Joseph B. Yavitt
jby1@cornell.edu

Specialty section:
This article was submitted to Biogeoscience, a section of the journal Frontiers in Earth Science

Received: *31 July 2020*
Accepted: *07 January 2021*
Published: *08 February 2021*

Citation:
Yavitt JB, Pipes GT, Olmos EC, Zhang J and Shapleigh JP (2021) Soil Organic Matter, Soil Structure, and Bacterial Community Structure in a Post-Agricultural Landscape. Front. Earth Sci. 9:590103. doi: 10.3389/feart.2021.590103

- Microbial functions, measured as gene abundance, distinguished between sites with well-drained soils and poorly drained soils, but only an upland site with alder trees had more similar values to a natural site than the present-day farm.

INTRODUCTION

Agriculture covers 38% of Earth's land surface with much of it on land that naturally supports forests and wetlands. However, converting forests and wetlands to agriculture often initiates a downward spiral in soil conditions (Kuzyakov and Zamanian, 2019). When drastic enough, agricultural production drops or fails altogether forcing abandonment. While many studies examine recovery of forest and wetland plant communities in post-agricultural landscapes (cf., Flinn and Vellend, 2005), a crucial uncertainty concerns how concomitant soils reclaim their natural conditions (Lal, 2015).

Although many studies have addressed individual mechanisms and specific drivers of soil degradation (cf., Bunemann et al., 2018), there are still no standards and comprehensive ways to differentiate between stages of degradation. Nonetheless, degraded soils experience to some degree: 1) loss of soil organic matter, 2) deterioration of soil structure, 3) scant or excessive levels of nutrients, and 4) altered microbial diversity and activity (Carter, 2002). The reclamation of each is still a matter of conjecture.

For example, the stock of soil organic matter represents the long-term balance between input of plant residue to the soil and decomposition of that residue by soil microorganisms. Agriculture has been shown to upset this balance, largely by increasing the rate of organic matter decomposition (Magdoff and Weil, 2004). One way that organic matter escapes microbial decomposers is by stabilization on the surfaces of soil minerals that are occluded within soil aggregates (Six et al., 2000; Lehmann et al., 2020). Tillage is especially destructive to soil aggregation and facilitates microbial access to organic matter. Thus, recovery of soil organic matter is linked to improved soil structure that restores the balance between inputs and decomposition of plant residue (Six et al., 2000).

A wide variety of approaches has been used to examine soil microorganisms, mostly in terms of community composition, diversity, and assembly mechanisms (Nemergut et al., 2013; Fierer, 2017). Yet additional information exists in the relative abundance of genes that soil microorganisms have and use, i.e., the soil metagenome. Although we know that genes alone do not determine microbial activity per se (Jansson and Hofmockel, 2018), we still expect a larger suite of genes to process plant residue that has a diverse biochemical composition or when nutrient fertilizers have been added compared to a uniform plant residue and nutrient poor soils (cf., Castañeda and Barbosa, 2017; Hermans et al., 2020).

Successful recovery of degraded soil also depends on knowing the endpoint that restoration is expected to achieve. When agriculture occurs on a landscape composed of different habitats, knowing the recovery endpoint can be complicated (Crews and Rumsey, 2017). For example, in many forested landscapes in temperate regions, the predominant forest established on mostly well-drained soil often also includes wet habitats with poorly drained soil. These wet habitats include permanent and seasonal pools, glades, stream-sides (riparian), and wetland marshes and swamps (Flinn et al., 2008; Cohen et al., 2016). Having comparable vestiges removes some of the uncertainty in the recovery endpoint. However, when agriculture is extensive and no natural sites exist, it is best to have more than one recovery endpoint for comparison with the restored site (Aronson et al., 1995).

The work described here is a survey of soil conditions in a post-agricultural landscape in central New York State. The landscape was originally upland forest with embedded wetlands that was converted to agriculture for ~70 years and then abandoned in the mid-1980s. Not long after agriculture ceased a restoration effort was undertaken. Natural stream flow across the site was restored. One portion of the study area (described below) was maintained as an old field dominated by herbaceous plants (Stover and Marks, 1998), whereas the other portion had more advanced succession and was dominated by speckled alder (*Alnus incana*) trees. Roots of alder are associated with soil microorganisms that 'fix' atmospheric nitrogen into a bioavailable form (Hurd et al., 2001), thereby adding nutrient nitrogen to the soil (Preem et al., 2012). This land use history is common in the region (Flinn and Vellend, 2005).

We focused on three soil parameters: 1) quantifying carbon and nitrogen in 11 sites including those with current agriculture (Farm), sites in the processes of recovery from agriculture (Restored), and sites with no previous agriculture (Reference); 2) measuring soil aggregation and aggregate stability in a subset of these soils; and 3) characterizing metagenomes to measure microbial gene abundances in the full suite of soils. We expected slow recovery of soil organic matter, in particular, if loss during agriculture created a large difference in levels between the Farm and Reference sites. We expected more rapid recovery of soil structure, which is promoted differently by different plant species (Scott, 1998) but especially by alder trees (Graf and Frei, 2013). Finally, although soil microorganisms have fast growth, we expected persistent legacy of agriculture on bacterial community structure as has been seen in the region (Hudgens and Yavitt, 1997).

MATERIALS AND METHODS

Study Site and Experimental Design

The research was conducted in central New York State. The region has a humid, continental climate with a mean monthly temperature of −4°C in January and 22°C in July. The mean frost-free season is 146 days, and mean annual precipitation is 890 mm, including 171 cm of snow. The vegetation falls into the Allegheny section of E. L. Braun's (in Dyer, 2006) hemlock–white pine–northern hardwoods region. Mesic, upland forests are dominated by sugar maple (*Acer saccharum*) and American beech (*Fagus grandifolia*).

The region lies on the glaciated Allegheny Plateau. Topography is a relatively flat plain at 300 to 450 m above sea

level. About 90% of the bedrock is overlain by glacial till of variable thickness and composition. Gravelly or sandy outwash and terraces of ice-contact stratified drift characterize the lowest lying land along streams and account for the remaining 10% of the landscape. Nearly all of the abandoned farmland is underlain by glacial till with low to medium carbonate content, whereas till with a great carbonate content are still in production. Our upland sites have coarse-loamy, well-drained soils formed from medium-lime tills and classified as Typic Dystrudepts. Our lowland sites have fine-loamy, poorly drained soils formed in low-to medium-lime till and classified as Aeric Fragiaquepts.

We established 11 study sites in total. Seven sites were within the Goetchius Wetland Preserve (42°23′18.114″N 76°18′1.9188″W). Here we established two sites in primary forest (Reference Upland) that had never been used for agriculture, as indicated by the pit and mound topography across the surface soil. Plowing levels this microtopography, which is not regained until mature trees, >100 years old begin to fall (Flinn and Marks, 2007). A portion of the Reference Upland has beech-maple forest with alder trees and was designated Reference Upland + alder and another portion has the beech-maple forest but no alder trees and was designated Reference Upland - alder. A third site was an active farm (Farm), the only one on the Preserve. Agriculture management on the Farm consists of 3-years continuous planting of corn followed by 3-years of perennial forage, alfalfa (*Medicago sativa*) plus reed canarygrass (*Phalaris arundinacea*). We sampled in the third year of the forage production. The fourth and fifth sites have relatively well-drained soil in which tillage ceased in 1989. A portion dominated by old-field, herbaceous plants was designated Restored Upland–alder, and a second old field with alder trees was designated Restored Upland + alder. The remaining two sites at Goetchius were associated with a small stream that cut across the site that had been diverted during the period of agriculture with natural flow restored in 1989. This area has poorly drained soil. One portion was dominated by cattails (*Typha latifolia*) and sedges (*Carex* sp.) growing in about 25 cm of open water and was designated Restored Wetland-alder, whereas the other has cattails and sedges with alder trees and was designated Restored Wetland + alder.

Since no Reference Wetlands occur in the Goetchius site, we used two other locations in the same region as references. One location was the Dorothy McIlroy Bird Sanctuary (42°40′09.9912″N 76°17′24.0792″W), which is the headwater of Fall Creek at the outlet of Lake Como. The wetland is a hummocky, streamside fen, dominated by sedges. One portion has sedges with the nitrogen-fixing shrub sweet gale (*Myrica gale*; Schwintzer, 1979) and was designated Reference Streamside Wetland + Myrica. A second portion has sedges but no Myrica and was designated Reference Streamside Wetland - Myrica. A second location was the headwater of Michigan Creek at the outlet of Jennings Pond (42°19′41.5128″N 76°28′41.0952″W). This wetland is a marshy, sedge fen (Bernard and Solsky, 1977), dominated by a dense cover of lake sedge (*Carex lacustris*). One portion has sedges with scattered alder trees and was designated Reference Depressional Wetland + alder, whereas a second portion has sedges with no alder trees and was designated Reference Depressional Wetland-alder. Soil in the depressional wetland is 1-m deep peat soil, whereas soil in the streamside wetland is mostly clay with no peat accumulation. Although no peat soil occurs in the Goetchius study site, we included the depressional location because this wetland type is common in the region (Ballantine and Schneider, 2009). Also, agricultural on peat soils is known to result in complete loss of the peat (Welsch and Yavitt, 2007).

Study 1: Bulk Soil

In each of the 11 study sites, we established three locations to collect soils. The locations were determined at random from a numbered x-y grid over a map of the site and a random number generator. At each sample location we collected 100 g of soil from three points (0 to 10-cm depth interval) that were combined to make a composite sample for a total of 33 samples. We measured moisture content gravimetrically on fresh portions of each soil, collected in early spring, i.e., the wettest time of the year. Other portions were air-dried before extracting available cations and phosphorus using the Mehlich III extractant solution (Mehlich, 1984): elemental analysis was done using atomic emission–inductively coupled plasma (AE–ICP) spectroscopy at Cornell University Laboratories.

Study 2: Soil Structure

We characterized the distribution of soil mass, carbon, and nitrogen in hierarchical aggregates from nine sites in the study area. We excluded peat soils from the Reference Wetland +/− alder, given the organic nature of the soil. Soil aggregates were fractionated by wet sieving of an air-dried portion (ca. 25 g) of the <2 mm fraction of soil following the scheme in Elliott (1986). Briefly, soil was spread evenly on a sieve with an opening of >250 μm, the sieve was immersed in water for 5 min (slaking). The sieve was then moved up and down at a rate of 50 strokes in 2 min. Floatable material was decanted and saved (designated free POM; fPOM) since it was part of the <2 mm fraction. Material that passed through the 250-μm sieve was allowed to collect on or pass through a sieve with an opening of 53 μm. The three fractions were washed into pre-weighed pans, i.e., macroaggregates (>250 μm), free microaggregates (53–250 μm), and free < 53 μM (silt and clay) fraction which were then oven-dried at 60°C.

A subsample of the macroaggregate fraction was further separated. Briefly, 15 g of oven-dried macroaggregates were slaked in deionized water for 5 min. These samples were then gently shaken with 50 stainless-steel bearings (4 mm dia.) while submerged on top of a 250-μm sieve until all macroaggregates were broken. A continuous stream of water flushed the <250 μm material through the mesh in order to avoid the disruption of occluded microaggregates released from the macroaggregates. Further sieving of the <250 μm fraction through a 53 μm sieve resulted in three size fractions isolated from the macroaggregates, i.e., occluded POM (>250 μm), occluded microaggregates (53–250 μm) and occluded <53 μm (silt and clay). Each of these fractions was rinsed into pre-weighed aluminum pans, oven-dried at 60°C.

Soil carbon and nitrogen concentration and isotopic composition were measured at the Cornell Stable Isotope Laboratory in Ithaca, NY, using a Finnigan MAT Delta Plus mass spectrometer following combustion with an elemental

analyzer (Carlo Erba NC2500; Thermo Finnigan, San Jose, CA, United States).

Study 3: Soil Metagenomics

We used soil from all 11 sites to assess environmental metagenomics. DNA was extracted using the MoBio PowerSoil DNA Isolation Kit following the manufacturer's protocol. Triplicate DNA extractions from the same soil core were combined to account for inner-core variability and to ensure sufficient DNA for sequencing. This was done for each of the three samples from the 11 sites, yielding a total of 33 DNA samples for sequencing. The DNA was sequenced at the Cornell University Institute of Biotechnology and was carried out using the NextSeq500 platform yielding 150 base long, single end reads.

Quality control was carried out using tools available at kbase (Arkin et al., 2018). Trimming of adapters and read quality assessment was carried out using trimmomatic using the kbase default settings (Bolger et al., 2014). Sample quality was then assessed using FastQC (Andrews, 2010), with default settings.

Sample dissimilarity analysis was performed using Mash with default settings on all reads. Mash utilizes a shared k-mer-based approach to compare sample read profiles and generate pairwise dissimilarity measures (Ondov et al., 2016). Sequence comparisons to identify reads derived from N-oxide genes were done using DIAMOND (Buchfink et al., 2015). For DIAMOND, sequence reads were used as a query in a blastx analysis against custom N-oxide protein data sets obtained from sequenced genomes available at JGI IMG. The maximum e-value for DIAMOND was set to 1×10^{-3} and downstream filtering limited alignments to those with a sequence identity of ≥60% and a contiguous match length of ≥25 amino acids. All reported read abundances are scaled to reads per million total reads to account for differing sequencing depths. Details are given in Nadeau et al. (2019).

Functional analysis of the metagenomic reads was determined using an open-sourced, stand-alone pipeline FMAP (Kim et al., 2016). Gene sequences were mapped to Kyoto Encyclopedia of Genes and Genomes (KEGG) Orthologies (KOs) database (Kanehisa et al., 2007, 2016) and were binned into pathways and modules. Default settings in FMAP were used to identify reads and to assign enrichment significance in the log2 (fold change) in the normalized read occurrence in comparisons of the triplicate samples between particular sites. In default mode differential abundances are determined using the Kruskal-Wallis rank-sum tests with normalization done using reads per kilobase per million.

Data Analyses

The preceding techniques produced three data sets: 1) carbon, nitrogen, pH and water content of bulk soil; 2) distribution of bulk soil among aggregate fractions; and, 3) gene abundances. We subjected all to simple exploratory analysis, calculating means +standard error (S.E., N = 3).

Site differences were evaluated with one-way Analysis of Variance (ANOVA). The low statistical power in the experimental design main effects (n = 11 sites; n = 2 +/− nitrogen fixers; n = 3 land use; n = 2 soil types) and interactions constrained our ability to draw real biological inferences with a full factorial ANOVA. Furthermore, the unbalanced experimental design with the present-day Farm, made it difficult to determine if non-significant results were caused by a true lack of differences or simply an artifact of sample size. Also, we follow the suggestion of Amrhein et al. (2019) and report means, estimates of variation, sample size, and p-values.

We used a repeated-measures ANOVA to evaluate how the aggregate fractions of soil varied across nine sites. A repeated measures design is the appropriate test because aggregate fractions are not independent of each other.

Differential responses by soils to the presence of nitrogen-fixing plants were assessed using Cohen's d effect sizes (Nakagawa and Cuthill, 2007). Cohen's d standardizes the direction and magnitude of the response by comparing where nitrogen-fixing plants (+ fixer) are present to the paired site with no fixer (− fixer). The units of d are Standard Deviations of the effect, and the effect is taken as statistically significantly different when the 95% confidence interval of d does not cross zero. This test is considered more informative than the t-test for paired comparisons, which provides only a dichotomous decision of significantly different, or not. The effect size test gives additional information on the magnitude of the difference (Sullivan and Feinn, 2012).

To examine the direct relationships, we calculated correlations among all pairs of variables in the data set. We examined both linear (Pearson r) and non-linear (Spearman rank rho) relationships. The large number of pairwise comparisons increased the likelihood of Type II errors (false negatives), and thus we used a Bonferroni correction (significance level P, times the number of variables, divided by the number of pairwise comparisons). This increased the confidence in positive findings at the cost of disregarding weaker correlations.

We did not employ higher-level multivariate statistical analysis for relationships among the data sets because assign variables to be dependent upon other variables could lead to spurious conclusions. Specifically, we now know there are feedbacks among soil organic matter, soil structure, and microbial community structure (Neal et al., 2020). For example, microbial community structure could depend upon soil organic matter and soil structure, whereas organic matter and soil structure could depend upon the soil microbial community involved in soil development. Therefore, correlation avoids spurious relationships.

Given the large number of genes in the metagenomic data set, we attempted to reduce the number of pairwise comparisons. To do this we relied on the KEGG database for orthhology and pathways (see below).

RESULTS

Study 1: Bulk Soils

Concentrations of carbon and nitrogen in bulk soils varied significantly across the 11 sites (**Table 1**). However, values in soils from both the Restored Upland and Restored Wetland sites

TABLE 1 | Carbon and nitrogen concentrations and pH of soils from the 11 sites investigated in this study.

	Carbon (g kg^{-1})	Nitrogen (g kg^{-1})	pH standard unit	Water content (% dry soil)
Farm	34.4 ± 1.0	3.2 ± 0.1	4.65	72 ± 4
Restored Upland				
– alder	31.2 ± 4.4	2.7 ± 0.4	4.88	63 ± 9
+ alder	27.1 ± 3.6	2.2 ± 0.2	4.12	66 ± 9
Reference Upland				
– alder	71.5 ± 18.6	5.2 ± 1.3	4.00	105 ± 17
+ alder	72.9 ± 24.1	5.3 ± 1.8	5.21	122 ± 35
Restored Wetland				
– alder	39.1 + 7.0	3.0 ± 0.5	5.13	71 ± 9
+ alder	43.4 ± 10.0	3.5 ± 0.2	5.05	84 ± 12
Reference Streamside Wetland				
– Myrica	126.8 ± 20.6	6.2 ± 1.1	5.03	213 ± 7
+ Myrica	66.1 ± 4.5	4.4 ± 0.2	4.85	128 ± 26
Reference Depressional Wetland				
– alder	354.2 ± 10.1	22.5 ± 0.4	5.17	1,052 ± 91
+ alder	158.4 ± 7.1	10.8 ± 0.5	4.92	359 ± 42
ANOVA $F_{10,32}$ =	56.25	63.04	10.11	73.94
p	<0.001	<0.001	<0.001	<0.001

Values are mean and one standard error from the mean. Sample size = 3; 0–10 cm depth interval.

TABLE 2 | Standardized mean effect sizes Cohen's *d* and 95% confidence intervals (CI) for the influence of nitrogen-fixing plants in five location on bulk soil carbon, nitrogen, and pH.

Location	Carbon	Nitrogen	pH
Restored Upland	**0.72 [0.26, 1.17]**	**0.97 [0.93, 1.00]**	**1.43 [1.07, 1.79]**
Reference Upland	–0.47 [–2.48, 2.39]	–0.43 [–0.22, 0.13]	**–2.86 [–3.03, –2.68]**
Restored Wetland	**–0.62 [–1.18, –0.05]**	**–0.93 [–0.97, –0.89]**	**0.25 [0.02, 0.51]**
Reference Streamside Wet.	**2.88 [1.19, 4.57]**	**1.65 [1.56, 1.74]**	0.31 [–0.14, 0.77]
Reference Depressional Wet.	**15.8 [14.8, 16.8]**	**18.9 [18.7, 19.0]**	0.32 [–0.29, 0.94]

Bold indicates a significant effect of nitrogen-fixing alder or Myrica. Positive values indicate lower concentrations or pH in the presence of nitrogen fixers; negative values indicate greater values. 0–10 cm soil depth interval.

were statistically similar to values in soils in the Farm (Ps > 0.05). In comparison, concentrations of carbon and nitrogen in soils from the Restored Upland sites were about 50% of the values in soils from the Reference Upland. Likewise, soils in the Restored Wetlands had significantly lower concentrations of carbon and nitrogen than soils in the Reference Wetlands.

Nitrogen-fixing plants had a significant effect on carbon and nitrogen in bulk soils for all of the pairs of sites, except for the Reference Upland (**Table 2**). Positive values for Cohen's *d* in **Table 2** indicate lower concentrations of carbon and nitrogen associated with nitrogen fixers, and thus the negative value in the Restored Wetland indicates that nitrogen-fixing alder enhanced concentrations of carbon and nitrogen in the bulk soils. Soil pH values ranged from about 4.00 to 5.21 with more acidic values associated with nitrogen fixers, except in the Reference Forest which had the highest pH among the soils measured. In the Reference wetlands, saturated soil water content was much less in sites with nitrogen fixers compared to paired sites without fixers.

Study 2: Soil Aggregates

The proportion of bulk soil in the four (free) aggregate fractions (**Table 3**) varied significantly across nine sites (repeated-measures ANOVA $F_{3,78} = 13.55$, $p < 0.0001$). Macroaggregates were the largest fraction in soil from the present-day Farm, followed by free microaggregates then free <53 μm size class. In the other sites macroaggregates also were the largest fraction but its proportion was significantly greater in soils with nitrogen-fixing plants. Without nitrogen fixers, macroaggregates were generally <50% of the bulk soil and free microaggregates and the < 53 μm size were about 2-times more abundant compared to the paired site with alder trees.

However, for the distribution of soil mass among the three fractions (occluded) within macroaggregates (**Table 4**), the analysis did not show a significant difference among sites (repeated-measures ANOVA $F_{2,52} = 0.33$, $p = 0.7194$). Yet a few patterns were evident. In the Restored Upland and Restored Wetland sites occluded microaggregates and the occluded <53 μm size class were about equal proportions in each site with values of about 15% each to 45% each. In contrast, in the Reference Upland and Reference Wetland sites, the occluded microaggregate fraction was larger than the occluded <53 μm size class.

For most of the aggregate fractions, concentrations of carbon and nitrogen as well as the natural abundance of their stable

TABLE 3 | Distribution of bulk soil mass in four free fractions of hierarchical aggregates from nine sites investigated in this study.

	Free POM (%)	Macroagg. (%)	Free microagg. (%)	Free <53 μM (%)
Farm	0.4 ± 0.1	71.3 ± 4.1	16.8 ± 1.8	11.5 ± 2.4
Restored Upland				
– alder	0.4 ± 0.1	43.7 ± 2.9	21.2 ± 2.1	34.6 ± 4.1
+ alder	0.6 ± 0.1	75.1 ± 1.4	9.5 ± 0.7	14.9 ± 1.6
Reference Upland				
– alder	1.0 ± 0.2	45.2 ± 5.0	37.4 ± 4.3	16.4 ± 1.0
+ alder	1.9 ± 0.4	74.2 ± 3.0	17.5 ± 1.6	6.3 ± 1.0
Restored Wetland				
– alder	3.5 ± 1.0	53.3 ± 2.6	22.3 ± 1.3	20.9 ± 1.3
+ alder	1.2 ± 0.4	73.3 ± 5.1	11.7 ± 2.5	13. 8 ± 2.9
Reference Depressional Wetland				
– alder	7.3 ± 2.0	56.7 ± 3.5	29.4 ± 1.7	6.4 ± 1.0
+ alder	4.5 ± 1.6	71.0 ± 2.7	13.5 ± 3.2	11.0 ± 1.0

TABLE 4 | Distribution of macroaggregate soil in three occluded fractions (occluded) from nine sites investigated in this study.

	Occluded POM (%)	Occluded microagg (%)	Occluded <53 μM (%)
Farm	15.4 ± 1.3	44.4 ± 2.2	39.7 ± 0.9
Restored Upland			
– alder	69.0 ± 6.9	14.2 ± 2.9	14.6 ± 3.8
+ alder	12.8 v 3.6	36.9 ± 4.6	35.3 ± 16.1
Reference Upland			
– alder	30.5 ± 7.8	44.0 ± 4.7	25.0 ± 2.4
+ alder	51.1 ± 14.2	32.8 ± 11.6	15.8 ± 3.3
Restored Wetland			
– alder	12.0 ± 3.7	39.7 ± 2.5	46.6 ± 1.7
+ alder	5.8 ± 2.2	42.6 ± 4.3	53.7 ± 0.3
Reference Depressional Wetland			
– alder	11.4 ± 10.3	55.7 ± 9.6	32.8 ± 4.2
+ alder	5.7 ± 11.0	56.5 ± 4.9	37.9 ± 3.5

TABLE 5 | Statistical *p* values averaged across nine sites investigated in this study for concentrations of nitrogen and carbon and natural abundance of stable isotopes in different fractions of hierarchical aggregates.

Fraction	Nitrogen	Delta ^{15}N	Carbon	Delta ^{13}C
Free POM	0.5119	**0.0001**	0.1975	0.4900
Free Macroaggregates	0.1156	**<0.0001**	0.0558	**0.0029**
Free microaggregates	**0.0006**	0.0112	**<0.0001**	**0.0004**
Free < 53 μm	0.0158	0.0567	**<0.0001**	**0.0021**
Occluded POM	**0.0027**	**0.0007**	**0.0033**	0.0970
Occluded Microagg.	0.0075	**<0.0001**	**0.0042**	**0.0006**
Occluded <53 μm	**0.0041**	**0.0058**	**0.0004**	**0.0033**

Statistically significant is indicated by bold, indicating site differences in the values.

isotopes varied statistically ($p < 0.0071$ Bonferroni Corrected) across the nine sites (**Table 5**). Across sites, the three occluded fractions accounted for more than 50% of soil carbon and soil nitrogen (**Figure 1**), with the proportion being more pronounced in the Restored sites than in the Reference sites. The distribution of carbon and nitrogen among these three occluded fractions varied considerably, with the occluded microaggregate fraction being the largest in some, but not all cases. Overall, however, more than 50% of the soil carbon and soil nitrogen was associated with free plus occluded microaggregate fractions.

The natural abundance of stable carbon and nitrogen isotopes showed lighter values in free POM than in the free microaggregate and free < 53 μm size class (**Figure 2A**). Notable, however, are enriched values for stable nitrogen isotopes in free POM from the soil from three sites: Farm, Restored Upland - alder, and Restored Wetland -alder. Although values for stable isotopes were more variable across the nine sites for occluded fractions, there was still a trend of heavier values between occluded POM vs. occluded microaggregates and occluded < 53 μm size class, except for stable carbon isotopes in soil from the Restored Upland - alder and Restored Wetland–alder (**Figure 2B**).

Study 3: Soil Metagenomics

A PCA plot based on a comparison of all the metagenomic reads (**Figure 3**) indicated that, with only a few exceptions, sites showed differences along axis one but there was some clustering of sites along axis 2. For example, the Restored Upland + alder site grouped with the Reference Upland along axis 1, whereas the Restored Upland-alder and the two Restored Wetland sites grouped with the Farm soil along axis 2. For the four Reference Wetland sites, the two streamside sites +/− Myrica clustered with each other, but for the Reference Wetland +/− alder the two sites were more dissimilar to each other.

Given the experimental design with sites +/− alder and the impact of added nitrogen, a more focused read analysis was made for the genes involved in denitrification (**Figure 4**). Reads from nitrate reductases, the initial step in denitrification, were in most sites mainly from the respiratory form (Nar) instead of the periplasmic form (Nap). The exceptions were the Restored Upland +/− alder and the Reference Upland-alder where occurrence of reads from both forms were similar. All sites had similar levels of reads assigned to *nap*. There was only limited variation in the occurrence of reads for *nirK*, which encodes the copper-containing nitrite reductase, with the Restored Wetland +/− alder having slightly higher read values than the other sites. Reads from the gene encoding the cd_1-type reductase, *nirS*, were relatively low in all sites and showed limited variation. Reads for the cytochrome *c*-oxidizing nitric oxide

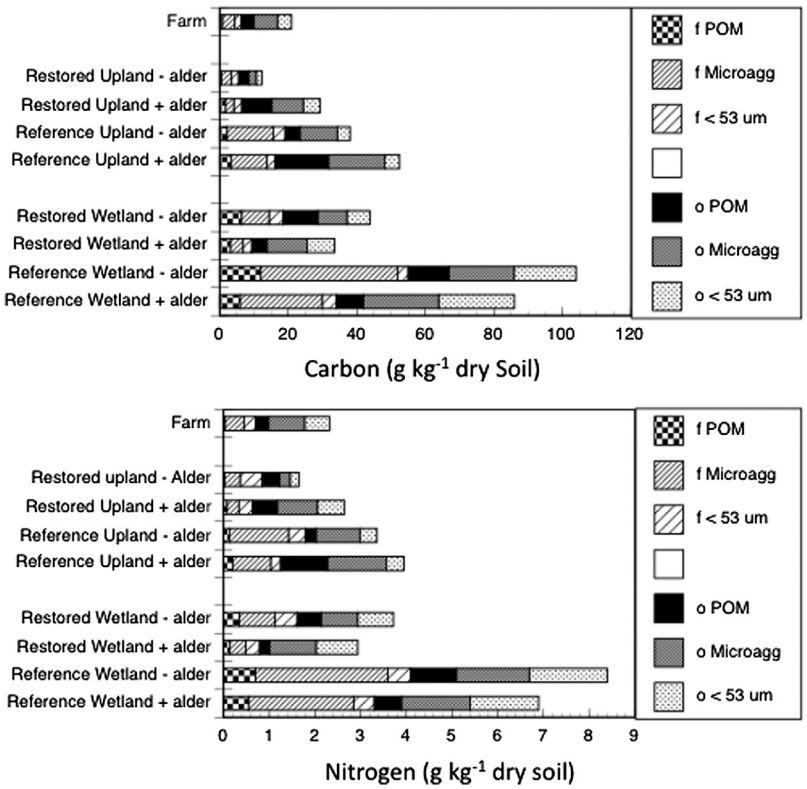

FIGURE 1 | Carbon and nitrogen in aggregate fractions of soil from nine sites. Bars are free fractions in bulk soil (f) and fractions occluded within macroaggregates (o).

reductase (Nor), *cnor*, showed a similar pattern to *nirS* in that they were relatively low occurrence in the reads and showed little difference between the sites. Reads from the quinol oxidizing Nor, *qnor*, occurred at significantly higher numbers than *cnor*. *qnor* reads also showed high variation within sample replicates, particularly in the Farm samples. Reads from the gene encoding the nitrous oxide reductase, *nosZ*, were relatively low in number but exhibited a somewhat similar pattern among sites as reads from the *nar* gene, in that samples from the reference upland +/− alder and the Reference Upland - alder had lower read occurrence than the other sites.

Given the experimental design with well-drained vs. poorly drained soil and potential methane production, a more focused read analysis was done for the *mcrA* gene as a marker for methanogenesis (**Table 6**). Reads coming from *mcrA* were most prominent in the Reference Wetland +/− alder, but significantly less in the portion where alder trees. Read abundance in the Reference Wetland +/- Myrica was lower than the Reference Wetland +/− alder and did not show a difference whether the nitrogen fixer, Myrica, was present, or not. Reads from *mcrA* were relatively more frequent in the Restored wetland and again with greater abundance in the situation without alder than when the tree was present. *mcrA* read abundance was below detection in the Farm and Upland sites. Reads from the methane oxidation gene *pmoA* were found in all 11 sites. The relative frequency of the gene was significantly less in the Restored Upland sites than in the Reference Forest sites. Interestingly, relative abundance of *pmoA* reads in the Restored Wetland sites were similar to values for the Reference Wetland sites.

To gain a broader view of bacterial community structure we used FMAP, which assigns function to reads using the KEGG ortholog database as reference (Kim et al., 2016). Given the experimental design with a large number of pairwise comparisons of sites (N = 55 pairs of sites), as well as the number of ortholog sequences in the KEGG database (>20,000), we only report the number of genes that were significantly enriched in some of the more relevant pairwise comparisons (**Table 7**). These differences serve as a proxy for similarities or differences in the physiological potential in the bacterial community. As expected, pairwise comparisons of sites that were adjacent in the PCA plot (**Figure 3**) generated relatively low numbers of orthologs with significant enrichment in one or the other of the paired sites. For example, for the Reference Streamside Wetlands +/− Myrica, which were fairly close on both PCA1 and PCA2, there were 93 orthologs that were significantly enriched in one or the other. In contrast, sites that showed large dissimilarity in the PCA plot had a relatively larger number of orthologs that showed significant enrichment in one or the other of the paired sites. For example, there were 2,286 significantly enriched orthologs in a pairwise comparisons of reads from the

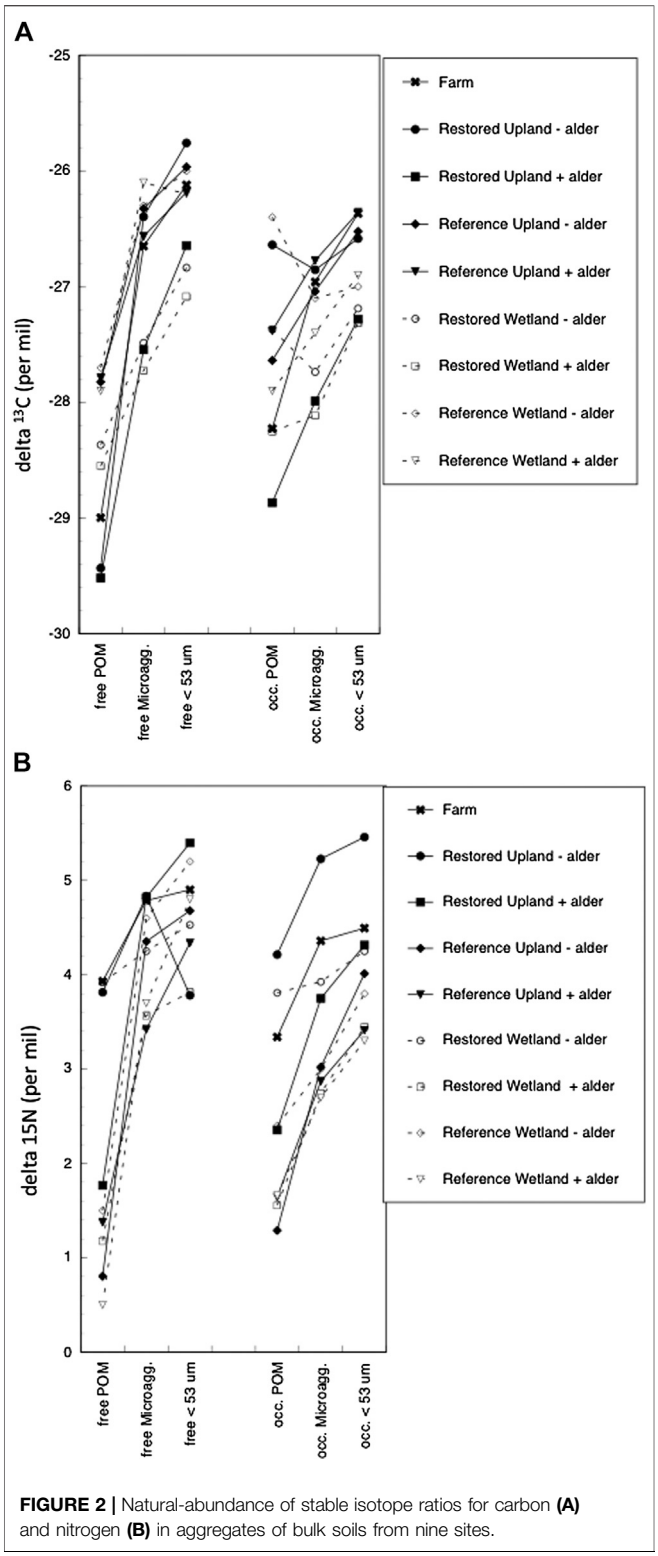

FIGURE 2 | Natural-abundance of stable isotope ratios for carbon **(A)** and nitrogen **(B)** in aggregates of bulk soils from nine sites.

Reference upland - alder sites to those from the Reference Depressional Wetland - alder.

The FMAP data (**Table 7**) also show that restoration of the soil bacterial community has progressed further in the uplands than in the wetlands. The restored uplands have only 382 KEGG orthologs with differential abundance between Restored and Reference, whereas there are still 536 KEGG orthologs with differential abundance between Restored and Farm. In contrast, the restored wetlands have 840 KEGG orthologs with differential abundance between Restored and Reference Streamside Wetland and 740 KEGG orthologs with differential abundance between Restored and Farm.

DISCUSSION

General

The recovery of post-agricultural land is undoubtedly related to its land use history (Bell et al., 2020). The work of Flinn and Marks (2007) provide a useful description of the agricultural history in the region that includes our study sites. Tompkins County in New York State was completely forested in 1790 prior to European colonization. Land use change for agriculture accelerated after 1850 reaching a peak in 1900. Dairy farming was the predominant form of agriculture resulting in a mix of pasture, hay and other crops. Woods, brush, and fallow were intermixed across the landscape. Widespread farm abandonment in the 1900s allowed forests to reclaim much of the landscape, and by 1995 forests covered 54% of the county (Flinn et al., 2005). Wetlands in the region were drained, mostly by ditching and dikes to channel water away and create more agricultural land (Walters and Shrubsole, 2003). Many of the wetlands were likely covered with soil that eroded from uplands (McCarty et al., 2009) that buried remnants of the original wetland, making it difficult to know the endpoint per se for wetland restoration.

A pertinent question in agriculture is the amount of nitrogen fertilizer used. Unfortunately, we do not have a complete record for the site. However, widespread use of synthetic fertilizers occurred mostly after 1960 (Davidson, 2009) and might not have been extensive in the region due to its excessive cost. Since synthetic fertilizers are produced by fixation of atmospheric nitrogen, they typically have a natural abundance for stable nitrogen isotope value of 0 (Nikolenko et al., 2018), similar to that for plants with symbiotic nitrogen fixation (Soper et al., 2015). But this did not dominate values for bulk soils or soil aggregates (discussed below). However, we cannot rule out manure having been applied to the soils, which generally has an isotope value of >+5 (Bateman et al., 2005), which is similar the that for decomposed organic matter.

Bulk Soils

Unfortunately, we also do not know the level of organic matter in bulk soil when agriculture was abandoned on the site. Nevertheless, comparison of the present-day Farm with the Reference Upland sites suggests that agriculture reduced bulk soil carbon by about 55%, whereas nitrogen was reduced by about 40% (**Table 1**). This reduction in soil carbon is larger than the reduction of 30% in soil carbon often assumed to occur as a consequence of cultivation (Davidson and Ackerman, 1993;

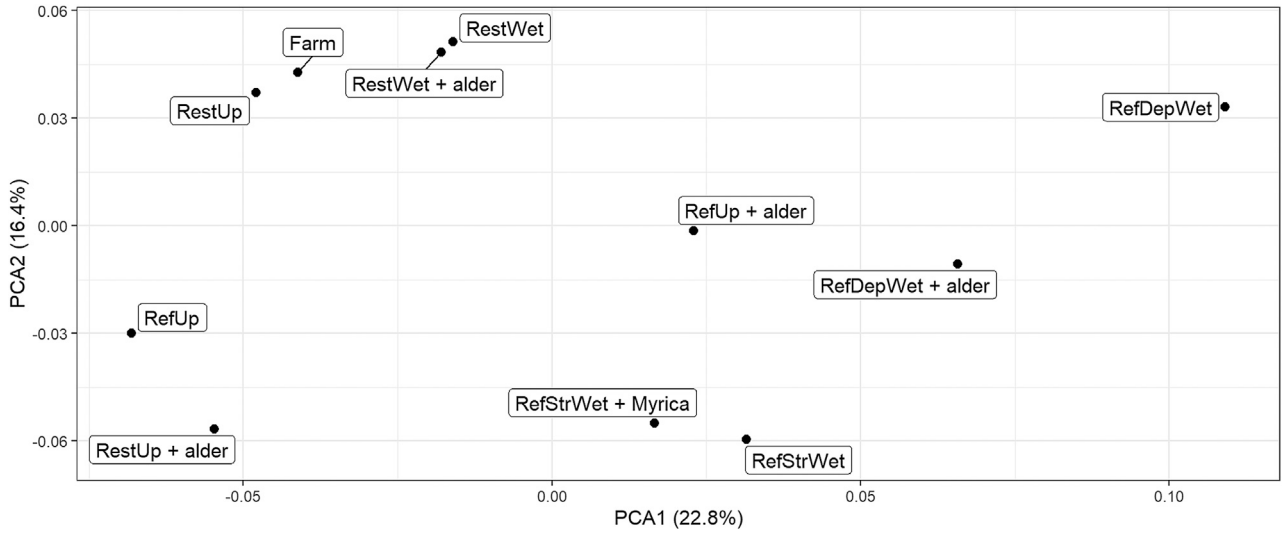

FIGURE 3 | PCA plot of metagenomic sample composition from the 11 sites using total metagenomic reads. Triplicate read sets were concatenated into one set for this comparison giving one point per site. Sample abbreviations are: RestUp–Restored Upland, RefUp–Reference Upland, RestWet–Restored Wetland, RefStrWet–Reference Streamside Wetland and RefDepWet–Reference Depressional Wetland.

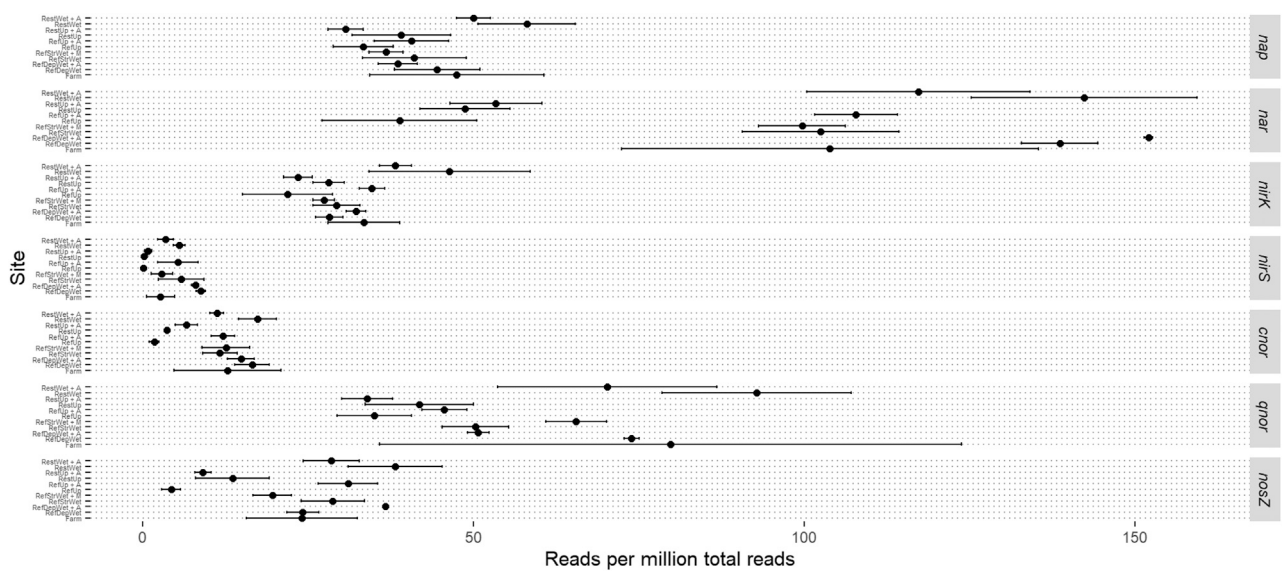

FIGURE 4 | Mean read abundance from individual denitrification genes. Sample abbreviations are: RestUp–Restored Upland, RefUp–Reference Upland, RestWet–Restored Wetland, RefStrWet–Reference Streamside Wetland and RefDepWet–Reference Depressional Wetland. Error bars represent one standard deviation from the mean.

Murty et al., 2002). Thus, over-worked soil is likely one reason agriculture was abandoned on the site.

For the poorly drained soils, our findings suggest bulk soils lost more than 80% of its carbon and 50% of its nitrogen as a result of agriculture (**Table 1**). There is some evidence in the literature that soils in poorly drained areas suffer less agriculture-induced soil carbon losses compared to better-drained soils (Jelinski and Kucharik, 2009). However, it is difficult to generalize about the fate of the missing carbon and nitrogen in the study area. For instance, agriculture increases the likelihood of wind erosion of the soil, in particular, for depressional wetlands. This occurred in relatively deep soils in depression wetlands along the south shore of Lake Ontario in New York State that were converted to agriculture and were productive for only about 50 years due to drastic loss of soil (Kojima, 1947), The rate of soil loss was much faster than

TABLE 6 | Occurrence of genes associated with either methane oxidation genes (pmoA) or methanogenesis (mcrA) and normalized ratio of genes from 11 sites investigated in this study.

	pmoA (RPM)	mcrA (RPM)	mcrA/(pmoA +mcrA) (%)
Farm	7.8 ± 10.3	0.7 ± 1.2	8
Restored Upland			
– alder	2.5 ± 0.3	0.0 ± 0.0	0
+ alder	5.4 ± 5.6	0.0 ± 0.0	0
Reference Upland			
– alder	16.0 ± 4.9	0.0 ± 0.0	0
+ alder	16.1 ± 4.2	4.3 ± 0.3	21
Restored Wetland			
– alder	27.7 ± 5.6	19.7 ± 14.2	42
+ alder	16.6 ± 9.3	8.6 ± 12.5	34
Reference Streamside Wetland			
– Myrica	9.3 ± 4.8	21.7 ± 3.4	70
+ Myrica	14.6 ± 6.1	25.4 + 17.5	64
Reference Depression Wetland			
– alder	31.9 ± 6.4	94.4 ± 8.5	74.7
+ alder	19.1 ± 1.7	9.2 ± 3.8	32.5
ANOVA $F_{10,32}$ =	6.64	32.48	
P	0.001	<0.001	

Values are mean and one standard error from the mean. Sample size = 3; 0–10 cm depth interval.

could be explained by microbial decomposition of plant residue and soil organic matter (Welsch and Yavitt, 2003, 2007) suggesting that the fine texture organic matter was wind eroded when fields were fallow.

Thus, our findings provide virtually no evidence that organic matter levels have recovered in the bulk soil samples since agricultural abandonment. This is perhaps not surprising as recovery of carbon and nitrogen in post-agricultural soils can be a slow process (McLauchlan, 2006), with estimates ranging from tens to several hundred years (Jandl et al., 2007; Krause et al., 2016). A slow recovery rate also suggests a long mean residence time for the pool of soil organic matter. According to reservoir theory (Eriksson, 1971), recovery from agricultural practices takes, at least, one residence time and three residence times for nearly complete recovery.

The findings here did not present a clear picture for alder contributions to restoration in these sites (**Table 2**). Typically, it is assumed that nitrogen added via fixation simulates plant production, which ultimately increases soil organic matter (Knops et al., 2002). Although this seems to be occurring in the Restored Wetland, there was no evidence for increased soil organic matter associated with alder in the Restored Upland site. Also, none of the Reference sites had greater amounts of soil organic matter from plants associated with nitrogen fixation. One possible explanation is that plants growing with nitrogen fixers do take-up the extra nitrogen, but the outcome is merely plant tissue that decomposes more readily (Hoogmoed et al., 2014; Averill and Waring, 2018)), without enhancing soil organic matter.

Soil Structure

Our study of soil aggregation produced several unanticipated findings. Despite the well-known finding that macroaggregates and, perhaps, even free microaggregates are disrupted by tillage (Six et al., 2000), macroaggregates were a prominent feature of bulk soils in the present-day Farm. The finding here is likely related to the type of agricultural practice used in the region, which is rotation of corn, hay, clover, and cover crops. At the time of sampling, the present-day Farm had a mixture of grasses and clover. Common pasture grasses tend to be colonized by arbuscular mycorrhizal fungi, some of which are very good at promoting soil aggregation (Lehmann et al., 2017). Indeed, Milne and Haynes (2004) showed that some grasses can restore aggregate stability quite quickly especially when tillage does not occur annually. In contrast, macroaggregates being a

TABLE 7 | Number of KEGG orthologs with statistically significant greater abundance in pairwise comparison between sites. KEGG Pathways affected by differential read abundance.

	KEGG orthologs	Pathways affected
Presence vs absence of nitrogen fixers		
Restored Upland	758	Aromatic metabolism Environ. Info. Process.
Reference Forest	1,291	Carbon metabolism Nitrogen metabolism
Restored Wetland	332	Genetic Info. Process. Environ. Info. Process.
Reference Depressional Wetland	776	Carbon metabolism Nitrogen metabolism Genetic Info. Process.
Reference Streamside Wetland	93	Environ. Info. Process.
Farm vs. Reference		
Reference Upland	795	Carbon metabolism Aromatic metabolism Environ. Info. Process.
Reference Streamside Wetland	812	Carbon metabolism Genetic Info. Process.
Restored vs. Reference		
Upland	382	Nitrogen metabolism Environ. Info. Process.
Depressional Wetland	1,484	Carbon metabolism Genetic Info. Process.
Streamside Wetland	840	Carbon metabolism Environ. Info. Process.
Farm vs Restored		
Restored Upland	536	Carbon metabolism Aromatic metabolism
Restored Wetland	740	Carbon metabolism Genetic Info. Process.
Soil drainage		
Ref. Upland vs. Depress. Wetland	2,286	Carbon metabolism
Restored Upland vs. Restored Wetland	1793	Carbon metabolism Genetic Info. Process.

smaller proportion of the bulk soil in the Restored Upland-alder site might be related to dominance by goldenrod plants (*Solidago* sp.) that have been shown to have little impact on soil structure (Zubek et al., 2020). The contrasts in soil aggregation among sites in our survey show there is still much to be learned about plant species' influences on soil aggregation.

For example, our findings show that alder roots are particularly good at promoting soil aggregation. This is likely related to the diversity of mycorrhizae associated with alder roots. Alder forms well-known relationships with ectomycorrhizal fungi (Põlme et al., 2013) and actinobacterial *Frankia*, which is responsible for the nitrogen-fixing capacity. However, young alder trees also often form associations with arbuscular mycorrhizal fungi (Chatarpaul et al., 1989) that are much better at soil aggregate formation. Indeed, Enkhtuya and Vosatka (2005) showed that mycorrhizae on young alder trees were able to make direct connections with grasses that further promoted soil aggregation. This suggests a benefit of alder promoting soil structure that goes beyond its nitrogen-fixing capability.

Across the sites, the predominance of soil carbon and nitrogen within macroaggregates is not surprising, given the well-known protection afforded organic matter when physically removed from soil decomposers (Lehmann et al., 2020). Furthermore, both free and occluded microaggregates had the largest amount of soil carbon and nitrogen. According to the hierarchy theory of aggregate formation (Tisdall and Oades, 1982) microaggregates form more readily within macroaggregates, and thus free microaggregates are thought to be those released from macroaggregates via disturbance, i.e., tillage. Although the timing of microaggregate formation depends on many soil factors (Totsche et al., 2018) it is generally believed to occur on a century rather than decade time scale. Thus, it is likely in our sites have not had enough time for complete formation of microaggregates occluded within macroaggregates. Therefore, the free microaggregates were likely inherited from pre-agriculture soil and released during the agricultural phase.

Although the stable isotope values for POM were generally lighter than values for microaggregates and <53 μm size class, of particular interest are the relatively large (enriched) values for stable nitrogen isotopes in free POM from the Farm and Restored Upland and Restored Wetland sites (**Figure 2**). The most likely explanation for heavier values in POM is extensive decomposition of the relatively fresh plant residue that is the origin of free POM in the mineral soil. For microaggregates and the <53 μm size class the relatively large (enriched) values for stable isotopes also suggest that protected organic matter is what remains after microbial decomposition. It is possible that the protected organic matter was derived from manure applied to the soil during the agricultural phase. Regardless of the source, and despite some evidence in the literature for fresher organic matter in occluded fractions in restored sites (cf., Kalinina et al., 2018), the results point to well decomposed organic material being protected with soil aggregation. This finding seems to apply across all the land uses, farm, restored, and reference, whereby fresher organic matter that is unprotected decomposes quickly. This is perhaps not surprising and has been observed in other systems (Liao et al., 2006).

Soil Metagenomes

Many studies have accessed the soil microbial community in terms of taxonomic identity of community members and statistical inference of turnover in community composition among treatment sites (cf., Turley et al., 2020). Here we focused on gene abundances instead of taxonomic identity as gene abundances provide deeper insight into the microbial processes that are occurring among sites, i.e., via metabolic pathways (cf. Yavitt et al., 2020).

As a result, we found that only one of the restored sites, the Restored Upland + alder, clustered with a plausible recovery endpoint, the Reference Upland − alder (**Figure 3**). The other three Restored sites showed closer affinity to the present-day Farm, suggesting relatively minor recovery of soil bacterial community structure. We have no a priori reason why the Restored Upland + alder site showed recovery. Since the site had alder, this gives a role for alder trees in restoration of post-agricultural soils that extends beyond the symbiotic nitrogen-fixing capacity of the tree.

Examination of gene abundances does help us resolve the appropriate endpoint for restoration of the post-agricultural wetlands, i.e., Depressional or Streamside. We do not know with certainty since the original wetland was lost long before we sampled the soils. However, the Restored Wetland had a soil bacterial metagenome with closer affinity to the Reference Streamside Wetland (+/− Myrica) than the Depressional Wetland (+/− alder). This conclusion is based on separation of the Restored Wetland from the Reference Depressional Wetland on the first axis of the PCA plot, whereas separation from the Reference Streamside Wetland occurred on the second axis. This indicates greater dissimilarity on the first axis (Lever et al., 2017). Another reason is there being fewer significantly different orthologs between the Restored Wetland and the Reference Streamside Wetland than a similar comparison but with the Reference Depressional Wetland (**Table 7**). Both types of wetlands occur in the region. Therefore, comparisons of metagenomes appear to be an insightful way to link habitats together at the landscape scale.

The examination of denitrification genes revealed only a few notable differences among sites. On one hand, this is surprising since the landscape contained soil ranging from well drained to poorly drained, with an a priori prediction of greater presence of denitrification genes in the poorly drained soils (Groffman and Tiedje, 1989). On the other hand, homogenization of the landscape during the agricultural period might have eliminated differences that have been slow to recover (Zhu et al., 2017). Moreover, there was no consistent effect of nitrogen fixers, alder or Myrica, on the abundance of denitrification genes. One notable exception was in the Reference Upland, where, for most of the denitrification genes, abundance was greater in the situations with alder than without. Presumably, this reflects the addition of fixed nitrogen to the well-drained soil with a long-established presence of alder.

For methane cycling, reads associated with methane oxidation (*pmoA*) but no reads associated with methane production (*mcrA*) in the well-drained soils suggest that the sole source of methane was atmospheric. This is well-known and has been observed many times in a wide range of soils (cf., Cai et la. 2016). Here greater abundance of *pmoA* reads in the Reference Forest than in Farm and Restored soils suggest that methane-oxidizing bacteria were impaired by agriculture and have been slow to recovery. There is evidence that the recovery of atmospheric methane consumption might take more than 50 years in post-agricultural soils (Hudgens and Yavitt, 1997). Although differences in the abundance of reads for *pmoA* occurred here, the three KEGG pathways associated with methane oxidation (M00344 xylulose monophosphate pathway; M00345 ribulose monophosphate pathway; and, M00346 serine pathway) did not show significant differences in any of the pairwise comparisons. Hence, further work is needed to assess whether rates of atmospheric methane consumption differ across the landscape.

All of the poorly drained soils showed *mcrA* reads, which is not surprising for wetland soils. Here the number of reads was statistically similar between the Restored Wetlands and Reference Wetland soils, suggesting rapid recovery of methane production capacity when wetland hydrology is restored. How *mcrA* persists in a landscape when, presumably, all of the wetlands have been drained, farmed, and allowed to dry is still unclear.

A straightforward interpretation of community structure provided by FMAP is an index of dissimilarity, in this case in gene abundances, between pairs of sites. This view of dissimilarity is akin to dissimilarity in community composition used by ecologists (Anderson et al., 2011). The largest differences, in our cases, between sites with different soil drainage (**Table 7**) makes sense since soil drainage, well drained vs. poorly drained, has shown to influence bacterial community composition (Suriyavirun et al., 2019). The FMAP analyses also support the conclusion that soil restoration is occurring faster for the Upland sites than the Wetland sites.

It is perhaps not surprising that most of the genes still showing differential abundances between pairs of sites were in KEGG pathways carbon and nitrogen metabolism, genetic and environmental information processing, and aromatic metabolism (**Table 7**). The Carbon Metabolism group likely reflects catabolism of new compounds in the soil derived from shifting patterns of plant species associated with farming, restoration, and natural vegetation. This is consistent with dissimilarity in the Environmental Information Processing pathway, which largely consists of genes involved in transport of a variety of compounds across cell membranes (Rice et al., 2014). Genetic Information Processing includes genes involved in repair of nucleic acids but also transposable elements. Transposable elements are often associated with the spread of novel catabolic genes within communities (Sun and Badgley, 2019).

Relationships in the Data Set

Admittedly, the study has a complex experimental design with 11 sites, two soil drainage classes, forested and non-forested sites, and current, past and not any agricultural practices. Although complex, such post-agricultural landscapes are common. A complication is how the three soil parameters examined here (organic matter, structure, and gene abundances in the bacterial community) are dependent on each other, which is less clear than often presented. We hesitate assigning cause and effect intuitively among the three parameters to avoid spurious relationships.

Therefore, we rely upon correlation analyses (**Table 8**). For example, our finding strong relationships between percentage of occluded microaggregates and abundance of denitrification reads (Pearson r = 0.49), *pmoA* reads (r = 0.62), and *mcrA* reads (r = 0.53) go along with the explanation that denitrification and methane cycling occur within these highly protected soil structures (cf., Neal et al., 2020). On the other hand, before labeling strong correlations between the percentage of occluded microaggregates and concentrations of carbon and nitrogen (r = 0.62) as organic matter protection, it is important to recognize that carbon and nitrogen compounds are the glue that hold microaggregates together.

CONCLUSION

It is an exciting time to study soil recovery from agricultural practices. The potential for carbon sequestration in soil organic matter has implications for atmospheric carbon cycling and global climate, despite still being uncertain (cf., Clark and Johnson, 2011). Long-term sequestration of nitrogen has implications for downstream water quality (cf., Van Meter et al., 2016). Increased genomic information is offering insight into the physiological potential of the bacterial community not possible even five years ago. Integrating bacterial functions with the dynamics of soil organic matter and soil structure is a challenge.

TABLE 8 | Correlation coefficients (Pearson r) for multiple comparisons among soil parameters.

	Total denitrify	pmoA gene	mcrA gene	pH	% Nitrogen	% Carbon	% Soil water	% Macroagg	% Microagg(o)
Total denitrify	1.00								
pmoA gene	0.69	1.00							
mcrA gene	0.44	0.70	1.00						
pH	0.27	0.45	0.40	1.00					
% Nitrogen	0.35	0.66	0.88	0.34	1.00				
% Carbon	0.34	0.63	0.90	0.35	0.99	1.00			
% Soil water	0.37	0.56	0.75	0.33	0.91	0.94	1.00		
% Macroagg	0.21	–0.02	–0.15	–0.59	–0.10	–0.15	–0.05	1.00	
% Microagg(o)	0.49	0.62	0.53	0.36	0.62	0.62	0.73	0.26	1.00

However, linking soil organic matter to structure to soil organisms will generate a robust understanding of soil recovery.

DATA AVAILABILITY STATEMENT

The datasets presented in this study can be found in online repositories. The names of the repository/repositories and accession number(s) can be found below: NCBI BioProject, accession no: PRJNA687526.

AUTHOR CONTRIBUTIONS

JY and GP conceived the study. JY, GP, EO, and JZ did the field work. GP, EO, and JZ carried out the laboratory analyze in support of the study. JY and JS analyzed the findings and wrote the initial manuscript. All authors contributed to the final version of the manuscript.

FUNDING

This work was supported by a USDA National Institute of Food and Agriculture, Hatch project (1477309). Any opinions, findings, conclusions, or recommendations expressed in this publication are those of the author (s) and do not necessarily reflect the view of the National Institute of Food and Agriculture (NIFA) or the United States Department of Agriculture (USDA).

ACKNOWLEDGMENTS

We thank the Finger Lakes Land Trust (https://www.fllt.org) for allowing access to the field locations for scientific research. We thank ad hoc reviewers for comments and suggestions that greatly improved the clarity of the presentation.

REFERENCES

Amrhein, V., Greenland, S., and McShane, B. (2019). Scientists rise up against statistical significance. *Nature* 567, 305–307. doi:10.1038/d41586-019-00857-9

Anderson, M. J., Crist, T. O., Chase, J. M., Vellend, M., Inouye, B. D., Freestone, A. L., et al. (2011). Navigating the multiple meanings of β diversity: a roadmap for the practicing ecologist. *Ecol. Lett.* 14, 19–28. doi:10.1111/j.1461-0248.2010.01552.x

Andrews, S. (2010). FastQC: a quality control tool for high throughput sequence data. *Reference Source*. doi:10.1109/hpcs.2010.5547068

Arkin, A. P., Cottingham, R. W., Henry, C. S., Harris, N. L., Stevens, R. L., Maslov, S., et al. (2018). KBase: the United States department of energy systems biology knowledgebase. *Nat. Biotechnol.* 36, 566. doi:10.1038/nbt.4163

Aronson, J., Dhillion, S., and Le Floc'h, E. (1995). On the need to select an ecosystem of reference, however imperfect: a reply to Pickett and Parker. *Restor. Ecol.* 3, 1–3.

Averill, C., and Waring, B. (2018). Nitrogen limitation of decomposition and decay: how can it occur?. *Global Change Biol.* 24, 1417–1427. doi:10.1111/gcb.13980

Ballantine, K., and Schneider, R. (2009). Fifty-five years of soil development in restored freshwater depressional wetlands. *Ecol. Applic.* 19, 1467–1480. doi:10.1890/07-0588.1

Bateman, A. S., Kelly, S. D., and Jickells, T. D. (2005). Nitrogen isotope relationships between crops and fertilizer: implications for using nitrogen isotope analysis as an indicator of agricultural regime. *J. Agr. Food Chem.* 53, 5760–5765. doi:10.1021/jf050374h

Bell, S. M., Barriocanal, C., Terrer, C., and Rosell-Melé, A. (2020). Management opportunities for soil carbon sequestration following agricultural land abandonment. *Environ. Sci. Pol.* 108, 104–111. doi:10.1016/j.envsci.2020.03.018

Bernard, J. M., and Solsky, B. A. (1977). Nutrient cycling in a Carex lacustris wetland. *Can. J. Bot.* 55, 630–638. doi:10.1139/b77-077

Bolger, A. M., Lohse, M., and Usadel, B. (2014). Trimmomatic: a flexible trimmer for Illumina sequence data. *Bioinformatics* 30, 2114–2120. doi:10.1093/bioinformatics/btu170

Buchfink, B., Xie, C., and Huson, D. H. (2015). Fast and sensitive protein alignment using DIAMOND. *Nat. Method.* 12, 59–60. doi:10.1038/nmeth.3176

Bünemann, E. K., Bongiorno, G., Bai, Z., Creamer, R. E., De Deyn, G., de Goede, R., et al. (2018). Soil quality–a critical review. *Soil Biol. Biochem.* 120, 105–125. doi:10.1016/j.soilbio.2018.01.030

Cai, Y., Zheng, Y., Bodelier, P. L., Conrad, R., and Jia, Z. (2016). Conventional methanotrophs are responsible for atmospheric methane oxidation in paddy soils. *Nat. Commun.* 7, 11728–11810. doi:10.1038/ncomms11728

Carter, M. R. (2002). Soil quality for sustainable land management. *Agron. J.* 94, 38–47. doi:10.2134/agronj2002.0038

Castañeda, L. E., and Barbosa, O. (2017). Metagenomic analysis exploring taxonomic and functional diversity of soil microbial communities in Chilean vineyards and surrounding native forests. *Peer J* 5, e3098. doi:10.7717/peerj.3098

Chatarpaul, L., Chakravarty, P., and Subramaniam, P. (1989). Studies in tetrapartite symbioses. *Plant Soil* 118, 145–150. doi:10.1007/bf02232800

Clark, J. D., and Johnson, A. H. (2011). Carbon and nitrogen accumulation in post-agricultural forest soils of western New England. *Soil Sci. Soc. Am. J.* 75, 1530–1542. doi:10.2136/sssaj2010.0180

Cohen, M. J., Creed, I. F., Alexander, L., Basu, N. B., Calhoun, A. J., Craft, C., et al. (2016). Do geographically isolated wetlands influence landscape functions?. *Proc. Natl. Acad. Sci. USA* 113, 1978–1986. doi:10.1073/pnas.1512650113

Crews, T. E., and Rumsey, B. E. (2017). What agriculture can learn from native ecosystems in building soil organic matter: a review. *Sustainability* 9, 578. doi:10.3390/su9040578

Davidson, E. A., and Ackerman, I. L. (1993). Changes in soil carbon inventories following cultivation of previously untilled soils. *Biogeochemistry* 20, 161–193. doi:10.1007/bf00000786

Davidson, E. A. (2009). The contribution of manure and fertilizer nitrogen to atmospheric nitrous oxide since 1860. *Nat. Geosci.* 2, 659–662. doi:10.1038/ngeo608

Dyer, J. M. (2006). Revisiting the deciduous forests of eastern North America. *Bioscience* 56, 341–352. doi:10.1641/0006-3568(2006)56[341:rtdfoe]2.0.co;2

Elliott, E. T. (1986). Aggregate structure and carbon, nitrogen, and phosphorus in native and cultivated soils. *Soil Sci. Soc. Am. J.* 50, 627–633. doi:10.2136/sssaj1986.03615995005000030017x

Enkhtuya, B., and Vosatka, M. (2005). Interaction between grass and trees mediated by extraradical mycelium of symbiotic arbuscular mycorrhizal fungi. *Symbiosis* 38, 261–277.

Eriksson, E. (1971). Compartment models and reservoir theory. *Annu. Rev. Ecol. Systemat.* 2, 67–84. doi:10.1146/annurev.es.02.110171.000435

Fierer, N. (2017). Embracing the unknown: disentangling the complexities of the soil microbiome. *Nat. Rev. Microbiol.* 15, 579–590. doi:10.1038/nrmicro.2017.87

Flinn, K. M., Lechowicz, M. J., and Waterway, M. J. (2008). Plant species diversity and composition of wetlands within an upland forest. *Am. J. Bot.* 95, 1216–1224. doi:10.3732/ajb.0800098

Flinn, K. M., and Marks, P. L. (2007). Agricultural legacies in forest environments: tree communities, soil properties, and light availability. *Ecol. Applic.* 17, 452–463. doi:10.1890/05-1963

Flinn, K. M., Vellend, M., and Marks, P. L. (2005). Environmental causes and consequences of forest clearance and agricultural abandonment in central New York, United States. *J. Biogeogr.* 32, 439–452. doi:10.1111/j.1365-2699.2004.01198.x

Flinn, K. M., and Vellend, M. (2005). Recovery of forest plant communities in post-agricultural landscapes. *Front. Ecol. Environ.* 3, 243–250. doi:10.1890/1540-9295(2005)003[0243:rofpci]2.0.co;2

Graf, F., and Frei, M. (2013). Soil aggregate stability related to soil density, root length, and mycorrhiza using site-specific Alnus incana and Melanogaster variegatus sl. *Ecol. Eng.* 57, 314–323. doi:10.1016/j.ecoleng.2013.04.037

Groffman, P. M., and Tiedje, J. M. (1989). Denitrification in north temperate forest soils: relationships between denitrification and environmental factors at the landscape scale. *Soil Biol. Biochem.* 21, 621–626. doi:10.1016/0038-0717(89)90054-0

Hermans, S. M., Taylor, M., Grelet, G., Curran-Cournane, F., Buckley, H. L., Handley, K. M., et al. (2020). From pine to pasture: land use history has long-term impacts on soil bacterial community composition and functional potential. *FEMS Microbiol. Ecol.* 96, fiaa041. doi:10.1093/femsec/fiaa041

Hoogmoed, M., Cunningham, S. C., Baker, P., Beringer, J., and Cavagnaro, T. R. (2014). N-fixing trees in restoration plantings: effects on nitrogen supply and soil microbial communities. *Soil Biol. Biochem.* 77, 203–212. doi:10.1016/j.soilbio.2014.06.008

Hudgens, D. E., and Yavitt, J. B. (1997). Land-use effects on soil methane and carbon dioxide fluxes in forests near Ithaca, New York. *Ecoscience* 4, 214–222.doi:10.1080/11956860.1997.11682398

Hurd, T. M., Raynal, D. J., and Schwintzer, C. R. (2001). Symbiotic N. *Oecologia* 126, 94–103. doi:10.1007/s004420000500

Jandl, R., Lindner, M., Vesterdal, L., Bauwens, B., Baritz, R., Hagedorn, F., et al. (2007). How strongly can forest management influence soil carbon sequestration?. *Geoderma* 137, 253–268. doi:10.1016/j.geoderma.2006.09.003

Jansson, J. K., and Hofmockel, K. S. (2018). The soil microbiome—from metagenomics to metaphenomics. *Curr. Opin. Microbiol.* 43, 162–168. doi:10.1016/j.mib.2018.01.013

Jelinski, N. A., and Kucharik, C. J. (2009). Land-use effects on soil carbon and nitrogen on a United States Midwestern Floodplain. *Soil Sci. Soc. Am. J.* 73, 217–225. doi:10.2136/sssaj2007.0424

Kalinina, O., Cherkinsky, A., Chertov, O., Goryachkin, S., Kurganova, I., de Gerenyu, V. L., et al. (2018). Post-agricultural restoration: implications for dynamics of soil organic matter pools. *Catena* 181, 104096. doi:10.1016/j.catena.2019.104096

Kanehisa, M., Araki, M., Goto, S., Hattori, M., Hirakawa, M., Itoh, M., et al. (2007). KEGG for linking genomes to life and the environment. *Nucleic Acids Res.* 36, D480–D484. doi:10.1093/nar/gkm882

Kanehisa, M., Sato, Y., Kawashima, M., Furumichi, M., and Tanabe, M. (2016). KEGG as a reference resource for gene and protein annotation. *Nucleic Acids Res.* 44, D457–D462. doi:10.1093/nar/gkv1070

Kim, J., Kim, M. S., Koh, A. Y., Xie, Y., and Zhan, X. (2016). FMAP: functional mapping and analysis pipeline for metagenomics and metatranscriptomics studies. *BMC Bioinf.* 17, 420. doi:10.1186/s12859-016-1278-0

Knops, J. M. H., Bradley, K. L., and Wedin, D. A. (2002). Mechanisms of plant species impacts on ecosystem nitrogen cycling. *Ecol. Lett.* 5, 454–466. doi:10.1046/j.1461-0248.2002.00332.x

Kojima, R. T. (1947). Soil organic nitrogen: I. Nature of the organic nitrogen in a muck soil from Geneva, New York. *Soil Sci.* 64, 157–165. doi:10.1097/00010694-194708000-00007

Krause, A., Pugh, T. A., Bayer, A. D., Lindeskog, M., and Arneth, A. (2016). Impacts of land-use history on the recovery of ecosystems after agricultural abandonment. *Earth Syst. Dynam.* 7, 745–766. doi:10.5194/esd-7-745-2016

Kuzyakov, Y., and Zamanian, K. (2019). Reviews and syntheses: agropedogenesis-humankind as the sixth soil-forming factor and attractors of agricultural soil degradation. *Biogeosciences* 16, 4783–4803. doi:10.5194/bg-16-4783-2019

Lal, R. (2015). Restoring soil quality to mitigate soil degradation. *Sustainability* 7, 5875–5895. doi:10.3390/su7055875

Lehmann, A., Leifheit, E. F., and Rillig, M. C. (2017). "Mycorrhizas and soil aggregation," in *Mycorrhizal mediation of soil*. Editors N. Collins Johnson, C. Gehring, and J. Jansa (Amsterdam: Elsevier), 241–262.

Lehmann, J., Hansel, C. M., Kaiser, C., and Markus, K., Kate, M., Stefano, M., et al. (2020). Persistence of soil organic carbon caused by functional complexity. *Nat. Geosci.* 13, 529–534. doi:10.1038/s41561-020-0612-3

Lever, J., Krzywinski, M., and Altman, N. (2017). Points of significance: principal component analysis. *Nat. Methods* 14, 641–642. doi:10.1038/nmeth.4346

Liao, J. D., Boutton, T. W., and Jastrow, J. D. (2006). Organic matter turnover in soil physical fractions following woody plant invasion of grassland: evidence from natural ^{13}C and ^{15}N. *Soil Biol. Biochem.* 38, 3197–3210. doi:10.1016/j.soilbio.2006.04.004

Magdoff, F., and Weil, R. R. (2004). "Soil organic matter management strategies," in *Soil organic matter in sustainable agriculture*. F. Magdoff and R. R. Weil (Boca Raton: CRC Press), 45–65.

McCarty, G., Pachepsky, Y., and Ritchie, J. (2009). Impact of sedimentation on wetland carbon sequestration in an agricultural watershed. *J. Environ. Qual.* 38, 804–813. doi:10.2134/jeq2008.0012

McLauchlan, K. (2006). The nature and longevity of agricultural impacts on soil carbon and nutrients: a review. *Ecosystems* 9, 1364–1382. doi:10.1007/s10021-005-0135-1

Mehlich, A. (1984). Mehlich 3 soil test extractant: a modification of Mehlich 2 extractant. *Commun. Soil Sci. Plant Anal.* 15, 1409–1416.

Milne, R. M., and Haynes, R. J. (2004). Soil organic matter, microbial properties, and aggregate stability under annual and perennial pastures. *Biol. Fertil. Soils* 39, 172–178. doi:10.1007/s00374-003-0698-y

Murty, D., Kirschbaum, M. F. M. M., and McGilvray, R. E. H. (2002). Does conversion of forest to agricultural land change soil carbon and nitrogen? A review of the literature. *Global Change Biol.* 8, 105–123. doi:10.1046/j.1354-1013.2001.00459.x

Nadeau, S. A., Roco, C. A., Debenport, S. J., Anderson, T. R., Hofmeister, K. L., Walter, M. T., et al. (2019). Metagenomic analysis reveals distinct patterns of denitrification gene abundance across soil moisture, nitrate gradients. *Environ. Microbiol.* 21, 1255–1266. doi:10.1111/1462-2920.14587

Nakagawa, S., and Cuthill, I. C. (2007). Effect size, confidence interval and statistical significance: a practical guide for biologists. *Biol. Rev.* 82, 591–605. doi:10.1111/j.1469-185X.2007.00027.x

Neal, A. L., Bacq-Labreuil, A., Zhang, X., Clark, I. M., Coleman, K., Mooney, S. J., et al. (2020). Soil as an extended composite phenotype of the microbial metagenome. *Sci. Rep.-UK* 10, 1–16. doi:10.1038/s41598-020-67631-0

Nemergut, D. R., Schmidt, S. K., Fukami, T., O'Neill, S. P., Bilinski, T. M., Stanish, L. F., et al. (2013). Patterns and processes of microbial community assembly. *Microbiol. Mol. Biol. Rev.* 77, 342–356. doi:10.1128/MMBR.00051-12

Nikolenko, O., Jurado, A., Borges, A. V., Knöller, K., and Brouyère, S. (2018). Isotopic composition of nitrogen species in groundwater under agricultural areas: a review. *Sci. Total Environ.* 621, 1415–1432. doi:10.1016/j.scitotenv.2017.10.086

Ondov, B. D., Treangen, T. J., Melsted, P., Mallonee, A. B., Bergman, N. H., Koren, S., et al. (2016). Mash: fast genome and metagenome distance estimation using MinHash. *Genome Biol.* 17, 132. doi:10.1186/s13059-016-0997-x

Põlme, S., Bahram, M., Yamanaka, T., Nara, K., Dai, Y. C., Grebenc, T., et al. (2013). Biogeography of ectomycorrhizal fungi associated with alders (Alnus spp.) in relation to biotic and abiotic variables at the global scale. *New Phytol.* 198, 1239–1249. doi:10.1111/nph.12170

Preem, J. K., Truu, J., Truu, M., Mander, Ü., Oopkaup, K., Lõhmus, K., et al. (2012). Bacterial community structure and its relationship to soil physico-chemical characteristics in alder stands with different management histories. *Ecol. Eng.* 49, 10–17. doi:10.1016/j.ecoleng.2012.08.034

Rice, A. J., Park, A., and Pinkett, H. W. (2014). Diversity in ABC transporters: type I, II and III importers. *Crit. Rev. Biochem. Mol. Biol.* 49, 426–437. doi:10.3109/10409238.2014.953626

Schwintzer, C. R. (1979). Nitrogen fixation by Myrica gale root nodules Massachusetts wetland. *Oecologia* 43, 283–294. doi:10.1007/BF00344955

Scott, N. A. (1998). Soil aggregation and organic matter mineralization in forests and grasslands: plant species effects. *Soil Sci. Soc. Am. J.* 62, 1081–1089. doi:10.2136/sssaj1998.03615995006200040032x

Six, J. A. E. T., Elliott, E. T., and Paustian, K. (2000). Soil macroaggregate turnover and microaggregate formation: a mechanism for C sequestration under no-tillage agriculture. *Soil Biol. Biochem.* 32, 2099–2103. doi:10.1016/s0038-0717(00)00179-6

Soper, F. M., Boutton, T. W., and Sparks, J. P. (2015). Investigating patterns of symbiotic nitrogen fixation during vegetation change from grassland to woodland using fine scale δ15 N measurements. *Plant Cell Environ.* 38, 89–100. doi:10.1111/pce.12373

Stover, M. E., and Marks, P. L. (1998). Successional vegetation on abandoned cultivated and pastured land in Tompkins County, New York. *J. Torrey Bot. Soc.* 125, 150–164. doi:10.2307/2997302

Sullivan, G. M., and Feinn, R. (2012). Using effect size—or why the P value is not enough. *J. Grad. Med. Educ.* 4, 279–282. doi:10.4300/JGME-D-12-00156.1

Sun, S., and Badgley, B. D. (2019). Changes in microbial functional genes within the soil metagenome during forest ecosystem restoration. *Soil Biol. Biochem.* 135, 163–172. doi:10.1016/j.soilbio.2019.05.004

Suriyavirun, N., Krichels, A. H., Kent, A. D., and Yang, W. H. (2019). Microtopographic differences in soil properties and microbial community composition at the field scale. *Soil Biol. Biochem.* 131, 71–80. doi:10.1016/j.soilbio.2018.12.024

Tisdall, J. M., and Oades, J. M. (1982). Organic matter and water-stable aggregates in soils. *J. Soil Sci.* 33, 141–163. doi:10.1111/j.1365-2389.1982.tb01755.x

Totsche, K. U., Amelung, W., Gerzabek, M. H., Guggenberger, G., Klumpp, E., Knief, C., et al. (2018). Microaggregates in soils. *J. Plant Nutr. Soil Sci.* 181, 104–136. doi:10.1002/jpln.201600451

Turley, N. E., Bell-Dereske, L., Evans, S. E., and Brudvig, L. A. (2020). Agricultural land-use history and restoration impact soil microbial biodiversity. *J. Appl. Ecol.* 57, 852–863. doi:10.1111/1365-2664.13591

Van Meter, K. J., Basu, N. B., Veenstra, J. J., and Burras, C. L. (2016). The nitrogen legacy: emerging evidence of nitrogen accumulation in anthropogenic landscapes. *Environ. Res. Lett.* 11, 035014. doi:10.1088/1748-9326/11/3/035014

Walters, D., and Shrubsole, D. (2003). Agricultural drainage and wetland management in Ontario. *J. Environ. Manag.* 69, 369–379. doi:10.1016/j.jenvman.2003.09.013

Welsch, M., and Yavitt, J. B. (2003). Early stages of decay of *Lythrum salicaria* L. and *Typha latifolia* L. in a standing-dead position. *Aquat. Bot.* 75, 45–57. doi:10.1016/s0304-3770(02)00164-x

Welsch, M., and Yavitt, J. B. (2007). Microbial CO_2 production, CH_4 dynamics and nitrogen in a wetland soil (New York State, United States) associated with three plant species (Typha, Lythrum, Phalaris). *Eur. J. Soil Sci.* 58, 1493–1505. doi:10.1111/j.1365-2389.2007.00955.x

Yavitt, J. B., Roco, C. A., Debenport, S. J., Barnett, S. E., and Shapleigh, J. P. (2020). Community organization and metagenomics of bacterial assemblages across local scale pH gradients in northern forest soils. *Microb. Ecol.* doi:10.1007/s00248-020-01613-7

Zhu, Y. G., Gillings, M., Simonet, P., Stekel, D., Banwart, S., and Penuelas, J. (2017). Microbial mass movements. *Science* 357, 1099–1100. doi:10.1126/science.aao3007

Zubek, S., Majewska, M. L., Kapusta, P., Stefanowicz, A. M., Błaszkowski, J., and Rożek, K. (2020). Solidago canadensis invasion in abandoned arable fields induces minor changes in soil properties and does not affect the performance of subsequent crops. *Land Degrad. Dev.* 31, 334–345. doi:10.1002/ldr.3452

Conflict of Interest: The authors declare that the research was conducted in the absence of any commercial or financial relationships that could be construed as a potential conflict of interest.

frontiers in Ecology and Evolution

ORIGINAL RESEARCH
published: 02 July 2021
doi: 10.3389/fevo.2021.553094

The Beautiful and the Dammed: Defining Multi-Stressor Disturbance Regimes in an Atlantic River Floodplain Wetland

Natalie K. Rideout[1], Zacchaeus G. Compson[2†], Wendy A. Monk[3], Meghann R. Bruce[4] and Donald J. Baird[2]*

[1] Department of Biology, Canadian Rivers Institute, University of New Brunswick, Fredericton, NB, Canada, [2] Environment and Climate Change Canada @ Canadian Rivers Institute, Department of Biology, University of New Brunswick, Fredericton, NB, Canada, [3] Faculty of Forestry and Environmental Management, Environment and Climate Change Canada @ Canadian Rivers Institute, University of New Brunswick, Fredericton, NB, Canada, [4] Canadian Rivers Institute, University of New Brunswick, Fredericton, NB, Canada

OPEN ACCESS

Edited by:
Matthias Peichl, Swedish University of Agricultural Sciences, Sweden

Reviewed by:
Richard Kingsford, Sydney Hospital, Australia
Mohammad Imam Hasan Reza, Independent Researcher, Chittagong, Bangladesh

***Correspondence:**
Natalie K. Rideout
nrideout@unb.ca

†Present address:
Zacchaeus G. Compson, Department of Biological Sciences, Advanced Environmental Research Institute, University of North Texas, Denton, TX, United States

Specialty section:
This article was submitted to Conservation and Restoration Ecology, a section of the journal Frontiers in Ecology and Evolution

Received: *17 April 2020*
Accepted: *31 May 2021*
Published: *02 July 2021*

Citation:
Rideout NK, Compson ZG, Monk WA, Bruce MR and Baird DJ (2021) The Beautiful and the Dammed: Defining Multi-Stressor Disturbance Regimes in an Atlantic River Floodplain Wetland. Front. Ecol. Evol. 9:553094. doi: 10.3389/fevo.2021.553094

Natural hydrological fluctuations within river floodplains generate habitat diversity through variable connections between habitat patches and the main river channel. Human modification of floodplains can alter the magnitude and frequency of large floods and associated sediment movement by interrupting these floodplain connections. The lower Wolastoq | Saint John River and its associated floodplain wetlands are experiencing anthropogenic disturbances arising from climate change, increased urbanization in the watershed, changing upstream agricultural landscape practices, and, most notably, major road and dam construction. By comparing digitized aerial images, we identified key periods of change in wetland extent throughout an ecologically significant component of the floodplain, the Grand Lake Meadows and Portobello Creek wetland complex, with significant erosion evident in coves and backwater areas across the landscape following dam construction and significant accretion around the Jemseg River following highway construction. Connectivity and hydrological regime also influenced other habitat components, namely nutrients and metals retention, as well as the composition of the local macrophyte community. These findings address two key aspects of floodplain management: (1) understanding how hydrological alteration has historically influenced floodplain wetlands can inform us of how the ecosystem may respond under future conditions, such as climate change, and (2) the mechanisms by which habitat diversity and disturbance regimes filter biological communities, with the potential for patches to host a rich biodiversity continuously supporting critical ecosystem functions.

Keywords: anthropogenic disturbance, multiple stressors, floodplain, wetlands, hydrological alteration, historical change

INTRODUCTION

River floodplains are subjected to habitat shaping disturbances, and as a result, spatiotemporal creation of patch diversity can promote high biodiversity through niche differentiation and environmental filtering (Ward et al., 1999; Amoros and Bornette, 2002; Tockner and Stanford, 2002). This reflects the Intermediate Disturbance Hypothesis (i.e., few taxa can survive in habitats with high disturbance and many taxa are outcompeted by competitive dominants in habitats with low disturbance; Connell, 1978). Floodplains constitute dynamic habitats, exhibiting a complex and seasonally variable natural stress regime for floodplain species; anthropogenic alteration of the natural state of a floodplain wetland can impose additional stress on these naturally resilient communities, with potentially negative consequences for local biodiversity and ecosystem integrity (e.g., Arias et al., 2018).

Essential characteristics of floodplains, such as shifting boundaries between lentic, lotic and terrestrial habitats, are driven by flood pulses (Junk et al., 1989). Flood pulses cause the vertical and horizontal inundation of the land surrounding rivers, as fed by groundwater, rain, snowmelt or ice jams (Junk et al., 1989). Although it was historically thought that flooding was a stress, (i.e., a chronic drain on the ecosystem that cannot be overcome by species replacement or adaptation), it is now realized, on the contrary, that flood pulses are an essential ecological disturbance, hydrologically linking the river and its floodplain, and replenishing sediment, nutrients and biological propagules to floodplain wetlands (Tockner et al., 2010). Natural hydrological fluctuations within the wetlands of intact floodplain-river ecosystems create habitat diversity through altered connectedness of floodplain patches to the river's main channel (Amoros and Bornette, 2002). Sediment deposition creates oxbows, swales, backwaters and levees in the wetlands (Venterink et al., 2006), while sediment composition and nutrient influx influence plant community structure (Rejmankova, 2011; Rooney et al., 2013). Varying degrees of hydrological connectedness of wetland patches also creates spatial heterogeneity in water temperature, suspended solids and turbidity, nutrient content, and substrate composition, all of which can influence biodiversity patterns (Amoros and Bornette, 2002).

The unpredictable timing of flood and drought years similarly creates a mosaic of patches at different stages of succession (Bayley and Guimond, 2008; Tockner et al., 2010). Water level directly influences submerged and emergent macrophyte dynamics. Deep, open water habitats are dominated by beds of submerged macrophytes and abundant planktonic communities (Brock et al., 1999). Comparatively, shallow wetlands, often protected from exposure, are characterized by diverse emergent plant communities, floating aquatic plants, and diverse associated vertebrate and invertebrate communities (Brock et al., 1999). As the floodplain shifts between flood and drought years, water levels in the associated wetlands create a changing mosaic of habitats, with the emergent edge community advancing on the submerged macrophyte beds as open water levels decrease (Brock et al., 1999).

Upstream water level manipulation of rivers by dam impoundment alters the natural dynamics of hydrological fluctuations within downstream floodplain wetlands. By reducing water flow through the system, dams and other impoundments can disconnect rivers from their floodplains, and consequently these floodplains no longer receive the seasonal inputs of sediment, nutrients and propagules required for healthy functioning (Kingsford, 2000; Tockner et al., 2008). For example, barriers, including dams, have been shown to impact dispersal of macrophytes (Jones et al., 2020) and migratory fish (Barbarossa et al., 2020), through altered longitudinal and lateral connectivity. Even when the connection between the river and the floodplain remains intact, water level manipulations can homogenize flows into wetlands (Tockner et al., 2008). Through hydropeaking, even run-of-the-river dams can significantly alter downstream hydrology; water may be released at regular intervals or steadily, unlike the variable flood pulses in a natural system (Almeida et al., 2020). In temperate rivers, where ice jams are an important driver of spring flood pulses (Tockner et al., 2010), dams can create physical barriers to ice, altering ice regimes by impacting the probability and location of ice jams, and thus the volume and timing of the spring freshet (Huokuna et al., 2020). Dams also change sediment dynamics in the river by trapping fine sediment behind impoundments, starving them of nutrients and leaving downstream riverbeds composed of greater proportions of gravel (Csiki and Rhoads, 2014). When water is released downstream, as in large flood years, the resulting flow can scour the floodplain (Galat et al., 1998; Csiki and Rhoads, 2014). In many rivers, hydrological isolation, or reduced connectivity of the river and its floodplain has drastically changed the landscape and reduced wetland extent (Galat et al., 1998; Tockner and Stanford, 2002). Altered flood regimes, a decrease in propagule rejuvenation, and a change in sediment composition and nutrient chemistry can create habitats where few species thrive, decreasing biodiversity within the ecosystem.

Due to lack of comparable global inventories, arising partly due to difficulty in determining wetland boundaries, a reliable pre-Anthropocene estimate of wetland extent has yet to be produced (Revenga et al., 2000). After an approximated loss of at least 50% of wetlands in the last century alone (Myers, 1997), current estimates put global coverage at 10% of the earth's surface, with floodplains comprising 15% of this (Tockner et al., 2008). Over the last three decades, almost 90,000 km^2 of permanent surface water has been lost, but overall, surface water has increased, due in large part to the creation of new permanent water bodies as hydropower reservoirs (Pekel et al., 2016). Our human footprint is most apparent in river floodplains; due to increasing human pressure and a desire to train rivers to meet our needs, almost 90% of floodplains in the Northern Hemisphere have been altered to the point of functional extinction (Tockner and Stanford, 2002). In fact, recent floodplain chronostratigraphy work by Brown et al. (2018) states that millenia-long interventions to river-floodplain systems in Europe have altered riverscapes to the point where it is no longer possible to identify their natural state. The prevailing model of lowland meandering channels with silt-clay floodplains may actually be a result of centuries of anthropogenic use,

including the construction of weirs and water mills, channel maintenance, controlled flooding and grazing pressure (Varga et al., 2013; Brown et al., 2018). Comparatively, in North America, modifications to rivers and their floodplains have taken place more recently (Brown et al., 2018), suggesting that it could be possible to protect the remaining wild rivers that still maintain connectivity with their floodplains.

The lower Wolastoq | Saint John River watershed is one of the last examples of a largely intact Atlantic river floodplain, acting as a vital reservoir for rare and endangered species and as an important nursery, nesting habitat and flyway for migratory and transitional species (Washburn and Gillis Associates Ltd, 1996). Despite its outstanding conservation value, it has nevertheless been subjected to multiple anthropogenic disturbances in the form of upstream dam construction and major local highway construction against a background of anthropogenic climate warming (Washburn and Gillis Associates Ltd, 1996; Canadian Rivers Institute, 2011; Stantec Consulting Ltd., 2015). In the past century, the hydrologic alteration of the watershed has proceeded during the construction and operation of 11 hydroelectric dams, 3 of which are located on the mainstem of the river (Canadian Rivers Institute, 2011). The most significant of these are Beechwood Hydroelectric Station ("BHS") and Mactaquac Generating Station ("MGS"). The construction of these run-of-the-river dams in the 1950s and 1960s created large reservoirs and altered downstream hydrology of the river (Canadian Rivers Institute, 2011; Stantec Consulting Ltd., 2015), and while the Wolastoq | Saint John River still maintains connectivity with its floodplain, alteration of water and sediment flows into its floodplain has almost certainly occurred. Like many floodplains globally, the lower Wolastoq | Saint John River and its associated floodplain wetlands, including the Grand Lake Meadows and Portobello Creek wetland complex (collectively denoted as the "GLM complex") have experienced an increase in the magnitude and frequency of large floods (Canadian Rivers Institute, 2011), thought to be linked to the hydrological alteration of the flood pulse. Understanding the present and future consequences of these hydrological alterations is critical for future mitigation of human impacts on the floodplain in an era of global human-driven climate change.

This study aimed to determine if there are areas that have experienced significant change to floodplain wetland extent associated with major anthropogenic disturbance within the Wolastoq | Saint John River watershed, and to determine if these areas are responding similarly in terms of habitat structure and environmental stressors. This was done by (1) quantifying how wetland habitat has changed over the last 70 years and identifying areas of highest change, (2) examining habitat diversity across the GLM complex and classifying areas that potentially experience higher levels of disturbance, and (3) determining if those high disturbance areas remain protected by current conservation protection measures. In answering these questions, we can identify habitat diversity and disturbance regimes that may dictate how the ecosystem and its communities will respond to future disturbance events. A key outcome of this work is to provide a habitat template for future studies examining the response of biodiversity-ecosystem function relationships to disturbance regimes. This has important policy implications as well, as outcomes may inform policy makers on where best to prioritize conservation efforts.

MATERIALS AND METHODS

Study Sites

This study was focused on Atlantic Canada's largest freshwater wetland complex, the Grand Lake Meadows and Portobello Creek wetland complex (the GLM complex; **Figure 1**). The region is part of the Atlantic Maritime ecozone, with average annual temperature of 5.6 ± 2.9°C and average annual precipitation of 1077.7 mm (Canadian Climate Normals data for station 8101500, calculated between 1981 and 2010; Government of Canada, 2020). The GLM complex is part of the floodplain of the Wolastoq | Saint John River; in the spring, driven by ice jams and the spring freshet, water overflows the banks of the river into the floodplain (Washburn and Gillis Associates Ltd, 1996; Cunjak and Newbury, 2005). Within the floodplain, over 85% of the GLM complex's 9,000 ha is flooded annually (Washburn and Gillis Associates Ltd, 1996), linking floodplain wetlands with the main river channel and allowing for the replenishment of sediment and nutrients. The annual flood pulse flows into the wetland complex through the westernmost streams and channels, draining from the floodplain back via the Jemseg River to the Wolastoq | Saint John River main channel (**Figure 1**; Washburn and Gillis Associates Ltd, 1996). Compared to other inland freshwater wetlands in the province, the GLM complex is extremely productive, fueled both by seasonal flooding from the spring freshest and an accelerated biogeochemical cycle from the process of wetting and drying (Washburn and Gillis Associates Ltd, 1996). The floodplain connects the Wolastoq | Saint John River to Grand Lake, the largest lake in the province; this lake is so large that it influences local climate, warming the surrounding area by several degrees, supporting the formation and maintenance of unique habitats for this region of the country, including extensive silver maple swamps (Washburn and Gillis Associates Ltd, 1996; Broster and Dickinson, 2015).

As part of the Wolastoq | Saint John River watershed, the GLM complex is subjected to the numerous anthropogenic influences that occur within the riverscape, including upstream dam construction (BHS is located 180 km upstream from the GLM complex and MGS is 45 km upstream), the construction of a new section of the Trans-Canada Highway through the downstream end of the wetland complex (constructed in 2001), agricultural activity, human settlement, and public recreational use. To minimize the potential impact of these threats, portions of these wetlands are protected by the New Brunswick Provincial Government, as the Grand Lake Meadows Protected Natural Area (GLM PNA) and by the Federal Government of Canada, as the Portobello Creek National Wildlife Area (PC NWA) (for more information on permitted activities within these protected areas see **Supplementary Table 1**). Across the edge of the GLM complex, 60 sites were sampled between June 2017 and August 2017 (**Figure 1**). Sites were distributed between three levels of protection: (1) unprotected (n = 12), (2) non-contiguous

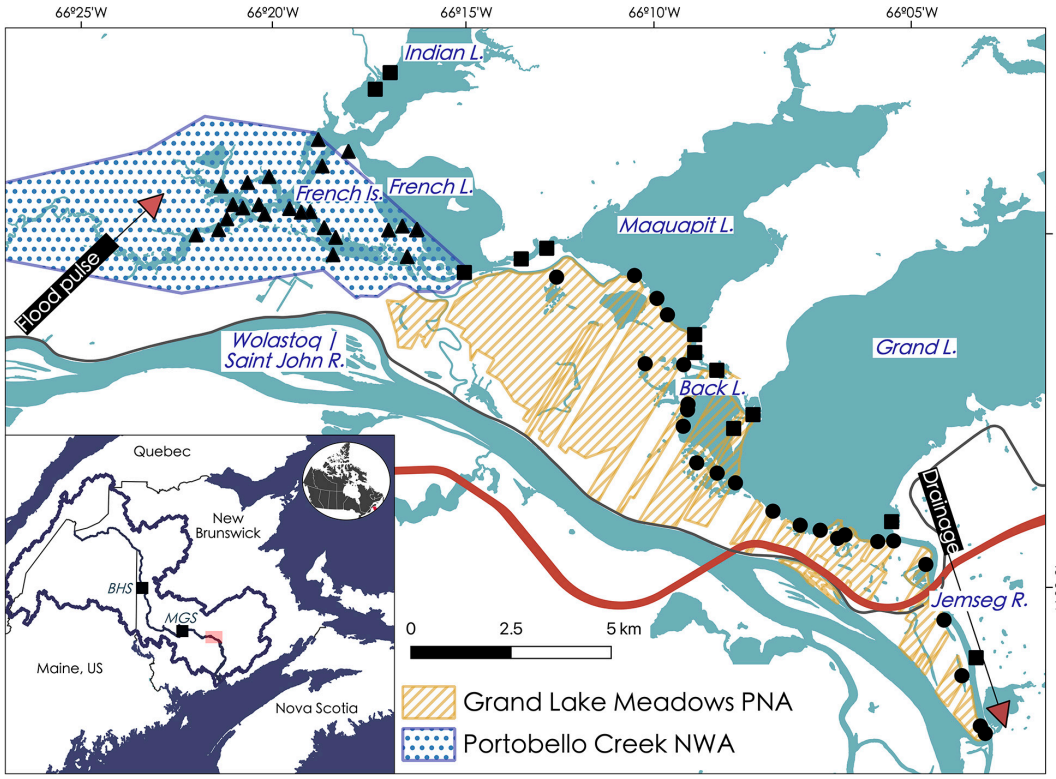

FIGURE 1 | Study sites within the GLM complex relative to different protection strategies, including Portobello Creek NWA (blue) and Grand Lake Meadows PNA (orange). Key locations are labeled. Sites are grouping into Portobello Creek NWA sites (triangles), Grand Lake Meadows PNA sites (circles) and sites in areas of no known protection strategy (i.e., "unprotected") (squares). The dominant flow of water into the wetland complex during the open water season is outlined by arrows. The old road (not raised and frequently overtopped) and the new Trans-Canada Highway (raised) are depicted in gray and red, respectively. Inset map shows location of sampling (red box) and upstream generation stations (BHS, Beechwood Hydroelectric Station; MGS, Mactaquac Generating Station) in relation to Wolastoq | Saint John River watershed and the mainstem of the river.

protection (GLM PNA; n = 24), and (3) contiguous protection (PC NWA; n = 24). All sites were accessible by boat from the lake edges but were disconnected from the main channel of the Wolastoq | Saint John River at the time of sampling. Each sampling site represented aquatic wetland habitat, consisting of emergent and submerged macrophytes, and extended from the edge of terrestrial high marsh vegetation to open water. A pair of bamboo poles marked the midpoints for each site and all biotic and abiotic samples were taken within 50 m of these poles for each site.

Determination of Historical Change in Wetland Extent

To determine change in wetland extent across the shoreline of the GLM complex since major human-driven change within the watershed, the historical shorelines were compared for pre- and post-construction of major dams (BHS, constructed in 1957, and MGS in 1968) and a portion of the Trans-Canada Highway (2001) in the Wolastoq | Saint John River watershed. Aerial photographs (processed at 1 m pixel resolution) from 3 years (1951, pre-dam construction; 1983, post-dam/pre-highway; 2014, post-highway; **Figure 2**) were obtained from the New Brunswick Department of Natural Resources and Energy Development, digitized, and georeferenced using ArcGIS (version 10.6.1; Environmental Systems Research Institute [ESRI], 2018) with a minimum of 10 control points per photograph. The shoreline for each year was digitized, closely following the wetland edge at a 1:25 scale, with a starting distance of 1.6 m between points, with quality control checks performed at regular intervals. An onshore baseline (**Figure 2**) from which to correct and measure historical shorelines was manually created with a new feature class in ArcGIS (version 10.6.1; Environmental Systems Research Institute [ESRI], 2018) following the recommendations of the USGS Digital Shoreline Analysis software protocol (Himmelstoss et al., 2018); subsequently, all measurement transects extended orthogonally from the baseline.

Since the aerial photographs were taken in different seasons depending on the year, the water levels for all shorelines required correction to a common mean water level (MWL). Final points along these lines were adjusted using the one-line shift method developed by Chen and Chang (2009), which shifts extracted shorelines on three sequential images to the corresponding shorelines based on MWL. The MWL was calculated for the open water season (May– October) between 2001 and 2017 for the Jemseg River (01AO004; mean = 1.734 m) and Lakeville (01AO010; mean = 1.810 m) gauging stations; these data

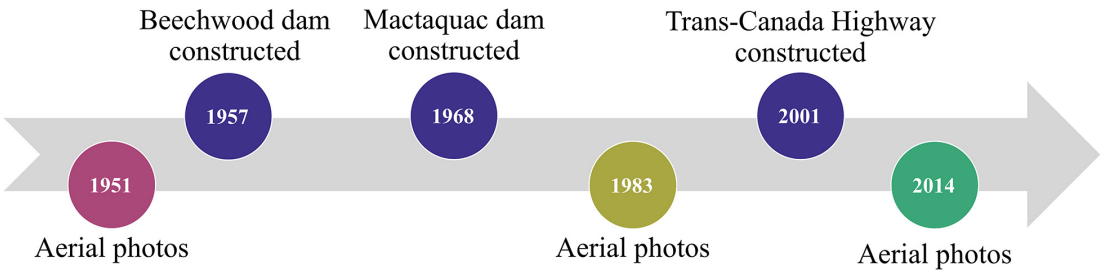

FIGURE 2 | Timeline of local anthropogenic alteration within the lower Wolastoq | Saint John River and the aerial photographs of the GLM complex which were digitized and used to assess historical change to wetland extent.

were accessed through the HYDAT database available from the Water Survey of Canada (2017). The 1950s photographs were taken before the Lakeville and Jemseg River gauges started recording so data were infilled using a regression between the two GLM complex gauges (01AO010 and 01AO004) and a nearby gauging station in Fredericton (01AK003) using all available open water data. Seventy percent of the data were randomly assigned to be used for calibration and 30% were saved for model validation, and the models were assessed using the Nash-Sutcliffe coefficient (Nash and Sutcliffe, 1970; 01AO010: calibration = 0.96, validation = 0.95; 01AO004: calibration = 0.94, validation = 0.93) and Root Mean Square Error (RMSE; 01AO010: calibration = 0.05 m, validation = 0.05 m; 01AO004: calibration = 0.03 m, validation = 0.04 m).

Perpendicular transects were generated every 25 m along the common onshore baseline and extended through all corrected historical shorelines (**Figure 3**). Shoreline change was measured for each perpendicular transect from the baseline to the shoreline and the change between 1951 and 1983, 1983 and 2014 and overall change (1951–2014) was calculated (**Figure 3**). For each set of measurements along a transect, the change was ranked from largest (1) to smallest (3) to compare during which period the most change occurred across a gradient of magnitudes. A categorical scatterplot (also known as a dot plot) was made with the resulting data to visualize how shoreline change was distributed across the time periods, with each measurement represented as an individual dot on the plot, and measurement classes grouped into bin sizes [plot made with the *ggplot2* package (version 3.2.1; Wickham, 2016) in R (version 3.5.3; R Core Team, 2019)]. The *y*-axis was log-scaled for easier visualization of the extreme ends of the data. To visualize historical change across the time periods, ArcGIS (version 10.6.1; Environmental Systems Research Institute [ESRI], 2018) was used to extend the calculated differences were along the baseline, splicing the polyline at each transect and applying the calculated value to that section; no values were assigned outside of a 200 m buffer around a given transect and areas without available measurements were assigned as "no data." Historical change values that were negative and positive were classified as "erosion" and "accretion," respectively.

Examination of plots of historical change across the time periods showed that extreme erosion or accretion events appeared to differ between time periods. To test this, the data were first filtered to areas that were exhibiting sensitivity to extreme change, defined as over 30 m of either erosion or accretion aligning with natural break points for at least one time period per transect. Data were separated for testing of erosion and accretion between the two periods, where erosion was hypothesized to be highest between 1951 and 1983 (n = 381 transects/period) and accretion was hypothesized to be highest between 1983 and 2014 (n = 459 transects/period) based on visual inspection of the plots of historical change. Both models violated parametric assumptions (Shapiro-Wilk normality tests: accretion $p < 0.001$, erosion $p < 0.001$; Levene's Test for Homogeneity of Variance: accretion $p = 0.0027$, erosion $p = 0.6345$), and so a paired, one-tailed Wilcoxon Signed-Rank test was performed for each in R (version 3.5.3; R Core Team, 2019) to test if change differed between periods.

Abiotic Variables

Grab samples for water chemistry were collected using the Canadian Aquatic Biomonitoring Network (CABIN) wetland protocol standard operating procedures (Armellin et al., 2019) in June and July 2017, 1 month apart (N = 2 sets of water samples per site; triplicate samples collected at 10% of sites), and analyzed at the Environment and Climate Change Canada's National Laboratory for Environmental Testing (NLET) for a standard suite of ions, metals, and nutrients (Environment and Climate Change Canada's National Laboratory for Environmental Testing, 2013). Due to the likelihood of fluctuations of spot measurements across space and time, measurements for each site were averaged prior to analysis. For a full analyte list of measured abiotic variables (see **Supplementary Tables 2, 5**).

Grab samples of wetland sediment (N = 1 per site; triplicate samples collected at 10% of sites) were collected following CABIN wetland protocol standard operating procedures (Armellin et al., 2019) and stored in the refrigerator in glass containers until transferred to RPC laboratory- New Brunswick's provincial research organization- in Fredericton, NB for analyses. Following EPA standards (United States Environmental Protection Agency, 1996) samples were analyzed for trace elements, total organic, and inorganic carbon, grain size, and composition (sand, silt, gravel, and clay).

The temperature profile of sites was measured over the sampling period using HOBO pendant temperature loggers (P/N UA 001 64) set to record every 5 min for the duration of the sampling period. Hourly water depth measurements were taken

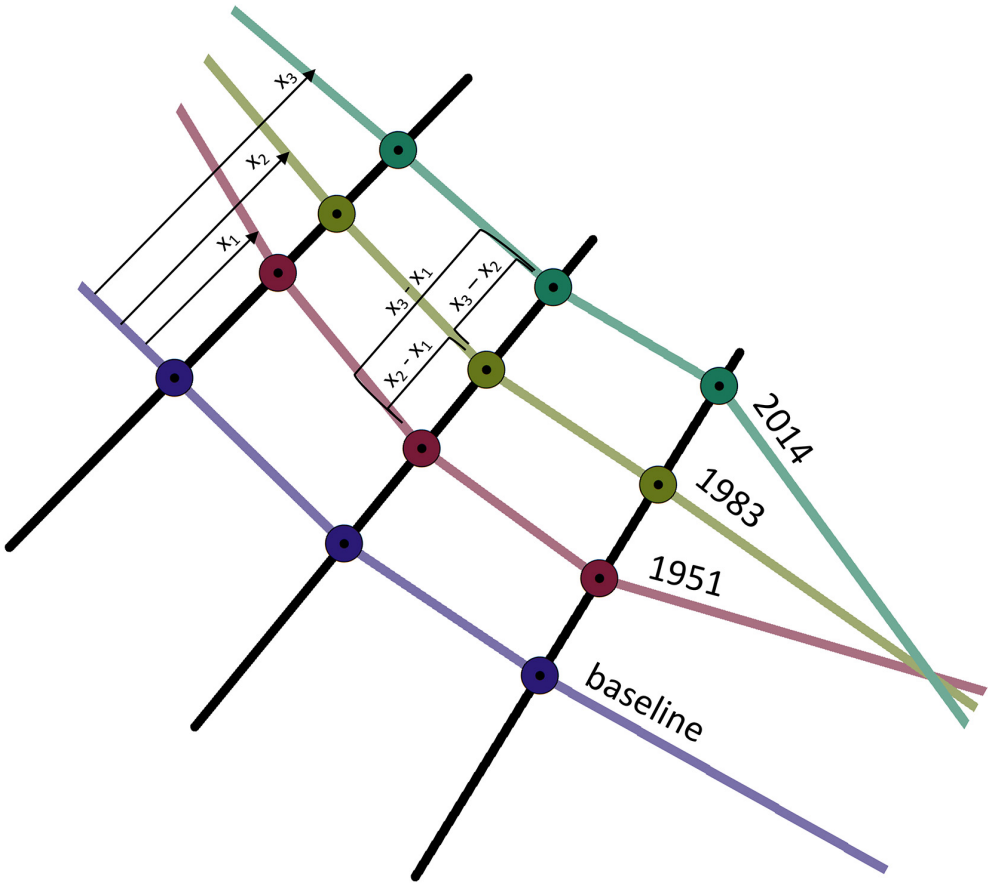

FIGURE 3 | Diagram depicting how historical change of wetland extent within the GLM complex was measured from the corrected shorelines derived from aerial photographs. Shorelines were calculated for the edge of the wetland where sites are shown in **Figure 1**. Transects extended from a manually created baseline through shorelines, resulting in measurements between 1951 and 1983 ($x_2 - x_1$), 1983 and 2014 ($x_3 - x_2$), and overall change ($x_3 - x_1$).

from HOBO water level loggers (range 0–4m, P/N 20-001-04) randomly assigned to 22 sites across the wetland complex; a total of 5 additional loggers were attached at known heights in the air in each lake or water body (corresponding to labeled water bodies in **Figure 1**) as calibration for air pressure. Water depth at sites without loggers was assigned from the nearest logger location. A suite of hydrologic variables was calculated from water depth data using the Indicators of Hydrologic Alteration software (Richter et al., 1996).

Macrophytes

Sampling for the submerged plant community (defined as aquatic vegetation that were either whole submerged or floating, and could be rooted or unrooted) was conducted by 2 observers for 15 min, sweeping in concentric rings around the poles (center of the site), as far as water depth allowed. If richness and abundance were so low that sampling had extended beyond the defined 50 m diameter of a site and no new morphotypes were found in 5 min, sampling was stopped, and the time and distance recorded. All unique morphotypes were collected for identification; the top three dominant species were designated, and the percent cover was estimated for each. Total percent cover was estimated by each observer and all numbers were compared for congruency. Emergent plant communities (comprising individuals with roots in the sediment, but the majority of the plant out of water) were assessed for the whole 50 m diameter site, focusing along the boundary between aquatic and terrestrial ecosystems. Specimens were collected of the top three dominant species, and their percent cover across the site was estimated.

Representative specimens of each macrophyte species present were collected and preserved as voucher specimens for subsequent taxonomic assessment. A subset of the voucher specimens collected were selected for subsequent genetic analysis to establish a reference specimen collection that was used to guide morphological based taxonomic identifications. For genetic analysis of reference specimens, dehydrated leaf tissue was sent to Canadian Centre for DNA Barcoding (CCDB) for DNA extraction, PCR amplification, and sequencing according to CCDB standardized protocols (Fazekas et al., 2012). To facilitate comparison of the genetic results with taxonomic data available on GenBank (NCBI Resource Coordinators, 2017) and the Barcoding of Life Data System (Ratnasingham and Hebert, 2007) two standard land plant DNA barcode markers, *rbc*L*A* and ITS2, were selected (Fazekas et al., 2012).

Visualizing Disturbance Regimes and Habitat Patches

All analyses and data visualization were completed in R (version 3.5.3; R Core Team, 2019). We reduced the number of abiotic variables based on Pearson correlation coefficients ($R > 0.70$; standard cutoff for a "strong correlation"; e.g., Dormann et al., 2013) retaining, among pairs, variables deemed the most ecologically relevant or having higher between-site variance. Variables were *z*-score standardized before Principal Components Analysis (PCA) using the *FactoMineR* package (version 2.3; Lê et al., 2008) to examine how environmental variables differed across the study area. PCA output was plotted on axes PC1 and PC2 as these had the most explanatory power with the *factoextra* package (version 1.0.5; Kassambara and Mundt, 2017). Hierarchical cluster analysis in *vegan* (version 2.5-4; Oksanen et al., 2019) was then performed to examine how environmental variables influenced the grouping of wetland sites, using the complete linkage method, which produces compact clusters with high similarities. Preliminary testing to determine the optimal clustering scheme was done using *NbClust* (version 3.0; Charrad et al., 2014), which tests all combinations of cluster numbers, distance measures and clustering methods; the majority of the produced metrics (8 out of 23) showed that the optimum number of clusters for analysis was three. A heatmap of the results, standardized to scale abiotic variables, was made to visualize results.

Habitat patches and spatial heterogeneity of patch quality in wetland habitat across the landscape was visualized by making individual radar plots for each site using the *fmsb* package (version 0.6.3; Nakazawa, 2018). Variables that were thought to have the most significant impact on biodiversity (e.g., Chipps et al., 2006) were chosen for the plot and *z*-score standardized to ensure that they were on the same scale; variables included in the plots were: silt, sediment and water metals (comprised of PCA axes as outlined below), overall change in shoreline location (absolute values), low pulse duration, the coefficient of variation for water temperature, macrophyte richness, macrophyte total percent cover, percent organic carbon in the sediment and total dissolved aquatic phosphorus. Sediment and water metal inputs were reduced for correlations above a Pearson correlation coefficient of 0.70 and condensed onto principal components axes (PC1 for each, with the sediment PC1 capturing 38.20% of the variance, and the water PC1 representing 44.87%) where higher values indicated increased metal concentrations. To examine differences among the three protection strategies, a separate radar plot was made using the mean values for each of the strategies.

RESULTS

After adjusting for differences in water levels across the years of aerial imagery, change in wetland extent across the GLM complex ranged from accretion of 400 m to erosion of −1450 m (mean = −6.48, $SD = 83.41$, $N = 2{,}500$ transects; among all 1951–2014 data). If change had continued in the same direction over the measured time periods, then the overall change was ranked highest for each transect; indeed, this is the case for most measurements, as indicated by the plot's teal coloring (**Figure 4**). High erosion (over 30 m) occurred between 1951 and 1983, which can be seen by the shift from yellow (lowest rank change) to dark blue (second rank; $n = 381$ transects, $Z = -14.19$, $p < 0.001$). The areas of highest erosion (depicted in shades of yellow to dark red according to magnitude) were located in backwater areas, such as in the coves off the west bank of the Jemseg River, Back Lake and Portobello Creek (**Figure 5A**).

Small shoreline changes (30 m) were greater between 1983 and 2014 than from 1951 to 1983, as shown by the measurements plotted in dark blue (**Figure 4**). These areas are plotted in shades of green on the maps and tend to extend over the edges of large lakes, such as Maquapit Lake and French Lake. Significant accretion (over 30 m) was evident through the period of 1983–2014, particularly across the Jemseg River area (**Figure 5B**; $n = 459$ transects, $Z = -18.60$, $p < 0.001$). During this period certain areas that had started to erode between 1951 and 1983, shifted and started to increase in their extent as they accreted sediment. This shift can be seen most clearly in the wetlands off the west bank of the Jemseg River, with shoreline changes from orange (erosion of −50–200 m) to dark blue (accretion of 100–400 m). Other areas of accretion, shown in shades ranging from aqua to dark blue, were evident across all time periods within the side channels of PC NWA (**Figure 5C**).

The first three axes of a Principal Components Analysis (PCA) explained 43.6% of the variation of abiotic variables among sites: PC1 explained 19.9%, PC2 explained 14.5%, and PC3 explained 8.3% of the variance (**Figure 6**). PC1 shows separation of samples based on micro- and macronutrients, with high scores aligning with increased dissolved nitrogen and total phosphorus concentrations in water samples, and increased molybdenum, potassium, aluminum and iron concentrations in sediment samples; low scores were associated with higher concentrations of barium (**Figure 6**). PC2 shows a separation of geographic regions of the GLM complex from east (low scores, areas plotted in shades of blue) to west (high scores, areas plotted in shades of pink; **Figure 6**). The variables most contributing to this axis were water temperature and metals, with low scores associated with maximum water temperature and high scores associated with alkalinity, minimum temperature, molybdenum and sodium concentrations in the water, and boron, magnesium and zinc concentrations in the sediment.

Cluster analysis grouped sites first by sediment iron, molybdenum and aluminum concentrations: sites located on French Island (P55 and P53) and two sites located at far ends of coves within PC NWA (P39 and P46) having the highest levels of the metals, shown in shades of blue near the bottom of the plot (**Figure 7**). The rest of the sites had generally lower concentrations, as depicted by the red coloring on the plot (**Figure 7**), with a sub-cluster of sites that were located along large lake edges and the edge of the Jemseg River consistently showing the lowest concentrations of sediment aluminum and molybdenum, visible as bands of dark orange (G17, G21, G23, G12, G05, U34, G19, G11, G16, U31, G10). The next significant cluster grouped the most northerly located sites, found in Indian Lake (U36 and U32) with the lowest levels of iron, aluminum, magnesium, potassium and boron in their sediment

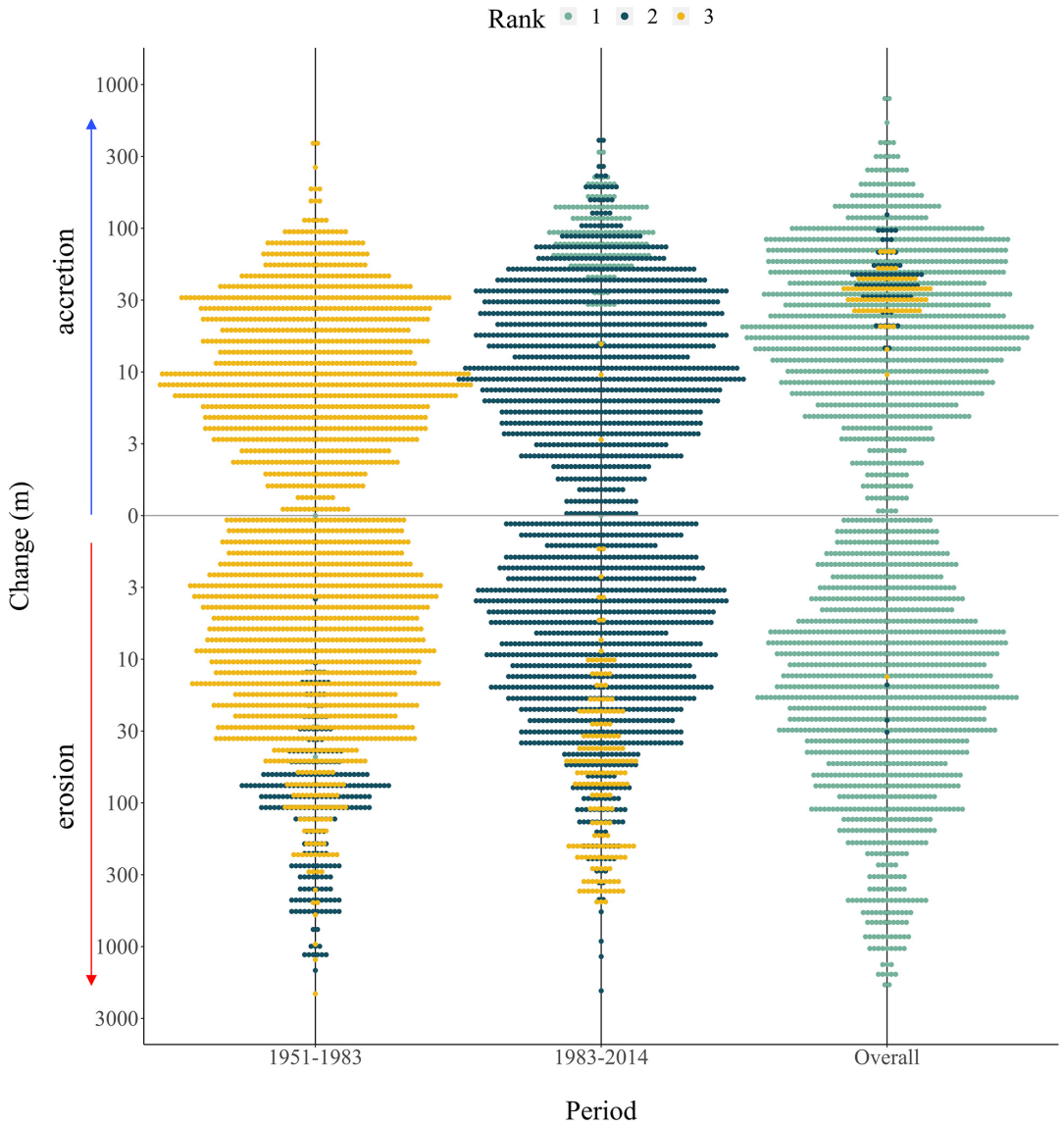

FIGURE 4 | Categorical scatterplot summarizing change in wetland extent in the GLM complex across measured time periods, showing which periods experienced the most erosion and accretion. At each measured point, the change between the periods was ranked, with a rank of 1 assigned to the period with the highest change. If change magnitude increased in the same direction (either erosion or accretion) then "overall change" would have a rank of 1 (i.e., highest change). Each dot represents a single measurement between shorelines, with wider bars indicating more measurements for that size bin. The *y*-axis was log-scaled for easier visualization of the extreme ends of the data.

(shown in dark red and burgundy). These sites also had similar levels of other environmental variables, such as molybdenum, potassium, nitrogen, copper, and barium concentrations in the water, molybdenum concentration and percent organic carbon in the sediment, and alkalinity, base flow rate and high pulse duration. Sites appeared to be grouped more by their hydrology and connectivity within the floodplain, than by geographic relationship alone.

Radar plots for each site are consistent with sites grouping by hydrologic connectivity (**Figure 8**). Sites in PC NWA had higher levels of most variables, particularly phosphorus, sediment and water metal and organic carbon, as indicated by the overall larger area of the individual radar plots, as well as the mean values for the whole protection level compared to GLM PNA and unprotected sites. The sites in PC NWA are more protected from wave exposure, as are the other sites that follow the same pattern of high overall levels of the chosen abiotic variables. Sites located along the edge of the large lakes, namely Indian Lake, Maquapit Lake and Grand Lake tended to have smaller radar plot areas overall, i.e., lower relative levels of measured variables. These sites tended to be located within the GLM PNA, where, compared to other protection levels, sites had on average lower levels of phosphorus, low pulse duration and silt. Unprotected sites, which were

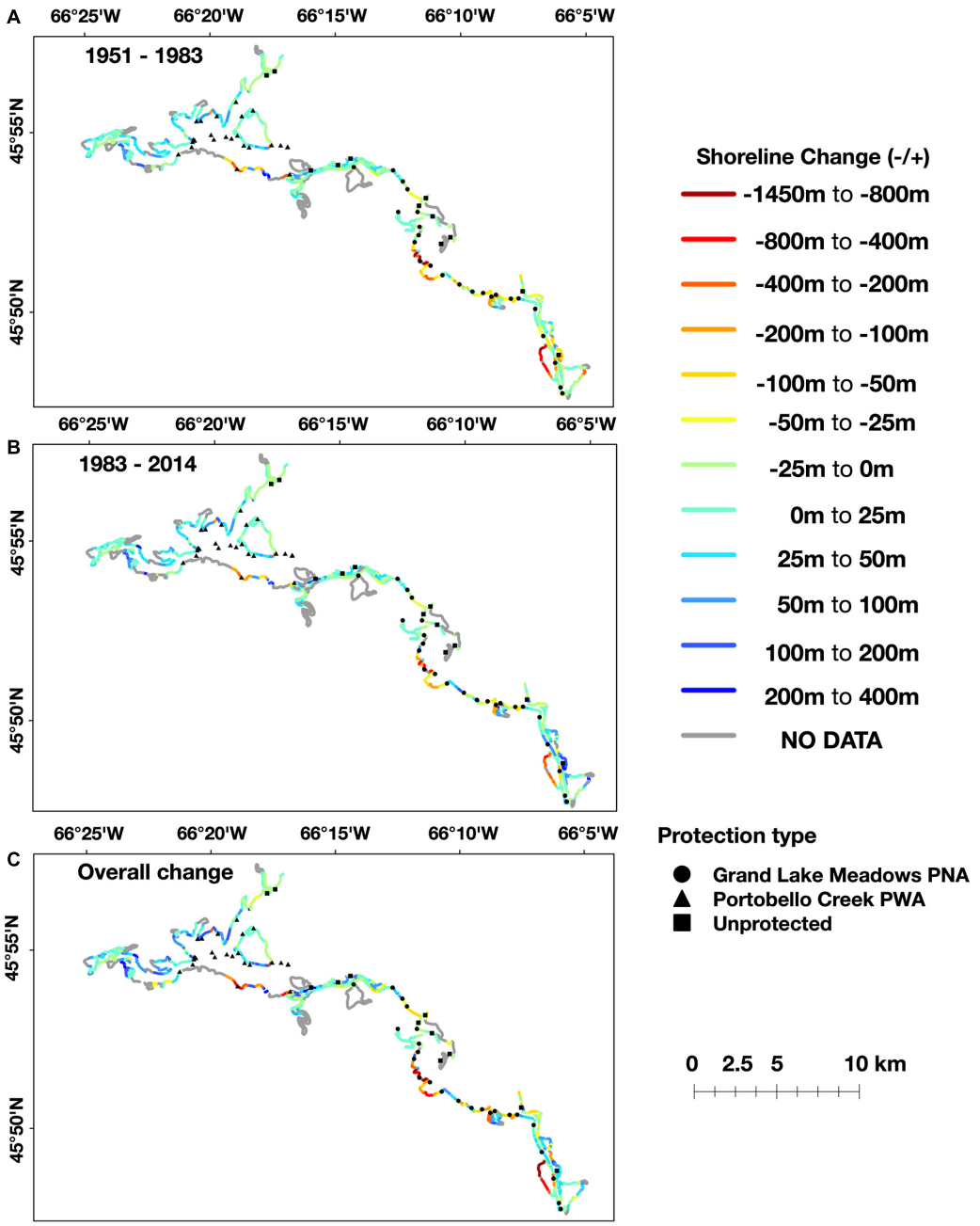

FIGURE 5 | Visualization of measured change in wetland extent in the GLM complex across periods of major anthropogenic change within the watershed, showing the difference between 1951 and 1983 **(A)**, 1983 and 2014 **(B)**, and overall cumulative change **(C)**. Sampling sites from 2017 are plotted on the maps to show distribution across different levels of historical change.

scattered throughout the study area, had a range of habitat patches, with the mean showing the lowest levels of water and sediment metals and organic carbon. Macrophyte richness and cover, overall historical change and the coefficient of variation of water temperature were similar across the GLM complex, regardless of protection level, suggesting that these variables are driven by the patchiness of flood pulse dynamics, rather than geographic proximity.

DISCUSSION

Anthropogenic Alteration of Floodplain Wetlands

Floodplains naturally experience channel migration and a shifting of wetland habitat boundaries over time as flood pulses vary from year to year (Bayley and Guimond, 2008); however, recent significant changes of wetland extent within the GLM

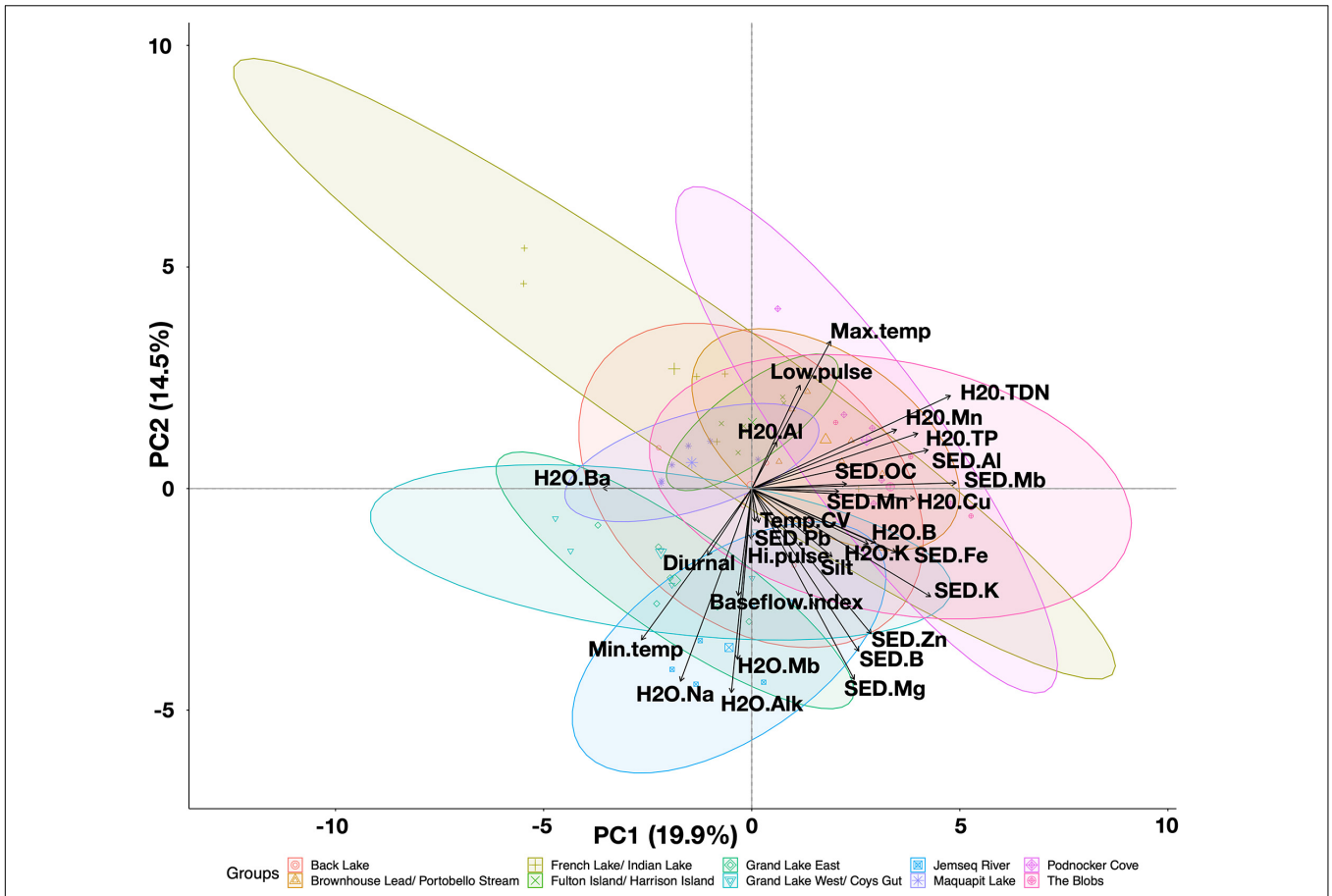

FIGURE 6 | Principal Components biplot projecting axes PC1 and PC2 for abiotic variables across 2017 sampling sites in the GLM complex. All variables were reduced first from correlations for below 0.7 collinearity before being subjected to the PCA. Sites are colored by geographic area with pink sites located furthest west within Portobello Creek and blue sites located in the east toward Grand Lake and Jemseg River. Acronyms for specific input variables listed in **Supplementary Table 6**.

complex can be linked to periods of major anthropogenic alterations in the Wolastoq | Saint John River watershed, appearing to follow the upstream construction of run-of-the-river dams and the construction of a new Trans-Canada Highway within the wetland complex. Erosional change was highest immediately following the period when the Beechwood (1957) and Mactaquac (1968) dams were constructed, suggesting support for the hypothesis that altered flood pulse and sediment deposition into the floodplain triggered significant erosion of the wetland. This was also during the period when agricultural land practices in the potato farming region located upstream of both Beechwood and Mactaquac began to change, shifting away from losing significant amounts of topsoil each year (Harvey, 1976; Chow et al., 2000); this landscape change could result in lower amounts of sediment being deposited in the floodplain wetlands with the flood pulse each spring, aiding erosion.

Erosion has continued, albeit at a diminished level, until recently, implying that those wetlands continued to experience shoreline change over time due to a perpetuation of the altered hydrologic and sediment deposition regimes. While the postulated change relating to hydroelectric dam construction was most significant for areas that experienced erosion, the most substantial change in recent years was accretional. This was associated with the construction of a section of the Trans-Canada Highway along the edge of the GLM complex and through wetland habitat near the Jemseg River; in this area of floodplain wetlands adjacent to the Jemseg River the most significant accretion was evident, supporting the hypothesis that the hydrologic isolation from highway construction has contributed to significant shoreline change in the area compared to other protection levels.

Floodplains are ecosystems with high spatial heterogeneity, characterized by a mosaic of habitat patches with varying levels of connectivity to the main channel and each other; these patches may be at different levels of ecological succession depending on the shifting boundaries of annual flood pulses (Junk et al., 1989; Ward et al., 1999). Any alteration of the flood pulse, namely the inundation of wetland habitat by flood waters and sediment deposition, therefore affects habitat patches differently, even across relatively small spatial scales. Since the construction of the run-of the-river dam, Mactaquac Generating Station, the frequency and magnitude

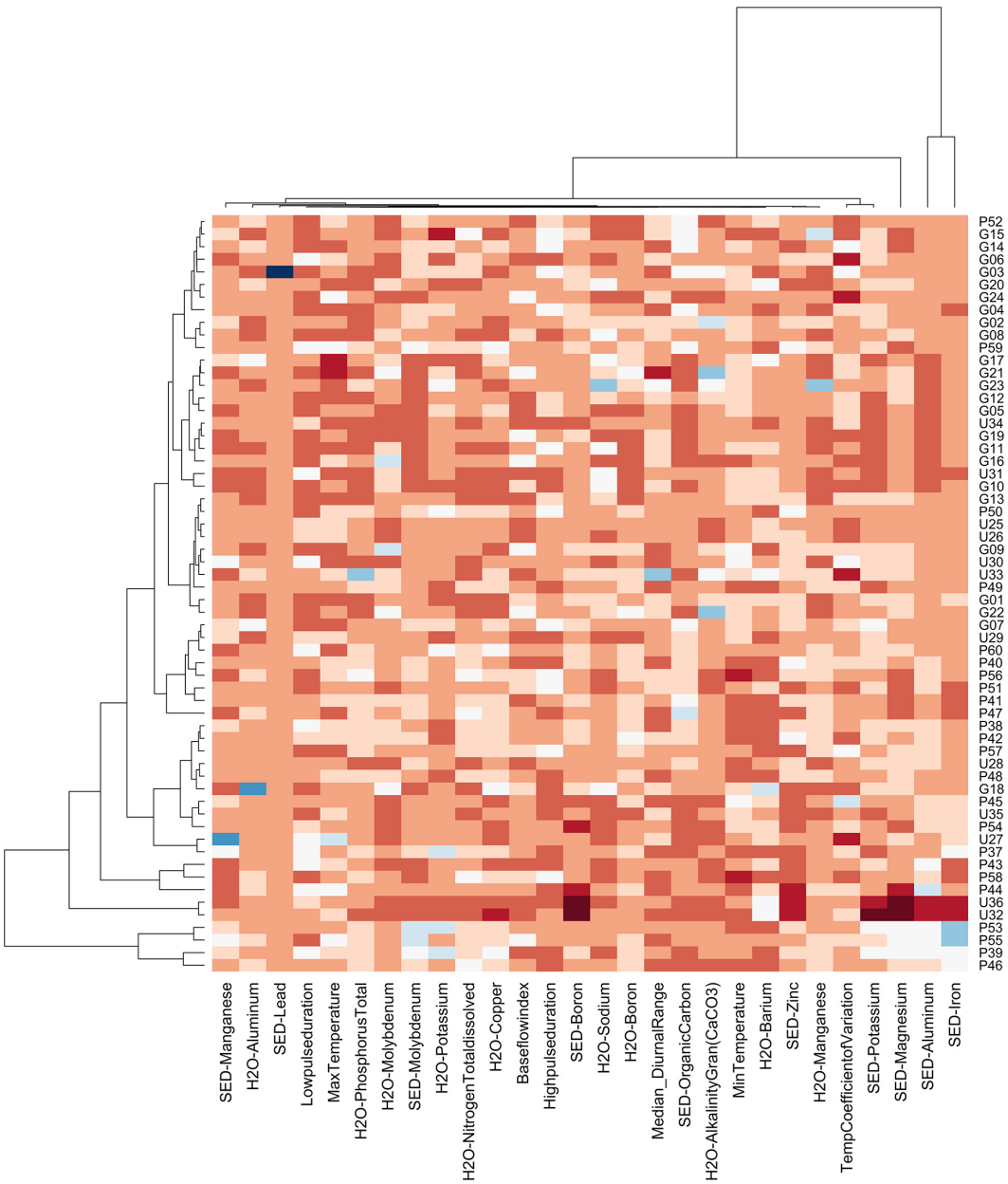

FIGURE 7 | Heat Map showing natural groupings of sampling sites in the GLM complex by abiotic variables with cluster analysis. All abiotic variables were reduced for correlations above 0.7; cells are colored according to their standardized value with lowest values depicted in dark red and highest in dark blue.

of large floods in the Wolastoq | Saint John River has increased, but this coincides with similar observations at the wider watershed scale (Canadian Rivers Institute, 2011). This suggests observed changes within the GLM complex are being compounded by other factors such as climate change and increased urbanization, and there is some evidence of limited sediment deposition behind Mactaquac Dam (Grace et al., 2017). Dam construction is, however, linked to the probability and location of ice jams, an important flood pulse mechanism in the Wolastoq | Saint John River (Canadian Rivers Institute, 2011; Huokuna et al., 2020). Although it is problematic to confirm without baseline measurements, the increased inundation period, as well as the sediment deprivation experienced in floodplains following upstream dam construction (Marren et al., 2014), likely had a role in the loss of wetland habitat that is evident in the GLM complex. The patches that experienced the most erosion were backwater and cove habitats, areas that tend to have more transient boundaries between wetland and high marsh habitat (unlike, for example, the edges of large lakes), where shallower slope facilitates amplified inundation and thus a transition to increasingly open water habitat.

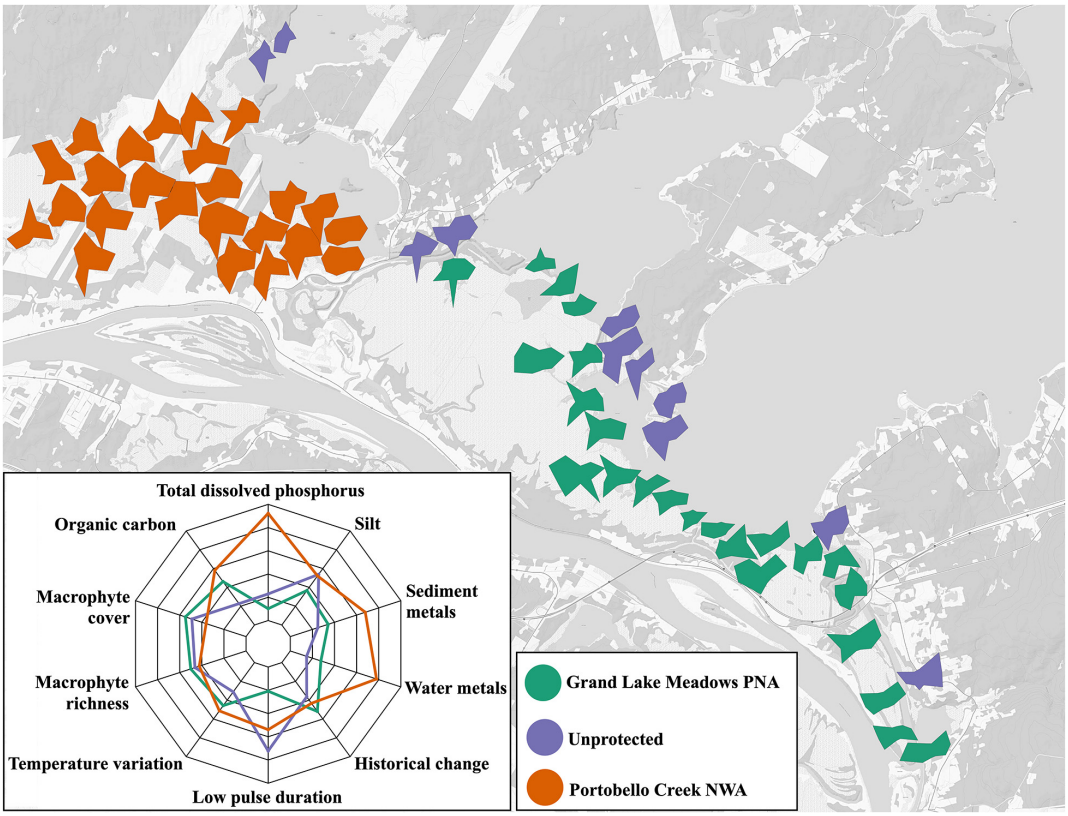

FIGURE 8 | Map of distribution of variables that are thought to have the greatest impact on shaping aquatic biodiversity in the GLM complex. Each site is depicted by a radar plot, where input variables are standardized to a scale of (0,1), and greater area of the radar plot indicates higher values of measured variables. The plot in the insert shows the mean for all sites within a protection classification.

In contrast, when the Trans-Canada Highway was constructed in 2001, 55 ha of floodplain wetland habitat adjacent to the Jemseg River was hydrologically isolated, thus no longer experiencing the same flood pulse dynamics (Washburn and Gillis Associates Ltd, 1996). Although an existing highway had already traversed the length of the GLM complex, it was frequently overtopped during flood pulse events, permitting transport of sediment, nutrients and biological propagules to the floodplain wetlands, albeit at a fraction of the level experienced in natural flood pulse events (Washburn and Gillis Associates Ltd, 1996). The new highway has a raised construction and was predicted to only be overtopped in a 1:20 years flood (Washburn and Gillis Associates Ltd, 1996); while the wetlands still flood, the transport of sediment and nutrients to certain habitat patches has been further diminished. The input and deposition of sediment and nutrients from flood pulses is particularly important in areas of sediment loss, such as the outflow from wetlands back into the main channel (e.g., the Jemseg River, which flows from Grand Lake into the Wolastoq | Saint John River) (Brinson, 1993). When the flow of the flood pulse into the wetlands was halted by the raised highway construction, these isolated areas were no longer inundated, transforming the aquatic wetland patches to terrestrial high marsh habitats. Trapped between two stretches of highway, accretional areas were most evident around the Jemseg River, where a combination of sediment loss and lack of hydrological connectivity led to an increase in upland habitat and a consequent loss of shallow aquatic wetlands.

Spatial Heterogeneity of Wetland Habitat Is Shaped by Connectivity

Depending on connectivity across the landscape, areas of accretion and erosion for all time periods were found across the entire GLM complex. Flood pulse dynamics were acting to both increase and decrease wetland extent, highlighting how significant the impact of connectivity and flow regimes are to these vital floodplain habitats. Connectivity and disturbance, subsequently, are important drivers of the biotic communities found within floodplain wetlands. Ward et al. (1999) hypothesized that biodiversity within floodplains would be highest at intermediate levels of both disturbance and connectivity, whereby at low connectivity, nutrients, sediment and organisms cannot be exchanged between communities, and at high connectivity, habitat heterogeneity is reduced, thus reducing niche availability. An updated model by Arias et al. (2018) combined principles from the Intermediate Disturbance Hypothesis (Connell, 1978) and the flood pulse concept (Junk et al., 1989), proposing that flooding patterns and disturbances within the watershed (both anthropogenic and

natural) can create spatial interactions to form a disturbance regime, shaping floodplain diversity along any disturbance gradient. Our study identifies the connectivity and disturbance regimes within floodplain wetlands of the Wolastoq | Saint John River, laying the groundwork for an exploration of the resulting consequences for floodplain biodiversity and associated ecosystem functions.

Beyond flood pulse dynamics and habitat boundaries, the ability to retain nutrients, filter metals and support complex macrophyte beds serving as habitat for invertebrate and fish communities directly depends on the hydrology and associated connectivity between habitat patches within the floodplain wetland complex. In the GLM complex, Principal Components Analysis revealed a grouping of sites from east to west, where sites experienced an overall change both in connectivity and hydrology. PC NWA, located in the west, is the most upstream part of the wetland complex, and as such is the first to experience the annual flood pulse; sites to the east, along the Jemseg River, drain first as the flood pulse moves through the floodplain back to the Wolastoq | Saint John River via the Jemseg River (Washburn and Gillis Associates Ltd, 1996).

Cluster analysis also supported the importance of hydrology and connectivity as factors grouping sites, as did the visual representation of patch diversity by radar plots (**Figure 7**). Sites located on lakes, which are open (i.e., fully connected) and exposed, tended to have lower levels of metal and nutrient accumulation, whereas backwater coves with decreased connectivity showed evidence of metal accretion in their sediments. Together, these factors have multiple consequences for provisioning of floodplain wetland ecosystem services. For example, it demonstrates that backwater coves are acting as sinks of potentially toxic metals, as depositional environments sheltered from wave exposure. This is also associated with retention of organic carbon, which can enhance metal storage capacity (Du Laing et al., 2009). Cadmium concentrations in the sediment had a high positive correlation with the percentage of organic carbon in the sediment, supporting this explanation. Beltaos and Burrell (2016) also found evidence for a strong metal association with the suspended sediment raised during ice jams in the Wolastoq | Saint John River, suggesting that flood pulses facilitate metal transport throughout the watershed. Moreover, their research indicated that measured aquatic concentrations of aluminum, iron and copper could be orders of magnitude higher during breakup conditions than open-water conditions (Beltaos and Burrell, 2016). This said, across the GLM complex, very few metals were above aquatic toxicity guidelines (Canadian Council of Ministers for the Environment, 2014; for average concentrations see **Supplementary Tables 2, 3**), with the exception of those few (e.g., iron and aluminum) that are naturally abundant crustal elements in the underlying geology of the Wolastoq | Saint John River watershed and are therefore found at high concentrations (Canadian Rivers Institute, 2011).

Through nutrient retention, sheltered coves also allow for the formation of diverse macrophyte communities with high complexity (Hansson et al., 2005), providing a variety of niches to invertebrate communities, thus supporting increased richness (Kovalenko et al., 2012; Walker et al., 2013). Moreover, some metals, such as iron, copper, nickel and molybdenum act as plant micronutrients, and as such are important components of wetland ecosystems (Merchant, 2010). The combination of macro- and micro-nutrients, organic carbon storage, and protection from wave exposure should lead to abundant macrophyte growth, however, despite seemingly suboptimal conditions, macrophytes were found at all sites in our study, just in varying degrees of abundance and richness. Spatial heterogeneity of habitat patches within the floodplain wetlands has led to differences in the structure of macrophyte communities across the wetland complex, forming important habitats for aquatic invertebrates and thus helping to shape community composition.

Current Protections and Impacts for Biodiversity

Due to its ecological significance, the GLM complex is protected by the provincial and federal government, but the extent of the protection, as well as the ease of enforcement, has important consequences for its habitat patches. PC NWA, with the most complete protection, had higher levels of macro-nutrients (particularly phosphorus) and micro-nutrients (i.e., some metals), more sites that were protected from wave exposure, and a larger build-up of organic carbon. Much of this is likely due to connectivity and the geographic location, rather than its protection strategy. While there are, indeed, more restrictions for recreational and commercial use in PC NWA, it is also harder to access, meaning less people are using the area, and it is easier to enforce protections.

Sites within the PC NWA are located along small coves and channels, rather than the exposed edge of the lakeshore as found for many sites in the GLM PNA and unprotected areas, meaning they will naturally have differences in the retention of vital abiotic building blocks, leading to the formation of highly productive wetland habitat. These differences are so substantial that until now the two areas (Portobello Creek and the Grand Lake Meadows) have been studied separately. For example, the most recent previous plant surveys of the area were completed by two separate groups, with Environment Canada's Canadian Wildlife Service performing a survey in the PC NWA (Blaney, 2003), and Papoulias et al. (2006) working on behalf of the New Brunswick Federation of Naturalists on an inventory of vascular plants within the Grand Lake Meadows (most of which is protected as the GLM PNA).

Historical change from erosion or accretion across the shoreline edge has put habitat patches at varying degrees of succession (Bayley and Guimond, 2008; Tockner et al., 2010). This implies that areas with significant change, found at a higher level within the GLM PNA (porous protection) and PC NWA (complete protection), are in earlier stages of succession (Lallias-Tacon et al., 2017), thus having a higher degree of disturbance. Sites within both protected areas had overall higher values for mean historical change, indicating that there are limitations to protection. While current protection can limit the introduction of invasive species, contamination and nutrient

runoff from agricultural areas, it does not currently mitigate altered flood pulse dynamics.

Changes to ecological succession from shoreline change may also have positive effects on wetland communities; following the Intermediate Disturbance Hypothesis, diversity of the biota that inhabit these habitat patches could positively benefit from introduced disturbance (Connell, 1978). Within floodplains, the flood pulse serves as an essential, natural ecological disturbance, creating spatial and temporal heterogeneity, increasing niche diversity, and thus functional richness (Ward et al., 1999; Tockner et al., 2010; Arias et al., 2018). With many patches at different stages of succession across the landscape, and experiencing a different regime of abiotic filters, the GLM complex has the capacity to play host to a wide variety of taxa that have a rich suite of traits. Communities with a diverse set of traits should more effectively utilize the ecosystem's resources as well as provide the ecosystem functions for which humans rely and floodplain wetlands provide.

CONCLUSION

A forthcoming study will examine how the relationships between biodiversity and ecosystem function are affected by the disturbance regimes operating on the Wolastoq | Saint John River floodplain wetland microhabitats. As climate change continues to bring increased levels of precipitation, earlier snow-melt and consequently flashier, potentially catastrophic flooding (Tockner and Stanford, 2002), understanding current disturbances and their effect on local communities is central in helping to predict the consequences for wetland communities. Although floodplain ecosystems are naturally resilient, communities that are already stressed due to anthropogenic disturbance may be ill-equipped to combat future climate-driven change. Furthermore, future studies within the GLM complex should examine how sediment deposition and erosion patterns have changed over time using sediment coring to more precisely link erosional and accretional wetland shoreline change with anthropogenic disturbances within the watershed. Although this is a complex system with multiple stressors potentially impacting flood pulse dynamics, more work in determining the role of upstream dam construction in historical habitat change is imperative as any decision that NB Power makes about the future of the failing Mactaquac Generating Station (Stantec Consulting Ltd., 2015) will have consequences for the downstream floodplain wetlands and their communities. Additional knowledge on how communities have already been affected by disturbance will help us to forecast how they will respond in the future, potentially aiding in the mitigation of lasting effects.

DATA AVAILABILITY STATEMENT

The datasets presented in this study can be found in online repositories. The names of the repository/repositories and accession number(s) can be found below: Dryad (doi: 10.5061/dryad.547d7wm5h).

AUTHOR CONTRIBUTIONS

NR, ZC, WM, and DB conceived and designed the experiment. NR and ZC conducted the field and lab work. MB led the identification of macrophytes. NR and WM performed the statistical analyses. NR wrote the first draft of the manuscript. All authors contributed to subsequent revisions.

FUNDING

Research support was provided by the Natural Sciences and Engineering Research Council of Canada Collaborative Research and Development Grant (NSERC CRD CRDPJ 462708-13) awarded to DB, WM and others, and a Natural Sciences and Engineering Research Council of Canada Discovery Grant awarded to DB and funding to DB from the federal Genomics Research and Development Initiative's Ecobiomics project.

ACKNOWLEDGMENTS

We thank members of CRI, ECCC, and the MAES team for valuable discussions and feedback in developing our study and manuscript. Additionally, CRI affiliates Z. O'Malley, C. Brooks, and S. Stefani helped with the substantial effort of scanning and digitizing aerial images. We also thank J. Ogilvie for all his help in getting the GIS part of this project off the ground, K. Heard for her invaluable help in the field, and to those at the New Brunswick Department of Energy and Resource Development, including D. Wilson, A. Robinson, D. Pardis-Lacey, and H. Loomer, who gave us access to the historical images and associated metadata. This research originally appeared in a thesis written by NR, as cited below.

SUPPLEMENTARY MATERIAL

The Supplementary Material for this article can be found online at: https://www.frontiersin.org/articles/10.3389/fevo.2021.553094/full#supplementary-material

REFERENCES

Almeida, R. M., Hamilton, S. K., Rosi, E. J., Barros, N., Doria, C. R. C., Flecker, A. S., et al. (2020). Hydropeaking operations of two run-of river mega-dams alter downstream hydrology of the largest Amazon tributary. *Front. Environ. Sci.* 8:120. doi: 10.3389/fenvs.2020.00120

Amoros, C., and Bornette, G. (2002). Connectivity and biocomplexity in waterbodies of riverine floodplains. *Freshw. Biol.* 47, 761–776. doi: 10.1046/j.1365-2427.2002.00905.x

Arias, M. E., Wittmann, F., Parolin, P., Murray-Hudson, M., and Cochrane, T. A. (2018). Interactions between flooding and upland disturbance drives species diversity in large river floodplains. *Hydrobiologia* 814, 5–17. doi: 10.1007/s10750-016-2664-3

Armellin, A., Baird, D. J., Curry, C., Glozier, N., Martens, A., and McIvor, E. (2019). *CABIN Wetland Macroinvertebrate Protocol Draft Version 1.0*. Canada: Environment and Climate Change Canada.

Barbarossa, V., Schmitt, R. J. P., Huijbregts, M. A. J., Zarfl, C., King, H., and Achipper, A. M. (2020). Impacts of current and future large dams on the geographic range connectivity of freshwater fish worldwide. *Proc. Natl. Acad. Sci. U.S.A.* 117, 3648–3655. doi: 10.1073/pnas.1912776117

Bayley, S. E., and Guimond, J. K. (2008). Effects of river connectivity on marsh vegetation community structure and species richness in montane floodplain wetlands in Jasper National Park, Alberta, Canada. *Écoscience* 15, 377–388. doi: 10.2980/15-3-3084

Beltaos, S., and Burrell, B. C. (2016). Characteristics of suspended sediment and metal transport during ice breakup, Saint John River, Canada. *Cold Reg. Sci. Technol.* 123, 164–176. doi: 10.1016/j.coldregions.2015.12.009

Blaney, S. (2003). *A Reconnaissance Vascular Plant Inventory of the Portobello National Wildlife Area*. Sackville, NB: Atlantic Canada Conservation Data Centre.

Brinson, M. M. (1993). Changes in the functioning of wetlands along environmental gradients. *Wetlands* 13, 65–74. doi: 10.1007/BF03160866

Brock, M. A., Smith, R. G. B., and Jarman, P. J. (1999). Drain it, dam it: alteration of water regime in shallow wetlands on the New England Tableland of New South Wales, Australia. *Wetl. Ecol. Manag.* 7, 37–46. doi: 10.1023/A:1008416925403

Broster, B. E., and Dickinson, P. C. (2015). Late Wisconsinan and Holocene development of Grand Lake Meadows area and southern reaches of the Saint John River Valley, New Brunswick, Canada. *Atl. Geol.* 51, 206–220.

Brown, A. G., Lespez, L., Sear, D. A., Macaire, J., Houben, P., Klimek, K., et al. (2018). Natural vs anthropogenic streams in Europe: history, ecology and implications for restoration, river-rewilding and riverine ecosystem services. *Earth Sci. Rev.* 180, 185–205. doi: 10.1016/j.earscirev.2018.02.001

Canadian Council of Ministers for the Environment (2014). *Canadian Environmental Quality Guidelines*. CCME. Available online at: http://ceqg-rcqe.ccme.ca/en/index.html#void (accessed June 19, 2019).

Canadian Rivers Institute (2011). in *The Saint John River: a State of the Environment Report*, eds S. D. Kidd, R. A. Curry, and K. R. Munkittrick (Fredericton, NB: Canadian Rivers Institute).

Charrad, M., Ghazzali, N., Boiteau, V., and Niknafs, A. (2014). NbClust: an R package for determining the relevant number of clusters in a data set. *J. Stat. Softw.* 61, 1–36.

Chen, W. W., and Chang, H. K. (2009). Estimation of shoreline position and change from satellite images considering tidal variation. *Estuar. Coast. Shelf Sci.* 84, 54–60. doi: 10.1016/j.ecss.2009.06.002

Chipps, S. R., Hubbard, D. E., Werlin, K. B., Haugerud, N. J., Powell, K. A., Thompson, J., et al. (2006). Association between wetland disturbance and biological attributes in floodplain wetlands. *Wetlands* 26, 497–508.

Chow, T. L., Rees, H. W., and Monteith, J. (2000). Seasonal distribution of runoff and soil loss under four tillage treatments in the upper St. John River valley New Brunswick, Canada. *Can. J. Soil Sci.* 80, 649–660. doi: 10.4141/S00-006

Connell, J. H. (1978). Diversity in tropical rain forests and coral reefs. *Science* 199, 1302–1310.

Csiki, S. J. C., and Rhoads, B. L. (2014). Influence of four run-of-river dams on channel morphology and sediment characteristics in Illinois, USA. *Geomorphology* 206, 215–229. doi: 10.1016/j.geomorph.2013.10.009

Cunjak, R. A., and Newbury, R. W. (2005). "Atlantic coast rivers of Canada," in *Rivers of North America*, eds A. Benke and C. Cushing (Cambridge, MA: Academic Press), 939–982.

Dormann, C. F., Elith, J., Bacher, S., Buchmann, C., Carl, G., Carré, G., et al. (2013). Collinearity: a review of methods to deal with it and a simulation study evaluating their performance. *Ecography* 35, 027–046. doi: 10.1111/j.1600-0587.2012.07348.x

Du Laing, G., Rinklebe, J., Vandecasteele, B., Meers, E., and Tack, F. M. G. (2009). Trace metal behaviour in estuarine and riverine floodplain soils and sediments: a review. *Sci. Total Environ.* 407, 3972–3985. doi: 10.1016/j.scitotenv.2008.07.025

Environment and Climate Change Canada's National Laboratory for Environmental Testing (2013). *Certified Reference Materials*. https://www.ec.gc.ca/inre-nwri/default.asp?lang=En&n=D3D76BEC-1 (Accessed July 7, 2013)

Environmental Systems Research Institute [ESRI] (2018). *ArcGIS Desktop: Release 10.6.1*. Redlands, CA: ESRI.

Fazekas, A. J., Kuzmina, M. L., Newmaster, S. G., and Hollingsworth, P. M. (2012). "DNA barcoding methods for land plants," in *DNA Barcodes. Methods in Molecular Biology (Methods and Protocols)*, Vol. 858, eds W. Kress and D. Erickson (Totowa, NJ: Humana Press), 223–252.

Galat, D. L., Fredrickson, L. H., Humburg, D. D., Bataille, K. J., Bodie, J. R., Dohrenwend, J., et al. (1998). Flooding to restore connectivity of regulated, large-river wetlands. *BioScience* 48, 721–733. doi: 10.2307/1313335

Government of Canada (2020). *Canadian Climate Normals 1981-2020 Station Data*. Available online at: https://climate.weather.gc.ca/climate_normals/results_1981_2010_e.html?stnID=6157&autofwd=1 (Accessed June 2020, 15).

Grace, M., Butler, K. E., Simpkin, P., and Yamazaki, G. (2017). *Reservoir Siltation and Quaternary Stratigraphy Beneath The Mataquac Headpond, New Brunswick, Canada, As Revealed By Acoustic And Ground Penetrating Radar Sub-Bottom Imaging. Atlantic Geology* **53**, Atlantic Geoscience Society Abstracts- 43 Colloquium & Annual General Meeting 2017. doi: 10.4138/atlgeol.2017.006

Hansson, L. A., Brönmark, C., Nilsson, P. A., and Åbjörnsson, K. (2005). Conflicting demands on wetland ecosystem services: nutrient retention, biodiversity or both? *Freshw. Biol.* 50, 705–714. doi: 10.1111/j.1365-2427.2005.01352.x

Harvey, H. H. (1976). Aquatic environmental quality: problems and proposals. *J. Fish. Res. Board Can.* 33, 2634–2670. doi: 10.1139/f76-315

Himmelstoss, E. A., Henderson, R. E., Kratzmann, M. G., and Farris, A. S. (2018). *Digital Shoreline Analysis System (DSAS) version 5.0 user guide: U.S. Geological Survey Open-File Report 2018–1179*. Reston, VA: USGS, 110. doi: 10.3133/ofr20181179

Huokuna, M., Morris, M., Beltaos, S., and Burrell, B. C. (2020). Ice in reservoirs and regulated rivers. *Int. J. River Basin Manag.* doi: 10.1080/15715124.2020.1719120

Jones, P. E., Consuegra, S., Borger, L., Jones, J., and de Leaniz, C. G. (2020). Impacts of artificial barriers on the connectivity and dispersal of vascular macrophytes in rivers: a critical review. *Freshw. Biol.* 65, 1165–1180. doi: 10.1111/fwb.13493

Junk, W. J., Bayley, P. B., and Sparks, R. E. (1989). "The flood pulse concept in river-floodplain systems," in *Proceedings of the International Large River Symposium (LARS)*, Vol. 106, ed. D. P. Dodge (Honey Harbour, ONT: Canadian Special Publication of Fisheries and Aquatic Sciences), 110–127.

Kassambara, A., and Mundt, F. (2017). *factoextra: Extract and Visualize the Results of Multivariate Data Analyses. R Package Version 1.0.5*. Available online at: https://CRAN.R-project.org/package=factoextra (Accessed April 2020, 1).

Kingsford, R. T. (2000). Ecological impacts of dams, water diversions and river management on floodplain wetlands in Australia. *Austral Ecol.* 25, 109–127. doi: 10.1046/j.1442-9993.2000.01036.x

Kovalenko, K. E., Thomaz, S. M., and Warfe, D. M. (2012). Habitat complexity: approaches and future directions. *Hydrobiologia* 685, 1–17. doi: 10.1007/s10750-011-0974-z

Lallias-Tacon, S., Liébault, F., and Piégay, H. (2017). Use of airborne LiDAR and historical aerial photos for characterising the history of braided river floodplain morphology and vegetation responses. *CATENA* 149, 742–759. doi: 10.1016/j.catena.2016.07.038

Lê, S., Josse, J., and Husson, F. (2008). FactoMineR: an R package for multivariate analysis. *J. Stat. Softw.* 25, 1–18. doi: 10.18637/jss.v025.i01

Marren, P. M., Grove, J. R., Webb, J. A., and Stewardson, M. J. (2014). The potential for dams to impact lowland meandering river floodplain geomorphology. *Sci. World J.* 2014, 1–24. doi: 10.1155/2014/309673

Merchant, S. S. (2010). The elements of plant micronutrients. *Plant Physiol.* 154, 512–515. doi: 10.1104/pp.110.161810

Myers, N. (1997). "The rich diversity of biodiversity issues," in *Biodiversity II: Understanding and Protecting Our Biological Resources*, eds M. L. Reaka-Kudla, D. E. Wilson and O. Wilson (Washington, DC: Joseph Henry Press), 125–138.

Nakazawa, M. (2018). *fmsb: Functions for Medical Statistics Book With Some Demographic Data. R Package Version 0.6.3*. https://CRAN.R-project.org/package=fmsb (accessed May 2021, 11).

Nash, J. E., and Sutcliffe, J. V. (1970). River flow forecasting through conceptual models. Part 1- A discussion of principals. *J. Hydrol.* 10, 282–290. doi: 10.1016/0022-1694(70)90255-6

NCBI Resource Coordinators (2017). Database resources of the national center for biotechnology information. *Nucleic Acids Res.* 45, D12–D14. doi: 10.1093/nar/gkw1071

Oksanen, J., Blanchet, F. G., Friendly, M., Kindt, R., Legendre, P., McGlinn, D., et al. (2019). *vegan: Community Ecology Package. R Package Version 2.5-4*. https://CRAN.R-project.org/package=vegan (Accessed November 2020, 28).

Papoulias, M. M., Chaplin, M., and Bishop, G. (2006). *Flora of the Grand Lake Meadows: Results of a Vascular Plant Inventory and Community Ecology Study Of The Grand Lake Meadows Project Boundary Area*. Fredericton, NB: New Brunswick Federation of Naturalists.

Pekel, J., Cottam, A., Gorelick, N., and Belward, A. S. (2016). High-resolution mapping of global surface water and its long-term changes. *Nature* 540, 418–422. doi: 10.1038/nature20584

R Core Team (2019). *R: A Language and Environment For Statistical Computing*. Vienna: R Core Team.

Ratnasingham, S., and Hebert, P. D. N. (2007). BOLD: the barcode of life data system (www.barcodinglife.org). *Mol. Ecol. Notes* 7, 355–364. doi: 10.1111/j.1471-8286.2006.01678.x

Rejmankova, E. (2011). The role of macrophytes in wetland ecosystems. *J. Ecol. Environ.* 34, 333–345. doi: 10.5141/jefb.2011.044

Revenga, C., Brunner, J., Henninger, N., Kassem, K., and Payne, R. (2000). *Pilot Analysis of Global Ecosystems: Freshwater Systems*. Washington, DC: World Resources Institute.

Richter, B. D., Baumgartner, J. V., Powell, J., Braun, D. P., Richter, B. D., Baumgartner, J. V., et al. (1996). A method for assessing hydrologic alteration within ecosystems. *Soc. Conserv. Biol.* 10, 1163–1174. doi: 10.1007/s13361-012-0389-8

Rooney, R. C., Carli, C., and Bayley, S. E. (2013). River connectivity affects submerged and floating aquatic vegetation in floodplain wetlands. *Wetlands* 33, 1165–1177. doi: 10.1007/s13157-013-0471-4

Stantec Consulting Ltd. (2015). *Mactaquac Project Comparative Environmental Review (CER) Report- Summary Document*. Fredericton, NB: Stantec Consulting Ltd.

Tockner, K., Bunn, S. E., Gordon, C., Naiman, R. J., Quinn, G. P., and Stanford, J. A. (2008). "Flood plains: critically threatened ecosystems," in *Aquatic Ecosystems: Trends and Global Prospects*, ed. N. Polunin (Cambridge: Cambridge University Press), 45–62.

Tockner, K., Pusch, M., Borchardt, D., and Lorang, M. S. (2010). Multiple stressors in coupled river-floodplain ecosystems. *Freshw. Biol.* 55, 135–151. doi: 10.1111/j.1365-2427.2009.02371.xR

Tockner, K., and Stanford, J. A. (2002). Riverine flood plains: present state and future trends. *Environ. Conserv.* 29, 308–330. doi: 10.1017/S037689290200022X

United States Environmental Protection Agency (1996). *Method 3050B Acid Digestion of Sediments, Sludges, and Soils*. Washington, DC: United States Environmental Protection Agency.

Varga, K., Dévai, G., and Tóthmérész, B. (2013). Land use history of a floodplain area during the last 200 years in the Upper-Tisza region (Hungary). *Reg. Environ. Change* 13, 1109–1118. doi: 10.1007/s10113-013-0424-8

Venterink, O., Vermaat, J. E., van der Lee, G. E. M., van den Hoorn, M. W., Pronk, M., Wiegman, F., et al. (2006). Importance of sediment deposition and denitrification for nutrient retention in floodplain wetlands. *Appl. Veg. Sci.* 9, 163–174. doi: 10.1111/j.1654-109X.2006.tb00665.x

Walker, P. D., Wijnhoven, S., and van der Velde, G. (2013). Macrophyte presence and growth form influence macroinvertebrate community structure. *Aquat. Bot.* 104, 80–87. doi: 10.1016/j.aquabot.2012.09.003

Ward, J. V., Tockner, K., and Schiemer, F. (1999). Biodiversity of floodplain river ecosystems: ecotones and connectivity. *Regul. Rivers Res. Manag.* 15, 125–139. doi: 10.1002/(SICI)1099-1646(199901/06)15:1/3<125::AID-RRR523<3.0.CO;2-E

Washburn and Gillis Associates Ltd. (1996). *Environmental Impact Assessment Trans-Canada Highway Fredericton to Salisbury: Component Study Report Grand Lake Meadows Wetland*. Fredericton, NB: Washburn and Gillis Associates Ltd.

Water Survey of Canada (2017). *National Water Data Archive: HYDAT*. Available online at: http://collaboration.cmc.ec.gc.ca/cmc/hydrometrics/www/ (Accessed July 2017, 5)

Wickham, H. (2016). *ggplot2: Create Elegant Data Visualisations Using The Grammar Of Graphics. ISBN 978-3-319-24277-4. R Package*. Available online at: https://ggplot2.tidyverse.org/ (accessed July 16, 2019).

Conflict of Interest: The authors declare that the research was conducted in the absence of any commercial or financial relationships that could be construed as a potential conflict of interest.

Advantages of publishing in Frontiers

OPEN ACCESS
Articles are free to read for greatest visibility and readership

FAST PUBLICATION
Around 90 days from submission to decision

HIGH QUALITY PEER-REVIEW
Rigorous, collaborative, and constructive peer-review

TRANSPARENT PEER-REVIEW
Editors and reviewers acknowledged by name on published articles

Frontiers
Avenue du Tribunal-Fédéral 34
1005 Lausanne | Switzerland

Visit us: www.frontiersin.org
Contact us: frontiersin.org/about/contact

REPRODUCIBILITY OF RESEARCH
Support open data and methods to enhance research reproducibility

DIGITAL PUBLISHING
Articles designed for optimal readership across devices

FOLLOW US
@frontiersin

IMPACT METRICS
Advanced article metrics track visibility across digital media

EXTENSIVE PROMOTION
Marketing and promotion of impactful research

LOOP RESEARCH NETWORK
Our network increases your article's readership